

PROCEEDINGS OF THE
INTERNATIONAL SYMPOSIUM ON
POLARIZATION PHENOMENA OF
NUCLEONS

Basel, 4-8 July, 1960

Editors: P. HUBER and K. P. MEYER



—1961

BIRKHÄUSER VERLAG BASEL
UND STUTTGART

FOREWORD

From 4-8 July 1960, following the 500th Anniversary Celebration of the University, a Symposium on 'Polarization Phenomena of Nucleons' was held in Basel under the sponsorship of the International Union of Pure and Applied Physics. In addition to the Union, the conference received financial support from the REGIERUNGSRAT BASEL-STADT, the SWISS NATIONAL FOUNDATION and the following industries: CIBA, ELEKTRIZITÄTWERK BASEL, GEIGY, HAEFELY, HOFFMANN-LA ROCHE, LONZA, and SANDOZ. The organizing committee consisted of:

P. HUBER, president
K. P. MEYER, secretary
E. BAUMGARTNER
L. BROWN
H. R. STRIEBEL
M. VERDE

The theme chosen for discussion was handled here for the first time by an international symposium. The organizers expected a small number of participants because of the special subject matter. Their expectations, however, were not fulfilled, as the meeting found considerable interest. It was fortunate, that nearly all physicists engaged in the development of artificial sources of polarized particles attended. The symposium gave an excellent survey of the present development of this new technique and allowed an intensive exchange of ideas between the various research groups. The production of polarized targets was also discussed, a problem whose realization will allow full utilization of sources of polarized ions. In addition to these new experimental techniques, which are being studied in several laboratories, the following topics came to discussion: Generation of polarized nucleons and deuterons by reactions; reactions and scattering of polarized particles; theories concerning polarization effects of nucleons. To keep the subject matter within reasonable limits, high energy physics was excluded except where its discussion was meaningful for the low energy areas.

The positive direction of polarization for particles of spin $1/2$ produced by reaction or scattering had not previously been unambiguously established, a situation obstructive for discussion and comparison of publications. The assembly adopted a convention—designated as the Basel Convention—at the suggestion of Prof. H. BARSCHALL and Prof. W. HÄBERLI eliminating this ambiguity. The general assembly of the International Union of Pure and Applied Physics later approved this clarification at the Ottawa meeting. The Basel Convention, defined at the end of this volume, has been used throughout.

The rapporteur system, which is often used at international conferences, was not selected. We thought it worthwhile to hear original communications from physicists who participated directly in the work reported. A survey talk formed the introduction to each section.

We wish to thank all authors for the rapid delivery of their manuscripts, the publisher for the careful printing of the proceedings and Miss E. HOFMANN and Mr. F. SEILER for their help in the correction of the proofs.

P. HUBER

TABLE OF CONTENTS

P. HUBER, Basel: Introduction	13
<i>I. Production of Sources and Targets of Polarized Nuclei</i>	
W. PAUL, University of Bonn, Germany and CERN, Geneva, Switzerland: Survey of Methods of Producing Sources of Polarized Protons	17
R. FLEISCHMANN, Phys. Institut, Erlangen, Germany: Production of Polarized Protons from a Beam of Atomic Hydrogen by Quadrupole Weak Field Separation of one Hyperfine Component	26
G. CLAUSNITZER, University of Minnesota, Minneapolis, USA: The Polarized Proton Source for the Minnesota Linear Accelerator	35
R. KELLER, L. DICK, and M. FIDECARO, CERN, Geneva, Switzerland: Production of Polarized Protons from a Beam of Atomic Hydrogen by Quadrupole Strong-to-Weak Field Separation of one Hyperfine Component	48
M. K. CRADDOCK, Clarendon Laboratory, Oxford, England: The Polarized Proton Source for the Harwell Proton Linear Accelerator.	59
Supplementary note	434
L. BROWN, E. BAUMGARTNER, P. HUBER, H. RUDIN, and H. R. STRIEBEL, Physical Institute of the University of Basel, Switzerland: The Production of Polarized Particles from an Atomic Beam by Quadrupole Strong Field Separation of Hyperfine Components.	77
V. W. HUGHES, C. W. DRAKE, JR., D. C. BONAR, J. S. GREENSBERG, and G. F. PIEPER, Yale University, New Haven, Conn. USA: Production and Detection of a Polarized Deuteron Beam Using the Atomic Beam Magnetic Resonance Method	89
Supplementary note	435
J. THIRION, R. BEURTEY et A. PAPINEAU, Centre d'Etudes nucléaires de Saclay, France: Etude d'une source de protons polarisés utilisant une transition haute fréquence pour un cyclotron.	108
C. F. HWANG and T. M. SANDERS, JR., University of Minnesota, Minneapolis, USA: Experiments on Dynamic Polarization of Protons in Polyethylene by the 'Solid Effect' - A Proposed Polarized Proton Target	122
I. ALEXEFF, Physikalisches Institut der Universität Zürich, Switzerland: Attempts to Produce H 2 S by Charge Exchange	134
J. EISINGER, Bell Telephone Laboratories, Murray Hill, New Jersey, USA; B. BEDERSON, K. RUBIN, and A. SALOP, New York University, New York, USA: An <i>E-H</i> Gradient Spectrometer	136
S. P. HEIMS, Raytheon Company, Wayland, Massachusetts, USA: Polarization of Nuclei by Macroscopic Rotation.	138
J. HEBERLE, Argonne National Laboratory, Argonne, Illinois, USA: Proposal for Detecting the Polarization of Slow Protons	140

M. BORGHINI et A. ABRAGAM, Saclay, France: Polarisation dynamique de noyaux.	143
N. W. TANNER, Clarendon Laboratory, Oxford, England and J. J. DOMINGO, California Institute of Technology: Polarization of Protons by an A. C. Sextapole Magnetic Field	146

II. Generation of Polarized Nucleons and Deuterons by Reactions

W. HAEBERLI, University of Wisconsin, Madison, Wisc., USA: Survey of Experiments on the Polarization in Reactions	149
C. C. JONKER, Naturkuundig Lab., Vrije Universiteit Amsterdam, Holland: Polarization Measurements of D-D Neutrons by a Solenoid	160
H. BRINKMAN, Naturkuundig Laboratorium der Rijks Universiteit, Groningen, Holland: Polarization in Some (d, n) and (d, p) Reactions. Principle of Ring Polarimeter.	166
H. B. WILLARD, Oak Ridge National Laboratory, Oak Ridge, Tennessee, USA: Detection of Deuteron Alignment with s-wave Reactions	175
J. P. SCANLON, A.E.R.E., Harwell, England: Production of Polarized Neutron Beams by (p, n) Reactions in Various Nuclei	181
B. HIRD, Liverpool University, Liverpool, England: Survey of Measurements in Stripping Reactions	193
L. G. PONDROM and J. W. DAUGHTRY, Aeronautical Research Laboratory, Wright-Patterson AFB, Ohio, USA: Detection of 900 KeV Vector Polarized Deuterons with the Reaction $\text{Li}^6(d, \alpha)\text{He}^4$	201
S. M. AUSTIN, University of Wisconsin, Madison, Wisc., USA and S. E. DARDEN, University of Notre Dame, South Bend, Ind., USA: Polarization of Neutrons from the $\text{Li}^7(p, n)\text{Be}^7$ Reaction.	214
A. BUDZANOWSKI, K. GROTOWSKI, H. NIEWODNICZAŃSKI, J. NURZYŃSKI, and M. SLAPA, Cracow Centre of Nuclear Physics, Cracow Poland: The Polarization of Neutrons from the Stripping of Deuterons on C^{12}	215
R. BARLOUTAUD, H. FARAGGI, A. GARIN et L. ROSEN, Centre d'Etudes nucléaires de Saclay, France: Left-Right Asymmetries in the $\text{D}(d, p)\text{T}$ Reaction with Polarized Deuterons.	217
G. IGO, Lawrence Radiation Laboratory, University of California, Berkeley, California, USA: Polarization of Nuclei in Direct Interaction Processes	219
J. E. BROLLEY, JR., J. L. GAMMEL, and L. ROSEN, Los Alamos Scientific Laboratory, Los Alamos, New Mexico, USA: Production of Spin Polarized Mass-Three Beams	220

III. Reactions and Scattering of Polarized Particles

H. H. BARSCHALL, University of Wisconsin, Madison, Wisc., USA: The Scattering of Polarized Particles	227
J. E. EVANS, A.E.R.E., Harwell, England: Measurements of Polarization in $\text{C}^{12}(p, p)$ Scattering.	239
J. SANADA, Institute for Nuclear Study, University of Tokyo, Japan: Polarization in Proton-Helium and Proton-Carbon Elastic Scattering	249
H. E. CONZETT, G. IGO and A. NIR, Lawrence Radiation Laboratory, University of California, Berkeley, Calif., USA: Polarization in $p\text{-He}^4$ and $p\text{-p}$ Scattering at 22 MeV	253

K. W. BROCKMAN, Jr., Institute for Nuclear Studies, Amsterdam, Holland: Proton Polarization Measurements around 17 MeV	259
S. E. DARDEN, C. A. KELSEY, and T. R. DONOGHUE, University of Notre Dame, South Bend, Ind., USA: Polarization of Neutrons Scattered from Li^6 and Li^7	269
H. R. BRUGGER, Laboratory for Nuclear Physics, Swiss Federal Institute of Technology, Zurich, Switzerland: Polarization Resulting from Elastic Nucleon Scattering below 4 MeV.	277
D. BROWN, A. T. G. FERGUSON, and R. E. WHITE, A.E.R.E., Harwell, England: Energy Variation of Neutron Polarization in Scattering from Zinc, Copper, Molybdenum and Cadmium.	291
F. L. HEREFORD, Department of Physics, University of Virginia, Charlottesville, Virg., USA: Polarization of Elastically Scattered 3.4-MeV Neutrons	303
L. CRANBERG, Los Alamos Scientific Laboratory, Los Alamos, New Mex., USA: Applications of Millimicrosecond Spectroscopy to Neutron Polarization Studies - Method and Results	311
G. W. GREENLEES and A. B. ROBBINS, University of Birmingham, Birmingham, England, Polarization of 9 MeV Protons Elastically Scattered by C, Mg and Al.	325
M. J. SCOTT, A.E.R.E., Harwell, England: A Survey of p - α Elastic Scattering as a Polarization Analyzer	332
R. E. WHITE, A.E.R.E., Harwell, England: D -Phase Dependence of Nucleon- Helium Polarization	335
K. BEARPARK, I. HALL, R. E. SEGEL, S. M. SHAFROTH and N. W. TANNER, Clarendon Laboratory, Oxford, England: Observation on the Reaction $\text{Li}^7(p, \alpha)\text{He}^4$ Using Polarized Protons	337
C. WEDDIGEN and H. SCHOPPER, University of Mainz, Mainz, Germany: The Reaction $\text{Li}^7(p, \alpha)\alpha$ with Polarized Protons	339

IV. Theories Concerning Polarization Effects of Nucleons

G. BREIT, Yale University, New Haven, Conn. USA: Nuclear Forces and Polarization Phenomena	343
J. L. GAMMEL, Los Alamos Scientific Laboratory, Los Alamos, New Mexico, USA: Stripping Theory in Operator Form.	359
L. C. BIEDENHARN, Duke University, Durham, North Carolina, USA and G. R. SATCHLER, Oak Ridge Nat. Lab., Oak Ridge, Tenn., USA: Polarization Phenomena in Deuteron Stripping Reactions	372
L. J. B. GOLDFARB, Department of Theoretical Physics, University, Manche- ster, England: Selection Rules for Polarization in Direct Interactions and Stripping Processes	402
J. L. GAMMEL, B. J. HILL, and R. M. THALER, Los Alamos Scientific Labora- tory, Los Alamos, New Mexico, USA: Elastic Scattering of Deuterons by He^4	409
J. L. GAMMEL and R. M. THALER, Los Alamos Scientific Laboratory, Los Ala- mos, New Mex., USA: Polarization Contours for $T - \alpha$ and $\text{He}^3 - \alpha$ Scattering	423
R. J. N. PHILLIPS, A.E.R.E., Harwell, England: Nucleon-Nucleon Polarization Experiments	425
R. J. N. PHILLIPS, A.E.R.E., Harwell, England: Deuteron Triple-Scattering Experiments	429
F. BJORKLUND, G. CAMPBELL, and S. FERNBACH, Lawrence Radiation Labo- ratory, Livermore, California, USA: Optical Model Analysis of Proton- Nucleus Elastic Scattering Data in the Energy Range 8-17 MeV	432

Introduction

By P. HUBER, Basel

It is indeed a privilege and a great joy for me, to be able to welcome so many of you today. In the name of our organizing committee I bid you a most cordial welcome and I hope that your stay in our city may be both pleasant and profitable.

Eleven years ago I had the pleasure of opening, here in Basel, the first part of an international congress of physics, which was later continued in Como under the auspices of our hospitable Italian colleagues. If we compare the subjects then discussed with those on our present agenda, we are amazed to find how far specialisation has progressed in the field of nuclear science. At our congress of 1949 it was still possible to discuss a wide part of what was then known of the subject of nuclear physics. Today we have to concentrate on a very small field of our knowledge, namely the very specific phenomena of the polarization of nucleons.

There is another change which has taken place in the course of the past eleven years: Some of the best known physicists, who honoured us by their presence in 1949, are no longer amongst us. I would only name such illustrious personages as Enrico Fermi, Wolfgang Pauli and Hans Cramers, of whom we think, together with many others, in grateful memory. On the other hand, students of physics, who at that time were listening with reverence and avid interest to the deliberations of those great scientists, have grown in stature during the ensuing years, and are today in a position to make eminently valuable and decisive contributions of their own to our knowledge of nuclear physics.

Basel has dared, for the second time, to prepare and to organize a symposium of the International Physical Union. Eleven years ago it was a hazardous enterprise to obtain consideration for being host to such a rare gathering. This time it was a question of how to justify that yet another congress should be added to the numerous events which are arranged for physicists all over the world. It was evident therefore, from the start, that we would have to find a theme which was of real interest to physicists everywhere. The choice was large, since scientific knowledge has grown rapidly, and the number of published papers has increased at

an alarming pace. This made it all the more important that we should choose an adequate theme, remembering the words of Erasmus of Rotterdam: Not everything which has been achieved in troublesome scientific work is necessarily important.

The main theme of the symposium has been chosen because we know that in various places work is in progress which is concerned with the production of sources of polarized nucleons. Since no international conference has discussed the theme so far, the moment for choosing it seemed propitious. That our choice was not altogether wrong seems to be proved not only by the interest which our program has found, but by a letter we recently received from the USA, stating that it had been intended to hold a conference on the same subject over there. The list of proposed speakers joined to that letter was almost identical with the names of our colleagues we had invited to read papers here. We are very happy in the knowledge that during the next few days nearly all the teams will be heard who are experimenting in the field which is the subject of our discussions.

A symposium is always awaited with a certain eagerness and expectation. Diverse personalities from all over the world are gathered together for a few days, thus creating an atmosphere of special character. One aspect is inherent in every symposium: it possesses a specifically human and cultural atmosphere which finds expression in friendly personal contacts. They lead to new bonds and strengthen old ones which reach far beyond the national frontiers and create in the truest sense a real worldwide community of physicists. In this way we attain an international unity without renouncing our personal individuality.

And now we are awaiting with particular interest the papers which are to be read. To all the contributors I should like to express, already now, our heartfelt thanks for the tasks which they have so kindly taken upon themselves. It is through their labours that the symposium has been made possible.

To all our guests and participants, who are gracing this event with their presence, I extend my very best wishes for an interesting and agreeable stay in our city. On this note I should like to open our symposium on polarization phenomena of nucleons.

I.

Production of Sources and Targets of Polarized Nuclei

Survey of Methods of Producing Sources of Polarized Protons

By W. PAUL, University of Bonn and CERN

Introduction

For a deeper understanding of the interaction of nucleons with complex nuclei it is extremely helpful to carry out experiments with beams of polarized particles. As always, it is first useful to define what polarized particles are. The nucleons have a spin $I = 1/2$ which is connected with a magnetic moment μ_I . In an external magnetic field there exist two states, with quantum numbers $m_I = \pm 1/2$, respectively, referring to the spin axis pointing parallel or anti-parallel to the field direction. We speak of a fully polarized beam when all of its particles are in only one of these states. If we have a mixture, we define the degree of polarization by the equation

$$P = \frac{N_{\uparrow} - N_{\downarrow}}{N_{\uparrow} + N_{\downarrow}}.$$

Thus 50% polarization ($P = 1/2$) means that $N_{\uparrow} = 3 N_{\downarrow}$: the number of particles with spin 'up' exceeds the number of particles with spin 'down' by a factor of 3.

The protons from all conventional ion sources are unpolarized. What are now the possibilities for producing polarized nucleons? We distinguish here three methods of production;

- 1) polarization by nuclear scattering, using the strong spin-orbit coupling of nuclear interactions;
- 2) production of polarized nucleons in nuclear reactions;
- 3) production of slow polarized protons in a special ion source and subsequent acceleration to the desired energy.

The first two methods work for both protons and neutrons. They will be dealt with during the next days. Today we shall discuss the third point. My task is to give a survey of the different proposals for these special ion sources. Some have already come into operation, as we shall see from the following papers. All methods have in common that they

polarize neutral H-atoms or H_2 -molecules in such a way that the spin of the bound proton has a preference direction in an external field. This polarization of the proton is maintained when the neutral particle is ionized by electron impact or by light. The polarization is conserved during the acceleration as well. If I may say so, none of these methods is new in principle; they are all based on well-known facts of atomic physics. In order to create some understanding, I have to give a refresher course about the hydrogen atom and the hydrogen molecule [1]¹⁾. Perhaps this is useful for some nuclear physicists of most strict observance.

Figure 1 gives the well-known energy levels of the hydrogen atoms. The ground state $1S_{1/2}$ splits into two hyperfine structure (hfs) levels $F = j \pm I = 0, 1$ with a separation $\Delta\nu = 1420$ Mc/s. The ionization energy amounts to 13.5 eV. The first excited state splits into the fine structure levels $2S_{1/2}$, $2P_{1/2}$ and $2P_{3/2}$; $2S_{1/2}$ and $2P_{1/2}$ are separated by the Lamb shift, $\Delta\nu = 178$ Mc/s i. e. $\Delta E \cong 7.3 \cdot 10^{-7}$ eV. The $2S_{1/2}$ state, in the absence of external fields, is metastable with a lifetime of

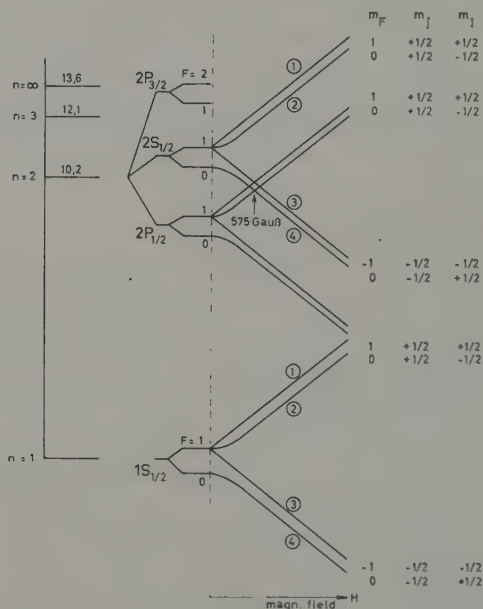


Figure 1

Energy levels and Zeeman splitting of the hyperfine structure states of atomic hydrogen.

¹⁾ Numbers in brackets refer to References, page 25.

about 0.1 second. The ionization energy in this state is only 3.3 eV. Both states, $1S_{1/2}$ and $2S_{1/2}$, can be used to produce polarized protons. We shall first consider the ground state.

1. Polarization Using the Hydrogen Ground State

1) By means of Static Magnetic Fields

If we bring the H-atoms into a magnetic field we observe the Zeeman effect of the hfs (see figure 1). Components 1 and 3 show a linear effect, whereas 2 and 4 have a quadratic dependence on the field strength H . If we are able to select particles in only one of these components, the first step of our task is solved, because m_I is defined. We can double the intensity if we use states $1 + 4$ or $2 + 3$.

The experiment was performed at first by RABI, KELLOGG and ZACHARIAS [2] using the molecular beam method and a Stern-Gerlach gradient field. The separation of the particles in the different levels is achieved by the force $\mu \cdot \partial H / \partial x$, where μ is the effective magnetic moment of the atom. It is plotted in figure 2 in units of the Bohr magneton μ_0 as a function of the magnetic field H . Components 1 and 3 have constant moments of opposite sign. Because of the decoupling of the electron spin from the proton spin, the magnetic moment of components 2 and 4 varies with H . At high fields it becomes very close to 1 magneton, but, unfortunately, the proton polarization in the components 1 and 2, or 3 and 4, respectively, has opposite sign. Therefore we can only use weak fields for the separation of the different components. To estimate the order of magnitude of the required field strengths, we have to remember that μ/μ_0 becomes about 0.5, when the interaction of the electronic moment with the external field $\mu_0 \cdot H$ is equal to $\mu_I \cdot H_k$ (H_k magnetic field at the place of the proton), which means $H \sim 500$ oersted. Low fields entail small gradients and hence the gradient field region has to be extended in order to get a minimum of spatial separation. This in turn gives rise to a small beam aperture and hence to relatively small intensities.

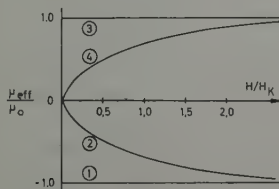


Figure 2

Variation of the magnetic moment with magnetic field for atomic hydrogen.

In order to overcome this aperture problem, it seems advantageous to use the separating properties of magnetic multipole fields, which can be treated as rotational symmetric lenses, focussing or defocussing, depending on the sign of the magnetic moment (FRIEDBURG, PAUL and BENNEWITZ [3]). The proposal to use such fields for a polarized proton source came from CLAUSNITZER, FLEISCHMANN and SCHOPPER [4].

The principle is the following (figure 3). Particles coming out of the oven slit are focused in a subsequent magnetic field if the force acting is $K = -cr$; in other words, if the potential energy is $\varphi \rightarrow r^2$.

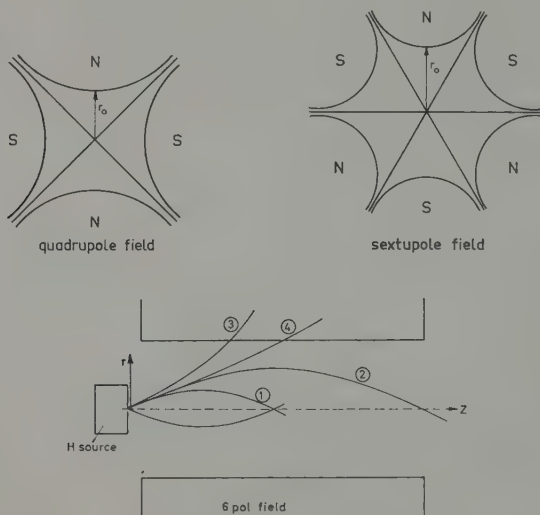


Figure 3

Schematic path of H atoms in the different Zeeman levels inside a sextupole field.

In the case of a linear Zeeman effect, the energy gain is $\Delta W = -\mu H$. From the focussing condition it is seen that H has to be proportional to r^2 and that only atoms with a negative magnetic moment are focused. This condition is fulfilled by a sextupole field (table I) for which $|H| = H_0 r^2 / r_0^2$. In such a field, H-atoms in state 1 are focused, whereas states 3 and 4 are defocused because the magnetic moment is positive. Particles in state 2 are focused as well, but with a weaker and anharmonic force. To get a harmonic force on these particles, which have a quadratic Zeeman effect at least up to 500 gauss, one must use a magnetic quadrupole field. For such a field is $|H| \sim r$ and because $\Delta W = -\alpha H^2$ the condition for a harmonic potential is fulfilled for states with negative α .

For the state 1 this leads to a constant force. The paths of the different particles are schematically shown in figure 3. The separation of the states is achieved by means of a diaphragm behind the field region.

Table I
General magnetic potential of a multipole field
 $\Phi \sim r^m \cos m \varphi$

4-pole	6-pole
$m = 2$	$m = 3$
$\Phi \sim r^2 \cos 2 \varphi$	$\Phi \sim r^3 \cos 3 \varphi$
$ H_r = \left(\frac{H_0}{r_0} \right) r$	$ H_r = \left(\frac{H_0}{r_0^2} \right) r^2$
$\text{grad } H = \frac{H_0}{r_0}$	$\text{grad } H = \frac{2 H_0}{r_0^2} r$
General force on an atom	
$F = -\text{grad } \omega = -\frac{\partial \omega}{\partial H} \cdot \frac{\partial H}{\partial r} = \frac{\mu}{\partial r} \frac{\partial H}{\partial r}$	
Force on component	
$F_1 = -\frac{\mu_0 H_0}{r_0}$	$F_1 = -\frac{\mu_0 2 H_0}{r_0} r$
$F_2 = -\frac{\mu_0 H_0}{r_0} \frac{\xi}{\sqrt{1 + \xi^2}}$	$F_2 = -\frac{2 \mu_0 H_0}{r_0} \frac{r \xi}{\sqrt{1 + \xi^2}}$
for $\xi = \frac{H}{H_K} < 1$	
$F_2 = -\text{const } r$	$F_2 = -\text{const } r^3$
$F_3 = -F_1$	$F_3 = -F_1$
$F_4 = -F_2$	$F_4 = -F_2$

The focal length of the lens depends on the velocity of the particles; as they come out of the oven with a Maxwellian distribution this gives rise to a strong chromatic error. HAMILTON and PIPKIN [5] have shown that this effect could be nearly cancelled by using a sextupole field with decreasing inhomogeneity in the z direction. This is achieved by increasing the pole diameter r_0 . FRIEDBURG [6] has shown that an achromatic lens can be obtained by using a time-of-flight focusing method. In this case the magnetic field is not constant in time but rather pulsed in such a way that slow and fast atoms reach the focal point at the same time. Perhaps this method can be used with pulsed accelerators.

It depends on the special arrangement whether quadrupole or sextupole fields are better. FLEISCHMANN was the first to propose the quadrupole; KELLER [7] discussed this question in detail by calculating the particle path in both field types. His arrangement consists of a strong field which adiabatically goes over into a weak one. For this arrangement a sextupole of a given length is slightly superior to a quadrupole. On the other hand, the sextupole field is more complicated to produce and needs more power.

2) Polarization by Means of an *rf* Field

As we have seen above, it is relatively easy to separate the two electronic states $m_j = \pm 1/2$ in a strong Stern-Gerlach or multipole field and to eliminate by means of a diaphragm all atoms in the states 3 and 4 (figure 2). Thus the beam contains only atoms in states 1 and 2 polarized according to the electronic moment but unpolarized in the proton moment.

ABRAGAM and WINTER [8] proposed to transfer all atoms in state 2 into state 4 by means of a radio-frequency field $H_1 \cos \omega t$ parallel to a constant field H_0 (adiabatic passage methods). Then the proton spin direction is the same for all atoms. For a transition frequency of 240 Mc/s they calculate for the necessary field strength $H_1 = 1$ gauss. Even if the population of the states 2 and 4 were equalized rather than interchanged by the *rf* field, the resulting proton polarization would be $1/2$.

For a Stern-Gerlach magnet separating the two electronic states, TIMOFEEV and FOGEL [9] propose a special field distribution with an exponential increase of H_z .

2. Polarization of Protons Using the Hydrogen 2S State

Proposals for polarizing protons using the $2S_{1/2}$ state came from ZAVOISKII [10] and MADANSKY and OWEN [11]. They make use of the Lamb shift. The principle of these methods is already contained in the famous paper of LAMB and RETHERFORD [12] on the fine structure of the excited hydrogen atom.

As already mentioned, the $2S_{1/2}$ and $2P_{1/2}$ states are separated by the Lamb shift. The lifetime of atoms in the $2P$ state is calculated to $\tau_p = 1.6 \cdot 10^{-9}$ s, whereas without external field the $2S$ state is metastable ($\Delta l = 0$). The decay time τ_s amounts to about 0.1 s which corresponds to a decay length of ~ 100 m at thermal velocity of the atom.

An external electrostatic field mixes the $2P$ into the $2S$ state, so that a field of 10 V/cm already reduces τ_s to about $5\tau_p$. The meta-

stable S level is therefore quenched and the decay length is shortened to ~ 0.01 mm.

A magnetic field has two effects upon the atom. At first we observe the Zeeman effect of the hyperfine structure, $S_{1/2}$ and $P_{1/2}$ levels split in four components as shown in figure 1. Secondly, a particle traversing a magnetic field sees a motional electric field of the order $E = (v/c)H$ which causes the quenching effect. At a field of 575 gauss the level ($m_j = -1/2$) of the $2S$ state crosses the $m_j = 1/2$ of the P state. An atom in either of the components 3 or 4 now has a decay length of ~ 0.5 mm, while for components 1 and 2 the decay length is still ~ 90 cm. It is obvious that this highly differential behaviour may produce a beam of particles in which the population of the $n = 2$ level is entirely in the states 1 and 2, which are polarized in the electron moment. Both proposals make use of these effects. They start with a beam of atomic hydrogen partially excited to the $n = 2$ level, which subsequently enters a field of 575 gauss. If the particles are removed adiabatically out of the field, the protons in component 1 remain completely polarized. The coupling between the electron and proton magnetic moments becomes effective again, so that at low fields the particles in component 2 are unpolarized because $m_f = 0$. By means of an νf resonance field, we can induce transitions between the state 2 and the corresponding P level. In this way one can, in principle, remove the unpolarized particles from the beam and achieve total polarization.

However, we have to take into consideration that the beam contains a large number of atoms in the ground state $n = 1$, all unpolarized. Only by a selective ionization of the particles in the $n = 2$ level we can get a 50% or higher polarized proton beam. For this selective ionization we use the fact that the ionization energies for the two levels are 3.3 and 13.5 eV respectively. So the energy of the ionizing electrons is restricted to $3.3 \rightarrow 13.5$ eV or, using photo-ionization, the wavelength of the ionizing light has to be $3700 > \lambda > 1260$ Å.

The available proton current depends mainly on the efficiency of the excitation of a H beam.

The normal methods, using electron impact or high temperature in the oven ($\sim 10^{-3}$ or less), are too inefficient to compete with the methods described in Section 1. For this reason the method proposed by MADANSKY and OWEN for obtaining a high intensity $2S$ beam is interesting. These authors propose to start with a beam of protons with an energy of the order of 10 keV. This beam is passed through a chamber filled with hydrogen or another gas (Cesium vapour would perhaps be effective) at a pressure of the order of 10^{-4} mm Hg. The cross-section ($\sim 0.1 \pi a_0^2$) for electron pick-up by a proton provides an efficient mechanism for the production of the metastable atoms. If this way proves to be successful,

the whole method of producing polarized protons is expressionally simpler and more elegant compared with the deflection methods of Section 1.

3. Polarization of Protons Using H_2 Molecules

Another possibility of getting polarized protons is by ionizing polarized ortho-hydrogen molecules. H_2 in the ortho-state has no electronic moment; the entire magnetic moment of the molecule is due to the protons, which have parallel spins. Because the lowest rotational state of the molecule allowed for the ortho-state is $j = 1$, the rotation effects have to be taken into account, but fortunately they are very small; thus a beam of ortho-molecules splits in a Stern-Gerlach field in three components $m_l = \pm 1, 0$. By selecting one state by means of an obstacle or diaphragm, we get a beam of H_2 with both proton spins pointing in the same direction. This method has two disadvantages; due to the low magnetic moment (only nuclear moments!) a strong inhomogeneity of an extended Stern-Gerlach field is necessary (see RAMSEY [1]). Secondly, the residual gas in the apparatus is the same as in the beam but unpolarized. No differential ionizing process is possible and the background problem seems hard to overcome.

GARWIN, who advocated this method [13], estimated that according to the results of RAMSEY, it should be possible to get $2 \times 10^{13}/s$ polarized H_2 molecules. Sending such a beam into a highly effective ion source, he hopes to get $0.1 \mu A$ of polarized protons. He discusses also the storage of such protons in the ion source for use in pulsed accelerators, but his calculations about the depolarization and the efficiency look too optimistic.

4. Depolarization Effects

We have seen that it is possible to obtain beams of neutral atoms or molecules containing polarized protons. The question is now whether their polarization is maintained during the ionizing process and the acceleration afterwards. The problem was discussed by MASSEY in his book 'Atomic Collisions', with the result that the interaction time of the atom with the ionizing electron or photon is too short for any appreciable depolarization. The already working proton sources of the CERN and Basel groups prove it. FRIEDMANN's [14] success in getting polarized photo-electrons from oriented potassium atoms is also a good check.

As TOLHOEK and DE GROOT [15] showed, the acceleration of protons by a pure electric field should not cause any depolarization. This is also true if a homogeneous magnetic field is present.

More serious are the following effects which need to be discussed in detail:

- i) depolarization by motion in an inhomogeneous magnetic field;
- ii) depolarizing collisions with hydrogen or other atoms or with electrons in the ion source.

SCHLIER treated this question in a summary [16], concluding that the collision effects, if any, can be avoided.

For the first point he found that during the acceleration of protons in a synchro-cyclotron like the CERN machine, the effect was negligible. In that special case, the probability of depolarization is only $P \sim 10^{-6}$. For synchrotrons, especially machines with field free sections or strong focusing machines, the depolarization could, however, become really serious.

REFERENCES

- [1] N. F. RAMSEY, *Molecular Beams*, Clarendon Press, Oxford (1956); H. KOPFERMANN, *Nuclear Moments*, Academic Press (1958).
- [2] I. I. RABl, J. M. KELLOGG and J. R. ZACHARIAS, *Phys. Rev.* **46**, 163 (1934).
- [3] H. FRIEDBURG and W. PAUL, *Naturwiss.* **38**, 159 (1951); H. G. BENNEWITZ and W. PAUL, *Z. Phys.* **139**, 489 (1954).
- [4] S. CLAUSNITZER, R. FLEISCHMANN and H. SCHOPPER, *Z. Phys.* **144**, 336 (1956).
- [5] D. R. HAMILTON, A. LEMONICK and F. M. PIPKIN, *Phys. Rev.* **95**, 1356 (1954).
- [6] H. FRIEDBURG, *Z. Phys.* **130**, 493 (1951).
- [7] R. KELLER, CERN Report 57-30.
- [8] A. ABRAGAM and J. WINTER, *Phys. Rev. Letters* **7**, 374 (1958).
- [9] A. D. TIMOFEEV and I. A. M. FOGEL, *Sov. Physics Techn. Phys.* **2**, 1974 (1957).
- [10] E. K. ZAVOISKII, *Sov. Physics JETP* **5**, 603 (1957).
- [11] L. MADANSKY and G. E. OWEN, *Phys. Rev. Letters* **2**, 209 (1959).
- [12] W. E. LAMB and R. C. RETHERFORD, *Phys. Rev.* **72**, 241 (1947).
- [13] R. L. GARWIN, *Rev. Sci. Instr.* **29**, 374 (1958).
- [14] H. FRIEDMANN, *Report on Electron Polarization*, Inst. Theor. Phys., München.
- [15] H. A. TOLHOEK and S. A. DE GROOT, *Physica* **17**, 1 (1951).
- [16] CH. SCHLIER, CERN Report 58-3.

Production of Polarized Protons from a Beam of Atomic Hydrogen by Quadrupole Weak Field Separation of one Hyperfine Component

By R. FLEISCHMANN, Phys. Institut, Erlangen

I should like to describe now which line we have followed in Erlangen to separate one of the four hyperfine components of hydrogen from a beam of atomic hydrogen.

We intend to separate one of the two components with constant magnetic moment. For this we need a weak inhomogeneous magnetic field with as strong a gradient as possible. This can be produced by a magnetic 4-pole field. We have used such a field in all our experiments. As a source of hydrogen atoms we first used a Wood's discharge, then we made a new step, namely by introducing a Laval nozzle. I will describe this later.

With our original atomic beam apparatus [1]¹⁾, it was found that the residual gas contains considerable amounts of hydrogen. This is present in the form of H_2 , H_2O and hydro-carbons from the oil vapours of the diffusion pumps. The H_2 and the H_2O coming mainly from the Wood's discharge can be removed by pumps with a higher pumping speed. The hydrocarbons from the oil vapor still remain. Even at a partial pressure of 10^{-8} Torr more protons would be produced in the ionizer from these molecules than from an atomic beam whose density corresponds to a pressure of 10^{-9} Torr. This results mainly from the fact that the electrons used for ionization occupy a much larger volume than the atomic beam. We have tried to overcome these difficulties in three ways.

Firstly we have replaced the oil diffusion pumps by high speed mercury pumps and have used very narrow channels.

Secondly we have increased the intensity of the atomic beam by using a Laval nozzle.

Thirdly: The volume which is crossed by the electrons in ionizing the beam is made as small as possible and the vacuum around the ionizer is being made extremely good and free of hydrogen. We intend doing this by a bakable thin walled can inside the vacuum. This can be separately

¹⁾ Numbers in brackets refer to References, page 34.

evacuated by a Vacion pump and heated by an electric current through the walls (800 A. at 8 V). The atomic beam will enter through a channel and will leave through a second channel into a second getter pump used as a beam catcher. Before showing a diagram of our setup, I should like to say something about the forming of an intense beam of hydrogen atoms. Which ways are there of forming an atomic H-beam?

Firstly one can use a simple opening in a thin wall. The admissible pressure is determined by the condition that the mean-free path is larger than (or equal to) the diameter of the opening. This is called the critical pressure. The atoms leave this opening with a cosine-distribution. At a certain distance a diaphragm is located to select the beam.

Secondly: In order to decrease the unused gas-flow one can use a long channel as beam-opening. This will produce similar intensities in the forward direction. Several such channels in close formation are called a Zacharias Oven.

Thirdly: As far back as 1941 it was stated by PAUL [2] that the pressure can be increased beyond the critical pressure. One has to use very strong pumps and small distances from the oven to the Abschäler, as we call it (i. e. peeler or beam separator). However the slope of increase of intensity is much smaller beyond the critical pressure than below. KELLER¹⁾ has obtained 12 times the intensity to be expected at the critical pressure. At higher pressures, however, the degree of dissociation of his HF source decreases. In all the atomic beam sources mentioned so far one can calculate the intensity of the atomic beam quite accurately. It can be shown that there is an upper limit which cannot be exceeded. Particularly in the weak field separation method where it is desired to produce a much stronger atomic beam, another way has to be found: One can use a *Laval nozzle*. This was introduced into the atomic beam technique by KISTIAKOWSKY and SLICHTER [3] and by W. BECKER, now in Karlsruhe [4] The nozzle can be described as follows: (figure 1).

The cross-section gradually decreases, reaches a minimum and continuously increases. Let the pressure at the intake end be called p_0 and the pressure at the exit end p_e . Now let us consider the conditions at the point *A* where the nozzle has its smallest cross section. A gas flow is called a 'Laval flow', if the velocity of the gas at *A* equals the velocity of sound under the conditions in *A*. We call this sound velocity $c(A)$. It depends especially on the temperature at *A*.

If we lower the pressure p_0 relatively to p_e until the velocity $v(A)$ at *A* equals $c(A)$, then the pressure in *A* is called 'Laval pressure p_L ' and becomes

$$p_L = \left(\frac{2}{k+1} \right)^{\frac{k}{k-1}} \cdot p_0, \quad \text{where } k = c_p/c_v.$$

¹⁾ This volume page 48.

If p_e is lowered further more, $v(A)$ is not influenced and also the particle flow remains the same. For a higher p_0 still $v(A)$ equals $c(A)$, but the particle flow is increased, mainly by the higher density of the gas.

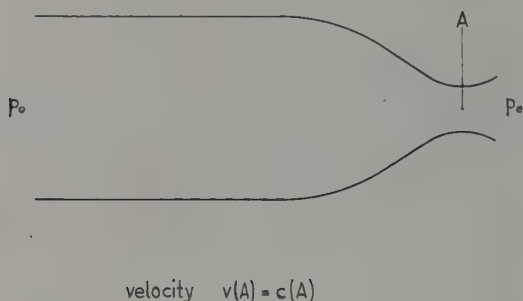


Figure 1

The *angle* of the opening of the nozzle behind the point of smallest cross-section must be chosen correctly, otherwise the beam is disturbed due to eddy phenomena.

The Laval beam has a characteristic *velocity distribution*. A forward velocity is superimposed on the Maxwellian distribution and the width of the distribution is diminished.

The *dissociation* ahead of the nozzle can be done by means of an electrical arc and this is what we have been trying so far.

But it is also possible to dissociate the hydrogen using high frequency. In this connection I should like to draw your attention to a technical development of the Valvo Company in Hamburg, which concerns a high frequency "electronic torch". In the high frequency plasma torch one finds a discharge similar to a direct current glow discharge, but which in this case is energized by high frequency. It can be used for every diatomic gas up to a pressure of one atmosphere. For the discharge one needs a high frequency of very high intensity. The electrodes can be designed in the form of a coaxial wave guide, which is water-cooled. The plasma torch itself is very clean but there are material problems connected with the use of it, and volume recombination by three particle collisions has to be taken into account. The high frequency of the Valvo-torch is 2400 MHz [5].

What is the difference between using a Laval nozzle and using a normal atomic beam?

Firstly: Much more gas enters the atomic beam vacuum and directly in front of the Laval nozzle much stronger pumps are required. Behind the first diaphragm, the Abschäler, as we call it, conditions remain prac-

tically the same as usual. This means that the Abschäler now acts as the new atomic oven opening, but there is a directed flow after the nozzle, instead of a cosine-distribution.

Secondly: Since the dissociation has to be done in a relatively high pressure volume recombination will heat up the gas and therefore the particles have a much higher velocity. This has the effect that the deflection of the particles is more difficult and that they remain only for a shorter time in the ionizing region of the ionizer. In this connection it should be noted that with a high frequency torch the gas temperature is lower than in an arc discharge. (It would appear not quite impossible that in an arc discharge with higher pressure fast atoms are formed by charge exchange and lead to the formation of neutral particles with an extremely high velocity.)

I will now describe *our experimental setup*. First of all I should like to mention the names of my collaborators: H. P. JOCHIM, W. KLINGER, G. FRITSCH, E. WEBER, W. FINK. The apparatus is shown in figure 2, from which can be seen the pumping speed in the different sections, the distances between the diaphragms, the position of the magnets and the location of the Molybdenumoxyd-detector and of the ionizing region.

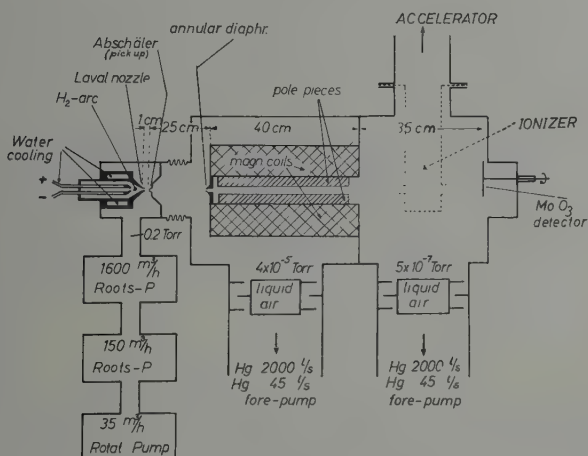
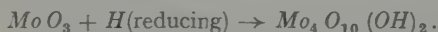


Figure 2

In the arc discharge we have 200 Torr of H_2 . The nozzle has a diameter of 0.2 mm and is made of a ceramic. The distance between the Laval nozzle and the Abschäler is evacuated to a vacuum of between 0.2 and 0.4 Torr by two high-speed mechanical Roots pumps in series. The total

pumping speed of this arrangement is 1600 m³/h or 450 l/s at a pressure of up to 1 Torr.

The length of the path in this section is kept as short as possible. However, the distance between the Laval nozzle and the Abschäler, the shape and the angles of the Abschäler and the adjustment are very sensitive because of possible eddy formation and production of shockwaves. This distance is about 10 mm in our arrangement. In the next section we use a mercury pump of 2000 l/s with a liquid air-trap, which decreases the pumping speed to about 1000 l/s. The pump evacuates this volume down to $5 \cdot 10^{-5}$ Torr. Then follows an annular diaphragm with an outer diameter of 2 mm. Then follows the 4-pole magnet with a length of 30 cm and a magnetic field strength gradient of 40000 Oe/cm at the entrance side and 15000 Oe/cm at the exit. These large gradients necessitates near the entrance the passage of particles through stronger fields. The magnet is so dimensioned that with a particle velocity of 5000 m/s the deflection of the component selected would be about 2 mm. If the velocity corresponded to 300° K, then the deflection of the maximum of the Maxwellian distribution would be about 6 mm. 30 cm further on is a Molybdenum-oxide detector. Figur 3 is a general view of our setup. One can see the Rootspumps, the arc source, the section containing the magnets and the section for the ionizer. There is a very important difference between the detection of an atomic beam by Molybdenum oxide using a Wood's discharge and using an electrical arc. With the latter source, it was noted that the blue colour did not come up before taking the Molybdenum-oxide out of the vacuum into the air. Apparently the presence of some water is important for the forming of the blue Mo-oxide. Therefore one cannot compare the intensities of the atomic beam in the Wood discharge with those in the Laval nozzle arrangement by means of the blue colouring of the Mo-oxide detector. The quantitative comparison will not be possible until we have used the Pirani manometer we have constructed. The process of forming blue Molybdenum oxide is according to a recent research work of chemists



The deflected patterns one gets by quadrupole weak field separation shows figure 4. It is taken using our former apparatus with a circular, not a annular diaphragm.

We want to separate by an opening the component which goes to the centre of the magnetic field, where the magnetic field strength is zero. CLAUSNITZER has checked experimentally in his thesis by using two 4-pole fields in series that this component remains polarized to $90 \pm 10\%$ after it has left the 4-pole field. It is thus shown that the polarization is not disturbed or destroyed by flipping processes under workable conditions.

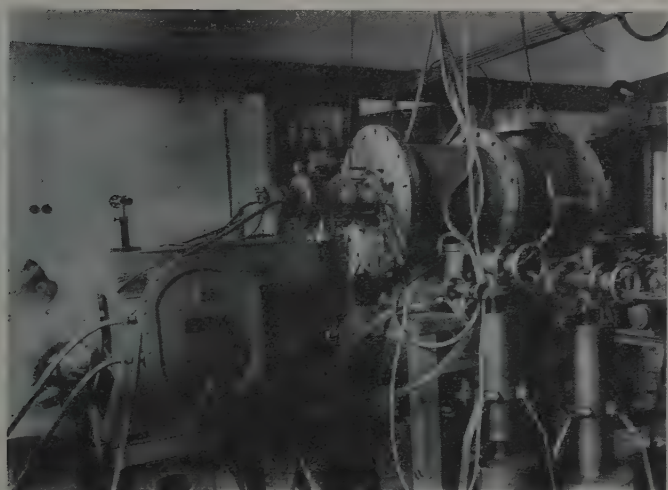


Figure 3

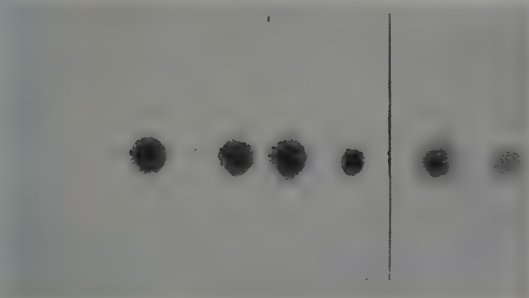


Figure 4

I should like to point to one more fundamental method to separate one hyperfine component which is not impaired by the Maxwellian distribution. BEDERSEN [6] has used superimposed inhomogeneous magnetic and electric fields of equal configuration. This will result in the vanishing of the deflecting force in the region where $\mu \sim H$. In this case the magnetic and the electric forces from the magnetic and electric induced dipole moment cancel out. He used this method for alkali atoms. However for hydrogen or deuterium this would need very high electrical fields. If it would work too for hydrogen, it would have the advantage that

the Maxwellian distribution has no more influence, however the focussing would not work.

Figure 5 shows some beam patterns obtained with the Laval beam apparatus and Molybdenum-oxide detector. In one experiment we removed the Abschäler and replaced it by the MoO-detector. A sharply defined area can be seen, the diameter of which is 3 mm (figure 5a). If it is known how many particles pass through the nozzle as well as the percentage of those, which enter the Abschäler we can determine the resulting beam intensity. We have measured the gas intake into the nozzle. This is $2,5 \cdot 10^{20}$ particles/s (200 Torr). The diameter of the Abschäler is 0.5 mm. Therefore we have $8 \cdot 10^{18}$ particles/s behind the Abschäler.

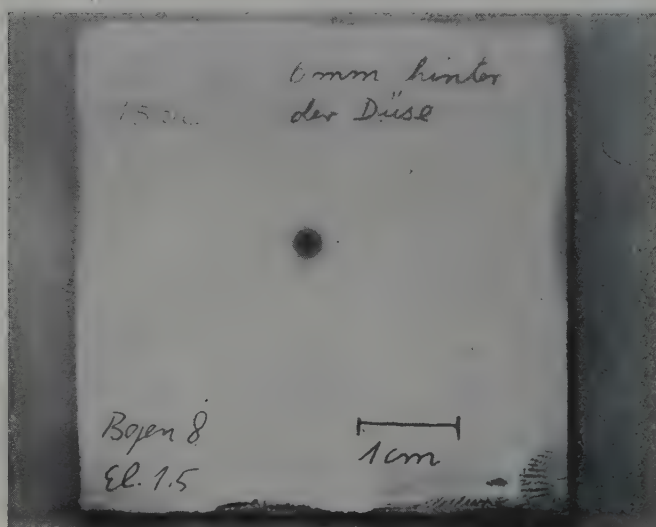


Figure 5a

Well-defined beam leaving the Laval-nozzle (no collimation!)

Of course, a separate measurement must be made to determine which percentage of the beam is dissociated. The degree of dissociation is small until now in our arc source. Figure 5b shows the beam at the end of the apparatus. A wire cross, which is located at the end of the magnets can be clearly seen.

For the ionization we have planned the following arrangement of electrodes in the electron bombardment ionizer which is shown in figure 6. It will be located in the space between the magnet and the Mo O₃ detector

in a can which is separately evacuated by a Vacion pump of 120 l/s for air, which is equivalent to 450 l/s of H_2 . A second getter pump is used as a beam catcher.

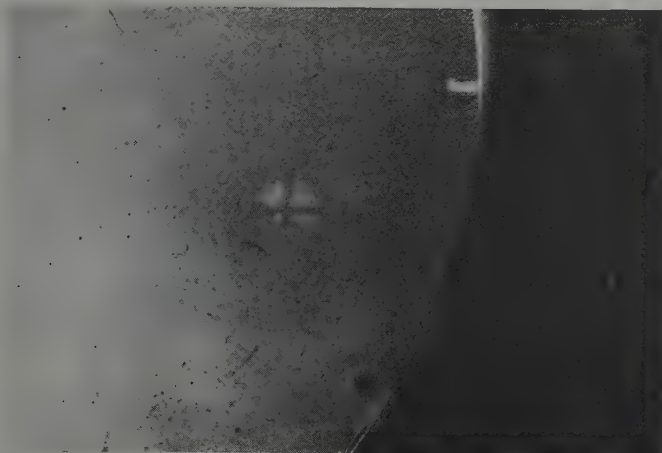


Figure 5b

Atomic beam showing crossed wires and a beam stop wire

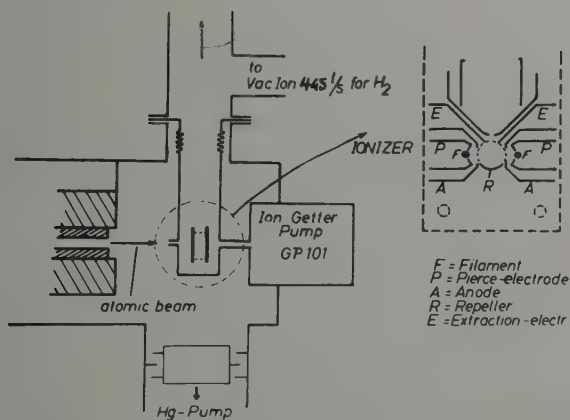


Figure 6

Our next step will be the insertion of the ionizer and especially the increase in the degree of dissociation.

REFERENCES

- [1] G. CLAUSNITZER, R. FLEISCHMANN, H. SCHOPPER, *Z. Physik* **144**, 336 (1956).
G. CLAUSNITZER, *Z. Physik* **153**, 609 (1958).
- [2] PAUL, *Z. Phys.* **117** (1941).
- [3] KISTIAKOWSKY and SLICHTER, *Rev. Sci. Instr.* **22**, 333 (1951).
- [4] W. BECKER, *Z. Naturf.* **9a**, 975 (1954).
- [5] G. CHRISTESCU and R. GRIGOROVICI, *Die Naturwissenschaften* (1941), S. 571;
and J. D. COBINE and D. A. WILBUR, *J. Appl. Phys.* **22**, 835 (1951).
- [6] B. BEDERSON, private communication.

The Polarized Proton Source for the Minnesota Linear Accelerator

By G. CLAUSNITZER, University of Minnesota¹⁾

Summary. The complete vacuum system with all essential parts is assembled in the final location and is working satisfactorily. The ion current extracted from the ionizer was measured with a collector, because the source is not yet connected to the accelerating column of the 500 kV injector. The result so far is a corrected (for residual pressure change) current increase of about 100% when the beam shutter is opened.

General Remarks

A source of polarized protons for injection into the Minnesota Linear Accelerator is being constructed. It is based on a principle mentioned in the work of CLAUSNITZER, FLEISCHMANN, SCHOPPER [1]²⁾. A neutral hydrogen atomic beam is passed through an inhomogeneous magnetic field in which the different magnetic states are separated. Because of intensity problems, no effort will be made to separate the four hyperfine structure components in a weak field. Instead a strong field deflection is used, where the decoupled spin states $m_j = 1/2$, $m_i = \pm 1/2$ are separated from the $m_j = -1/2$ states. Then the beam passes into a weak magnetic field, where it is ionized. The atoms follow the field adiabatically [2], forming coupled states $f = 1$, $m_f = 1, 0$ resulting in a nuclear spin orientation of 0.5. With this method it is possible to shorten the field considerably, allowing therefore a greater aperture of the beam. By ionizing these atoms in a weak field, polarized protons can presumably be extracted.

Since the injector of the Linear Accelerator is on a positive 500 kV potential, the whole ion source has to be on this potential. This seems to involve great difficulties because of weight, space and power needs of this special source. The finally accepted design is shown in figure 1.

The neutral hydrogen atoms are polarized on ground potential, leaving the whole high speed vacuum system there. The hydrogen beam is allowed to travel a distance of 2 meters in an insulating column and is ionized at the high potential by electron bombardment.

¹⁾ On leave of absence from Universität Erlangen, Germany.

²⁾ Numbers in brackets refer to References, page 47.

The necessary pit underneath the injector for the atomic beam apparatus was finished in January 1960, the equipment moved in, connected and aligned afterwards. The ionizer chamber with two Vacion pumps was fitted into the very limited space of the injector. The connection of the two systems is made by a Pyrex glass column. The whole system was completely assembled in June 1960 and test runs were made.

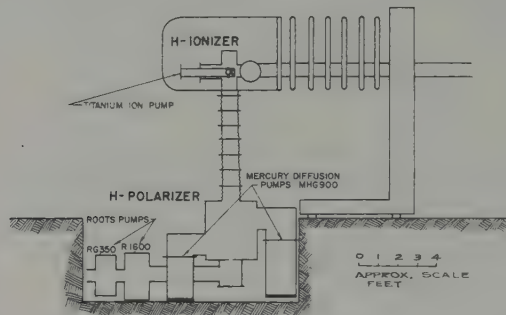


Figure 1

General design schematic of the polarized proton source

The cross section of the source is shown in figure 2; the details will be discussed in the following sections.

The Dissociation Chamber

In order to produce an intensive hydrogen atomic beam, we followed the work of BECKER and BIER [3] and KISTIAKOWSKY and SLICHTER [4], who showed that high intensity beams can be produced by using a supersonic mass flow through specially shaped nozzles. The dissociation is made by a low voltage arc discharge, which the molecules have to traverse.

This chamber was first built up according to the design described in the Progress Report of 1958 [5]. Extensive tests with different filament geometries and materials, nozzle geometries, electrode distances and gas mixtures (Helium admixtures) gave a hydrogen beam with a maximum dissociation degree of about 5%. From gas consumption measurements one could derive a flux of about 10^{21} particles/s through the first nozzle. Besides other troubles (Teflon insulators start burning when the pressure drops below 10 mm and discharge occupies the whole chamber) this scheme seemed rather unsatisfactory, because with the chosen pump units one could not obtain the necessary atomic beam intensity.

For the new design (see figure 3) the two filament supports were replaced by one water cooled support for the negative arc electrode, which was adjustable to change the electrode distance. A Pyrex plate was used for insulation and rubber O-rings for gasketing. The inner part of the nozzle was changed, so that the closest distance of the electrodes was very near to the hole of about .6 mm diameter. The size of the nozzle is not critical, because the pressure in chamber No. 1 can always be

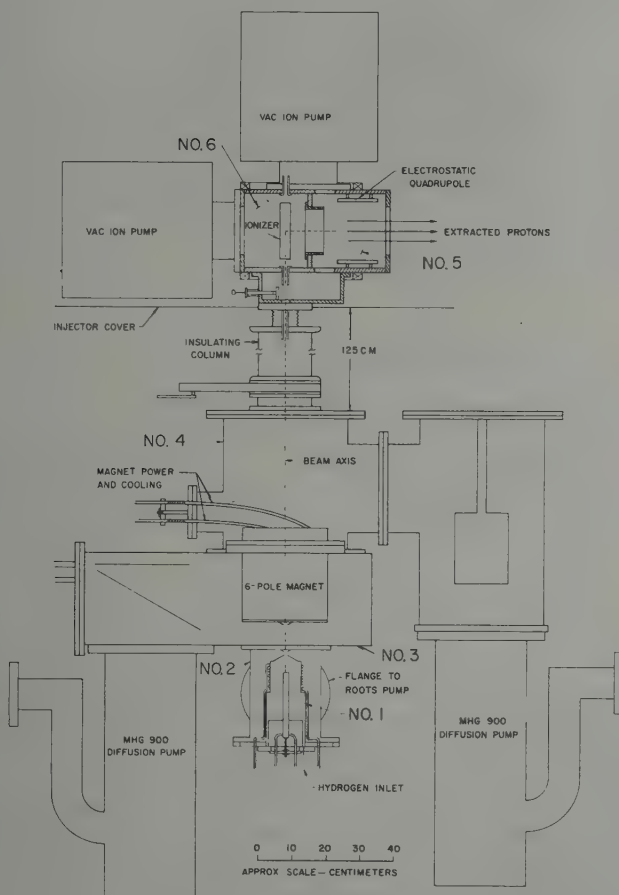


Figure 2

Detailed cross section of the polarized proton source. (Numbers are to identify the differential pumping system as explained in the text).

adjusted to give a suitable working condition. The power supply for the arc discharge can give — 500 volts, 5 amps, which is necessary for starting a glow discharge at low pressure (about 10 mm Hg). A pressure increase to 300 mm (100 to 600 mm, depending on nozzle diameter) change the discharge to an arc with typical working conditions of 100 volts and 3 amps. A voltage of 300 to 400 volts is dropped across a series resistor which stabilizes the arc.

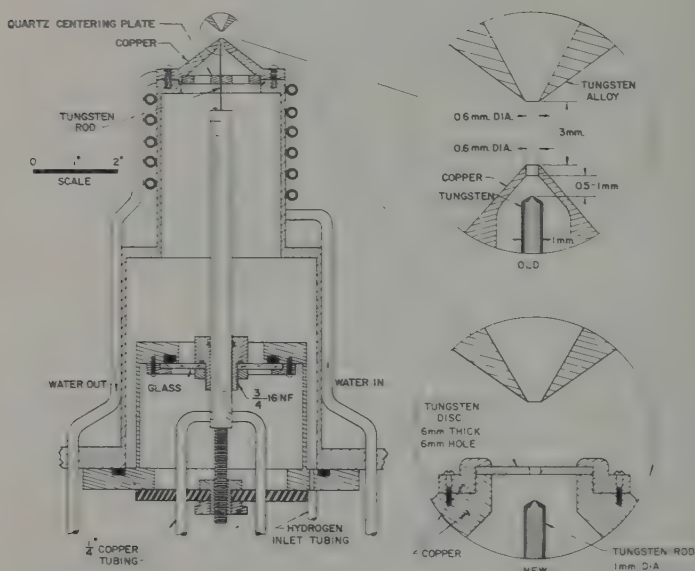


Figure 3

The dissociation chamber with old and new arc electrodes

The presently used cathode is a tungsten rod of 1 mm diameter which is set to a distance of .5 to 1 mm from the anode (nozzle). To maintain stable working conditions, it is necessary to reset the cathode every day; the tungsten consumption is about 1 mm³ 10 hours of discharge.

The arc discharge can be obtained in two different modes depending on the electrode distance. If the distance is 1 mm, the arc will burn between the electrodes and the dissociated molecules have a high chance to recombine at the walls. This results in a beam with about 5% dissociation degree and small velocity (wall temperature). If the distance is .5 mm or smaller, the plasma will be blown through the nozzle into the low pressure chamber No. 2 (.2 mm Hg) which is pumped by the Roots-

pump unit. In this mode the beam is highly dissociated (more than 50%), but the velocity of the atoms is about 12×10^5 cm/s (corresponding to a temperature of about 5000° K). This increased velocity is a disadvantage because the deflection in the magnet and the ionization probability are decreased. We tried to decrease the recombination rate in the first working condition in order to get a high intensity beam with a small velocity, by covering the nozzle inside with Pyrex glass. This melted out in the first second and only a Vicor insert could stand the discharge for about 10 minutes. A stable working condition was obtained by modifying the anode of the arc discharge as shown in figure 3 (new). The arc burns against a tungsten sheet and heats the center part to a white glow. Because of the hot aperture the recombination rate is decreased, resulting in a beam of about 8×10^5 cm/s velocity (corresponding to a temperature of about 3000° K). A beam picture with this arc condition is shown in figure 5. The arc discharge worked erratically sometimes but well enough for the test runs. The tungsten disc anode had to be exchanged after about 50 hours of running time. The system will presumably be modified to meet the requirements of stability necessary for this ion source.

The Differential Pumping System

In figure 2 the vacuum chambers are numbered according to the steps to lower pressures. Chamber No. 1, the arc chamber, is connected to a hydrogen supply (cylinder) and the flow rate can be adjusted with a needle valve to give the pressure of 300–400 mm Hg in working condition. Chamber No. 2 is pumped by two Roots pumps (in series) and a Kinney pump (KD 30).

The choice of the heavier Roots pump RG 350 for backing the high speed pump R 1600 was found necessary. Even in this arrangement the water cooling of the R 1600 is not sufficient, when the pump compresses large amounts of hydrogen. Additional cooled flanges are necessary to maintain safe operation.

The next chamber (No. 3) is rectangular with 1 2" stainless steel walls so that no additional flanges are needed. The connected chambers are bolted to the walls of chamber No. 3. This design gives the shortest possible connection, which is necessary to obtain maximum pumping speed. The chosen mercury diffusion pump MHG 900 did not give satisfactory working pressures because of incomplete baffling. Improved baffles would have cut down the pumping speed to an intolerable value, so that a change to an oil diffusion pump was necessary for this chamber.

The equilibrium pressure in working condition is 10^{-4} mm Hg, which is satisfactory to step down to the low pressure region of the magnet

chamber. With this pump unit it is possible to produce a pressure difference from 300 mm Hg to 10^{-4} mm Hg within a distance of a few millimeters.

The chamber No. 3 has adjustable steel legs so that it can be exactly connected to the Roots pump unit. All the other parts are mounted onto this rectangular chamber. The magnet drops in from the top and the diffusion pump is bolted on from underneath. The distance between the entrance aperture (beam defining aperture) to the magnet chamber and the source (nozzle) will be 5 to 10 cm (variable for best beam geometry). The following detection measurements have been made in this chamber at the pressure of 10^{-4} mm Hg.

The results of the different detectors indicate a flux of 10^{18} atoms/sec-cm² about 8 cm behind the source. The beam was first detected with molybdenum oxide (MO) which gave an indication of the above mentioned flux and dissociation degree (this was roughly found from gas consumption measurements and blackening time of the detector, using a calibration from Erlangen with the nearly 100% dissociated beam of a Woods discharge).

The high flux was also detectable with an electron bombarder and following mass analysis. The signal obtained from the beam (10 cm distance from the source) was the same as that from a pressure change of 10^{-5} mm Hg in this chamber (produced by pressure increase in chamber No. 1). This gives a rough means to calculate the flux. With an assumed velocity of 5×10^5 cm/s, one also gets the above mentioned value.

The measurement of recombination heat of the hydrogen atoms was not convincing because one cannot easily eliminate effects of radiation, heat, conduction change of the residual gas, tungsten condensation and ion recombination. It would need some work, to make it dependable.

The flux was measured again with a microbalance, an open microammeter in a vacuum with a 1 cm² aluminium foil glued to the needle, rectangular to the beam. Calibrated with a milligram weight it can measure directly the momentum of the beam particles, or for a known momentum, the flux. For the molecular beam the result was 2×10^{18} particles/sec-cm² at 8 cm distance from the source (the deflection of the needle was about 1 cm). For the measurement of the atomic beam one needs two informations, the velocity of the atoms and the dissociation degree. The deflection of the scale for a typical atomic beam condition was 2 cm. This would give the order of magnitude of the above mentioned flux.

The entrance aperture of the magnet chamber has a diameter of $3/64$ " with an inner stopper with a diameter of $1/64$ ", thus giving a ring-shaped area of about 1 mm². Therefore about 10^{16} atoms/sec will enter the magnet chamber.

Measurements of the magnetic field strength were made with a little calibrated Hall probe (figure 4c). This measurement shows that the typical 6-pole field properties ($|H| \propto r^2$) are only obtained in a region $-1/2 a < r < 1/2 a$, where $2a$ is the distance between opposite pole pieces. For $|1/2 a| < r < |a|$ the field is linearly proportional to the distance r from the symmetry axis, so that the gradient is constant. Because of intensity reasons, the whole region between the pole pieces is used for the beam. The middle part of the beam is stopped with the $1/64''$ insert in the beam defining aperture because the field gradient drops to zero on the symmetry axis and no separation takes place. This insert also prohibits molecules and atoms of the unwanted component from entering the ionizer region. Only atoms which have been deflected toward the axis can enter the ionizer chamber.

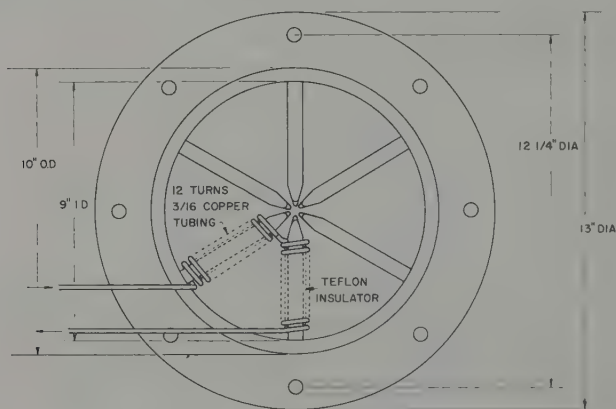


Figure 4b

The 6-pole magnet, top view

The measured field gradient on the entrance side was 85,000 gauss/cm (in the region where $|H| \propto r$) and on the exit side 12,000 gauss/cm for 300 amps current through the coils (see figure 4c).

The magnet was built with a fixed welded-on flange for support, so that one can use appropriate distance rings between the rectangular chamber (No. 3) and the magnet, to change the beam geometry.

To increase the field gradient, the pole pieces of the 6-pole magnet were shimmed with tapered steel sheets, which decreased the distance between opposite pole pieces by 0,6 mm at the entrance side and by 3,5 mm at the exit. (New dimensions 2,5 mm at entrance, 9 mm at exit). This increased the available deflecting force by approximately 50%.

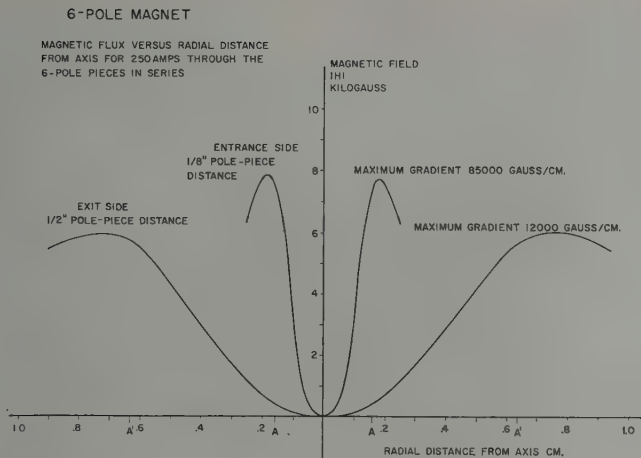


Figure 4c

The 6-pole magnet, field measurements. ($2A$ is the distance between opposite pole-pieces on the entrance side, $2A'$ on the exit side.)

The Detector

The vacuum chamber for the magnet (No. 4) was made out of stainless steel, welded from the inside to avoid cracks. The beam deflection pictures were taken either in this chamber or at the end of a 1.2 meter glass column (ionizer position).

For detection of the hydrogen atoms we used the chemical reduction of yellow molybdenum oxide to a blue oxide with less oxygen content. Thin layers of molybdenum oxide were produced by burning a molybdenum sheet metal in a gas-oxygen flame and condensing the produced vapor on a cold glass plate. One can derive a sensitivity of this detector, from earlier measurements of 10^{16} atoms/sec entering the magnet chamber, the exposed area of 10 cm^2 , and the necessary 6 seconds for the first visibility. This is assuming that no atoms are lost on a path of 0.5 meters in a vacuum of 10^{-5} mm Hg . The involved definition of the first visibility of the picture contains some error, but nevertheless allows an order of magnitude measurement of the atomic flux. For example, a flux of 10^{14} atoms/sec- cm^2 produces a visible picture after a one minute exposure.

Pictures were taken from the undeflected beam at different distances from the source (first nozzle), to measure the divergence of the beam. With the magnet switched on, the same exposures were made again.

On the pictures of the deflected beam, one can recognize a rather sharp border-line between a region of high and one of low intensity. The diameter of this borderline was measured in the pictures taken at different distances from the source and a divergence of the deflected component was derived. From the change of divergences of the undeflected and deflected beam, an approximate velocity was calculated. The velocity values given above were obtained in this way. This measured velocity is connected to the unknown velocity distribution of the beam, but since this outer borderline of the wanted component defines our entrance aperture to the ionizer very well, this is the necessary information.

Figure 5 shows a beam picture taken 1 meter behind the field end with magnet off (left) and magnet on (right). The exposure time was 1 minute, first visibility 10–15 seconds indicating a flux of about 4×10^{14} atoms/s.cm². With a velocity of 8×10^5 cm/s this represents a beam pressure of 2×10^{-8} mm Hg.

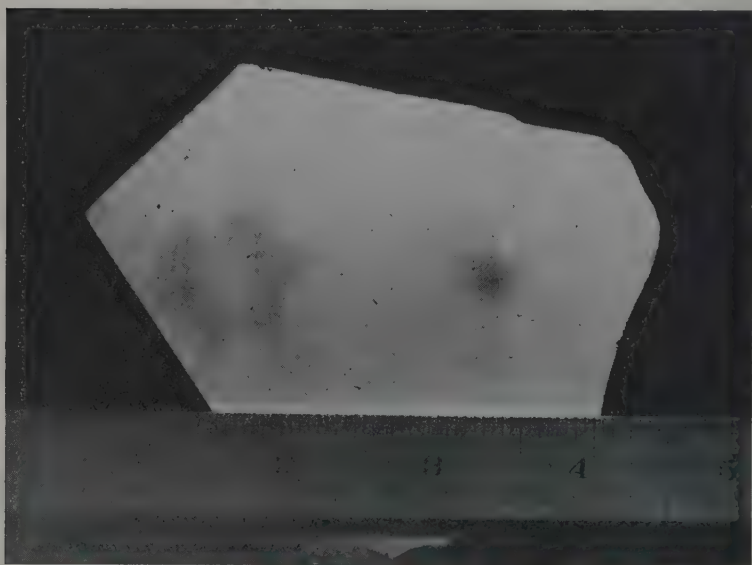


Figure 5

Beam pictures; magnet off (left), magnet on (right),

detector position: 1 meter behind field end

exposure time: 1 minute

First visibility: 10–15 seconds

The Ionizer Chamber

Because the beam pressure is expected in the order of 10^{-8} mm Hg, the residual gas pressure in the ionizer region has to be lower than this value in order to get as satisfactory polarization degree. Therefore the ionizer chamber (No. 6, figure 2) will be pumped down by an Vacion-pump of 100 liters/sec pumping speed for air. The unused (not ionized) atomic beam will leave this chamber again and will be pumped away by a second Vacion-pump of the same type, which also serves to pump the region around the ionizer chamber (No. 5). The chambers are connected with channels of low flow rate, which allow a pressure difference of a factor 10 between chamber No. 4 and No. 5 and also between chamber No. 5 and No. 6.

The Vacion pumps are working satisfactorily; we were able to pump down below 10^{-7} mm Hg within one day after the system had been open to air. After about 3 days of pumping and baking (the ionizer was used as a heat source) the pressure was below 10^{-8} mm Hg. These values were taken from current curves measured by the manufacturer.

The gasketing is done with pure aluminium wire of 0,6 mm diameter, welded together and clamped between flat polished flanges. The wire is compressed to about 0,2 mm and the bolts have to be tightened a few times because the aluminum flows during baking. The pressure readings with the beam going into the ionizer chamber were $< 10^{-7}$ mm Hg in chamber No. 5 and $< 10^{-8}$ mm Hg in chamber No. 6 after about 5 days of pumping.

The Ionizer

An electron bombarder ionizer was built following in principle the design of FRICKE [6] and BERNHARD [7].

The length was chosen to be 10 cm, the ionized volume is then about 10 cm^3 . For this large volume a careful Pierce cathode design seemed rather difficult. The system is designed to stand high temperatures during operation and baking. It is assembled on four stainless steel posts insulated with a Vicor tubing. The different parts are then insulated with Vicor spacers fitting over the tubing. The geometry is shown in figure 6.

The six tungsten filaments (0.4 mm diameter) are heated in parallel by a current of 60 to 80 amps A.C. The grid consists of thin tungsten wires in order to obtain a maximum electron current through the atomic beam volume. Presumably the electrons will oscillate and therefore increase the current density and so the ionization probability.

Cathode-grid potentials up to 400 volts were used and the produced ions extracted at right angles to the atomic beam as a flat bundle. With

electron currents of 1 A we were able to extract $0,8 \mu$ A in a residual gas pressure of 10^{-7} mm Hg. So far this was our ultimate pressure for this high emission because the chamber was heated up. With 0,1 A emission current the ultimate pressure was below 10^{-8} mm Hg. At this pressure we could detect a signal from the beam without a mass analysis of the ion current. Opening the beam shutter increased the collector current (extracted ions) by a factor 2,5. The pressure in the ionizer chamber increased by a factor 0,3 due to back streaming of hydrogen from the chamber No. 5. This leaves a signal/noise ratio (beam signal/residual gas noise) of approximately 1.

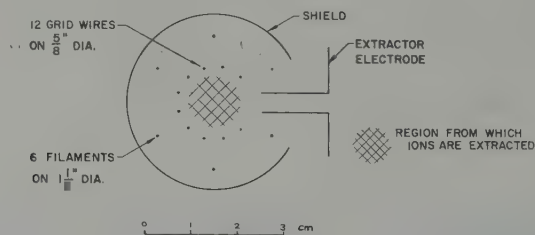


Figure 6

Cross section of the electron bombarder ionizer

Tests were so far made without the 6-pole magnet working and without the beam stopper in the beam defining aperture, so that molecules could not be distinguished from atoms. The polarization direction of the protons is defined by the direction of the magnetic field which acted on the neutral atoms before they were ionized. A field of about 30 gauss is furnished by two Helmholtz coils outside the ionizer chamber. This provides an easy means to make asymmetry measurements because one does not have to use two counters. A change of the field direction provides the same information as a counter changed to the negative angle. In order to avoid troubles because of polarization fluctuations one can change the spin direction fast (every machine pulse) and switch the signal in phase into different channels for counting.

Acknowledgment

Important contributions to the success of this project have been made by DAVID NORDBY and BAILEY DONNALLY. Special thanks are due to the Physics machine shop for their careful fabrication of the leak tight stainless steel vacuum chambers. The author wishes to acknowledge the support of the U. S. ATOMIC ENERGY COMMISSION and of the LINEAR ACCELERATOR staff in making this project possible.

Note added in Proof. During the first weeks of November 1960 protons were accelerated to 10 MeV and the polarisation was detected by left-right (and spin up-down) asymmetry measurements of the 150° scattered protons from aluminium. From the first experiment together with Rosen's data on aluminum the polarisation is estimated to 0.15 ± 0.04 . The useful current beam in this experiment was $2 \cdot 10^{-13}$ amps.

From signal/noise measurements (at 10 MeV) with the atomic beam on/off and sixpole-magnet on/off one can estimate a polarisation of 0.25. The discrepancy can be caused by stray fields from the filaments and Vacionpumps because the guide field of the Helmholtz coils is only 10-15 gauss.

REFERENCES

- [1] G. CLAUSNITZER, R. FLEISCHMANN, H. SCHOPPER, Z. Phys. 144, 336 (1956).
- [2] G. CLAUSNITZER, Z. Phys. 153, 609 (1959).
- [3] E. W. BECKER, K. BIER, Z. Naturf. 9a, 975 (1954).
- [4] KISTIAKOWSKY, SLICHTER, Rev. Sci. Instr. 22, 332 (1951).
- [5] Annual Progress Report, University of Minnesota (1958).
- [6] G. FRICKE, Z. Phys. 147, 166 (1955).
- [7] F. BERNHARD, Z. angewandte Phys. 9, 68 (1957).

Production of Polarized Protons from a Beam of Atomic Hydrogen by Quadrupole Strong-to-Weak Field Separation of one Hyperfine Component

By R. KELLER, L. DICK et M. FIDECARO, CERN

La source de protons polarisés en construction au CERN est destinée pour le synchro-cyclotron de 600 MeV. Le système consiste en la production d'un jet d'hydrogène atomique. Le jet est dirigé sur l'axe du synchro-cyclotron où il rencontre un pinceau d'électrons qui l'ionise partiellement. Dans la région centrale du SC, où a lieu l'ionisation, le vide n'est jamais bon et le gaz résiduel ionisé donnerait une quantité appréciable de protons non polarisés. Notre travail a été, par conséquent, centré sur la production d'un faisceau atomique aussi intense que possible, et en même temps la question du vide a été particulièrement soignée.

Nous allons décrire les différentes parties de notre appareil [1, 2]¹⁾.

Le dissociateur d'hydrogène

La dissociation de l'hydrogène a lieu dans un tube de verre Pyrex, parcouru par un courant de haute fréquence. Dans la figure 1 on remarque le tube en Pyrex, de 0.5 cm de rayon, en forme d'épingle à cheveux, dont les deux branches ont une longueur de 25 cm, avec un renflement à l'extrémité. La décharge se fait par couplage capacitif. Des électrodes d'argent serrées sur le renflement sont alimentées par un générateur de haute fréquence dont la puissance est de 1 kW et la fréquence de 20 MHz. Le renflement a comme effet de diminuer l'échauffement diélectrique du verre. Comme les électrodes sont à l'extérieur il n'y a pas de pulvérisation cathodique.

Un canal latéral soudé au milieu du tube de décharge conduit l'hydrogène atomique dans une tuyère de Laval. De l'air comprimé dirigé sur le canal, refroidit le gaz jusqu'à une température de 40° C environ.

Le taux de dissociation atteint une valeur de 95%.

¹⁾ Les chiffres entre crochets renvoient à la bibliographie, page 58.

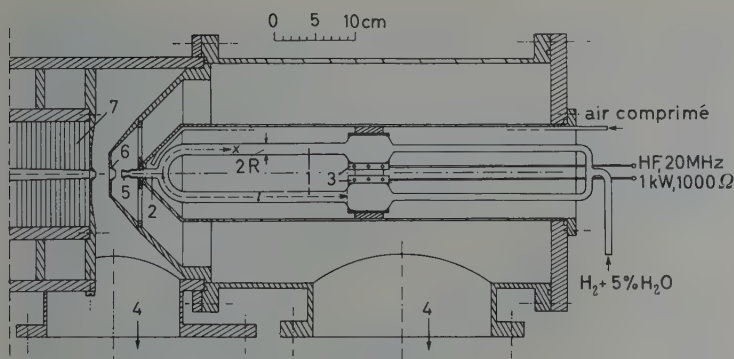


Figure 1
Dissociateur

- | | |
|----------------------------|------------------------|
| 1 tube Pyrex | 5 tuyère de Laval |
| 2 canal | 6 éplucheur |
| 3 électrodes en argent | 7 aimant quadrupolaire |
| 4 pompes 1000 l/s pour air | |

La tuyère de Laval

Pour des raisons d'intensité l'hydrogène atomique est éjecté par une tuyère de Laval [3]. On obtient ainsi un effet directionnel de 14, c'est-à-dire l'intensité du faisceau vers l'avant est 14 fois supérieure à celle qu'on obtiendrait avec un simple orifice non profilé.

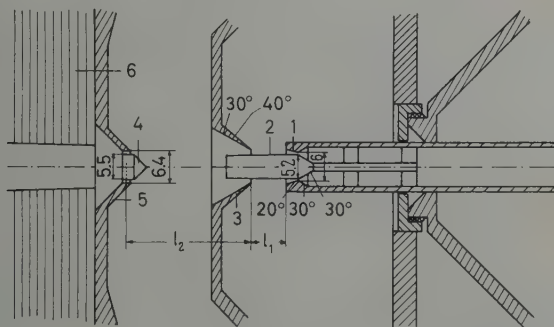


Figure 2
Tuyère de Laval

- | | |
|------------------|-----------------|
| 1 cône extérieur | 4 cloison |
| 2 cône intérieur | 5 paroi conique |
| 3 éplucheur | 6 quadrupôle |

Le séparateur magnétique nécessite un faisceau annulaire. La tuyère est donc en forme de double cône concentrique comme l'indique la figure 2. Les atomes partent d'une couronne dont le rayon intérieur est de 2.6 mm et le rayon extérieur de 3 mm.

Avant d'entrer dans le séparateur magnétique le faisceau passe par un éplucheur (voir figure 2). Deux pompes de 2400 l/s évacuent les deux régions, entre tuyère et éplucheur, et entre éplucheur et séparateur magnétique.

Le séparateur magnétique

Pour séparer la composante $F = 1$, $m = 1$ des 4 composantes de structure hyperfine de l'atome d'hydrogène, on se sert d'une longue lentille magnétique. C'est un aimant permanent quadrupolaire qui aura 7 m de long, un premier tronçon de 1,40 m est illustré dans la figure 3. Le reste n'est pas encore construit. Les pièces polaires sont profilées suivant l'axe. L'entre-fer va en augmentant de façon à produire un champ décroissant régulièrement de 3400 à 170 gauss. Cette lentille possède les propriétés suivantes:

- 1) champ intense à l'entrée, d'où grand angle solide et grande intensité du faisceau,
- 2) passage continu du champ intense au champ faible, sans perte de particules,
- 3) réduction de l'angle solide du faisceau, donc parallélisation,
- 4) achromatisme, c'est-à-dire tout le spectre de Maxwell est conservé (sauf la partie rapide constituant 2% de l'intensité totale du faisceau).

Démonstration de l'achromatisme

L'équation des trajectoires est nonlinéaire dans un quadrupôle, tandis qu'elle est linéaire dans un sextupôle. Pour des raisons de simplicité nous allons calculer le cas du sextupôle. Il est aisé de démontrer que le comportement des trajectoires est le même dans le cas d'un quadrupôle [1].

La force que subit un atome dans l'état $F = 1$, $m = 1$ est égale à

$$F = -\mu_B H', \quad (1)$$

où μ_B est le magnéton de Bohr et H' le gradient de la valeur absolue du champ magnétique. Cette force est centrale, donc dirigée vers l'axe du sextupôle. H' est proportionnel à l'élongation r (voir figure 4). La projection de la force sur le plan xy sera

$$F_y = -\mu_B H'' y, \quad (2)$$

où H'' est égal à $d^2|H|/dr^2$.

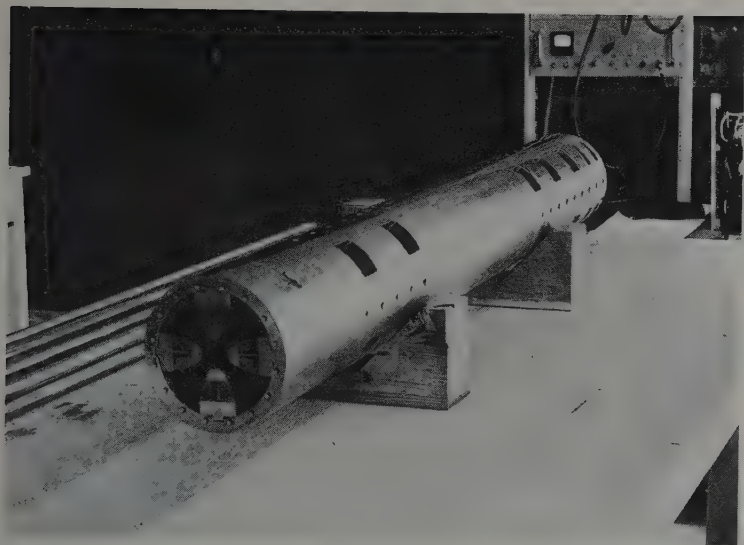
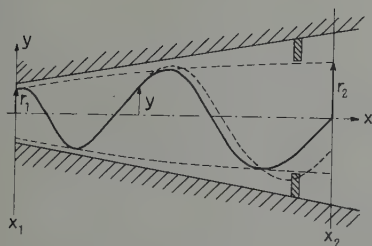


Figure 3

Figure 4
Trajectoires

La projection du mouvement des particules dans le plan xy obéit à l'équation

$$\dot{m} \ddot{y} + \bar{\mu}_B H'' y = 0 \quad (3)$$

et la forme de la trajectoire est, avec $\ddot{y} = v^2 y''$, v étant la vitesse de l'atome:

$$y'' + \frac{\mu_B H''}{mv^2} y = 0. \quad (4)$$

Introduisons maintenant un certain profil donnant une variation de H'' en fonction de x comme suit:

$$H'' = H_1'' \left(\frac{x_1}{x} \right)^n, \quad (5)$$

où n est un exposant plus grand que l'unité.

L'équation devient

$$y'' + b \frac{y}{x^n} = 0, \quad (6)$$

avec

$$b = \frac{\mu_B H_1'' x_1^n}{mv^2} = \frac{\mu_B H_2'' x_2^n}{mv^2}. \quad (7)$$

Les indices 1 et 2 marquent l'entrée et la sortie de la lentille. Les solutions de l'équation différentielle (6) sont

$$y = A \sqrt{\frac{x}{x_1}} Z_p \left(2p \sqrt{b} x^{\frac{1}{2p}} \right), \quad (8)$$

où Z_p est une fonction de Bessel d'ordre p . L'ordre p est donné par

$$p = \frac{1}{2-n}. \quad (9)$$

La constante A est choisie de telle sorte que $y = r_1$ pour $x = x_1$ et pour chaque valeur de b , c'est-à-dire pour chaque valeur de la vitesse v des atomes. En examinant les fonctions de Bessel on remarque que les trajectoires données par (8) forment des courbes ondulatoires dont les enveloppes coïncident par définition vers $x = x_1$ (à l'entrée de la lentille). Mais les enveloppes pour les différentes vitesses des atomes diffèrent légèrement lorsque x croît.

Il existe pourtant des fonctions pour lesquelles l'enveloppe est identique pour n'importe quelle valeur de v , ce sont les fonctions d'ordre ∞ , donc pour un exposant n égal à 2. Les solutions de l'équation (6) deviennent alors

$$y = r_1 \sqrt{\frac{x}{x_1}} \cos \left[\sqrt{b - 1/4} \ln \frac{x}{x_1} \right]. \quad (10)$$

Ce sont les solutions d'une équation d'Euler.

L'enveloppe des trajectoires est maintenant la même pour toutes les vitesses, soit

$$r = r_1 \sqrt{\frac{x}{x_1}}. \quad (11)$$

C'est un paraboloïde de révolution.

Considérons maintenant les atomes se trouvant dans l'état $F = 1$, $m = 0$. D'après le diagramme de Breit-Rabi [4] la force est

$$F^* = -\mu_B H' \frac{\gamma}{\sqrt{\left(\frac{H_0}{H'}\right)^2 + \gamma^2}} \quad (12)$$

où $H_0 = 507$ gauss.

C'est aussi une force focalisante, mais qui décroît plus vite que la force F , formule (1), lorsque x augmente. Les trajectoires de ces atomes forment aussi une enveloppe, mais celle-ci croît plus vite que l'enveloppe précédente, formule (11). Il est alors possible de placer une série de diaphragmes dans la lentille, qui coupent cette dernière enveloppe et laissent passer la première. Ainsi l'on peut éliminer ce dernier état et polariser entièrement le faisceau. (Les deux autres états $F = 1$, $m = -1$ et $F = 0$ sont défocalisés).

La séparation est seulement possible si les enveloppes des trajectoires correspondantes à toutes les vitesses sont identiques, donc pour le cas d'Euler, $n = 2$. Dans ce cas la lentille est *achromatique*.

La figure 5 montre le rapport d'amplitude des deux trajectoires (figure 5 de référence [1]) en fonction de H_0/H . Afin d'avoir une bonne séparation nous avons choisi le rapport égal à 1.35, ce qui correspond à $H_0/H = 3$. Le champ dans la lentille doit donc diminuer jusqu'à une valeur de 170 gauss.

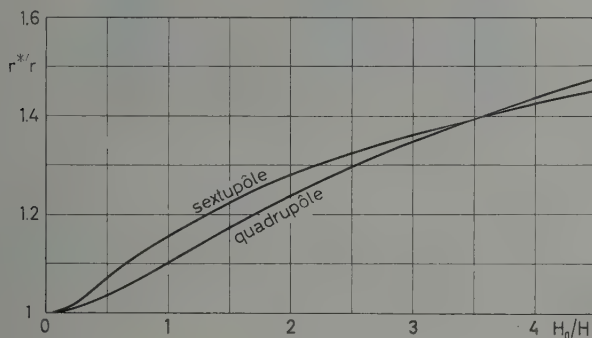


Figure 5

Le choix des dimensions de la lentille magnétique

Afin que la lentille ne soit pas trop difficile à construire nous avons choisi un agrandissement pas trop grand, soit

$$\frac{\gamma_2}{\gamma_1} = 4.5. \quad (13)$$

Le rapport x_2/x_1 devient égal à 20.25 en vertu de (11). Comme le champ H est égal à $-H'' r^2/2$, on obtient, avec (5):

$$\frac{H}{H_1} = \left(\frac{r}{r_1}\right)^{-2}. \quad (14)$$

Cela donne un champ à l'entrée égal à 3400 gauss si le champ à la sortie est de 170 gauss.

Dans un quadrupôle le gradient H' est égal à H/r , d'où

$$\frac{H'}{H_1} = \left(\frac{r}{r_1}\right)^{-3} = \left(\frac{x}{x_1}\right)^{-3/2}. \quad (15)$$

Le choix de r_1 et r_2 a été fixé à 0.31 et 1.4 cm respectivement. Les gradients deviennent ainsi, d'après (15): $H'_1 = 11000$ gauss/cm et $H'_2 = 120$ gauss/cm.

Voici comment nous avons choisi r_2 :

L'angle d'ouverture du faisceau pour la moyenne des vitesses du spectre de Maxwell est donné par

$$\alpha = \sqrt{\frac{\mu_B H}{2 k T}}. \quad (16)$$

On constate que l'angle fois l'amplitude, αr , est une constante, comme le théorème de Liouville l'exige. Il y a parallélisation du faisceau. En introduisant les valeurs on obtient $\alpha_2 = 1/230$.

En franchissant la distance qui sépare la lentille du centre du synchrocyclotron, distance au moins égale à 3 m pour notre machine de 2.5 m de rayon, le faisceau diverge en moyenne de $300 \text{ cm} \times \alpha_2$ ce qui fait 1.3 cm. Si l'on exige que le faisceau ne diverge pas plus d'un facteur 2 il faut que son rayon à la sortie de la lentille soit supérieur à 1.3 cm. Nous avons choisi $r_2 = 1.4$ cm.

La longueur de la lentille est fixée de telle sorte que les atomes possédant la plus grande vitesse comprise dans 98% du spectre de Maxwell, parcourant au moins une demi-longueur d'onde dans la lentille. D'après l'expression (10) il faut poser

$$\sqrt{b - 1/4 \ln \frac{x_2}{x_1}} \geq \pi. \quad (17)$$

La vitesse maximum considérée est donnée par $mv^2/2 \cong 5 kT$. En introduisant ceci et l'expression (7), pour $n = 2$, on obtient

$$\left(\frac{x_2}{r_2}\right)^2 \geq 1.35 \cdot \frac{5 kT}{\mu_B H_0} \cdot \frac{H_0}{H_2}. \quad (18)$$

Avec $kT/\mu_B H_0 = 8800$ et $H_0/H_2 = 3$ on obtient $x_2 = 420$ $r_2 = 590$ cm. La longueur minimum de la lentille devient égale à $x_2 - x_1 = 531$ cm.

Nous avons choisi un peu plus, soit 700 cm, à cause de l'augmentation des vitesses provoquée par la tuyère de Laval (voir aussi [6]).

Ionisation et accélération du faisceau atomique

Actuellement nous avons construit le premier tronçon de la lentille magnétique, dont la longueur est de 1.40 m. Le faisceau obtenu est de $1.5 \cdot 10^{16}$ atomes par seconde. Une photographie du faisceau, faite au moyen d'une couche d'oxyde de molybdène, est reproduite dans la figure 6.

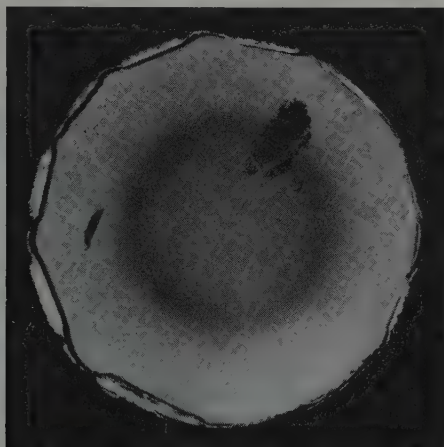


Figure 6

Photographie du faisceau atomique

L'ionisation du faisceau atomique a été étudiée à l'intérieur d'un petit synchro-cyclotron de 4.4 MeV, que nous avons construit spécialement. Le faisceau d'atomes est dirigé sur l'axe du synchro-cyclotron, où il croise un pinceau d'électrons de 3 mA émis par une cathode de tungstène. Deux raisons majeures nous ont dicté le choix d'un tel accélérateur:

La source de protons polarisés est prévue pour être installée sur le synchro-cyclotron de 600 MeV. Les phénomènes d'ionisation et d'accélération initiale sont très particuliers. Pour les étudier il est nécessaire de se placer dans des conditions aussi semblables que possible.

La mesure de la polarisation ne peut s'effectuer facilement qu'avec des protons accélérés à quelques MeV diffusés sur des noyaux d'hélium ou de carbone.

La principale difficulté rencontrée lors de l'ionisation est la présence d'une pression appréciable de gaz résiduel, en particulier de la vapeur d'eau. La pression limite est de $2 \cdot 10^{-6}$ mm Hg tandis que la pression du faisceau est inférieure à 10^{-6} mm Hg. On obtient de ce fait autant de protons non polarisés provenant du gaz résiduel que de protons provenant du faisceau. Pour abaisser la pression du gaz résiduel nous avons refroidi le dummy-*D* et la partie centrale du *D* avec de l'air liquide. Dans la figure 7 on remarque le dummy-*D* semi-circulaire fixé à un tube dans lequel passe l'air liquide. Deux autres plaques semblables sont fixées par des supports de saphir au dummy-*D* et pénètrent à l'intérieur du *D*. Le saphir possède une conductibilité thermique aussi grande que le cuivre, ainsi tout le système devient froid en moins de 20 minutes.

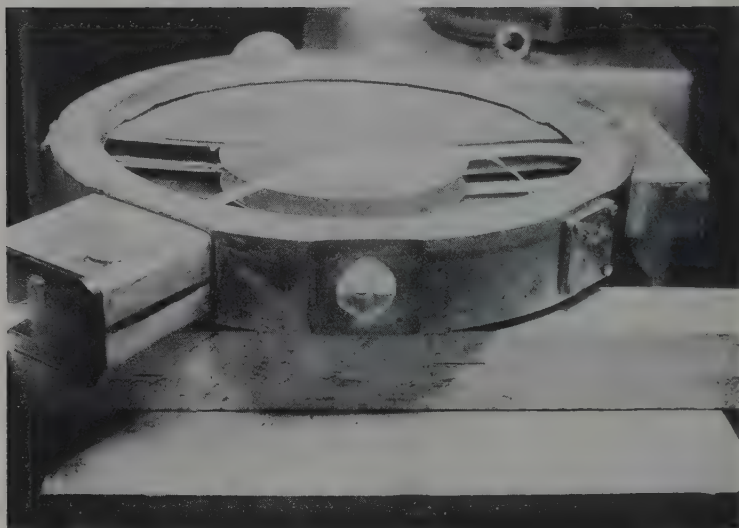


Figure 7

Avec les électrodes refroidies les protons accélérés provenant du gaz résiduel ne représentent que les 3% du faisceau total.

Les protons de 4.4 MeV sont comptés avec un photomultiplicateur joint à un scintillateur. Avec une paire de quadrupôles nous focalisons environ 1% du faisceau interne du petit accélérateur. L'intensité mesurée est de 10^7 protons par seconde.

Nous allons pouvoir augmenter cette intensité car le pinceau d'électrons ionisants est actuellement limité à 3 mA pour des raisons de charge

d'espace. Nous projetons d'ioniser le faisceau au moyen d'un plasma d'argon ou d'hélium de 300 mA. Ainsi nous aurons 100 fois plus, soit 10^9 protons par s.

Dans le synchro-cyclotron de 600 MeV la situation se présentera d'une façon analogue, sinon plus favorable. Nous pouvons donc espérer d'obtenir un faisceau de 10^9 protons polarisés par s, accéléré à 600 MeV.

Mesure préliminaire de la polarisation des protons par diffusion nucléaire

Nous avons effectué une mesure préliminaire de la polarisation du faisceau de protons de 4.4 MeV diffusés par une cible de polyéthylène, sous des angles de 45° .

En effet il est possible d'obtenir un faisceau d'atomes partiellement polarisés dans le premier tronçon de 1.40 m, avec une tuyère de Laval simple (non annulaire) et en disposant trois diaphragmes sur les trajectoires. Deux des diaphragmes se trouvent au 1^{er} et au 2^e tiers du quadrupôle. Leurs diamètres sont suffisamment petits pour limiter les trajectoires dans un espace où le champ est faible. Le 3^e, placé à l'extrémité du quadrupôle, arrête partiellement la composante $F = 1$, $m = 0$ la moins focalisée. Cette disposition semblable à celle de BENNEWITZ, PAUL et FRIEDBURG [5], doit nous permettre d'obtenir un degré de polarisation du faisceau de 40% environ, avec une intensité réduite d'un facteur 8.

Dans notre dispositif de diffusion les angles solides de détection à 45° sont de $20/_{00}$. Le nombre d'événements mesurés dans chaque voie est de l'ordre de 3 par min. Avec une expérience de 3 h nous avons obtenu une asymétrie gauche-droite pour le C^{12} de $(10 \pm 3)\%$. Les défauts géométriques du système de diffusion sont éliminés en faisant la même expérience avec des protons non polarisés. La possibilité de cette mesure de l'effet zéro présente un grand avantage sur les expériences où les particules polarisées sont produites par une diffusion nucléaire.

Les protons diffusés par le carbone ont été identifiés par un télescope à temps de vol, ce qui permettait en plus de supprimer complètement le bruit de fond.

La dissymétrie que nous avons observée, comparée à la valeur de 20% donnée par R. E. WARNER et W. P. ALFORD [7], permet de déduire une polarisation de $(50 \pm 15)\%$, valeur qui était prévue par la disposition de nos diaphragmes.

Dans la version définitive du polariseur, tuyère annulaire et longueur de quadrupôle de 7 m, la polarisation sera voisine de 100%. D'après les résultats obtenus nous pouvons conclure qu'une expérience de 10 heures permettra de mesurer la polarisation avec une précision de 3%.

RÉFÉRENCES

- [1] R. KELLER, *Projet d'une source d'ions polarisés*, Rapport CERN 57-30.
- [2] R. KELLER, L. DICK et M. FIDECARO, *Une source de protons polarisés, - état actuel de la construction*, Rapport CERN 60-2.
- [3] E. W. BECKER et K. BIER, *Die Erzeugung eines intensiven, teilweise monochromatisierten Wasserstoff-Molekularstrahles mit einer Laval-Düse*. Z. Naturf. 9A, 975 (1954).
- [4] N. F. RAMSEY, *Molecular Beams* (Oxford 1956).
- [5] H. G. BENNEWITZ et W. PAUL, Z. Phys. 139, 489 (1954). - H. FRIEDBURG et W. PAUL, Naturwiss. 38, 159 (1951).
- [6] R. L. CHRISTENSEN et D. R. HAMILTON, Rev. Sci. Instr., 30, 356 (1959).
- [7] R. E. WARNER and W. P. ALFORD, *Feasibility of Proton Polarisation Measurement with a Carbon Polarimeter*, NYO - 8576 (1958).

The Polarized Proton Source for the Harwell Proton Linear Accelerator

By M. K. CRADDOCK, Clarendon Laboratory, Oxford

The polarized proton source to be described has been built at Harwell for the National Institute for Research in Nuclear Science. It is to be installed on the 50 MeV proton linear accelerator at the Rutherford Laboratory there later this year.

Principle

In this source polarized protons are produced by the ionization of hydrogen atoms which have been partially polarized in passing through a strong inhomogeneous magnetic field. In a strong magnetic field, where the electron and proton spins are decoupled figure 1 shows that it is the spin state of the electron which principally determines the energies W of the hyperfine states, and their effective magnetic moments,

μ_z .

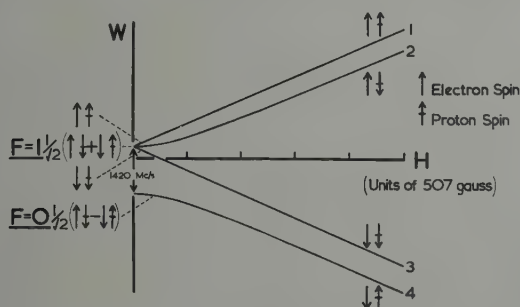


Figure 1

Energy levels of the hydrogen atom in a magnetic field

These are related by

$$W = -\boldsymbol{\mu} \cdot \mathbf{H} = -\mu_z |H|$$

and over a large range of magnetic field ($H \gg 500$ gauss)

$$\mu_z \sim \pm \mu_0$$

where μ_0 is the Bohr magneton.

Thus when the atoms are passed through a strong inhomogeneous field states 1 and 2 ($+\mu_0$) are separated from 3 and 4 ($-\mu_0$). Although the two halves of the beam are completely polarized with regard to electron spin there is as yet no proton polarization. If, however, the atoms pass into a zero field region adiabatically (i.e. without changing states) those in state 1 (1, 1) have complete, and those in state 2 (1, 0) zero proton polarization. Ionization of these atoms would thus result in a 50% polarized proton beam.

In practice ionization has to be carried out in a weak magnetic field in order to define the direction of polarization. In a field of 50 gauss the polarization is reduced to 45%.

The use of an R.F. transition at about 1500 Mc/s between states (1, 0) and (0, 0), followed by ionization in a strong field is even more promising. The transition efficiency is 75% for atoms with a Maxwellian velocity distribution and this should result in 75% proton polarization instead of 50%. Furthermore, ionization should be more efficient in a strong magnetic field.

Sextupole Magnet Principle

A sextupole magnet has been used to provide the inhomogeneous separating field. The field in an ideal sextupole, at distance r from the axis,

$$|H| = \alpha r^2$$

where α is a constant if the pole tip radius does not change.

The force acting on an atom

$$\mathbf{F} = -\text{grad } W = \text{grad } \mu_z |H|$$

i.e. a radial force

$$F_r = \frac{\partial}{\partial r} [\mu_z |H|] = 2\alpha \mu_z r.$$

If the field is 'strong' over most of the magnet aperture an atomic hydrogen beam will be split into two parts, one attracted to the axis, the other repelled from it, as $\mu_z = \pm \mu_0$.

If the magnet is sufficiently long the atomic beam will leave almost completely polarized in electron spin; the rejected, or 'defocused' atoms will have recombined to form molecules on the magnet surfaces, and been pumped away.

In spite of its greater complication the sextupole was preferred to a quadrupole, because of

- 1) its greater focusing power,
- 2) the simpler transition to a dipole field at the ionizer.

Both have the advantage over the dipole that they exert focusing forces on the beam of selected atoms.

Construction

The apparatus is shown diagrammatically in figure 2. Hydrogen is dissociated into atoms in a radio-frequency «ring» discharge powered by

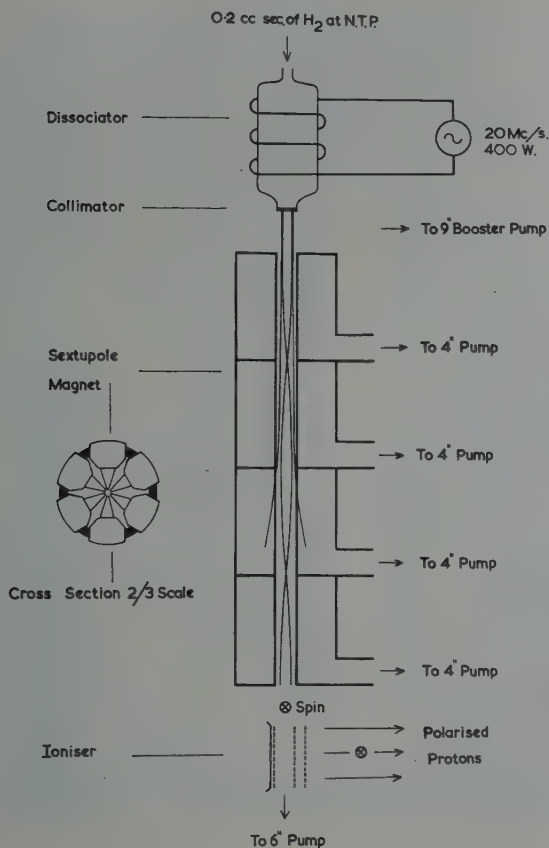


Figure 2

Schematic diagram of source

the 20 Mc/s oscillator which operates the conventional ion source. A multichannel glass 'collimator' then forms an atomic beam (90% dissociated) down the axis of the sextupole separating magnet. The polarized atoms are ionized by electron-bombardment and the protons are extracted at right angles to the atomic beam and accelerated into the linac.

The resultant polarization is horizontal, but a solenoid will be used to rotate the proton spins and give vertical polarization. Then the polarization should not be affected by the beam's passage through the

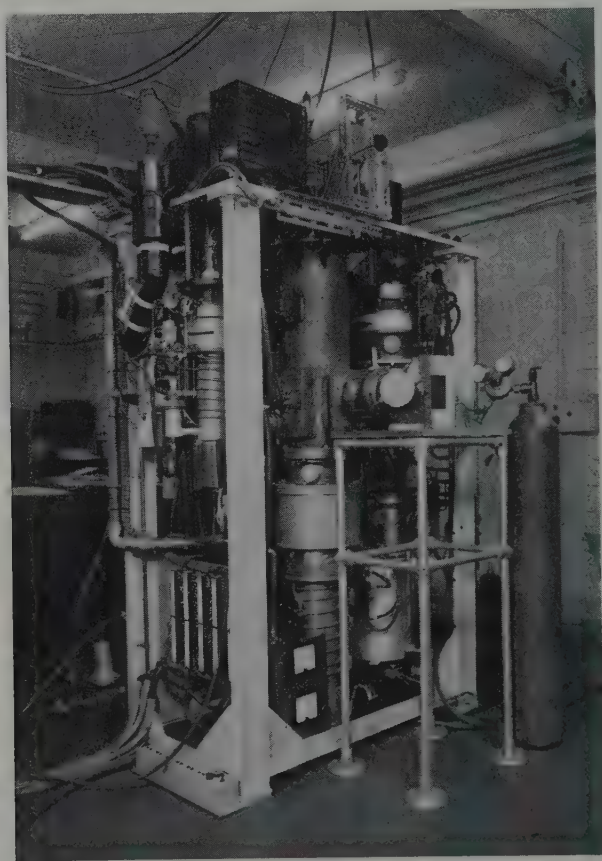


Figure 3
The polarized proton source

bending magnet, which has a vertical magnetic field and provides several radial positions for experiments on the linac. As the solenoid will be located between the ionizer and the linac injector, where the proton energy is only 1 keV, it can be short and of simple design. The combination of solenoid and bending magnet should make any direction of polarization available.

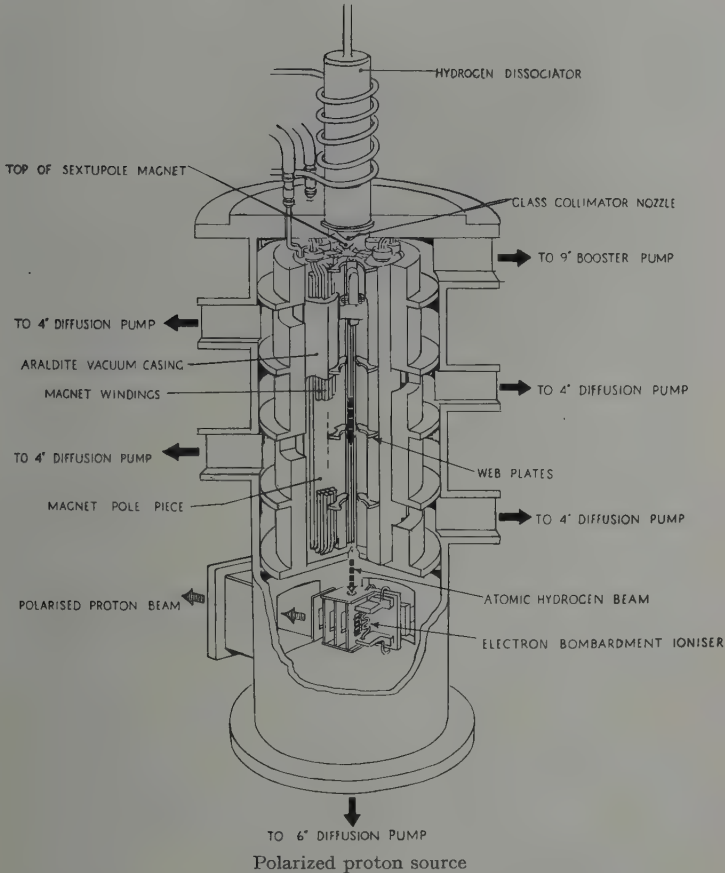


Figure 4
Cut-away diagram

Figure 3 shows the source as it appears in the laboratory. The most striking external feature is the pumping system: 6 oil diffusion pumps

and their automatic control systems and services surround the main vacuum vessel containing the magnet and ionizer.

In the laboratory experiments a simple 60° mass spectrometer has been used to distinguish the H^- and H_2^- components of the ion beam.

The Sextupole Magnet

Details of the magnet construction are shown in the cut-away diagram (figure 4). The poles are of mild steel, 40 cm long, and there is no shaping, the pole-tip radius being 4 mm throughout. Under running conditions the field at the pole-tips is ~ 6000 gauss, and the field gradient there 30000 gauss/cm. The exciting current of 140 A at 2 V d.c. is carried by a 1/4-inch water cooled copper tube coiled six times around each pole-piece. The windings are encased in araldite.

Proof that the separating magnet does produce polarized atoms is found in the variation of proton current from the ionizer (measured by the mass spectrometer) with sextupole field (figure 5). As the current in the magnet windings is raised to its running value of 140 A the proton current increases by a factor 4, reflecting the fourfold increase in the atomic beam under the focusing action of the sextupole.

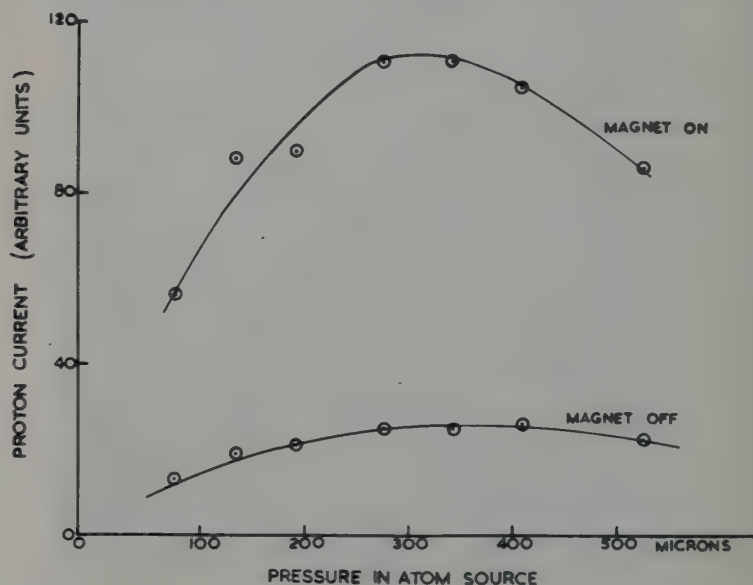


Figure 5

Proton currents - magnet on and off

Those atoms which can pass through the magnet lie within the solid angle

$$\delta\omega = \frac{2\pi\mu_0 H_m}{mv^2} \sqrt{1 - \left(\frac{r_0}{r_m}\right)^2}$$

if they enter at radius r_0 , and H_m is the field at the pole tip radius r_m . The linearity of this formula in H_m is confirmed in the linearity of the graph (figure 6). For $H_m = 6$ kg, $T = 400^\circ\text{A}$, then $\delta\omega = 2.1 \times 10^{-3}$ sterad (half-angle 1.49°), and this would suggest a focusing factor of 4.3. If the atoms leave the source at 400°A only 2% of the rejected states should be passed by the magnet and the resultant proton polarization is 48%.

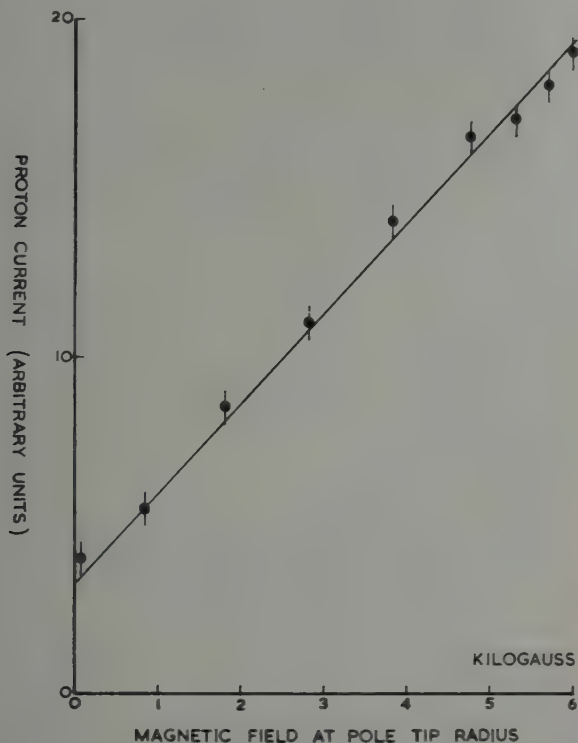


Figure 6
Focusing effect of sextupole magnet

Pumping System

The main vacuum chamber is a mild steel cylinder of 10 inches diameter. The magnet is held vertically inside this, and the space above the magnet and below the source of atoms is pumped by an Edwards 9B3 Booster pump. Most of the gas from the discharge is pumped away here and a pressure of 8×10^{-4} mm is maintained with a pressure of 340μ in the discharge. The gas flow is then $180 \text{ l}\mu/\text{s}$. Plates fitted

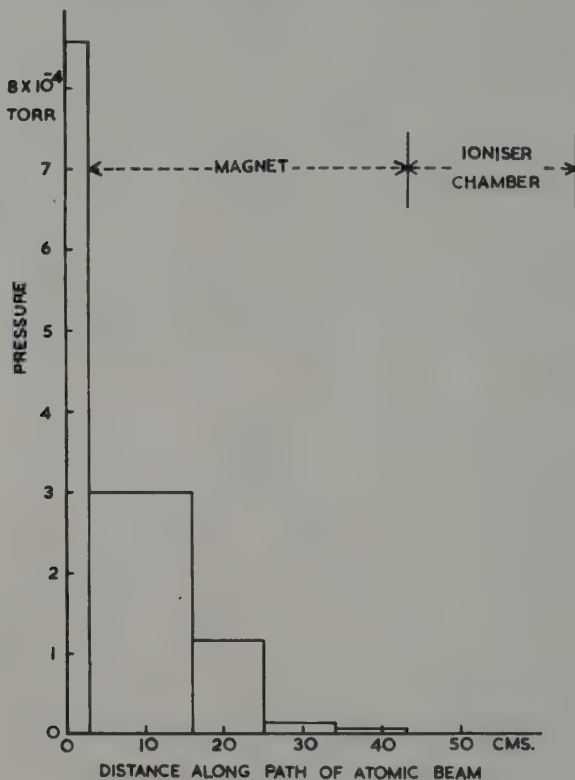


Figure 7

Residual gas pressures along the path of the atomic beam

between the pole pieces at right angles to the magnet axis divide it into four pumping sections. Each of these is pumped by an Edwards F403 oil diffusion pump. The ionization chamber, beneath the magnet, is pumped by an Edwards F603 pump. The pumping speeds of these

pumps for hydrogen are quoted by the makers as 1800, 300 and 900 l/s respectively. All these pumps are backed by a single Edwards ISC 450 rotary pump and all were originally fitted with chevron baffles refrigerated by freon at -40°C .

The residual gas pressures in the different pumping sections along the path of the beam have been estimated from the readings of ionization gauges in the pumping lines, allowing for the conductances of the pumping paths. These pressures are plotted in figure 7 for a discharge pressure of $340\ \mu$. The area under each step of the graph indicates the scattering power of each section.

By varying this 'gas thickness' it has been possible to estimate the attenuation of the beam in its passage from collimator to ionizer. Figure 8 shows a typical mass spectrometric analysis of H^+ and H_2^+ components of the ion beam, plotted against pressure in the dissociator. The beam intensity rises with dissociator pressure until the increased gas flow into the magnet chamber causes sufficient pressure rise there for the scattering to lower it again. At the optimum pressure 30% of the beam is lost by scattering.

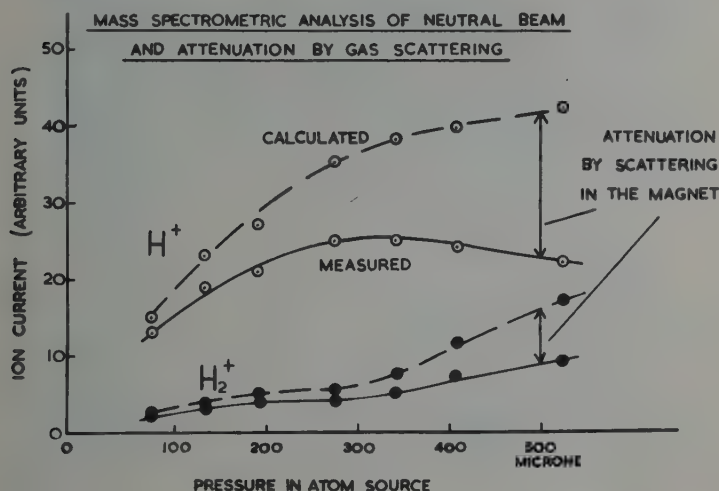


Figure 8

Mass spectrometric analysis of neutral beam and attenuation by gas scattering

The Collimator

The atomic beam is produced by a glass 'collimator' (figure 9) consisting of about 1000 capillary channels $1/8\text{ mm} \times 2\text{ mm}$ forming a disc

2 mm thick and of 8 mm diameter. About 35% of the disc is open to gas flow. These were made on the lines of the Born-Kessel jet used in oxygen blowpipes: the glassblower drew down capillaries, stacked them in a tube and then drew down the whole matrix to a diameter of 8 mm. This requires some practice. Collimator discs were then cut off with a diamond saw and mounted on the conical pyrex flanges (figure 10) which form the base of the discharge tube.

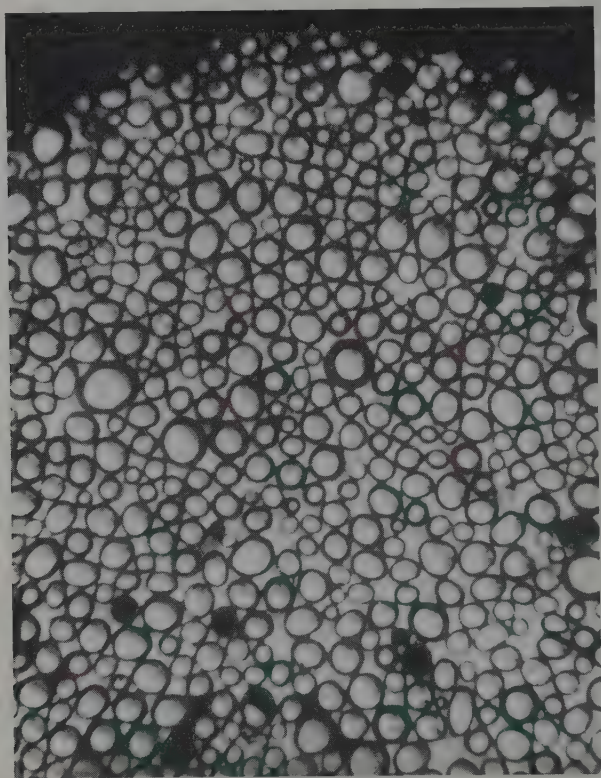


Figure 9

A section through part of the glass collimator (4 mm across)

An impression of the collimating effect of these multichannel discs is given in figure 11 where their polar diagram is compared with the cosine diagram of an infinitely thin aperture of the same area. The continuous line has been measured; the dotted part is estimated. While

the waste gas flow is reduced by a factor of more than 10 the intensity in the forward direction is not impaired. The collimator must be accurately aligned with the magnet axis.

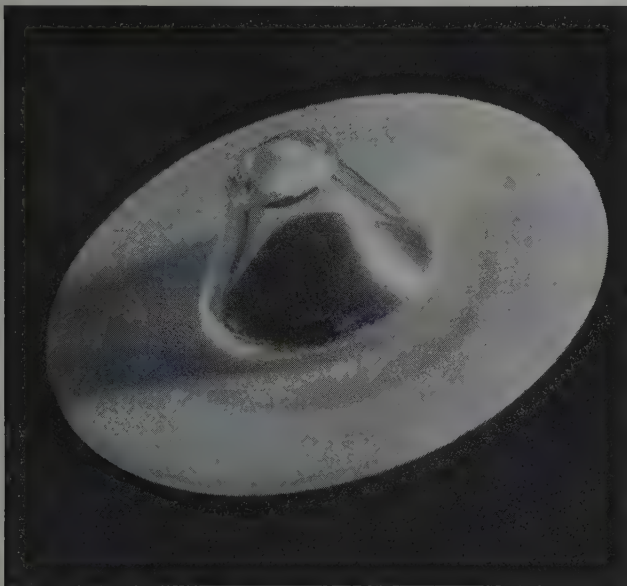


Figure 10

The collimator mounted on a 2 inch glass flange

A large single aperture of the same area could not be used in any case, for only a very low discharge pressure is allowable if molecular flow is to be maintained. The mean free path for atomic hydrogen equals the channel length, 2 mm, at a pressure of about 80μ . Contrary to expectation no decrease in beam because of cloud formation behind the collimator has been observed at this pressure; the limitation to discharge pressure, at 340μ , is attributable to attenuation of the beam by gas scattering.

The Dissociator

Pyrex glass has been used in the construction of both discharge tube and collimator; pyrex has the lowest recombination coefficient of any measured material for atomic hydrogen. Its use should result in the highest dissociation and best atomic beam for a given pressure in the dis-

charge. The tubes have furthermore been treated in various ways and the beam dissociation attainable with them is plotted against pressure in figure 12. The dissociation is calculated from the results of mass spectrometric analysis, allowing for the different ionization cross-sections of hydrogen atoms and molecules. A coating of methyl-trichlorosilane was found to be most successful, and air cooling increased the dissociation by a further 10% to over 90%.

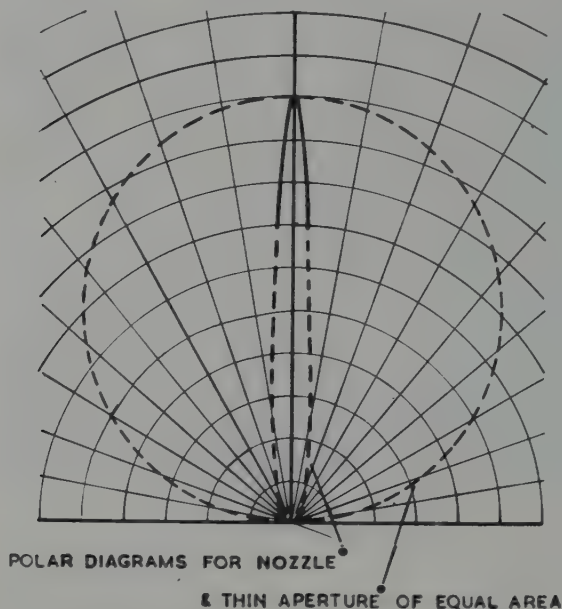


Figure 11

Collimating effect of multichannel glass nozzle

The power absorbed in the discharge has been measured roughly using a water jacket. Figure 13 shows that much more power is required at high, than at low, pressures to produce the same dissociation.

The Ionizer

This is seen in figure 14. The atomic beam, containing between 1 and 5×10^{15} atoms/s, has a 9 mm diameter and passes from left to right between the two plates nearest the camera. Electrons are drawn off the tantalum wire filament and accelerated to 250 V across a 2 mm gap

by a grid of 0.020" tantalum wires into the atomic beam. Although the nearest two plates are held at the same potential, field penetration from the further plates and the focusing effect of electron space charge cause extraction of the ion beam away from the camera. The plates are all 6×3 cm tantalum sheets with 2×1 cm holes for the beam to pass through; only the first has an actual grid of wires. Under the optimum working conditions the potentials on the filament and four plates are + 1000 V, 1250 V, 1250 V, 1200 V, 0 V respectively.

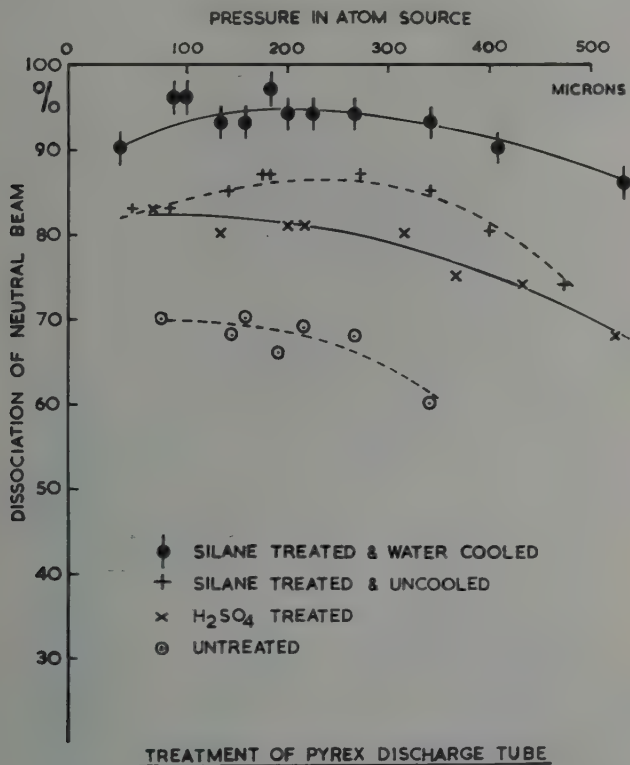


Figure 12

Dissociation of neutral beam for different treatments of discharge tube

The filament is heated to 2200°C by 36 A a.c., and about 200 mA of electrons pass through the first grid. 1 mm tantalum wire has been found to be the most reliable material; tungsten is not easily workable and oxide coated cathodes are too short-lived.

The mass analysis of the ion beam may be used to calculate the proton component of the total ion current produced by the ionizer from the neutral beam. The results of a typical measurement are given in figure 15. The best proton current there is $0.12 \mu\text{A}$ or 7×10^{11} protons/s. The efficiency of the ionizer is thus between 2 and 8×10^{-4} . The polarized proton flux available for experiments depends on how much of this can be accepted by the accelerator.

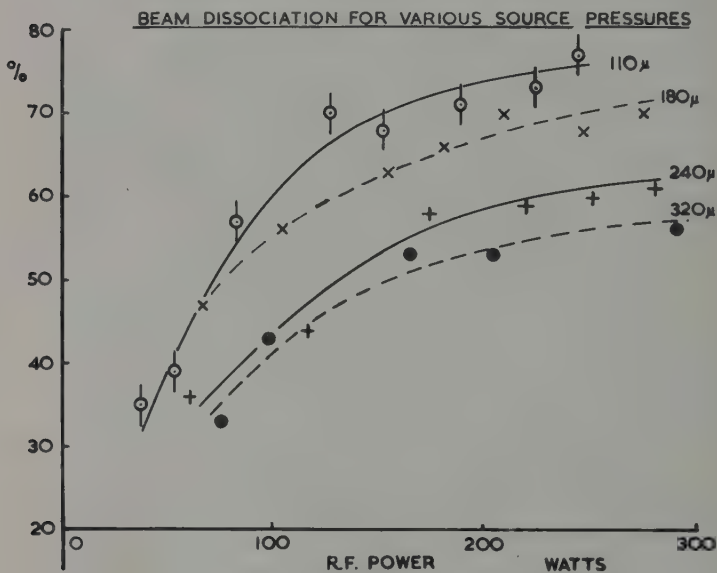


Figure 13

Dissociation of neutral beam as a function of R. F. power

Experiments on the shape of the 2×1 cm ion beam have shown that 50% of the protons travel at $< 3^\circ$ to the axis, and that it should be possible to focus 50% into the linac injector. With a transmission factor of 8×10^{-4} a mean current of 2×10^8 protons/s at 50 MeV is expected.

Background

Protons arising from the beam and from the residual gases have been distinguished using a shutter to cut off the beam. This does not alter the residual gas pressure significantly, and the difference of the two readings gives the contribution of the beam.

At first no better beam: background ratios than 1:1 could be obtained, with residual gas pressures of 2×10^{-6} mm. These protons were known not to arise from hydrogen molecules, because of the small cross-section for this process and the low population of molecules indicated by measurement of the H_2^+ current. Also, liquid-air-trapped and untrapped gauges gave quite different readings, indicating the presence of a condensable vapour. The freon baffle on the 6 inch pump was replaced by a liquid air trap, and lower pressures were obtained. No trouble has been experienced with protons from pump oil either in a test-rig or in this apparatus.

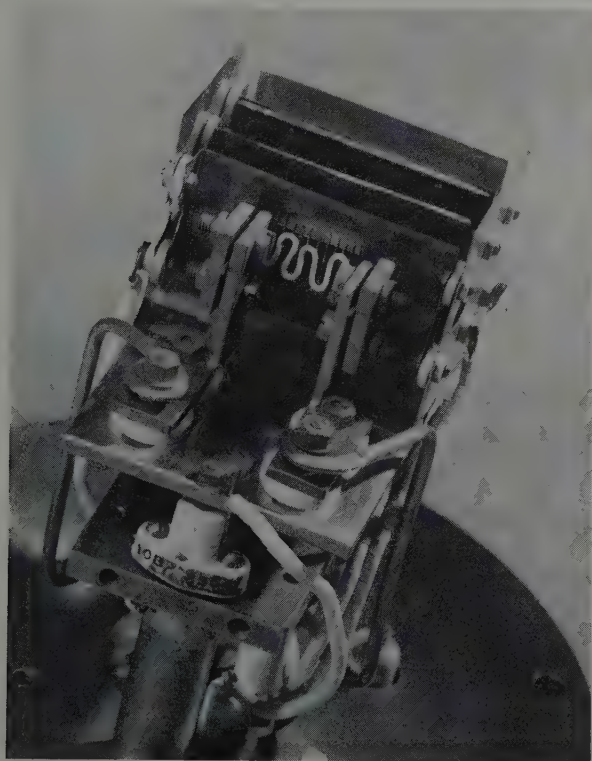


Figure 14
The ionizer

The pressure was found to rise by a factor of 3 or 4 after the ionizer had been working for a few hours. About 300 watts are dissipated by the

ionizer and the chamber walls soon reach 60°C outside. Cooling the vacuum chamber, even with an air blast was found to reduce the residual gas pressure by a factor 3. Under these conditions the pressure now rises from 2 to 8×10^{-7} mm when the ionizer is switched on and a beam: background ratio of 5:1 is obtainable (figure 16). The chamber has

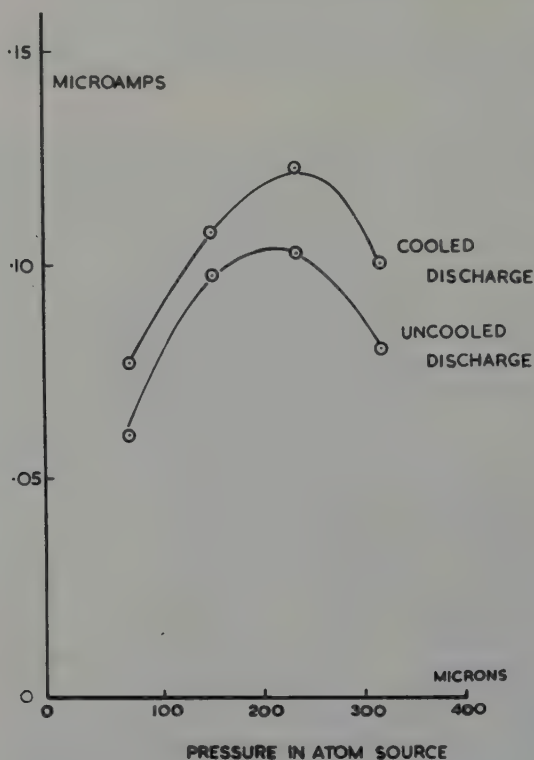


Figure 15
Total proton current

never been baked out at red heat in vacuo although it has been heated to $\sim 100^{\circ}\text{C}$ with infra red lamps, yielding considerable gas. In any future design we should use a stainless, and not mild, steel chamber. The ionizer has now been enclosed in a cooled box which will shield the chamber walls from radiation heating. It is hoped that this will improve the beam: background ratio to 10:1 but no results are yet available.

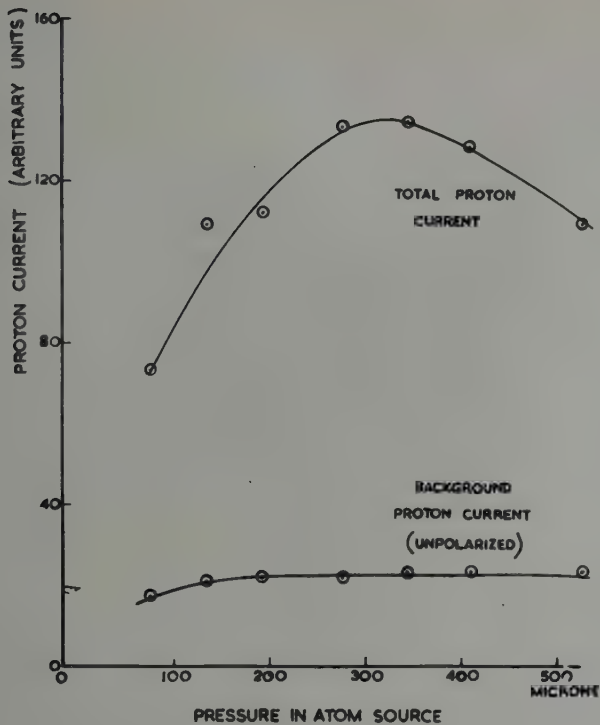


Figure 16

Proton currents from neutral beam and from background gas

Polarization

If a fraction β of the protons arise from the background the latent polarization P of the atomic beam only results in a polarization $P(1-\beta)$ of the proton beam. A 50 gauss field applied at the ionizer to swamp the stray fields of the sextupole and the filament, and define the proton spin direction, reduces the 48% polarization produced by the magnet to 43%. A background of 10% brings this down to 39%, or of 20% to 34%. It is clearly very important to keep the background and the stray fields at the ionizer as low as possible. Short of any unforeseen depolarizing action it is hoped to obtain a polarization of 40%.

Elastic scattering from He^4 at 10 MeV will be used to measure and monitor the polarization but acceleration of the beam for this purpose awaits the installation of the source on the linac.

Installation on the P. L. A.

The linac injector is supplied by a 520 kv Cockcroft-Walton H.T. generator, and the entire proton source has been designed to operate at this potential.

This has necessitated the construction of a new H.T. stand to carry the source and its associated equipment, which together weigh 2 tons. This stand will be connected to the injector by a short pipe, containing the solenoid, and which will be removable to allow conversion to a conventional ion source. This change-over should take less than 24 hours.

The services on the stand include a recirculating water chilling unit, refrigerating units for pump baffles, a traversing mechanism for beam alignment and 20 cu. ft. of electrical equipment. A 30 H.P. motor drives a 15 kW generator by belt up one of the legs of the stand; and control of the apparatus is effected by rod drive mechanisms in the legs.

Conclusion

A polarized proton source which will produce over $.1 \mu\text{A}$ of protons has been built. The polarization has not yet been measured but 40% should be attainable.

The most satisfactory points of this design seem to be

- (i) the short, strong-field magnet, which gives good intensity;
- (ii) the glass collimator which reduces the pumping requirements to a tolerable level.

The chief disadvantage is the situation of the whole source at 520 kv; however, this is outweighed by intensity considerations. The greatest opportunity for development lies with the ionizer, which has an efficiency of less than 10^{-3} .

Acknowledgements

This work has been performed with Mr. J. M. DICKSON and Mr. D. C. SALTER of the Rutherford Laboratory, and Mr. J. BOON has supervised the engineering design and construction. We are most grateful to all those in the Clarendon and Rutherford Laboratories who have contributed to the project, and to Dr. K. F. SMITH, Dr. G. H. STAFFORD and Dr. D. ROAF for many helpful discussions.

The Production of Polarized Particles from an Atomic Beam by Quadrupole Strong Field Separation of Hyperfine Components

By L. BROWN, E. BAUMGARTNER, P. HUBER, H. RUDIN, and H. R. STRIEBEL
Physical Institute of the University of Basel

Abstract. A device has been constructed for the production of polarized deuterons from an atomic beam. The design of the source is described. The alignment of the 10^{-8} A deuteron beam was established by observing the anisotropy of neutron distribution from the $T(d, n)He^4$ reaction. Experiments indicate its usefulness as a source of polarized protons, if the proton content of the residual gas ions is reduced.

General

The objective of this work is the production of a beam of partially polarized protons or deuterons. The probable existence of unforeseen technical difficulties led us to a simple design with large margins of error. Possible future applications in Basel allow the source to be operated at earth potential, hence no serious restrictions on size and energy consumption need consideration. An important simplification for the first development stage is made possible by the anisotropy of distribution and the polarization of the neutrons from the $T(d, n)He^4$ reaction [1]¹⁾ produced by aligned and polarized deuterons. The resonance cross section of 5 b allows small currents to be employed. The deuteron resonance energy of 107 keV is convenient, and the target may be placed at high voltage with the neutron detectors at earth potential.

The course of the particles through the device is shown in figure 1. Atoms of hydrogen or deuterium are allowed to diffuse from a high frequency discharge tube through a region of differential pumping into a strong magnetic quadrupole field. The pole shoes of the magnet are parallel to the beam axis. Half of the hydrogen or deuterium atoms diverge in this field; the other half is confined to a circular cylindrical region defined by the pole shoes. The beam so formed passes into an orienting homogeneous field weak enough to allow strong coupling of electron and nucleus. A small part of it is ionized there by electron bombardment.

¹⁾ Numbers in brackets refer to References, page 88.

Protons so produced should have a polarization of at most 50%. Deuterons should have spin populations for $m_d = +1, 0, -1$ of $4/3, 4/3, 1/3$ respectively for the ideal case. The resulting ions are accelerated to produce the desired nuclear reaction.

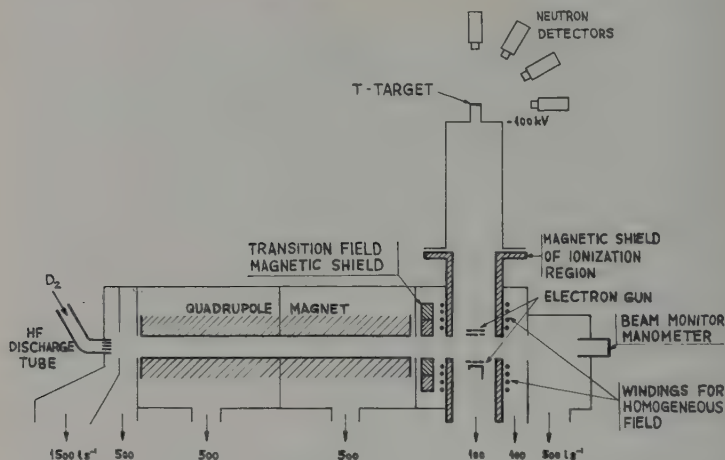


Figure 1

General scheme of the apparatus

The Gas Discharge and the Differential Pumping System

Hydrogen or deuterium gas, saturated at atmospheric pressure with H_2O or D_2O , is admitted into both legs of a V-shaped Pyrex tube of 11 mm inside diameter. An oscillator is capacitively coupled to the tube by two cylindrical electrodes, each located 110 mm from the notch of the V. The oscillator has a frequency of 20 MHz and dissipates about 200 W in the tube. Investigations of the dissociation have been undertaken with a calorimeter [2] and indicate a high degree of dissociation. The degree of dissociation is not sensitive to changes of either oscillator power, electrode position or gas current for usual operating conditions. The tube is cooled by air streams. Deuterium gas is produced by electrolysis of a heavy water solution of NaOD.

The atomic gas produced in the tube diffuses through an annular opening [3] at the notch into the first pumping compartment. Its course may be seen in figure 2. A small fraction of the atoms passes through an aperture into a second pumping compartment, and still a smaller fraction passes into the quadrupole field. The first compartment is pumped by a Leibold 1500 l/s diffusion pump operated at booster pump conditions.

The second compartment and the two compartments of the magnet tank are each pumped by Balzers 500 l/s diffusion pumps. Typical operating conditions: gas inlet of H_2 saturated with H_2O is 0.3 Torr l/s; pressures in the discharge tube and the four compartments are respectively 0.3, 6×10^{-4} , 2×10^{-4} , 6×10^{-6} and 4×10^{-6} Torr. All pumps use silicon oil of type Dow Corning DC 704. All Balzers pumps are operated with heater power 1/3 greater than the catalog value.

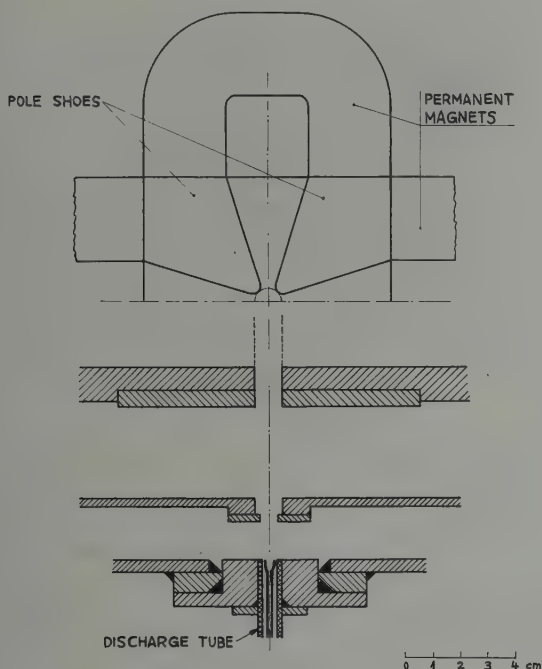


Figure 2

Gas inlet, apertures, magnet tank entrance and magnet cross section.

The Atomic Beam and the Quadrupole Magnet

The intensity of the atomic beam is calculated with the following assumptions: the magnitude of the field is proportional to the distance from the axis [4]; the atoms in the discharge tube have a Maxwellian velocity distribution; they enter the field through a ring opening with a mean radius equal to half the radius of the cylinder defined by the pole shoes (a maximizing condition); the weak field region of the quadrupole is

negligible; those atoms whose trajectories pass outside the pole shoe cylinder are lost from the beam. The convergent atoms will be confined to the beam, if their initial velocity vectors fall within a solid angle that varies inversely as the square of the velocity. Averaging this solid angle over the velocity distribution gives

$$\Omega = 1.39 \frac{\mu_0 H_0}{kT}$$

where μ_0 is the Bohr magneton, H_0 the magnetic field at the pole shoe, k the Boltzmann constant and T the absolute temperature. The intensity [5] of the beam in atoms per unit time for completely dissociated gas is

$$I = \frac{n}{2} \bar{v} F \frac{\Omega}{4\pi}$$

where n is the density of atoms in the discharge tube, \bar{v} the mean velocity of the atoms, $F = \pi r_0 \varepsilon$, the area of the annular opening, r_0 the pole shoe cylinder radius, ε the slit width and m the mass of the atom. The usual rule for estimating the maximum intensity of an atomic beam assumes the density n corresponds to a mean free path equal to the slit width, i. e.

$$\varepsilon = \frac{1}{\sqrt{2}n\sigma}$$

where σ is the collision cross section. A slit width of 1 mm was used. Application of this rule gives

$$I = \frac{1.39}{\sqrt{\pi m k}} \frac{\mu_0}{\sigma} \frac{H_0 r_0}{\sqrt{T}}$$

Evaluation of this formula for c. g. s. units (the value of σ has been taken for H_2) gives

$$I = 3.3 \times 10^{14} \frac{H_0 r_0}{\sqrt{A T}} \text{ s}^{-1}$$

where A is the atomic weight. The density of the beam is

$$\rho = 6.2 \times 10^9 \frac{H_0}{T r_0} \text{ cm}^{-3}.$$

The substitution of the experimental values $H_0 = 10^4$ gauss, $T = 300$ K and $r_0 = 0.5$ cm with a correction factor of 0.7 to account for the location of the discharge tube exit ring outside the quadrupole field, gives an intensity for hydrogen of $5.4 \times 10^{16} \text{ s}^{-1}$ and a density of $2.3 \times 10^{11} \text{ cm}^{-3}$; this corresponds to a pressure in the beam of 7×10^{-6} Torr.

The length L of the quadrupole insures the removal from the beam of all divergent atoms that have no angular momentum relative to the axis (the most difficult case) and speeds less than 2.5 times the mean velocity in the beam. This gives

$$L = \frac{5}{\sqrt{2}} (1 + \sqrt{2}) \sqrt{\frac{kT}{\mu_0 H_0}} r_0$$

or again evaluating,

$$L = 1.04 \times 10^3 \sqrt{\frac{T}{H_0}} r_0 \text{ cm.}$$

For the conditions mentioned earlier $L = 90$ cm.

Permanent magnets attached to four pole shoes of 90 cm length produce the field. Figure 2 shows the shape and arrangement of the magnets. The 32 permanent magnets are spaced far enough apart to give a pumping resistance with reasonable relationship to the speed of the pumps. The permanent magnets were magnetized in place on the pole shoes. The manufacturer [6] surpassed by 10% the original goal of 10^4 gauss at the pole shoes.

A longer quadrupole presents only the disadvantage of attenuation by scattering. A quadrupole field may be utilized for containing an atomic beam that must be transmitted to a high potential terminal; a series of permanent quadrupole magnets are spaced to divide the total voltage, and the confining property of the quadrupole field is essentially maintained.

Measurements of the Atomic Beam Intensity

Intensity measurements have been made by directing the beam into an ionization manometer. To interpret the manometer reading a correction must be made for pressure build-up in the glass cylinder of the gauge, the ionization cross section of hydrogen and the divergence of the beam outside of the quadrupole field. Recombination of atoms is not considered, since the ionization cross section of H_2 is nearly twice that of H . The correction for beam divergence is the weakest part of the interpretation. The molecular beam obtained when no gas discharge is present has also been measured for comparison, although its intensity is much lower.

The compartment in which the measurements are made has an entrance for the beam, a liquid air trap, a second manometer located out of the beam path to monitor the residual gas pressure and a 500 l/s diffusion pump. The small increases in residual gas pressure are subtracted from the reading of the inpath manometer. This compartment follows the ionization compartment, thereby reducing the diffusion of beam gas back into the ionization region and serving as an atomic beam monitor. A beam of predicted value would raise the residual gas pressure by

1×10^{-6} Torr. The residual pressure without beam is of the order of 10^{-7} Torr.

The measured maximum intensity is 15% of the predicted value. Intensity plotted against gas inlet shows saturation at the same gas currents for the H and H_2 beams; furthermore, the maximum H_2 beam is about 20% of its predicted value. These measurements indicate beam loss due to a scattering, incomplete dissociation, erroneous interpretation of the manometer reading and incorrect assumptions for the predicted value.

The Homogeneous Field

Ionization of the atoms takes place in a weak homogeneous field, which determines the direction and the magnitude of the polarization or alignment. To minimize the effects of beam divergence, ionization occurs as near the exit of the quadrupole as possible. Choosing the direction of the homogeneous field parallel to the direction of ion acceleration simplifies the magnetic shielding. This has no disadvantages for the $T(d, n)He^4$ reaction, as it is produced by S-wave deuterons, but a 90° rotation of spin is required for a proton experiment. The magnetic shielding is shown

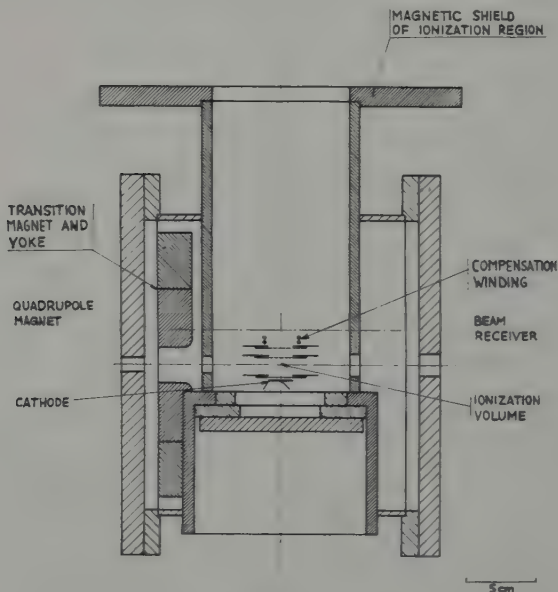


Figure 3
Ionization compartment

in figure 3. It consists of an iron ring of 9.2 cm^2 cross section and 15 cm mean diameter; it is located 2.6 cm beyond the quadrupole. The ring is dimensioned to absorb the entire measured stray flux of the quadrupole. The ring also serves as the yoke for a transition dipole field of about 60 gauss. Non-adiabatic transitions are not feared, if the field does not become too weak, since changes of the magnetic field direction experienced by the atoms are slow compared to the Larmor period. The beam passes next into the ionizing region, which is enclosed in an iron cylinder. The ring-cylinder combination reduces the field in the ionization region to 0.6 gauss, but the field direction is not the cylinder axis. Additional current windings on the cylinder correct this, thereby increasing the field to 5 gauss. From the point the beam enters the transition field to the point where it leaves the ionization cylinder, the field is essentially parallel and directed downward.

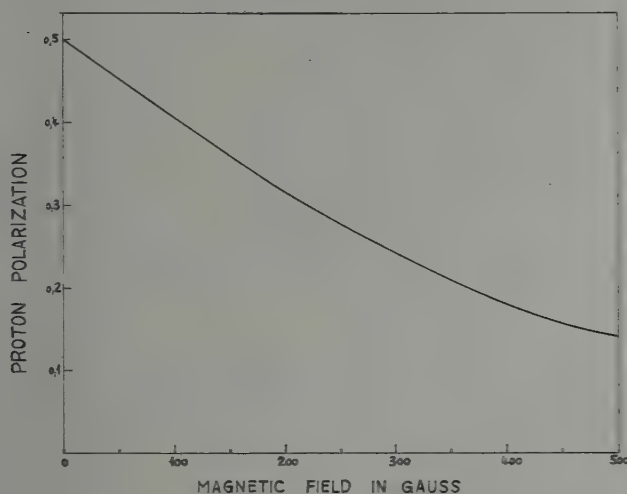


Figure 4

Proton polarization as function of field strength

The magnetic field of the heater current in the electron gun is not negligible. Its spiral form allowed an approximate calculation of its field in the ionization volume [7]. An additional winding is mounted on an electrode of the electron gun; the field resulting from the spiral and compensation winding is similar to that of a Helmholtz coil, has a value of 5.5 gauss at the center of the beam and has no angular deviations greater than 30° .

The nuclear spin populations of the hyperfine components of the beam that are mixed states were calculated as functions of magnetic field. For H atoms this is conveniently expressed as proton polarization and is shown in figure 4. For D atoms the populations of the three m_d states are plotted in figure 5.

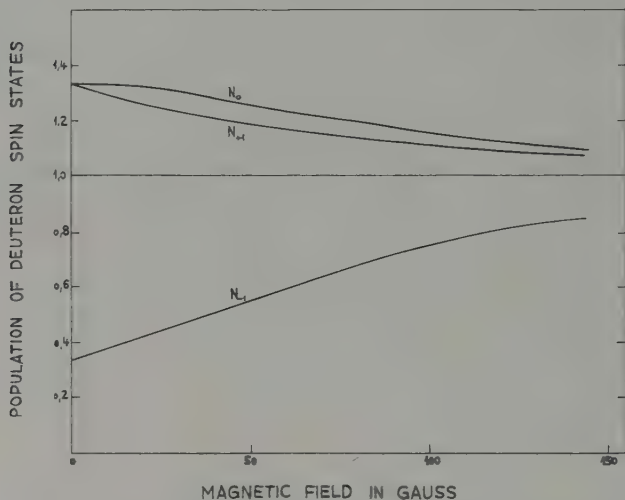


Figure 5

Populations of m_d states as function of field strength

Ionization, Residual Gas Ions

Electron bombardment ionizes the atoms of the beam virtually without depolarization [8]. Measurements of the atomic ionization cross section [9] σ_i show that for electrons with energy U greater than 100 eV a value satisfactory for design purposes is

$$\sigma_i = \frac{1.37 \times 10^{-15}}{U} \ln \frac{U}{0.325} \text{ cm}^2.$$

The current i_p of ions from the beam, bombarded at right angles by a cylindrical electron beam of the same diameter D , is

$$i_p = j \sigma_i V \rho$$

where V is the volume common to both beams (0.67 cm^3), j the electron current density. For the measured density, electrons of 300 eV and an electron current density of 0.1 A cm^{-2} , the ion current from the atomic beam would be $0.075 \mu\text{A}$. Figure 3 shows the arrangement of the elec-

trodes in the electron gun. The plate holding grid no. 1 and the supports of the tungsten filament are liquid cooled. A weak electric field between grids 1 and 2 accelerates the ions out of the ionizing region; a stronger field between grids 2 and 3 stops the electrons and further accelerates the ions. Potentials for the electrodes are as follows: cathode 0; grid 1, + 300 V; grid 2, + 125 V; grid 3, - 475 V. The volume in which the residual gas is ionized is larger than the bombarded volume of the beam by a factor of 1.6.

Residual gas in the ionization compartment constitutes an obstacle for application of the device as a polarized proton source. Five separately pumped vacuum compartments precede the iron cylinder enclosing the electron gun. The ionization cylinder and its surrounding tank are each pumped by a Balzers 100 l/s diffusion pump. The diffusion pumps of the ionization compartment and beam receiver have a mechanical pump separate from the other diffusion pumps. All seals use rubber *O*-rings, and degassing procedures are correspondingly limited. Large surfaces at liquid air temperature are maintained in the vicinity of the gun. Calculation indicates little diffusion of H_2 or D_2 into the ionization cylinder. This is substantiated by no observable rise in pressure ($\Delta p < 5 \times 10^{-8}$ Torr) in the cylinder when an operational gas current is admitted to the first compartment. Protons constitute 2% of the residual gas ions, molecular hydrogen about 1%. Experiments with a residual gas primarily of molecular hydrogen gave the ratio $H^+/H_2^+ = 0.15$; this was reduced to 0.08 by use of an oxide cathode, indicating that processes other than dissociation of H_2 by the tungsten filament are important. These measurements lead us to suspect hydrogenous compounds as the origin of a large part of the protons.

An increase in the proton current and a decrease in the molecular hydrogen ion current are observed when the gas discharge is switched on. These changes are roughly in the right proportion to indicate the replacement of the molecular by the atomic beam. The proton increase, which immediately follows the switching of the oscillator, is independent of compartment pressure; the proton current from the residual gas is 5 to 10 times greater than the increase, depending on the compartment pressure. The large proportion of residual gas protons makes the device unsuitable in its present condition as a source of polarized protons but allows observation of the neutrons produced by deuterons from the atomic beam.

Application to the $T(d, n)He^4$ Reaction

The ions produced by the electron gun are accelerated through 100 kV without deflection onto a thick target of tritium in titanium. No separation of ions is made, since few molecular deuterium ions are expected

from the residual gas and other ions produce no radiation that might be confused with 14 MeV neutrons. This causes rapid formation of a carbon layer on the target. The disadvantages are offset by additional simplicity and the elimination of a large scatterer near the target. The large volume in which the ions originate is responsible for a beam of about 15 mm diameter at the target.

Neutrons are detected by photomultipliers with plastic scintillators located 30 cm from the target. Unpolarized deuterons are obtained by admitting molecular deuterium into the ionization compartment. The ratio of reaction cross sections $\sigma(0)/\sigma(\theta)$ is measured by comparing the neutron counting rates produced by deuterons from the atomic beam and from the molecular gas admission. Corrections for the different distributions in the laboratory coordinate system for the 100 keV and 50 keV deuterons are negligible when compared with the resolving power of the detectors. No appreciable increase in neutron counting rate from residual gas ions is observed to result from previous admission of molecular deuterium to the ionization compartment. Typical neutron counting rates: atomic beam ionized 530 min^{-1} ; residual gas ionized with normal gas admission to the first compartment but no atomic beam 200 min^{-1} ; residual gas ionized without gas admission 180 min^{-1} ; no ionization but accelerating voltages present 50 min^{-1} .

These results show that more than twice as many neutrons originate from ions of the atomic beam as from the residual gas and molecular beam. The partial pressure of the atomic beam may be calculated by comparing the neutron counting rates for the atomic beam and the unpolarized deuterium, taking into consideration different yields and ionizing volumes. The result agrees with the pressure measured by the manometer that monitors the atomic beam. The current on the target can be estimated from the fraction of the total pressure attributed to the atomic beam and the total positive ion current. This calculation gives a value of 10^{-8} A.

We have investigated the effect of various field conditions on the value of $\sigma(0^\circ)/\sigma(90^\circ)$, using two detectors simultaneously. The magnetic shielding and the field from the cathode prevent a controlled change of the direction of the homogeneous field, and the magnitude could not be increased to values allowing a significant change of $\sigma(0^\circ)/\sigma(90^\circ)$ with increase of the magnetic field without changing the field coils. Nevertheless, $\sigma(0^\circ)/\sigma(90^\circ)$ showed values close to unity, if the field in the iron cylinder was decreased below 1 gauss.

Three points of the angular distribution were measured simultaneously with four scintillation counters. Figure 6 shows the measured values of $\sigma(0)/\sigma(\theta)$. A convenient parameter, G , is the population ratio of spin state 0 to the sum of the populations of states $+1$ and -1 . For ioniza-

tion in a weak parallel field, G is very nearly $4/5$. A value of G was calculated for each experimental point; the weighted average is 0.73 ± 0.02 . Curves for $G = 0.8$ and 0.73 are also shown in Figure 6. The average value is smaller than 0.8 , as one might expect, since the homogeneous field in the ionization volume is not exactly parallel; we think all other sources of depolarization are less important.

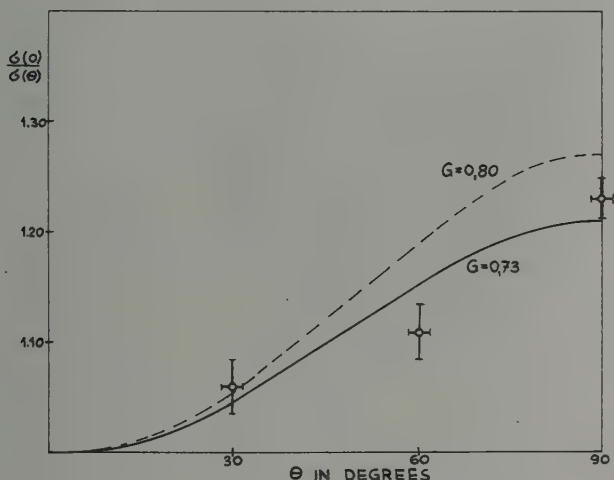


Figure 6
Angular distribution measurements

Conclusions

The experiments show that polarized deuterons can be obtained from an atomic beam in sufficient numbers for useful purposes. The device operated satisfactorily with little attention from the operators. The individual runs give no evidence for fluctuations of $\sigma(0)/\sigma(\theta)$ except those due to counting statistics. A reduction in size and energy consumption as well as an increase in polarized current seem technically possible, as does the elimination of the large number of protons from the residual gas.

Acknowledgments

We have had the help and encouragement of many persons in this work, all of whom we wish to thank. Special thanks, however, must be directed to Mr. H. WEYENETH of the mechanical shop and to Mr. F. ABT of the electrical shop together with their personnel.

REFERENCES

- [1] A. GALONSKY, H. B. WILLARD, and T. A. WELTON, Phys. Rev. Let. 2, 349 (1959).
- [2] H. G. POOLE, Proc. Roy. Soc. 163 A, 404 (1937).
- [3] R. KELLER, CERN 57-30 (August 1, 1957); R. KELLER, L. DICK, and M. FIDECARO, CERN 60-2 (January 29, 1960).
- [4] H. FRIEDBURG, Z. Phys. 130, 493 (1951); H. G. BENNEWITZ, and W. PAUL, Z. Phys. 139, 489 (1954); G. CLAUSNITZER, R. FLEISCHMANN, and H. SCHOPPER, Z. Phys. 144, 336 (1956).
- [5] N. F. RAMSEY, *Molecular Beams*, Oxford (1956).
- [6] Gesellschaft der Ludwig von Roll'schen Eisenwerk AG., Klus, Switzerland.
- [7] C. L. BARTBERGER, J. Appl. Phys. 21, 1108 (1950).
- [8] N. F. MOTT and H. S. W. MASSEY, *The Theory of Atomic Collisions*, Second Edition, p. 65, Oxford (1949).
- [9] W. L. FITE and R. T. BRACKMANN, Phys. Rev. 112, 1141 (1958).

Production and Detection of a Polarized Deuteron Beam Using the Atomic Beam Magnetic Resonance Method¹⁾

By V. W. HUGHES, C. W. DRAKE, JR., D. C. BONAR, J. S. GREENBERG,
and G. F. PIEPER, Gibbs Laboratory, Yale University

1. Introduction

The development of nuclear physics and particle physics has reached the stage where it is useful, possible, and perhaps necessary to consider the production of polarized accelerated beams of various kinds of particles. Use of such beams would allow the careful study of spin dependent interactions and tests of various symmetries and invariances in nuclear and particle physics.

Polarized particles can be produced by scattering unpolarized particles from nuclei, and a great deal of work has been done with polarized particles obtained in this way. However, the intensities of polarized particle beams so obtained are small, even when substantial energy and angular spreads are accepted. Furthermore, the energies at which polarized beams can be obtained and the magnitudes of the polarization depend on the particle-nucleus interaction and so are not readily controllable.

If a polarized ion source is produced and then the ions are accelerated, it is anticipated that a much higher intensity beam of polarized particles can be achieved than by the scattering method. The energy and the geometrical characteristics of the beam will be determined by the accelerator, and the magnitude of the polarization should be independent of energy. Hence much greater versatility should be available for experiments.

The present paper reports the progress of work at Yale on the production and detection of an accelerated beam of deuterons. This paper is the content of a report to the Basel International Symposium on Polarization Phenomena of Nucleons, 1960. Our approach has been to use the classic atomic beam magnetic resonance method to produce polarized atoms,

¹⁾ This research has been supported in part by the U. S. Atomic Energy Commission and the Office of Naval Research.

to ionize the atoms by electron bombardment, to accelerate the deuterons in an electrostatic accelerator, and finally to test for the deuteron polarization by use of the spin dependence of the nuclear reaction $T(d, n) \text{He}^4$.

The use of magnetic resonance to select polarized atoms, as opposed to the method using only deflection by inhomogeneous magnetic fields, has some advantages. Fast modulation techniques involving the alternate use of a polarized beam and an unpolarized beam are possible and should aid greatly in the subtraction of background counts. The use of magnetic resonance makes possible less critical requirements on the inhomogeneous magnetic fields and the use of larger fields and field gradients in the deflecting magnets. The resonance technique also allows different ions (for example, protons and deuterons) to be used with only a change in the frequency of the radiofrequency generator. The addition of a magnetic resonance transition is a negligible complication to the overall apparatus.

2. Theory of Experiment

2.1 *Production of Polarized Atoms Using the Atomic Beam Magnetic Resonance Method*

The production of polarized atoms by the use of inhomogeneous magnetic deflecting fields dates from the classic experiments of STERN and GERLACH [1,2] in 1922 in which a beam of silver atoms was split into its two electronic magnetic substates $-^2S_{1/2}$, $m_J = -1/2$ and $^2S_{1/2}$, $m_J = +1/2$. The magnetic field they used was of the type shown in Figure 1.

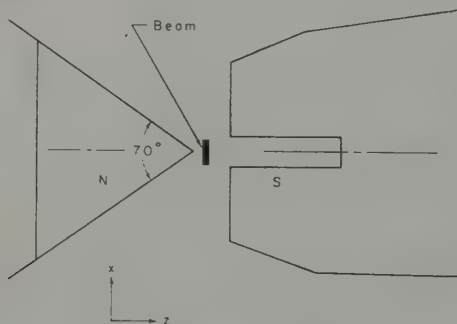


Figure 1

Magnet to produce inhomogeneous field of the type used in the Stern-Gerlach experiment. The force on an atom acts predominantly in the z direction

²) Numbers in brackets refer to References, page 106.

Several other types of inhomogeneous magnetic fields have been widely used to produce a spatial separation of the different polarization components of an atomic beam. The ideal geometry for the two wire deflecting field and its more practical realization with magnetic equipotentials are shown in figures 2 and 10, respectively [2]. This field is suitable for a beam of rectangular, ribbon-like cross section. Another type of field is a six-pole magnetic field [3] as shown in figure 3. This field is suitable for a beam having a circular or ring-shaped cross section.

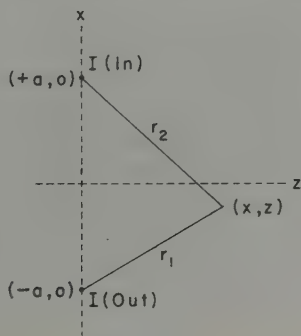


Figure 2

Geometry of two-wire deflecting field. The force on an atom acts predominantly in the z direction

For an atom with angular momentum quantum number J , which has only an electronic magnetic moment, there are $2J + 1$ polarization states – an example is ${}^4_2\text{He}$ in the 3S_1 electronic state with 3 different states of polarization. If the nucleus of the atom has a nuclear magnetic moment associated with the spin quantum number I , the total number of states of polarization is $(2I + 1)(2J + 1)$. Hence for hydrogen in the $1^2S_{1/2}$ ground electronic state with $I = 1/2$ there are 4 states of polarization and for deuterium in the $1^2S_{1/2}$ state with $I = 1$ there are 6 states of polarization.

The spatial separation of atoms in states of different nuclear polarization is more difficult than the separation of atoms in states of different electronic polarization, because a nuclear magnetic moment is much smaller than an electronic magnetic moment. Still the spatial separation of an atom in a particular state of nuclear polarization can be achieved in practice, particularly with the use of inhomogeneous magnetic fields having low average field values. This is possible in general because the effective magnetic moments of all the polarization states may differ by a significant fraction of a Bohr magneton at intermediate magnetic

field values where the hyperfine structure interaction is comparable in magnitude to the interaction of the atom with the external magnetic field.

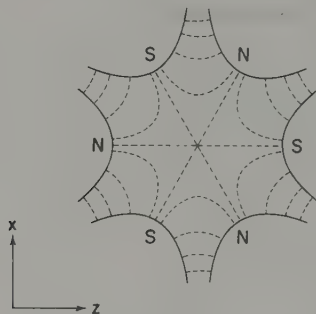


Figure 3a

Field and potential lines for a magnetic field which varies as the square of the distance from the axis. Field lines are dashed (---); potential lines are solid (—); axis is through the geometrical center of diagram perpendicular to figure. The force on an atom acts in the radial direction

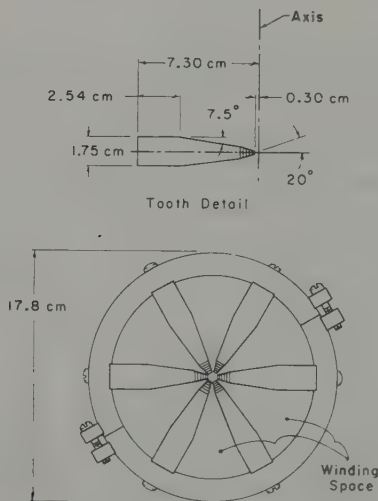


Figure 3b

Six-pole magnet to produce an inhomogeneous magnetic field of the type shown in figure 3a, view of the soft-iron structure. Magnet windings (not shown) fill space between teeth. Striations near tips of individual teeth correspond to the longitudinal shaping of the magnet

An alternative but related method of selecting an atom in a particular state of nuclear polarization involves the use of the well known atomic beam magnetic resonance method [4, 5]. The general scheme is indicated in figure 4. A discussion of the method can be given with reference to figures 5 and 6, which present the energy levels and magnetic moments of the hydrogen atom in an external magnetic field. The A- and B-regions have inhomogeneous magnetic fields and the C-region has a homogeneous magnetic field. The magnetic fields in the A- and B-regions are sufficiently high so that an adequate approximation of the hydrogen atom either has a magnetic moment of $+\mu_0$ or $-\mu_0$ ($\mu_0 =$ Bohr magneton). Hence in the A-region the hydrogen atoms are separated into two groups which follow different trajectories. Figure 4 indicates this situation and how it can be used to obtain polarized atoms. A wire stop is placed after the collimator between the B- and the C-regions so that only atoms with magnetic moment $-\mu_0$ in the A-region, i. e., atoms in the states with $m_J = -1/2$ ($m_J =$ magnetic quantum number associated with the electronic angular momentum) pass by the wire; atoms with magnetic moment $+\mu_0$ in the A-region, i. e., atoms in the states with $m_J = +1/2$ will strike the wire. Hence with the inhomogeneous A-magnet and the wire stop atoms in two magnetic substates are selected.

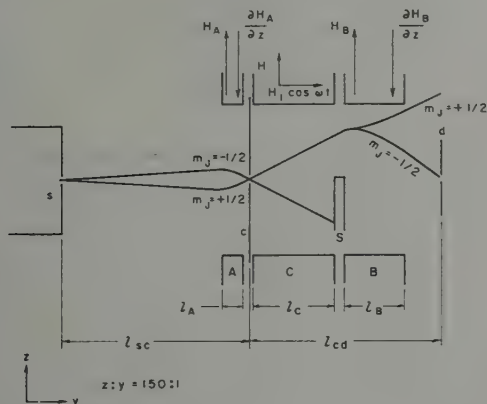


Figure 4

Schematic diagram of atomic beam magnetic resonance spectrometer. s is the source chamber with source slit. c is the collimator slit. The A- and B-regions are regions of inhomogeneous magnetic field. The C-region contains the oscillating electromagnetic field, and, in addition, a constant homogeneous field. d is the detector region. S is a wire stop. Trajectories of atoms in different m_J states are shown. $l_{sc} = 19.7$ cm, $l_{cd} = 16.3$ cm, $l_A = 2.0$ cm, $l_C = 8.0$ cm, and $l_B = 6.0$ cm.

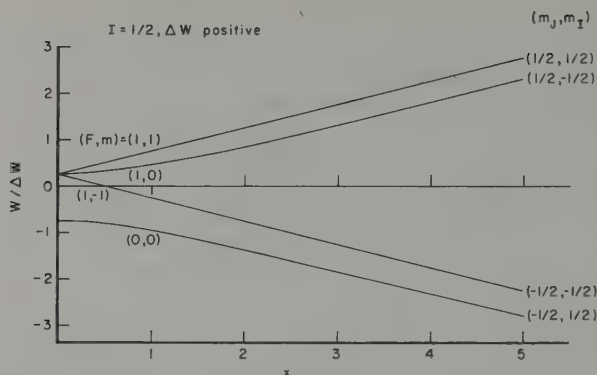


Figure 5

Energy level diagram for hydrogen in a magnetic field H , obtained from the Breit-Rabi equation:

$$W_{F=I \pm 1/2, m} = -\frac{\Delta W}{2(2I+1)} + \mu_0 g_I H m \pm \frac{\Delta W}{2} \left[1 + \frac{4m\kappa}{2I+1} + \kappa^2 \right]^{1/2}$$

ΔW is the zero field hfs separation between the states

$$F = I + 1/2 \text{ and } F = I - 1/2 \quad [\Delta W = W_{I+1/2}(H=0) - W_{I-1/2}(H=0)];$$

$\kappa = (g_J - g_I) \mu_0 H / \Delta W$; g_J and g_I are the electronic and nuclear g -values in units in which $g_J \simeq 2$; μ_0 = Bohr magneton. For hydrogen, $J = 1/2$, $I = 1/2$, $\Delta W/h = \Delta\nu = 1420.4$ Mc/s, $g_J = 2.002$, $g_I = -0.0030$. The levels are designated by both their weak field quantum numbers (F, m) and their strong field quantum numbers (m_J, m_I)

The remainder of the apparatus including the C- and B-regions is designed to select only one of these two magnetic substates. This can be done in one of two ways. The first involves selection of the substate $(F, m) = (1, 1)$. In the C-region a constant, homogeneous magnetic field H is present. In addition, a radiofrequency field is applied of the proper frequency and amplitude so as to cause a transition of atoms in the magnetic substate $(F, m) = (1, 0)$ to the magnetic substate $(1, -1)$. Atoms in the magnetic substate $(F, m) = (1, 1)$ remain unaffected. If the B-field is high and if the direction of its field gradient is opposite to that of the A-field (this is not the condition shown in figure 4), then atoms in the state $(F, m) = (1, 1)$ (high field quantum numbers are $m_J = +1/2$, $m_I = +1/2$) can be refocussed onto a detector region, whereas atoms which are in the substate $(F, m) = (1, -1)$ (high field quantum numbers $m_J = -1/2$, $m_I = -1/2$) will be deflected elsewhere. This scheme is often called the «flop-out» method because atoms which undergo the transition do not arrive at the detector. Because of the

velocity distribution in the atomic beam, the maximum fraction of the atoms which will theoretically undergo a transition is 0.77. Hence the atomic beam arriving at the detector region is composed of a mixture of the states $(F, m) = (1, 1)$ and $(1, 0)$. Since the relative numbers of the atoms in the states $(1, 1)$ and $(1, 0)$ are 1 and 0.23, respectively, the average nuclear polarization of the beam in the weak magnetic field region at the detector is³⁾:

$$P_N = \frac{\bar{I}_z}{I} = 0.81$$

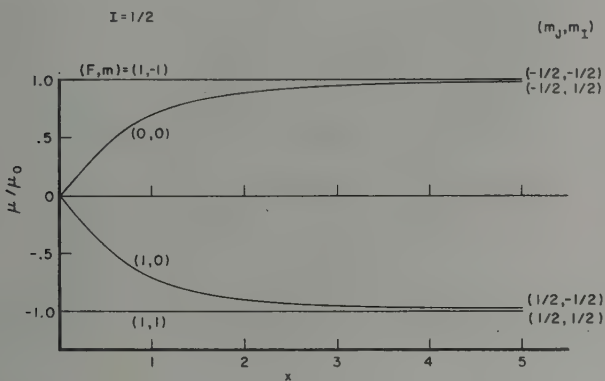


Figure 6

The magnetic moments of the magnetic sublevels of the hfs states of hydrogen with $J = 1/2$ and $I = 1/2$ as a function of magnetic field H , obtained from the equation:

$$\frac{\mu_{F-I \pm 1/2, m}}{\mu_0} = -\frac{1}{\mu_0} \frac{\partial W_{F, m}}{\partial H} = -g_I m \mp \frac{x/2 + m/(2I+1)}{[1 + 4m x/(2I+1) + x^2]^{1/2}} (g_J - g_I)$$

$$\text{for } m = I - 1/2, I - 3/2, \dots, -(I - 1/2),$$

$$\frac{\mu_{F-I \pm 1/2, m \pm (I+1/2)}}{\mu_0} = \mp (g_J/2 + g_I I)$$

The levels are designated by both their weak field quantum numbers (F, m) and their strong field quantum numbers (m_J, m_I)

A second method involves selection of the magnetic substate $(F, m) = (1, -1)$. As in the first method a transition is induced in the C-region from the state $(F, m) = (1, 0)$ to $(1, -1)$. Now, however, the direction

³⁾ The discussion in this section is idealized in that slits of infinitesimal width or magnets with infinite deflecting power are assumed. The actual case is discussed in Section 3.1.

of the B-magnetic field gradient is the same as that of the A-field (this is the condition shown in figure 4), so that only the atoms which have undergone the transition $(F, m) = (1, 0) \rightarrow (1, -1)$ and hence have $m_J = -1/2$ in the B-region will be refocussed onto the detector region. This scheme is often called the «flop-in» method because atoms which undergo the transition do arrive at the detector. The entire beam at the detector will be in the magnetic substate $(F, m) = (1, -1)$ and the average nuclear polarization of the beam is $P_N = -1.0$. This second method is the one we are presently employing.

The «flop-out» scheme as discussed selects primarily the substate $(F, m) = (1, +1)$. Without change in the magnetic fields a «flop-out» scheme can also select primarily the substate $(F, m) = (1, -1)$. This can be accomplished by moving the wire stop so that only atoms with magnetic moment $+\mu_0$ in the A-region - i. e., atoms in the states with $m_J = -1/2$ - pass by the wire and by inducing the transition $(F, m) = (0, 0) \rightarrow (1, +1)$.

The «flop-in» scheme as discussed selects the magnetic substate $(F, m) = (1, -1)$. However, it can also select the magnetic substate $(F, m) = (1, +1)$ without changing the magnetic fields by moving the wire stop and by inducing the transition $(0, 0) \rightarrow (1, +1)$.

The above discussion has been illustrated by the case of hydrogen. The principles are the same for obtaining other polarized atoms. In particular, our work is being done with deuterium. The energy levels and magnetic moments of the deuterium atom in an external magnetic

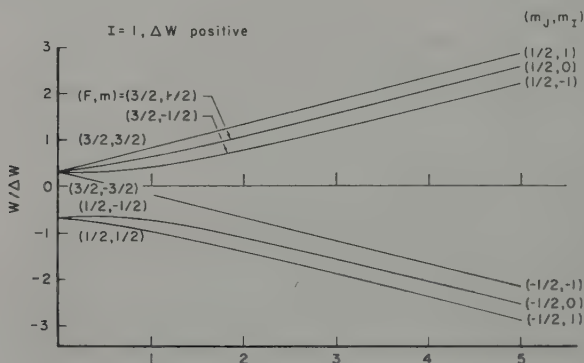


Figure 7

Energy level diagram for deuterium in a magnetic field H , obtained from the Breit-Rabi equation as given in caption to figure 5. For deuterium, $J = 1/2$, $I = 1$, $\Delta\nu = 327.38$ Mc/s, $g_J = 2.002$, and $g_I = -0.00047$. Further description is the same as for figure 5

field are shown in figures 7 and 8. We are using a «flop-in» scheme which selects the magnetic substate $(F, m) = (3/2, -3/2)$ and hence in principle produces an atomic beam with complete nuclear polarization, $P_N = -1$.

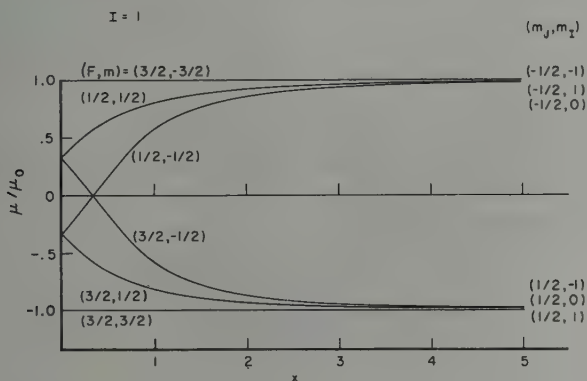


Figure 8

The magnetic moments of the magnetic sublevels of the hfs states of deuterium with $J = 1/2$ and $I = 1$ as a function of magnetic field H , obtained from the equations given in the caption to figure 6. Further description is the same as for figure 6

2.2 Ionization of Polarized Atoms

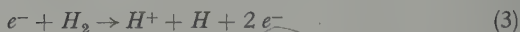
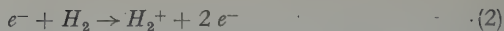
In order to be suitable for injection into an accelerator the polarized atoms must, of course, be ionized to produce polarized nuclei. The practical and obvious method is to ionize the polarized atoms by electron bombardment. Important questions in practice are the magnitude of the ionization cross sections both for the atom of interest and for other atoms or molecules which might constitute important ionic background and the realizable characteristics of an electron gun. The only question in principle is whether, or to what extent, the nuclei may lose their polarization in the process of ionization of the atom.

The ionization cross section of a hydrogen atom by an electron,



has been measured recently [6] by an atomic beam method. The cross section as a function of energy is shown in figure 9a. The cross section for the ionization of deuterium will be the same as that of hydrogen.

Other processes which may contribute in an important way to the background are the following:



The cross section for process (2) is shown in figure 9a. The cross section for process (3) is shown [7, 8] in figure 9b. Processes (2) and (3) may constitute an important source of background because of the presence of molecular hydrogen or deuterium. Process (3) clearly produces an unpolarized proton as background. Process (2) may also be troublesome unless the scheme for detection of polarization clearly distinguishes between the atomic and molecular ions. Indeed, in our experiment with deuterium, in which the $T(d, n) \text{He}^4$ nuclear reaction is used, the principal background will be from D_2^+ .

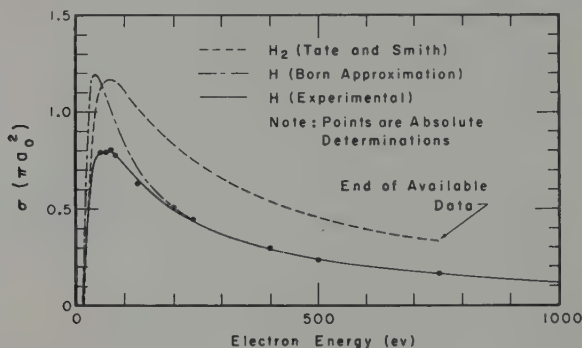


Figure 9a

Ionization cross sections for atomic and molecular hydrogen as a function of electron bombarding energy. The solid (—) and dot-dash (— · —) curves refer to the process: $e^- + H \rightarrow 2e^- + H^+$. The dashed (---) curve refers to the process:



The probability for the loss of nuclear polarization in the atomic ionization process is believed to be negligibly small. A qualitative argument is that the ionization occurs primarily through an electrostatic interaction; magnetic effects, which are required for reorientation of the nuclear spin, are expected to be relatively unimportant since the electrons have non-relativistic velocities. An alternative view is that the nucleus will experience a disorienting magnetic field due to the electrons during the collision. A characteristic value for this field is $\mu_0/a_0^3 \sim 10^5$ gauss (μ_0 = Bohr magneton; a_0 = Bohr radius for hydrogen) and a characteristic time for the collision is $2a_0/v \sim 5 \times 10^{-17}$ s (v = electron velocity $\simeq 2 \times 10^8$ cm/s). The angle of precession of a proton magnetic

moment in a 10^5 gauss field in a time of 5×10^{-17} s is only 10^{-7} radian and hence the change in the direction of the proton magnetic moment is negligible. Since the ionization process produces two free electrons and a free proton, electron exchange effects will not contribute to a change in proton polarization.

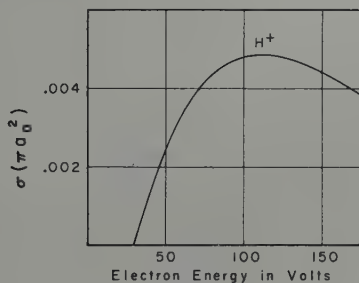
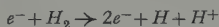


Figure 9b

Ionization cross section for molecular hydrogen as a function of electron bombarding energy. The curve refers to observed cross sections for the process:



Although the nuclear moment will not change its orientation during the ionization process, once it is free of the hydrogen electron and the associated large magnetic field, its orientation will be determined by the relatively small magnetic field in which it may find itself. If the nucleus moves slowly enough through a region where the magnetic field is not zero so that it does not experience a substantial frequency component at the frequency characteristic of the Larmor precession of the nucleus in the field, then the nuclear spin direction will follow adiabatically the external field direction [9].

Design and Operation of Apparatus

3.1 Atomic Beam Magnetic Resonance Apparatus

For our initial experiments a relatively standard atomic beam magnetic resonance apparatus for hydrogen work has been constructed. Because of the scheme we plan to use for the detection of polarized nuclei, the work is actually being done now with deuterium rather than with hydrogen. Figures 4 and 13 show the essential features of the apparatus including pertinent dimensions.

The source of deuterium atoms is a water-cooled Wood's discharge tube, operated at 10 000 volts ac with a current of 240 ma. The pressure

in the discharge tube as estimated from the flow rate and slit area is 0.35 mm of Hg. The slit in the discharge tube is 1 cm high by 0.013 cm wide. (The collimator slit is the same as the source slit.) Hence for the source temperature of 300° K, the particle flux from the source is $7 \times 10^{18}/\text{s}$. In the absence of the static and radiofrequency fields, the fraction of these particles which enter through the opening of 1 cm by 0.015 cm to the detector region is 3.5×10^{-6} [Detector area/ π (source to detector distance)²].

The positions and lengths of the magnets are indicated in figure 4. A detailed drawing of the A-magnet is shown in figure 10. It is a permanent magnet (Alnico) with high permeability (Permendur) pole tips and soft iron (Armco) return path as indicated. A magnetic field of 7.5 kilogauss and a field gradient of 11 kilogauss/cm is achieved at the position of the atomic beam. The B-magnet is identical in structure except that its length is 6.0 cm. A detailed drawing of the C-magnet is shown in figure 11. It is designed to produce a homogeneous magnetic field of about 100 gauss.

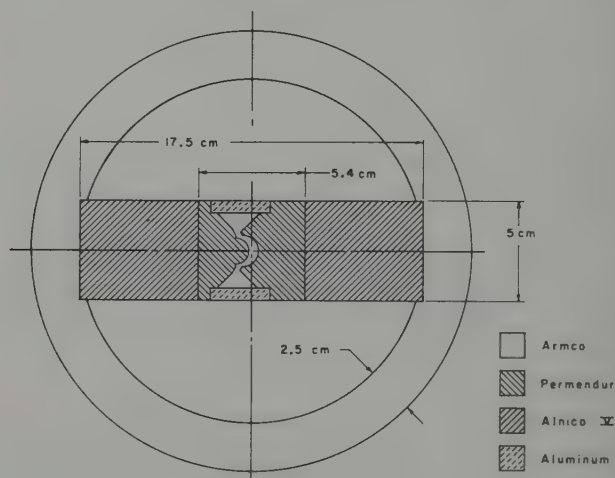


Figure 10a

Cross section of iron deflecting magnet, complete view.
Length of A-magnet is 2.0 cm

A radiofrequency field with a component of magnetic field perpendicular to the static C-field is introduced through a loop in the C-region extending for a length of 0.3 cm along the direction of beam propagation. In order to obtain resonance for the transition in deuterium from

$(F, m) = (3/2, -1/2)$ to $(3/2, -3/2)$ in a field $H = 101$ gauss, a frequency of 155 Mc/s is chosen. The radiofrequency is generated by a Hewlett-Packard 608D oscillator, amplified, and fed through a double stub tuner to the rf loop. The observed width of the resonance line is 700 kc/s whereas the natural width associated with the transit time of the atoms through the rf region is 560 kc/s; the excess width over the natural width is due to magnetic field inhomogeneity.

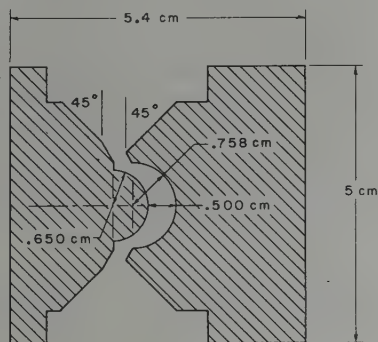


Figure 10b

Cross section of iron deflecting magnet, details of pole faces

The operation of the atomic beam magnetic resonance apparatus has been studied with the use of a Pirani gauge of a usual modern design as a detector [10]. The dimensions of the entrance slit to the Pirani gauge are 0.32 cm by 0.0025 cm. The absolute sensitivity of the Pirani gauge for D atoms was obtained by observing the Pirani signal when a beam of D_2 molecules is allowed to effuse from the slit of the discharge tube. (No voltage is applied to the discharge tube so only deuterium molecules are present.) From a knowledge of the rate of the total flow of D_2 gas from the reservoir feeding the discharge tube and of the dimensions of the system the number of D_2 molecules entering the Pirani detector per unit time can be calculated by use of the kinetic theory of gases, and hence the Pirani gauge sensitivity can be determined for D_2 molecules. To obtain the sensitivity for D atoms the assumption is made that two D atoms produce the same effect as one D_2 molecule [10]. The sensitivity of our Pirani gauge, including its associated circuitry, is 1 cm of deflection on a galvanometer scale for 4×10^9 D_2 molecules entering the gauge per second.

With the use of this measured sensitivity of the Pirani gauge and the known entrance area of the Pirani gauge, the observed resonance signal

can be converted into the number of polarized atoms per second that would enter the larger detector area (0.015 cm^2) actually to be used as the entrance to the ionizer. The flux of polarized deuterium atoms in the state $(F, m) = (3/2, -3/2)$ is thus measured to be 10^{12} atoms per second. This figure agrees with the theoretical design value within the experimental uncertainty of about 30%. Deuterium atoms in other magnetic substates have only a small probability of entering the detector region. Thus the deflection, s_z , of an atom which is in any one of the magnetic substates with $m_J = +1/2$ in the strong B-field away from the center of the detector opening is $3.8 \times 10^{-2} \text{ cm}$ for an atom having the most probable velocity of an atom in the source. This value of s_z implies that the fraction of the atoms in the $m_J = +1/2$ state in the B-field which enter the detector region is only about 0.2. In practice the fraction will depend on the position of the wire stop and can be made smaller than 0.2. Atoms which were in the $m_J = -1/2$ states in the A-field should be blocked by the wire stop. All atoms in the $m_J = -1/2$ state in the B-field (low field state $(F, m) = (3/2, -3/2)$) should enter the detector. Hence the relative numbers of atoms entering the detector region in the states $(F, m) = (3/2, -3/2), (3/2, -1/2), (3/2, +1/2)$, and $(3/2, +3/2)$ are 0.8, 0.05, 0.2 and 0.2. The nuclear polarization of the beam entering the detector region should then be $P_N = -0.44$. By proper positioning of the wire stop a larger negative value of polarization can be obtained.

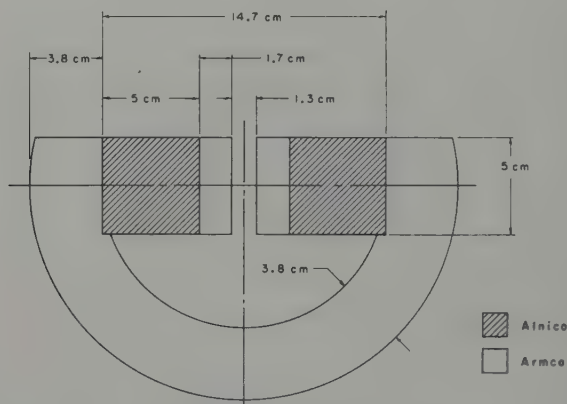


Figure 11

Cross section of homogeneous C-magnet, complete view

A major practical problem is the background of unpolarized hydrogen or deuterium present in the ionization region. For our deuterium experiment since the eventual detected event is the product of a specific

nuclear reaction induced by an accelerated deuteron, the only troublesome background will be due to unpolarized deuterium in the ionization region. The unpolarized deuterium may be present either as molecules or as unpolarized atoms.

With a view in particular to the production of a polarized proton source, our apparatus is provided with freon-cooled mercury pumps and liquid nitrogen traps (see figure 12). Conventional oil mechanical pumps are used. The vacuum envelope is constructed of stainless steel. There is provision for metal gaskets and for baking out the entire apparatus including the magnets at 250°C , although it has been convenient thus far to take data with the use of polyethylene gaskets and no bake-out has been attempted. The vacuum system is divided into three separately pumped sections – the source chamber, the interchamber, and the main chamber, which includes the atomic beam magnetic resonance components, the ionizer, and the attached electrostatic accelerator. These sections are separated by small openings which allow passage of the atomic beam.

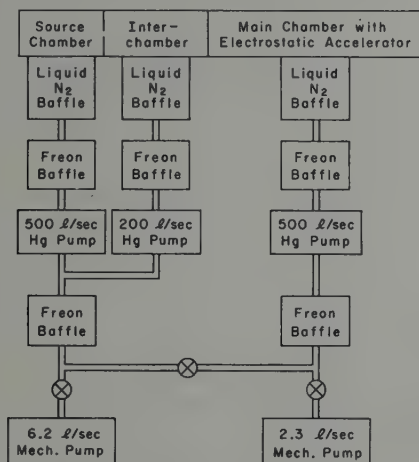


Figure 12

Schematic diagram of vacuum system

With no flow of deuterium gas into the vacuum system, an ionization gauge placed near the beam ionizer region indicates a pressure of 3×10^{-7} mm of Hg. With the customary rate of flow of deuterium gas through the discharge tube, the pressure increases to 3.3×10^{-7} mm of Hg. The increase in pressure of 3×10^{-8} mm of Hg is a measure of the pressure of unpolarized deuterium – presumably predominantly

molecular deuterium. This pressure corresponds to a density of 2×10^9 particles/cm³. The background of unpolarized deuterium atoms in the ionization region is contributed principally by those atoms in the magnetic substates with $m_J = +1/2$ in the B-field which are not deflected away from the detector opening. As discussed in the previous paragraph, the number of atoms in these states which enter the detector opening depends on the geometry of the atomic beam and upon s_α and is about 5×10^{11} atoms/s.

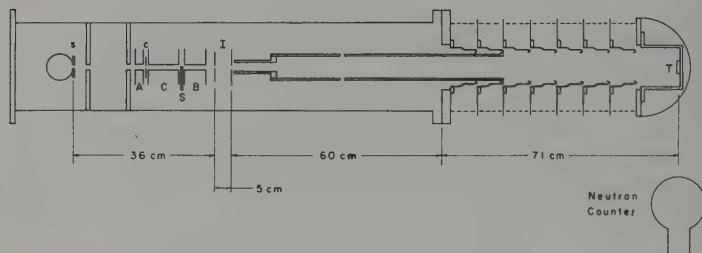


Figure 13

Schematic diagram of entire experimental setup, showing atomic beam magnetic resonance spectrometer, ionizer, electrostatic accelerator, and neutron counters

3.2 The Ionizer

The polarized deuterium atom flux entering the ionization region is 10^{12} atoms/s as was mentioned in section 3.1. Since the average velocity of the deuterium atoms from a discharge tube at 300° K is 2×10^5 cm/s and the opening for the beam into the ionization region is 0.015 cm², the density of polarized atoms will be 3×10^8 /cm³. It was noted in section 3.1 that the background density of D₂ molecules is 2×10^9 /cm³ and of D atoms in unwanted magnetic substates about 1.5×10^8 /cm³. If the energy of the electron beam in the ionizer is 200 ev, then in view of the cross sections as given in figure 9, the relative numbers of D⁺ nuclei of the desired polarization, D⁺ nuclei of undesired polarization, and D₂⁺ molecular ions are 1, 0.5, and 11.

The ionizer is now under development. Studies have been made of an electrostatic Pierce-type gun [11] in which the electron beam travels in a direction perpendicular to that of the atom beam and parallel to the long dimension of the ribbonlike beam. The objective was to obtain an electron beam of several hundred ev energy which has a current density of 100 ma/cm² and a width approximately that of the atom beam or 0.02 cm. We have found it difficult to achieve this operation with any degree of reliability.

At présent we are experimenting with another ionizer [12] which bombards in a direction perpendicular to that of the atom beam propagation and parallel to the short dimension of the beam. The ionizer has a large cathode area (1 cm high by 5 cm long). The design value of the electron current density is 0.5 amp/cm^2 at an energy of 80 ev. The electrons are accelerated through a grid to a collector plate at the grid potential. The atomic beam runs through the space between grid and collector. Advantage is to be taken of the potential minimum due to space charge effects in order to trap the ions and then accelerate them out the exit end of the ionizer. The electric field in the direction of the atom beam propagation is obtained by varying the grid to plate spacing.

3.3 Acceleration of deuterons and the detection of polarization

The $T(d, n) \text{He}^4$ reaction with *s*-wave deuterons provides a convenient and sensitive detector of the polarization of an accelerated deuteron beam [13]. This reaction [14] has a broad resonance centered about 107 keV, and the thick target yield for a deuteron bombarding energy of 150 keV is approximately 4×10^{-6} per incoming deuteron for a 5 Curie T-Zr target. The angular distribution, in the center of the mass system, for the outgoing neutrons, when the reaction is induced by deuterons which are partially polarized in the transverse *z* direction, is given by

$$W(\theta) = (P_1 + P_{-1}) (3 \sin^2 \theta + 2) + P_0 (6 \cos^2 \theta + 2) .$$

The angle θ is measured with respect to the deuteron polarization axis in the plane perpendicular to the beam axis, and the quantities P_1 , P_{-1} , and P_0 are the probabilities for the deuteron to have $m_l = +1$, -1 , and 0, respectively. For the completely polarized deuterons, the anisotropy $W(90^\circ)/W(0^\circ)$ will be 2.5. However, as discussed in section 3.2, before acceleration one expects 11 times as many unpolarized D_2^+ as polarized D^+ . With a terminal voltage of 150 kv on the accelerator, the ratio of the thick target yields for D^+ and D_2^+ is approximately 1.5 since the D_2^+ are accelerated only to 75 keV. The expected asymmetry with this D_2^+ background, as well as with the background of D^+ in magnetic substates other than the desired one (see section 3.2), then becomes $W(90^\circ)/W(0^\circ) \simeq 1.08$. Solid angle effects and scattering will tend to reduce this somewhat.

The accelerator column consists of seven spinnings separated by ceramic insulators 3 inches long. It was kindly provided by Drs. N. HEYDENBERG, G. TEMMER, and J. WEINMAN of the Department of Terrestrial Magnetism Laboratory in Washington, D.C. The deuterons are focussed into the accelerator column from the ionizer by a single electrostatic lens.

Plastic scintillators are used for neutron detection. They have an intrinsic efficiency of approximately 10% for the 14 MeV neutrons produced in the $T(d,n)He^4$ reaction. The spectrum produced by the recoil protons has a reasonably sharp cut-off at maximum energy. With appropriately chosen bias levels the counter can be made quite insensitive to gamma rays below a few MeV.

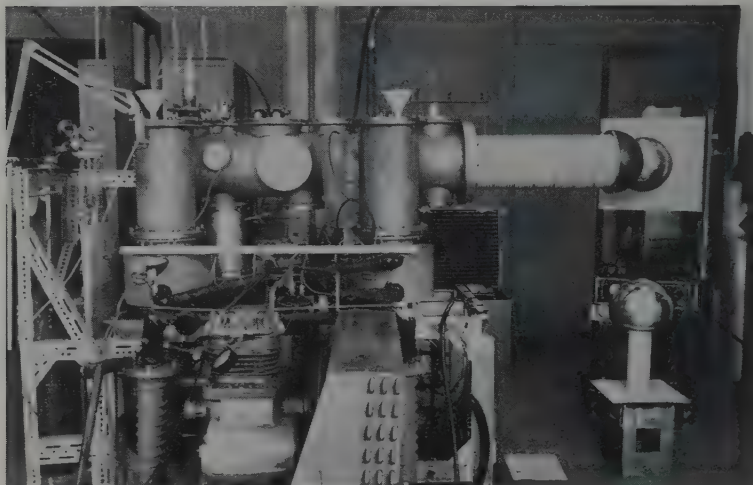


Figure 14
Photograph of entire apparatus

Acknowledgements

We are particularly indebted to Drs. N. HEYDENBERG, G. TEMMER, and J. WEINMAN of the Department of Terrestrial Magnetism, Carnegie Institution, Washington, D.C., for supplying the electrostatic accelerator tube and for encouragement and collaboration. It has been our mutual intention to install the polarized ion source in their Van de Graaff accelerator.

REFERENCES

- [1] W. GERLACH and O. STERN, *Ann. Phys.* 74, 673 (1924); W. GERLACH and O. STERN, *Z. Phys.* 8, 110 (1921–1922).
- [2] P. KUSCH and V. W. HUGHES, *Encyclopedia of Physics* (Springer, Berlin 1959), Vol. XXXVII/1, p. 41.
- [3] P. KUSCH and V. W. HUGHES, *Encyclopedia of Physics* (Springer, Berlin 1959), Vol. XXXVII/1, p. 51.

- [4] P. KUSCH and V. W. HUGHES, *Encyclopedia of Physics* (Springer, Berlin 1959), Vol. XXXVII/1.
- [5] N. F. RAMSEY, *Molecular Beams* (Oxford: Clarendon Press, 1956).
- [6] W. L. FITE and R. T. BRACKMANN, *Phys. Rev.* **112**, 1141 (1958).
- [7] H. S. W. MASSEY and E. H. S. BURHOP, *Electronic and Ionic Impact Phenomena* (Oxford: Clarendon Press, 1952), p. 247.
- [8] H. E. NEWHALL, *Phys. Rev.* **62**, 11 (1942).
- [9] I. I. RABI, *Phys. Rev.* **49**, 324 (1936).
- [10] A. G. PRODELL and P. KUSCH, *Phys. Rev.* **88**, 184 (1952).
- [11] J. R. PIERCE, *Theory and Design of Electron Beams* (D. Van Nostrand Co., New York 1949), p. 167.
- [12] K. R. SPANGENBERG, *Vacuum Tubes* (McGraw-Hill, New York, 1948), pp. 248–265.
- [13] A. GALONSKY, H. B. WILLARD, and T. A. WELTON, *Phys. Rev. Letters* **2**, 349 (1959).
- [14] J. B. MARION and J. L. FOWLER, *Fast Neutron Physics* (Interscience Publishers, Inc., New York 1960), Vol. IV/1, p. 90 and p. 692.

Etude d'une source de protons polarisés utilisant une transition haute fréquence pour un cyclotron

Par J. THIRION, R. BEURTEY et A. PAPINEAU
Centre d'Etudes nucléaires de Saclay

Introduction

Ce projet a été réalisé afin de définir les meilleures conditions possibles pour l'adaptation d'une source de protons polarisés à un cyclotron. Le but consiste à diriger un faisceau d'atomes aussi dense que possible vers la région d'ionisation au centre du cyclotron, le faisceau devant contenir des spins nucléaires polarisés à une valeur voisine de 1. Les deux facteurs essentiels sont donc, d'une part la pression interne du jet d'atomes à une distance de la source correspondant au centre du cyclotron, d'autre part, la valeur de la polarisation.

La méthode utilisée dans le cas des protons peut être envisagée pour celui des deutons, ainsi qu'on l'examinera plus loin. Les problèmes non encore étudiés sont ceux de l'ionisation et des difficultés liées au vide résiduel. Ces dernières sont moins dramatiques dans le cas des deutons: d'une part, les conditions de résonance de l'accélération opèrent une sélection (champ magnétique légèrement différent du cas des molécules d'hydrogène une fois ionisées H^{2+}) et d'autre part, la séparation complète du faisceau sorti de deutons est possible.

I. Principe

Nous étudions d'abord le cas des protons. La méthode choisie consiste à polariser les protons d'un jet d'atomes et à le diriger vers la région ionisante du centre du cyclotron. En supposant que l'ionisation [1¹⁾], puis l'accélération [2] sont deux processus non dépolarisants, on obtient ainsi un faisceau de protons complètement polarisés en principe. L'opération comporte trois étapes:

1. Production d'un jet atomique.

¹⁾ Les chiffres entre crochets renvoient à la bibliographie, page 121.

2. Séparation par effet STERN et GERLACH [3]. Le diagramme de RABI (figure 1) donne la variation de l'énergie des états hyperfins d'un atome d'hydrogène dans un champ magnétique. Il est relativement facile de séparer les composantes (1) et (2) des composantes (3) et (4). A la sortie de l'aimant STERN et GERLACH, les protons ont une polarisation nulle dans un champ élevé (populations égales de (1) et (2)).

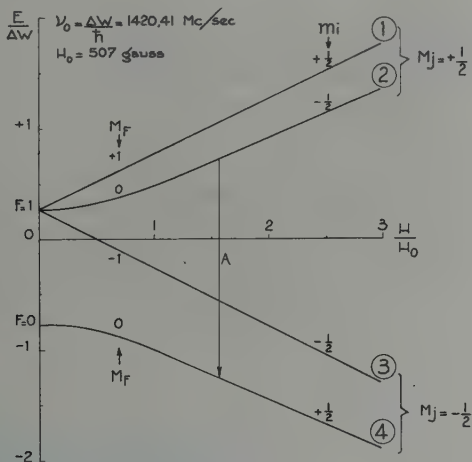


Figure 1
Structure hyperfine de l'atome d'hydrogène

3. Transition de radiofréquence. Cette partie est due à MM. ABRAGAM et WINTER [5]. La transition a lieu à un champ assez faible et il est plus exact de la noter suivant les valeurs F et M_F du spin total de l'atome et de sa projection sur la direction du champ magnétique. La transition notée A (figure 1) fait passer les atomes de l'état $F = 0, M_F = 0$ à l'état $F = 1, M = 0$. En principe, la méthode du passage adiabatique [4, 5] permet un rendement voisin de 100%. Les états (1) et (4) étant seuls peuplés la polarisation des protons en champ magnétique élevé (centre du cyclotron) sera pratiquement complète.

II. Formation du jet atomique

a) Dissociation des molécules d'hydrogène

Nous avons employé la méthode développée par KELLER [6]. Une tension de haute fréquence (20 MHz) est appliquée en deux zones d'un tube en verre Pyrex en forme de V. La sortie du jet s'effectue par une

tuyère placée au milieu du tube. L'hydrogène moléculaire entrant est mouillé par passage dans un flacon d'eau; la proportion de vapeur d'eau est ajustée autour de 10%. La longueur optimum des branches est de 15 cm environ. L'état de surface interne du tube est important pour éviter la recombinaison d'atomes sur les parois. Divers procédés, dont celui du nettoyage à l'acide fluorhydrique, semblent donner de bons résultats. La dissociation a été observée en mesurant l'échauffement d'une plaque de cuivre située à 5 mm de la sortie du tube. Pour 2 mm Hg de pression d'hydrogène et un taux de vapeur d'eau de 10%, la dissociation est, qualitativement, complète. Nous n'avons pas procédé à une étude précise. La puissance haute fréquence est de l'ordre de 1 kW.

b) Formation du jet d'atomes

L'ensemble est représenté figure 2. L'écoulement des atomes à la sortie du tube en Pyrex se fait par la succession de deux orifices inspirés des travaux de BECKER [7] et CLAUSNITZER [8]. Le premier est une tuyère

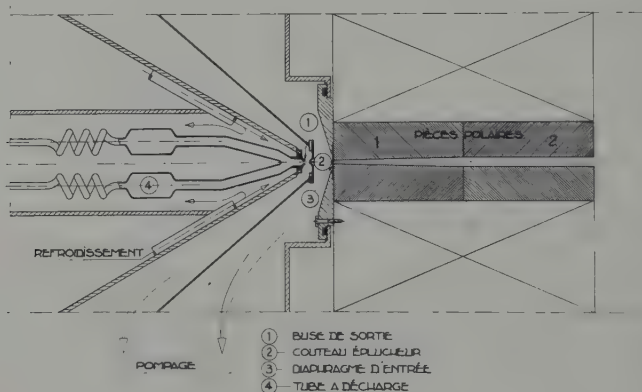


Figure 2

Production et injection des atomes

en Pyrex, déjà mentionnée, de 2 mm de diamètre. Le second est un «couteau éplucheur» en tantale, de forme conique très effilée, situé à 5 mm environ de l'extrémité de la tuyère. Le cône a 3 mm de long, les angles d'ouverture interne et externe sont 50° et 70° respectivement; le trou central est de 1 mm et sert d'objet pour la lentille sextupolaire qui compose l'aimant STERN et GERLACH. L'espace intermédiaire est vidé par une pompe Roots (Haereus) 1600. La pression y est de l'ordre de 10^{-2} mm Hg dans les conditions de fonctionnement. L'ensemble

donne une concentration du jet et un spectre des vitesses théoriquement plus étroits ainsi qu'une intensité axiale plus grande que dans le cas d'un simple trou cylindrique [9]. Ces avantages sont cependant réduits par le fait que la vitesse moyenne est augmentée (voir paragraphe 3), ce qui rend plus difficiles les conditions de fonctionnement de l'aimant séparateur STERN et GERLACH. L'angle solide d'entrée dans l'aimant est ensuite défini par un compartiment de vide poussé de $P = 10^{-4}$ mm Hg en fonctionnement, et de longueur 25 mm, terminé par un diaphragme. Le pompage se fait dans ce compartiment par une pompe 2000 litres Leybold.

Le nombre d'atomes dans un angle solide de $1/1000$ de stéradian est de $3 \cdot 10^{16}$ par seconde.

III. Elimination des états $F = 1$, $M_F = -1$; $F = 0$, $M_F = 0$

L'aimant STERN et GERLACH de séparation est un électroaimant sextupolaire [10] représenté figures 2 et 3. La culasse est cylindrique et l'intérieur de cette culasse ($\varnothing 500$) est entièrement sous vide; les bobines noyées dans l'araldite comportent 20 tours et sont formées de tube

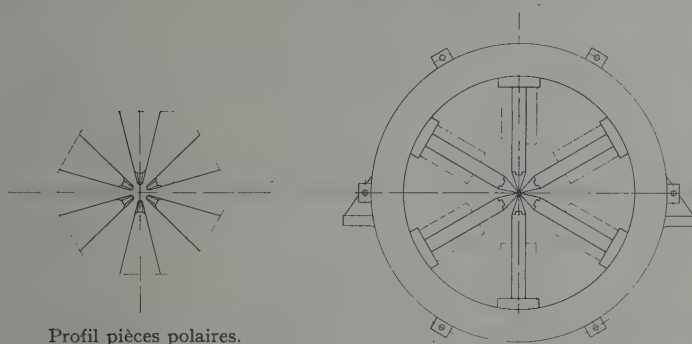


Figure 3
Aimant sextupolaire

carré refroidi intérieurement à l'eau. La saturation débute vers 80 ampères. Le champ magnétique varie comme le carré de la distance à l'axe (nous avons constaté qu'en réalité cette forme de variation n'était valable que jusqu'à la moitié du rayon r_0 limité par les pièces polaires, après quoi le gradient tend vers une constante. Nous négligerons cette anomalie dans le calcul.

Le champ magnétique au bord des pièces polaires H_0 était de 8000 gauss partout. L'aimant se décompose en deux parties I et II indiquées sur la figure 2.

Le champ magnétique étant élevé, on peut distinguer en première approximation deux sortes de trajectoires, celles pour lesquelles le spin de l'électron de l'atome est «en haut» et celles pour lesquelles il est «en bas» par rapport au champ magnétique. Les premières sont celles d'atomes soumis à une force dirigée vers l'axe (focalisantes); les secondes soumises à une force qui part de l'axe divergent progressivement. Dans l'approximation utilisée, on peut écrire les équations de ces trajectoires, les symboles de dérivation se rapportant au temps:

$$m y'' \pm \left(2 \mu_B \frac{H_0}{r_0^2} \right) \cdot y = 0, \quad (1)$$

v étant la vitesse parallèle à l'axe Ox et y la distance à l'axe:

$$y'' = v^2 \cdot \frac{d^2 y}{dx^2},$$

d'où

$$\frac{d^2 y}{dx^2} = 2 \mu_B \frac{H_0}{m v^2 r_0^2}. \quad (2)$$

Dans la partie I,

$$r_0 = 0,2 \cdot \frac{X}{10} \quad (3)$$

et dans la partie II,

$$r_0 = C t e = 0,5 \text{ cm}.$$

L'équation des trajectoires devient:

Partie I:

$$\frac{d^2 y}{dx^2} \pm b \frac{y}{\left(\frac{X}{10} \right)^2} = 0 \quad (4)$$

avec

$$b = 2 \mu_B \frac{H_0}{m v^2} \cdot 0,2^2 \quad (5)$$

$$y = \sqrt{\frac{X}{10}} \left[\alpha \cos \left(\sqrt{b - \frac{1}{4}} \log \frac{X}{10} \right) + \beta \sin \left(\sqrt{b - \frac{1}{4}} \log \frac{X}{10} \right) \right]$$

pour les trajectoires «convergentes» ($S_{ez} = + \hbar/2$)

$$y = \sqrt{\frac{X}{10}} \left[\gamma \operatorname{ch} \left(\sqrt{b - \frac{1}{4}} \log \frac{X}{10} \right) + \delta \operatorname{sh} \left(\sqrt{b - \frac{1}{4}} \log \frac{X}{10} \right) \right] \quad (6)$$

pour les trajectoires «divergentes» ($S_{ez} = - \hbar/2$)

Partie II:

$$\frac{d^2y}{dx^2} \pm \frac{b}{6,25} y = 0 \quad (7)$$

Trajectoires:

$$y = A \cos \frac{\sqrt{b}}{2,5} x + B \sin \frac{\sqrt{b}}{2,5} x \quad (\text{convergentes}) \quad (8)$$

$$y = C \operatorname{ch} \frac{\sqrt{b}}{2,5} x + D \operatorname{sh} \frac{\sqrt{b}}{2,5} x \quad (\text{divergentes}) \quad (9)$$

Les calculs sont faits avec les paramètres suivants: $H_0 = 8000$ gauss partout; objet: couteau éplucheur de diamètre zéro placé à 10 cm du sextupole.

En faisant le raccordement entre I et II pour des vitesses et des positions d'objet différentes, nous avons recherché quelle portion du spectre des vitesses pouvait passer au centre du cyclotron (c'est-à-dire à une distance de 150 cm du bord de sortie des pièces polaires), dans une surface circulaire de 1 cm de diamètre. On trouve que cette proportion, pour un angle solide limité en cours de trajectoires par le cercle tangent aux pièces polaires (environ 10^{-3} stéradian), correspond à une zone du spectre des vitesses incidentes située autour d'une certaine vitesse moyenne, quelle que soit la forme du spectre, dans une bande de largeur approximative de $\pm 13\%$. Chaque fraction de zone est à pondérer pour les variations des angles solides utiles, lesquelles sont faibles dans la bande définie. Ensuite, il faut tenir compte des probabilités des vitesses.

Le calcul de la proportion effective d'atomes focalisés dans la surface choisie ne peut avoir lieu avec réalisme que si l'on connaît la forme du spectre de vitesses des atomes, c'est-à-dire a) le fonctionnement de l'ensemble «supersonique» tuyère de Laval – couteau éplucheur; b) la température des atomes à l'intérieur du tube Pyrex du dissociateur.

Pour avoir une idée des défauts chromatiques de notre sextupole d'essai, on peut faire la supposition pessimiste d'un spectre des vitesses v à l'intérieur du faisceau de la forme

$$N \sim \eta^3 \exp(-\eta^2)$$

valable pour l'émission par un trou cylindrique ($\eta = v/v_m$ où v_m est la vitesse moyenne dans l'enceinte avant le trou). On recueille, en admettant la ponctualité du couteau (objet), une proportion de 16% du nombre d'atomes $S_{zz} = \hbar/2$ faisant partie de l'angle solide «utile» indiqué plus haut.

Il reste une fraction de «divergents» ($S_{zz} = -\hbar/2$) de 3% environ. Cette fraction provenant des atomes qui passent au voisinage de l'axe

du sextupole peut d'ailleurs être éliminée par une aiguille fine placée sur l'axe.

Il est inutile de pousser le calcul plus à fond car le problème se complique du fait que:

1) le champ réel du sextupole actuel ne varie comme r^2 que pendant la moitié du rayon du cercle tangent aux pièces polaires;

2) l'objet a une dimension finie et l'appareil possède un grandissement de 6 à 10 selon les « vitesses utiles » et positions légèrement différentes de l'objet, pour une distance image de 150 cm;

3) la forme du spectre des vitesses v que l'on sait être approximativement [9]

$$\exp \left\{ -m \frac{(v - V)^2}{2 k T_1} \right\}$$

serait une gaussienne plus étroite en valeur relative qu'un spectre $\eta^3 \exp(-\eta^2)$, T_1 étant la température du jet au couteau épilucheur et V étant la vitesse moyenne d'écoulement du jet. En se basant sur les résultats de BECKER [7] dans le cas moléculaire, on peut admettre que $V \simeq 5200$ m/s en prenant 400° K pour la température des atomes dans le tube Pyrex dissociateur.

Nous avons donc procédé à l'expérience dans les conditions suivantes: distance objet-entrée sextupole = 25 mm; diaphragme d'entrée $\simeq 3$ mm; diaphragme de sortie $\simeq 15$ mm; on a observé, sur l'oxyde de molybdène déposé sur verre, placé successivement à une distance de sortie $D = 30, 100, 180$ cm, des images telles que celle présentée figure 4 et qui correspond à $D = 30$ cm. Nous focalisons, dans ces conditions, à $D = 180$ cm la partie du spectre située autour de $v = 3600$ m/s. On a ensuite remplacé cette détection qualitative par un tube à compression suivi d'une jauge à ionisation; le facteur de compression est $f = 60$ environ en utilisant la formule de KNUDSEN [11]. Le résultat des variations en intensité ΔI mesurées à la jauge (Leboeuf = $TK2$) est indiqué dans le tableau I. Ces mesures correspondent à l'augmentation de pression dans la jauge lorsqu'on passe de $H_0 = 0$ à $H_0 = 8000$ gauss. En tenant compte du rapport (lecture jauge/pression réelle) pour l'hydrogène atomique, on déduit, à 180 cm, un flux mesuré d'atomes $F = 10^{15}/s \cdot cm^2$. Notons que le diamètre du jet est, à cette distance, de l'ordre de 1 cm.

Tableau I

D	30 cm	100 cm	180 cm
ΔI (μA)	1,45	0,85	0,4

Les pièces polaires actuelles sont en acier doux; on peut espérer gagner en gradient en les remplaçant par des pièces en Armco ou mieux

en un acier du genre «Permendur». Le profil des pièces polaires doit pouvoir être également amélioré (voir par exemple réf. 10c).

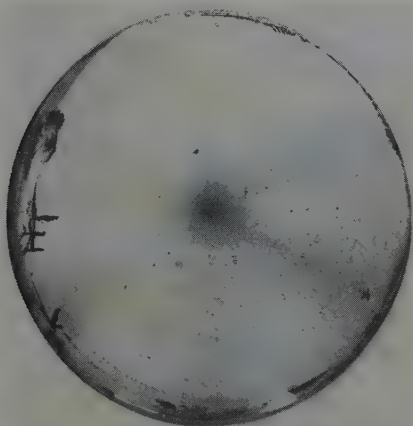


Figure 4

IV. Transition en passage adiabatique $0 \rightarrow 0$

Le dépeuplement intégral de l'état ($F = 1$, $M_F = 0$) au profit de ($F = 0$, $M = 0$) du diagramme de Rabi se fait par la méthode de passage adiabatique proposée par ABRAGAM et WINTER [5] dont nous rappelons brièvement les conclusions. Le passage se fait en faisant traverser aux atomes une cavité de radiofréquence fonctionnant sur la fréquence ν correspondant à la transition au champ \mathfrak{H}_0 existant au centre de la cavité. Les atomes «voient» un champ $\mathfrak{H}_0 + \Delta H$, à l'entrée de la cavité, $\mathfrak{H}_0 - \Delta H$ à la sortie, le passage de l'un à l'autre ayant lieu à peu près linéairement. Si $H_1 e^{i\omega t}$ ($\omega = 2\pi\nu$) est le champ magnétique oscillant dans la cavité, on doit remplir deux conditions:

a) *condition d'adiabaticité*

$$\frac{2 \Delta H}{l} v_m < \frac{2 \pi v_0}{4} \frac{H_1^2}{H^*} \frac{1}{y \sqrt{1+y^2}} \quad (10)$$

où v_0 la fréquence de structure fine (~ 1420 Mc/s), $H^* = h\nu_0/2 \mu_B \cong 507$ gauss ($\mu_B = 1$ magnéton de BOHR), $y = \mathfrak{H}_0/H^*$

b) *condition de polarisation*

$$\Delta H \gg H_1. \quad (11)$$

Dans ce cas, la polarisation est à peu près égale à

$$P = 1 - \left(\frac{H_1}{\Delta H} \right)^2.$$

Choisissant $\Delta H \simeq 4 H_1$ ($P \sim 94\%$), on obtient pour $l = 3$ cm, $v_m \sim 3,6.10^5$ cm/s, $\mathfrak{H}_0 \sim 880$ gauss, la condition suivante pour le passage adiabatique

$$H_1 > 0,76 \text{ gauss} \quad (12)$$

On réalise ces conditions en faisant passer les atomes dans un tube en quartz ($\varnothing 20$ mm) situé au milieu d'une cavité rectangulaire fonctionnant en régime $TE_{01,2}$. La puissance y est injectée par un magnétron Raythéon RJK 62; on a mesuré une puissance dans la cavité d'environ 70 watts, ce qui permet de calculer le champ H_1 oscillant, d'après la formule (valable pour une cavité rectangulaire):

$$H_1 = \sqrt[4]{40 \frac{P \text{ (watt)} Q}{v \text{ (Mc/s)} V \text{ (cm)}^3}} \quad (13)$$

où P est la puissance injectée dans la cavité, Q le coefficient de surtension de celle-ci, ν la fréquence, V le volume de la cavité. Ici $P \simeq 70$ watts, $Q \sim 350$, $\nu \simeq 2850$, $V = 324$ cm³. Donc,

$$H_1 = 1,03 \text{ gauss} \quad (14)$$

Prenant alors $\Delta H = 4,12$ gauss, les conditions (10) et (11) sont remplies.

La fréquence de la cavité ν_0 , mesurée à 0,5 Mc près par un ondemètre AMEP 1403 était finalement de 2859,5 Mc et le champ $\mathfrak{H}_0 = 884,5$ gauss. Le champ $\pm \Delta H$ était réalisé à l'aide de 4 bobines correctrices placées sur les faces polaires de l'aimant et le champ \mathfrak{H}_0 mesuré par résonance magnétique nucléaire.

V. Détection de polarisation

La détection de la polarisation obtenue se fait qualitativement de la manière suivante (voir figure 5 et 8). Sur le trajet du faisceau, après passage dans la cavité de radiofréquence, se trouve un diaphragme étroit (5×1 mm) permettant de définir un mince pinceau d'atomes à peu près parallélisé. Ce pinceau aborde obliquement, selon une méthode suggérée par RABI [12], le champ de fuite des pièces polaires d'un électro-aimant incliné d'un angle θ par rapport à la direction du faisceau incident. Les atomes des deux composantes $S_{ez} = \pm \hbar/2$ subissent, dans

le gradient de champ approximativement perpendiculaire à leur direction initiale, des forces défléctrices opposées.

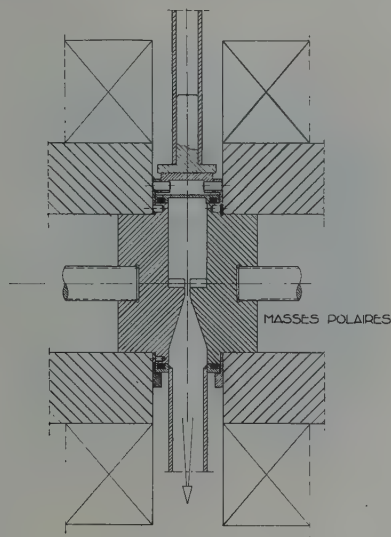


Figure 5

Stern et Gerlach. Coupe

Quand l'aimant sextupolaire seul fonctionne, on doit apercevoir, sur de l'oxyde de molybdène placé à la suite de cet aimant, une seule tache image ($S_{ez} = \hbar/2$). Si l'on opère alors la transition $M_F = 0 \rightarrow 0$, on doit observer à nouveau deux taches d'intensités à peu près égales. La distance prévue de ces deux taches à 35 cm du centre de l'aimant, pour une variation de champ vue de 12000 gauss et $\theta = 1/20$, est donnée par

$$s \simeq 21 \delta \simeq \frac{2 H l}{m v^2 \theta} \sim 0,6 \text{ cm.} \quad (15)$$

Sur la figure 6 on aperçoit la tache obtenue sur l'oxyde de molybdène avec l'aimant sextupolaire seul (faisceau direct), surmontée de celle obtenue avec déflexion finale sans radiofréquence. On constate bien que seuls, les atomes $S_{ez} = + \hbar/2$ existent. En opérant la transition désirée, on observe une deuxième tache (figure 7) correspondant à la réapparition d'atomes dans l'état $F = 0$, $M_F = 0$. La tache supérieure possède une forme plus étroite, la tache inférieure une forme plus large que la tache de référence (tache inférieure de la figure 6) à cause de l'existence d'un gradient de champ transversal, « focalisant » pour une

composante ($S_{zz} = \hbar/2$), «défocalisant» pour l'autre ($S_{zz} = -\hbar/2$). Nous avons constaté le maintien de l'existence des deux taches en faisant varier \mathfrak{H}_0 seul de ± 2 gauss. L'ensemble de l'appareillage est représenté figure 8.

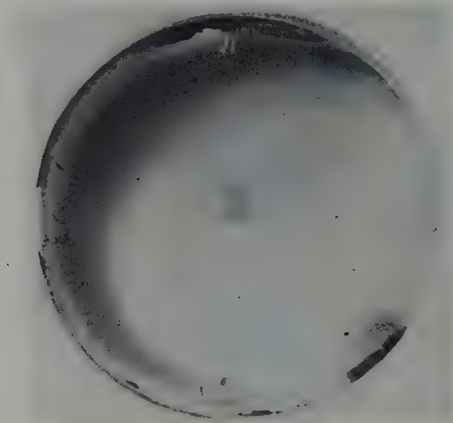


Figure 6

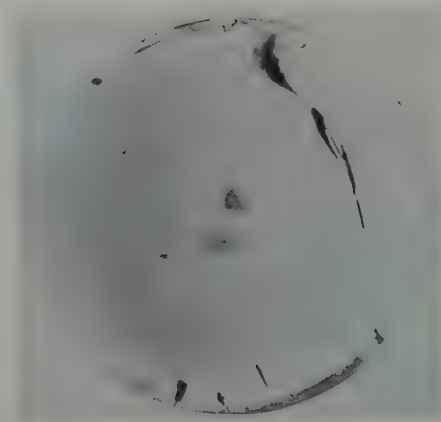


Figure 7

La mesure de la valeur de la polarisation a été effectuée de la façon suivante: Un tube de compression (\varnothing 8 mm, L = 150 mm) suivi d'une jauge à ionisation a été installé à l'endroit de la tache supérieure. Les

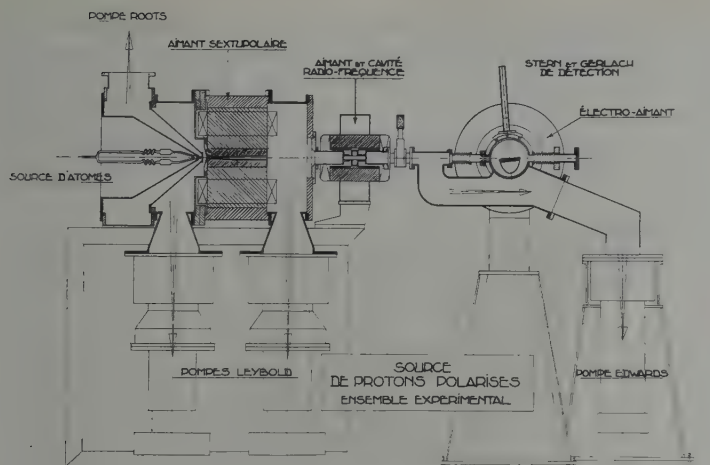


Figure 8

lectures du courant de la jauge ont été faites en fixant le champ à la résonance de la transition de radiofréquence puis nettement en dehors. Nous en déduisons la valeur de la polarisation $P = 0,62 \pm 0,1$ dans les conditions actuelles.

VI. Améliorations possibles

Les résultats donnés plus haut ne correspondent pas aux conditions optimums. De nouvelles pièces polaires du sextupole doivent être essayées afin d'obtenir une forme de gradient meilleure pour la vitesse moyenne la plus probable (5000 à 6000 m/s). La limitation du nombre d'atomes proviendra ensuite des conditions de vide dans la zone centrale du sextupole. Il est possible d'augmenter le nombre utile en donnant au couteau éplucheur un diamètre plus grand. Des essais préliminaires ont montré que le gain est presque proportionnel à la surface de l'orifice (\varnothing variant de 1 à 1,4 mm), donc que, ni le grandissement, ni les pressions ne sont limitatifs dans les conditions actuelles. On peut raisonnablement escompter un gain possible d'un facteur de l'ordre de 3.

La valeur de la polarisation peut certainement être améliorée en augmentant le champ H_1 , soit par la puissance de la radiofréquence, soit par l'accroissement du coefficient de surtension de la cavité.

VII. Cas des deutons

Le diagramme relatif au deutérium (figure 9) donne les transitions possibles (A, B, C) et conduisant, après élimination des états (4) (5) et passage adiabatique, à une polarisation partielle des deutons en

champ magnétique élevé. La différence d'énergie en champ zéro, ΔW , étant plus faible que dans le cas de l'hydrogène léger, le champ H_1 oscillant doit être nettement plus grand si l'on veut conserver le même domaine de fréquence ν et satisfaire à (10) (voir réf. [5], éq. 1). Ceci nécessiterait probablement l'emploi de magnétrons plus puissants.

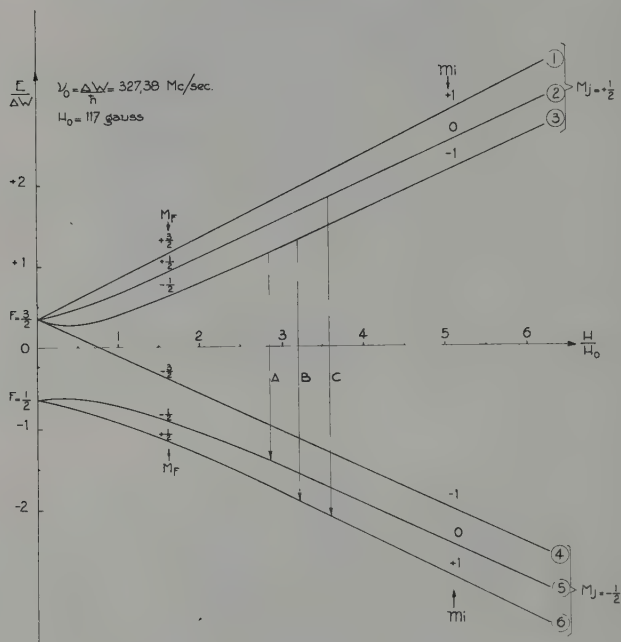


Figure 9
Structure hyperfine de l'atome de deutérium

On voit qu'en définitive on peut obtenir les mélanges suivants d'états, où le chiffre entre parenthèses indique la projection du spin du deuteron en champ magnétique élevé :

$$\frac{2}{3} (0) + \frac{1}{3} (1) \quad (\text{transition } A)$$

$$\frac{2}{3} (1) + \frac{1}{3} (0) \quad (\text{transition } B)$$

$$\frac{2}{3} (1) + \frac{1}{3} (-1) \quad (\text{transition } C)$$

Nous tenons à remercier MM. ABRAGAM et WINTER pour l'intérêt qu'ils ont porté à ce travail et les fructueuses discussions que nous avons eues à ce sujet; M. KELLER pour ses nombreux conseils, particulièrement sur la méthode de dissociation dont nous nous sommes beaucoup inspirés; M. CLAUSNITZER qui a attiré notre attention sur l'injection des atomes suivant la méthode de Becker. Le présent travail a été possible grâce à la participation essentielle de MM. TOMASSO, RE, MAILLARD, D'AGOSTINO, KNITTNER, DRUAUX, BENEZECH et DUVAL pour la réalisation d'ensemble. Mlle FAURE, MM. CATILLON et CHAMINADE ont participé à la mise au point de la transition de radiofréquence. A tous, nous exprimons notre profonde gratitude.

Note ajoutée sur épreuves (octobre 1960). — Les résultats actuels sont les suivants: la polarisation finale mesurée des protons est supérieure à 90%; un effet avec du deutérium dans les mêmes conditions a permis un basculement de 40% pour la transition A.

BIBLIOGRAPHIE

- [1] N. F. MOTT et H. S. W. MASSEY, *Theory of Atomic Collisions*, Clarendon Press, Oxford 1949; CH. SCHLIER, Rapport C.E.R.N. 58-3.
- [2] M. CARASSI, *Nuovo Cim.* 10, 955 (1957); BUDIANSKY *et al.*, *Atomnaia Energia* 6, 306 (1959).
- [3] GERLACH et O. STERN, *Ann. Physik* 74, 673 (1924) et 76, 163 (1925).
- [4] F. BLOCH, *Phys. Rev.* 70, 460 (1946).
- [5] A. ABRAGAM et J. M. WINTER, *Phys. Rev. Letters* 1, 375 (1958).
- [6] R. KELLER, L. DICK et M. FIDECARO, Rapport C.E.R.N. 60-2.
- [7] E. W. BECKER et K. BIER, *Z. Naturf.* 9a, 975 (1954).
- [8] G. CLAUSNITZER, University of Minnesota, Annual Report, (Nov. 1959), p. 52.
- [9] A. KANTROWITZ et J. GREY, *Rev. Sci. Instr.* 22, 228 (1951).
- [10] a) H. FRIEDBERG et N. PAUL, *Naturwiss.* 38, 199 (1951); b) LEMONICK, PIPKIN et HAMILTON, *Rev. Sci. Instr.* 26, 1112 (1955); c) R. L. CHRISTENSEN et HAMILTON, *Rev. Sci. Instr.* 30, 356 (1959).
- [11] Voir par exemple N. F. RAMSEY, *Molecular Beams*, p. 15.
- [12] I. I. RABI, *Nature* 123, 163 (1929).

Experiments on Dynamic Polarization of Protons in Polyethylene by the 'Solid Effect' — A Proposed Polarized Proton Target¹⁾

By C. F. HWANG and T. M. SANDERS, JR.²⁾, University of Minnesota

Introduction

We wish to report here on the «state of the art» with regard to the polarization of nuclei, in particular of protons, in environments suitable for use as polarized targets for scattering experiments. The program of this talk will be to discuss:

1. design criteria for a polarized proton target;
2. possible methods of polarization;
3. recent experimental work in various laboratories which encourages one to believe that a useful polarized target can be realized;
4. the studies made at the University of Minnesota on this subject.

We wish to emphasize that our experimental work is still in a preliminary state. Although the prospect of a useful polarized proton target is encouraging, we have not at this moment such a target in final form.

Design Criteria for a Polarized Proton Target

Many nuclear physics experiments utilizing oriented nuclei, a typical example being that by C. S. Wu *et al.* [1]³⁾, have already been performed. Elegant angular correlation and other experiments involving radioactive decay of oriented nuclei have yielded many results. However, it is clear after some reflection that most of the orientation methods which have been applied in these radioactive decay experiments are not

¹⁾ This work is jointly supported by AEC Contract No. AT(11-1)-50 and USAF Contract No. 49(638)-811.

²⁾ ALFRED P. SLOAN Foundation Research Fellow.

³⁾ Numbers in brackets refer to References, page 133.

suitable for producing a polarized target for scattering experiments. We will state now the criteria, or perhaps the prejudices, we have applied in our thinking about possible polarized targets. These criteria are as follows:

A. The number of target nuclei must be large enough and the polarization must be sufficiently great to produce detectable asymmetries in scattered beams. For this reason we have restricted our consideration to condensed matter, and we have felt that only polarizations above ten percent would be useful. This separation at ten percent polarization is of course rather arbitrary and the position of the demarkation line actually depends on the particular experiment that is contemplated. In considering p - p scattering at 40 and 68 Mev – the available energies of the Minnesota proton linear accelerator – we have assumed that the polarization of the incident beam might be of the order of thirty percent. Since asymmetries below one percent are for all practical purposes unobservable, we felt that a minimum target polarization of ten percent would be necessary.

B. The polarization must be maintained in the presence of the incident beam. This is the consideration which makes the decay experiments so different from scattering experiments. A useful figure to keep in mind is that if each particle loses 1 Mev in the target, a beam current of one microampere will deliver one watt to the target. This means that with this energy loss per particle a beam of 10^{10} particles per second dissipates approximately one milliwatt in the target. This need to handle power inputs in the range of a few milliwatts and to maintain a constant polarization over the long time intervals required to obtain counting statistics eliminates from consideration all orientation methods requiring such very low temperatures as can only be achieved by the method of adiabatic demagnetization.

C. The material containing the target nucleus to be studied (e.g. protons) should be simple enough so that the scattering process to be studied (e.g. p - p scattering) can be separated from background scattering by other nuclei. In the experiments involving radioactive decay the radioactive nuclei may be embedded in a medium containing several different nuclear species without any complications ensuing. In the case of scattering experiments, however, each scattering process by nuclei other than those under study provides an undesirable background. If in addition, other nuclei with spins (which may or may not be oriented with the target nuclei) are present, spin correlation experiments become even more difficult. Of course energy discrimination will be helpful to distinguish beam particles scattered by protons from those scattered by other nuclei in the case of p - p or n - p experiments. Nevertheless even energy discrimination may not be adequate if foreign nuclei

possessing many low level excited states are present. Therefore we decided at the outset of our work that we would look into the question whether useful polarization can be produced in very simple materials. We have not explored the question whether there may be other less simple materials in which larger polarizations are realizable. (Work at other laboratories shows that larger polarization can indeed be achieved in various materials.)

D. It should be possible to fabricate the material readily into a suitable form for use as a target. This is not really a very serious criterion, involving as it does only questions of engineering design. However, on this basis we have excluded from consideration some otherwise fairly promising techniques. We have not considered for example, a target composed of hydrogen atoms dissociated in a discharge tube and deposited in a solid rare gas matrix at liquid helium temperatures.

Possible Methods of Polarization

We divide the possible polarization methods into two categories, static and dynamic [2]. In the static method, polarization is produced in a material in thermal equilibrium subject only to time-independent external magnetic fields. In the dynamic methods, time-dependent external magnetic fields are used.

A. *The static methods applicable to nucleus with spin $I = 1/2$*

1. Polarization in an external field (the «brute force» method). This method requires $H_0 = 10^5$ gauss and $T = 0.02^\circ K$ in order to produce polarization of approximately 50%. Thus this method is out of the question since adiabatic demagnetization is required to reach such low temperatures.

2: Polarization in an internal field («Rose-Görter method»). This method is not completely out of the question if one could find a material with $H_{int} \cong 10^6$ gauss. However for an election in the $1s$ state about a proton, the internal field is $H_{int} \cong 1.5 \times 10^5$ gauss. Thus $T = 0.03^\circ K$ is necessary to achieve a polarization of approximately fifty percent. The internal fields in ferromagnetic media are also typically of the same order of magnitude. Hence it seems unlikely that large proton polarization can be produced by static methods without the use of adiabatic demagnetization. As we have seen, this means that it is not likely that a useful polarized proton target can be achieved by this method. The situation will be more favorable for polarization of nuclei of high Z value where the internal field at the nucleus can be considerably higher.

B. *Dynamic Methods of Polarization*

Dynamic polarization of nuclei has been produced by many methods, some of which have been applied to radioactive decay experiments. Among the names of authors associated with the different methods are OVERHAUSER [3], ABRAGAM [4], JEFFRIES [5], FEHER [6] and others. Some of the methods have steady-state characteristics, producing polarization which can be maintained at a constant level for long periods. Others, notably two methods associated with the names of ABRAGAM and FEHER, are transient methods producing a polarization which decays with time. The time constant of decay is equal to the nuclear spin-lattice relaxation time which may be many minutes at low temperatures. We will not consider the transient methods here.

A common characteristic of the steady-state methods is, that the material containing the nuclei to be polarized must also be one which contains unpaired electron spins. The system is perturbed by time-dependent (radio-frequency or microwave) magnetic fields which induce transitions. The transitions of the Overhauser Effect involve the flip of the electron spin only. On the other hand, the transitions of the Jeffries method involve the simultaneous flip of both the electron and the nuclear spins. These transitions are possible due to the magnetic interaction between the nuclei and the electrons. In either case the system is allowed to come to a perturbed equilibrium state in the presence of the ν_f field and the thermal relaxation processes. Under favorable conditions the population distribution over the nuclear energy levels is no longer a Boltzmann distribution with characteristic energy $\hbar\omega_p$ but now involves an energy of the order $\hbar\omega_e$ where $\nu_e = \omega_e/2\pi$ and $\nu_p = \omega_p/2\pi$ are the Larmor frequencies of the electron and proton respectively in a field H_0 .

Thus the nuclear polarization in the perturbed equilibrium state can be of the order of the electron polarization in thermal equilibrium, and a sizeable polarization can exist at a temperature obtainable without adiabatic demagnetization.

The original proposal by OVERHAUSER was for nuclear polarization in metals. Shortly after his work however, BLOCH [7], KITTEL [8], ABRAGAM [9] and others showed that the method has wider applicability. Since then, the Overhauser method has been applied to align nuclei in metals [10], free radicals [11], solvent nuclei in solutions of free radicals [12] and other materials. The proton-bearing materials to which this method might be applied appear generally to fail our criteria A (large polarization) and/or C (simple enough material).

The Jeffries method was originally applied by him to polarization of nuclei in paramagnetic ions, and as so applied also fails our criteria A

and C, for the paramagnetic ions must themselves be present in rather small concentration in a matrix of diamagnetic material.

C. Polarization by the Solid Effect

The method which appears to give hope that a polarized proton target can be realized was discovered in 1958 when ABRAGAM and PROCTOR [13] and ERB, MOTCHANE and UEBERSFELD [14] independently announced the observation of dynamic polarization of nuclei in various solids containing unpaired electron spins [15]. The observations indicated that polarization occurred not just in the vicinity of a paramagnetic center, but could spread throughout a sample of bulk material. The explanation of this effect, given by ABRAGAM and PROCTOR, indicated that such spreading of polarization could be the case and that this method of polarization should be a very general method of polarizing nuclei. The method, named «l'Effet Solide» or the «Solid Effect» by ABRAGAM, is like that of JEFFRIES in that it employs a microwave magnetic field which induces transitions in which an electron spin and a nuclear spin are simultaneously flipped. A nuclear polarization results when a perturbed equilibrium state is achieved in the presence of the relaxation process. Unlike the Jeffries method, however, the nuclear spins flipped by the microwave field can be rather distant from the paramagnetic center, and communicate with it only via the magnetic dipolar interaction between electron and nuclear spins. The internal magnetic field at such a nucleus is very nearly the external magnetic field. Thus these nuclei, after being polarized, can transmit the polarization to other nuclei far away from the paramagnetic center by inducing flips of the more distant nuclei due to the dipolar interaction among the nuclei themselves. The polarization thus spreads away from the paramagnetic centers by a «spin-diffusion» process. We may see in detail the process by which a nucleus reasonably near the paramagnetic center becomes polarized, as is shown in figure 1. We have drawn the figure for the relevant case where the nuclear Zeeman energy $\hbar\omega_p$ is much greater than the interaction energy E_i between the electron and the nuclear moments. The allowed transition occurs at circular frequency ω_e . However, because of the electron-nucleus dipolar interaction m_i is not a rigorously good quantum number and the forbidden transitions A and B, at frequencies $\omega_B = \omega_e \pm \omega_p$ can be induced, with a matrix element lower than that for the «allowed transitions» by a factor of order $E_i/\hbar\omega_p$. We suppose that the applied microwave field is sufficiently strong so that the «forbidden transition» is saturated, i.e. the population of the initial and final states of the transition are equalized. This will always be the case for a sufficiently strong microwave field because the trans-

ition probability of induced emission always equals that for absorption (Microwave power of the order of one milliwatt is sufficient for our case at 1.2 °K). The presence of this microwave field now «short-circuits» some of the relaxation processes. The fastest of these processes is generally that which keeps the electron spins in thermal equilibrium with the lattice at temperature T . The transition probabilities associated with these thermal relaxation process must have such values as to maintain the ratio of the populations in the upper and the lower states of the «allowed transitions» at the electron Boltzmann factor $\epsilon_e = \exp(-\hbar\omega_e/kT)$. Thus the result of saturating a «forbidden transition» will be to enhance greatly the nuclear polarization, since the distribution over the nuclear energy levels is now governed by the electron Boltzmann factor. The polarization now spreads to nuclei more distant from the magnetic centers by the «spin-diffusion» process mentioned earlier. It is clear from figure 1 that saturation of the «forbidden transition A» yields polarizations of equal magnitude but opposite sign to that due to the saturation of the «forbidden transition B». Hence polarization of nuclei by the «Solid Effect» has the added advantage that the sign of the polarization can be reversed easily by changing the microwave frequency from ν_A to ν_B .

PROTON		POLARIZATION FORBIDDEN TRANSITIONS	BY SATURATION OF TRANSITIONS		
STRONG FIELD QUANTUM NOS.			POPULATIONS $(\epsilon_e = \frac{\hbar\omega_e}{eKT}, \epsilon_p = \frac{\hbar\omega_p}{eKT})$		
m_s	m_I		THERMAL EQUIL.	A SATURATED	B SATURATED
+	-		$N_1 \epsilon_e \epsilon_p$	$N_2 \epsilon_e$	N_3
+	+		$N_1 \epsilon_e$	N_2	$N_3 \epsilon_e$
-	-		$N_1 \epsilon_p$	N_2	N_3 / ϵ_e
-	+		N_1	N_2 / ϵ_e	N_3
POLARIZATION $\equiv \frac{\langle I_z \rangle}{I}$			$= \frac{1 - \epsilon_p}{1 + \epsilon_p}$ $= \tanh \frac{\hbar\omega_p}{2KT}$ $\equiv \frac{\hbar\omega_p}{2KT}$	$= \frac{1 - \epsilon_e}{1 + \epsilon_e}$ $= \tanh \frac{\hbar\omega_e}{2KT}$ $\equiv \frac{\hbar\omega_e}{2KT}$	$= \frac{\epsilon_e - 1}{\epsilon_e + 1}$ $= -\tanh \frac{\hbar\omega_e}{2KT}$ $\equiv -\frac{\hbar\omega_e}{2KT}$
ENHANCEMENT FACTOR			$= 1$	$\equiv \frac{\omega_e}{\omega_p} = 660$	$\equiv \frac{\omega_p}{\omega_e} = 660$

Figure 1
Schematic Diagram of the «Solid Effect»

Now the nuclear physicist may ask, since neither radioactive decay nor scattering experiments have been performed, how is the nuclear polarization produced by this method measured? The answer is by measuring the strength of a nuclear magnetic resonance signal produced by these nuclei. The equality of transition probabilities for absorption and induced emission guarantees that the rate of power absorption in a nuclear resonance experiment performed with a fixed number of nuclei is proportional to the nuclear polarization which is defined as

$$P = \frac{\langle I_z \rangle}{I} = \frac{N_+ + N_-}{N_+ - N_-}$$

and which has the value

$$P = \tanh \frac{\hbar \omega_p}{2 kT} \approx \frac{\hbar \omega_p}{2 kT}$$

at thermal equilibrium.

Thus we know the absolute polarization if we measure the ratio of the power absorption of the nuclear magnetic resonance in the presence of the microwave field to that occurring in the absence of the microwave field.

Observation of nuclei polarized by the «Solid Effect» has now been reported by several workers and on a variety of substances. Protons in water of hydration in paramagnetic crystals have been polarized at Oxford [16], Berkeley [17] and Saclay [18]. Nuclei in damaged crystals [16], and polymers [17] [18] have also been polarized as have nuclei in a polymer doped with free radicals [18].

A Proposed Polarized Proton Target

We have made some preliminary studies hoping to achieve a polarized proton target by the use of the «Solid Effect». These studies require an apparatus in which a nuclear magnetic resonance signal may be observed while a microwave magnetic field is applied to the sample. Workers in this field have not to date published the details of how this may be accomplished, but the method we have used (after trying other techniques with varying degrees of failure) is shown in figure 2. We wind a coil for use in the nuclear resonance measurement directly on the sample and place both inside a rectangular microwave cavity (slotted to break eddy current paths) resonating in the TE_{012} mode. Our nuclear resonance circuitry is shown in figure 3 and is notable only for its crudity, which is permissible because of the large nuclear resonance signal encountered here. Earliest measurements were made with a marginal oscillator circuit which was considerably more sensitive

than this arrangement is. However, we grew to mistrust the linearity of the marginal oscillator over the wide range of nuclear resonance absorption and emission strength encountered here. In figure 4 we show a copy of a typical recorder tracing which shows a base-line, the thermal equilibrium nuclear magnetic resonance signal, and the enhanced nuclear magnetic resonance signal. The ratio of these signals is called the enhancement factor.

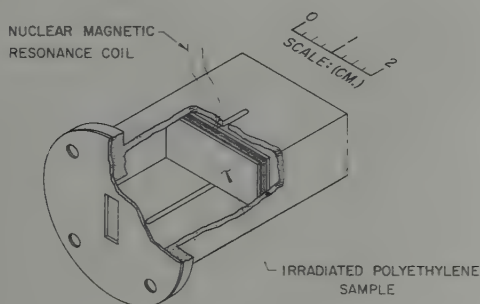


Figure 2

Microwave cavity with sample and nuclear magnetic resonance coil

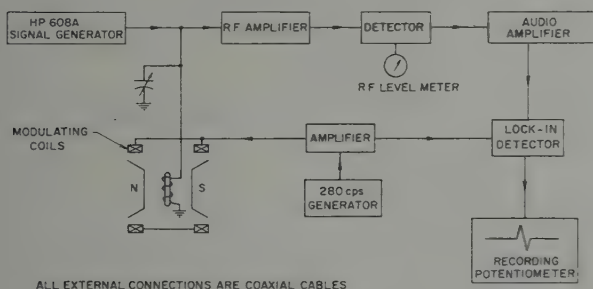


Figure 3

Block diagram of nuclear magnetic resonance spectrometer used for measurement of proton polarization

We have concentrated our attention on the study of proton polarization in polyethylene. We chose polyethylene as the target material because it is simple, containing no other nuclear species than C^{12} which has spin zero and a few low level excited states. Moreover polyethylene also has a very high proton density (0.14 g of proton per cm^3 as compared to 0.07 g of proton per cm^3 for liquid hydrogen). Paramagnetic

centers are introduced successfully via radiation bombardement of the sample by fast neutrons or 40 Mev protons. Table 1 gives a summary of our results to this date. All data tabulated were obtained at $H_o \cong 3200$ gauss, $\nu_e \cong 9$ kmc/s and $T = 1.2^\circ$ K. Note that even the largest enhancement factor observed at liquid helium temperature, which is forty (corresponding to $P = 1.2\%$), falls short of the theoretical expectation which is approximately six hundred sixty. One may well ask what are the factors which limit the enhancement. In the case of polyethylene, one of the limitations may be readily seen by examining the shape of the electron spin resonance line. The absorption line is primarily due to the allowed transitions which we have previously considered to occur at one frequency ν_e , for a given external magnetic field H_o . The observed electron spin resonance absorption line actually has a width $.1H_o$ of approximately 60 gauss for ν_e fixed at 9 kmc/s, or correspondingly a frequency width $\Delta\nu_e = \Delta\omega_e/2\pi = H_o \cdot d\nu_e/dH_o = 150$ mc/s. The line shape of the electron spin resonance here represents the distribution of the ν_e values for the various paramagnetic centers. This distribution results from the fact that near each paramagnetic center are many

Table 1
Proton Polarization in Irradiated Polyethylene

Radiation	Dosage	Sample	Temp.	Max. Enhancement
			$^\circ$ K	
40 MeV Proton	$\sim 2 \times 10^7$ rad	High Density	77	45
1.3 MeV γ of Co^{60}	1.4×10^7 roentgen	High Density	77	10.5
Fast Neutron (Brookhaven)	6 h	High Density	77	8
Fast Neutron (Brookhaven)	12 h	High Density	77	15
Fast Neutron (Brookhaven)	60 h	High Density	77	36
Fast Neutron (Argonne)	Light Brown Color	Low Density	77	4
Electrons	10^7 rad	Low Density	77	1
Fast Neutron (Argonne)	Lemon Color	Low Density	2.1	2
Fast Neutron (Argonne)	Light Brown Color	High Density	2.1	40
40 MeV Proton	$\sim 2 \times 10^7$ rad	High Density	1.2	22
1.3 MeV γ of Co^{60}	1.4×10^7 roentgen	High Density	1.2	5
Fast Neutron (Argonne)	Light Brown Color	High Density	1.2	40
	24 h			
Fast Neutron (Brookhaven)	6 h	High Density	1.2	3
Fast Neutron (Brookhaven)	12 h	High Density	1.2	8
Fast Neutron (Brookhaven)	60 h	High Density	1.2	20

Radiation dosage of fast neutrons are given either in terms of the color of the sample or the length of bombardment time at a given location in the reactor.

protons, each of which may have its spin up or down, and each of which produces a contribution to the total internal magnetic field at the paramagnetic center. In any event we have an ensemble of paramagnetic centers with a distribution of ν_e values, whose width is 150 mc/s. We also have corresponding distributions for $\nu_A = \nu_e - \nu_p$ and $\nu_B = \nu_e + \nu_p$ each with a width of 150 mc/s. Thus for a given value of H_o and ν , we will satisfy the condition $\nu = \nu_e$ for some centers, $\nu = \nu_A$ for others and $\nu = \nu_B$ for still others. Consequently we can never find a condition in which we saturate only one type of transition. It has been shown by ABRAGAM [13] that saturation of the «allowed transition» ($\nu = \nu_e$) does not affect nuclear polarization. However, as we have shown previously, saturation of the two «forbidden transitions» will produce competition between centers. Some centers tend to produce enhanced polarization of one sign, whereas others tend to produce enhanced polarization of opposite sign. The most favorable condition in such a case is that which maximizes the difference between the numbers of centers of types A and B. This difference is proportional to the slope of the absorption line shape times ν_p if $\nu_p \ll \Delta\nu_e$. Both the electron spin resonance absorption derivative and the enhancement are plotted against H_o in figure 5 for a fixed frequency ν . Materials in which $\nu_p > \Delta\nu_e$ also exist and may be expected to yield larger enhancements. Such materials have been and are being studied at Saclay [18] as is reported elsewhere in these proceedings.

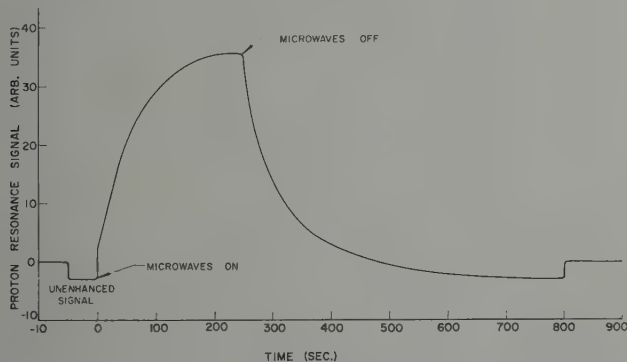


Figure 4

Copy of a typical enhancement observation

For a material like polyethylene the electron spin resonance line shape and $\Delta\nu_e$ are independent of H_o , whereas ν_p is proportional to H_o . Thus we would expect to observe increasing enhancement as we increase H_o [19]

(and ν_e) so long as we continue to satisfy $\nu_p < \frac{1}{2}\nu_e$. Our next step is therefore to perform similar measurements at higher values of H_0 and ν_e . We hope to see proton polarization in the range of 5–15% at 12,000 gauss and 1.2° K. The 5% figure assumes no increase of enhancement factor upon raising H_0 . As it is rather simple today to extract power inputs of the order of a few milliwatts at temperatures as low as 0.4–0.5° K by using He^3 as the refrigerant, we are designing our present apparatus accordingly and hope to gain an additional factor of two to three in proton polarization by lowering the temperature.

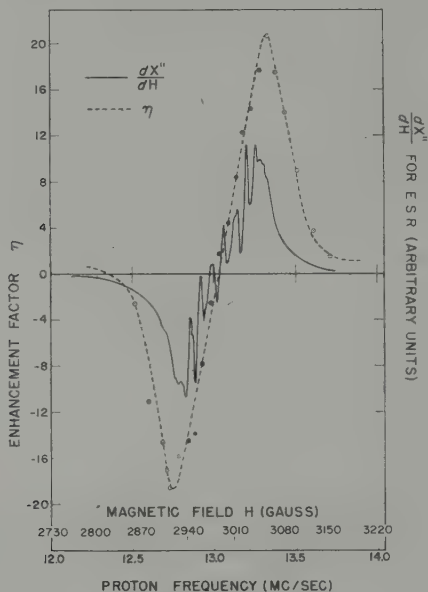


Figure 5

Plot of electron spin resonance line shape (absorption derivative) and enhancement factor for protons in radiation damaged polyethylene at 1.2° K.

In summary the study of the dynamic polarization of protons by the «Solid Effect» in radiation damaged polyethylene at Minnesota has yielded a proton polarization of 1.2% using $H_0 \cong 3200$ gauss, $\nu_e \cong 9$ kmc/s. and $T = 1.2^\circ$ K. It appears to be quite feasible to produce proton polarization of 10% or more using $H_0 \cong 12,000$ gauss, $\nu_e \cong 36$ kmc/s and $T = 0.5^\circ$ K. Such a polarized proton target can then be used for scattering experiments. Unfortunately we do not have an operating polarized proton target at this moment, but the design and construction work are now under way.

REFERENCES

- [1] C. S. WU, E. AMBLER, R. W. HAYWARD, D. D. HOPPES, and R. P. HUDSON, *Phys. Rev.* **105**, 1413 (1957).
- [2] For a review of methods of polarizing nuclei, see M. J. STEENLAND and H. A. TOLHOEK, *Progress in Low Temperature Physics*, P. 292f, ed. by C. J. Gorter, North Holland Publishing Co. (1957).
- [3] A. OVERHAUSER, *Phys. Rev.* **89**, 689 (1953); **92**, 411 (1953).
- [4] A. ABRAGAM, *C. r.* **242**, 1720 (1956).
- [5] C. D. JEFFRIES, *Phys. Rev.* **106**, 164 (1957).
- [6] G. FEHER, *Phys. Rev.* **103**, 500 (1956).
- [7] F. BLOCH, *Phys. Rev.* **93**, 944 (1954).
- [8] C. KITTEL, *Phys. Rev.* **95**, 589 (1954).
- [9] A. ABRAGAM, *Phys. Rev.* **98**, 1729 (1955).
- [10] T. P. CARVER and C. P. SLICHTER, *Phys. Rev.* **92**, 212 (1953).
- [11] H. G. BELJERS, VAN DER KINT, and J. S. VAN WIERINGEN, *Phys. Rev.* **95**, 1683 (1954).
- [12] A. ABRAGAM, J. COMBRISSE, and I. SOLOMON, *C. r.* **245**, 157 (1957).
- [13] A. ABRAGAM and W. G. PROCTOR, *C. r.* **246**, 2253 (1958).
- [14] E. ERB, J. MOTCHANE, and J. ÜEBERSFELD, *C. r.* **246**, 2121 (1958).
- [15] The solid effect was foreshadowed in the work of N. BLOEMBERGEN and P. P. SOROKIN, *Phys. Rev.* **110**, 865 (1958).
- [16] M. ABRAHAM, M. A. H. McCausland, and F. N. H. ROBINSON, *Phys. Rev. Letters* **2**, 449 (1959).
- [17] P. L. SCOTT, O. S. LEIFSON, and C. D. JEFFRIES, *Bull. Amer. phys. Soc.* **4**, 453 (1959).
- [18] M. BORGHINI and A. ABRAGAM, *C. r.* **248**, 1803 (1959); A. ABRAGAM and J. M. WINTERS, *Phys. Rev. Letters* **1**, 374 (1958); M. BORGHINI and A. ABRAGAM, communications at the Basel Conference.
- [19] Note added in proof: Measurements performed at 3,000 gauss and 4,500 gauss and 1.2° K verified the fact that the enhancement factor is approximately proportional to H_0 .

Attempts to Produce H 2 S by Charge Exchange

By I. ALEXEFF¹⁾, Physikalisches Institut der Universität Zürich

The 2 S state of atomic hydrogen is a possible basis for producing 50% polarized protons. Continuing along the line of MADANSKY²⁾ and co-workers, we attempted to produce, and subsequently to ionize, metastable atomic hydrogen by charge exchange in hydrogen gas. By operating in the energy range 150–600 ev, it was hoped to get more protons from the metastable charge exchange process than from the competing ground state process. It was hoped that the ground state stripping cross section would have dropped well below its maximum value, while the metastable stripping cross section remained high.

Rough measurements of the ground state stripping cross section are listed below:

600 ev	$= 2 \times 10^{-17} \text{ cm}^2/\text{atom}$	Accuracy –
300 ev	$2 \times 10^{-17} \text{ cm}^2/\text{atom}$	a factor of 2
150 ev	$1 \times 10^{-17} \text{ cm}^2/\text{atom}$	

Thus the cross section has not dropped appreciably from the constant value of $4.20 \times 10^{-17} \text{ cm}^2$ that extends from 4 to 9 kev [1]³⁾.

Results for the metastable double charge exchange process showed nothing within the sensitivity of the apparatus. The sensitivity at 600 ev, the worst case, would have shown an effect if $\sigma_{-0} = \sigma_{0-}^*$ and $\sigma_{0-} = \frac{1}{2} \sigma_{0-}^*$.

Next studied was the metastable production process alone. It was not possible to detect any metastable beam above the threshold of sensitivity of the apparatus – one metastable atom for 20 ground state atoms. Further work with a Lyman – α photon counter also showed no buildup of a metastable beam.

A reason for the negative results is suggested by the work of FITE *et al.* [2]. For metastable hydrogen atoms of about 0.3 ev energy in hydrogen gas, a de-excitation cross section of $0.7 \times 10^{-14} \text{ cm}^2$ was found.

¹⁾ U.S.A. National Science Foundation Postdoctoral Fellow.

²⁾ c/o Physics Department, Johns Hopkins University, Baltimore, Md., U.S.A.

³⁾ Numbers in brackets refer to References, page 135.

If a similar value holds in the region of 150–600 ev, where the electron pick up cross section is about 10^{-16} cm^2 , more than one metastable atom for every 100 incident protons could not be expected.

REFERENCES

- [1] ALLISON, SAMUEL K., *Revs. Modern Phys.* **30**, 1137 (1958).
- [2] FITE, WADE L., BRACKMANN, HUMMER, STEBBINGS, *Phys. Rev.* **116**, 363 (1959).

An E - H Gradient Spectrometer

By J. EISINGER, Bell Telephone Laboratories, Murray Hill, New Jersey,
B. BEDERSON, K. RUBIN, and A. SALOP, New York University

We shall in our remarks stress nuclear polarization though it will become evident that the instrument we will describe can be employed for electronic polarization and hence atomic beam magnetic resonance experiments as well. As is well known a beam of atoms is split into $(2I+1)$ $(2J+1)$ beams on passing through a magnetic field H with a gradient ∇H . The deflecting force is $\mu_{eff}\nabla H$ where μ_{eff} , the effective magnetic moment of the atom, is a function of H , the field in the particular region of the gap traversed by the beam. When $H < \Delta W/2\mu_0$ (ΔW is the zero field hyperfine splitting) and $J \neq 0$, atoms in different nuclear magnetic substates (m_I) have different effective moments of the order of a fraction of μ_0 . Such an inhomogeneous field is therefore in principle a means of producing a polarized beam as has been pointed out by several speakers before me. In practice the two main difficulties are 1) the deflected beam has many times the width of the original beam due to the thermal velocity distribution, and 2) only narrow beams can be used since μ_{eff} is a function of H and H necessarily varies across the gap. These (and other) difficulties can be overcome by applying an electric field E across the magnetic polefaces which must of course be insulated from the magnet yoke. The electric field therefore has a gradient ∇E (proportional to ∇H) and exerts a deflecting force $\alpha E \nabla E$ on an atom with an atomic polarizability α . By satisfying the balance condition $\mu_{eff}(m_I)\nabla H = \alpha E \nabla E$ for any particular state m_I , a beam of atoms in that state suffers no deflection and hence no broadening on passing through the field. Moreover it can have finite width since the balance condition can be satisfied over a wide range of H , by choosing an H for which μ_{eff} is nearly proportional to H .

The balance condition in the intermediate field region can be satisfied for most atoms (e. g. alkalis) with fields whose gradients are of the same order of magnitude commonly employed in atomic beam experiments (i. e. $\nabla H/H = \nabla E/E \approx 3 \text{ cm}^{-1}$) with values of E below the breakdown field. For hydrogen whose polarizability is about fifty times less than that of alkalis the situation is unfortunately less favorable and it may be necessary to work in the low field region ($\mu_{eff} \approx 0.1 \mu_0$) in order to satisfy

the balance condition with feasible E -fields and still retain a favorable geometry and the advantages offered by the E - H spectrometer. Although it has not been tried it seems likely that the resolution of such a system for hydrogen atoms can be greatly increased by running the hydrogen discharge at a low temperature.

An E - H gradient spectrometer has been built at New York University and is being used to measure α of alkalis [1]. Polarized beams with essentially the same width as that of the original beam width and their theoretical intensities have been obtained. This is illustrated in figure 1 where the beam profile of a K^{39} beam with and without deflecting fields

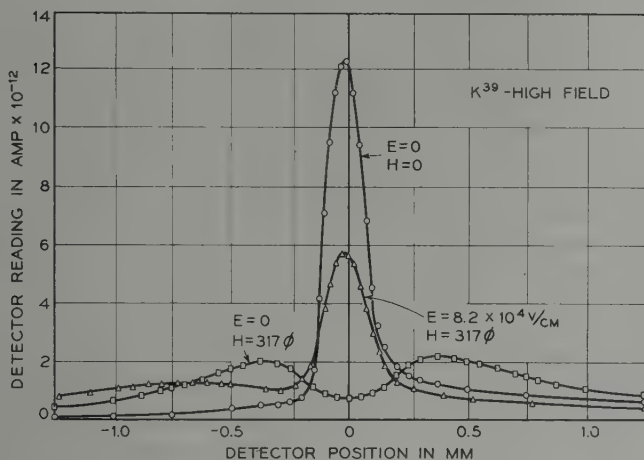


Figure 1

The beam profile of a K^{39} atomic beam at the detector position with and without applied E and H fields. $\nabla H/H = \nabla E/E = 2.6 \text{ cm}^{-1}$. Note that the beam width with E and H applied is almost the same as the width of the unseparated beam ($E = H = 0$).

is shown. Note that the H field by itself causes considerable broadening of the deflected beams but that the effect of the simultaneous application of the E and H fields is to re-establish the beam width of the undeflected beam.

We have confined our remarks to dipole fields but it can readily be seen that these ideas are applicable to higher multipole fields as well.

REFERENCE

- [1] A. SALOP, E. POLLACK, B. BEDERSON, and J. EISINGER, Bull. Amer. Phys. Soc., June 15-17, (1960).

Polarization of Nuclei by Macroscopic Rotation

By S. P. HEIMS, Raytheon Company, Wayland, Mass. USA

A theoretical study [1]¹⁾ has been made of the polarization of the nuclei in a crystal by means of a rapid rotation of the crystal [2]. The corresponding polarization of electrons (Barnett effect) has been known for a long time. Assuming that some mechanism for reaching equilibrium inside the crystal exists, one obtains for the equilibrium density matrix describing a spin \mathbf{I} in a crystal rotating with angular velocity $\boldsymbol{\omega}$ and acted upon by an external magnetic field \mathbf{H}

$$\varrho = \frac{\exp(-\beta \mathfrak{H} - \boldsymbol{\lambda} \cdot \mathbf{I})}{\text{Tr} \exp(-\beta \mathfrak{H} - \boldsymbol{\lambda} \cdot \mathbf{I})}; \quad \beta = 1/kT, \quad \boldsymbol{\lambda} = \boldsymbol{\omega}/kT \quad (1)$$

where \mathfrak{H} is the Hamiltonian of the spin, and T the temperature of the crystal. The expectation value of the spin is

$$\langle \mathbf{I} \rangle = \text{Tr} \varrho \mathbf{I} = \beta \hbar (\gamma \mathbf{H} + \boldsymbol{\omega}) \frac{I(I+1)}{3}, \quad \beta \hbar |\gamma \mathbf{H} + \boldsymbol{\omega}| \ll 1. \quad (2)$$

From (2) it is seen that the action of the field and the rotation are additive and equivalent:

$$\nu = \frac{\omega}{2\pi} \longleftrightarrow g_n \frac{eH}{4\pi Mc} = 762 g_n H \frac{\text{rev}}{\text{sec}},$$

if H is expressed in gauss and g_n is the nuclear g -factor. Some corrections to (2) are obtained by considering the coupling of the single spin with the rest of the crystal. A possible mechanism for bringing about the polarization is the tensor (dipole-dipole) interaction between nuclei. The interaction will depend on time because the relative position vector connecting two nuclei is rotating in space. If \mathfrak{H}_{12} is the dipole coupling for the stationary crystal, then the time-dependent interaction in the rotating crystal may be written $G(t) = U^{-1}(t) \mathfrak{H}_{12} U(t)$, with $U(t) = \exp(i/\hbar \mathbf{S} \cdot \boldsymbol{\omega} t)$ where \mathbf{S} is the total spin. With this plausible hypothesis

¹⁾ Numbers in brackets refer to References, page 139.

one may show that the transformed Schroedinger wave function $\psi' = U(t)\psi$ and the energy levels for the rotating crystal in a fixed magnetic field differ from that of a fixed crystal in a rotating magnetic field essentially only through an additional effective field ω/γ_k acting along the axis of rotation at nucleus k . As an explicit example, consider a pair of spins of magnitude $1/2$, rigidly connected, each associated with a nucleus lying on the z -axis, and the whole system rotating about the x -axis; by integration of the Schroedinger equation, and averaging over oscillations, one obtains the polarization of the system $\langle S_x \rangle = 9 E_0 \hbar \omega (1/4 - p) [(3 E_0)^2 + (2 \hbar \omega)^2]^{-1}$, where $E_0 = (\hbar \gamma)^2 / 2 r_{12}^3$ measures the strength of the dipole coupling and p the probability that initially the system was in the state $S = 1, m_s = 0$. The spin vector will precess around the x -axis in non-circular orbits for finite initial temperatures. The more general time-dependent behavior of a spin in thermal contact with other spins or a lattice may be treated by adapting the Wangness-Bloch theory of magnetic resonance to the rotating crystal. The theory then yields the equilibrium density matrix (1). The formal expression for relaxation times are the same as those applying to magnetic field cases; however numerically one will find different values whenever processes involving the coupling of two spins with different gyromagnetic ratios are important. Experimental observation of nuclear polarization by means of macroscopic rotation of a crystal is expected to be possible by modifying some of the nuclear magnetic resonance experiments usually performed with a stationary crystal in an external magnetic field.

I am indebted to Dr. E. T. JAYNES, with whom many of the features of this effect have been discussed.

REFERENCES

- [1] S. P. HEIMS, Ph. D. Dissertation, Stanford University (1960).
- [2] E. T. JAYNES, Phys. Rev. *106*, 620 (1957).

Proposal for Detecting the Polarization of Slow Protons¹⁾

By J. HEBERLE, Argonne National Laboratory

Summary. A method is proposed for measuring the polarization of protons with a kinetic energy of about 10 keV. It is based on the properties of metastable hydrogen atoms.

In view of the current interest in sources of polarized protons, a method for detecting the polarization of slow (about 10 keV) protons would be useful in testing such sources.

It is here proposed that the protons, whose degree of polarization is P , be partly converted into metastable hydrogen atoms by acceleration to about 10 keV and passage through a suitable donor gas [1, 2]. For brevity the hyperfine components ($F = 1$, $m_F = +1$), $(1, 0)$, $(1, -1)$, and $(0, 0)$ of the 2 S state are denoted by 1, 2, 3, and 4, respectively. The fractional populations of the states 1, 2, 3, and 4 will be $(1 + P)/4$, $1/4$, $(1 - P)/4$, and $1/4$, respectively. Any one of the three tests described below will reveal the differences between these populations and result in an approximate determination of P . The metastable atoms may be detected by quenching them in an electric field and observing the Lyman-alpha photons with a Geiger counter [1, 2] or an Allen tube [3]. Let I_0 be the detector signal in the absence of perturbing fields.

1. The simplest test is to insert a magnetic analyzer [4] between the donor gas and the detector. Let A , $A-a$, B , and $B-b$ denote the probabilities that atoms in states 1, 2, 3, and 4, respectively, are *not* quenched in passing through the analyzer, where $0 < a \ll A$ and $0 < b \ll B$ for analyzing fields below 575 gauss. Then the detector signal in the presence of the analyzing field is

$$I_m = \frac{I_0}{4} [2(A + B) - (a + b) + P(A - B)].$$

Let $K_p \equiv I_m/I_0$. Next measure the corresponding ratio K_u for a proton beam known to be unpolarized. Then

$$P = \left(\frac{K_p}{K_u} - 1 \right) \frac{2(A + B) - (a + b)}{A - B}.$$

¹⁾ Work performed under the auspices of the U. S. Atomic Energy Commission.

²⁾ Numbers in brackets refer to references, page 142.

It would be exceedingly difficult to compute A , B , a , and b because among other reasons the existing theory [4, 5] of magnetic analysis is valid only for motional electric fields so weak that the rate of quenching is very much smaller than the decay rate γ of the $2P$ state. This condition is not realized in the present case because of the relatively high velocity of the atoms. LAMB and RETHERFORD [5] show that for increasing electric fields the quenching rates of all the metastable states approach $\gamma/2$ so that A becomes equal to B . For the present purpose, however, it is essential to achieve the condition $B \ll A$ by reducing the electric field experienced by the atoms. This can be done by operating the magnetic analyzer well below 575 gauss, by reducing the angle between the beam direction and the magnetic lines of force, and by providing a compensating electric field.

Then

$$P \approx 2 \left(\frac{K_p}{K_u} - 1 \right) \left[1 + \frac{2B}{A} - \frac{a}{2A} \right],$$

where the bracketed expression is nearly equal to one.

2. A more convincing test is to induce a magnetic resonance [4]. An rf magnetic field of frequency ν is inserted between the donor gas and the magnetic analyzer with the rf field perpendicular to the very weak magnetostatic field. As the resonances are very wide because of the high velocity, it is possible by setting $\nu = \Delta\nu$ ($2S$) = 177.6 Mc/s to induce the (1, 4) and (4, 3) resonances simultaneously with the result that the populations of states 1 and 3 are exchanged at optimum rf amplitude. Then the detector signal is

$$I' = \frac{I_0}{4} [2(A + B) - (a + b) - P(A - B)]$$

and

$$P = \frac{I_m - I'}{I_m + I'} \frac{2(A + B) - (a + b)}{A - B}$$

$$\approx 2 \left[1 + \frac{2B}{A} - \frac{a}{2A} \right] \frac{I_m - I'}{I_m + I'}.$$

The same result is obtained by setting $\nu = (x/2) \Delta\nu$ (where x is the usual magnetic-field parameter) and inducing the (1, 2) and (2, 3) resonances. At either frequency the optimum rf current is about 60 A rms for 10-keV protons.

3. In place of the magnetic analyzer, an rf state selector [6, 7] may be employed to detect a magnetic resonance. The frequency and intensity of the rf electric field in the state selector are so adjusted that state 1 is quenched more strongly than state 4. The frequency of the rf magnetic field is set on the (1, 4) resonance; the static field must be

large enough to separate the (1, 4) from the (4, 3) line. The optimum νf current is smaller than that in the second test by a factor $[2 + 2\alpha/(1 + \alpha^2)^{-1/2}]^{-1/2}$. According to the theory [7] of νf state selection, turning on the νf magnetic field will change the detector signal by an amount

$$\Delta I = \frac{PI_0}{4} [\exp(-\lambda_4 t) - \exp(-\lambda_1 t)]$$

This change is at a maximum, $\Delta I = 0.190 PI_0$, when the frequency of the state selector is set at 1100 Mc/s and the amplitude is adjusted so that $U^2 t/\gamma = 0.769$. The notation not defined here is that of NOVICK and COMMINS [7].

Since the required νf powers are proportional to the proton energy, it would be advantageous to perform these tests at a lower proton energy if sufficient intensity of metastable atoms can be obtained.

REFERENCES

- [1] L. MADANSKY and G. E. OWEN, Phys. Rev. Lett. 2, 209 (1959).
- [2] T. A. CHUBB and H. FRIEDMAN, Rev. Sci. Instr. 26, 493 (1955).
- [3] NOVICK, LIPWORTH and YERGIN, Phys. Rev. 100, 1153 (1955).
- [4] HEBERLE, REICH and KUSCH, Phys. Rev. 101, 612 (1956).
- [5] LAMB and RETHERFORD, Phys. Rev. 79, 549 (1950).
- [6] See footnote 12 of Reference 4.
- [7] R. NOVICK and E. D. COMMINS, Phys. Rev. 111, 822 (1958).

Polarisation dynamique de noyaux

Par M. BORGHINI et A. ABRAGAM, Centre d'études nucléaires de Saclay

Nous avons utilisé la méthode dite de «l'effet solide» pour polariser des spins nucléaires. L'échantillon contient à la fois les spins nucléaires à polariser I et des spins électroniques libres S , généralement en faible concentration. Nous supposons $I = S = 1/2$. On applique à l'échantillon un champ magnétique constant H_0 et un champ de radiofréquence H_1 , perpendiculaire à H_0 , de fréquence $\Omega = \omega_e \pm \omega_n$, où $\omega_e = \gamma_e H_0$ et $\omega_n = \gamma_n H_0$ sont les fréquences de Larmor électronique et nucléaire. On montre [1]¹⁾ que dans ces conditions la polarisation dynamique nucléaire $\langle I_z \rangle / I$ peut être considérablement accrue, jusqu'à une valeur théorique maximum égale à plus ou moins la polarisation électronique correspondant à l'équilibre thermodynamique $\langle S_z \rangle_0 / S$. (La généralisation aux cas où I ou S sont différents de $1/2$ se fait sans difficulté).

Soient T_e et T_n les temps de relaxation électronique et nucléaire, N_e et N_n les concentrations en spins électroniques et nucléaires, $\Delta\omega_e$ la largeur de la raie électronique, W la probabilité d'un renversement simultané électron-noyau induite par le champ de radiofréquence H_1 . La polarisation maximum est obtenue si les inégalités suivantes sont satisfaites:

$$\Delta\omega_e \ll \omega_n, \quad (1)$$

$$\frac{1}{T_n} \ll W \ll \frac{N_e}{N_n} \frac{1}{T_e}. \quad (2)$$

La première inégalité (2) exprime que la transition de radiofréquence court-circuite la relaxation nucléaire, et la seconde qu'elle est négligeable par rapport à la relaxation électronique.

Si (1) est satisfaite, mais non (2), la polarisation dynamique nucléaire est donnée par:

$$\frac{\langle I_z \rangle}{I} = \frac{\langle S_z \rangle_0}{S} \frac{W T_n}{1 + \left(1 + \frac{N_n}{N_e} \frac{T_e}{T_n}\right) W T_n} \quad (3)$$

ou encore, si

$$T'_e = \frac{N_n}{N_e} T_e;$$

¹⁾ Les chiffres entre crochets renvoient à la bibliographie, page 145.

$$\frac{\langle I_z \rangle}{I} = \frac{\langle S_z \rangle_0}{S} \frac{W T_n}{1 + W(T_n + T_e)}$$

Résultats expérimentaux

Les conditions expérimentales sont les suivantes: $\Omega = 33500$ MHz; $H_0 = 12000$ à 14000 Oe; température: $1,5^\circ$ K. On a alors: $\langle S_z \rangle_0/S = 50\%$.

La polarisation des noyaux est mesurée par l'amplitude du signal de résonance magnétique nucléaire; le spectromètre est un pont dont la bobine de self-inductance est disposée, près des parois de la cavité, autour de l'échantillon.

Dans des échantillons de polystyrène contenant un radical paramagnétique dissous (DPPH), nous avons obtenu dans les meilleures conditions un accroissement de la polarisation nucléaire par un facteur 60, c'est-à-dire une polarisation absolue des protons de $\pm 5\%$, suivant que $\Omega = \omega_e \pm \omega_n$.

Dans des échantillons de FLi irradiés par des neutrons thermiques, nous avons obtenu un accroissement de la polarisation nucléaire par un facteur 75, soit une polarisation absolue des noyaux de fluor de $\pm 6\%$.

Dans un monocristal de $\text{La}_2\text{Mg}_3(\text{NO}_3)_{12} \cdot 24 \text{H}_2\text{O}$ contenant $0,1\%$ de cérium [2], nous avons obtenu, dans un champ de 13700 Oe, un accroissement par un facteur 200 de la polarisation des protons, c'est-à-dire une polarisation absolue de $\pm 19\%$.

Indiquons que la densité en protons de cet échantillon est environ les $2/3$ de celle de la glace, et que l'échantillon de $0,5 \times 1 \times 4$ mm contient $8 \cdot 10^{19}$ protons.

Les figures 1 montrent les signaux de dispersion de la résonance des protons: 1a) sans irradiation à la fréquence Ω ; 1b) avec irradiation.

Dans cet échantillon où l'on a $N_n/N_e = 24000$, nous avons mesuré $T_n = 360$ s, $T_e = 8 \cdot 10^{-3}$ s. De la valeur expérimentale: $\langle I_z \rangle / \langle S_z \rangle_0 = 0.38$, on tire par (3): $W T_n \cong 1$.

Nous avons également mesuré le temps de polarisation t qui exprime le taux de croissance de $\langle I_z \rangle$ en présence de la radiofréquence. Théoriquement t est donné par la formule

$$\frac{1}{t} = \frac{1}{T_n} + \frac{W}{1 + W T_e} \quad \text{ou} \quad 1 - \frac{t}{T_n} = \frac{\langle I_z \rangle}{\langle S_z \rangle_0} \quad (4)$$

Avec les valeurs précédentes des paramètres on trouve par (4): $t = 220$ s. La valeur mesurée est 180 s.

La probabilité de transition croît avec la puissance de radiofréquence d'une façon complexe due à différents phénomènes comme la diffusion de spin, etc., dont l'étude sera précisée dans une autre publication.

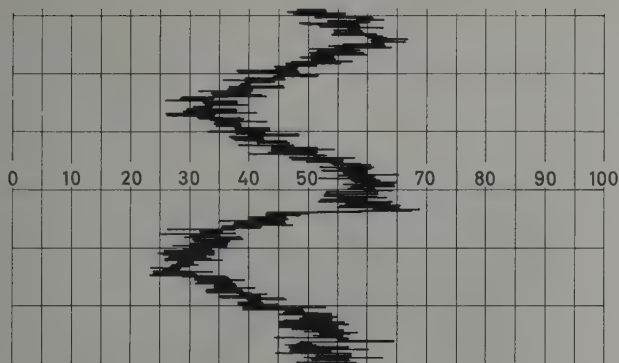


Figure 1a

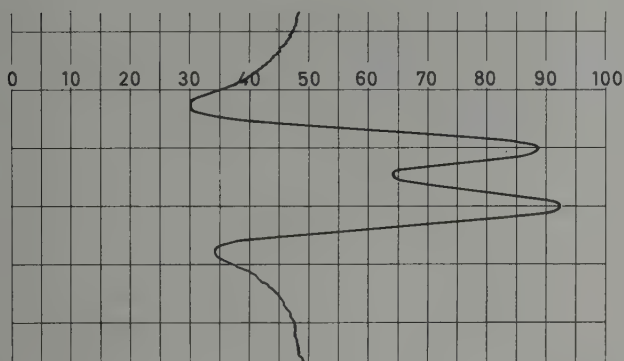


Figure 1b

Des études sont en cours pour permettre à l'échantillon polarisé de servir de cible à un cyclotron, et pour étendre cette méthode à d'autres noyaux, en particulier à des noyaux lourds, en conjonction avec des neutrons lents polarisés.

Ces résultats n'ont pu être obtenus qu'avec la collaboration de toute l'équipe de résonance magnétique de Saclay et plus particulièrement M.M. RYTER, WINTER et COMBRISSE.

RÉFÉRENCES

- [1] A. ABRAGAM et W. G. PROCTOR, *Comptes Rendus*, 246 (1958), p. 2253.
- [2] Nous remercions le Professeur C. D. JEFFRIES qui nous a suggéré l'emploi de cette substance.

Polarization of Protons by an A.C. Sextapole Magnetic Field

By N. W. TANNER, Clarendon Laboratory, and
J. J. DOMINGO, California Institute of Technology

The d.c. sextapole magnetic field has been proposed as a method of polarizing atomic hydrogen, the motion of the atoms being sinusoidal for one orientation of the atomic magnetic dipole and exponentially divergent for the other. If the polarized atomic hydrogen is ionized in a weak magnetic field, a nuclear polarization of 50% can be achieved.

It appears likely that nuclear polarizations of $> 50\%$ can be achieved with an a.c. sextapole field of the form

$$|H| = \alpha (1 - \cos \omega t) r^2,$$

which gives an equation of motion for a magnetic dipole

$$m \ddot{r} = -2\mu_{eff} \alpha (1 - \cos \omega t) r.$$

The solutions of this equation are Mathieu functions [1], for $\mu_{eff} = \pm \mu_0$, and, presumably, similar functions for $\mu_{eff} = \pm \mu_0 H (H^2 + H_0^2)^{-1/2}$. For $\mu_{eff} < 0$ the solutions diverge rapidly. For $\mu_{eff} > 0$ the solution may be stable or divergent oscillations depending on the values of α and ω and it appears likely that one of the two positive values of μ_{eff} could be kept stable while the other is divergent.

Putting $\alpha = 4 \times 10^4$ gauss/cm² and $\omega/2\pi = 7.55$ kc/s, the component with $\mu_{eff} = +\mu_0$ would be diverged by a factor of $\sim e^4$ in 1 m while at least some part of the other positive component would remain stable. Alternatively, for $\alpha = 4 \times 10^4$ gauss/cm² and $\omega/2\pi = 6.16$ kc/s, the component $\mu = -\mu_0 H (H^2 + H_0^2)^{-1/2}$ might be largely diverged.

REFERENCE

- [1] N. W. McLACHLAN, *Theory and Application of Mathieu Functions*, O.U.P., (1947).

II.

Generation of Polarized Nucleons and Deuterons by Reactions

Survey of Experiments on the Polarization in Reactions

By W. HAEBERLI, University of Wisconsin

The possibility to polarize fast neutrons by scattering from suitable nuclei was first suggested by SCHWINGER [1]¹⁾. Shortly thereafter WOLFENSTEIN [2] proposed that neutrons produced in a reaction might already be polarized. This suggestion was based on a paper by KONOPINSKI and TELLER [3] who had shown that the interpretation of the $d-d$ reaction requires a large amount of p -wave interaction with strong spin-orbit coupling.

The polarization of neutrons or protons produced in a reaction can be detected by the arrangement shown in figure 1. An unpolarized beam \mathbf{k}_0 from an accelerator is incident on target 1. The polarization P_1 of the outgoing nucleons \mathbf{k}_1 is normal to the reaction plane. The magnitude

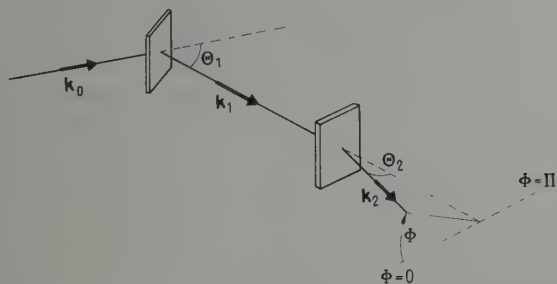


Figure 1

An unpolarized beam from an accelerator is incident in the direction \mathbf{k}_0 . Neutrons or protons originating in the first target move in the direction \mathbf{k}_1 . Particles emitted by the second target in the direction \mathbf{k}_2 are detected.

of the polarization is defined as $(N_+ - N_-)/(N_+ + N_-)$, where N_+ and N_- are the numbers of nucleons with spin up and spin down, respectively. Two conventions are in use as to which direction is to be called «up».

¹⁾ Numbers in brackets refer to References, page 158.

SCHWINGER chose $\mathbf{k}_1 \times \mathbf{k}_0$ as the «up» direction, while WOLFENSTEIN and others chose the opposite convention. In this paper WOLFENSTEIN's convention will be used.

The second target serves to detect the polarization of the nucleons emitted by the first one. Without making specific assumptions about the reaction mechanism one can predict that the flux of particles from the second target at a fixed reaction angle θ_2 will depend on the azimuthal angle ϕ . The azimuthal dependence of the cross section in the second reaction is given by

$$\sigma(\theta_2, \phi) = \sigma_0(\theta_2) [1 + P_1 \cdot A(\theta_2) \cos \phi], \quad (1)$$

where $\sigma_0(\theta_2)$ is the differential reaction cross section. The quantity $A(\theta_2)$ depends on the particulars of the second reaction. It usually is called the «analyzing power» or the «asymmetry» of the reaction. SIMON [4] showed that A is equal to the polarization of the outgoing nucleons of the inverse reaction, induced with an unpolarized beam: $A = P_{\text{inverse}}$. For the case of elastic scattering there is no difference between the reaction and its inverse. In this case A of equation (1) is usually replaced by the symbol P_2 . The analyzing properties of different scatterers will be discussed in session 3 of this symposium. In the following it will be assumed that there are scatterers available for which P_2 is known.

The first experiments which showed that nucleons produced in a reaction are polarized were reported in 1952 for the $d-d$ reaction. BISHOP and others [5] observed the polarization of protons, while HUBER and BAUMGARTNER [6, 7] and RICAMO [8] experimented with neutrons.

The experimental arrangement which HUBER and BAUMGARTNER used is shown in figure 2. Neutrons originating from the $D(d, n) \text{He}^3$ reaction were scattered from a graphite sample. Neutrons scattered to the «left» ($\phi = 0$) and the «right» ($\phi = \pi$) were detected with scintillation counters. From the left-to-right ratio of counting rates and the known value of $P_2 = A$ the polarization P_1 of $d-d$ neutrons can be found by means of equation (1).

In a number of recent experiments the polarization of $d-d$ neutrons was measured over a wider range of energies. Figure 3 shows the results of PASMA [9], MEIER *et al.* [10], LEVINTOV *et al.* [11] and BAICKER [12] for a neutron emission angle of about 45° . Except for one, all experiments used helium as an analyzer. A recent experiment [13] at a deuteron energy of 8.2 MeV indicates that the polarization above 4 MeV remains almost constant. For protons from the $d-d$ reaction measurements have been reported for deuteron energies of 0.3, 0.64 and 1.2 MeV [5, 14, 15]. The magnitude of the proton polarization is systematically larger than the neutron polarization at the same angle and energy, but in view of the experimental uncertainties the difference is probably not significant.

BEIDUK, PRUETT and KONOPINSKI [16] tried to explain the energy dependence of the $d-d$ reaction cross section by simple assumptions. They showed that the variation of the cross section with energy can be attributed entirely to the energy variation of the barrier penetrability for deuterons of different orbital angular momentum. For deuteron energies up to a few hundred kilovolts only s - and p -waves are effective. For this energy region BLIN-STOYLE [17] and CINI [18] predicted that the polarization as a function of angle should be of the form $P \sim (\sin 2\theta)/\sigma(\theta)$. The measurements by MEIER *et al.* [10] and McCORMAC *et al.* [19] for a deuteron energy of 600 KeV agree well with this prediction. No such measurements have been reported for higher bombarding energies. At higher energies terms containing $\sin 4\theta$, $\sin 6\theta \dots$ may be expected.

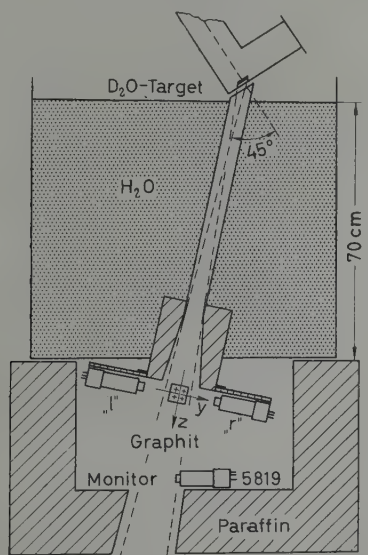


Figure 2

Arrangement used by HUBER and BAUMGARTNER (references [6] and [7]) to detect the polarization of neutrons from the $d-d$ reaction.

PRUETT, BEIDUK and KONOPINSKI [20] discussed the question whether the strong spin-orbit coupling which they found necessary to interpret the $d-d$ reaction could be accounted for by the nucleon-nucleon tensor force. The results were inconclusive. However, if the tensor force mainly provides the spin-orbit coupling, FIERZ [21] showed that the angular and energy dependence of the polarization is predictable up to about

2 MeV deuteron energy. The angular dependence should remain the same as that at low energies. At a fixed angle, the energy dependence of the product $P\sigma(\theta)$ should be given by the function σ_1 of reference [16] i.e. by the reaction probability of $l = 1$ deuterons. In figure 4 the points of figure 3 are replotted in this way. The differential reaction cross sections $\sigma(\theta)$ were taken from a number of different sources [22, 23, 24]. The agreement is better than can be expected from the experimental uncertainties of σ and of P .

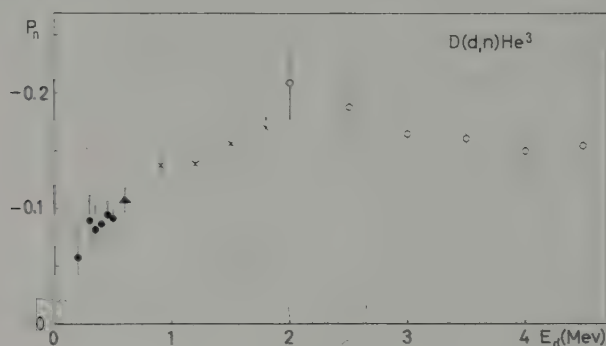


Figure 3

Polarization of neutrons from the $D(d, n)He^3$ reaction as a function of bombarding energy. In order of increasing energy the data are by PASMA, MEIER *et al.*, LEVINTOV *et al.*, BAICKER *et al.* (references [9, 10, 11, 12]) and apply to laboratory angles of 47°, 50°, 49° and 40°, respectively.

Another reaction which has been widely used as a source of neutrons is the $Li^7(p, n)Be^7$ reaction which has a threshold of 1.88 MeV. The polarization of the outgoing neutrons has been investigated extensively by BARSCHALL's group at Wisconsin. Recent results for proton energies up to 3.1 MeV and a neutron emission angle $\theta = 50^\circ$ are shown in figure 5. After the early work by ADAIR [25] at Wisconsin and WILLARD [26] at Oak Ridge there remained the question if in the vicinity of 2.1 MeV the polarization varies appreciably with energy or not. The recent measurements by DARDEN [27] show a very rapid rise between 2 and 2.1 MeV which is followed by a maximum and a slow decrease. The polarization seems to pass through a minimum at 2.5 MeV and then rises slowly. The trend of the curve at higher energies was established by the experiments of CRANBERG [31] and of BAICKER [12]. The results are shown in figure 6, together with the low energy data. For proton energies above 4 MeV the measurement did not discriminate against neutrons to the first excited state of Be^7 . For comparison the $Li^7(p, n)Be^7$

total cross section [32] is also shown in figure 6. It is apparent that the variation in the polarization near 2.2 MeV is associated with the well known resonance at 2.25 MeV. The variation near 5 MeV may be caused by the broad resonance which appears in the $\text{Li}^7(p,n)$ cross section at this energy. An interpretation of the $\text{Li}^7(p,n)$ differential reaction cross section and the polarization in terms of the virtual states of Be^8 was attempted by DARDEN and AUSTIN. Some results of this analysis will be presented in another paper at this symposium.

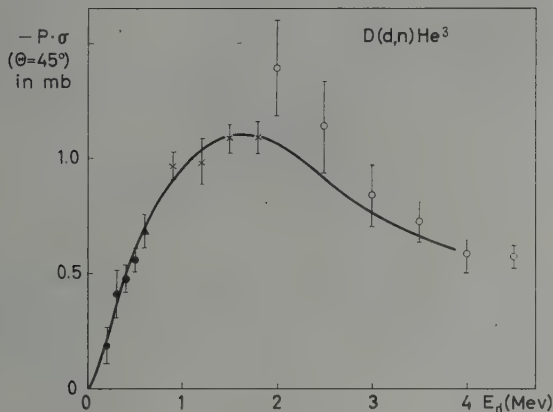


Figure 4

The polarization of neutrons from the $\text{D}(d, n)\text{He}^3$ reaction, multiplied by the reaction cross section (in units of 10^{-27} cm^2) as a function of deuteron bombarding energy. The points are those of figure 3. The solid curve is the function σ_1 of reference 16, multiplied by an arbitrary scale factor.

In the experiments summarized so far the polarization was measured by scattering from light nuclei like helium, carbon or oxygen. The analyzing power $A = P_2$ is computed from phase shifts which are obtained from an analysis of differential cross section experiments. This procedure is rather indirect and it usually is difficult to estimate the uncertainty of the computed analyzing power. A method which eliminates this problem was proposed by BARSCHALL [33]. In this method the polarization of neutrons or protons from a reaction is measured by using the inverse reactions as an analyser. Thus to observe the polarization of $\text{T}(p, n)\text{He}^3$ -neutrons, He^3 would be used as the second target. Since the analyzing power of a reaction is equal to the polarization in the inverse reaction, and the two successive reactions are chosen to be the inverse of each other, P_1 and A of equation (1) are equal to each other.

This, of course, presumes that both reactions take place at the same center of mass angle and energy, i. e. the velocity of the neutron relative to the He^3 nucleus is to be the same in both reactions. For a given bombarding energy there is at most one reaction angle for which

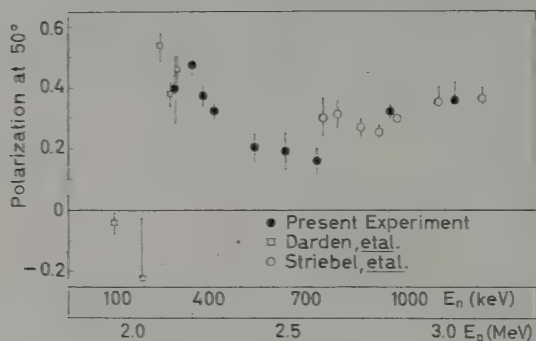


Figure 5

Polarization of neutrons emitted by the $\text{Li}^7(p, n)\text{Be}^7$ reaction at 50° for proton energies between the threshold and 3.1 MeV. In order of increasing bombarding energy the measurements are those of DARDEN *et al.*, AUSTIN, and STRIEBEL *et al.* (references [27, 28] and [29]). The figure is taken from reference [28].

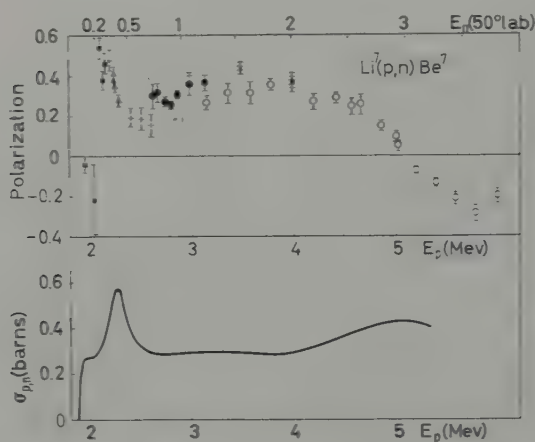


Figure 6

Polarization of neutrons emitted by the $\text{Li}^7(p, n)\text{Be}^7$ reaction at 50° for proton energies up to 6 MeV. The data are from references [27] (■), [28] (+), [29] (●), [30] (▲), [31] (·), [12] (○).

this condition is satisfied. Whether there is such an angle or not depends on the Q -value of the reaction, the masses and the bombarding energy.

In a recent experiment ARTEMOV, VLASOV and SAMOILOV [34] used BARSCHALL's method to study the $T(p,n)$ reaction for proton energies between 6 and 10 MeV. For $E_p = 10$ MeV a scattering angle of 16.5° has to be chosen to satisfy the conditions of the method. At this angle the polarization was found to be quite small, so that the asymmetry (which depends on the square of the polarization) was difficult to measure. Most measurements were carried out for a reaction angle of 40° . At this angle the neutrons have an energy of 7.7 MeV rather than the required 8.8 MeV. However the conditions of the method still apply approximately because the polarization in this reaction presumably varies rather slowly with energy. The results of the experiment are shown in figures 7

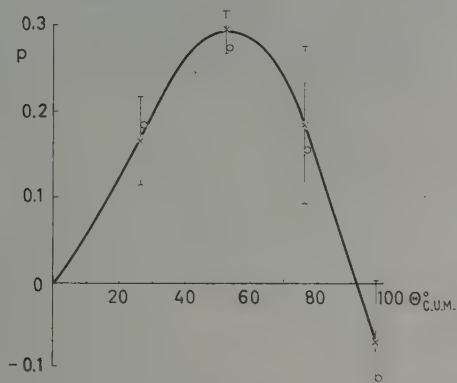


Figure 7

Polarization of $T(p,n)\text{He}^3$ neutrons as a function of center of mass angle for $E_p = 9.9$ MeV, obtained from measurements of the asymmetry in the $\text{He}^3(n,p)T$ reaction for four different angles of proton emission. $\times \theta_1 = 40^\circ$, $E_n = 7.7$ MeV; $\circ \theta_1 = 16.5^\circ$, $E_n = 8.8$ MeV. The figure is from reference [34].

and 8. The angular dependence (figure 7) indicates a maximum polarization of 0.3 for a center of mass reaction angle of about 50° . For 8 MeV proton energy a similar angular dependence was found. Figure 8 shows the dependence of the polarization of neutrons from the $T(p,n)\text{He}^3$ reaction and of the asymmetry parameter A in the $\text{He}^3(n,p)T$ reaction as a function of incident particle energy for an angle of 40° . The polarization increases with energy up to a value of 0.3 at 9.9 MeV proton energy. This corresponds to a neutron energy of 7.7 MeV. The sign of the polarization is not known.

Brief mention should be made of two experiments on the $T(d,n)He^4$ reaction, since it is a widely used source of high energy neutrons. For deuteron energies up to 300 keV, PASMA [9] detected no polarization. Measurements were also made with 1.8 MeV deuterons, for a number of neutron emission angles by LEVINTOV, MILLER and SHAMSHEV [35]. The largest observed polarization²⁾ was $.12 \pm .03$ for 67.5° . According to the authors this value is to be considered a lower limit of the polarization because the nonisotopic angular distribution of the neutrons causes instrumental asymmetries which in this experiment tended to give too small a polarization. Of course the problem of distinguishing between instrumental asymmetries and true polarization effects arises in all polarization experiments. An elegant method to avoid this problem was proposed by HILLMAN, STAFFORD and WHITEHEAD [36]. It makes use of the fact that a magnetic field between the first and second target changes the direction of the polarization vector but does not affect the intensity distribution of the neutrons. The method has recently been applied by DUBBELDAM, JONKER and BOERSMA [37] to 3 MeV neutrons from the $d-d$ reaction.

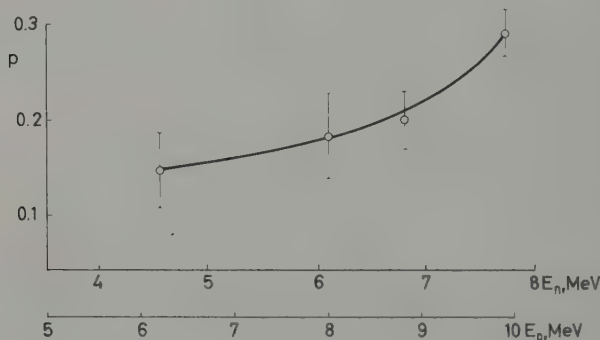


Figure 8

Polarization of neutrons from $T(p, n)He^3$ and asymmetry of protons from $He^3(n, p)T$ as a function of incident particle energy at 40° in the laboratory system. The figure is from reference [34].

Little needs to be reported here on proton polarization experiments. Proton beams of high degree of polarization can be prepared by elastic scattering, in particular from helium and carbon. Consequently there has been little reason to search for reactions which produce highly polarized protons. The main motivation to study polarization in proton

²⁾ Reference [35] does not define the direction of positive polarization.

producing reactions has been the possibility of obtaining information about the reaction mechanism. Indeed a considerable number of such experiments has been reported, but practically all of them pertain to the study of (d, p) stripping reactions. This topic will be discussed at this symposium in a paper by HIRD. In some cases it has been found that stripping reactions are useful sources of polarized nucleons. In an experiment on the $C^{12}(d, n)N^{13}$ reaction HAEBERLI and ROLLAND [38] found that neutrons emitted near the forward peak of the angular distribution have a relatively high degree of polarization. The angular distribution of polarization is shown in figure 9 for two different bombarding energies. The Liverpool group [39, 40] found the $C^{12}(d, p)C^{13}$ reaction to be a useful source of 9 MeV polarized protons. For a reaction angle of about 45° the polarization reaches nearly 0.5. To obtain maximum proton yield the internal deuteron beam of the cyclotron was used to bombard a graphite target. The proton beam was focussed into a chamber several meters away from the cyclotron.

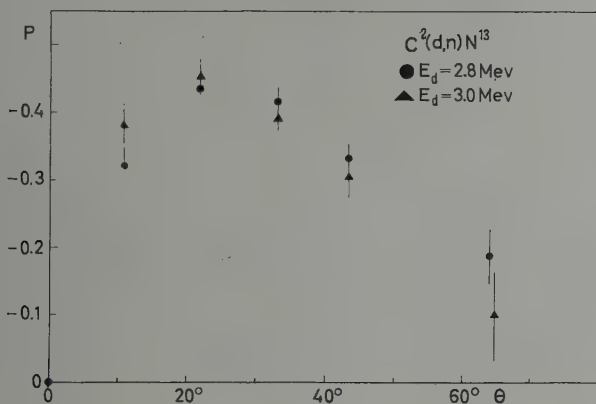


Figure 9

Polarization of neutrons from the $C^{12}(d, n)N^{13}$ reaction as a function of center of mass angle of neutron emission for two different bombarding energies. The data are from reference [38].

One may well ask what has been accomplished so far in the study of polarization in reactions. In the first place one now has available sources of polarized neutrons of any energy between 0.2 and 8 MeV. In figure 10 the polarization in different neutron producing reactions is shown as a function of neutron energy. Over much of the energy range neutron sources of higher degree of polarization are obviously needed.

The curves of figure 10 are not to be taken literally since the uncertainties are still rather large.

Another accomplishment of these experiments has been the development of techniques to measure the polarization of nucleons. This development clearly is not completed but much progress has been made during the last eight years.

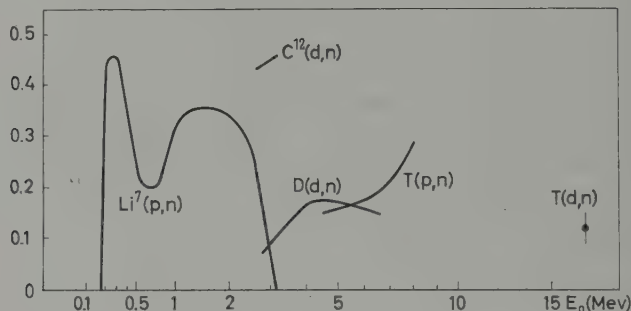


Figure 10

Dependence of the neutron polarization on neutron energy for different reactions. The curves are not to be taken literally, since the experimental uncertainties are rather large.

Finally an obvious conclusion from the experiments summarized here is that polarization in reactions is a very common phenomenon. Since spin-orbit coupling is a necessary condition for polarization to occur one may say that the experiments provide rather direct evidence for the importance of spin-orbit coupling. Thus one has become more cautious about accepting calculations based on the assumption of central forces. It would appear, therefore, that polarization experiments have helped to make the interpretation of reactions more realistic.

REFERENCES

- [1] J. SCHWINGER, Phys. Rev. 69, 681 (1946); and Phys. Rev. 73, 407 (1948).
- [2] L. WOLFENSTEIN, Phys. Rev. 75, 342 (1949).
- [3] E. J. KONOPINSKI and E. TELLER, Phys. Rev. 73, 822 (1948).
- [4] A. SIMON, Phys. Rev. 92, 1050 (1953).
- [5] G. R. BISHOP, G. PRESTON, J. M. WESTHEAD, and H. H. HALBAN, Nature 170, 113 (1952).
- [6] P. HUBER and E. BAUMGARTNER, Helv. Phys. Acta 26, 420 (1953).
- [7] E. BAUMGARTNER and P. HUBER, Helv. Phys. Acta 26, 545 (1953).
- [8] R. RICAMO, Helv. Phys. Acta 26, 423 (1953).
- [9] P. J. PASMA, Nucl. Phys. 6, 141 (1958).
- [10] R. W. MEIER, P. SCHERRER, and G. TRUMPY, Helv. Phys. Acta 27, 577 (1954).

- [11] I. I. LEVINTOV, A. V. MILLER, E. Z. TARUMOV, and V. N. SHAMSHEV, *Nucl. Phys.* **3**, 237 (1957).
- [12] J. A. BAICKER, K. W. JONES, and B. TELL, *Bull. Amer. Phys. Soc., Ser. II*, **4**, 62 (1959); J. A. BAICKER and K. W. JONES, *Nucl. Phys.* **17**, 424 (1960).
- [13] W. W. DAHEHNICK, *Phys. Rev.* **115**, 1008 (1959).
- [14] R. E. SEGEL and S. S. HANNA, *Phys. Rev.* **106**, 536 (1957).
- [15] B. MAGLIĆ and J. VUKOVIĆ, *Nucl. Phys.* **6**, 443 (1958).
- [16] F. M. BEIDUK, J. R. PRUETT, and E. J. KONOPINSKI, *Phys. Rev.* **77**, 622 (1950).
- [17] R. J. BLIN-STOYLE, *Proc. Phys. Soc.* **A65**, 949 (1952).
- [18] M. CINI, *Nuov. Cim., Ser. IX*, **8**, 1007 (1951).
- [19] B. M. MCCORMAC, M. F. STENER, C. D. BOND, and F. L. HEREFORD, *Phys. Rev.* **104**, 718 (1956).
- [20] J. R. PRUETT, F. M. BEIDUK, and E. J. KONOPINSKI, *Phys. Rev.* **77**, 628 (1950).
- [21] M. FIERZ, *Helv. Phys. Acta* **25**, 629 (1952).
- [22] PRESTON, SHAW, and YOUNG, *Proc. Roy. Soc.* **A226**, 206 (1954).
- [23] FULLER, DANCE, and RALPH, *Phys. Rev.* **108**, 91 (1958).
- [24] J. L. FOWLER, and J. E. BROLLEY, JR., *Rev. Mod. Phys.* **28**, 103 (1956).
- [25] R. K. ADAIR, S. E. DARDEN, and R. E. FIELDS, *Phys. Rev.* **96**, 503 (1954).
- [26] H. B. WILLARD, J. K. BAIR, and J. D. KINGTON, *Phys. Rev.* **95**, 1359 (1954).
- [27] S. E. DARDEN, T. R. DONOGHUE, and C. A. KELSEY, *Bull. Amer. Phys. Soc., Ser. II*, **5**, 17 (1960), and *Nucl. Phys.* (to be published).
- [28] S. M. AUSTIN, Thesis, University of Wisconsin, (1960), and *Nucl. Phys.* (to be published).
- [29] H. R. STRIEBEL, S. E. DARDEN, and W. HAEBERLI, *Nucl. Phys.* **6**, 188 (1958).
- [30] A. OKAZAKI, *Phys. Rev.* **99**, 55 (1955).
- [31] L. CRANBERG, *Phys. Rev.* **114**, 174 (1959).
- [32] J. H. GIBBONS, and R. L. MACKLIN, *Phys. Rev.* **114**, 571 (1959).
- [33] H. H. BARSCHALL, *Helv. Phys. Acta* **29**, 145 (1956).
- [34] K. P. ARTEMOV, N. A. VLASOV, and L. N. SAMOILOV, *Zh. eksper. teor. Fiz.* **37**, 1183 (1959) (transl. *Soviet Phys. - JETP* **37** (10), 841 (1960)).
- [35] I. I. LEVINTOV, A. V. MILLER, and V. N. SHAMSHEV, *Zh. eksper. teor. Fiz.* **34**, 1030 (1958) (transl. *Soviet Phys. - JETP* **34** (7), 712 (1958)).
- [36] P. HILLMAN, G. H. STAFFORD, and C. WHITEHEAD, *Nuov. Cim.* **4**, 67 (1956).
- [37] P. S. DUBBELDAM, C. C. JONKER, and H. J. BOERSMA, *Nucl. Phys.* **15**, 452 (1960).
- [38] W. HAEBERLI and W. W. ROLLAND, *Bull. Amer. Phys. Soc.* **2**, 234 (1957).
- [39] M. S. BOKHARI, J. A. COOKSON, B. HIRD, and B. WEESAKUL, *Proc. Phys. Soc.* **72**, 88 (1958).
- [40] M. A. AL-JEBOORI, M. S. BOKHARI, B. HIRD, and A. STRZALKOWSKI, *Proc. Phys. Soc.* **74**, 705 (1959).

Polarization Measurements of D-D Neutrons by a Solenoid

By C. C. JONKER, Naturkuundig Lab., Vrije Universiteit Amsterdam

The following is a short survey of the work of DUBBELDAM *a.o.* [1, 2, 3¹⁾] on the measurement of the polarization of D-D neutrons. The accuracy up till now obtained with the familiar method of turning the detectors 180° around the primary neutron beam is not very great. This is caused mainly by the possibility of introducing false asymmetries and insufficient shielding. This can be avoided by using a method due to HILLMAN [4] *a.o.* Hillman determined the polarization of 100 MeV neutrons with fixed detectors by turning the polarization vector with a solenoid.

In applying this method to the case of 3 MeV D-D neutrons, some difficulties arise, concerning the collimation and the intensity of the neutrons. It is obvious that the intensity is very important. Therefore it is necessary that the solenoid is as short as possible and has a rather large inner diameter determined by the need of having not too small scatterers. Therefore a very compact solenoid with forced air cooling was designed with a great current density: 4.6 A/mm² while the normal value for technical coils is 2 A/mm². The length of the solenoid is 780 mm, the inner diameter is 46 mm. The required current of 57 A was stabilized to better than 1%. The maximum dissipated power was about 8 kW. There is an influence of the magnetic field of the solenoid on the pulse height of the photomultipliers. The resulting correction can be determined experimentally and amounts to about 3%. The experimental set-up is given in figure 1.

The neutrons were produced in a gold drive-in target, a carbon scatterer was used as analyzer and stilbene crystals mounted on E.M.I. photomultipliers as detectors. The polarization vector was turned 90° to the left, and then 90° to the right, by reversing the current through the solenoid.

With this set-up first of all the left-right asymmetry for $E = 450$ keV and $\vartheta_{\text{lab}} = 50^\circ$ was measured as a function of the current through

¹⁾ Numbers in brackets refer to References, page 165.

the solenoid and an accuracy of 5% in the asymmetry was easily obtained.

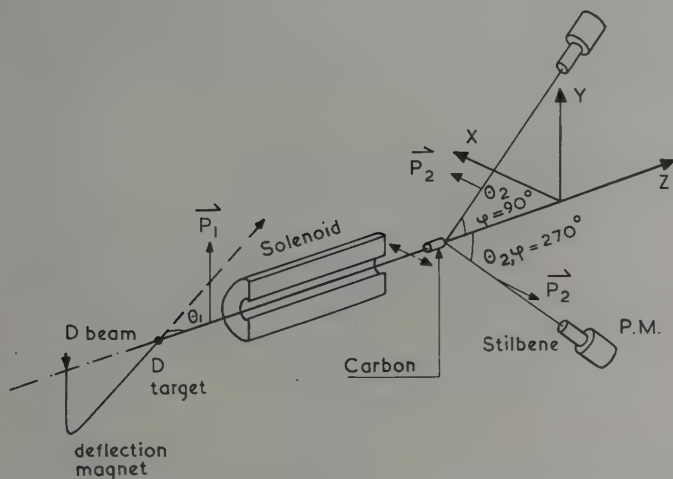


Figure 1

Schematic view of the experimental set-up

Next the polarization of D-D neutrons as a function of the deuteron energy for two different values of ϑ_1 was measured. The values for ϑ_1 were chosen for the following reason: the polarization of D-D neutrons can be described by the formula due to FIERZ [5]

$$\Pi(E_D, \vartheta_1) = \sigma_1 a \sin 2 \vartheta_1 + \sqrt{\sigma_0 \sigma_2} \alpha \sin 2 \vartheta_1 + \sigma_2 \beta \sin 2 \vartheta_1 (3 \cos^2 \vartheta_1 - 1)$$

where Π is the differential polarization defined as the product of the polarization and the differential cross-section; σ_0 , σ_1 and σ_2 are the 'approach cross sections' for the $l = 0, 1$ and 2 waves defined and computed by BEIDUK, PRUETT and KONOPINSKI [6]; E_D is the deuteron energy and α, β and a are constants. The second and third term disappear if in the nucleon-nucleon interaction only central and tensor forces are present. Without these terms there is a $\sin 2 \vartheta_1$ dependence. If a deviation of this $\sin 2 \vartheta_1$ dependence is found one can say something about a possible spin-orbit coupling in the nucleon-nucleon interaction. For that purpose ϑ_1 was chosen: 50° and $22^\circ 30'$, the angles where the third term is zero and extreme.

The polarization P_1 of the neutrons can be obtained from the measured asymmetry R by $R = P_1 P_2$ with P_2 defined as the polarization of the

neutrons resulting from the scattering of an unpolarized neutron beam by carbon. The value found for P_1 depends on the known values for P_2 . There are two computations of P_2 from different phase analyses, one by MEIER [7] *a.o.* and an other by WILLS [8] *a.o.* In figure 2 the two sets of values for P_2 are given, they show appreciable differences – in the place of the positive peak and in the large negative values on each side of the peak.

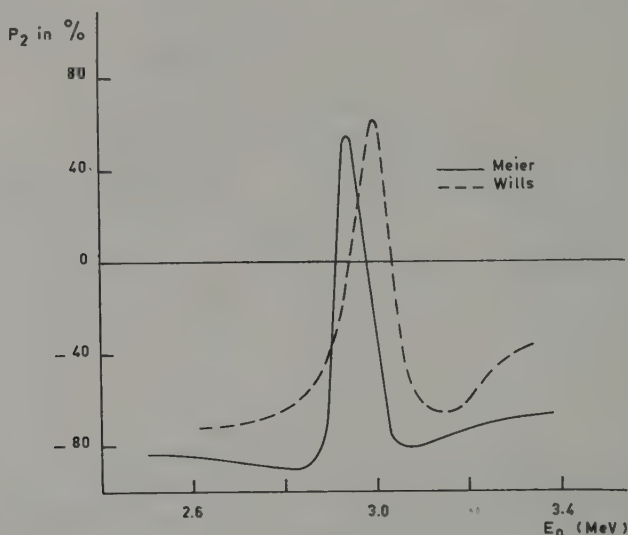


Figure 2

$P_2(\vartheta_2 = 45^\circ)$ as a function of the neutron energy from phase analyses of MEIER and WILLS

As a thick drive-in target was used average values for the asymmetry were obtained. It is rather difficult to interpret these values. Therefore we computed with the thin target data from the literature and P_2 of MEIER and of WILLS the asymmetry that can be expected for a thick target and compared this with our measurements. The computation is as follows:

The differential cross section for the carbon scatterer is in the case of a solenoid,

$$\sigma_c(\vartheta_2, \varphi) = \sigma_c(\vartheta_2) \left(1 \pm P_1(E_D, \vartheta_1) P_2(E_n, \vartheta_2) \sin \frac{a I}{\sqrt{E_n}} \right)$$

as is evident from the formula of WOLFENSTEIN, $\sigma_c(\vartheta_2)$ is the unpolarized differential cross section, $a I / \sqrt{E_n}$ is the angle over which the polarization

vector is turned by the solenoid with a a constant, I the current through the solenoid and $\sqrt{E_n}$ the square root of the neutron energy which is proportional to the velocity for the neutrons, The (+) sign is for the rotation of 90° to the right, the (−) sign for 90° to the left.

The numbers of neutrons are in the two cases:

$$N_{\pm} = \varepsilon K \int_0^{E_D \max} \sigma_c(E_n, \vartheta_2) \left(1 \pm P_1(E_D, \vartheta_1) P_1(E_n, \vartheta_2) \sin \frac{a I}{\sqrt{E_n}} \right) N(E_D) dE_D$$

with $N(E_D)$ the neutron spectrum, ε the efficiency and K a constant. One finds from the definition of R :

$$R_{av} = \frac{N_+ - N_-}{N_+ + N_-} = \frac{\int_0^{E_D \max} \sigma_c(E_n, \vartheta_2) P_1(E_D, \vartheta_1) P_2(E_n, \vartheta_2) \sin \frac{a I}{\sqrt{E_n}} N(E_D) dE_D}{\int_0^{E_D \max} \sigma_c(E_n, \vartheta_2) N(E_D) dE_D}$$

For $\sigma_c(E_n, \vartheta_2)$ are taken the values of MEIER [7]. In this formula the neutron spectrum is not yet known; it can be found approximately in the following manner

$$\begin{aligned} N(E_D) dE_D &= \text{const } \varrho_D(z) \sigma(E_D, \vartheta_1) dz \\ &= \text{const } \varrho_D(z) \sigma(E_D, \vartheta_1) \left(\frac{dE_D}{dz} \right)^{-1} dE_D ; \end{aligned}$$

ϱ_D is the deuteron density in the target at the depth z .

For the stationary case holds $\varrho_D = Q_z/\alpha$ where α is the diffusion constant for deuterons in gold and Q the deuteron source strength. The range-energy relation gives that dE_D/dz is nearly a constant. $\sigma(E_D, \vartheta_1)$ can be taken linear with energy for E_D is less than 500 keV. So the spectrum is the product of two linear terms, i.e. a parabola.

From the thin target measurements of MEIER, PASMA and LEVINTOV we determined that to a good approximation:

$$P_1(E_D, \vartheta_{1 \text{ lab}} = 50^\circ) = \sqrt{0.18 E_D} \%, \quad E_D \text{ in keV},$$

the result of this computation is given in figure 3.

The points are our measurements. The curve computed with MEIER's data agrees much better with this measurement than that with the values of WILLS. For $\vartheta_1 = 22^\circ 30'$ the same computation is made (see figure 4). P_1 is computed with the $\sin 2 \vartheta_1$ dependence of the differential polarization, that is the first term of the formula of FIERZ.

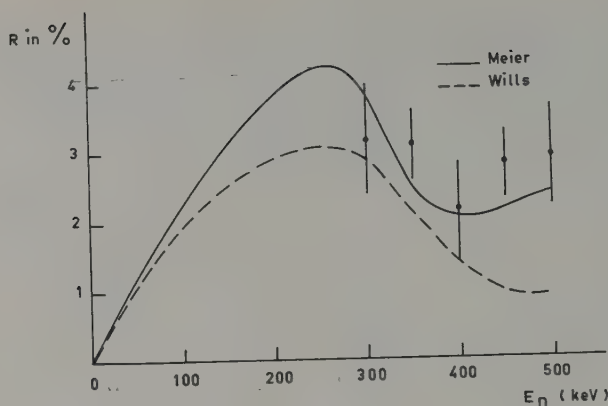


Figure 3

R_{av} as a function of E_D at $\vartheta_{1lab} = 50^\circ$. The curves are computed as explained in the text

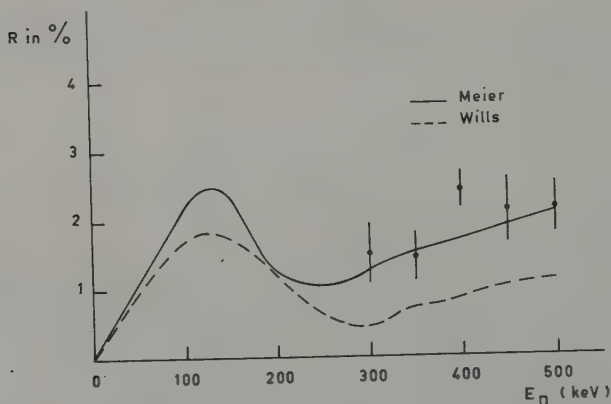


Figure 4

R_{av} as a function of E at $\vartheta_{1lab} = 22^\circ 30'$. The curves are computed as explained in the text

Again MEIER agrees better with the experimental points than WILLS. Further it is evident from the figures 3 and 4 that the $\sin 2 \vartheta_1$ dependence is not contradictory to the thick target measurements. Therefore it is impossible to decide for the existence of the spin-orbit coupling in the nucleon-nucleon interaction. It is, however, also impossible to conclude to the non-existence. Therefore, the measurements are continued with a thin target and for several values of ϑ_1 .

REFERENCES

- [1] P. S. DUBBELDAM, C. C. JONKER, and F. J. HEEMSKERK, *Nucl. Instr.* **4**, 234 (1960).
- [2] P. S. DUBBELDAM, C. C. JONKER, and H. J. BOERSMA, *Nucl. Phys.* **15**, 452 (1960).
- [3] P. S. DUBBELDAM (Thesis Free University Amsterdam, 1959).
- [4] P. HILLMAN, G. H. STAFFORD, and C. WHITEHEAD, *Nuovo Cim.* **4**, 67 (1959).
- [5] M. FIERZ, *Helv. Phys. Acta* **25**, 629 (1952).
- [6] F. M. BEIDUK, J. R. PRUETT, and E. J. KONOPINSKI, *Phys. Rev.* **77**, 622 (1950).
- [7] R. W. MEIER, P. SCHERER, and G. TRUMPY, *Helv. Phys. Acta* **27**, 577 (1954).
- [8] J. E. WILLS, J. K. BAIR, H. O. COHN, and H. B. WILLARD, *Phys. Rev.* **109**, 891 (1958).
- [9] P. J. PASMA (Thesis Groningen 1958).
- [10] P. J. PASMA, *Nucl. Phys.* **6**, 141 (1958).
- [11] I. I. LEVINTOV, A. V. MILLER, E. Z. TARUMOV, and V. N. SHAMSHEV, *Nucl. Phys.* **3**, 237 (1957).

Polarization in Some (d, n) and (d, p) Reactions Principle of Ring Polarimeter

By H. BRINKMAN, Natuurkundig Laboratorium der Rijks Universiteit, Groningen

1. Introduction

In the past years we studied the polarization of neutrons from the $D(d, n)He^3$ and $T(d, n)He^4$ reactions (Pasma [1]¹⁾), and the polarization of protons from the $Be^9(d, p)Be^{10}$ and $Li^6(d, p)Li^7$ reactions (van BEEK and ANDRÉ [2]). In each case we shall report the results of our thin target measurements, only briefly indicating the method used for measuring the polarization. Finally a new geometry for the measurement of nucleon polarization will be discussed.

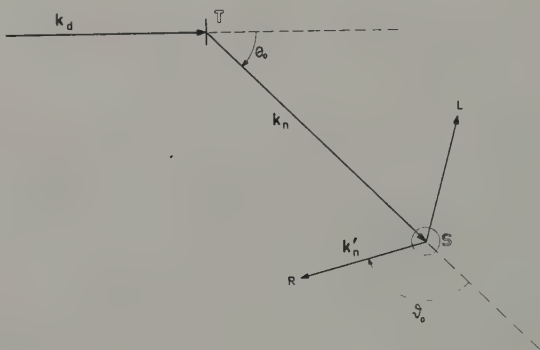


Figure 1

We are dealing with nuclear reactions in which the incident particles and the target nuclei are unpolarized, whereas the observed outgoing particles are nucleons (spin $1/2$). Polarization of these nucleons may result from spin-orbit coupling. The polarization vector P_n is always normal to the reaction plane, defined by the paths of incoming and outgoing

¹⁾ Numbers in brackets refer to References, page 174.

particle. If \mathbf{P}_n has the direction of $\mathbf{k}_d \times \mathbf{k}_n$ the polarization is called positive. The degree of polarization is a function of the energy of the incident particles E_d and the angle of emission θ_0 (lab. system) of the nucleons. The value of P_n is found from the left-right asymmetry in scattering the nucleons by spin zero nuclei. We used He^4 as the scatterer.

When an unpolarized beam of spin 1/2 particles is scattered by a zero spin scatterer, the beam becomes polarized, the polarization vector \mathbf{P}_s being perpendicular to the scattering plane, its magnitude a function of the energy E_n and the scattering angle ϑ_0 (lab. system), the left hand scattering being equal to the right hand scattering. The function $P_s(E_n, \vartheta)$ is called the *polarization efficiency* or 'analyzing power' of the scatterer. If \mathbf{P}_s has the direction $\mathbf{k}_n \times \mathbf{k}_n'$ the polarization is called positive.

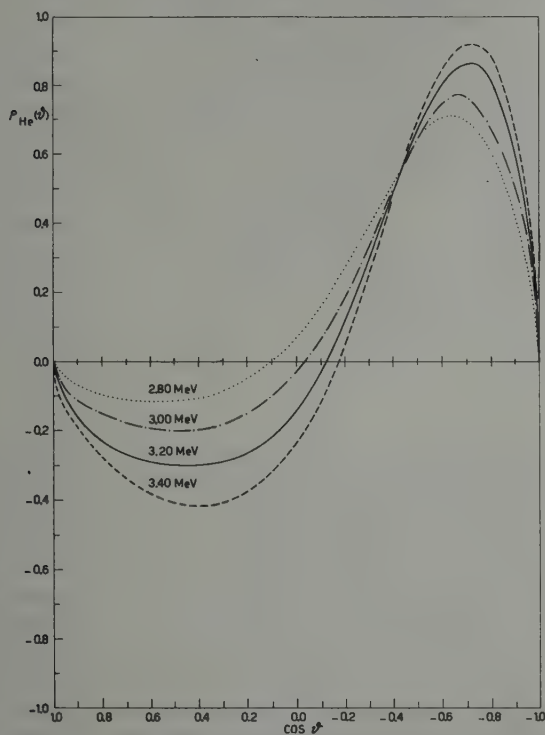


Figure 2

Neutron polarization by n - α scattering as a function of c. m. angle ϑ
(VAN WAGENINGEN [3])

However, if the nucleons incident on the scatterer have the polarization degree P_n , and if we take the scattering plane normal to the vector P_n , then the left scattering with intensity L is no longer equal to the right scattering R (fig. 1). The left-right asymmetry, defined as

$$\varepsilon = \frac{L-R}{L+R} \quad (1)$$

turns out to be

$$\varepsilon(E_d, \theta_0, \vartheta_0) = P_n(E_d, \theta_0) \cdot P_s(E_n, \vartheta_0) \quad (2)$$

From the measured value of ε the value of P_n can be found if the polarization efficiency P_s of the scatterer is known. This is for instance the case for He^4 . Figure 2 shows, by way of example, the value of $P_s(\vartheta)$ for 2.8–3.4 MeV neutrons scattered by He^4 (ϑ is the scattering angle in the c. m. system). Similar curves exist for higher neutron energies. These curves, calculated by VAN WAGENINGEN [3], are consistent with those computed by LEVINTOV [4] *et al.*, and are based on the accurate measurements of the differential neutron scattering cross sections for helium by SEAGRAVE [5]. Also in the case of proton scattering reliable curves for the polarization efficiency of He^4 exist. In actual experiments one has to use average values of P_s , accounting for a spread in the scattering angles due to the finite size of the scatterer and of the detectors at R and L. Further one has to correct the measurements for possible geometrical asymmetries, differences in sensitivity of the counters, background counts and the like. In positions where the left-right asymmetry must be essentially zero (either P_n or P_s being zero), test measurements were made.

2. Results

$D(d, n)\text{He}^3$. For this reaction the neutron polarization was determined from the left-right asymmetry, induced when the neutrons are scattered elastically by He^4 nuclei. The experimental arrangement is shown in figure 3. The well collimated neutron-beam ($\theta_0 = 47^\circ\text{--}50^\circ$) is scattered by the helium-filled gas scintillation counter S. The neutrons, scattered over 123° in the reaction plane, are detected by the two liquid scintillation counters R and L when in coincidence with the gas scintillation counter S. The choice of helium as the scatterer enabled us to employ this coincidence technique.

The angular distribution of neutrons (in the c. m. system) from the $D(d, n)\text{He}^3$ reaction is rather pronounced, even at low deuteron energy showing that P -waves of the incident deuteron are involved in the reaction. The differential cross section is proportional to $1 + A(E_d) \cdot \cos^2\theta$. The degree of polarization P_n is a function of the c. m. angle θ of the

emitted neutron and the deuteron energy E_d . According to BLIN-STOYLE [6] we have at low energies ($E_d < 0.5$ MeV), where only S - and P -waves are effective:

$$P_n(E, \theta) = C \cdot \frac{A(E_d) \cdot \sin \theta \cos \theta}{1 + A(E_d) \cdot \cos^2 \theta}. \quad (3)$$

Thus we have $P_n = 0$ at $\theta = 0$ and $\theta = \pi$, what follows from general symmetry conditions already. Since the colliding particles are identical in this reaction, we must also have $P_n = 0$ at $\theta = \pi/2$, in accordance with the

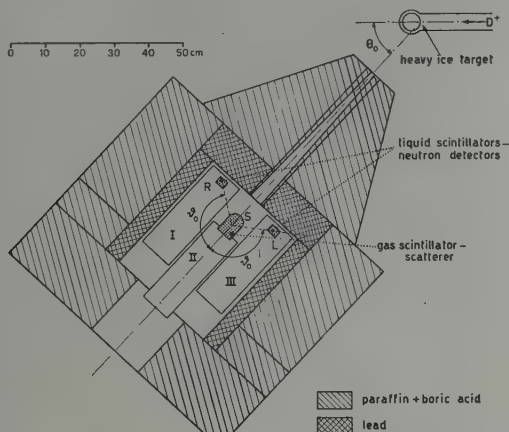


Figure 3

Arrangement used in $D(d, n)\text{He}^3$ neutron polarization experiments by PASMA [1]

formula. At low deuteron energies the maximum polarization P_n^{\max} can be expected near $\theta_0 = 50^\circ$ ($\theta = 58^\circ$). The highest value of ε occurs if P_s is maximum; this corresponds to $\vartheta_0 = 123^\circ$ ($\cos \vartheta = -0.7$; $\vartheta = 135^\circ$) and P_s about $+80\%$. The results obtained by PASMA [1] are summarized in figure 4. The 3 MeV neutrons, emitted under 47° to 50° from thin heavy ice targets (50 keV) show a negative polarization P_n^{\max} of 6 to 9% depending on the deuteron energy, varied between 200 and 500 keV. In the same figure the maximum values of P_n , calculated from the thin target results obtained by MEIER, SCHERRER, and TRUMPY [7] at 600 keV (using C^{12} as a scatterer) and those obtained by LEVINTOV and coworkers [4] at energies between 900 and 1800 keV deuteron energy (He^4 scatterer) are shown. The thin target polarization data, obtained by various authors using different experimental techniques, appear to fit in a smooth curve. At low deuteron energies the measured polarizations are in accordance

with theoretical values, calculated by CINI [8] and BLIN-STOYLE [6]. The recent experiments by DUBBELDAM [9] at deuteron energies between 300 and 500 keV, using the solenoid method for determining the neutron polarization, yield values in accordance with PASMA's curve. Recent thick target measurements by KANE [10] at an average deuteron energy of 93 keV and emission angles of 43° and 53° in the laboratory system yield rather high P_n^{max} values of about -10% . This would be in disagreement with the curve of figure 4, when extrapolated to low energies. Including the thin target and thick target results published by various authors, KANE concludes that the polarization of neutrons from the DD-reaction is independent of the deuteron energy between 93 keV and 700 keV. We believe this conclusion and his measurement to be incorrect.

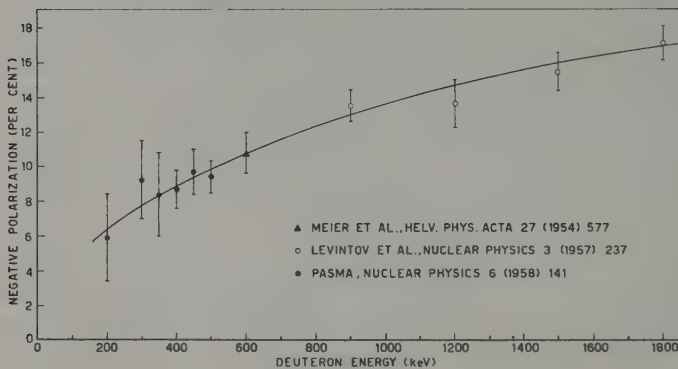


Figure 4

Thin target $D(d, n)He^3$ neutron polarization data as a function of deuteron energy

$T(d, n)He^4$. The 14.8 MeV-neutrons from this reaction, emitted under 45° (θ_0) from a tritium loaded zirconium target, bombarded with deuterons of 100 to 300 keV, showed no polarization, as can be expected. The measurements (PASMA [1]) were done with the same equipment as described for the DD-neutrons. The accuracy in the measured left-right-asymmetries was less, however, due to a much larger background and the lower scattering cross section of He^4 for fast neutrons. The polarization efficiency of helium for 14.8 MeV neutrons has a pronounced minimum at $\vartheta_0 = 76^\circ$ ($\cos \vartheta = -0.1$) and a pronounced maximum at $\vartheta_0 = 123^\circ$ ($\cos \vartheta = -0.7$). Measurements in both circumstances proved the degree of polarization of the DT-neutrons to be zero ($\pm 2\%$). This result is in accordance with the zero angular momentum of the resonance in the

reaction cross section at 110 keV. At higher energies (1800 keV) LEVINTOV and coworkers [11] measured maximum polarizations of about 10%.

$Be^9(d, p)Be^{10}$ and $Li^7(d, p)Li^7$. VAN BEEK (Groningen) and ANDRÉ (Trondheim) [2] measured the polarization of the protons to the ground state of Be^{10} and to the ground state and first excited state of Li^7 . A beam of $5 \mu A$ 1.63 MeV deuterons, produced with the Van de Graaff generator of the Physical Institute of the Norwegian Technical University at Trondheim, was bombarding thin Be^9 and Li^6O_2 targets ($90 \mu g/cm^2$ and $130 \mu g/cm^2$ respectively, supported by a 0.12 mm copper backing) for about 10 hours. The protons emitted under 40° entered the scattering chamber through a 10μ nickel foil. The chamber was filled with helium of 2.5 and 1.5 atm respectively (fig. 5). The scattered protons, the scattering angle of 67.5° being defined by slits, are hitting the photographic plates under 15° (dip angle). Between target chamber and scattering chamber a paraffin-borax shielding reduced the neutron background. An area of 14×17 mm of the left and the right plate has been scanned, carefully selecting the appropriate proton tracks. The degree of polarization has been calculated from the left-right asymmetry, using the p, α polarization efficiencies given by BROCKMAN [12]. In our experiments P_{He} amounted to -43% (beryllium reaction) and -54% and -42% respectively (lithium reaction). The accuracy of our proton polarization measurements is rather unsatisfactory, since only a small number of tracks could be used and a disturbing background existed.

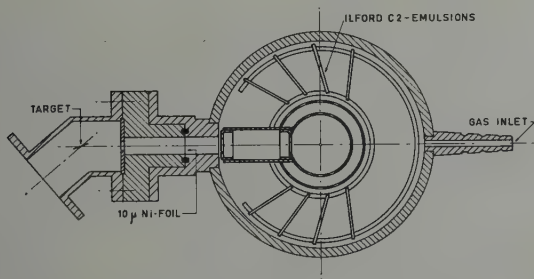


Figure 5

Scattering chamber used by VAN BEEK and ANDRÉ [2]

The ground state protons of $Be^9(d, p)Be^{10}$ showed a very weak polarization if any; we found $P_p = 1(\pm 7)\%$ at $\theta_0 = 40^\circ$. The ground state protons and the first excited state protons of Li^7 could just be resolved ($\Delta E = 0.48$ MeV). We found a negative polarization of both proton

groups: $P_p^{(0)} = -48 (\pm 16)\%$ and $P_p^{(1)} = -63 (\pm 14)\%$ at $\theta_0 = 40^\circ$, that is near the stripping peak (ANDRÉ [2]).

3. Ring Geometry for Polarization Measurements

In determining the degree of polarization from the left-right asymmetry, one compares the left intensity L (at $\varphi = 0$) proportional with $1 + P_n P_s$ and the right intensity R (at $\varphi = \pi$) proportional with $1 - P_n P_s$. Both intensities are observed at the *same* scattering angle ϑ , preferably chosen at an extremum of the polarization efficiency or 'analyzing power' of the scatterer.

However, since the complete polarization efficiency function $P_s(\vartheta)$ is known, one may in principal just as well compare any two intensities corresponding to *different* scattering angles ϑ_1 and ϑ_2 , for which the polarization efficiencies are P_{s1} and P_{s2} respectively, taking the azimuthal angle *either* $\varphi = 0$ *or* $\varphi = \pi$. Before comparing these intensities one has to account for the differences in the scattering cross sections at ϑ_1 and ϑ_2 , for differences in geometry and for possible differences in the response of the two counters due to the change in energy of the scattered nucleons. This reduction of the measurements to 'identical geometry' offers no principal difficulties, however. Denoting the *reduced* intensities as I_1 and I_2 , one finds:

$$\varrho = \frac{I_1 - I_2}{I_1 + I_2} = \frac{P_n (P_{s1} - P_{s2})}{2 + P_n (P_{s1} + P_{s2})}. \quad (4)$$

In the usual left-right asymmetry arrangement with $\varphi_L = 0$, $\varphi_R = \pi$ and $\vartheta_1 = \vartheta_2$ one has $P_{s1} = -P_{s2} (= P_s)$, so that $\varrho_{LR} = \varepsilon = P_n P_s$. In the more general case of $\vartheta_1 \neq \vartheta_2$ and constant φ it can be concluded from equation (4) that optimal values of ϱ are obtained at angles ϑ_1 and ϑ_2 for which the nominator is large and the denominator small. If P_n has a small value it is important only to make $P_{s1} - P_{s2}$ large, that is to choose ϑ_1 and ϑ_2 such that P_{s1} is a maximum and P_{s2} a minimum of the polarization efficiency curve (or vice versa). If P_n has a high value, one may try to find with the aid of the given $P_s(\vartheta)$ -curve other values of ϑ_1 and ϑ_2 for which ϱ is optimal. The ϱ -values can be made about as large as the ε -values in the usual left-right asymmetry set-up. If the geometry corresponding with optimal ϱ would become unpractical, one might measure at a ϑ_1 with large $|P_{s1}|$ and a ϑ_2 with $P_{s2} = 0$ (or vice versa).

We can take advantage of the mentioned more general possibility of measuring the polarization degree of nucleons emitted in a nuclear reaction by using the *ring geometry* schematically shown in figure 6. It is easy to see that in each plane through the direction of incidence of the bombarding particles, the arrangement of scatterer and counter is equally sensitive to the polarization of the emitted nucleons. If by way of example

the polarization of 3.4 MeV DD-neutrons, emitted under 45° , must be determined, using helium as the ring scatterer, one should take $\vartheta_1 \approx 120^\circ$ (P_{s1} max) and $\vartheta_2 \approx 65^\circ$ (P_{s2} min) for optimal ϱ , which is quite feasible. However one can choose other ϑ values as well or one may place more than two counters along the axis of the ring polarimeter, combining the intensities belonging to different $P_s(\vartheta)$ values. It will be obvious that the principle of the ring polarimeter is applicable for all reaction angles θ_1 . Under suitable circumstances one may use two (or more) coaxial ring scatterers and measure simultaneously at angles θ_1 and θ_2 , using an additional pair of counters.

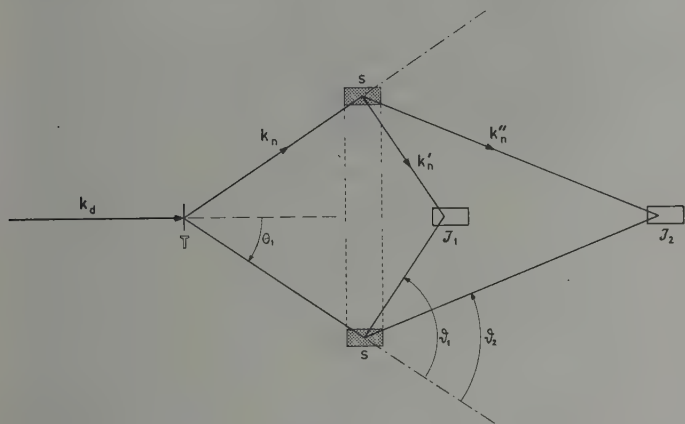


Figure 6
Principle of ring polarimeter

In the ring geometry of figure 6 the counters are in line with the primary beam, hence instrumental asymmetries are unlikely to occur, whereas it will be relatively easy to shield the counters from stray radiation. An important advantage of the ring polarimeter is the appreciable increase of the measured intensity of scattered particles for a given geometry. A disadvantage is that a coincidence technique, as employed in the neutron polarization measurements by PASMA, may give practical difficulties. If polarization measurements of charged particles are envisaged, specially shaped scintillation crystals or semiconductor counters may be necessary. This ring geometry will be applied in polarization measurements in the Groningen Physical Institute. The proposed ring geometry has great advantages over the one obtained when rotating figure 1 about the direction of incidence of the bombarding particles, in which case one would need extensive ring counters except at very small angles θ and ϑ .

REFERENCES

- [1] P. J. PASMA, Thesis Groningen (1958), and Nucl. Phys. *6*, 141 (1958).
- [2] A. M. K. VAN BEEK, and G. O. ANDRÉ, Nucl. Phys. 1961 (to be published).
- [3] R. VAN WAGENINGEN, Internal Report 15 (Groningen 1954).
- [4] I. I. LEVINTOV, A. V. MILLER, and V. N. SHAMSHEV, Nucl. Phys. *3*, 221 (1957);
I. I. LEVINTOV, A. V. MILLER, E. Z. TARUMOV, and V. N. SHAMSHEV, Nucl. Phys. *3*, 237 (1957).
- [5] J. D. SEAGRAVE, Phys. Rev. *92*, 1222 (1953).
- [6] R. J. BLIN-STOYLE, Proc. Phys. Soc. *A 64*, 700 (1951), and *A 65*, 949 (1952).
- [7] R. W. MEIER, P. SCHERRER, and G. TRUMPY, Helv. Phys. Acta *27*, 577 (1954).
- [8] M. CINI, Nuovo Cimento *8*, 1007 (1951).
- [9] P. S. DUBBELDAM, Thesis Amsterdam (1959) and Nucl. Phys. *15*, 452 (1960).
- [10] P. P. KANE, Nucl. Phys. *10*, 429 (1959).
- [11] I. I. LEVINTOV, A. V. MILLER, and V. N. SHAMSHEV, Soviet Phys. JETP *34*, 712 (1958).
- [12] K. W. BROCKMAN, Phys. Rev. *170*, 163 (1958).
- [13] G. O. ANDRÉ, Nucl. Phys. *15*, 464 (1960).

Detection of Deuteron Alignment with s-wave Reactions

By H. B. WILLARD, Oak Ridge National Laboratory

Abstract. A brief review is made of some properties possessed by oriented deuteron beams with tensor moments up to rank 2. In particular, it is pointed out that angular distributions may result from aligned deuteron beams, even though the reaction may be initiated by s-waves and/or proceed through the contribution from a single element of the reaction matrix. Specific calculations are carried out for the 107-keV resonance in the $T(d, n)He^4$ reaction, the 430-keV resonance in the $He^3(d, p)He^4$ reaction, and the 940-keV resonance in the $C^{12}(d, p)C^{13}$ reaction. Several suggestions are made for these reactions as analyzers of deuteron alignment.

It is evident from the agenda for this symposium that many laboratories are currently engaged in the fascinating, albeit difficult, problem of producing polarized particle beams by two distinct methods, (a) polarized ion sources suitable for post acceleration to any desired energy, and (b) polarized beams of second-order intensity obtained through reactions and scattering. The present paper is concerned primarily with deuteron orientation, alignment, and polarization processes.

The theoretical aspects of orientated beams with particle spins higher than $1/2$ have been formulated by DALITZ [1]¹⁾, and applied to the case of the deuteron by LAKINS and WOLFENSTEIN [2, 3]. General treatment of the higher order tensor moments has been given by SIMON and WELTON [4, 5], and GOLDFARB [6]. Numerous other theoretical treatments [7-13] are of value in understanding the tensor orientation problem, and in particular the review articles of WOLFENSTEIN [14], DEVONS and GOLDFARB [15], BLIN-STOYLE and GRACE [16], and BREIT and MCINTOSH [17] are very comprehensive.

In contrast to the polarization of spin $1/2$ particles, a physical picture for spin 1, or higher becomes considerably more complex. A particle of spin i will, in general, have non-zero irreducible tensor moments (T_q^k) up to a maximum rank of $2i$. A beam of rank zero is unoriented, a beam with only odd rank components is termed polarized (rank 1 corresponds to the usual vector polarization), a beam with only even rank components we call aligned (not necessarily along a single axis),

¹⁾ Numbers in brackets refer to References, page 179.

and a beam containing both even and odd tensor components is said to be oriented. Thus the general orientation of a deuteron beam will have $(2i+1)^2$ tensor components of rank 0 (one scalar normalized to unity), 1 (the three components of a pseudo-vector, the total spin), and 2 (the five components of an irreducible tensor). If \hat{i} is chosen along the beam (z) axis, then $T_1^{\pm 1} = 0$. Furthermore, the oriented states produced in simple reactions (two colliding particles in both entrance and exit channels) will have the spin and a principal axis of the tensor along the normal to the reaction plane, hence all values of $T_q^{\pm 1}$ vanish. Even so, it is apparent that considerable experimental information is required to uniquely determine all tensor components of the orientation.

Oriented deuterons may be produced from ionized atomic beams. There is, in particular, a group at the Oak Ridge National Laboratory engaged in such a project. J. E. SHERWOOD, R. F. KING, and S. J. OVENSCHINE [18] have under construction a machine of the Rabi-type where selection of the appropriate atomic hyperfine states is made by means of the «flop-in» technique. Presently the expected difficulties with the ionization stage of the problem are being investigated.

Scattering and reactions are also possible sources of oriented deuterons. Elastic deuteron scattering in He^4 (at the 1.069-Mev resonance as first suggested by GOLDFARB [6, 19,] see also PONDROM [20] and PHILLIPS [21]) and C^{12} , (p, d) and (n, d) reactions, whether proceeding by compound nucleus formation or «pick-up», (He^3, d) and (He^4, d) reactions are all possible sources of highly oriented deuterons. Thermal neutron capture in hydrogen has also been suggested [22] as an aligned deuteron source. The point is that there are many ways to obtain oriented deuteron beams, and hence convenient methods of analysis are desirable. In particular, an analyzer for low energy deuterons would serve as a great impetus in the development of oriented ion sources for injection into accelerators.

Before considering specific reactions, there are two important special conclusions that can be drawn regarding alignment with rank 2. First of all, the general expression [4, 5, 6] reveals that reactions, or scatterings induced by s-wave deuterons with even rank tensor alignment can give rise to non-isotropic angular distributions, provided that the compound state has total angular momentum greater than 1/2, and the emitted wave of particles has orbital angular momentum greater than 0. This is in contrast to spin 1/2 particles which can have only «vector» polarization (rank 1), and hence produce only spherically symmetrical angular distributions, independent of their state of polarization.

Secondly, alignment depends upon the real part of $R_1 R_2^*$, while odd rank polarization is a function of the imaginary part of $R_1 R_2^*$. (Here R_i is the usual reaction matrix element.) Thus, alignment can arise

from a *single* matrix element (single level of definite spin and parity formed (and decaying) by unique values of orbital angular momentum and channel spin). Furthermore, since the unoriented angular distribution also depends upon the real part of $(R_1 R_2^*)$, the alignment resulting from a single matrix element will be independent of the dynamics of the process (compound nucleus formation, pick-up process, etc.). It will be characterized by the geometry only. On the other hand, odd rank polarization is essentially an interference phenomena and hence requires at least two different elements in the reaction matrix.

A particularly good reaction illustrating both the above conclusions was first pointed out by GALONSKY, WILLARD, and WELTON [23] (see also GOLDFARB [24]). The $T(d, n)\text{He}^4$ reaction [25] has an isolated resonance at a deuteron bombarding energy of 107 kev. This state of total angular momentum $J = 3/2^+$ is formed by s-wave deuterons and decays by d-wave neutron emission. Unoriented beam angular distributions are isotropic up to about 500 kev, and the total reaction cross section is well fitted in this region by assumption of a single level. If aligned deuterons formed in the pure spin state $m_d = \pm 1$ interact with tritium, the angular distribution of the emitted neutrons will have a 0° to 90° asymmetry ratio of 2 to 5 (in the center of mass system where the axis of quantization has been taken along the incident beam direction). If the deuterons are produced in the pure spin state $m_d = 0$, this ratio will be 4 to 1. (Note that the distribution depends upon the expectation value of m_d^2 , and hence is identical for $m_d = +1$ and $m_d = -1$.) More general types of tensor alignment [6, 24] also produce large asymmetries, and because of its large cross section (5 barns at resonance) this reaction should serve as a useful analyzer of deuteron alignment from about 25-kev to 500-kev deuteron energy. It should be possible to detect very weak beams of low alignment by discriminating against the usual troublesome gamma-ray background in high efficiency neutron detectors, with pulse shape differentiation [26]. Finally, under suitable choice of the second rank tensor components of the deuteron alignment, this reaction may serve as a source of completely polarized 14-MeV neutrons.

The mirror reaction $\text{He}^3(d, p)\text{He}^4$ has also an isolated resonance of similar properties [25], except displaced to about 430 kev and reduced in peak cross section to about 0.7 barns by the Coulomb barrier. Unoriented angular distributions for this reaction are spherically symmetric up to about 800 kev, and this reaction should serve as a useful alignment analyzer from 250 kev up to the former energy. Furthermore, the higher efficiency for proton detection (100 per cent) will approximately compensate the lower cross section. Background discrimination should be extremely favorable.

These two reactions are most attractive for aligned deuteron ion source development, since it is possible to construct the apparatus at ground potential where unlimited space and power are available. The oriented beam can be accelerated to a few hundred kev in an air operated Cockcroft-Walton, or similar machine, and the asymmetry then measured in the terminal. Such a scheme is planned at Oak Ridge [18].

A third possible choice for s-wave analysis of deuteron alignment is provided by the $C^{12}(d, p)C^{13}$ reaction, long a source of polarized protons. In particular, there is a broad (140 kev) $J = 1^+$ level at 940 kev formed by s-wave deuterons and emitting p-wave protons [25]. We have used the formalism of GOLDFARB [6] to calculate the angular distribution of protons for a deuteron beam of arbitrary orientation. The analysis is somewhat complicated by the two possible combinations of exit channel angular momenta. This is because oriented beams may, in general, interfere coherently in the exit channel spin, thus the usual simplifications in this representation are lost. We find that

$$W = W_0 \left[1 - \frac{(1/2 + \sqrt{2}x)}{1 + x^2} \right] \left\{ P_{33} P_2^{(0)}(\cos \theta) + 2/3 (P_{13} \cos \chi + P_{23} \sin \chi) P_2^{(1)}(\cos \theta) + \frac{1}{6} [(P_{11} - P_{22}) \cos 2\chi + 2 P_{12} \sin 2\chi] P_2^{(2)}(\cos \theta) \right\}$$

where W_0 is the angular distribution of an unoriented beam (isotropic), x is the mixing ratio of $j_{out} = 1/2$ to $j_{out} = 3/2$, j is the vector addition of outgoing particle spin and orbital angular momentum,

$$P_{ij} \equiv \frac{3}{2\hbar^2} [\vec{i}_i \cdot \vec{i}_j + \vec{i}_j \cdot \vec{i}_i] - 2 \delta_{ij},$$

$\vec{i} = \hbar \mathbf{P}$ is the *vector* spin orientation of the deuteron,

χ is the angle between the y-axis used to describe the orientation of the incident beam (z-axis) and the normal to the plane of the reaction, and

$P_2^{(k)}(\cos \theta)$ is an associated Legendre polynomial.

The results in channel spin representation can easily be obtained from the unitary transformation equation of SATCHLER [27]. For example, a beam with pure channel spin zero has $x = 1/\sqrt{2}$, and pure channel spin one has $x = -\sqrt{2}$.

In the pure spin states $m_d = \pm 1$, $P_{11} = P_{22} = -2$, $P_{33} = +1$, and $P_{12} = P_{23} = P_{13} = 0$. The angular distribution then simplifies to

$$W = W_0 \left[1 - \frac{(1/2 + \sqrt{2}x)}{(1+x^2)} \cdot P_2(\cos \theta) \right].$$

Similarly, the pure $m_d = 0$ state has $P_{11} = P_{22} = +1$, $P_{33} = -2$, and $P_{12} = P_{23} = P_{13} = 0$, with the resultant distribution

$$W = W_0 \left[1 + \frac{(1+2\sqrt{2}x)}{(1+x^2)} \cdot P_2(\cos \theta) \right].$$

It is quite apparent then that this reaction will have large observable asymmetries over the deuteron energy range 800 to 1100 kev. However, the assumption of an isolated resonance used in the above calculations is not as well justified as in the first two reactions considered. There is, in fact, a broad $J = 2^-$ level at 1.16 MeV [25] which produces interference in the unoriented angular distribution. The effect of neighboring levels will be considered in a more detailed treatment to appear later.

Thus the three reactions considered in this paper will serve as convenient analyzers of second rank tensor deuteron alignment over the energy range 25 to 1100 kev. Because of their broad character, the first two reactions may be used as general analyzers of almost any energy deuterons, since the deuterons may be slowed down by foils to the effective energy interval.

Although, first considered for their utility in oriented beam ion source development, these reactions may also serve as the second stage reaction in a double «scattering» experiment, where the first stage may be, for example, (p, d) «pickup», [28, 30] or (He^3, d) stripping. In particular it may be of some interest to orient deuterons by the $\text{C}^{13}(p, d)\text{C}^{12}$ reaction and then analyze by the inverse reaction, $\text{C}^{12}(d, p)\text{C}^{13}$. In a two stage process, care must be taken in the transformation of the spin tensors from the laboratory to the center of mass system [29]. In addition, conversion of tensor components by deflection in magnetic fields [3, 29] may be helpful in unraveling the complicated tensor alignment. Experiments of this general nature are in the planning stage at Oak Ridge.

REFERENCES

- [1] R. H. DALITZ, Proc. Phys. Soc. *A* **65**, 175 (1952).
- [2] W. LAKINS and L. WOLFENSTEIN, Phys. Rev. *90*, 365A (1953).
- [3] W. LAKINS, Phys. Rev. *98*, 139 (1955).
- [4] A. SIMON and T. A. WELTON, Phys. Rev. *90*, 1036 (1953).
- [5] A. SIMON, Phys. Rev. *92*, 1050 (1953). *Erratum*, Phys. Rev. *93*, 1435E (1954).
- [6] L. J. B. GOLDFARB, Nuclear Phys. *7*, 622 (1958).
- [7] H. STAPP, Phys. Rev. *107*, 607 (1957).
- [8] S. W. MACDOWELL, Ann. Acad. Brasil. de Ciencias *28*, 71 (1956).
- [9] S. W. MACDOWELL and J. TIOMNO, Ann. Acad. Brasil. de Ciencias *28*, 157 (1956).

- [10] O. D. CHEISHVILI, JETP (USSR) 3, 974 (1957), 5, 1009 (1957).
- [11] S. WATANABE, Rev. Mex. de Fisica 6, 59 (1957).
- [12] C. B. VAN WYK, Nuovo cimento (10) 9, 270 (1958).
- [13] S. WATANABE, Nuclear Phys. 8, 484 (1958).
- [14] L. WOLFENSTEIN, Ann. Rev. Nuclear Sci. 6, 43 (1956).
- [15] S. DEVONS and L. J. B. GOLDFARB, *Angular Correlations*, Handb. d. Physik XLII, 443 (Springer 1957).
- [16] R. J. BLIN-STOYLE and M. A. GRACE, *Oriented Nuclei*, Handb. d. Physik XLIII, 555 (1957).
- [17] G. BREIT and J. S. MCINTOSH, *Polarization of Nucleons Scattered by Nuclei*, Handb. d. Physik XLI, 466 (1959).
- [18] J. E. SHERWOOD, R. F. KING, and S. J. OVENSCHINE, Bull. Southeastern Section Amer. Phys. Soc., April 1960.
- [19] L. J. B. GOLDFARB and J. R. ROOK, Nuclear Phys. 12, 494 (1959).
- [20] L. G. PONDROM, Phys. Rev. Letters 2, 346 (1959).
- [21] R. J. N. PHILLIPS, Phys. Rev. Letters 3, 101 (1959).
- [22] M. E. ROSE, Phys. Rev. Letters 3, 387 (1959).
- [23] A. GALONSKY, H. B. WILLARD, and T. A. WELTON, Phys. Rev. Letters 2, 349 (1959).
- [24] L. J. B. GOLDFARB, Nuclear Phys. 12, 657 (1959).
- [25] F. AJZENBERG-SELOVE and T. LAURITSEN, Nuclear Phys. 11, 1 (1959).
- [26] F. D. BROOKS, Nuclear Instr. 4, 151 (1959).
- [27] G. R. SATCHLER, Proc. Phys. Soc. (London) 66A, 1081 (1953).
- [28] G. R. SATCHLER, Nuclear Phys. 6, 543 (1958).
- [29] G. R. SATCHLER, Oak Ridge National Laboratory Report ORNL-2861 (unpublished) (1960).
- [30] K. E. GREIDER, Nuclear Phys. 14, 498 (1960).

Production of Polarized Neutron Beams by (p, n) Reactions in Various Nuclei

By J. P. SCANLON, A.E.R.E., Harwell

Introduction

The work that is the subject of this talk was carried out at the Atomic Energy Research Establishment, Harwell, by a team consisting of the following people,

P. H. BOWEN, G. C. COX, G. B. HUXTABLE, J. P. SCANLON,
J. J. THRESHER, A. E. R. E., Harwell;
A. LANGSFORD, Clarendon Laboratory, Oxford, .

and we were also assisted for some time by H. APPEL, on leave from the University of Mainz.

The production and measurement of high energy polarized neutron beams was part of a programme of research carried out using a neutron time-of-flight spectrometer in conjunction with the Harwell cyclotron. Using this equipment, measurements had previously been made with unpolarized neutrons, including the determination of neutron total cross-sections in the energy range 15–125 MeV for a wide range of elements, and the angular distribution of neutron-proton scattering in the range 30–120 MeV. A source of polarized neutrons covering a similar energy range was needed in order to extend this work.

Neutron Time-of-Flight Spectrometer

The apparatus has been described in detail (SCANLON, STAFFORD, THRESHER and BOWEN [1]¹), so the remarks here will be confined to a brief outline.

Neutrons are produced by allowing 143 MeV protons to strike an internal target in the cyclotron (figure 1). As each accelerated proton bunch reaches a mean radius of 112 cm it is deflected electrostatically onto a target which is placed above the magnetic median plane and hence

¹) Numbers in brackets refer to References, page 192.

is not in the path of the undeflected protons. In this way, 200 bursts of neutrons are produced per s at the target, and the duration of each burst is 9 ns measured as a full width at half height.

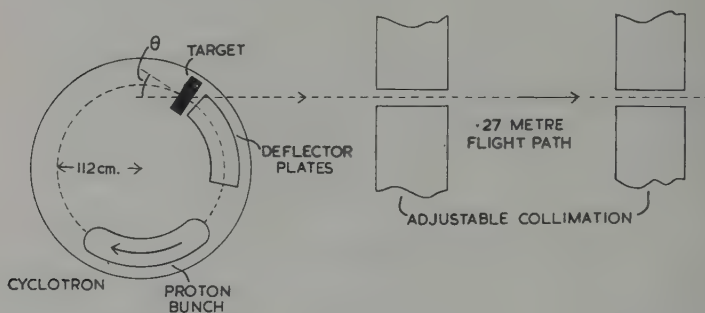


Figure 1

The collimated flight path is 27 m long, and the energy of any neutron which is detected at the end of the flight path is determined by measuring its time of flight over the known distance from the target. This time is obtained from the interval between two pulses, the first corresponding to the deflection of the proton bunch, and the second to the detection of the neutron. The energy resolution depends on the duration of the neutron burst and the length of the flight path. The figures quoted above correspond to $13\frac{1}{2}\%$ at 130 MeV and $3\frac{1}{2}\%$ at 30 MeV.

One big advantage of this technique is that providing the necessary neutrons come along the flight path and that suitable neutron detectors are used, one can cover a large range of neutron energies in a single experiment.

Production of a Polarized Neutron Beam

In general, some degree of polarization will be expected in the neutrons scattered at angles other than 0° from targets bombarded by high energy protons. However, to achieve the most useful beam it is necessary to maximize the quantity $P_1^2 N$, where P_1 is the polarization of the beam and N the intensity. For doing this with a given geometry, three possible variable parameters were target material, target thickness and angle of scattering. On the basis of previous work one could say that in the range of scattering angles $\theta = 0 - 45^\circ$, N might be expected to decrease and P to increase as θ increased.

The first target material to be tried was lithium deuteride, as this had given the largest neutron yield for 0° scattering of all materials used.

Furthermore it was hoped that a reasonable degree of polarization might result from 'quasi-free' p - n scattering in deuterium. The target thickness was 28 MeV, and scattering angles of 25° , 35° , and 45° were used. A similar set of measurements was made with an aluminium target of 55 MeV thickness, and one thick enough to stop the incident protons completely was tried at 35° . Finally, to try to gain a little more insight into the physical processes involved, some measurements were made of the neutrons produced from thin (~ 3 MeV) targets of lithium hydride, lithium deuteride and aluminium.

The Polarization Analyser

The technique used was that suggested by SCHWINGER [2]. It depends on the fact that the small angle scattering of neutrons by nuclei is polarized due to the interaction of the magnetic moment of the neutron with the Coulomb field of the target nucleus. The magnitude of the effect can be estimated with reasonable accuracy, and it occurs at scattering angles small enough for the polarization from nuclear interactions to be negligible. The basic principle was therefore to measure the asymmetry between left and right scattering through an angle θ of the polarized beam by a suitable target (figure 2).

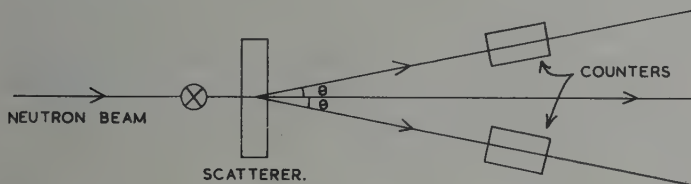


Figure 2

In order to find out the best conditions for doing this, the scattering process must be considered in rather more detail. The neutron will see an effective magnetic field as it rushes past the electric charge of the nucleus, so that its magnetic dipole will have a potential energy $V = -\boldsymbol{\mu} \cdot \mathbf{H}$. This can be regarded as a small perturbation to the specifically nuclear interaction, and assuming the nuclear part of the scattering amplitude to be unpolarized, a plane wave Born approximation calculation gives the differential cross-section at angle θ as

$$\sigma(\theta) = \left[|f_0(\theta)|^2 + \gamma^2 \cot^2 \frac{\theta}{2} \right] - 2 \operatorname{Im} \{f_0(\theta)\} \gamma \cot \frac{\theta}{2} \cdot \mathbf{n} \cdot \mathbf{P}_1 \quad (1)$$

where θ is the C of M scattering angle, $f_0(\theta)$ is the nuclear scattering

amplitude, \mathbf{n} is the unit vector defining the plane of scattering, \mathbf{P}_1 is the polarization vector of the incident beam, and $\gamma = \frac{1}{2} |\mu_n| Z e^2 / M c^2$ where the intrinsic magnetic moment μ of the neutron is defined as $\mu = -|\mu_n| \sigma e \hbar / 2 M c$, σ being the Pauli spin matrix. The asymmetry for left-right scattering is

$$A = \frac{-2 \operatorname{Im} \{f_0(\theta)\} \gamma \cot \frac{\theta}{2} \cdot \mathbf{n} \cdot \mathbf{P}_1}{\left[|f_0(\theta)|^2 + \gamma^2 \cot^2 \frac{\theta}{2} \right]} = P_2 (\mathbf{n} \cdot \mathbf{P}_1). \quad (2)$$

The denominator is the unpolarized differential cross-section, which can be measured. Also, for sufficiently small angles ($\sim 1^\circ$) we may say

$$\operatorname{Im} \{f_0(\theta)\} \simeq \operatorname{Im} \{f_0(0)\} \simeq \frac{K \sigma_T}{4 \pi}$$

by the optical theorem. We can measure σ_T .

P_2 which may be called the analysing efficiency of the system, varies as shown in figure 3, having a maximum amplitude in the neighbourhood of $1/4^\circ$. This is not necessarily the best angle at which to measure the scattering however, from the following considerations. Suppose a counter of finite size is placed as close as possible to the transmitted beam, also of finite size (figure 4); the optimum position for the counter will be that which gives the maximum value of the quantity $P_2^2 \Omega \cdot \sigma(\theta)$ where Ω is the solid angle subtended at the scatterer by the counter. If θ is varied by changing the distance between the counter and scatterer the following type of curve is obtained (figure 5). Substantial gains can be made by moving out as far as 2° or so. There are still several reasons why θ should be kept as small as possible however.

a) The approximation $\operatorname{Im} f_0(\theta) = \operatorname{Im} f_0(0)$ will break down at larger angles.

b) Nuclear polarization will cease to be negligible as θ increases.

c) The effect of false asymmetries is reduced by keeping P_2 as large as possible.

d) The plane wave Born approximation calculation becomes less valid as θ is increased.

e) The calculation of P_2 assumes a point nucleus. The error in this assumption increases rapidly as θ is increased.

From these considerations it was decided to use a scattering angle of 1° , and because $P_2 \propto \gamma \propto Z$, Uranium was used as the scattering material.

The experimental arrangement is shown schematically in figure 6. The beam was approximately 2 cm by 5 cm in cross-section and the Uranium scatterer was 2.5 cm thick. The scattering was measured simultaneously on both sides of the beam by two liquid scintillation

counters 48 cm long 2.5, cm thick and 7.5 cm wide. In addition, the magnetic field from a solenoid was used to reverse the polarization direction of the neutron beam. As the angle through which the neutron spin precesses in a given integrated magnetic field depends upon the neutron velocity, it was possible to turn it through $+$ and $- 90^\circ$ for only one energy. This was chosen to correspond to the mean velocity of the spectrum between 20 and 120 MeV, which corresponded to 42 MeV. For other energies, if $\pm \alpha$ is the angle of precession of the neutron spin, the value of P_1 calculated from the measured asymmetry has to be multiplied by $\text{cosec } \alpha$. The correction amounts to about 25% at 120 MeV and 20% at 20 MeV.

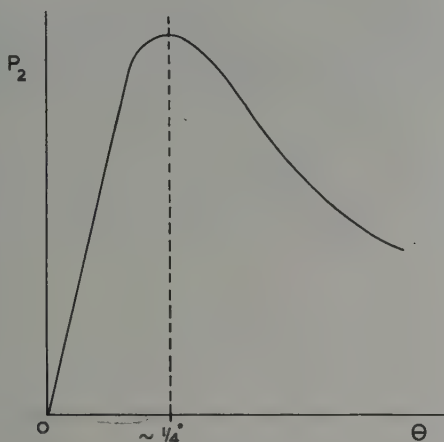


Figure 3

To minimize scattering from the 'straight through' beam into the counters, a hydrogen path was used, and the neutrons travelled a further 6 m into a beam trap. The residual background rates, which amounted to about 25% of the total counting rates were determined by putting 40 cm of steel directly in front of the counters to block the neutrons scattered from the uranium.

There are a number of advantages in using the system of two counters together with a solenoid. If the counter efficiencies are defined as ϵ_1 and ϵ_2 , the number of neutrons scattered left and right per unit incident flux as L and R , and I^+ and I^- the incident fluxes for measurements made with clockwise and anti-clockwise precession, the ratio of neutrons detected in the two counters is $I^+ L \epsilon_1 / I^- R \epsilon_2$, and for anti-clockwise precession $I^- R \epsilon_1 / I^+ L \epsilon_2$. Dividing these two ratios together gives L^2 / R^2 from which

A can be calculated. The result is independent of changes in beam intensity, so that the system is self-monitoring, and also independent of the counter efficiencies, so long as they remain constant.

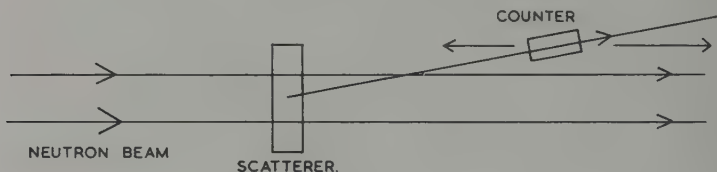


Figure 4

A monitor is still needed to normalize the measurements of backgrounds, but as this is only some 25% of the total, the monitoring can be proportionately less accurate.

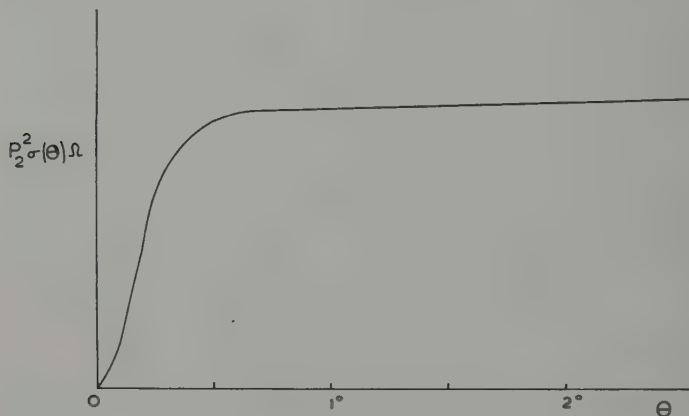
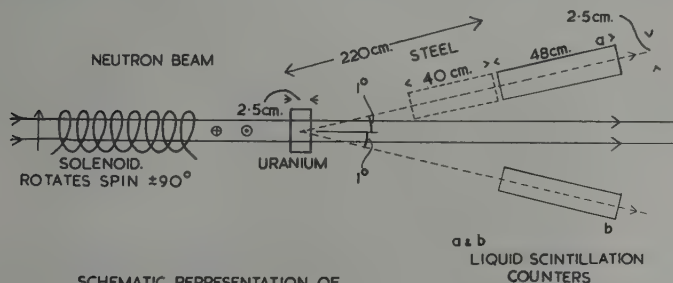


Figure 5

An even more important advantage lies in the greater precision with which the geometry may be defined. The centre line of the neutron beam can certainly not be defined to better than 1 mm, so this limits the accuracy to which the angle of a single counter can be set. However, when two counters are used, the angle between them can be set to a much greater accuracy, and any false asymmetries which result if they are not placed symmetrically about the beam line cancel out to first order when measurements are made with the polarization vector reversed. For conditions which would give a 5% false asymmetry using a single counter, the error is reduced to 0.1% for a double counter system.

Finally, by using two counters the information is obtained in half the time that would be taken using a single counter.



SCHEMATIC REPRESENTATION OF
POLARIZATION ANALYSER

Figure 6

The total neutron cross-section of Uranium was measured over the energy range 15–120 MeV by a transmission experiment in good geometry, and the 1° differential cross-section was determined by comparing the number of neutrons scattered at 1° with the number in the incident beam, using an unpolarized beam and the same experimental arrangement.

Corrections

Eq. (1) and (2) may be expressed more simply as

$$\sigma(\theta) = X(\theta) + Y(\theta) P, \quad (3)$$

$$P_2 = \frac{Y(\theta)}{X(\theta)}. \quad (4)$$

and these relations apply strictly to a point source and scatterer. In practice these conditions were not fulfilled owing to the finite extent of the scatterer and counters, and neutrons were detected which had been scattered over a range of angles in different scattering planes. This was further complicated by the variation in intensity of the neutron beam over its cross-sectional area, and a small variation of efficiency over the area of the counters. The last two effects were determined by subsidiary measurements. There was also a 10% probability that a scattered neutron would be scattered at least once more before leaving the uranium.

However, it is still true to say that

$$(\text{observed scattering}) = x + y P_1, \quad (5)$$

$$(\text{effective analysing power}) = \frac{y}{x} \quad (6)$$

so that if the cross-section measurement is made in the same geometry as the asymmetry measurements, what actually is measured is x . Thus when calculating the effective analysing efficiency of the system no corrections have to be applied to x , and the only corrections which must be considered are those applying to y . The geometrical effects result in the effective value of P_2 being reduced by about 25%.

The effects of multiple scattering are very difficult to evaluate but the most pessimistic estimate gives a 2% correction.

Experimental Results

Figure 7 shows the values of P_2 obtained as a function of energy. These are fairly constant at a value of about 0.25 for energies down to 80 MeV, and then rise fairly sharply to 0.3 or more. The rise is correlated with a fall in the measured value of the differential scattering cross-section which

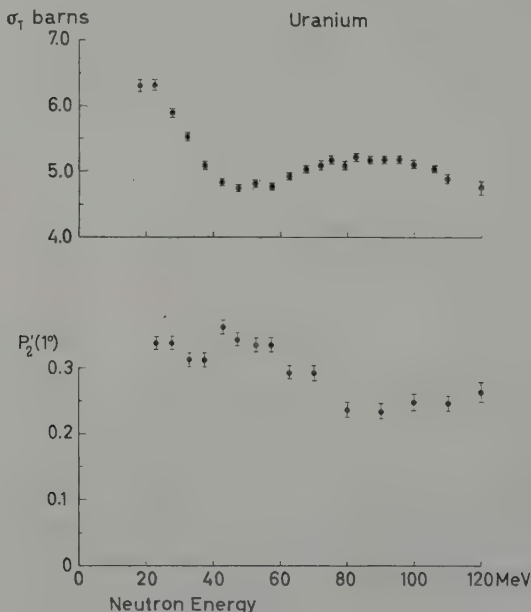


Figure 7

occurs at the energy of the maximum in the total cross-section curve. Such a variation is consistent with the optical model picture of nuclear scattering.

Figure 8 shows values of neutron polarization obtained as a function of energy for 25° scattering from the 28 MeV lithium deuteride target and the 55 MeV aluminium target.

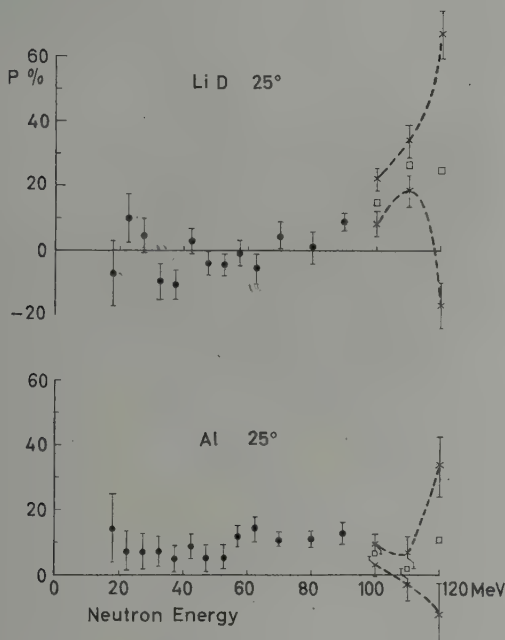


Figure 8

For lithium deuteride the polarization is effectively zero between 20 and 80 MeV, but becomes positive at higher energies. The result for aluminium is rather more encouraging, there being a polarization of about 10% at most energies. The alternative extreme values shown for energies of 100 MeV and above are due to a shortcoming in one of our earlier techniques. The velocities of neutrons detected in the two counters were analysed in separate timing channels, and as the number of neutrons per MeV was a rapidly varying function of energy in this region, a small uncertainty in the lining up of the two timing channels led to a large but systematic uncertainty in the measured asymmetries.

Figure 9 shows results for scattering at 45° from the same targets. Here the polarization of neutrons from lithium deuteride actually changes sign and becomes negative below 55 MeV. From aluminium the polarization is consistently positive, varying smoothly between about 0.15 at 20 MeV and 0.40 at 120 MeV.

The results obtained for a scattering angle of 35° lie in between those shown for 25° and 45° , and the effect of using a thicker aluminium target which completely stops the incident protons is simply to reduce slightly the number of high energy neutrons escaping from the target, and to reduce P_1 slightly at lower energies.

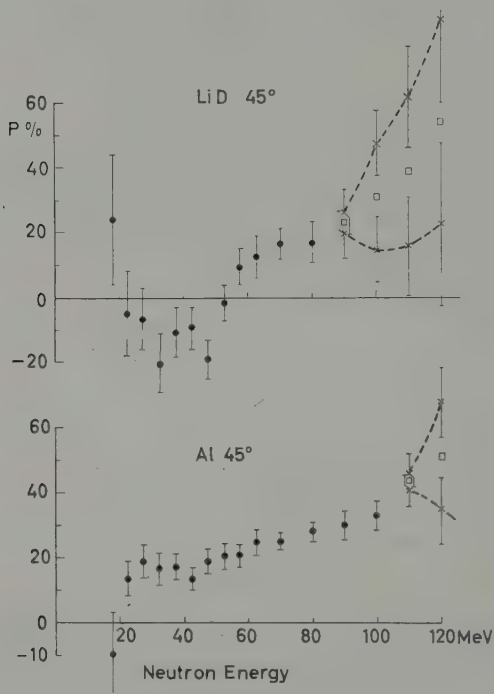


Figure 9

The foregoing results rule out the first choice of lithium deuteride as a polarizing target, and comparing the performance of aluminium at different angles, the most useful beam is obtained at 45° . The fall in intensity between 25° and 45° is more than compensated by the increase in polarization. Some results of CARPENTER and WILSON [3] indicate that a slight further increase of polarization might be obtained by observing scattering at about 55° , but it is doubtful whether this would compensate for the decrease in intensity which would result. Their results also indicate that no significant increase in P_1 would be obtained by using elements heavier than aluminium. It was therefore decided to use a

55 MeV target of Aluminium observed at 45° as the standard polarized neutron source.

Figure 10 shows the results obtained for neutron scattering from thin targets at 45° . The results for deuterium were obtained as the difference between those for lithium, deuteride and lithium.

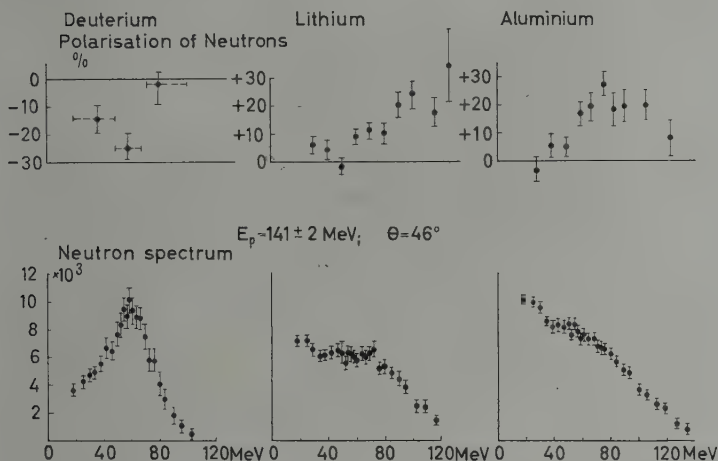


Figure 10

The peak at 60 MeV in the neutron spectrum from deuterium is consistent with quasi-free $p-n$ scattering, as is the sign and magnitude of the corresponding polarization. For lithium and aluminium the expected energy for quasi-free $p-n$ scattering at 45° would be approximately 50 MeV, but at this energy instead of a negative polarization the value is in fact close to zero, while at higher energies both give a large positive polarization.

A qualitative explanation of this has been given by SQUIRES [4]. He regards the scattering process as a quasi-free $p-n$ scattering within the nucleus, and considers the modifications introduced by the nuclear potential and by double and higher order scattering. He concludes that the effect of the nuclear potential could not change the sign of polarization observed, but that multiple scattering within the nucleus is liable to predominate and can easily give the opposite sign. For instance in the present case of $\theta = 45^\circ$, the most likely type of double scattering to give 45° is made up from two single scattering of about $22\frac{1}{2}^\circ$ each. At that angle the signs of $p-n$, $p-p$ and $n-n$ polarizations are positive so that

the outgoing neutrons produced in this way will have a positive polarization.

The large difference between polarizations produced by deuterium and by heavier elements is explained therefore by the greater likelihood of multiple scattering in the larger nuclei, and the low polarizations from our lithium deuteride target are simply due to the fortuitous cancellation of the effects from deuterium and lithium.

REFERENCES

- [1] J. P. SCANLON, G. H. STAFFORD, J. J. THRESHER, and P. H. BOWEN, R. S. I. 28, 749 (1957).
- [2] J. SCHWINGER, P. R. 73, 407 (1948).
- [3] S. G. CARPENTER and R. WILSON, P. R. 113, 650 (1959).
- [4] E. J. SQUIRES, Proc. Phys. Soc. 72, 433 (1958).

Survey of Measurements in Stripping Reactions

By B. HIRD, Liverpool University

I want first to state some rules which current stripping theories provide before I describe the measurements so that I can make comparisons as I go along.

The simplest stripping theory, BUTLER's or BORN Approximation, the one often used by nuclear spectroscopists to find spins and parities, gives always zero polarization, so polarization measures the inadequacies of this theory directly.

The next lowest order approximation, and one which has received extensive theoretical treatment supposes the incoming deuteron and emitted nucleon to pass through a distorting potential which is purely central. The emitted nucleon polarization then obeys the following rules:—

$$P \leq \frac{1}{3}$$

$$P_{l=0} = 0$$

$$\begin{aligned} \left[\left(j + \frac{1}{2} \right) P \right]_{j=l+1/2} &= - \left[\left(j + \frac{1}{2} \right) P \right]_{j=l-1/2} = \left[\frac{1}{3} \left(j + \frac{1}{2} \right) P_{nuc} \right]_{j=l-1/2} = \\ &= \left[\frac{j(j+1/2)}{3(j+1)} P_{nuc} \right]_{j=l+1/2} \end{aligned}$$

$$A = 3 P \cdot P_d$$

for reactions with the same l and the same distorting potentials.

here j and l refer to the captured nucleon, the parameters which spectroscopists are finding when they do stripping. The relations involving P_{nuc} , the polarization of the final nucleus, are restricted to spin zero target reactions. The last formula relates the asymmetry A in stripping with polarized deuterons which have vector polarization P_d to the emitted nucleon polarization produced by the same reaction with unpolarized

deuterons. It also seems from semiclassical pictures and actual calculations that the deuteron and emitted nucleon distortions each give opposite signs of polarization, and the resulting sign is to some extent a measure of their relative importance.

Spin dependence in the deuteron, or emitted nucleon distorting potential, invalidates all these relations and there then seem to be no general rules, except perhaps for $P_{l=0}$ reactions when we have rules which are effectively extensions of those for scattering processes, with the polarization coming from the spin dependence of the distorting potentials and not depending directly on the properties of the captured nucleon.

The measurements fall into three distinct energy regions, which I will discuss separately starting at the lowest energies.

JURIĆ and ĆIRILOV [1]¹⁾ have measured the energy dependence of the $C^{12}(d, p)C^{13}$ polarization around 1 MeV (figure 1). The differential cross section at these energies shows strong resonances and its angular variation is completely different from a Butler type curve, showing a forward and backward peak. JURIĆ and ĆIRILOV measured near these peaks, at 20° and 140° . There is a resonance at 1.16 MeV and they varied the bombarding energy across it.

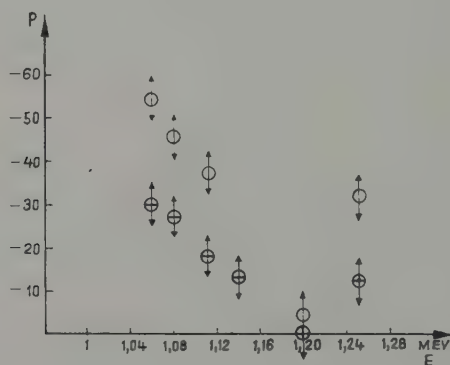


Figure 1

Their experimental method was to analyse the polarization of the protons by scattering them from carbon. The phase shifts for this are known in the appropriate energy region. Carbon offers obvious experimental advantages over helium as an analyser, but the phase shift analysis is yet not as accurate (EVANS and GRACE [2]). It is quite

¹⁾ Numbers in brackets refer to References, page 200.

obvious that here resonance effects predominate, and it may not be valid to consider this with a direct interaction theory at all. However quite good theoretical fits to the differential cross section have been made by including the Coulomb distortions in the deuteron and proton interactions and assuming the resonance to occur in the orbital angular momentum 2 partial wave of the emitted protons. Perhaps this theoretical approach will also succeed in fitting the polarization if some appropriate total spin for the partial wave is assumed.

Most polarizations have been measured at somewhat higher energies where stripping is well established as the main mechanism and the differential cross sections show in most cases clearly defined stripping peaks.

With one exception, all measurements in this medium energy region have been made by substantially the same method, differing only in details. I will show one particular arrangement as typical. Figure 2 shows the apparatus of JUVELAND and JENTSCHKE [3]. Some workers include a strong focussing magnet to focus the protons into the helium analyser, this seems worthwhile doing because it can give a factor 50 increase in the proton to background ratio. The helium analysers vary in detail. Sometimes a venetian blind slit system is used to define the scattered proton direction, and sometimes this is deduced from the directions of the emulsion tracks. The phase shifts for the helium scattering are now known sufficiently well over all this energy region to predict its analysing power to perhaps a few percent.

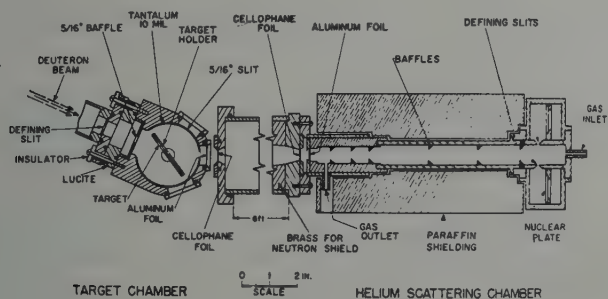


Figure 2
Schematic diagram of the apparatus

The reaction most investigated is $C^{12}(d, p)C^{13}$. Figure 3 shows a combined plot of all measurements on the ground state proton polarization. Ignoring the 1.06 MeV points which are from JURÍĆ and ĆIRILOV

data, the only evidence of resonance behaviour is the 4 MeV point obtained by HILMAN otherwise the energy variation seems to be too slight to identify clearly from these results. Obvious features of the polarization are that it is fairly small near the stripping peak which is somewhere near 20 to 30° at these energies, and then a rise to a magnitude which is definitely more than the $1/3$ predicted by the central distortion theory. At larger angles still we have only one point to indicate the change of sign which is expected theoretically at some angle near to the minimum of the differential cross section. This sign change comes from assuming that the distortion effects provide a small perturbation to the simple stripping, so that the sign of the polarization changes with the sign of the simple stripping amplitude.

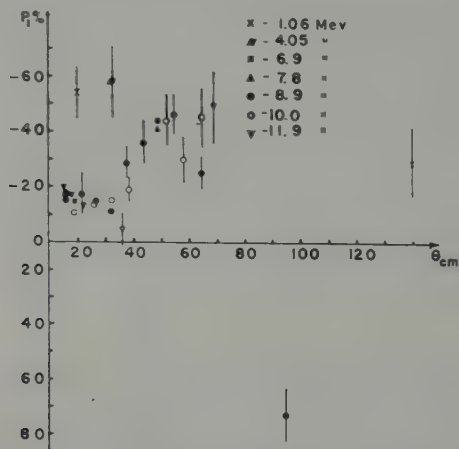


Figure 3

All known polarization measurements on $C^{12}(d, p)C^{13}$

The overall experimental sign of the polarization indicates that the deuteron central distortion effects predominate over the proton distortion effects in producing this polarization.

There is rather fragmentary experimental data on a range of other reactions in this energy region, mostly obtained by the same experimental system as for the carbon measurements. An exception to this is the method used by CHASE and IGO [6] to find the sign of the B^{12} polarization from the $B^{11}(d, p)B^{12}$ reaction. They looked at the forward-backward asymmetry of the β decay of the B^{12} final nucleus. On the central force distortion theory, the final nucleus has the same sign polarization

as the outgoing protons when $j = l + 1/2$ and the opposite sign when $j = l - 1/2$.

The results in the medium energy range can be summarised by saying that, apart from two reactions, the sign of the polarization has always been found to indicate predominating deuteron distortions. One of the exceptions is $B^{10}(d, p)B^{11}$ to the first excited state. HENSEL and PARKINSON [7] showed that this has opposite sign to the ground state. This reaction has an $l = 1$ angular distribution but a spin change of $5/2$ is required to fit the energy level spins. Two theories have been suggested for this reaction, both of which would predict the anomalous proton polarization. One is that a normal $l = 1$ transition is followed by spin flip of the emitted proton interacting with the final nucleus. This process would of course require a noncentral proton interaction. The other suggestion is exchange stripping, where the two nucleons from the deuteron are both absorbed and the emitted proton, with opposite spin direction, comes from the initial nucleus.

The other exception to the polarization sign rule is $Ca^{40}(d, p)Ca^{41}$, which should be $l = 3$ and $j = 7/2$, but has been found to emit protons with positive polarization in the stripping peak. Distorted wave calculations have not yet been made for nuclei as large as calcium. A possible explanation of the sign is that some size resonance effect in the distorted waves could make the polarization produced by the proton distortion the more important in these larger nuclei. It should be possible to investigate this both theoretically and experimentally.

There are some measurements on $l = 0$ reactions. Any polarization here cannot be caused by the central distorting potentials. HENSEL and PARKINSON [7] measured the polarization of the proton group corresponding to stripping to the 3.09 MeV level in C^{13} . At 15° the polarization was found to be zero, but when they measured further away from the forward stripping peak, at 45° , they found $\pm 21\%$ polarization.

Very little has been done on (d, n) stripping polarization. I am excluding consideration here of the $D(d, n)He^3$ reaction which has been discussed by HAEBERLI. There are some measurements in progress by a group in Cracow using a helium counter as a polarization analyser and taking coincidences between the recoil helium and the scattered neutron in a separate counter.

In Liverpool we have been doing some measurements with polarized deuterons of about 6 MeV.

The deuterons were first polarized by scattering them from carbon and we then measured the left-right asymmetry in $Be^9(d, p)Be^{10}$. The angular variation of the ground state and first excited state group asymmetries is shown in figure 4. The ground state polarization angular distribution seems to be quite similar in shape to that found for the

proton polarization in $C^{12}(d, p)C^{13}$, as should be expected from the last of the central distortion theory rules, since the stripping peaks and minima of the two reactions occur at roughly similar angles. The opposite signs of the asymmetries of the ground and first excited state groups is also expected from the central distortions because the neutron coupling of one is $j = l + 1/2$, it could be mainly $j = l - 1/2$ in the other. This opposite sign would not be produced by the spin dependent part of the distortions, which ought to be very similar for both proton groups and give similar polarizations. Unfortunately the deuteron vector polarization was not known in these measurements and also tensor polarization have an unknown effect. To make a real test of the last of the central distortion theory rules it will be necessary to measure the asymmetry using deuterons which have known polarization on a reaction where the proton polarization has already been measured. It is possible that the rule might be more generally valid than the central distortion theory but with the factor 3 modified somewhat.

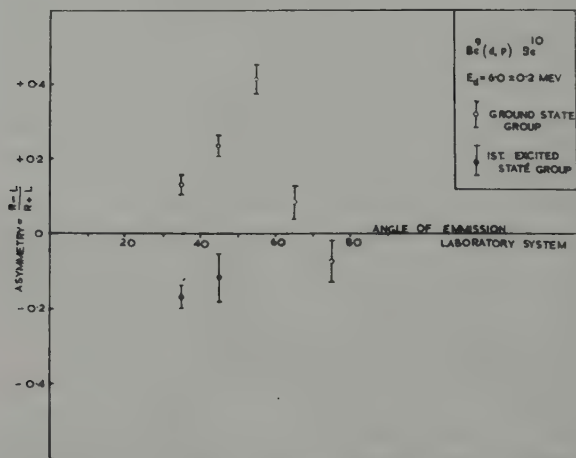


Figure 4
Proton Stripping Asymmetry with Polarized Deuterons

Lastly I want to mention some measurements at much higher energies which I think are relevant. These are (p, d) pick up asymmetry measurements at 145 MeV on carbon by COOPER and WILSON [8] made with a polarized proton beam. They represent the inverse of the stripping polarization measurements. At these energies the energy spectrum

of the deuterons shows a peak corresponding to the production of the C^{11} nucleus in its ground state. COOPER and WILSON measured the angular distribution of the asymmetry of these deuterons and their results are shown on figure 5. The line is a theoretical calculation by GREIDER where the neutron spin coupling is entirely neglected and where the asymmetry arises purely through the spin dependence of the proton and deuteron distorting potentials. As is well known from elastic scattering processes the oscillations in the differential cross section and polarizations which are seen at medium energies are smoothed out when the energy becomes high enough for the wavelengths to be of the order of many times the nuclear surface thickness. The same thing seems to have happened here where there is no sign of an $l = 1$ peak at some small angle in the pick-up differential cross section. Oscillations in the asymmetry which might have been associated with this peak in the same angular region are completely absent. The asymmetry is certainly very small at forward angles.

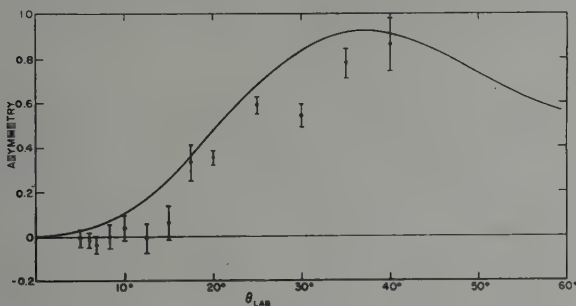


Figure 5

Asymmetry in the reaction $C^{12}(p, d)C^{11}$ by a 100% polarized beam.
The theoretical curve is a fit by GREIDER.

The general situation in stripping polarization measurements is that they have established the central distortion theory as being qualitatively but only qualitatively valid for most reactions in the medium energy region. The agreement is sufficiently good however that polarization measurements could probably be used with a fair degree of certainty in this energy region to fix the predominating j of the captured nucleon.

On the other hand a comparison of polarization measurements with a full theoretical calculation, including spin dependent forces, could give information about the optical model potential which would supplement that obtained more directly from scattering measurements.

REFERENCES

- [1] S. D. CIRILOV and M. K. JURIC., *Bull. Inst. Nuclear Science «Boris Kidrich»* 9, 39 (1959).
- [2] J. E. EVANS and M. A. GRACE, *Nucl. Phys.* 15, 646 (1960).
- [3] A. C. JUVELAND and W. JENTSCHKE, *Phys. Rev.* 110, 456 (1958).
- [4] R. G. ALLAS and F. B. SHULL, *Phys. Rev.* 116, 996 (1959).
- [5] P. HILMAN, *Phys. Rev.* 104, 176 (1956).
- [6] L. F. CHASE and G. IGO, *Phys. Rev.* 116, 170 (1959).
- [7] J. C. HENSEL and W. C. PARKINSON, *Phys. Rev.* 110, 128 (1958).
- [8] P. F. COOPER and R. WILSON, *Nucl. Phys.* 15, 373 (1960).

Detection of 900 KeV Vector Polarized Deuterons with the Reaction $\text{Li}^6(d, \alpha)\text{He}^4$

By L. G. PONDROM¹⁾ and J. W. DAUGHTRY

Aeronautical Research Laboratory, Wright-Patterson AFB, Ohio

Abstract. The existence of vector polarized deuterons after elastic scattering through 45° in the center of mass from He^4 at the 1.070 MeV resonance energy has been demonstrated by observing a right-left asymmetry in the alpha particles from the reaction $\text{Li}^6(d, \alpha)\text{He}^4$. The polarization has the correct energy dependence through the resonance. Viewing the second reaction at 45° in the lab, if we let $R = I_0(1 - \varepsilon)$ and $L = I_0(1 + \varepsilon)$, then for a left scattered polarized beam $\varepsilon = -0.065 \pm 0.010$. Similar measurements on $\text{H}^2(d, p)\text{H}^3$ at 45° give $\varepsilon = -0.03 \pm 0.025$.

Introduction

The possibility of producing vector and tensor polarized deuterons by using the $J = 3^+$ resonance occurring in $d\text{-He}^4$ elastic scattering at an incident deuteron energy of 1.070 MeV has been discussed by several authors [1, 2, 3¹⁾]. The resonance level is only about 40 keV wide, and the recoil alpha particle absorbs more than 40 keV for deuteron scattering angles exceeding about 15° in the laboratory. Since the magnitude of the polarization drops sharply off the resonance, a double scattering experiment is impractical if deuterons are accelerated on helium gas. Polarization prediction for backward hemisphere scattering angles can be checked by accelerating alpha particles on deuterium gas and then re-scattering the deuterons in helium. The vector polarization is especially large in the forward hemisphere [3], however, and thus a measurement at a center of mass angle of 45° was considered profitable. In order to perform such a measurement, a suitable deuteron reaction on a light nucleus must be found which is sensitive to deuteron vector polarization.

Experimental limitations require a deuteron reaction with $Q > 0$ and $d\sigma/d\Omega \geq 5$ mb/sterad. Four target nuclei used as analyzers of deuteron polarization are reported here: H^2 , Li^6 , B^{10} , and C^{12} . The reaction $\text{Li}^6(d, \alpha)\text{He}^4$ is indeed polarization sensitive, verifying the existence of vector polarization, but not its magnitude.

¹⁾ Now at Columbia University, New York, N. Y.

²⁾ Numbers in brackets refer to References, page 213.

Experimental Equipment

Figure 1 shows the gas scattering chamber configuration. The scattering angle in the polarizing reaction was fixed at 30° , or 45° in the center of mass. The predicted behavior of the cross section and the polarization components at this angle is given in reference [2]. The entrance and exit nickel foils were cooled by circulating the target gas through liquid nitrogen, and extracting it with a Kinney pump [4]. The target volume and gas pressure were adjusted to give a target approximately 40 keV thick. The monitor counter looked at the right scattered beam, and allowed a precise setting of the mean energy of the incident beam in the target volume by using the cross section resonance. The beam energy could be re-set to ± 10 keV, and remained constant to ± 3 keV for a run. The solid angle for the left scattered beam was 5×10^{-3} sterad, giving a polarized beam intensity on the analyzing target of the order of 10^7 particles/s. The analyzing reaction could be studied at angles of 45° and 135° . For 135° the $1/2'' \times 1-1/2''$ CsI(Tl) crystals were rotated about the target center. The solid angle for each counter was ~ 0.10 sterad., and ~ 5 counts/min were obtained in counters *R* and *L*.

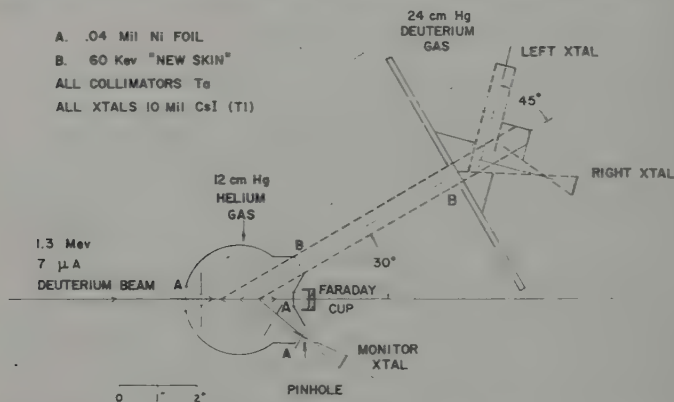


Figure 1

Double scattering chamber configuration. The 'New-Skin' windows are collodion films 60 keV thick for 900 keV deuterons.

The electronics is shown in figure 2. The display scaler in the monitor circuit counts for one second, displays, re-sets, and repeats about every five seconds. An RIDL 256 channel analyzer split into two sets of 128 channels was used to record the pulse height spectra simultaneously from the right and left counters, which look at the analyzing reaction.

Figure 3 shows a monitor counter scan as the incident beam energy is varied through the resonance. The beam energy shown was measured

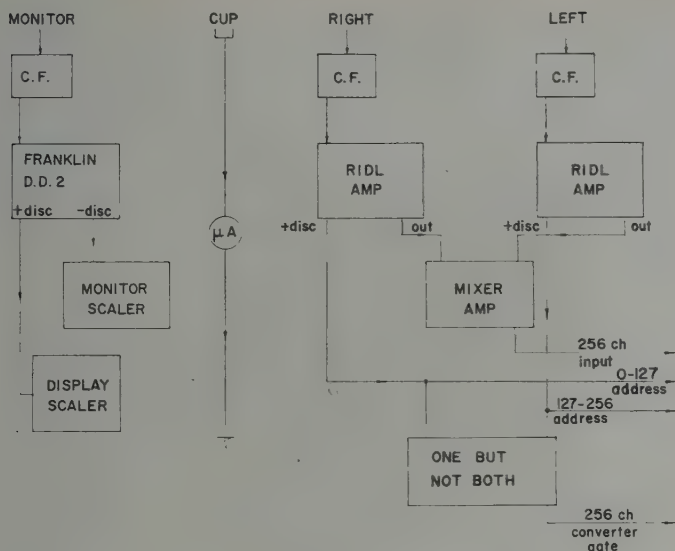


Figure 2
Block diagram of the electronics

by the Van de Graaff generating voltmeter, and therefore indicates a 230 keV loss in energy in the entrance foil and the target gas. Subsequent resonance scans have been made by measuring the excitation of the Van de Graaff bending magnet, which allows a more precise setting of relative beam energy. The uncorrected monitor counts showed a high energy tail because of background noise in the monitor counter. An integral discriminator as set to eliminate this noise at 1.20 MeV, but more background was counted as the energy increased.

Inherent asymmetries in the analyzing system were studied by using argon gas, cooled by liquid oxygen, in the first scattering chamber. At a generating voltmeter energy of 1.30 MeV and an argon pressure of 4 cm of mercury the scattered deuteron beam energy coincided with the energy normally obtained in resonance scattering from helium. This energy, after the beam left the polarizing chamber, was 900 ± 20 keV. The beam coulomb scattered from argon was normally about ten times as intense as the polarized beam. Argon runs always precede and followed helium runs to check for changes in the behavior of the experimental apparatus.

There was inherent asymmetry in the analyzer due to the intensity structure of the polarized beam, caused by the increase in the cross section towards forward angles. When the deuteron beam was coulomb

scattered from argon the right side of the beam on the second target exceeded the left in intensity by about 30%. The net effect observed in over 100 argon runs, each to about 3% statistical accuracy, was that R/L for the analyzer reaction varied between 1.00 and 1.10. Thus $R/L \geq 1$, independent of such systematics checks as exchanging counters, reversing the target, turning the scattering chamber upside down, and reversing the electronics. All of these tests have been performed several times with the various targets used as analyzers.

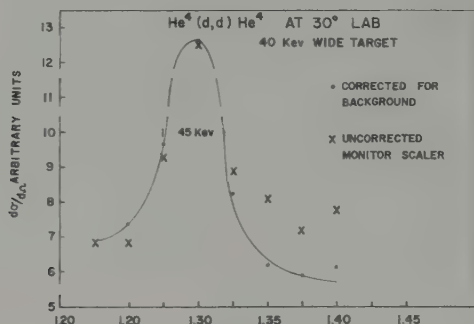


Figure 3

Typical scan of the scattering resonance with the monitor counter. The uncorrected tail represents low energy noise in the counter spectrum. The energy scale is the potential of the Van de Graaff dome.

The 130 keV thick deuterium gas analyzer is shown in figure 1. To study Li^6 , B^{10} , or C^{12} as an analyzer a solid target of about 1 mg/cm^2 thickness was placed at the center of the gas target volume, and the «New Skin» window and defining slits were removed. Solid targets were prepared on 0.02 mil nickel foil backing; C^{12} and B^{10} were deposited by evaporating the water from a «dag» suspension. Li^6 was evaporated on the nickel foil in metallic form.

The technique for observing a polarization effect involved measuring R/L at the analyzer for deuteron energies on, above, and below the polarizing resonance, and using the argon R/L as a relative normalization. An «on-resonance minus off-resonance» difference in the asymmetry indicated both a polarized beam and a sensitive analyzer.

Results

Figure 4 shows a typical set of helium resonance runs with Li^6 as the analyzer at angles of 45° and 135° in the lab. The energy is set 10 keV below the peak rate determined as in figure 3, to correspond to the

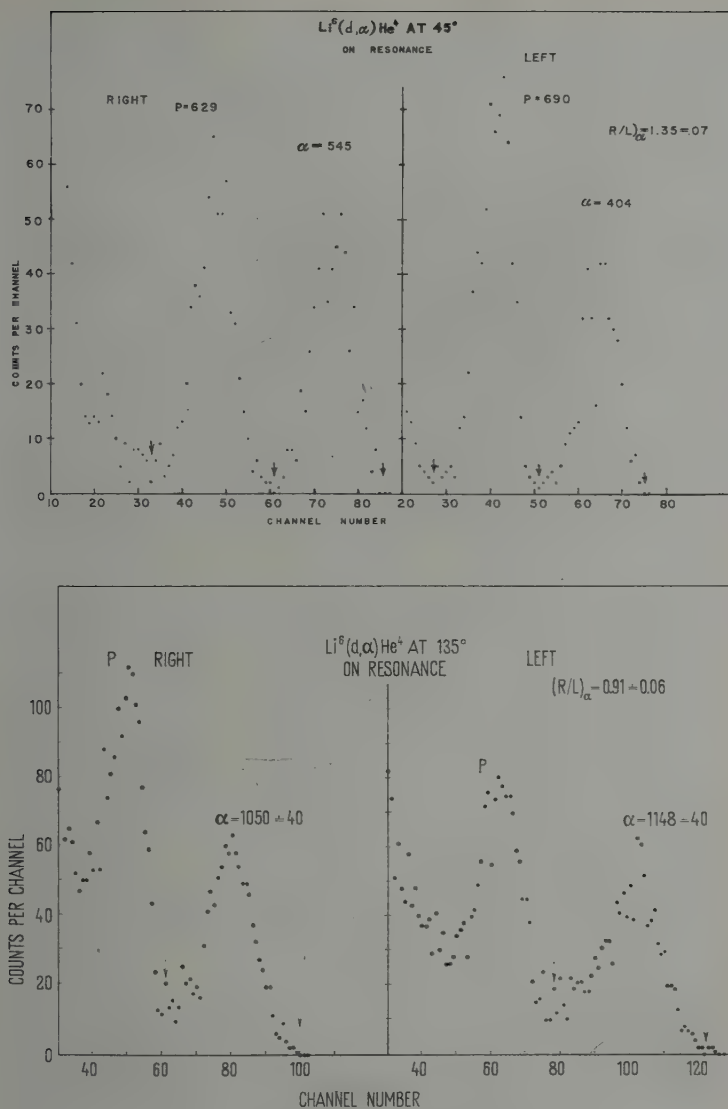


Figure 4

Typical pulse height spectra obtained from the asymmetry counters for $\text{Li}^6(d, \alpha)\text{He}^4$ at 45° and 135° with the polarized deuteron beam. 'On resonance' refers to the polarizing reaction energy.

expected position of the maximum polarization, as described in reference [2]. The low energy peak of each counter shown in figure 4 represents the two unresolved proton groups from $\text{Li}^6(d, p)\text{Li}^7$ and $\text{Li}^6(d, p)\text{Li}^{7*}$, where Li^{7*} is the first excited state, at 0.478 MeV. [6]. The 135° run lasted three hours; the 45° run lasted 70 minutes. Because the counters were much closer to the incident beam at 135° , the proton peaks appear on a large background. The second peak in each spectrum is alpha particles from $\text{Li}^6(d, \alpha)\text{He}^4$. The background is completely negligible for both protons and alphas at 45° , and only represents about 3% of the alpha rate at 135° . Since this 3% is essentially the same in both R and L , it is ignored in computing R/L . The poor separation between protons and alphas at 135° is therefore a resolution problem, and not due to background. Error in estimating this separation is included in the errors for 135° asymmetries.

Table I gives a resume of all of the helium runs performed with Li^6 as an analyzer. E refers to the energy of the incident beam at the center of the helium target. Both targets were about 1 mg/cm², or 400 keV thick for 900 keV deuterons, neglecting the stopping power of the unknown

Table I
 R/L for $\text{Li}^6(d, p)\text{Li}^7$ and $\text{Li}^6(d, \alpha)\text{He}^4$ with deuterons initially scattered from helium gas

Li ⁶ TGT	E	θ'	$R/L)_\alpha$	$R/L)_p$
A	1.07	45°	1.26 ± 0.07	0.95 ± 0.05
A	1.07	45°	1.08 ± 0.06	1.04 ± 0.04
A	1.07	45°	1.19 ± 0.05	1.02 ± 0.04
A	0.97	45°	1.37 ± 0.07	1.07 ± 0.06
B	0.97	135°	1.00 ± 0.07	—
B	1.06	135°	0.92 ± 0.06	—
B	1.06	135°	0.89 ± 0.06	—
B	1.06	135°	0.91 ± 0.05	—
B	1.17	135°	1.02 ± 0.07	—
B	1.17	135°	1.03 ± 0.06	—
B	0.97	135°	1.09 ± 0.11	—
B	0.97	135°	0.98 ± 0.11	—
B	1.06	45°	1.40 ± 0.10	1.10 ± 0.07
B	1.10	45°	1.10 ± 0.07	0.97 ± 0.06
B	0.97	45°	1.16 ± 0.07	1.10 ± 0.06
B	1.17	45°	1.02 ± 0.06	1.09 ± 0.05
B	0.97	45°	1.06 ± 0.06	1.03 ± 0.05
B	1.06	45°	1.35 ± 0.07	0.91 ± 0.06
B	1.06	45°	1.16 ± 0.05	1.02 ± 0.04
B	0.97	45°	1.05 ± 0.05	1.02 ± 0.05
B	1.17	45°	1.07 ± 0.07	1.09 ± 0.06

quantity of oxygen contamination. Table II gives the weighted average helium results, and the average normalization results obtained by replacing the helium in the first scattering chamber with argon. Each argon number represents about ten runs, but an error of 3% is nevertheless assigned because of possible systematic effects when windows are changed or pressures varied slightly. Both parameters could effect the beam structure, and have never been studied to better than 3%. Window changes occurred quite frequently during a series of runs. R/L for protons at 135° is not recorded because of the background. The essential features to note are that the argon runs in all cases result in $R/L)_\alpha \sim R/L)_p \sim 1.04$, and that $R/L)_p \sim 1.00$ for a helium scattered beam at the resonance energy, while $R/L)_\alpha \sim 1.15$ for $\theta' = 45^\circ$ and $R/L)_\alpha \sim 0.90$ for $\theta' = 135^\circ$ with the same resonant scattered beam.

Table II
Weighted average results for $\text{Li}^6(d, \alpha)\text{He}^4$

Li TGT	E	θ'	$R/L)_\alpha$	$R/L)_p$	Gas
A	1.070	45°	1.17 ± 0.03	1.00 ± 0.03	He
A	0.970	45°	1.37 ± 0.07	1.07 ± 0.06	He
A	1.070 ^{a)}	45°	1.04 ± 0.03	1.04 ± 0.03	Argon
B	1.060	135°	0.91 ± 0.03	—	He
B	0.970	135°	1.02 ± 0.04	—	He
B	1.170	135°	1.03 ± 0.04	—	He
B	1.070 ^{a)}	135°	1.02 ± 0.03	—	Argon
B	1.060	45°	1.25 ± 0.04	1.01 ± 0.03	He
B	0.970	45°	1.08 ± 0.04	1.06 ± 0.04	He
B	1.103	45°	1.10 ± 0.07	0.97 ± 0.06	He
B	1.170	45°	1.04 ± 0.05	1.09 ± 0.04	He
B	1.070 ^{a)}	45°	1.09 ± 0.03	1.07 ± 0.03	Argon

^{a)} The argon energy is adjusted to give a scattered beam energy equal to the energy of the beam scattered from helium on the resonance, or 1.070 MeV. This scattered energy is 900 keV after leaving the gas target.

Simple kinematics requires that in the center of mass system every alpha particle appearing at θ' , ϕ' must be accompanied by an alpha at $\pi - \theta'$, $\pi + \phi'$, regardless of initial polarization. Thus if we observe a right-left asymmetry ε , defined at $\theta' = 45^\circ$ by

$$R = (1 - \varepsilon) \quad \frac{R}{L} \cong 1 - 2\varepsilon \quad (1a)$$

$$L = (1 + \varepsilon)$$

then the asymmetry at $\theta' = 135^\circ$ must have the form

$$\begin{aligned} R &= (1 + \varepsilon) \\ L &= (1 - \varepsilon) \quad \frac{R}{L} \cong 1 + 2\varepsilon. \end{aligned} \quad (1b)$$

Hence $\theta = 45^\circ$ and $\theta' = 135^\circ$ measure the same asymmetry parameter, and the R/L ratio must be less than unity at 135° by the same amount by which it exceeds unity at 45° , or the converse.

Using the notation of LAKIN [6], the differential cross section in the center of mass system for a reaction initiated by vector polarized deuterons is

$$I(\theta, \phi') = I_0(\theta') + i\langle T_{11} \rangle C(\theta') \sin \theta' \cos \phi' \quad (2)$$

where $i\langle T_{11} \rangle = -i\sqrt{3/2} \langle S_x + iS_y \rangle$ for the incident deuteron beam, $I_0(\theta')$ is the unpolarized cross section, and $C(\theta')$ is a polynomial in $\cos \theta'$ with a maximum power $(\cos \theta')^{2L-1}$, L being the highest incoming orbital angular momentum participating in the reaction. Since a state which decays into two alpha particles can have only even orbital angular momentum, let us assume for $\text{Li}^6(d, \alpha)\text{He}^4$ that $L = 2$. Then the two alpha particle final state requires

$$C(\theta') = (a + b \cos^2 \theta') \cos \theta' \quad (3)$$

or

$$I(\theta', \phi') = I_0(\theta') + i\langle T_{11} \rangle (a + b \cos^2 \theta') \sin \theta' \cos \theta' \cos \phi'. \quad (4)$$

Therefore ε defined by equations (1) is given by

$$\varepsilon = i\langle T_{11} \rangle (a + \frac{1}{2}b) / 2 I_0(45^\circ) \quad (5)$$

for s and d waves contributing to the reaction. The coordinate systems for this experiment are shown in figure 5 for $\theta' = 45^\circ$. The center of mass to lab transformation amounts to a 3° change in angle, which produces no appreciable effect because of the $\sin \theta' \cos \theta'$ factor in equation (4).

Figure 6a shows a plot of the weighted averages of $(R/L - 1)$ from table II, where each number has been normalized to the corresponding average argon number. From the above discussion we see that we can combine all of the results into one graph of ε versus $E - E_0$ if we divide each $(R/L - 1)$ by two, and change the sign of each 135° datum. This has been done in figure 6b. Since $R/L > 1$ at 45° , ε is negative. The predicted form of the polarization from reference 2 with the experimental target width folded in is also sketched in figure 6b. The height of the

polarization curve is normalized to the maximum value of ε ; no energy shift in the prediction has been made. The finite resolution decreases

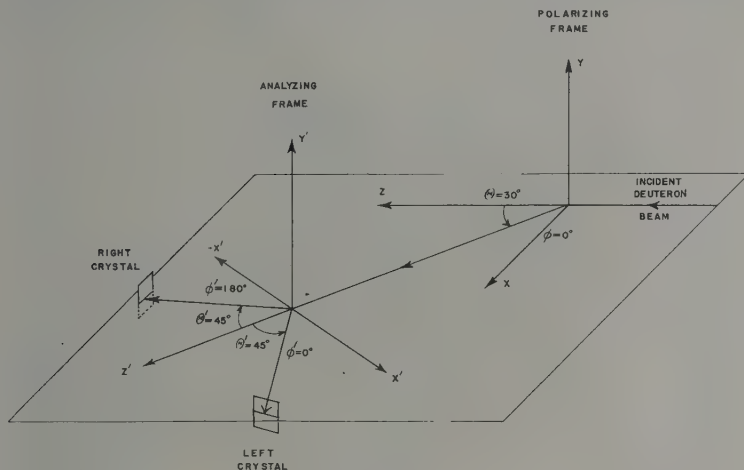


Figure 5

Diagram of the two coordinate systems for the double scattering. The analyzer angle is shown at 45° .

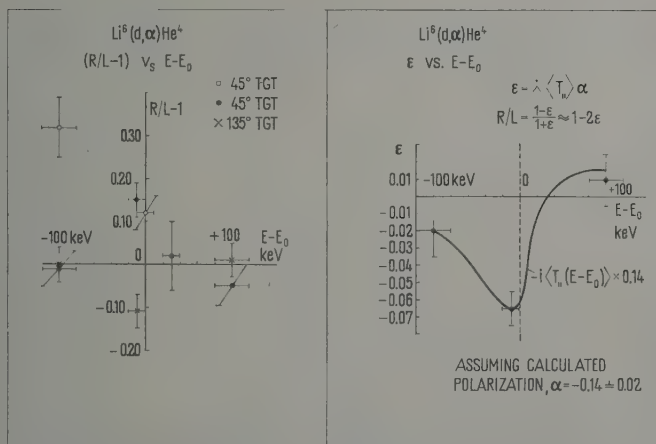


Figure 6

Final weighted average results for $\text{Li}^6(d, \alpha)\text{He}^4$ asymmetry as a function of the deuteron energy on the polarizing target. $E_0 = 1.070$ MeV. The quantity ε is defined in the text.

the predicted maximum of the polarization from 0.57 to 0.47. Using 0.47 as the maximum, $\varepsilon = -0.065 \pm .01$ from figure 6b gives

$$(a + 1/2 b)/2 I_0 = -0.14 \pm 0.02, \quad (6)$$

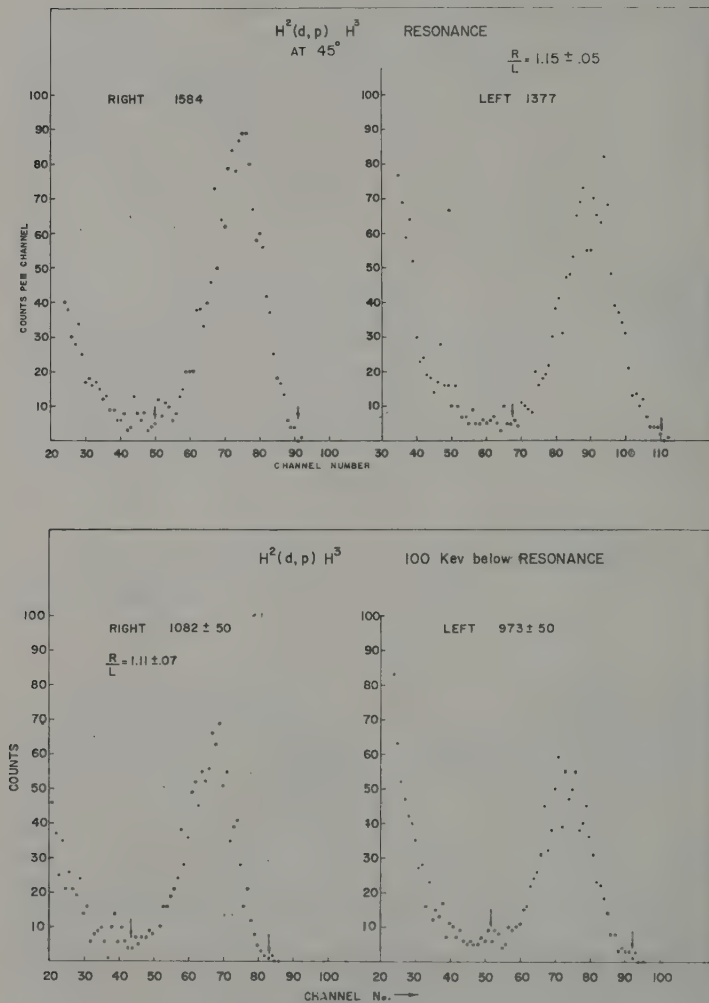


Figure 7

Typical pulse height spectra for $H^2(d, p)H^3$ on and off the polarizing resonance at 45°

This result represents an average value for incident deuteron energies from 900 keV to 500 keV, since the target is approximately 400 keV thick. Figure 6b can be interpreted as indicating, however, that a , b , and I_0 are slowly varying functions of energy in this range, since the energy

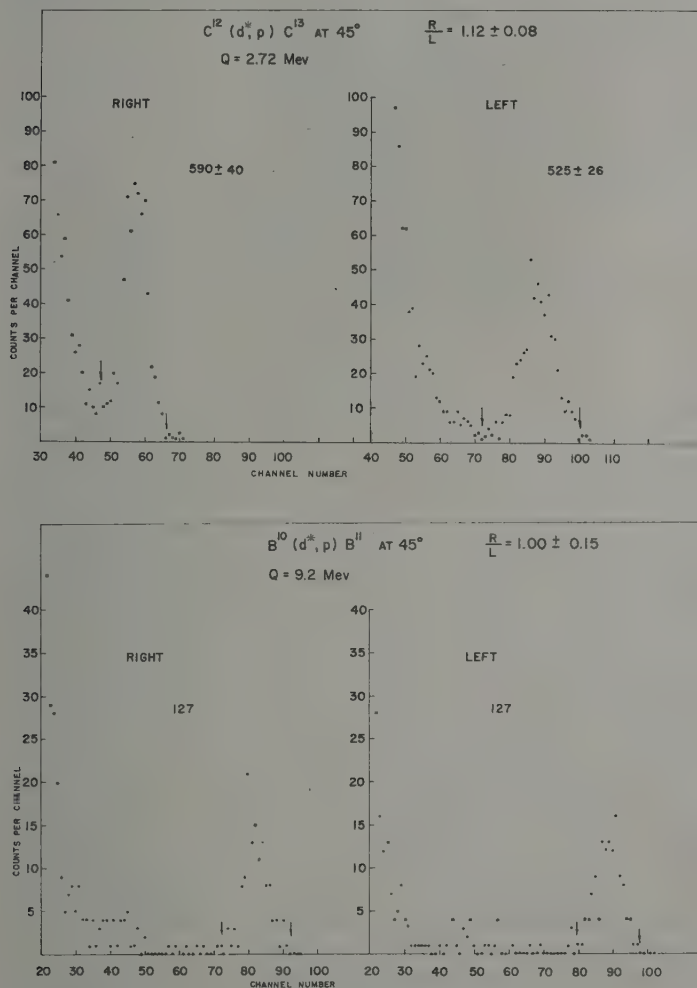


Figure 8

Typical pulse height spectra for $B^{10}(d,p)B^{11}$ and $C^{12}(d,p)C^{13}$ at 45° with the polarized beam on resonance.

dependence of $i T_{11}$ completely accounts for the observed energy dependence of ϵ .

Figure 7 shows typical results of similar asymmetry runs made on and off the polarizing resonance with deuterium gas as the analyzing target. Defining ϵ as in equation (1a), the final results for $H^2(d, p)H^3$ at $\theta' = 45^\circ$ and resonance scattered deuterons are

$$\epsilon = -0.03 \pm 0.025. \quad (7)$$

Figure 8 shows resonance runs on $C^{12}(d, p)C^{13}$ and $B^{10}(d, p)B^{11}$. These reactions have not been carefully studied, for there has never been any indication of a positive effect. Our results at 45° on resonance are as follows:

$$B^{10}(d, p)B^{11}, \quad \epsilon = +0.02 \pm 0.07 \quad (8a)$$

$$C^{12}(d, p)C^{13}, \quad \epsilon = -0.02 \pm 0.04 \quad (8b)$$

Conclusions

The reaction $Li^6(d, \alpha)He^4$ has a broad resonance at 600 keV incident deuteron energy, which is attributed to a resonant state of Be^8 occurring at $E_d = 350$ keV with $T \approx 500$ keV $^{-1}$ 5, 7. The energy spread of the polarized beam across the target, from 900 to 500 keV, brackets the peak of this resonance⁷, which is consistent with an analyzer sensitivity which varies slowly with energy. It seems likely, therefore, that it is this level which is sensitive to the vector polarization. Hence unless there is interference with some neighbouring level with spin two, this level cannot have spin zero, but must have spin of at least $J = 2^-$.

Further studies of this reaction are contemplated. It is hoped that the energy dependence of the polarization can be studied in detail. Confidence in the correct magnitude of the vector polarization can be strengthened by checking the magnitude of the predicted tensor polarization with the reaction $He^3(d, p)He^4$ ⁸. There is a weak indication from these data that the protons from $Li^6(d, p)Li^7$, Li^{7*} show a small positive ϵ . Since the ground state of Li^7 is $J = 2.3^-$ and the first excited state is $J = 1.2^+ 5$, one might expect opposite proton asymmetries from the two levels, and hence a cancellation effect on the total peak asymmetry. The two peaks can be resolved with this apparatus if a thinner Li^6 target is used, about 0.2 mg/cm².

We have profited by discussions with Dr. R. E. SEGEL and Dr. J. W. OLNESS during all phases of this work. Thanks are due to Mr. DAVID BREITENBECHER for efficient maintenance of the 2 MeV Van de Graaff accelerator.

Note added in proof: The authors have recently measured the polarization component $\langle T_{20} \rangle$ produced by this d -He⁴ scattering resonance using He³(d, p)He⁴ as an analyzer (Physical Review, to be published). This component was found to have the correct magnitude and sign. A term $3/8 \sqrt{2} \langle T_{20} \rangle B(\theta)$ should appear in the R - L asymmetry expression, equation (2) above. It was ignored because $3/8 \sqrt{2} \langle T_{20} \rangle = -0.12$, only 25% of the magnitude of $i \langle T_{11} \rangle$. The conclusion $J \geq 2^+$ for the 22.6 MeV state of Be⁸ is slightly weakened, for $B(\theta) \sim \cos \theta$ if $J = 0^+$. However, for $J = 0^+$ the observed asymmetry would have to come exclusively from $B(\theta) \sin \theta / I_0(\theta) \sim 0.8$, an improbably large sensitivity.

REFERENCES

- [1] L. J. B. GOLDFARB, Nucl. Phys. 7, 622 (1958).
- [2] LEE G. PONDROM, Phys. Rev. Letters 2, 346 (1959).
- [3] L. J. B. GOLDFARB and J. R. ROOK, Nucl. Phys. 12, 494 (1959).
- [4] M. J. SCOTT and R. LINDGREN, Rev. Sci. Instr. 28, 1090-N (1957).
- [5] F. AJZENBERG-SELOVE and T. LAURITSEN, Nucl. Phys. 11, 1 (1959).
- [6] W. LAKIN, Phys. Rev. 98, 139 (1955).
- [7] W. WHALING and T. W. BONNER, Phys. Rev. 79, 258 (1950).
- [8] L. J. B. GOLDFARB, Nucl. Phys. 12, 657 (1959).

Polarization of Neutrons from the $\text{Li}^7(p, n)\text{Be}^7$ Reaction

By S. M. AUSTIN, University of Wisconsin, and
S. E. DARDEN, University of Notre Dame

Using previously described methods [1], further polarization measurements have been performed on neutrons from the $\text{Li}^7(p, n)\text{Be}^7$ reaction. Angular distribution measurements of the polarization (P_n) were carried out at proton energies of 2.2, 2.6, and 3.0 MeV, covering angular ranges (laboratory system) of 30° to 70° , 30° to 115° , and 30° to 70° respectively. For the neutrons emitted at 50° , additional measurements have been made on the energy dependence of P_n between 1.95 and 3.00 MeV proton energy. The angular distribution data indicate that the polarization reaches a maximum in the vicinity of 60° . At a proton energy of 2.6 MeV, the polarization is near zero for angles of 105° and 115° , suggesting that two states with the same initial channel spin and $l_1 + l_2 \geq 2$ are contributing to the cross-section. As a function of energy, P_n at 50° has a minimum near 2.45 MeV and increases with decreasing proton energy to a maximum value of about 0.5 at 2.1 MeV, below which it decreases abruptly. For energies below 2.5 MeV, the observed variation with energy of P_n is similar to that calculated assuming the reaction proceeds primarily via a 3^+ and a 2^- state in Be^8 . If the level parameters which fit the total cross-section in this energy region are used, the calculations can be brought into qualitative agreement with experiment only by drastically altering the hard sphere phases near threshold. Fair agreement can also be obtained by introducing a 1^- level near threshold.

REFERENCES

- [1] STRIEBEL, DARDEN, and HAEBERLI, Nuclear Physics **6**, 188 (1958).
- [2] NEWSON, WILLIAMSON, JONES, GIBBONS, and MARSHAK, Phys. Rev. **108**, 1294 (1294).

The Polarization of Neutrons from the Stripping of Deuterons on C^{12} ¹⁾

By A. BUDZANOWSKI, K. GROTOWSKI, H. NIEWODNICZAŃSKI,

J. NURZYŃSKI, and M. SLAPA

Cracow Centre of Nuclear Physics, Cracow

The polarization of neutrons emitted in the stripping reaction $C^{12}(d, n)N^{13}$ has been investigated at deuteron energy 12.9 MeV and different reaction angles. The polarization was found to be:

Reaction angle in LAB system	Polarization
15°	− (39 ± 11)%
30°	+ (3 ± 8)%
45°	+ (25 ± 8)%
60°	+ (55 ± 20)%

The positive direction of polarization is that of the product $\mathbf{k}_{in} \times \mathbf{k}_{out}$, \mathbf{k}_{in} and \mathbf{k}_{out} indicating the wave-vectors of the incident and outgoing particle respectively.

The resolution of the apparatus was not sufficient to provide the separation of groups of neutrons connected with different energy levels of the resultant N^{13} nucleus. Therefore the figures given above represent the superposition of the polarization effects for several energy groups of neutrons which are related also to different amounts of the angular momentum transferred to the resultant nucleus.

Measurements of the energy spectrum of neutrons at different reaction angles were performed using the nuclear emulsion technique. The knowledge of the result of these measurements is however not sufficient to enable the determination of the polarization of particular groups of neutrons, due to their comparable abundance. New experimental data of the angular dependence of the polarization of at least one separate

¹⁾ The experiments reported in this communication represent the further development of the previous work: A. BUDZANOWSKI, K. GROTOWSKI, H. NIEWODNICZAŃSKI and J. NURZYŃSKI, *Bulletin de l'Académie Polonaise des Sciences, Série des sci. math., astr. et phys.*, 7, 583 (1959).

energy group of neutrons from the $C^{12}(d, n)N^{13}$ reaction are necessary. Experiments having this purpose are now in progress.

At the reaction angle $\theta_{lab} = 15^\circ$ the predominant number of neutrons corresponds to the 3.58 MeV excited level of the N^{13} nucleus. The results of measurements of the energy spectrum of neutrons at this angle gave the following relative numbers of neutrons connected with the first three energy states of the resultant N^{13} nucleus:

Ground state	0.19
2.36 MeV excited state	0.20
3.58 MeV excited state	1.00

Taking into account these figures and the energy dependence of the efficiency of the counter we obtain the following value of the polarization of neutrons connected with the 3.58 MeV energy state of the N^{13} nucleus: $-(39_{-11}^{+21})\%$.

So the negative sign of the polarization of neutrons would be connected with the $l = 2$ transition.

Taking into account the results obtained by JUVELAND and JENTSCHKE, HENSEL and PARKINSON, HILLMAN, and HIRD for the level of the nucleus with $l = 1$ the negative sign of polarization suggests for the energy level 3.56 MeV of N^{13} the value of spin $3/2^+$.

Alternatively, the negative sign of the polarization of protons from the reaction $C^{12}(d, p)C^{13}$ corresponding to the second excited level $5/2^-$ of the C^{13} nucleus with $l = 2$ permits us to suppose that in both these cases the negative sign of the polarization determines the value $j = l - 1/2$. This could be connected with the preponderance of the distortion of the wave of the outgoing nucleon.

Left-Right Asymmetries in the $D(d, p)T$ Reaction with Polarized Deuterons

By R. BARLOUTAUD, H. FARAGGI, A. GARIN et L. ROSEN¹⁾

Centre d'Etudes nucléaires de Saclay

A 1.4 ± 0.3 MeV deuteron beam, almost purely vectorially polarized, obtained by α -D elastic scattering [1], has been used to study the angular dependence of left-right asymmetry for protons from $D(d, p)T$. Protons emitted right (R) and left (L) from a 0.8 mg/cm^2 heavy paraffin target were detected by nuclear emulsions. A separate run, with a 1 mg/cm^2 polytene target, made under identical experimental conditions, gave the contribution from $C^{12}(d, p)C^{13}$ protons. Figure 1 gives the R and L

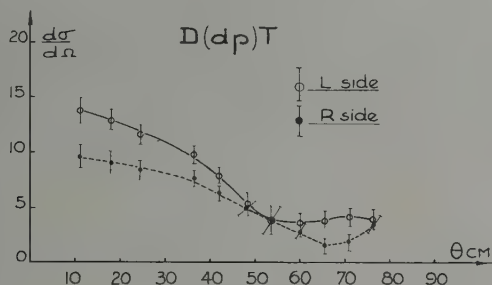


Figure 1

angular distributions, showing that the deuterons are effectively polarized, and figure 2 gives the angular dependence of $\varepsilon = (R - L)/(R + L)$. If $P_d \sim +0.33$ is the deuteron vector polarization [1], P'_d the deuteron polarization for $T(p, d)D$ with unpolarized protons, we must have rigorously [2, 3]: $\varepsilon = 3/2 P_d P'_d \cong P'_d/2$. Moreover if P_p is the proton polarization for $D(d, p)T$ with unpolarized deuterons ($P_p \sim \sin 2\Theta/(R + L)$ [3]), the stripping approximation [2] without symmetrization for $d-d$ reaction shows that $\varepsilon = 3 P_d P_p \cong P_p$ (broken curve in figure 2).

¹⁾ On leave from Los Alamos.

For $35^\circ < \theta_{CM} < 45^\circ$, P_p values so deduced are in fair agreement with previous measurements [4] but the stripping approach does not seem to hold for all angles.

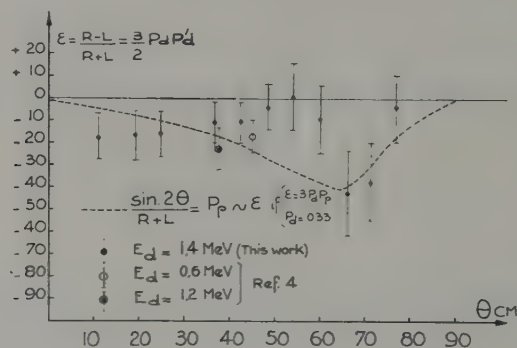


Figure 2

REFERENCES

- [1] R. J. N. PHILIPPS, Private communication, R. BARLOUTAUD, H. FARAGGI, L. ROSEN and S. M. SHAFROTH, J. Phys. Rad. 27, 369 (1960).
- [2] G. R. SATCHLER, Nucl. Phys., 6, 543 (1958). – RODBERG, Private communication.
- [3] M. FIERZ, Helv. Phys. Acta, 25, 629 (1952).
- [4] R. E. SEGEL, and S. S. HANNA, Phys. Rev., 106, 536 (1957). – B. MAGLIĆ and J. VUKOVIĆ, Nucl. Phys., 6 443 (1958).

Polarization of Nuclei in Direct Interaction Processes

By G. IGO, Lawrence Radiation Laboratory, Univ. of Calif.

The residual nuclei following a direct interaction process are left in a polarized state in general. The observation of an up-down asymmetry in the emission of beta-particles, the polarization of internal conversion electrons, the circular polarization of gamma rays emitted from the residual nucleus depend on the nuclear polarization moments. The experiment of CHASE and IGO [1] is an example of the first type of observation. The theories of the second and third type of measurement have been developed by BECKER and ROSE [2] and by SATCHLER [3] respectively. The angular correlation of an inelastically scattered particle or reaction product with a gamma ray emitted from the residual nucleus also depends on the polarization moments. An example is the $(p, p'\gamma)$ reaction which has been summarized by LEVINSON and BANERJEE [4].

In a (d, p) reaction, the distorted wave direct interaction (DWDI) theory predicts the polarization of the residual nucleus $B(\theta)$ may reach 100% whereas the proton polarization cannot exceed $33\frac{1}{3}\%$. However the proton polarization in the $C^{12}(d, p)C^{13}$ reaction at MeV at a scattering angle of 70 degrees has been found to exceed $33\frac{1}{3}\%$ [5]. There is also evidence from the $Be^9(d, p)Be^{10}$ reaction [3] and the $C^{12}(d, p\gamma)C^{13}$ correlation [3] that the DWDI theory is inadequate without at least the addition of spin orbit coupling.

A test of the DWDI theory can be made by measuring the asymmetry $A(\theta)$ of the scattered deuterons in the $N^{14}(p, d)N^{13}$ when polarized protons are incident on N^{14} , and the polarization $B(\theta)$ of N^{13} in the $H^1(N^{14}, N^{13})H^2$ reaction at the same center of mass energy. The DWDI theory predicts that $A(\theta)/B(\theta)$ is a constant independent of the scattering angle θ . A source of 10^6 sec.^{-1} 100% polarized protons has been prepared at Berkeley to study the pick-up reaction.

REFERENCES

- [1] L. F. CHASE, Jr. and G. IGO, Phys. Rev. *116*, 170 (1959).
- [2] R. L. BECKER and M. E. ROSE, Nuovo Cimento *13*, 1182 (1959).
- [3] G. R. SATCHLER (private communication).
- [4] C. A. LEVINSON and M. K. BANERJEE, Ann. Physics *2*, 471 (1957), *3*, 67 (1958).
- [5] A. C. JUVELAND and W. JENTSCHKE, Phys. Rev. *110*, 456 (1958).

Production of Spin Polarized Mass-Three Beams

By J. E. BROLLEY, JR., J. L. GAMMEL, and L. ROSEN¹⁾

Los Alamos Scientific Laboratory

It is quite desirable to obtain as much information as possible on the non-central part of the nuclear force field. So far most of the direct information has come from the scattering of protons and neutrons on nuclear systems ranging from mass-one upwards. There is also a smaller body of information relative to the deuteron. Studies with polarized mass-three beams may provide additional illumination and perhaps be germane to three body spin orbit calculations [1]²⁾.

To observe polarization of mass-three particles we have considered double-scattering experiments in the classical pattern [2].

Guidance for such an observation might be expected from the phase shift analysis of mass-three scattering by He^4 analogous to the case of proton- He^4 [3]. Differential cross section input data for this procedure were supplied by a survey of triton and helium [3] scattering conducted by us [4], over a bombarding alpha energy range of 12 to 28 MeV. In the accompanying note of J. L. GAMMEL and R. M. THALER some of these data have been analyzed in conjunction with the data of MILLER and PHILLIPS [5].

This analysis, graphically depicted in figure 1, indicates quite strong polarization in the 90° center-of-mass region over quite a range of input scattering energies.

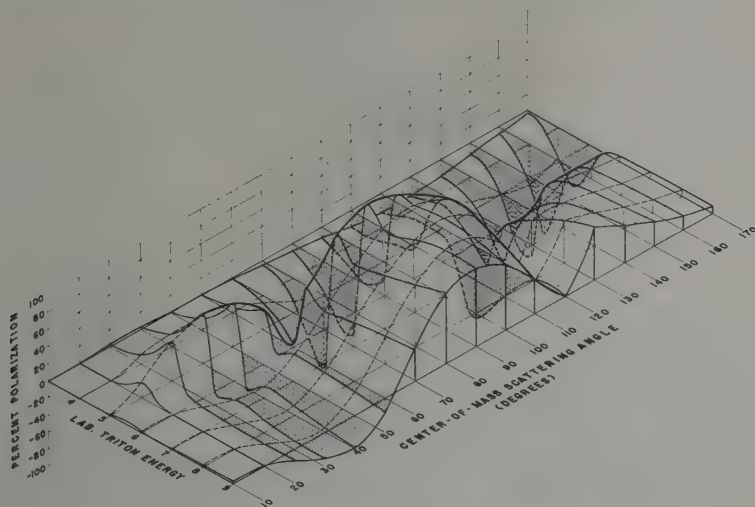
Experiment

Whilst measurements on tritons or helium [3] particles are essentially equivalent we have chosen to use tritons because of their lower rate of energy loss. The first scattering of the tritons occurred in a small

¹⁾ On leave as a Guggenheim fellow at le Centre d'Etudes Nucléaires de Saclay, France.

²⁾ Numbers in brackets refer to References, page 223.

vessel containing tritium at a pressure of 140 cm Hg. Alpha particles from the Los Alamos cyclotron entered through a 0.4 mil molybdenum window. The cyclotron was adjusted so that the alpha particle energy in the collision volume [6] was about 16.4 MeV. Tritons recoiling at 90° center-of-mass or 45° forward in the laboratory with a spread of $\pm 2^\circ$ emerged from the target vessel via a quarter mil permalloy window and proceeded in vacuo to the second scattering chamber. They entered through a quarter mil nylon window and scattered off He^4 which filled



T- α POLARIZATION MAP

Figure 1

the chamber to a pressure of 119 cm Hg. 7.2 MeV tritons scattering at $53 \pm 11^\circ$ in the laboratory, again 90° in the center-of-mass, were detected in a tandem proportional counter filled with a mixture of argon plus 5% CO_2 to a pressure of 3.4 cm Hg as indicated in figure 2. The isolating window was quarter mil permalloy. The ambient nuclear radiation field was of such proportions as to make the detection of the tritons quite difficult. This condition was considerably mitigated by imposing a coincidence requirement between the triton and its associated alpha particle. The latter was detected by a one mil aluminized organic plastic scintillator viewed by a DuMont 6292 photomultiplier. The triple coincidence circuit had $1/2$ microsecond resolving time. Juxtaposed about each triton counting run in either left or right station was a background

run. In the latter type run the first scattered tritons were intercepted prior to entering the second scattering chamber.

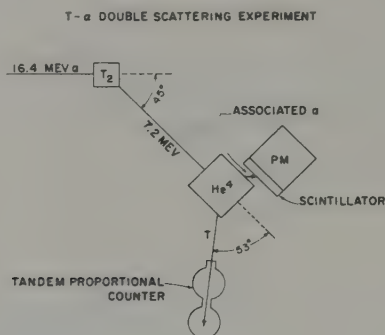


Figure 2

Results

Four separate runs produced the results of table 1 which lead to a left-right counting asymmetry ratio of $3.3 \pm 35\%$. To compare this with the expectations from the phase shift analysis it is necessary to fold in the scattering cross sections and polarizations into the finite geometry. When this is done and a slight extrapolation is made for the polarization in the first scattering, we obtain a ratio of 4. Evidently the experimental results and the expected value are compatible and we are observing peak polarizations in the vicinity of 80 to 90%.

Table 1

Counts	Left	Right
Stopper in	93	83
Stopper out	234	125
Corrected counts .	141	42

Clearly further measurements are indicated, but on the basis of this result it is reasonable to contemplate a number of experiments: the scattering of polarized mass-three nuclei by other heavy nuclei to supplement the differential cross section data in optical model analyses; possible spin correlation experiments in reactions and scattering; $D + D \rightarrow P + T$, $P + T \rightarrow P + T$ for example; polarization produced in scattering $He^3 + T$ for example.

REFERENCES

- [1] See for example: J. FUJITA and H. MIYAZAWA, *Prog. Theor. Phys.* **17**, 366 (1957).
- [2] M. HEUSINKVELD and G. FREIER, *Phys. Rev.* **85**, 80 (1952).
- [3] C. L. CRITCHFIELD and D. C. DODDER, *Phys. Rev.* **76**, 602 (1949).
- [4] Some of these data are summarized in: J. E. BROLLEY, JR., L. ROSEN and L. STEWART, *Proceedings of the 1959 International Conference on the Few Nucleon Problem*, London, Pergamon Press (to be published).
- [5] P. D. MILLER and G. C. PHILLIPS, *Phys. Rev.* **112**, 2048 (1958).
- [6] The desirability of this sequence is discussed: L. ROSEN and J. E. BROLLEY, JR., *Phys. Rev.* **107**, 1454 (1957).

III.

Reactions and Scattering of Polarized Particles

The Scattering of Polarized Particles

By H. H. BARSHALL, University of Wisconsin

The scattering of polarized particles has been the subject of several recent reviews from which the present survey greatly benefited, particularly FAISSNER's article in the «Ergebnisse der Exakten Naturwissenschaften» [1]¹⁾ and Rosen's report to the International Conference on the Nuclear Optical Model [2].

That beams of scattered particles might be partially polarized was first predicted by MOTT [3] for electrons. The mechanism discussed by MOTT is that the energy of interaction between the magnetic moment of the electron and the electromagnetic field produced by the nuclear charge depends on which side of the nucleus the electron passes the nucleus. This prediction was verified after previous unsuccessful attempts in a double scattering experiment by SHULL, CHASE, and MYERS [4] in 1943.

In 1948 SCHWINGER [5] pointed out that the same effect should be observable in the small-angle scattering of fast neutrons by heavy nuclei. This effect was clearly demonstrated at Harwell in 1956 [6] in the scattering of very high energy neutrons. Its importance lies in the fact that it should be possible to calculate the magnitude of this polarization so that unknown polarizations can be measured by this method. For neutron energies which are to be discussed at the present conference, MOTT-SCHWINGER scattering is much more difficult to observe. GORLOV, LEBEDEVA, and MOROSOV [7] at the Atomic Energy Institute in Moscow studied in 1957 the Mott-Schwinger scattering by Pb of partially polarized 3.7-MeV neutrons from the $D + D$ reaction and deduced from this measurement the polarization of the neutrons. Mott-Schwinger scattering of protons should also occur, but the predominant effect of RUTHERFORD scattering makes it difficult to observe this effect.

A second mechanism which produces polarization in the scattering of particles by nuclei was also first suggested by SCHWINGER [8], *i.e.*,

¹⁾ Numbers in brackets refer to References, page 238.

spin-orbit coupling. SCHWINGER suggested that this could be observed in a double scattering experiment of neutrons by He. SCHWINGER thought that the observed anomaly in the scattering of 1-MeV neutrons by He could be accounted for by a $P_{1/2} - P_{3/2}$ doublet in He^5 with a splitting of 0.4 MeV. He predicted a large asymmetry in the double scattering of neutrons which had an energy corresponding to the upper member of the doublet in the first collision, and to the lower energy level in the second collision. Schwinger's idea was not pursued experimentally because a double scattering experiment with 1-MeV neutrons appeared too difficult to carry out. Actually the splitting of the $P_{1/2} - P_{3/2}$ doublet in He^5 is much larger than SCHWINGER had thought. On the other hand polarization in scattering does not depend on the particular circumstances originally discussed by SCHWINGER, but occurs quite generally whenever there is interference between two partial waves, at least one of which has a phase shift which depends on the spin orientation of the scattered particle with respect to its orbital motion. As a consequence some polarization is expected in almost all nuclear scattering of particles with spin provided the energy is high enough so that the scattering involves partial waves with angular momentum greater than zero.

Although it was not possible to perform the double scattering experiment on He suggested by SCHWINGER with neutrons, it was pointed out by WOLFENSTEIN [9] that a similar effect would be expected in the scattering of protons by helium since the mirror nucleus Li^5 should also exhibit a large splitting between the $P_{1/2}$ and $P_{3/2}$ levels formed by protons of energies around 2 MeV. This experiment was performed by Williams' group at the University of Minnesota [10] using the experimental arrangement shown in figure 1. A collimated beam of 3.25-MeV protons from an electrostatic accelerator is scattered in helium gas through a CM angle of about 90° . The scattered protons are scattered again by He and are detected in photographic emulsions. By observing the direction of the protons in the photographic emulsion, those protons which were scattered approximately through 90° (CM) in the second collision could be selected. The number of tracks observed in the two emulsions differed by a factor of about two. Thus the polarization in the scattering of fast nucleons was first demonstrated.

From experiments on (p, α) scattering carried out at Minnesota, CRITCHFIELD and DODDER [11] had deduced phase shifts. The data could be fitted by two sets of phase shifts, one corresponding to the assumption the $P_{3/2}$ level in Li^5 lies above the $P_{1/2}$ level, the other corresponding to the opposite order. Under the two assumptions quite different polarizations are expected. In one case, the forward plate would show more tracks, in the other the backward plate. The experiments clearly showed

that the $P_{1,2}$ level must lie above the $P_{3,2}$ level, which agreed with an earlier analysis by ADAIR [12] based on (n, α) scattering.

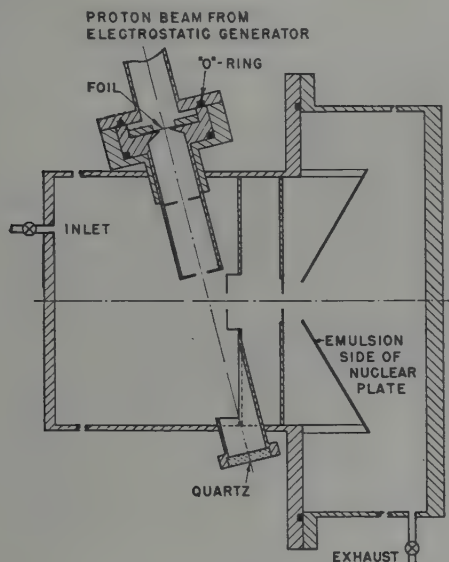


Figure 1

The arrangement used in the experiment of HEUSINKVELD and FREIER [10]. Polarization of protons scattered by helium was observed in a double scattering experiment

It should be pointed out that because of the energy loss in elastic scattering a double scattering experiment of protons (or neutrons) does not permit the determination of the polarization directly from the observed asymmetry, but determines only the product of the polarizations in the two collisions which occur at different energies. A method which allows an absolute determination of a polarization in a double scattering experiment of protons was used by Miss SCOTT [13] at Brookhaven. In this experiment advantage is taken of the fact that charged particles remain polarized when they are slowed down in passing through a foil. By measuring three products of polarizations involving protons of three different energies it was possible to calculate the individual polarizations. In one of the three combinations the proton is slowed down in a foil (figure 1a).

It is thought that the phase shifts for (p, α) scattering are sufficiently well known to enable one to calculate polarizations from (p, α) scattering

with an accuracy of the order of ten percent. Figure 2 shows a plot of the calculated polarizations in (p, α) scattering taken from a paper by BROCKMAN [14]. Over most of the energy range there are scattering angles at which the polarization reaches more than 90 percent. That the polarization of protons scattered by helium exceeds 95 percent at certain angles was shown experimentally by ROSEN and BROLLEY [15] for 6.25- and 10-MeV protons.

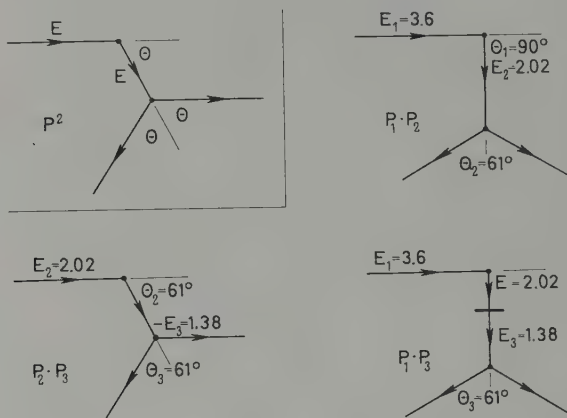


Figure 1a

The only other nucleus for which the proton scattering phase shifts are well enough known to deduce polarizations reliably appears to be C^{12} . Figure 3 shows a plot prepared by TOMBRELLO, BARLOUTAUD, and PHILLIPS [16] in which calculated polarizations in $p-C^{12}$ scattering are given for protons between 1.5 and 5 MeV. These polarizations were computed after adjusting the phase shifts to fit recent experiments at Harwell [17] on the scattering or polarized protons by C^{12} . The more rapid variation of polarization with energy and angle and the occurrence of energy regions in which there is very little polarization makes carbon a less useful polarizer or analyzer than helium in this energy range. On the other hand for some experiments the availability of carbon as a solid target is a great advantage. At higher proton energies the polarization of protons scattered by carbon varies more slowly with energy so that carbon is a more desirable analyzer and polarizer. It was shown by BROCKMAN [14] that between 16 and 18 MeV the polarization is of the order of 50 percent for protons scattered through 45° .

For neutrons double scattering experiments have so far not been possible because of intensity and background difficulties. All experi-

ments on the scattering of polarized fast neutrons have used polarized neutrons from a reaction. These neutrons are then scattered and the left-right asymmetry in the scattering is observed. The application of this procedure to the study of nuclear reactions was discussed at an earlier session. At the present session it will be assumed that we have learned how to produce beams of partially polarized fast neutrons.

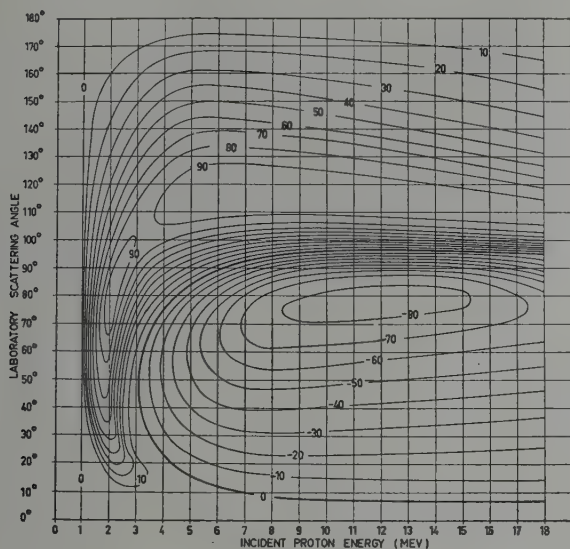


Figure 2

Polarizations calculated by BROCKMAN [14] for the scattering of protons by helium

Polarization in the scattering of fast neutrons was discovered by HUBER and his co-workers in Basel in 1953 [18] and at about the same time by RICAMO [19] and SCHERRER's group [20] in Zürich. Both groups demonstrated asymmetries in the scattering of $d-d$ neutrons from carbon. Shortly thereafter asymmetries in the scattering of $\text{Li}(p, n)$ neutrons scattered from oxygen were observed at our laboratory [21]. Figure 4 shows the experimental arrangement which has been used at Wisconsin.

As analyzers of the polarization of neutrons several light nuclei have been used. As in the case of the scattering of protons, helium is a particularly useful analyzer. The polarizations expected in (n, α) scattering are shown in figure 5. This figure is taken from a paper by LEVINTOV, MILLER, and SHAMSHEV [22], and is based on the phase shifts given by SEAGRAVE [23]. It is apparent that the polarization varies slowly with

neutron energy and is almost 100% for a CM scattering angle of 135° for neutron energies from 4 to 20 MeV. The difficulty of preparing helium samples of high density is in the case of neutrons an even greater disadvantage than in the case of protons.

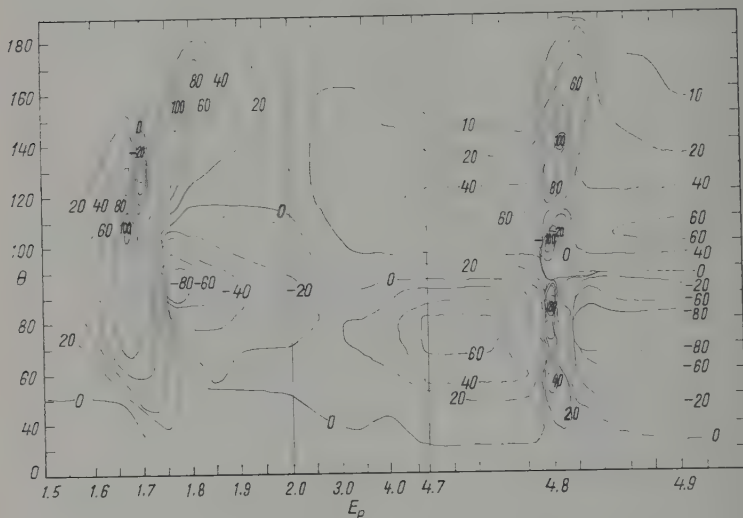


Figure 3

Polarizations calculated in [16] for the scattering of protons by carbon

Although it is difficult to prepare dense helium scatterers, it is easy to detect helium recoils from fast neutrons in counters. The polarization can then be measured by observing a left-right asymmetry of α -particles recoiling in a given direction. This has been done particularly successfully with thin proportional counters by LEVINTOV [22] and co-workers.

Other nuclides for which polarizations in neutron scattering can be calculated fairly well in certain regions are C^{12} and O^{16} . Figure 6 shows calculated polarizations at two angles in the scattering of neutrons by O^{16} [24]. Although the polarization varies rapidly with neutron energy, oxygen has been useful as an analyzer for neutrons of energies around 1 MeV and lower.

In view of the fact that polarization experiments are relatively difficult to carry out and frequently give rather inaccurate results, it is well to examine what experiments on the scattering of polarized particles are likely to give information which cannot be obtained more easily by simpler experiments.

The original Minnesota p - α scattering experiment [10] is an example of an ideal application of the scattering of polarized particles. Only the sign of the polarization needed to be determined to decide the sign of a phase shift difference. Polarization measurements are generally useful to check phase shift analyses, based on angular distribution measurements.

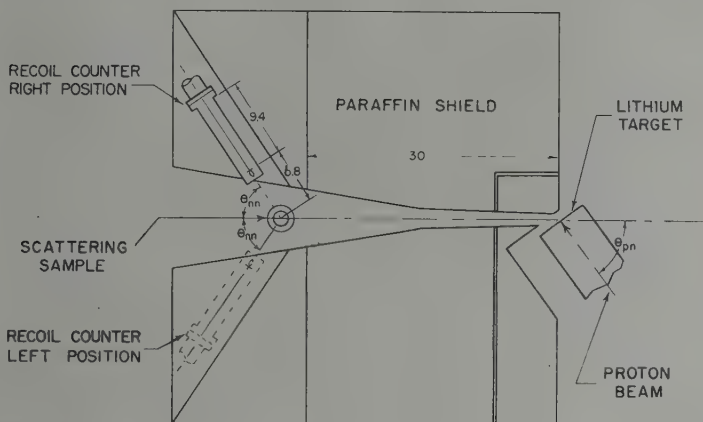


Figure 4

Experimental arrangement
used for observing the scattering of polarized neutrons [24]

The fact that the polarization depends on the interference of partial waves has the effect that the polarization is strongly affected by the presence of partial waves which undergo only a small phase shift. Measurement of the polarization, therefore, enables one to discover the effect of phase shifts which are too small to be noticeable in the angular distribution. An example of a measurement with this aim is the recent determination of the polarization of 3.3-MeV protons scattered by protons carried out by ALEXEFF and HAEBERLI [25]. The experimental arrangement is shown in figure 7. Protons are scattered by hydrogen in the region *B* and the scattered protons are scattered again by helium in the region *D*. The doubly scattered protons are detected in two counter telescopes. As an indication of the accuracy that can be obtained in double scattering experiments with protons, a typical result was that 3.3-MeV protons scattered by protons through a CM angle of 45° have a polarization of $(0.25 \pm 0.16)\%$. Measurements of the polarization of scattered neutrons have so far reached only accuracies which are an order of magnitude worse.

Another area in which scattering of polarized particles has produced useful information is the general question of the importance of spin-orbit interactions in nuclear collisions. In general, the scattered particles will be polarized if spin-orbit interactions are present. The observation of polarization will, therefore, indicate the presence of such interactions, although one can construct circumstances under which the absence of polarization does not prove the absence of spin-orbit forces.

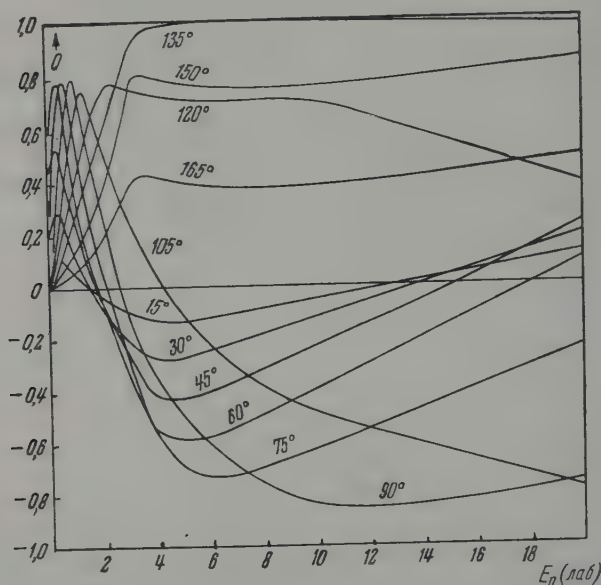


Figure 5

Polarization in the scattering of neutrons by helium taken from [22], and based on the phase shifts of [23]

This aspect became of interest in the development of the nuclear optical model. When the optical model was first developed to account for the observed giant resonances in the scattering of fast neutrons by heavy nuclei, the optical potential which was used did not contain a spin-orbit term. Since the shell model had shown the importance of spin-orbit forces, it appeared that the optical model which is related to the shell model should include a spin-orbit term. The optical model contained, however, too many adjustable parameters to enable one to deduce even the need for a spin-orbit term from the measured cross sections alone. An attempt was made, therefore, to observe the polari-

zation of neutrons scattered by heavy elements and this effect was observed at our laboratory in 1954 for 0.4-MeV neutrons [21]. Since that time more accurate measurements of the scattering of neutrons by heavy elements have been performed at our laboratory both at 0.4 and 1.0 MeV [26]. Typical results are shown in figure 8. It is apparent that spin-orbit effects are important especially for elements around $A = 100$ for which it is known that there is a P -wave giant resonance at this energy. Similar measurements have been performed with $D + D$ neutrons at several laboratories, particularly at the ETH Zürich [27] and at the University of Virginia [28].

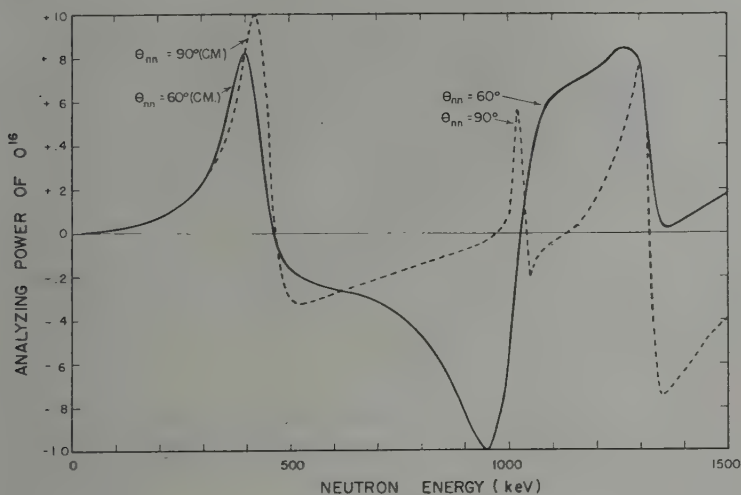


Figure 6

Polarizations in the scattering of neutrons by oxygen taken from [24]

Excellent measurements on the scattering of polarized protons from intermediate and heavy nuclei have been performed at the ETH Zürich at 4 MeV [29], at the University of Rochester [30] for 6- and 7-MeV protons, at Los Alamos [2] at 8 and 10 MeV, and at Princeton University [31] at 17 MeV. Typical results are shown in Figure 9 where the polarization of 17-MeV protons scattered by zinc is plotted against scattering angle. The polarizations are much larger than those observed in low-energy neutron scattering. The solid curve shows an optical model fit to the measurement.

It was recently shown by RODBERG [32] that according to the optical model the polarization should be proportional to the derivative of the

angular distribution, *i.e.*, it is zero at the maxima and minima of the angular distribution, in good agreement with experimental results on proton scattering. The magnitude of the spin-orbit term in the potential can be deduced from the magnitude of the polarization and the derivative of the angular distribution for scattering angles near 90° .

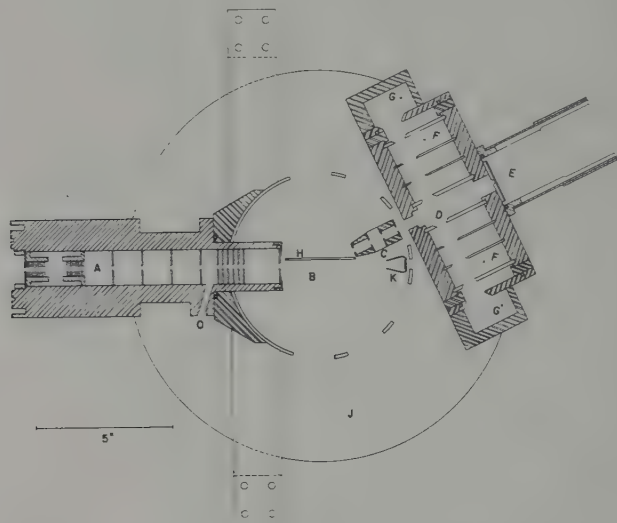


Figure 7

Experimental arrangement used in the measurements of the polarization in proton-proton scattering (from [25])

Many experiments have been performed on the scattering of polarized nucleons by deuterons. Since neutron-deuteron scattering is anisotropic even at quite low neutron energies, one knows that this interaction involves angular momenta different from zero. One might expect, therefore, to observe appreciable polarization in nucleon-deuteron scattering experiments. Experiments have failed, however, to show much, if any, polarization in either neutron or proton scattering by deuterons [33-38]. This result is rather surprising.

In summary, there are a number of applications for which measurements of the polarization of scattered particles give information not readily obtainable by other means. On the other hand, one should examine carefully in each case whether the desired information cannot be obtained by means other than the polarization measurements which are usually rather difficult to perform.

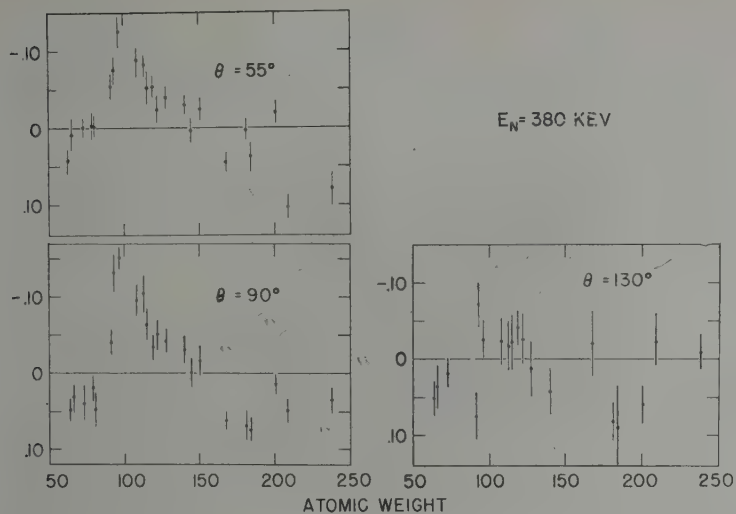


Figure 8

Polarizations measured for the scattering of 350-keV neutrons by intermediate and heavy elements as a function of atomic weight for three scattering angles [26].

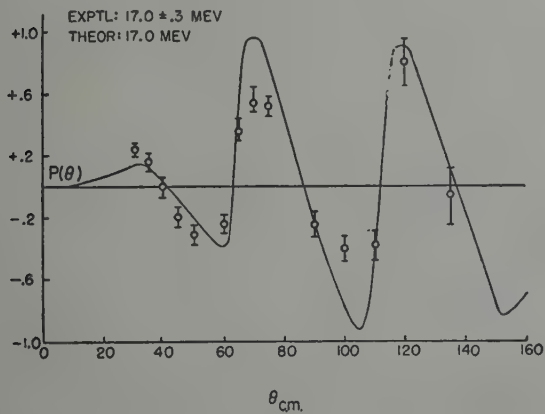


Figure 9

Angular distribution of the polarization of 17-MeV protons by zinc measured by BLANPIED [31]

REFERENCES

- [1] H. FAISSNER, *Ergeb. d. Exakten Naturw.* **32**, 180 (1959).
- [2] L. ROSEN, *Proceedings of the International Conference on the Nuclear Optical Model*, p. 27 (1959).
- [3] N. F. MOTT, *Proc. Roy. Soc. A* **724**, 425 (1929).
- [4] C. G. SHULL, C. T. CHASE, and F. E. MYERS, *Phys. Rev.* **63**, 29 (1943).
- [5] J. SCHWINGER, *Phys. Rev.* **73**, 407 (1948).
- [6] R. G. P. VOSS and R. WILSON, *Phil. Mag.* **1**, 175 (1956).
- [7] G. V. GORLOV, N. S. LEBEDEVA, and V. M. MOROSOV, *Conference on Nuclear Reaction at Low Energies*, Moscow 1958, p. 93.
- [8] J. SCHWINGER, *Phys. Rev.* **69**, 681 (1946).
- [9] L. WOLFENSTEIN, *Phys. Rev.* **75**, 1664 (1949).
- [10] M. HEUSINKVELD and G. FREIER, *Phys. Rev.* **85**, 80 (1952).
- [11] C. L. CRITCHFIELD and D. C. DODDER, *Phys. Rev.* **76**, 602 (1949).
- [12] R. K. ADAIR, *Phys. Rev.* **82**, 750 (1951).
- [13] M. J. SCOTT, *Phys. Rev.* **110**, 1398 (1958).
- [14] K. W. BROCKMAN, *Phys. Rev.* **110**, 163 (1958).
- [15] L. ROSEN and J. E. BROLLEY, *Phys. Rev.* **107**, 1454 (1957).
- [16] T. A. TOMBRELLO, R. BARLOUTAUD, and G. C. PHILLIPS, *Phys. Rev.* **119**, 761 (1960).
- [17] J. E. EVANS and M. A. GRACE, *Nucl. Phys.* **15**, 646 (1960).
- [18] P. HUBER and E. BAUMGARTNER, *Helv. Phys. Acta* **26**, 420 (1953).
- [19] R. RICAMO, *Nuovo Cim.* **10**, 1607 (1953).
- [20] R. W. MEIER, P. SCHERRER, and G. TRUMPY, *Helv. Phys. Acta* **27**, 577 (1954).
- [21] R. K. ADAIR, S. E. DARDEN, and R. E. FIELDS, *Phys. Rev.* **96**, 503 (1954).
- [22] I. I. LEVINTOV, A. V. MILLER, and V. N. SHAMSHEV, *JETP* **32**, 274 (1957).
- [23] J. D. SEAGRAVE, *Phys. Rev.* **92**, 1222 (1953).
- [24] S. M. AUSTIN, Thesis, University of Wisconsin, 1960.
- [25] I. ALEXEFF and W. HAEßERLI, *Nucl. Phys.* **15**, 609 (1960).
- [26] J. D. CLEMENT, F. BORELI, S. E. DARDEN, W. HAEßERLI, and H. R. STRIEBEL, *Nucl. Phys.* **6**, 177 (1958).
- [27] A. E. REMUND, *Helv. Phys. Acta* **29**, 545 (1956).
- [28] M. F. STEUER, W. P. BUCHER, and F. L. HEREFORD, *Congrès International de Physique Nucléaire*, Paris 1959, p. 545.
- [29] J. X. SALADIN and P. MARMIER, *Helv. Phys. Acta* **33**, 299 (1960).
- [30] R. E. WARNER and W. P. ALFORD, *Phys. Rev.* **114**, 1338 (1959).
- [31] W. A. BLANPIED, *Phys. Rev.* **113**, 1099 (1959).
- [32] L. S. RODBERG, *Nucl. Phys.* **15**, 72 (1960).
- [33] S. E. DARDEN, C. A. KELSEY, and T. R. DONOGHUE, *Nucl. Phys.* **16**, 351 (1960).
- [34] M. BRÜLLMANN, H. J. GERBER, D. MEIER, and P. SCHERRER, *Helv. Phys. Acta* **32**, 511 (1959).
- [35] W. P. BUCHER, W. B. BEVERLY, G. C. COBB, and F. L. HEREFORD, *Nucl. Phys.* **13**, 164 (1959).
- [36] L. CRANBERG, *Phys. Rev.* **114**, 174 (1959).
- [37] J. E. BROLLEY, T. M. PUTNAM, L. ROSEN, and L. STEWART, *Phys. Rev.* **117**, 1307 (1960).
- [38] S. M. SHAFROTH, R. CHALMERS, E. N. STRAIT, and R. E. SEGEL, *Phys. Rev.* **118**, 1054 (1960).

Measurements of Polarization in $C^{12}(p,p)$ Scattering

By J. E. EVANS, A.E.R.E., Harwell

1. Introduction

There are two good reasons for investigating the polarization produced in $C^{12}(p,p)$ scattering. One is to provide the data for using C^{12} as an analyser of proton polarization, and in this connection it is worth mentioning that a solid carbon analysing target has several advantages over gaseous helium. These are:

1. A target in the form of a plane sheet allows better geometry than a volume of gas.
2. No energy is lost in target-containing windows.
3. Less energy is lost to the recoiling carbon nucleus than to a helium nucleus. 2 and 3 imply that the final protons are detected in the presence of less background and with better resolution.

The second reason for measuring $C^{12}(p,p)$ polarization is to provide a sensitive check on the accuracy of phase shifts derived from the $C^{12}(p,p)$ angular distribution, and we include an application of this.

2. Experiments with the 5 MV Electrostatic Generator

This work was reported recently. It was done in collaboration with Dr. M. A. GRACE [1]¹). The $C^{12}(p,p)$ polarization was measured at 60° (lab.) in the energy range 2.3–4.3 MeV using helium as an analyser. Figure 1 shows the arrangement used. The self supporting carbon target was made by spraying a suspension of colloidal graphite in alcohol on to a glass slide. The carbon film (2 mg/cm^2) was floated off after evaporation of the alcohol.

The CsI crystals used for detecting the protons were milled down to $.0025''$ in order to minimize the background. The technique for doing this was described [1]. The pulse height spectrum of the observed protons is shown in figure 2.

¹) Numbers in brackets refer to References, page 248.

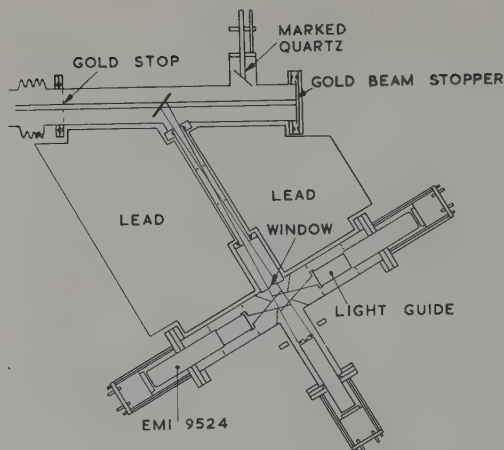


Figure 1
The first scattering chamber and the helium polarimeter

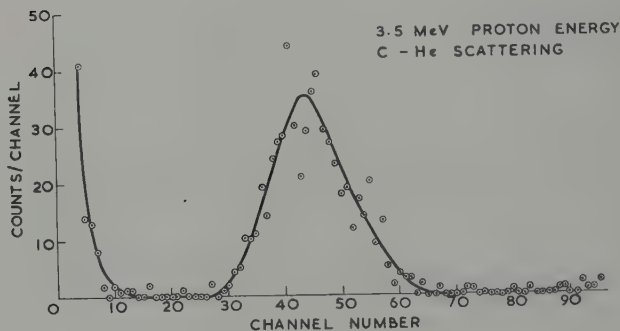


Figure 2
The pulse height spectrum of protons after double scattering from carbon and helium.
The initial energy was 3.5 MeV.

The results for the polarization are shown in figure 3 along with two points obtained by double scattering from C^{12} at 60° . The polarization predicted from a phase shift analysis due to REICH, PHILLIPS and RUSSELL [2] is also shown. In this region the polarization is extremely sensitive to changes in the splitting of the two d -waves, but not to the s - and p -wave phase shifts. A change of 6° in the separation of the two d -wave phases is sufficient to account for the large discrepancy observed

in the polarization at 4 MeV but the corresponding change in the cross section as measured by REICH *et al.* is only of the order of their experimental error. We sent our results to Dr. G. C. PHILLIPS at the Rice Institute who deduced a very similar correction to the phase shifts [3]. Figure 4 shows the effect on the polarization of varying the d -wave separation.

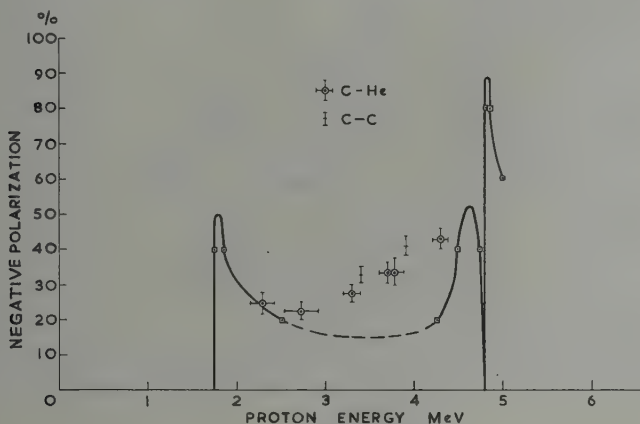


Figure 3

Experimental results for $C^{12}(p, p)$ Polarization at 60° (lab.) with the polarization predicted from the phase shift analysis

3. Experiments with the 12 MV Tandem Electrostatic Generator

Dr. J. H. MONTAGUE has collaborated in much of this work which is being done to extend the energy range of the measurements. As a complementary programme Drs. DEARNALEY, MONTAGUE and WHITEHEAD have made angular distribution measurements of the elastic scattering for a phase shift analysis. A carbon polarimeter has been incorporated in a 30" scattering tank, after a suggestion by Dr. E. PAUL. It is shown in figure 5. The polarimeter can be rotated from outside the evacuated tank, so that the first scattering angle is continuously variable. Each CsI crystal is suspended within a reflecting enclosure, normal to the surface of the photo-cathode of a 2" EMI tube. With an arrangement such as in figure 5, the flux of protons striking the first target is perhaps a factor of 10^{14} times the flux of protons being detected. This means that the polarimeter must be screened to prevent protons reaching the detectors by devious paths after being scattered from the walls of the tank.

The energy of the beam from the Tandem Generator was calibrated after scattering from a thin carbon foil into the back counter shown in figure 5. For this purpose we used the results of REICH *et al.* for the scattered intensity near the 4.8 MeV resonance in the elastic scattering. This enabled us to relate the analyser magnet field as measured with a proton resonance magnetometer to the beam energy.

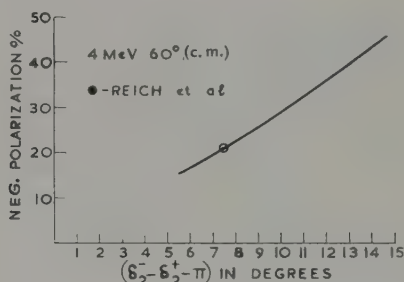


Figure 4

$C^{12}(p, p)$ polarization at 4 MeV and 60° (c.m.) as calculated from the phase shifts of REICH (*et al.* [2]) with the d -wave splitting varied

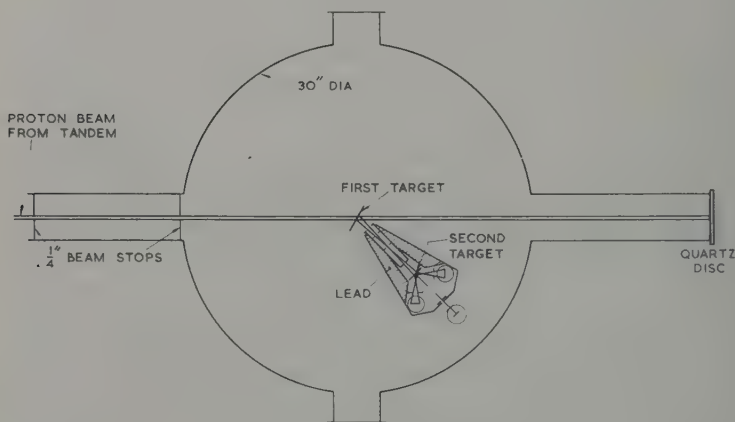


Figure 5

Scattering tank with carbon polarimeter

The most efficient way to use a polarimeter is to incorporate large solid angles so as to keep the counting rate high. The effective polarization P_2 for analysing is then inferred from a calibration in which well-

collimated protons of known polarization P_1 enter the polarimeter, to produce a measured right-left asymmetry. The calibration so obtained remains good for subsequent experiments so long as polarization and cross-section do not vary between the angular limits set by the entrance slit of the polarimeter.

We required accurate values of P_1 in order to calibrate the polarimeter. It is readily seen that the product $P_1 \bar{P}_2$ should be as large as possible for good accuracy. If X is the right-left ratio, then $\delta(P_1 \bar{P}_2)/P_1 \bar{P}_2 \simeq 2 \delta X/X^2$ for $X \gg 1$.

It is known from the work of WARNER and ALFORD [4] carried out with a helium polarimeter, that the polarization in $C^{12}(p, p)$ at 45° (lab.) is very high in the region of 5.5 MeV. We used a different method to check their results and to provide values of P_1 with which to calibrate the polarimeter. This method, which is not new [5] has the advantage of being self-consistent. First, good geometry in the polarimeter was achieved by setting small circular apertures ($3/16''$) in front of the counters at 1.55 inches from the carbon analysing target. These then defined a mean value of 48° for the second scattering angle. The beam entering the polarimeter was of circular section and well collimated ($\pm 0.7^\circ$ R.M.S. deviation). Then a good approximation to the angular detector efficiency (in arbitrary units) is given by

$$I(x) = \int_{x-1}^1 \left[(1-y^2) \left(1 - \frac{x^2}{y^2} \right) \right]^{1/2} dy$$

where x is proportional to the deviation from 48° . This function was tabulated by the Computer Group and the R.M.S. deviation found to be $\pm 2.4^\circ$.

Three experiments on double scattering of protons on C^{12} at 48° (lab.) were now performed.

The good geometry made a low counting rate inevitable. With $2 \mu A$ of protons hitting the first target, the counting rate in the depleted detector was about one per minute. The counter resolution however was excellent. The spread in the peak of double scattered protons was $6\frac{1}{2}\%$ at half height. The CsI crystals were $.010''$ thick and the background was negligible.

The mean scattering energies E_1, E_2 for the three experiments were arranged to be

E_1 (MeV)	E_2 (MeV)
5.59	5.16
6.04	5.16
6.04	5.59 .

For the second experiment an aluminium foil was placed between the carbon targets. To ensure that E_1 , E_2 were as tabulated, the energy loss in each target was measured using the back counter shown in figure 5, in a subsidiary experiment. A foil support was made which could be moved in front of a gold target placed at the centre of the scattering chamber. Protons were reflected into the back counter which was calibrated by varying the machine energy. Then the carbon targets which had been fixed to the support were moved in turn into the scattered beam and the consequent energy loss measured. The required thickness for the aluminium foil was then calculated and a suitable foil obtained and its thickness confirmed in the same way.

In order to deduce the three polarization products ($P_1 P_2$) from the experiments it was necessary to take account of the asymmetry due to mechanical inaccuracies in the polarimeter as well as that due to the angular spread of the beam entering the polarimeter. Another subsidiary experiment was done in which a gold target (5 mg/cm²) was used to scatter protons into the polarimeter. These protons are not expected to be polarized [1] so that any difference in the detector counting rates which is not statistical must be due to the asymmetry described above. The effect of the angular spread of the first scattered beam is calculable (see 4 below) and was removed from the counting rate ratio of the two detectors. The amended ratio was found to be $0.97 \pm .025$ ($\theta_1 = -48^\circ$) and $0.97 \pm .025$ ($\theta_1 = +48^\circ$) where θ_1 is the first scattering angle. The counter efficiencies were thus taken to be in the ratio of 0.97:1. One can distinguish three separate effects which may determine this ratio.

- a) The two detectors may subtend unequal solid angles.
- b) The polarimeter carbon target may be non-uniform.
- c) The scattering angles set by the two detectors may be unequal.

The three experimental right-left ratios for the carbon double scattering were obtained with the first scattering angle set at $+48^\circ$ and again at -48° . Each ratio was corrected first using the efficiency ratio of 0.97:1. The products $P_1 P_2$ were then deduced using the formula of 4 below. For this purpose the angular distributions of polarization and cross-section at 5 MeV were taken from the literature [2, 3]. The three products then allowed calculation of the polarization in $C^{12}(p, p)$ at 48° (lab.) at the three different energies tabulated.

So long as asymmetry of type (c) above is not present one expects to find that each product $P_1 P_2$ deduced as described should not depend on the sign of the first scattering angle. In fact no such dependence was found within the counting statistics. It is worth noting that only a special type of asymmetry due to (c) will be revealed by the experiment with a gold first target. (This special type occurs when the rotation

from -48° to $+48^\circ$ does not take place about the first target as centre. Our results do not indicate the presence of this special type.) In order to obtain consistent results, it was found necessary to ensure that the beam entering the scattering chamber, did so only after completely filling the $1/4''$ apertures. The reason for this is clear when it is realised that at 48° the C^{12} differential scattering cross-section is changing at the rate of 5% per degree so that a misalignment of 1° in the polarimeter produced a 10% effect in the right-left ratio.

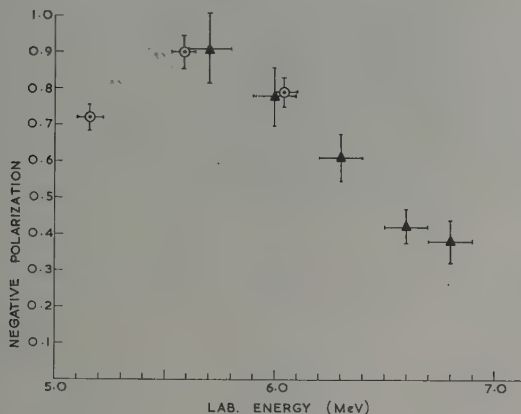


Figure 6

$C^{12}(p, p)$ polarization. The present results at 48° (lab.) are shown as open circles. The full triangles represent the results of WARNER and ALFORD at 45° (lab.).

The effect of the angular spread in the second scattering was examined. If the first scattering geometry is regarded as perfect (apart from the asymmetry effects considered in [4]) then the second polarization as measured is a mean polarization defined by

$$\bar{P}_2 = \frac{\int \sigma_2(\theta_2) P_2(\theta_2) \phi(\theta_2) d\theta_2}{\int \sigma_2(\theta_2) \phi(\theta_2) d\theta_2}$$

where θ_2 is the angle of second scattering and $\phi(\theta_2)$ is the angular detector efficiency introduced earlier. A numerical integration using the forms for $P_2(\theta_2)$ and $\sigma_2(\theta_2)$ in the literature [2, 3] showed however that P_2 was only 1% less than $P_2(48^\circ)$. This implied that the three values of the polarization in $C^{12}(p, p)$ at 48° (lab.) as calculated were only $\frac{1}{2}\%$ low. These values were

Lab. Energy (MeV)	Polarization
6.04	$-0.79 \pm .04$
5.59	$-0.90 \pm .045$
5.16	$-0.72 \pm .036$

They are shown plotted in figure 6 and the results of WARNER and ALFORD at $45^\circ \pm 2.3^\circ$ also plotted for comparison. The experiment we have described does not give the sign of the polarization. We were in no doubt about this however even without the results of WARNER and ALFORD because we had done preliminary experiments with a polarimeter of poor geometry using our earlier results (figure 3) for calibrating the polarimeter. The polarization found was always negative when defined by the vector $\mathbf{K}_{in} \times \mathbf{K}_{out}$.

The results of figure 6 are now being used for an accurate calibration of the polarimeter, used with poor geometry. Absorber foils will then be used to extend the polarization measurements if possible to the maximum energy available with the Tandem Generator (11.5 MeV).

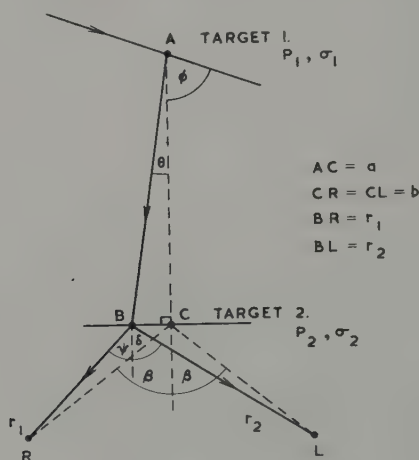


Figure 7

The effects of an extended second target in a double-scattering experiment

4. The Asymmetry due to an Extended Second Target

Figure 7 shows the arrangement of a double scattering experiment. It may be seen that the right/left ratio observed is given by

$$\frac{R}{L} = \frac{+\theta_1 \int \sigma_1(\phi+\theta) \sigma_2(\psi-\theta) \cdot S(\theta) \cdot \frac{1}{r_1^2} [1 + P_1(\phi+\theta) \cdot P_2(\psi-\theta)] d\theta}{-\theta_1 \int \sigma_1(\phi+\theta) \sigma_2(\delta+\theta) \cdot S(\theta) \cdot \frac{1}{r_2^2} [1 - P_1(\phi+\theta) \cdot P_2(\delta+\theta)] d\theta}$$

where $S(\theta)$ is a source term which depends on the shape of the second target. After expanding, this ratio turns out [6] to be as given in figure 8 where σ_1, σ_2, P_1 and P_2 and their derivatives with respect to angle are evaluated at the mean angles set by the apparatus. A calculation which applies to the good geometry experiment described gives for 5 MeV protons.

$$\frac{R}{L} = \frac{1 + 0.022 + P_1 P_2 (1 - 0.011)}{1 + 0.044 - P_1 P_2 (1 + 0.005)}$$

The parameters were:

$$\begin{aligned} a &= 7.0 \text{ inches} \\ b &= 1.55 \text{ inches} \\ \beta &= 48^\circ \\ \theta_1 &= .027 \text{ radians.} \end{aligned}$$

Figure 8
Effect of an extended second target

$$\frac{R}{L} = \frac{1 + (R+S) \frac{\theta_1^2}{n} + P_1 P_2 \left\{ 1 + [(V+PT+QU+R) + (W+QT+UP+S)] \frac{\theta_1^2}{n} \right\}}{1 + (R-S) \frac{\theta_1^2}{n} - P_1 P_2 \left\{ 1 + [(V+PT+QU+R) - (W+QT+UP+S)] \frac{\theta_1^2}{n} \right\}}$$

where $n = 3$ for a rectangular target

$n = 4$ for a circular target

$$P = \frac{\sigma'_1}{\sigma_1}$$

$$Q = 2B \sin \beta - \frac{A \sigma'_2}{\sigma_2}$$

$$R = \frac{A^2}{2} \frac{\sigma''_2}{\sigma_2} - \frac{B^2}{2} \sin 2\beta \frac{\sigma'_2}{\sigma_2} + \frac{\sigma''_1}{2\sigma_1} - B^2 - 2AB \sin \beta \frac{\sigma'_2}{\sigma_2}$$

$$S = \frac{\sigma'_1}{\sigma_1} \left[2B \sin \beta - A \frac{\sigma'_2}{\sigma_2} \right]$$

$$T = \frac{P'_1}{P_1}$$

$$U = -A \frac{P'_2}{P_2}$$

$$V = \frac{A^2}{2} \frac{P''_2}{P_2} - \frac{B^2}{2} \sin 2\beta \frac{P'_2}{P_2} + \frac{P''_1}{2P_1}$$

$$W = -A \frac{P'_1 P'_2}{P_1 P_2}$$

and $A = \frac{a \cos \beta}{b} + 1$

$$B = \frac{a}{b}$$

REFERENCES

- [1] J. E. EVANS and M. A. GRACE, Nucl. Phys. *75*, 646 (1960).
- [2] C. W. REICH, G. C. PHILLIPS, and J. L. RUSSELL, JR., Phys. Rev. *104*, 143 (1956).
- [3] T. A. TOMBRELLO, R. BARLOUTAUD, and G. C. PHILLIPS, Submitted for publication in Physical Review.
- [4] R. E. WARNER and W. P. ALFORD, Phys. Rev. *114*, 1338 (1959).
- [5] M. J. SCOTT, Phys. Rev. *110*, 1398 (1958).
- [6] J. E. EVANS, A calculation of the asymmetry due to an extended second target in experiments to determine nuclear spin polarization. A.E.R.E. Report R 3347.

Polarization in Proton-Helium and Proton-Carbon Elastic Scattering

By J. SANADA, Institute for Nuclear Study, University of Tokyo

Proton-Helium Scattering

We have made measurements of the polarization in proton-helium scattering near 10 MeV with the INSJ 160 cm variable energy cyclotron [1]¹⁾ and an usual double scattering chamber [2]. Three interdependent polarization products, $P_1 P_2$, $P_2 P_3$ and $P_3 P_1$, were measured. The individual polarizations may be stated in terms of observed quantities [3] as:

$$P_1 = \left(\frac{P_1 P_2 \cdot P_3 P_1}{P_2 P_3} \right)^{1/2}, \quad P_2 = \left(\frac{P_1 P_2 \cdot P_2 P_3}{P_3 P_1} \right)^{1/2}, \quad P_3 = \left(\frac{P_2 P_3 \cdot P_3 P_1}{P_1 P_2} \right)^{1/2}.$$

The results of the individual polarizations are: P (7.8 MeV, 117°) = 0.92 ± 0.11 , P (11.4 MeV, 50°) = -0.45 ± 0.06 and P (14.4 MeV, 50°) = -0.45 ± 0.06 , where energies and angles are those in the laboratory system. The measurements of the differential cross sections in the same energy region [4] showed that there is no D-state resonance and the differential cross sections are fitted almost with S- and P-waves, from the phase shift analysis. The values of the polarization calculated from phase shifts are: P (7.8 MeV, 117°) = 1.00, P (11.4 MeV, 50°) = -0.47 , P (14.4 MeV, 50°) = -0.39 , which agree with experimental values. Thus we can use the proton-helium scattering as a standard analyzer of the polarization of protons even up to 15 MeV.

Series Polarimeter

As the next step, we have investigated the polarization in proton-carbon elastic scattering. At that time, we devised a series polarimeter, which is composed of two polarimeters in a row, the one for carbon target and the other for helium target. Figure 1 shows its photograph. The main

¹⁾ Numbers in brackets refer to References, page 252.

purpose of this device is the saving of time in taking data. In general, data concerning an unknown target are taken and the analysing of the polarization of the incident beam are made simultaneously.

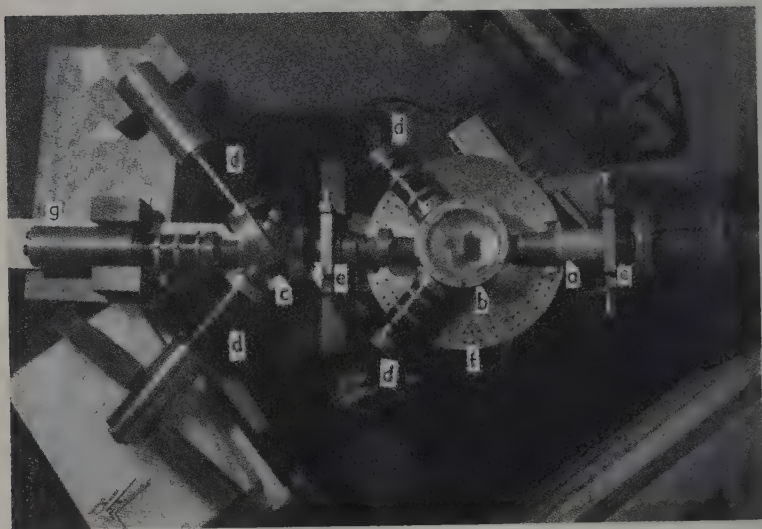


Figure 1

The photograph of the 'Series polarimeter'.

a: collimator tube, b: target chamber, c: gas chamber, d: scintillation detector, e: ball bearing, f: disk for setting detectors, g: monitor counter.

The polarized beam, which was obtained from some kind of the first scattering, entered the collimator. The collimator has two slits of 10 mm wide and 20 mm high. Each is separated by 300 mm. Behind the collimator, a target chamber is installed. A graphite target foil was set at its center. The chamber has in its inside an annular slit ring, which has 9 pairs of slit holes arranged symmetrically about the direction of the beam. A gas chamber is attached to the end of the target chamber. Between these two chambers, a stainless steel foil of 35 microns thick is inserted and sustains the high gas pressure. The gas chamber and this foil were tested up to 15 atmospheric pressure. A pair of double slits, which defines the scattering angle, the target thickness and the solid angle, of the proton-helium scattering, was set at an angle of 50° .

The whole instruments above described, including the scintillation counters, can be rotated through 180° about its own axis, in order to eliminate the asymmetry due to instrumentation.

Proton-Carbon Scattering

The measurements of the differential cross sections in the energy range of 7 to 16 MeV [5] showed a sharp resonance at 9 MeV and a broad resonance at 10.5 MeV. The shape of the angular distribution of the differential cross sections resembled those derived from the optical potential, except at the resonances above described. Then, it is in interesting to investigate the polarization in the same energy region.

The measurements of the angular distribution of the polarization in proton-carbon elastic scattering were made by ROSEN *et al.* [6] at 11.5 MeV, by YAMABE *et al.* [7] at 14 and 16 MeV, and by BROCKMAN at 17.7 MeV [8]. The main feature of these results resemble also those derived from the optical potential [9].

In the present work, we have made a measurement of the angular distribution of the polarization at 10.5 MeV, with the series polarimeter. Figure 2 shows the result. Since the width of the energy of protons in the scattering was not so small, ± 0.5 MeV, some averaging effects may occur over the resonance region. But the result shows the pattern, which is essentially different from the one derived from the optical potential.

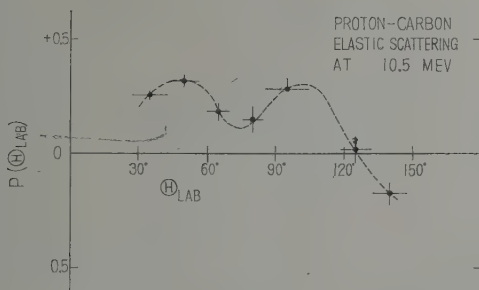


Figure 2
The angular distribution of the polarization.

To determine the energy dependence of the polarization, we have measured the polarization at an angle of 50° in the laboratory system, varying the energy of protons. The result is shown in figure 3. $P(50^\circ)$ is almost constant and about 70 percent from 12 MeV to 17 MeV. This character may show the usefulness of proton-carbon elastic scattering as the sub-standard analyser in the energy region above. Below 12 MeV, the energy dependence of the polarization is remarkable. $P(50^\circ)$ changes its sign at 11 MeV.

The present work has been done by the collaboration with Drs. S. SUWA, I. HAYASHI, K. NISIMURA, N. RYU and H. HASAI. The more details will be given in elsewhere.

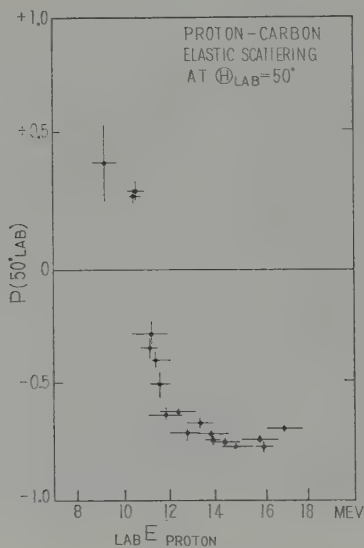


Figure 3
The energy dependence of $P(50^\circ_{\text{LAB}})$.

REFERENCES

- [1] S. KIKUCHI *et al.*, J. Phys. Soc. Japan **15**, 41 (1960).
- [2] SANADA, NISIMURA, SUWA, HAYASHI, FUKUNAGA, RYU, and SEKI, J. Phys. Soc. Japan **15**, 754 (1960).
- [3] M. J. SCOTT, Phys. Rev. **170**, 1398 (1958).
- [4] J. SANADA, J. Phys. Soc. Japan **14**, 1463 (1959).
- [5] Y. NAGAHARA, J. Phys. Soc. Japan, to be published.
- [6] L. ROSEN, *Proceedings of the International Conference on the Optical Model*, The Florida State University (1959).
- [7] S. YAMABE *et al.*, J. Phys. Soc. Japan, to be published.
- [8] K. W. BROCKMAN, Phys. Rev. **170**, 163 (1958).
- [9] G. W. ERICKSON and W. B. CHESTON, Phys. Rev. **171**, 891 (1958).

Polarization in $p\text{-He}^4$ and $p\text{-}p$ Scattering at 22 MeV

By H. E. CONZETT, G. IGO and A. NIR¹⁾

Lawrence Radiation Laboratory, University of California, Berkeley

We have developed a beam of 22-MeV protons, using $p\text{-He}^4$ scattering as the polarizing mechanism. We have followed the method first used by ROSEN and BROLLEY [1]²⁾ three years ago, but before describing a few details of the method, I should like to summarize briefly the information available on $p\text{-He}^2$ scattering as a proton polarizer. This can be done most conveniently in terms of the following table.

Table

E_{LAB} (MeV)	Data		Reference
	(θ)	$P(\theta)$	
0.95-18	X	—	K. W. BROCKMANN, Phys. Rev. 108, 1000 (1957) contains a list of authors whose work is referred to here. M. K. RUSSELL and J. H. WILLIAMS, Phys. Rev. 106, 286 (1957).
39.8	X	—	
1.37	—	one angle	M. J. SCOTT, Phys. Rev. 110, 1398 (1958).
2.02	—	one angle	
3.58	—	one angle	J. SANADA <i>et al.</i> , J. phys. Soc. Japan, to be published.
7.8	—	one angle	
11.4	—	one angle	
14.4	—	one angle	
10	—	10 angles	Reference 1.

Phase shifts derived from analyses of the very complete differential cross section data have been used to calculate the polarizations; and finally, description of the $p\text{-}\alpha$ interaction in terms of an effective two-body potential with a central and a spin orbit term has resulted in inter-

¹⁾ On leave from the Weizmann Institute, Rehovoth, Israel.

²⁾ Numbers in brackets refer to References, page 258.

polations and predictions of the phase shifts, and thus the polarizations, up to 40 MeV [2]. It should be noted here (table) that the polarization measurements at these energies are sparse; and, since the polarizations are more sensitive than the angular distributions of the differential cross sections to uncertainties in the phase shifts, it is important to extend these measurements in order to provide further checks on theory, and thus enable experimenters to use the calculated values more confidently. The results of GAMMEL and THALER's optical-model potential calculations are shown in figure 1. I want to call your attention to the fact that between 10 and 11 MeV $P(130^\circ) > +90\%$, and in fact, ROSEN and BROLLEY's [1] measured value at 10 MeV is $P(130^\circ) = +99_{-2}^{+1}\%$. It is precisely this measurement that we use in setting up our polarized proton beam; that is, we have incident on a H_2 gas target a 43.1 MeV α -particle beam of about $1 \mu A$ intensity. Protons knocked on at a laboratory angle of 25° are in fact equivalent to 10.8 MeV (lab. energy) protons scattered from He^4 at a centre-of-mass angle of 130° .

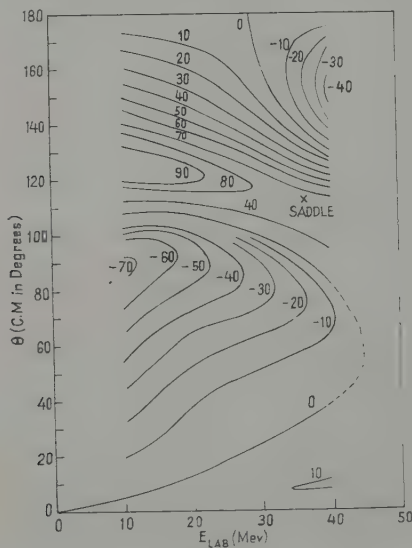


Figure 1

Figure 2 shows a sketch of our experimental set up. The region of the first scattering is imbedded in paraffin to reduce the high-energy neutron background that is most troublesome. This is shown by the dotted line. After passing through the H_2 gas target, the α -beam passes through a shielding wall, is stopped in a Faraday Cup and monitored.

The protons knocked on at 25° with respect to the incident beam are collimated into the second scattering chamber. Measured left-right asymmetries in the second scattering then give us P_2 , the polarization

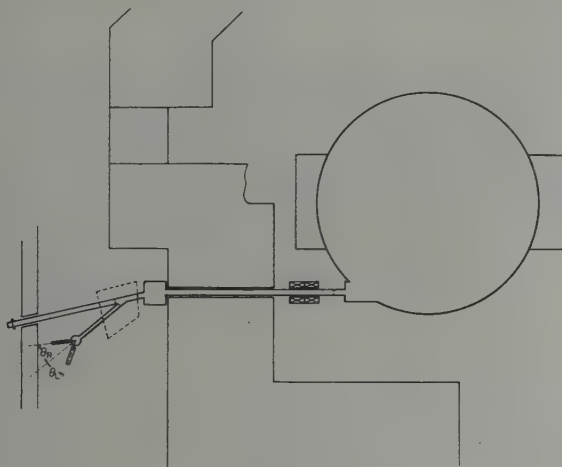


Figure 2

that would be induced in the second scattering if the proton beam were unpolarized. Figure 3 is a schematic drawing of our scattering geometry; the α -particle energy of 45.5 MeV is that just on the downstream side of the entrance foil. The following conditions apply:

1. First scattering: 8 atm. of H₂, $E_\alpha = 43.1$ MeV, $E_p = 23$ MeV.
2. Second scattering: 6 atm. of He⁴ or H₂, $E_p = 22$ MeV, Polarization essentially 100%, and a beam of $\approx 6 \cdot 10^6$ protons/s.
3. $\Delta\theta_1$, the angle subtended at the first scattering volume by the 11.16" collimator defining the proton beam, is about 1.4° . This angular spread is kept small in order to minimize the inherent asymmetry in the second scattering due to non-uniform illumination across the second target.
4. $\Delta\theta_2$, the angular resolution of our counters, including beam width, is about 9° .
5. This geometry gives us second-scattered counting rates in each counter of about 3000/h in p -He⁴ scattering at an angle of 45° .
6. We use a simple coincidence counting arrangement to reduce the background to the point where it constitutes no problem, at least for measurements in the forward hemisphere. A pulse from the plastic scintillator-photomultiplier tube is used to gate on the pulse-height

analyzer which records the pulses from the CsI crystal counter. Figure 4 shows a spectrum of the second-scattered protons, note the small background measured with a brass absorber placed in front of the counter.

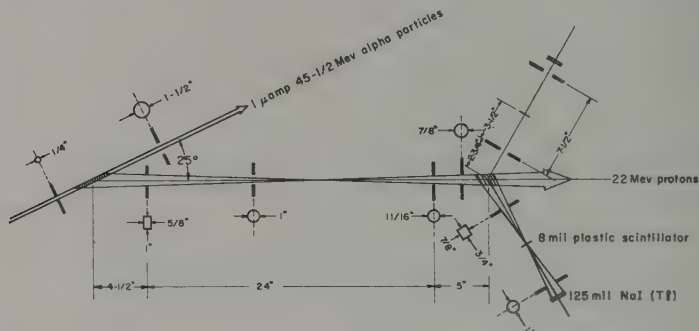


Figure 3

A measurement of P_2 comes directly from the asymmetry measurement because $\varepsilon = (L - R)/(L + R) = P_1 P_2$ and our P_1 is 100% within something like 2 or 3% figure 5 shows, then our results to date on p -He⁴ polarization at 22 MeV. The probable errors indicated are statistical. The solid curve represents GAMMEL and THALER's calculated values. This experiment is in progress and we will extend the measurements to the backward angles and will reduce the statistical errors on the points measured on this first run. We can also degrade our proton beam and extend the measurements to lower energies.

With the relatively high 2nd-scattered yields we have available, it was overwhelmingly tempting to try a quick measurement of the p - p polarization before this conference convened; especially, since in principle it was necessary only to change the gas in the 2nd-scattering chamber. Our preliminary result is

$P(50^\circ) = (+0.6 \pm 1.0)\%$ at 22 MeV to be compared with

$P(60^\circ) = (+1.2 \pm 2.0)\%$ at 17.7 MeV [3] and

$P(50^\circ) = (0.6 \pm 0.5)\%$ at 16.2 MeV [4].

Our probable error is that due to counting statistics alone, and we have not yet refined our equipment to the point where we can claim that the other sources of error are small in comparison. In fact, a qualitative estimate is $\pm 4\%$ due to the other sources, the major contribution coming from the fact that an electronic difficulty during part of a run made the data from one counter unuseable. Thus we had data from each counter only in one position and not with the counters inter-

changed, and so the differences in counter-detection efficiencies were not cancelled out.

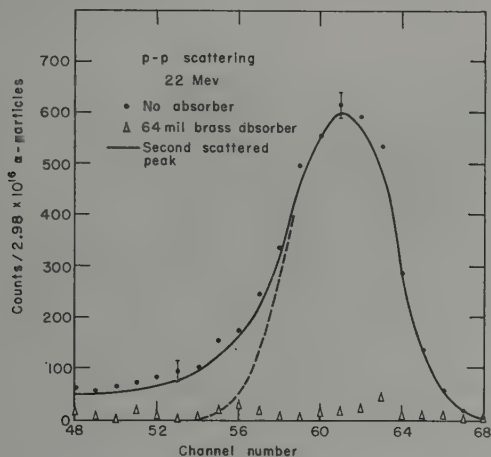


Figure 4

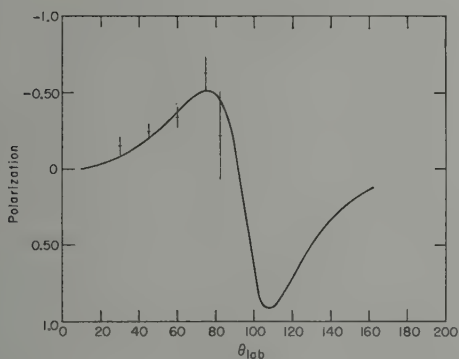


Figure 5

This raises the question of the importance of a measurement of the p - p polarization at these energies. MAC GREGOR's phase-shift analyses [5] of the differential cross section data result in four possible solutions, i.e. sets of phase shifts. Two of them predict small negative polarizations in the energy and angular regions of the above results and hence, seem to be ruled out by the polarization measurements. The other two solu-

tions predict small positive polarizations and even a very precise measurement cannot distinguish between them. Hence, in closing, we would welcome any expression of theoretical opinion on this question.

REFERENCES

- [1] L. ROSEN and J. E. BROLLEY, Jr., *Phys. Rev.* **107**, 1454 (1951).
- [2] J. L. GAMMEL and R. M. THALER, *Phys. Rev.* **109**, 2041 (1958).
- [3] K. W. BROCKMAN's result quoted in reference 2.
- [4] W. A. BLANPIED, *Phys. Rev.* **116**, 738 (1959).
- [5] M. H. MACGREGOR, *Phys. Rev.* **113**, 1559 (1959).

Proton Polarization Measurements around 17 MeV

By K. W. BROCKMAN, Jr.

Institute for Nuclear Studies, Amsterdam

Abstract. The work done on proton polarization at Princeton University for energies around 17 MeV is reviewed. The greatest emphasis is given to the work on proton-alpha polarization, but the other work of the author and his successor, W. A. BLANPIED, is discussed.

This paper is a review of the polarization work done at Princeton University using protons with energies around 17 MeV [1, 2, 3]¹⁾. The work was begun and carried through an initial phase by the author. In this period the instruments and techniques for measuring proton polarization in this energy region were developed and a few measurements were made. The second phase of the work was performed by W. A. BLANPIED. He continued the work and has made an important series of polarization measurements. While the results of Dr. BLANPIED will be recalled here, the paper will deal mainly with the work of the author.

The work was begun in 1955. It was motivated by the results that were at that time being found at very high energies. The idea was simply that the same sort of thing might be found at medium energies. There were theoretical reasons to support the idea, but there was little theoretical guidance concerning what might be expected, i.e., where to look and what magnitude might be found.

One way of proceeding might have been to set up a double scattering apparatus and to try various target materials and various scattering angles until an effect was found. The pit fall in this is that the asymmetry, which is the measured quantity, is the product of the polarizations for the two scattering events. Unless these polarizations are large, the asymmetry will be small. With no guarantee that polarizations in this energy region were large, and it was generally thought at that time that they might be rather small, this sort of procedure seemed a risky thing to try.

A much better technique is to use an event with a large known polarization for either the first or second scattering event. In 1955 there was only one suitable event that was known and tested. This was the scattering of protons by helium. The polarization to be expected in

¹⁾ Numbers in brackets refer to References, page 268.

this process had been calculated from the nuclear scattering phase shifts deduced from cross section measurements for energies up to 3.5 MeV [4]. The existence of the predicted polarization had been confirmed by a double scattering experiment [5]. This polarization measurement was in fact a crucial test deciding between two mathematically equivalent sets of phase shifts extracted from the scattering data.

Figure 1 shows a contour plot of the polarization in proton-alpha scattering as a function of laboratory energy and angle for energies up to 18 MeV. The values here have been calculated from phase shifts deduced from differential cross section measurements. Measured values of polarization played no role in the construction of the chart. No great accuracy is claimed for the values shown. The purpose of the calculations that are represented here was only to serve as a guide in the design of experimental apparatus.

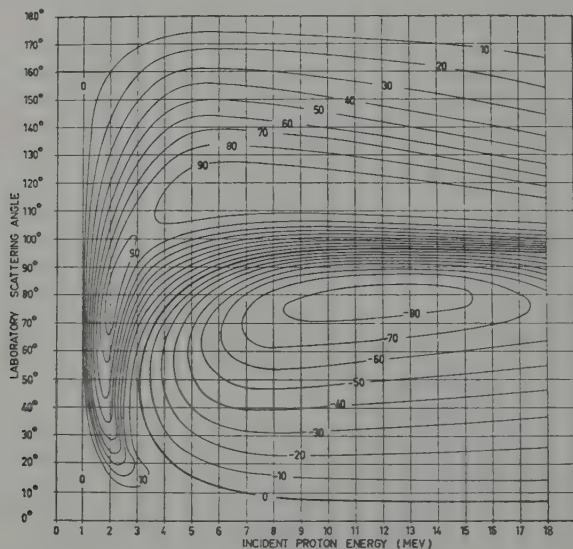


Figure 1

Contour plot of proton alpha polarization as a function of laboratory energy and laboratory scattering angle

The region of the chart below 3.5 MeV was the part for which values of polarization had been published in 1955. We tried to set up an experiment using only this information. An apparatus was built in which the first scatterer was the material under investigation. Scattered particles were then reduced in energy to the region of 2.5 MeV by letting them pass through foils and were scattered the second time by helium at 90.

The apparatus was a complete failure for nothing recognizable was ever observed. The reason for the failure lay in the fact that counters were used as detectors. Success might have been achieved with nuclear emulsions.

When the attempt to use the 2.5 MeV polarization failed it was decided to investigate the polarization predicted by scattering data for higher energies. Phase shifts for measured cross sections had been found for energies up to 9.5 MeV [6]. A calculation using these values revealed the part of the chart up to this energy. A strong maximum appeared to be developing in the region of 60° to 80° , and it seemed that this maximum might persist up to still higher energies. A region of strong polarization at more forward angles is experimentally favorable for two reasons: First, the scattering cross section is larger for smaller angles. Second, less energy is lost by the scattered proton to the recoil of the alpha particle, and detection problems are simpler. It was desirable now to try to extend the prediction of polarization to the region of 18 MeV, the region of the proposed experiments. The only analysable proton-alpha cross section measurement above 9.5 MeV was due to the author [7]. The only phase shift analysis of that data was also due to the author and this was thought to be incorrect. It was necessary therefore to investigate the problem of extending the lower energy phase shifts from the region of 9.5 MeV to the region of 18 MeV.

If a thorough analysis of the data at 17.5 MeV is carried out, one must expect to find more than one set of phase shifts fitting the data. The reason for this is that the formula for the cross section in terms of the phase shifts is the squared magnitude of the amplitude function which itself involves the phase shifts as the arguments of trigonometric functions. Besides a possible ambiguity arising from the periodicity of trigonometric functions, there is the more serious problem that extraneous roots may appear due to the non linearity of the cross section formula. Thus unless one has additional information he will not know which set of roots at the higher energy corresponds to those known to apply at the lower energies.

One method that might be used to match the lower energy results to higher energy ones is to fit the lower energy ones with a model, such as an optical model, and to use the model to extrapolate the phase shifts to the higher energy. Such a procedure may seem risky. When optical models are used with heavier nuclei, the parameters used are found to vary with energy. In the present case the extrapolation required is over a region in which the energy almost doubles. In addition to this there is the opinion of many theorists that optical models should not be applied to very light nuclei. In spite of these difficulties, GAMMEL and THALER have used a potential model for this purpose with some success [8].

Their model allows them not only to connect the low energy measurements with those at 17.5 MeV but also with those at 40 MeV. We shall comment on these results later but will first describe our own procedure for the extension of the lower energy phase shifts to the region of 18 MeV.

We use the fact that the phase shifts must be continuous functions of the energy. Then if several measurements of the cross section are made at energies intermediate to 9.5 MeV and 17.5 MeV and a phase shift analysis is made for each of these measurements, then one may follow the correct phase shifts up in energy using only the condition of continuity. Accordingly, a scattering chamber was set up to measure the cross section at a set of fixed angles at a number of energies between 11 and 18 MeV [9]. Figure 2 shows the proton helium scattering cross section at three energies. The vertical lines show the angles chosen for the new measurements. When these angles were chosen it was thought that they were a sufficient set for the purpose of phase shift determinations. This turned out to be a serious error in judgement. Apparently it is necessary to have measurements at still smaller angles to be able to determine the D wave phase shifts. If one smaller angle, say 20° , had been included, everything might have been all right. A least squares procedure was used to fit S and P phase shifts to the data. The fits obtained were very good, but when the phase shifts thus found were used to calculate the 17.5 MeV cross section it was found that the old data was not fitted in the small angle region. It was clear that the inclusion of D phase shifts was required at this energy

PROTON-ALPHA DIFFERENTIAL CROSS SECTIONS

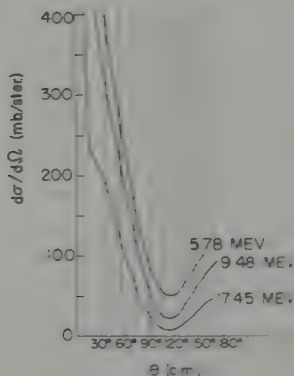


Figure 2

Proton alpha differential scattering cross section at three energies. Vertical lines show angles at which intermediate measurements were made

(this was, of course, expected from the beginning) but that the new data was not sufficient to find them. A least squares procedure including D waves was also tried with the new data but this failed to converge in practically every case. The failure of the D wave procedure to converge was attributed to experimental error and to the lack of data at a smaller angle.

Figure 3 shows S and P phase shifts as a function of energy. Those below 10 MeV are due to previous work while those above are the results of the analyses made here in terms of S and P phase shifts only. The lines drawn have no theoretical significance but were drawn by eye to pass through the points. Values were taken from these lines however to calculate the expected polarization in this region. The question that arises now is what sort of confidence can one have in polarization calculations based on such values. If one observes the scatter of the points and considers the criterion used to draw the line, and if one considers the fact that D wave phase shifts which must be present in this energy range have been neglected, then he cannot have too much faith in the exact values calculated. It is highly probable, however, that in this energy region the D phase shifts are small, probably no greater than 10° . Thus while the calculations cannot be expected to provide a very accurate prediction of the polarization, they can nevertheless be used as a guide to the sort of thing that may be expected.

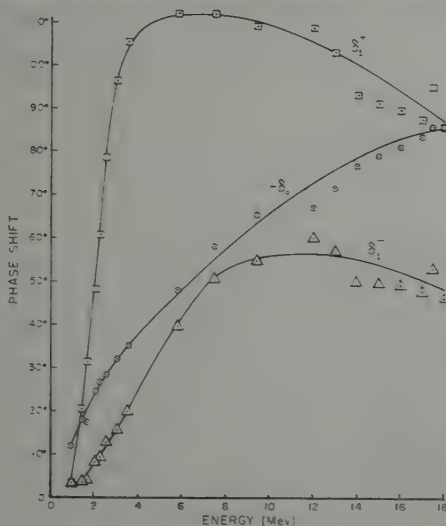


Figure 3

S and P phase shifts for proton alpha scattering as a function of energy

Figure 4 shows the angular distribution of polarization for 17.5 MeV proton-alpha scattering calculated with four sets of phase shifts. Curve 2 of the drawing was calculated using only the S and P phase shifts taken from the lines in figure 3. Curve 4 is calculated from GAMMEL and THALER's solution 5 [8]. This was their best fit to the 17.5 MeV data using S , P and D phase shifts. The remarkable agreement of these two calculations can only be regarded as fortuitous. Curve 3 was calculated from the phase shifts used to calculate the polarization chart of figure 1. They are closely related to one of GAMMEL and THALER's other solutions and were in fact chosen using some information received from them. Curve 1 was plotted from values read from GAMMEL and THALER's contour plot of polarization between 10 and 40 MeV [8]. This chart is based on the phase shifts calculated from their potential model which fits the data at 9.5, 17.5 and 40 MeV. The measurements shown are some of the measurements obtained by us which will be discussed a little later. They are not all at the same energy. Those at 30° and 45° were at about 17.5 MeV, but those at 65° and 115° were at about 15.5 MeV. Polarization at a particular angle does not vary very rapidly with energy in this region however so they still may be used to compare with the calculations. The interesting point to note here is the seeming superiority of GAMMEL and THALER's fit including only D waves (curve 4) to the results obtained from their potential mode (curve 1). While one of their purposes in choosing this model may have been to use it as an interpolation device, part of their motivation must have been to be able to account for the still higher order phase shifts which one feels

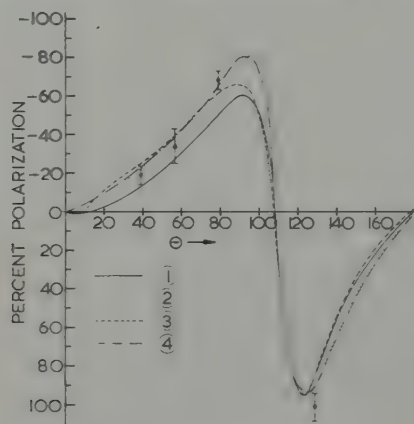


Figure 4

Angular distribution of polarization for 17.5 MeV proton alpha scattering. The various curves are identified in the text

must be present. It is curious that when they try to account for these higher order partial waves that the results should be inferior to those when they are ignored. This difficulty introduced with their model also shows up in the scattering cross section. They refer to this as the forward scattering problem. Figure 5 shows the proton alpha differential cross section at 17.5 MeV in the region of the nuclear-coulomb interference. Here the cross section calculated from the model – the line in the drawing – shows a much more pronounced dip than the data will allow. Failure of the model to fit the data in this region again would indicate that the model in fact fails to account for the higher order phase shifts correctly. GAMMEL and THALER have discussed these shortcomings and have concluded that the polarization chart found by them may still be used as a guide, however the extent to which the accuracy of the figures may be trusted is not clear.

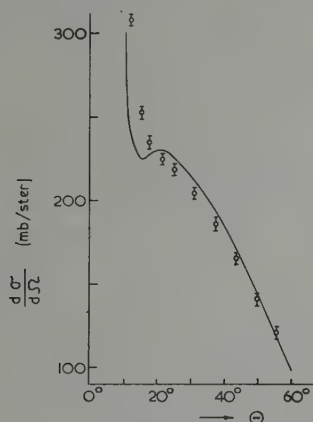


Figure 5

Proton alpha differential cross section at 17.5 MeV in the region of nuclear-coulomb interference. Theoretical curve is due to GAMMEL and THALER

We shall now return to the polarization measurements that were made around 17 MeV. The information that was found from the calculations concerning proton-alpha polarization was used to build a polarization analyzer based on the scattering of protons by helium at 65°. Figure 6 shows a drawing of the instrument. The first scattering target which was usually the material under investigation was placed about 2 inches in front of the first collimator. The second scattering was in helium gas at a pressure of about 7 atmospheres between the collimation vanes. The set up with the vanes to define the gas scattering geometry was chosen to get as high a counting rate as possible consistent with a

reasonable efficiency and a reasonable energy resolution. Detection of the doubly scattered protons was by cesium iodide scintillation counters.

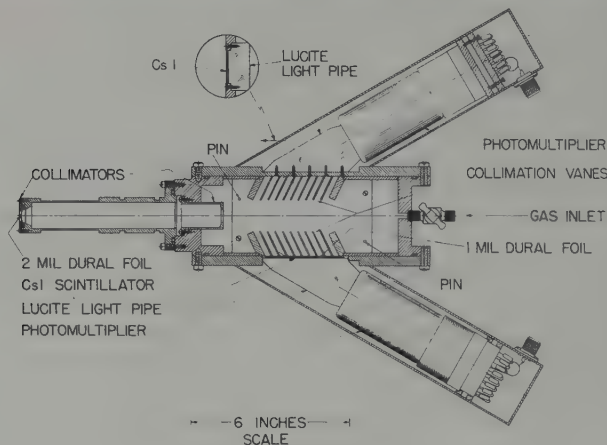


Figure 6

Helium polarization analyzer

Among the first measurements undertaken were those to calibrate the polarization analyzer and to check the calculated helium polarizations. It is possible to do a series of measurements involving three polarization events and to determine the magnitude of the polarization in each of the three. In our experiments the procedure was as follows: An experiment (experiment 1) was done in which an asymmetry A_1 was measured for two consecutive scatterings by carbon at 45° . Each of these scatterings is a separate event since the energy at the second target is lower than at the first. $A_1 = P_1 P_2$, where P_1 is the polarization of the first event and P_2 that of the second. Two more measurements were made. In these scattering by carbon at 45° was the first event and scattering by helium the second. The energy of protons incident on the helium target was adjusted to be the same for these two experiments by the use of foils. But in the first experiment of the two the energy at the carbon target was made the same as the energy incident on the first target in experiment 1, while in the second experiment it was made equal to the energy incident on the second target in experiment 1. The two asymmetries measured then are $A_2 = P_1 P_{He}$ and $A_3 = P_2 P_{He}$. The three asymmetries connect the three polarizations in three equations which may be solved for the polarizations. Calibration in this way is of the greatest value since it frees one of having to use the results of a theoretical calculation. Scattering by carbon at 45° was used in the calibration procedure because it was found early in our work that the

polarization for this event was large and because the use of this event was experimentally simpler.

The results of measurements done to verify the predicted proton-alpha polarization have been shown in figure 4. The values obtained at 65° and 115° were found by using scattering by carbon at 45° as the first event and scattering by helium in the helium analyzer as the second. The 115° point was obtained by turning the collimation vanes of the analyzer around. The values obtained at 30° and 45° were found using a gas cell containing helium as the first scatterer. The helium analyzer was used for the second event.

The next series of measurements was to measure the angular distribution of polarization in the scattering of protons by carbon. The results of these measurements are shown in figure 7. Here the polarization measured for both the elastic scattering and the inelastic scattering with excitation of the 4.43 MeV level of carbon are shown. The lines have no significance and merely connect the points. The upper part of the figure shows the differential cross section for the two processes.

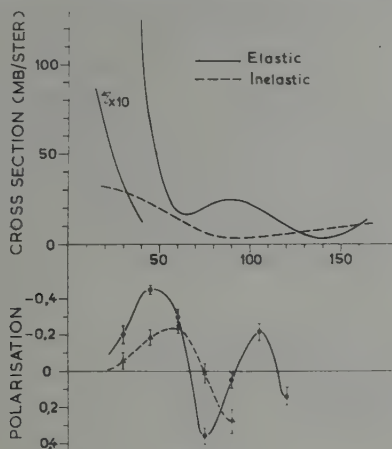


Figure 7

Angular distribution of polarization in the scattering of protons by carbon. Data are shown for elastic scattering and for inelastic scattering with 4.43 MeV excitation. Upper part of figure shows the associated differential cross sections

BLANPIED continued measurements of this type. He has measured the angular distribution of proton polarization in scattering by magnesium, calcium, copper, silver and gold. The polarization patterns are oscillatory like those shown for carbon. He shows that the positions of the maxima and minima for all the measurements follow a systematic scheme. This

is that they come at a certain set of values of $A^{1/3} \sin \theta/2$ which is proportional to the product of the nuclear radius and the momentum transfer in elastic scattering.

The third sort of experiment undertaken was an attempt to measure polarization in proton-proton scattering. This is an important measurement because it serves to differentiate between several sets of phase shifts that have been found to fit measured proton-proton cross sections. At the time when the measurement was first done there was very little theoretical guidance in the literature except that it should be small. A measurement was attempted scattering by hydrogen gas at 30° and analysing with the helium analyzer. The value obtained was $(1.2 \pm 2)\%$ which is consistent with zero.

BLANPIED has also remeasured the proton polarization but with an improved technique. The improvement regarded a method of eliminating the spurious asymmetries arising from the finite scattering geometry. The idea is as follows: It was found that protons scattered at around 45° from carbon and copper have a magnitude of polarization around 40% but the polarizations are of opposite sign. On the other hand the ratio of the slope of the cross section to the value of the cross section is about the same for these two targets at that angle. Now let carbon and copper be used alternately as the first target of a double scattering experiment and the material under investigation is used as the second target. The asymmetry arising from the effects of finite geometry, which is proportional to the slope to cross section ratio, is the same for either carbon or copper first target, but the asymmetry due to polarization changes sign with the alternation of targets. If then the asymmetry obtained with a carbon first target is subtracted from the asymmetry found with the copper, the finite geometry part drops out but the polarization part remains.

BLANPIED set up his experiment at 25° and used an energy of 16.2 MeV. The result obtained was $(0.6 \pm 0.5)\%$. While this value still may be said to be consistent with zero, it is a significant result for the problem of the proton-proton interaction.

REFERENCES

- [1] K. W. BROCKMAN, *Phys. Rev.* **170**, 163 (1958).
- [2] W. A. BLANPIED, *Phys. Rev.* **173**, 1099 (1959).
- [3] W. A. BLANPIED, *Phys. Rev.* **176**, 738 (1959).
- [4] C. L. CRITCHFIELD and D. C. DODDER, *Phys. Rev.* **76**, 602 (1949).
- [5] M. HEUSINKVELD and G. FREIER, *Phys. Rev.* **85**, 80 (1952).
- [6] D. C. DODDER and J. L. GAMMEL, *Phys. Rev.* **88**, 520 (1952).
- [7] K. W. BROCKMAN, *Phys. Rev.* **102**, 391 (1956).
- [8] J. L. GAMMEL and R. M. THALER, *Phys. Rev.* **109**, 2041 (1958).
- [9] K. W. BROCKMAN, *Phys. Rev.* **108**, 1000 (1957).

Polarization of Neutrons Scattered from Li^6 and Li^7

By S. E. DARDEN, C. A. KELSEY, and T. R. DONOGHUE, University of Notre Dame

I. Introduction

I should like to discuss briefly some asymmetry measurements we have performed on the scattering of polarized neutrons from Li^6 and Li^7 in the few hundred keV energy region. The instigation for these measurements was a desire to extend previous data on the polarization of neutrons from the $\text{Li}^7(p,n)\text{Be}^7$ reaction to lower energies. The results as pertain to the $\text{Li}(p,n)$ reaction were presented in a short communication, and here I should like to elaborate slightly on the use of Li^6 and Li^7 as polarization analyzers.

Both of these isotopes of lithium have prominent resonances in their neutron total cross-sections near 250-keV bombarding energy. These are shown in figure 1. In both cases the resonances correspond to states formed by neutrons having one unit of orbital angular momentum. The spins and parities of the compound states are for Li^7 and Li^6 , $5/2^-$ and

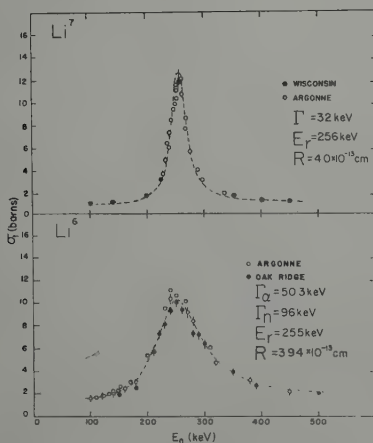


Figure 1

3⁺ respectively, which means that in both cases only the larger of the two possible channel spin states are involved: i.e. 3/2 for $\text{Li}^6 + n$, and 2 for $\text{Li}^7 + n$. Cross sections calculated using the parameters given in the figure are also shown. The level parameters used are those given by WILLARD *et al.* [1¹]. If the assumption is made that all of the non-resonant cross-section arises from the interaction of *s*-wave neutrons with these nuclei, these data combined with other scattering data can be used to obtain information on the *s*-wave scattering phase shifts. In the case of Li^7 these data exist in two forms: the angular distribution of elastic scattering and the low energy coherent scattering data. In principle, the *s*-wave phases can be obtained from the differential cross-sections alone, but it is very difficult in practice to measure angular distributions with sufficient accuracy to provide precise phase shifts. It was pointed out by THOMAS and coworkers [2] that the coherent scattering length, which depends linearly on the two *s*-wave phase shifts, δ_0^1 and δ_0^2 , and the low energy total cross-section, which depends quadratically on the same, admit two possible sets of phases. For one set, the parallel spin phase shift is the dominant one, with δ_0^1 being quite small. With the other set the converse is true. Differential cross-sections measured above and below the resonance energy exhibit a large asymmetry about 90°, indicating appreciable interference between the resonant scattering and the channel spin-2 *s*-wave scattering. This excludes the set of phases for which δ_0^2 is small and indicates that the *s*-wave interaction occurs predominantly in the channel spin-2 state at low energies. On the basis of just the measured asymmetry about 90° in the differential cross-sections WILLARD and coworkers [1] concluded that both channel spins were of approximately equal importance in the *s*-wave scattering. In any case, the presence of appreciable channel spin-2 *s*-wave scattering which interferes with the resonant scattering will produce appreciable polarization in the scattered neutrons. This is illustrated in figure 2, in which polarizations produced in the scattering through a c.m. angle of 90° are shown as a function of neutron energy. The positive direction of polarization is given by the vector $\mathbf{k} \times \mathbf{k}'$, where \mathbf{k} and \mathbf{k}' are incident and outgoing wave numbers respectively. These curves were calculated using the level parameters shown in the preceding figure and assuming that the *s*-wave interaction is either entirely in the parallel channel spin state or equally strong in both channel spin states for the broken and solid curves respectively. It can be seen that $P(\theta)$ should be appreciable for Li^7 between about 250 and 400 keV. Using 280 keV neutrons from the $\text{Li}^7(p, n)$ reaction, WILLARD's group [3] has shown that appreciable polarization is indeed present.

¹) Numbers in brackets refer to References, page 276.

On the basis of the low energy coherent scattering data and the angular distribution measurements one would expect $P(\theta)$ to be somewhere between these two curves.

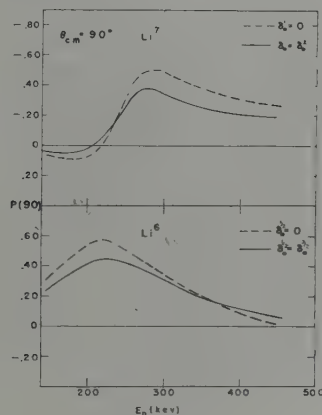


Figure 2

The situation for Li^6 is complicated by the presence of the competing (n, α) reaction. If one represents the s-wave elastic scattering again by real phase shifts consistent with the background elastic scattering cross-section, then the choice of phase shifts which reproduce the differential cross-section involves something like a statistical mixture of channel spins and the corresponding polarization is that given by the solid curve.

II. Measurements

In this investigation the asymmetries in the scattering of polarized $\text{Li}^7(p, n)$ neutrons from samples of natural lithium and Li^6 enriched to 96% have been measured. Neutrons emitted at a laboratory angle of 50° with respect to the incident proton beam and having an average energy spread of 45 keV were used. The experimental procedure used for the first set of measurements is shown in figure 3. This is the conventional arrangement for such experiments. A magnetically analyzed proton beam from the electrostatic accelerator is incident on an evaporated lithium target, producing neutrons which are collimated at an angle of 50° with respect to the proton beam by the paraffin shield. A hydrogen-filled proportional counter detected neutrons scattered to the left and right by the lithium scatterers. Most of the data were taken for a laboratory scattering angle of 88° . Cylindrical scatterers 8 cm high and 3 cm

in diameter were used. The entire procedure was checked from time to time by using a carbon scatterer to ensure that no experimental asymmetries were creeping in. As is generally the case, the most serious limitation on the accuracy with which data could be obtained was imposed by the large background counting rate present when the scatterers are removed. This background, which was enhanced by the unfavorable environment in which the measurements were carried out, varied from 35 to 75% of the counting rate with scatterers present. It is necessary to apply a number of corrections to data obtained in this way. Principal among these are the corrections for the variation in neutron flux across the sample, the presence of the other isotope, and the effect of multiple scattering. The effect of multiple scattering is mitigated by the fact that the doubly scattered neutrons are on the average substantially less energetic than those which have been scattered only once, and are, therefore, detected with much less efficiency, since the pulse height discrimination used was such as to detect with zero efficiency neutrons having energies less than about 40% of the incident neutron energy.

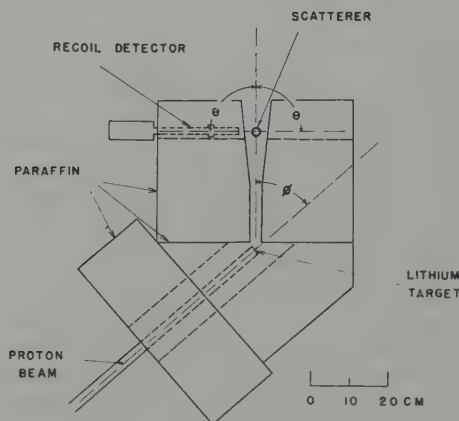


Figure 3

More recently, additional measurements have been made using a different procedure, illustrated in figure 4. With this arrangement the necessity of moving the detector from side to side is eliminated by the use of a magnetic field transverse to the direction of the neutron's flight path between source and scatterer. Instead of rotating the detector from one side to the other, the intensity of scattered neutrons is measured with the field alternately shut off and turned on to a value sufficient

to permit precession of the neutron's magnetic moment through 180° as the neutrons pass from source to scatterer. The advantages of this approach have been discussed elsewhere and will not be dwelt upon here. One obvious disadvantage is that the substitution of iron for paraffin in the region between source and scatterer results in an increased neutron background at the detector. This difficulty was circumvented by increasing the distance between source and scatterer and inserting additional paraffin shielding, and by using a somewhat larger scatterer. As before, asymmetries were measured from time to

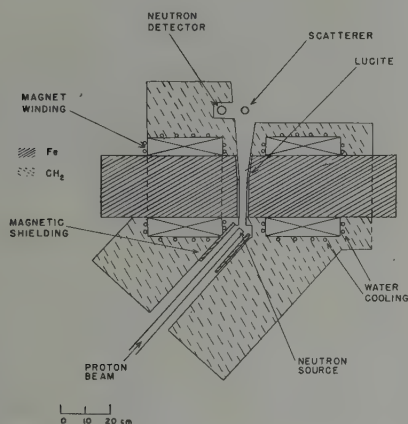


Figure 4

with time carbon to ensure that no spurious effects were being introduced by the magnetic field. An additional check was provided by measuring asymmetry versus magnetic field in one case. The results are shown in figure 5. The ordinate is proportional to the product of the polarization of the incident neutrons and the analyzing power of the Li^7 as given by the expression

$$P_1 P_2 = \frac{\frac{L}{R} - 1}{\frac{L}{R} + 1}. \quad (1)$$

Here L/R refers to the ratio of the scattered intensities measured with the magnet alternately off and on. The $P_1 P_2$ as defined above is, of course, the correct one only when the magnetic field rotates the neutron spins through 180° . The points were obtained from the measured asymmetries using Eq. (1), while the shape of the curve represents the $P_1 P_2$

calculated from the asymmetries expected on the basis of the measured values of the magnetic field. For the point farthest to the right, the field strength was that required to rotate the neutron spin vector through 360° . The correspondence between the points and the curve indicates that the neutron spins are being rotated by the magnetic field as expected.

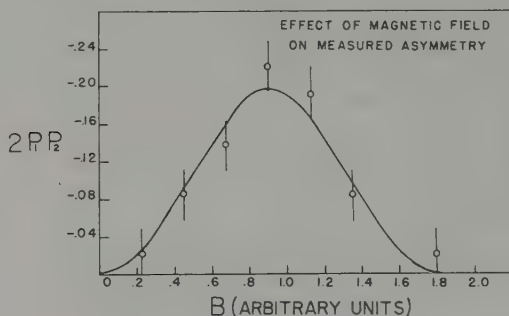


Figure 5

III. Results and Discussion

Results of the measurements for both Li^6 and Li^7 are shown in the last figure. The points represent values of P_n , the polarization of the incident neutrons, times $P(\theta)$ for the scatterer and are given as a function of neutron energy. These were obtained from the corrected experimental asymmetries using Eq. (1). In addition to statistical uncertainties, an uncertainty of about one third the value of the corrections to the data has been included in the error bars shown. The solid circles represent data obtained by rotating the neutron detector from side to side, while the open circles correspond to data taken using the electromagnet. On the right are given the ordinate scales for the curves, which are the calculated polarizations assuming the s -wave interaction is all channel spin-2 for Li^7 , and assuming equal phases for both channel spin states in the case of Li^6 . The normalization between the left and right hand ordinate scales is such that the points should coincide with the curves wherever P_n is equal to 0.40, providing the curve gives the correct value of $P(\theta)$.

If, for Li^7 , the curve is assumed to represent $P(\theta)$ correctly in the energy interval between 300 and 400 keV, values of P_n close to .40 are obtained, in agreement with the results obtained using oxygen analyzers. This agreement, together with the evidence from the scattering length data discussed in the introduction, would indicate that the channel

spin-2 *s*-wave interaction is predominant for neutron energies below about 400 keV. Consequently, $P(\theta)$ below 400 keV was taken to be given by the curve shown to within about 10%, and the data below 400 keV were used to determine P_n . The positive value of $P_n P(\theta)$ found at 190 keV suggests that P_n changes sign somewhere between 200 and 250 keV. Unfortunately, the small magnitude of $P(\theta)$ together with the large experimental uncertainties prevent any very quantitative determination of P_n at 190 keV. The change in sign of P_n is also evident in the Li^6 data, since the measured $P_n P(\theta)$ reverses sign while the analyzing power does not. This conclusion does not depend on a detailed knowledge of the *s*-wave phase shifts for Li^6 , since the shape of the $P(\theta)$ curve, i.e. the slow variation with energy near 200 keV, is quite insensitive to the relative magnitude of the two *s*-wave phases. The fact that these measured points for Li^6 fall somewhat below the curve suggests the channel spin 1/2 interaction may be somewhat stronger than the channel spin 3/2 interaction.

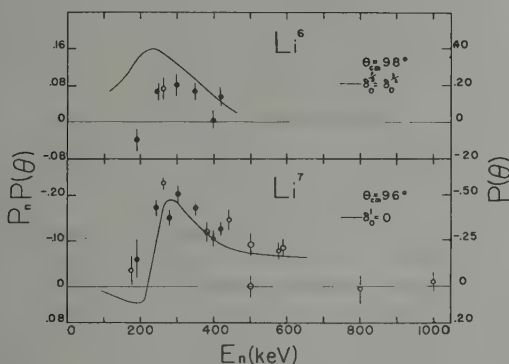


Figure 6

Over the energy interval from about 420 to 600 keV, the observed asymmetries for Li^7 are generally greater than would be expected if the curve shown really represented $P(\theta)$. The polarization of the incident neutrons is known from oxygen measurements to be about .20 in this energy region. Dividing the experimental $P_n P(\theta)$ by .20 yields $P(\theta)$ values at least twice as large as those calculated using just the 3^+ resonant phase and an *s*-wave phase obtained from the total cross-section. It is not immediately obvious what causes this increased polarization. Additional *P*-wave phases may become important at these energies. Also, the threshold for inelastic scattering to the first excited state in Li^7 , which occurs around 550 keV, may affect the polarization in the

vicinity of the threshold. At present however the data are too sparse and inaccurate to permit much to be said about the phases above 400 keV.

This work was supported in part by the joint program of the Office of Naval Research and the U. S. Atomic Energy Commission.

REFERENCES

- [1] WILLARD, BAIR, KINGTON, and COHN, *Phys. Rev.* **101**, 765 (1956).
- [2] R. G. THOMAS, M. WALT, R. B. WALTON, and R. C. ALLEN, *Phys. Rev.* **101**, 759 (1956).
- [3] WILLARD, BAIR, COHN, and KINGTON, *Bull. Amer. Phys. Soc.* **1**, 54 (1956).

Polarization Resulting from Elastic Nucleon Scattering below 4 MeV

By H. R. BRUGGER

Laboratory for Nuclear Physics, Swiss Federal Institute of Technology,
Zurich

Herein are described two experiments undertaken at the Swiss Institute of Technology, the first as carried out by H.-J. GERBER¹⁾ *et al.* and the second by J. SALADIN²⁾ *et al.*: a) The elastic scattering of polarized neutrons from deuterons at 3.3 MeV, and b) the polarization of 3.9-MeV protons elastically scattered by medium-heavy nuclei.

The elastic scattering of low-energy neutrons by deuterons has for many years been of great interest both from an experimental and a theoretical point of view. Two-nucleon theory for these low energies is not able to give much information on nuclear forces since practically only s-waves are involved.

The situation is much improved if one considers the three-nucleon problem associated with neutron-deuteron scattering. Three main reasons are responsible for this: a) This reaction includes neutron-neutron interaction and hence could yield information of great value such as is very difficult to derive from other experiments. b) The exchange forces are not very well known at energies below 10 MeV. Neutron-deuteron scattering experiments assist in distinguishing between different approaches. c) These experiments could, furthermore, provide information on three-nucleon forces, if the latter exist.

Several calculations on low-energy neutron-deuteron scattering have recently been published which involve a tensor force or an explicit spin-orbit coupling apart from a central exchange potential. DELVES and BROWN [1]³⁾, who included the effects of both tensor force and the distortion of the deuteron in their approximation, predict a polarization of nearly zero for 2-MeV neutrons. BOSE [2] uses in his article a spin-orbit-coupling. BRANSDEN *et al.* [3], assuming central exchange plus

¹⁾ Now Physics Dept., University of Illinois, Urbana, Illinois, USA.

²⁾ Now Physics Dept., University of Wisconsin, Madison, Wisconsin, USA.

³⁾ Numbers in brackets refer to References, page 290.

tensor force, report in their latest paper that extensive numerical calculations of the neutron-deuteron cross section are in progress. WATANABE [4] has included a spin-orbit term and published a general formulation of the problem as an intermediate report; detailed calculations are to follow. Earlier theoretical work has been reviewed in an article by VERDE [5].

The aim of our experiments was to measure the polarization produced on elastic scattering of polarized neutrons by deuterons. This polarization was evaluated by measuring the left right-asymmetry of the differential cross section using a neutron beam of known polarization.

The relation is [6]:

$$P_1 P_2 = \frac{\sigma(\theta, 0) - \sigma(\theta, \pi)}{\sigma(\theta, 0) + \sigma(\theta, \pi)} \quad (1)$$

P_1 is the (transverse) polarization of the incident neutrons. P_2 is the polarization of an originally unpolarized neutron beam elastically scattered by deuterons. By definition, P is taken to be positive if the polarization vector is parallel to the normal $[\mathbf{k}_1 \times \mathbf{k}_2]$ of the reaction plane, \mathbf{k}_1 and \mathbf{k}_2 being respectively the momentum vectors of the incident and the scattered neutron. $\sigma(\theta, \varphi)$ is the differential cross section for elastic neutron-deuteron scattering, where θ is the scattering angle and φ the angle between \mathbf{P}_1 and $[\mathbf{k}_1 \times \mathbf{k}_2]$. Formula (1) holds for target nuclei with spin = 0 assuming time-reversal invariance for the scattering process [6].

Figure 1 shows the general assembly (for a more detailed description of the experiment see GERBER *et al.* [7]). We normally use a 15- μ A beam of magnetically analyzed deuterons. The polarized neutrons are produced by the D - D -reaction using a thin heavy ice target. The neutrons have an energy of (3.27 ± 0.04) MeV and a polarization of 11% as given by the measurements of MEIER [8], LEVINTOV [9] and PASMA [10]. The neutron energy is just below the threshold for deuteron break-up, so that elastic scattering is the only possible reaction. The scatterer is cylindrical and consists of deuterated benzene C_6D_6 with the addition of 3 g/l p-terphenyl and 0.1 g/l POPOP. The production of deuterated benzene has been described by MEIER *et al.* [11]. This mixture has the property of acting as a liquid scintillator; its proton-to-deuteron ratio is 1.3 percent. Each scattering event is detected both via the recoil deuteron in the liquid scintillator and via identification of the coincident neutron in a plastic scintillator.

The advantages of this method are obvious. One of the difficulties of nearly all fast-neutron experiments is the high background due to extraneous scattering of neutrons from walls etc., gamma rays, particles which pass through the shield etc. This background is reduced to a very small percentage if only those neutron counter pulses are accepted which

coincide with the recoil signal. The second advantage is that one uses the full beam current of the accelerator, not only a small fraction as in some time-of-flight experiments. Of course there is also a great disadvantage: This method is applicable only to those few cases where the scattering material scintillates or can be mixed with a scintillator.

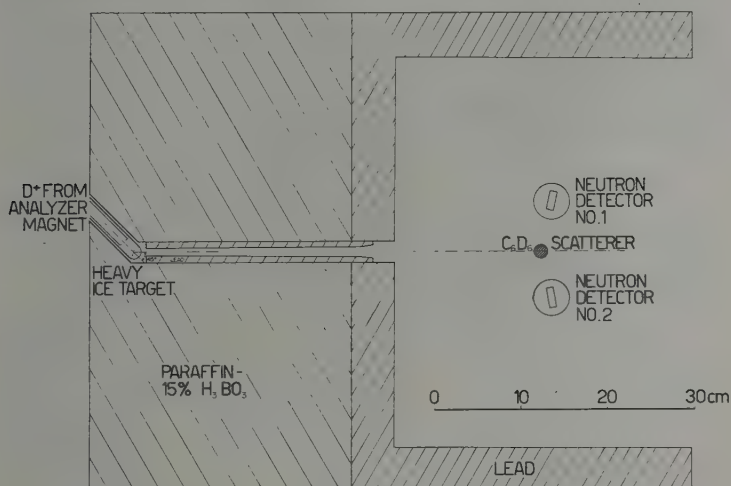


Figure 1

General assembly for neutron-deuteron scattering

This arrangement has been used for two completely independent experiments with different circuitry. In the first, one uses a time-of-flight apparatus, in the second, one simply measures the coincidences between deuteron recoil counter and neutron counter.

The time-of-flight experiment has been carried out in the following manner (figure 2): Start and stop pulses are delivered by deuteron counter and neutron counter respectively. The anode pulses of an RCA 6810 photomultiplier go through a limiter and a fast discriminator and are then clipped to give rectangular pulses of exactly uniform height and length. The neutron and the recoil pulses then have the same shape; they are mixed in a pentagrid tube, so that the resulting anode pulse height is a measure of the overlapping of the two rectangular pulses and hence a measure of the neutron flight time between recoil and neutron counter. The resolving time has been found, using coincident ^{60}Co gamma rays, to be 3.3 ns full width at half height. Very probably the resolving time is essentially determined by the relatively large time-spread of the photomultiplier.

The time-of-flight experiment serves two purposes: a) it is an independent measurement of the polarization; b) it provides a check of whether carbon recoils in the scatterer could produce light pulses of sufficient intensity to influence the measurement of polarization. As is well known [8], carbon is a good polarizer in this energy range and hence could well disturb measurements. If we count neutrons scattered by carbon, then the measured polarization is an indefinite sum of the polarizations produced in deuterium and carbon scattering. This point has been investigated in a separate experiment. However, the test showed that neutrons scattered by carbon are not detected even if the photomultiplier voltage is raised.

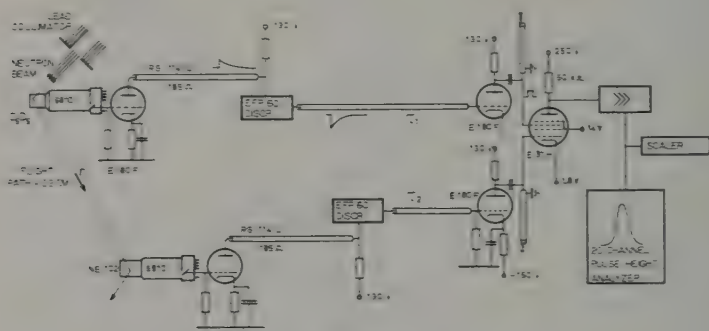


Figure 2

Block diagram of the time-of-flight circuitry for the neutron-deuteron polarization experiment

The results of the polarization measurement as obtained by the time-of-flight experiment agree within experimental error with those of the second experiment (termed the "coincidence experiment"). Thus these results will be discussed together with the latter.

The coincidence experiment mentioned earlier consists simply in counting the coincidences from recoil and neutron counter as can be seen in figure 3. Most of the results have been obtained by this and not by the time-of-flight method thanks to the shorter neutron flight path and hence improved counting rate. The use of two neutron counters has the double advantage of improving counting statistics and of eliminating effects due to variations in intensity of the neutron beam.

Very considerable care has been given to the geometrical adjustments both in this and in the time-of-flight experiments, as it is well known that small misalignments are able to simulate a large polarization if the differential cross section varies markedly with scattering angle. As an

example of all the tests, I mention the measurements of the polarization of neutrons scattered by protons. This experiment has been carried out simultaneously with the measurement of the neutron-deuteron scattering simply by replacing the deuterated scatterer by a similar one containing ordinary benzene C_6H_6 . The measured neutron-proton polarization at a scattering angle $\theta_{Lab} = 64^\circ$ is (2.2 ± 3) percent as compared with the theoretical value of practically zero at these energies.

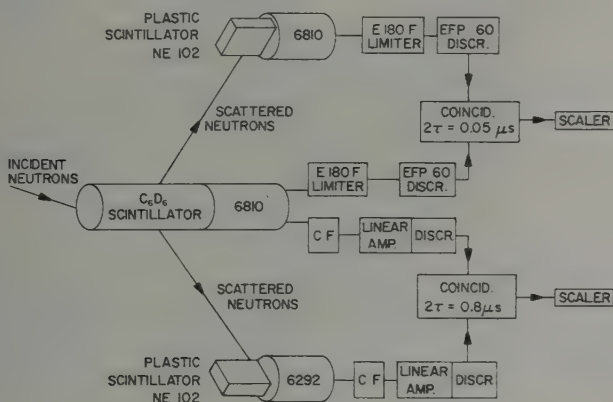


Figure 3

Block diagram of the electronic circuit for the neutron-deuteron polarization experiment, using coincidences between the deuteron-recoil counter and the neutron counter. Two identical neutron counters were used simultaneously.

The measurements have been corrected for the effects of finite geometry, for background, fortuitous coincidences and for multiple scattering. Of all these corrections, only multiple scattering has a perceptible effect on polarization since there are neutrons scattered first by a carbon nucleus, which is a good polarizer, and afterwards by a deuteron. This effect has been evaluated and taken into account.

Figure 4 shows our experimental results [7] together with those of other authors [12–16]. The full circles represent the mean value of the coincidence and the time-of-flight experiment. The values of different authors are in good agreement except for the single value of WHITE *et al.* [14]. It can be seen that the polarization of 2-to-3-MeV neutrons scattered by deuterons is practically zero for all scattering angles. The same seems to be true for proton-deuteron scattering. The experimental values agree essentially with the calculations of DELVES and BROWN [1] (indicated by the solid line). However, DARDEN *et al.* [12] who measured

the n-d polarization at 1 MeV also find a small value which is in disagreement with the results of Delves.

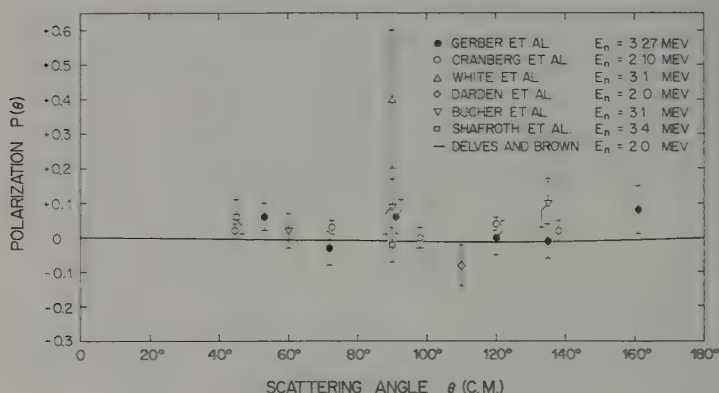


Figure 4

Polarization of nucleons scattered elastically by deuterons. Neutron data are taken from GERBER *et al.* [7], CRANBERG [13], WHITE *et al.* [14], DARDEN *et al.* [12], BUCHER *et al.* [15]. Also included are the proton data of SHAFROTH *et al.* [16]. Energies are given in lab system. The full curve was calculated by DELVES and BROWN [1].

Figure 5 shows the differential cross section of n-d-scattering at an energy of 3.27 MeV (laboratory system), measured at the same time as the polarization. The values show good agreement with those published by SEAGRAVE and CRANBERG [17]. The figure includes the theoretical results of BUCKINGHAM, HUBBARD and MASSEY [18] and of CHRISTIAN and GAMMEL [19], these having been calculated on the basis of a pure central exchange force for the nucleon-nucleon interaction. It is difficult to decide whether the inclusion of a tensor force or a spin-orbit coupling improves the agreement with the experiment since different approximations can be made.

Finally, it can be said that the polarization of neutrons elastically scattered by deuterons around 3 MeV is at all angles smaller than - 10 percent as established by different authors using different methods.

In contrast with the preceding work, this which now follows deals with the many-nucleon problem. SALADIN [20] measured the polarization of protons elastically scattered by magnesium, aluminum, titanium and vanadium. This was undertaken at 4 MeV which is, to our knowledge, the lowest proton energy at which a polarization has been found for

medium heavy nuclei. Similar work has been carried out at 6 MeV [21] 9 MeV [22], 10 MeV [23] and 18 MeV [24, 25].

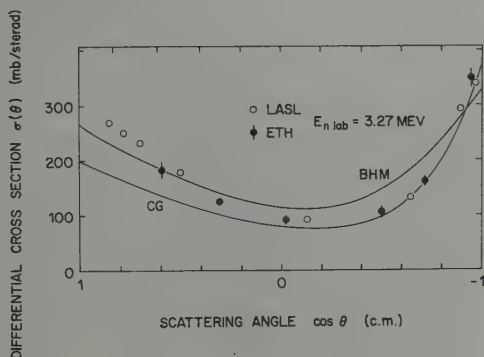


Figure 5

Differential cross section of neutrons elastically scattered by deuterons. Full circles are results due to GERBER *et al.* [7], open circles to SEAGRAVE and CRANBERG [17]. The solid curves represent theoretical results of BUCKINGHAM, HUBBARD, and MASSEY [18] (BHM) and of CHRISTIAN and GAMMEL [19] (CG).

In recent years, the optical model of the nucleus has extensively and with fair success been used to calculate both differential cross sections and polarizations of nucleons elastically scattered by nuclei. (See for example [26].) For a wide range of energies and atomic numbers this model has proved able to account quantitatively for the experimental data.

The measurements to be described now have been undertaken as a test of whether the optical model would apply to scattering even in this low-energy region. There are three main points of interest: a) the value of the parameters describing both the central and the spin-orbit term of the potential; b) the role of compound-elastic scattering which is not well known [26]; c) the influence of the relatively large level separation for light nuclei. Thus if one examines the optical model assumptions, one sees that many levels must contribute to the scattering, and this may not be the case for Mg and Al.

The polarization P_1 has been measured in the usual way by measuring the asymmetry in a double scattering experiment, the second scatterer being helium, whose polarization P_2 is well known [24]. The relation between asymmetry and polarization P_1 is given by equation (1).

Figure 6 shows the general arrangement. The E.T.H. cyclotron was operated at a proton energy of (4.05 ± 0.05) MeV with a mean external beam intensity of $0.8 \mu\text{A}$. After passing through a narrow collimator,

the protons are scattered by a target foil thinner than 3 mg cm^{-2} . One might regard this as the polarizer. Thereafter, the protons pass through a tantalum foil to enter the scattering region of the polarimeter. The protons are there scattered through approximately 70° by helium under a pressure of 4 atmospheres, being finally detected by nuclear photo plates.

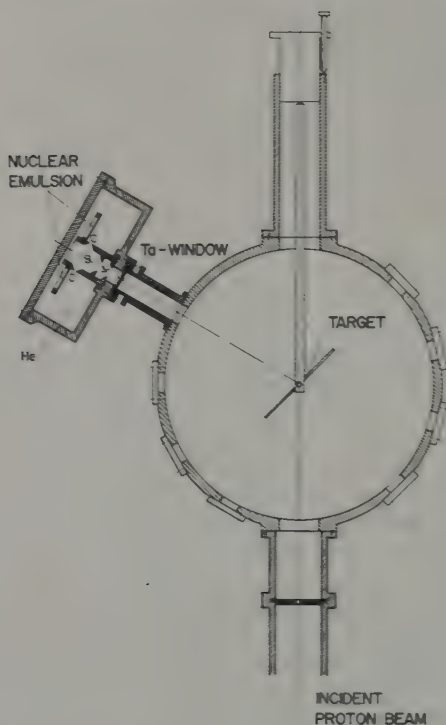


Figure 6

Scattering chamber and helium polarimeter used for polarization measurements on 4-MeV protons elastically scattered by Mg, Al, Ti, V.

As is well known one must take great care either to avoid or at least to take account of any instrumental asymmetry which could falsify the measurements. One of the most important requirements is that the center of the target lie at the intersection of the beam axis with that of the polarimeter. That this was the case at every scattering angle was established to within 0.5 mm optically. The resulting asymmetry was smaller than 1.5° , which would throughout be smaller than the statis-

tical error. Secondly, one must ensure symmetry of the helium polarimeter; the mechanical precision of some critical parts approached 0.02 mm. A correction had also to be made for the fact that the beam intensity at the entrance of the helium polarimeter was not uniform due to the rapid variation of cross section for the first scattering event with angle. The resulting asymmetry was measured using gold as a first scatterer (this produces no polarization since only Coulomb scattering is effective). It was found never to exceed 8%, which agrees sufficiently with the estimated value. This effect has been taken into account in all measurements.

Several tests have been undertaken to ensure absence of instrumental asymmetries: a) The helium polarimeter was turned through 90° and then through a further 180° , to make the second scattering plane perpendicular to the first. No asymmetry should occur in such a case. With gold as a first scatterer the asymmetry was found to be $\epsilon = 0.004 \pm 0.014$ and $\epsilon = -0.004 \pm 0.007$ for the two polarimeters respectively. b) The polarisation of carbon was measured at angles of 95° and 152.5° (c.m.) and compared with the values calculated from known phase shifts [27]. Results agree within the experimental error of 6%.

Two other effects could spoil the polarisation measurements, namely production of recoil protons in the nuclear emulsion by neutrons and inelastic scattering of protons in the target material. The former effect proved to be negligible except for vanadium. By shielding stringently with paraffin and cadmium its effect could be reduced to insignificance. The inelastically scattered protons also proved to be altogether un-

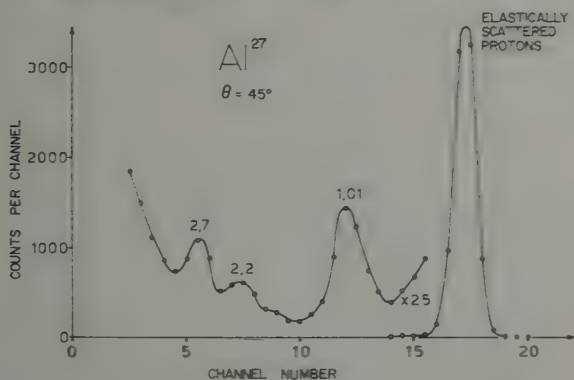


Figure 7

Pulse height spectrum due to 4-MeV protons scattered by Al, as determined using a CsI(Tl) crystal. Scattering angle $\theta = 45^\circ$ lab. The peak figures indicate the energy loss, in MeV, of the protons.

important. Their intensity was only a few percent of the elastically scattered protons and practically all of them lost 1 MeV or more in the target, as can be seen from figures 7 and 8. These show the energy spectra

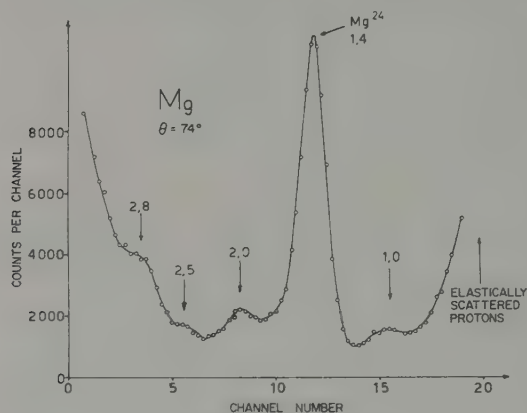


Figure 8

Pulse height spectrum due to 4-MeV protons scattered by Mg, as determined using a CsI(Tl) crystal. Scattering angle $\theta = 74^\circ$ (lab). The peak figures indicate the energy loss, in MeV, of the protons.

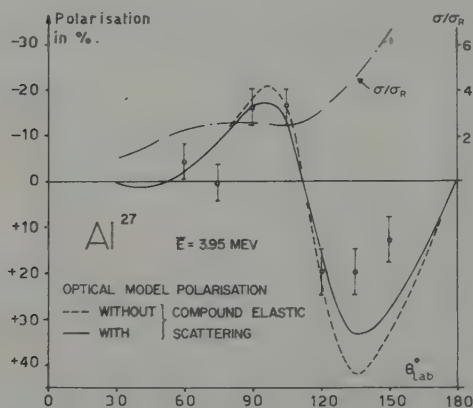


Figure 9

Polarization of 3.95-MeV protons elastically scattered by Al (open circles). The dot-dashed curve represents the ratio of observed elastic scattering to Rutherford scattering. The full and the dashed curves are results of optical model computations by BJÖRKLUND *et al.* 28 with and without the inclusion of an isotropic compound-elastic scattering term.

of the scattered protons, on replacing the helium polarimeter by a CsI(Tl)-detector. It should be noted that those protons which lost more than 800 keV were rejected in scanning the photo plates.

In figure 9 the results for aluminum are shown. The open circles represent the measured polarization together with the experimental error. Polarizations as high as 20% have been found. The dot-dashed line represents the ratio of observed scatter to Rutherford scatter as measured with a CsI(Tl) crystal and a multichannel pulse height analyzer. It is arbitrarily normalized to unity at 30° in this and in figures 11 and 12. The full and the dashed curves represent the optical model calculations for the polarization with and without the inclusion of an isotropic compound-elastic scattering term of 4 mb/ster. We are indebted to Dr. BJORKLUND and Dr. CAMPBELL [28] for these computations, which

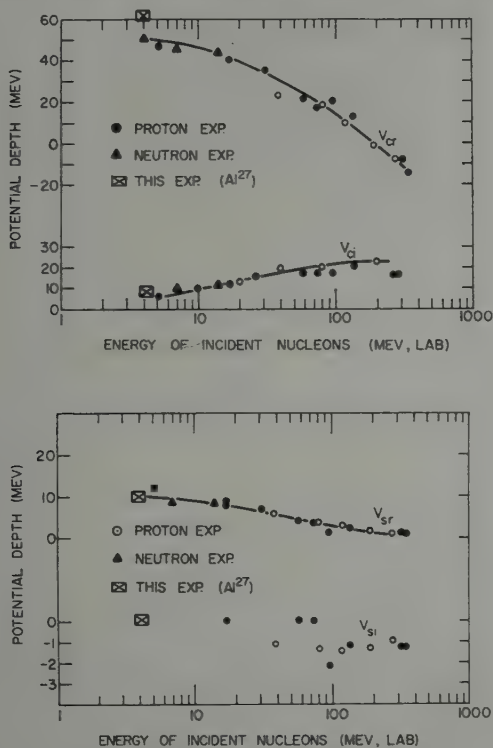


Figure 10

Values of the optical model parameters using the potential of BJORKLUND *et al.* [26]. The values marked by crosses were found to fit the polarization measurement on Al.

they kindly undertook using their rounded potential with surface absorption and a real spin orbit term. As can be seen, good agreement was attained with the experimental data except at back-scattering angles. This may be due to the influence of compound-elastic scattering which can only rather roughly be taken into account. The parameters used in this fit can be seen in Figure 10, together with those at higher energies. The values fit smoothly on to those at energies up to 300 MeV, with the possible exception of V_{cr} which characterises the real central potential. Those parameters which define the diffuseness of the surface have been chosen to be the same as for proton experiments of similar energy.

Figure 11 shows the polarization and the differential cross section for natural magnesium. The polarization data differs markedly from that of aluminum and it seems unlikely that a good fit could be obtained with an optical model calculation using similar parameters as in the case of aluminum. The reason may be that the number of resonances involved in the scattering process is small. The mean level separation is of the same order as the energy spread of the incident protons, thus leaving one of the main assumptions of the optical model unfulfilled. GREENLEES *et al.* [22] in discussing the polarization results of 9-MeV protons elastically scattered by Mg, has come to a similar conclusion.

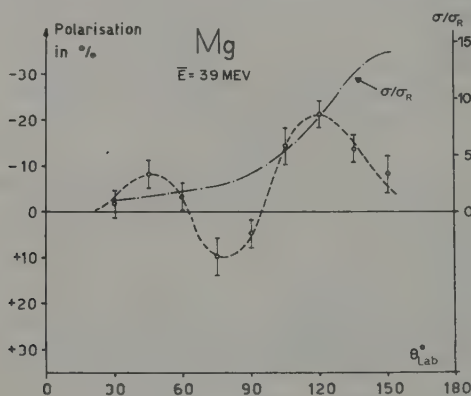


Figure 11

Polarization of 3.9-MeV protons elastically scattered by Mg (open circles). The dot-dashed curve represents the ratio of observed elastic scattering to Rutherford scattering.

The results for natural titanium are represented in figure 12. Counting statistics were rather bad for this element owing to the rapidly decreasing differential cross section. Only small polarization, if any, was observed.

The same holds for vanadium, shown in Figure 13. This behaviour is not unexpected since the Coulomb barrier is high on comparison with the relatively low proton energy.

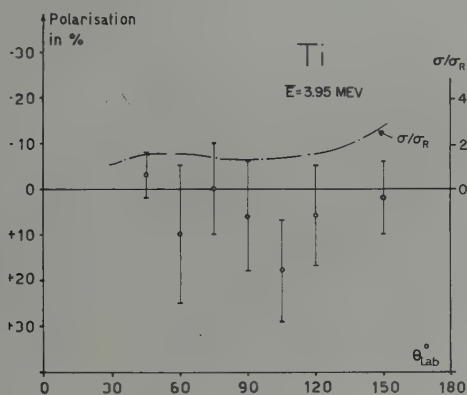


Figure 12

Polarization of 3.95-MeV protons elastically scattered by Ti (open circles). The dot-dashed curve represents the ratio of observed elastic to Rutherford scattering.

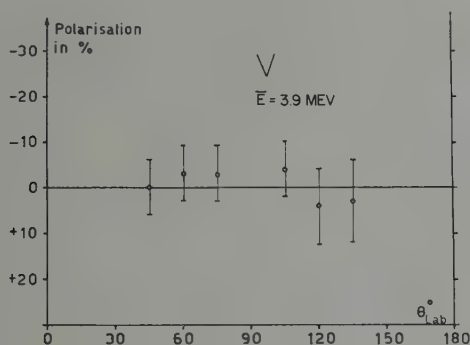


Figure 13

Polarization of 3.9-MeV protons elastically scattered by V (open circles).

In conclusion, polarization has been found to attain as much as 20% for medium heavy nuclei at a proton energy of 3.9 MeV. The optical model, in so far as its assumptions be satisfied, is able on inclusion of a spin-orbit term to account satisfactorily for the results obtained.

The author wishes to acknowledge the very helpful interest of Dr. ERIC SHELDON of our Laboratory for Nuclear Physics.

REFERENCES

- [1] L. M. DELVES, D. BROWN, *Nucl. Phys.* **77**, 432 (1959).
- [2] A. K. BOSE, Thesis, Georg-August-Universität, Göttingen (1957).
- [3] B. H. BRANDEN, K. SMITH, C. TATE, *Proc. Roy. Soc.* **247**, 73 (1958).
- [4] S. WATANABE, *Nucl. Phys.* **14**, 429 (1959).
- [5] M. VERDE, *Handb. der Physik* (Flügge) (Springer, Berlin), **39**, 144 (1957).
- [6] L. WOLFENSTEIN, *Ann. Rev. Nucl. Sci.* **6**, 43 (1956); H. FAISSNER, *Erg. ex. Naturw.* **32**, 180 (1959).
- [7] M. BRÜLLMANN, H.-J. GERBER, D. MEIER, P. SCHERRER, *Helv. Phys. Acta* **32**, 511 (1959).
- [8] R. W. MEIER, P. SCHERRER, G. TRÜMPY, *Helv. Phys. Acta* **27**, 577 (1954).
- [9] I. I. LEVINTOV, A. V. MILLER, E. Z. TARUMOV, V. N. SHAMSHEV, *Nucl. Phys.* **3**, 237 (1957).
- [10] P. J. PASMA, *Nucl. Phys.* **6**, 141 (1958).
- [11] M. BRÜLLMANN, H. J. GERBER, D. MEIER, *Helv. Chim. Acta* **41**, 1831 (1958).
- [12] S. E. DARDEN, C. A. KELSEY, T. R. DONOGHUE, *Nucl. Phys.* **16**, 351 (1960).
- [13] L. CRANBERG, *Phys. Rev.* **114**, 174 (1959).
- [14] R. E. WHITE, A. CHISHOLM, D. BROWN, *Nucl. Phys.* **7**, 233 (1958).
- [15] W. P. BUCHER, W. B. BEVERLY, G. C. COBB, F. L. HEREFORD, *Nucl. Phys.* **13**, 164 (1959).
- [16] S. M. SHAFROTH, R. A. CHALMERS, E. N. STRAIT, R. E. SEGEL, *Phys. Rev.* **118**, 1054 (1960).
- [17] J. D. SEAGRAVE, L. CRANBERG, *Phys. Rev.* **105**, 1816 (1957).
- [18] R. A. BUCKINGHAM, S. J. HUBBARD, H. S. W. MASSEY, *Proc. Roy. Soc. A* **211**, 183 (1952).
- [19] R. S. CHRISTIAN, J. L. GAMMEL, *Phys. Rev.* **91**, 100 (1953).
- [20] J. SALADIN, P. MARMIER, *Helv. Phys. Acta* **33**, 299 (1960).
- [21] R. E. WARNER, W. P. ALFORD, *Phys. Rev.* **114**, 1338 (1959).
- [22] A. B. ROBBINS, G. W. GREENLEES, *Phys. Rev.* **118**, 803 (1960).
- [23] L. ROSEN, J. E. BROLLEY, *Int. Conf. on the Peaceful Uses of Atomic Energy A/Conf. 15/P/668* (1958).
- [24] K. W. BROCKMAN, *Phys. Rev.* **110**, 163 (1958).
- [25] W. A. BLANPIED, *Phys. Rev.* **113**, 1099 (1959).
- [26] *Proceedings of the Int. Conf. on the Nuclear Optical Model*, ed. by A.E.S. GREEN, C.E. PORTER, D.S. SAXON. The Florida State Univ., Tallahassee (1959).
- [27] R. E. WARNER, W. P. ALFORD, Univ. of Rochester NYO-8576; C. W. REICH, G. C. PHILLIPS, J. L. RUSSEL, JR., *Phys. Rev.* **104**, 143 (1956).
- [28] F. BJORKLUND, G. CAMPBELL, private communication.

Energy Variation of Neutron Polarization in Scattering from Zinc, Copper, Molybdenum and Cadmium

By D. BROWN¹⁾, A. T. G. FERGUSON, and R. E. WHITE, A.E.R.E., Harwell

1. Introduction

The polarization of neutrons of energy less than 2 MeV scattered from medium and heavy nuclei has been studied by a number of workers [1, 2, 3, 4²⁾]. Measurements have been restricted to only two energies – 380 KeV and 980 KeV and three angles – 55°, 90° and 130°. The variation of polarization with respect to the parameter A , the atomic weight, has been relatively extensively explored. The most comprehensive set of results in this field is that of CLEMENT *et al.* [5], at neutron energies of 380 KeV and 980 KeV. They found that an optical model with spin-orbit coupling gave a general description of their results giving the change in sign indicative of the p -wave size resonance.

BJORKLUND, using a refined optical model with spin-orbit coupling reported attempts [6] to fit the data in more detail. He found that the calculated polarizations were in general too large, and the parameters required to fit the data fluctuated considerably from element to element.

The present series of measurements was undertaken to explore the variation with energy in more detail. For four elements measurements have been made at 50 KeV intervals from 350 KeV up to 1600 KeV. These measurements were made at 55° and 90° scattering angles, these angles being chosen for the comparison with the results of earlier workers.

Using the optical model potential proposed by BJORKLUND and FERNBACH the polarization was computed for the cases of interest. The general overall agreement was poor though it was clear that reasonable parameters could be found to fit particular points.

¹⁾ On leave from Dept. of Physics, University of Auckland, New Zealand.

²⁾ Numbers in brackets refer to References, page 301.

2. Experimental Procedure

The experimental arrangement used is shown in figure 1. Protons from the Harwell 5.5 MeV Electrostatic Generator are brought to a focus through a 5 mm diameter collimator onto a target of Li_3N . This material was chosen because of its high lithium content and low yield of high energy gamma rays. Neutrons from the reaction $\text{Li}(p, n)\text{Be}^7$ emitted at an angle $\phi = \pm 50^\circ$ to the proton beam pass through a collimator to the scatterer 50 cm distant. The neutron energy spread due to target thickness is about 40 KeV. The main shield is formed of boron loaded paraffin. The first half of the collimator is slightly tapered with a mean width of 2 cm, the second half broadens out into a trumpet shape such that no part was nearer to the sample than 5 cm. The sides of the collimator were fitted with carbon liners to depth of 2.5 cm to reduce small angle scattering.

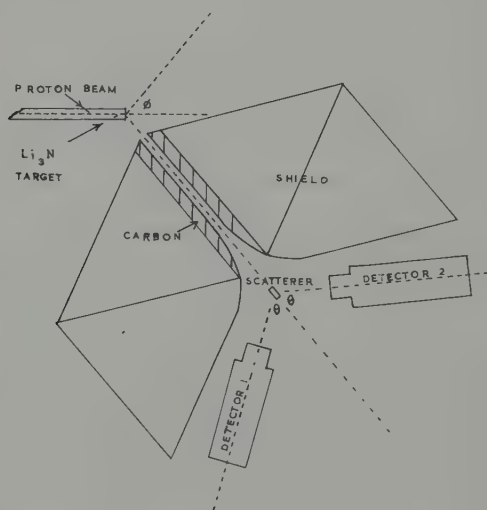


Figure 1
General arrangement of the apparatus

The scatterers were rectangular blocks $1.9\text{ cm} \times 3.2\text{ cm} \times 7.5\text{ cm}$. The two detectors were scintillation counters consisting of cylinders of stilbene 4 cm diameter by 2.5 cm long mounted on E.M.I. type 6097 photomultipliers. The distance from the centre of the scatterer to the centre of each detector was 12 cm. The response of the two detectors was closely similar (though this was not in fact essential). Pulse shape

discrimination [7, 8] was used in the detector in order to distinguish neutrons from gamma rays. The circuitry used for this purpose was similar to that described by OWEN [8]. The voltage between the last dynode and the collector (~ 2 –3 volts) was supplied from a battery and potentiometer. This voltage was adjusted so that the integrated pulse at the last dynode had a positive sign for a neutron pulse and a negative sign for a pulse due to a γ -ray. A linear pulse was derived from an earlier dynode so that normal pulse height selection could also be applied. Thus only those events satisfying the two criteria of having linear amplitude between appropriate limits, and giving a positive pulse at the last dynode, were counted as neutrons. This procedure enabled low energy neutrons and gamma rays to be excluded from the counters. This feature greatly assisted in the reduction of background.

In order to reduce background due to neutrons scattered from the floor, and surroundings, the experiments were conducted at a target position 320 cm above the floor in a large aircraft hangar. The shields and counters were supported on a light framework which was pivoted, so that the whole apparatus could rotate about the target as centre.

With the pulse height selection set so as to exclude neutrons from the reaction $\text{Li}^7(p, n)\text{Be}^7$ and neutrons which had lost energy by inelastic scattering, the background, measured by removing the sample, was found to be $\sim 30\%$ of the total count at incident neutron energies of 400 KeV, rising to about 50–60% for neutrons of 1600 KeV. A «long-counter» was used as a monitor to relate the «scatterer in» runs to those with scatterer out.

The experiment was carried out by measuring N_1 and N_2 the true counts, *i.e.* total counts minus background, in each of the counters 1 and 2 with the assembly in a position corresponding to $\phi = +50^\circ$. The measurement was then repeated with $\phi = -50^\circ$ giving N_1^1 and N_2^1 . Clearly, if the incident polarization in the first case is P_1 then in the second it is $-P_1$. Also if L/R is the true asymmetry

$$\left(\frac{N_1}{N_2}\right) \left(\frac{N_2^1}{N_1^1}\right) = \left(\frac{L}{R}\right)^2 ;$$

it is this quantity L/R that we have chosen to plot.

At a later stage in the experiment a simpler method was used. Here ϕ was kept constant. The positions of detectors 1 and 2 were adjusted so that their geometrical efficiencies were identical. Instead then of moving to $-\phi$ counters 1 and 2 were interchanged. The method of analysis is very similar to that described above.

The sign convention used in this paper is that the positive direction of the polarization is in the direction $\mathbf{n} = \mathbf{k}_0 \times \mathbf{k}$,

where \mathbf{k} = momentum vector of the outgoing particle,

\mathbf{k}_0 = momentum vector of the incident particle.

In evaluating P_2 we have assumed a constant value of $P_1 = +0.40$ throughout the energy range. ADAIR [1], and OKAZAKI [3] found polarization values of $+0.40 \pm 0.02$ in the range 210 KeV to 600 KeV. STRIEBEL *et al.* [9] give the value $+0.30 \pm 0.02$ for the range 700 KeV to 1.5 MeV but this is not well supported by CRANBERG [10] who finds $+0.44 \pm 0.03$ at 1.494 MeV, and $+0.37 \pm 0.05$ at 1.95 MeV.

The polarization of neutrons scattered from carbon for neutrons of energies less than 1 MeV should be zero as there are no strong p -wave or higher resonances in this region. This material was used as a check that we had eliminated artificial asymmetries. This topic is discussed in some detail in the Appendix.

3. Results

Using the methods described above, the asymmetry has been measured at scattering angles $\phi = 55^\circ$ and $\phi = 90^\circ$ for copper and molybdenum. In view of the somewhat surprising nature of the results considerable pains were taken to ensure their consistency and reliability. Measurements were made using both methods described above and within the errors there appeared to be good agreement. Carbon checks were made during the course of these measurements. The results at 55° are shown in figures 2 and 3.

Since over a large part of the energy region the two materials have opposite signs of polarization a further check was to make alternate measurements with copper and molybdenum. These measurements were again consistent with our previous measurements. There can be little doubt that the polarization is not a smooth monotonic function of energy. This is confirmed by the measurements at 90° which are shown in figures 4 and 5. In order to investigate these effects further the experiments were repeated for zinc and cadmium. Here fewer points have been taken (figures 6 and 7) but the same general features appear.

Taking the assumptions described above the polarizations were calculated. These have not been corrected for the effect of multiple scattering in detail. The order of magnitude of this correction is estimated to be about 30%, i.e. the observed polarization should be increased by about 30%. When this correction is taken into account there is in general fair agreement between our measurements and those of CLEMENT *et al.* though there are one or two discrepancies well outside the experimental error.

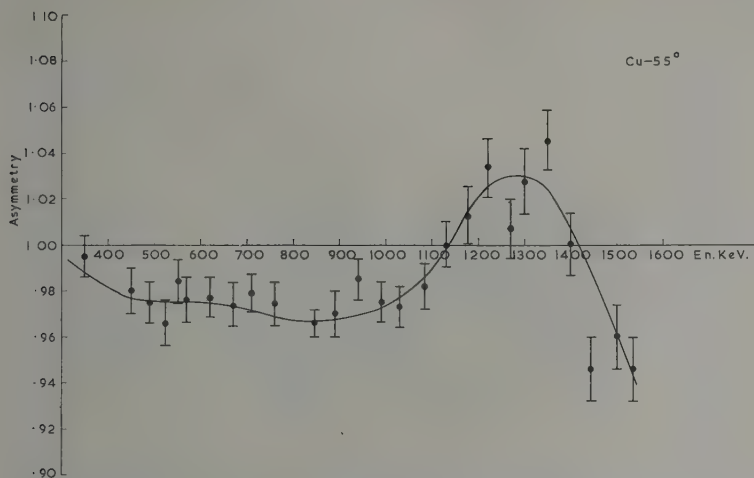


Figure 2. The variation of the polarization of neutrons scattered from copper at 55°

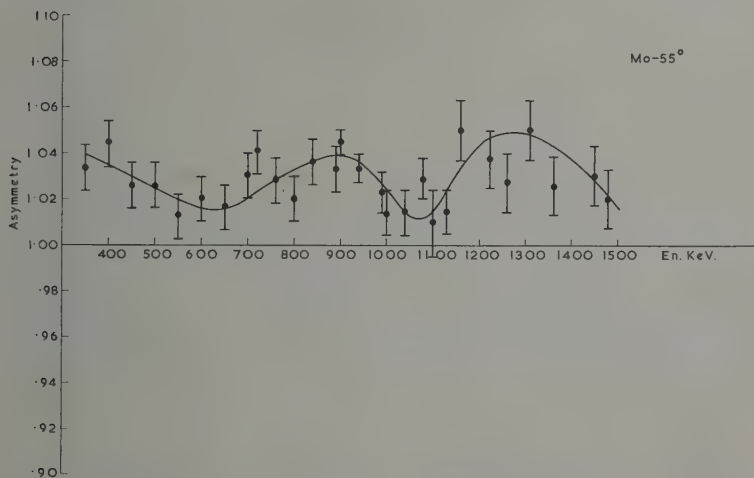


Figure 3. The variation of the polarization of neutrons scattered from molybdenum at 55°

4. Discussion

Calculations were made using the version of the optical model with spin orbit coupling proposed by BJORKLUND and FERNBACH. The para-

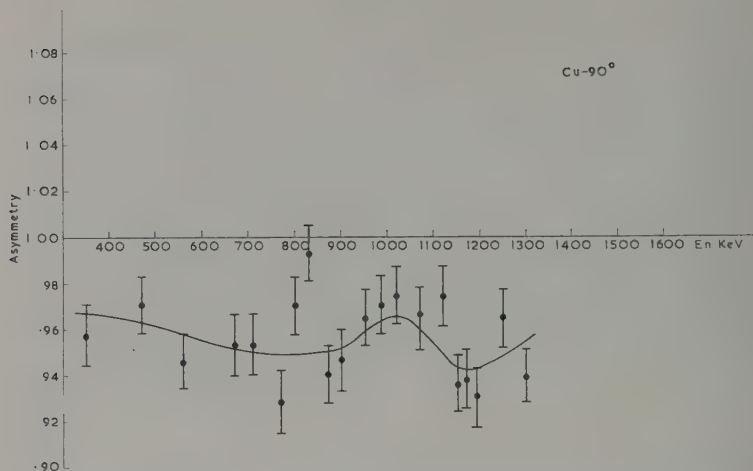


Figure 4. The variation of the polarization of neutrons scattered from copper at 90°

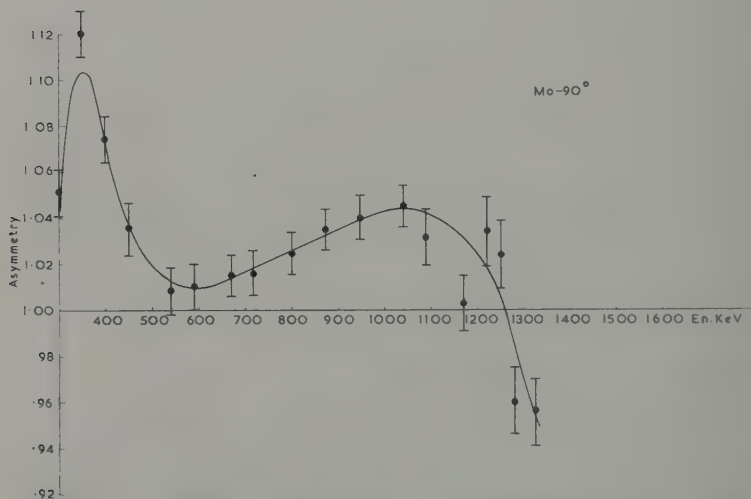


Figure 5. The variation of the polarization of neutrons scattered from molybdenum at 90°

meters were taken from their summary of best values given at the Florida Conference in 1959. They were $V_{en} = 56$ MeV, $V_{ei} = 2$ MeV,

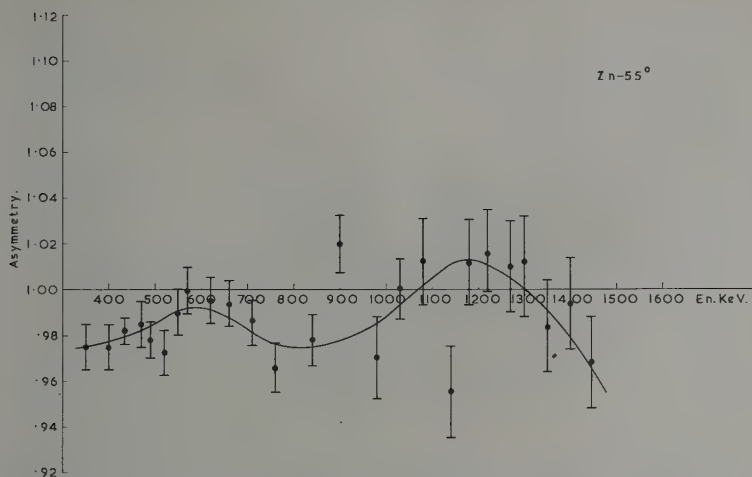


Figure 6. The variation of the polarization of neutrons scattered from zinc at 55°

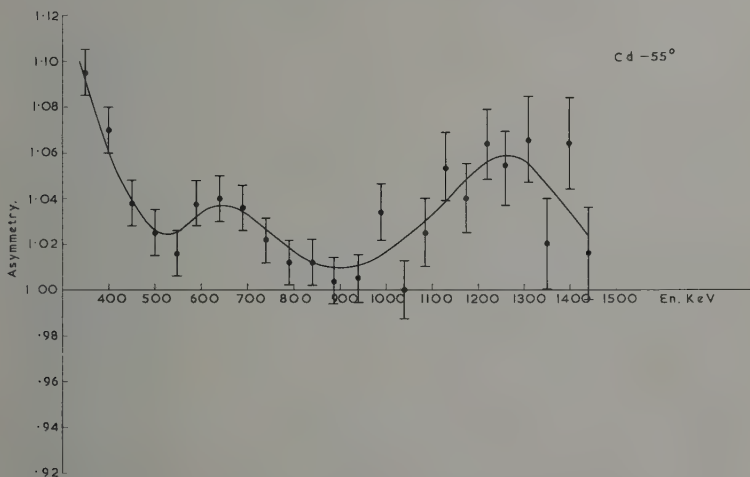


Figure 7. The variation of the polarization of neutrons scattered from cadmium at 55°

$V_{sn} = 10$ MeV, $a = 0.65$ or 0.4 , $b = 1.0$, using the notation of these authors. The comparison of these calculations with the data is shown

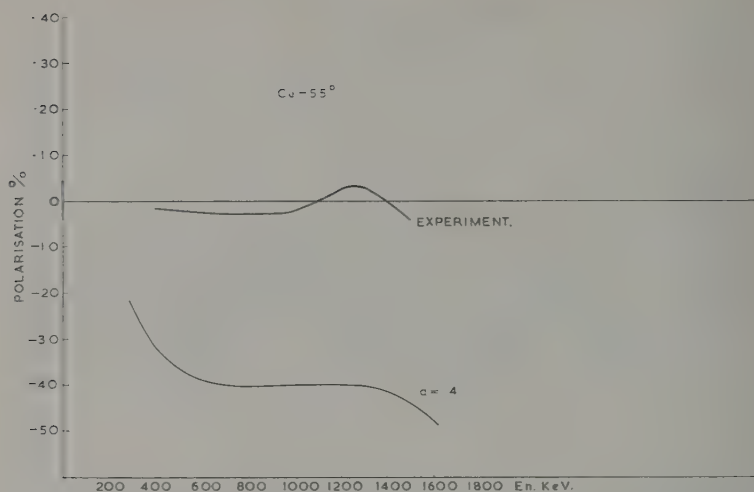


Figure 8. Comparison of the experimental polarization on scattering from copper at 55° with calculation on the basis of the optical model

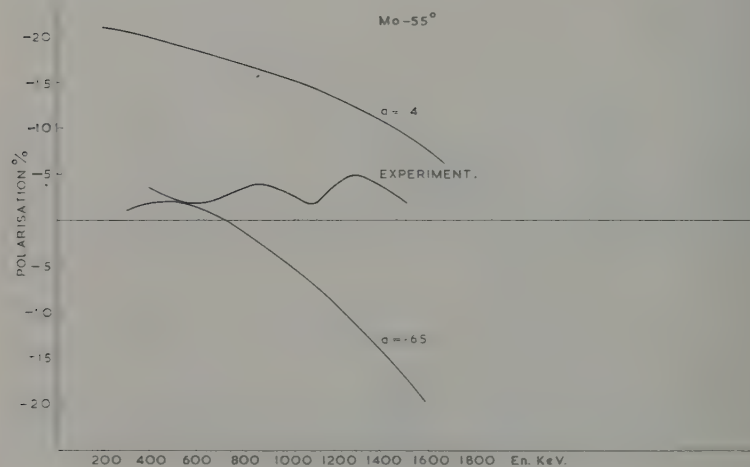


Figure 9. Comparison of the experimentally measured polarization on scattering from molybdenum at 55° with calculations on the basis of the optical model

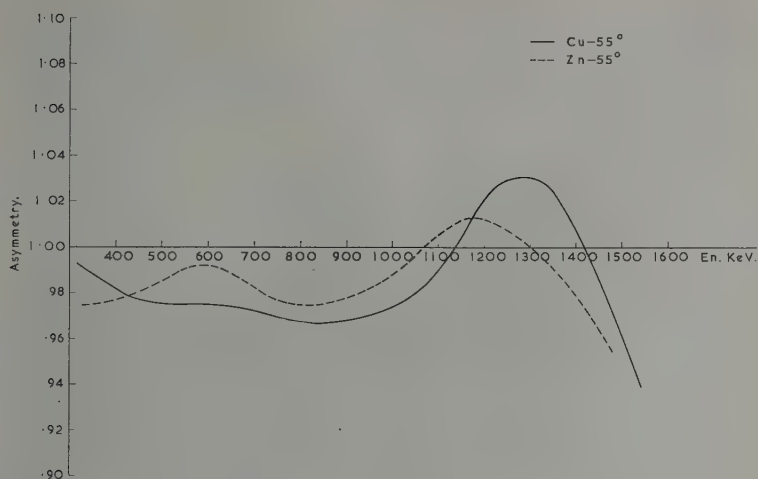


Figure 10. Comparison of the experimentally measured polarizations for scattering from copper and zinc at 55°

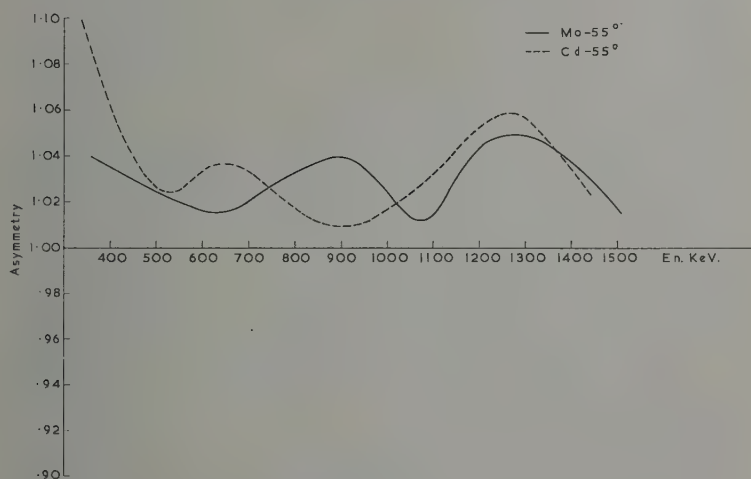


Figure 11. Comparison of the experimentally measured polarizations for scattering from molybdenum and cadmium at 55°

in figures 8 and 9. It is clear that the optical model cannot reproduce the detailed features observed. Although no serious exploration of the

parameter space could be undertaken through lack of computer time, it appeared that with some quite reasonable variation of the parameters each point could be fitted. Using the same parameters the calculated angular distribution of scattered neutrons at 1 MeV fitted the work of WALT and BARSCHALL [12] fairly well.

The question then arose as to whether the variation with energy observed was simply peculiar to the individual nuclei or whether there was some greater regularity. As a first step in investigating this point the measurements on zinc and cadmium were made. Figures 10 and 11 show this comparison. Though not conclusive there is sufficient similarity present to make us anxious to pursue this matter further.

In terms of the optical model division of elastic scattering into shape elastic and compound elastic, it is fairly certain that any explanation of these phenomena will primarily concern the compound elastic processes. An explanation could be in terms of a departure from the statistical distribution of levels in the compound nucleus allowing one or two dominant levels to decide the polarisation, i.e. the compound elastically scattered neutrons may be polarised. There is as yet, however, too little data to provide a worthwhile basis for computation. It is our intention to extend this work to a further series of elements using a transverse magnetic field to rotate the spins of the incident neutron.

Appendix

False Asymmetries

Many of the asymmetries which may be observed in scattering experiments arise from causes other than polarization. The principal causes of these may be summarized as under:

- a) Unequal efficiency of the two counters.
- b) Uneven illumination of the sample due to:
 - i. Variation of the cross-section for the $\text{Li}(p, n)$ reaction with angle.
 - ii. Unequal scattering off the sides of the collimator due to displacement of the source.
- c) The variation of the polarization of the incident neutrons P_1 across the sample.
- d) The variation of P_2 with angle of scattering.

The experimental procedure described above clearly eliminates (a) in this case. (The somewhat simpler procedure of interchanging the two counters also eliminates (a)). In principle (b)ii is also eliminated. However, precise rotation of the assembly about the target spot is difficult to achieve and unless this effect is made small false asymmetries may

appear. This may be achieved by keeping the width of the sample small compared with mean width of the collimator and by lining the latter with carbon. The effects mentioned at (b) i, (c) and (d) have been considered in detail by EVANS [11]. He shows that the expression for the asymmetry may be written

$$\frac{R}{L} = \frac{1 + (\alpha - \beta) \frac{\theta_1^2}{3} + P_1 P_2 \left[1 + (\gamma + \delta) \frac{\theta_1^2}{3} \right]}{1 + (\alpha + \beta) \frac{\theta_1^2}{3} + P_1 P_2 \left[1 + (\gamma - \delta) \frac{\theta_1^2}{3} \right]}.$$

The functions α and β depend only on the angular distribution $\sigma(\theta)$ of the neutrons from the $\text{Li}(p, n)$ reaction and $\sigma'(\theta)$ its derivative with respect to θ . The functions γ and δ contain not only σ and σ' but also P and its derivative with respect to θ , P' . θ_1 is the angle subtended by the scatterer at the source.

If we consider scattering from carbon we should expect that for neutrons less than 1 MeV P_2 should be zero: in those circumstances

$$\frac{R}{L} = \frac{1 + (\alpha - \beta) \frac{\theta^2}{3}}{1 + (\alpha + \beta) \frac{\theta^2}{3}}.$$

We have measured the quantity R/L for carbon for several energies up to 900 KeV and find that within our statistical errors it is unity. Consequently the terms in α and β which contain only the parameters of the $\text{Li}(p, n)$ reaction must be negligible with the solid angles used.

Insufficient data is available to compute γ and δ precisely but using reasonable estimates it would seem unlikely that these terms would give rise to significant asymmetry. Experimentally, the use of a magnet to rotate the spins of the incident neutrons would eliminate the effect due to this cause. Until this is done there must remain a residual uncertainty on this point.

From this discussion, the checks using carbon as a scatterer would appear to remove the main uncertainties and to give reasonable confidence that only true asymmetries were being observed.

REFERENCES

- [1] ADAIR, DARDEN, and FIELDS, *Phys. Rev.* **96**, 503 (1954).
- [2] WILLARD, BAIR, and KINGTON, *Phys. Rev.* **98**, 669 (1955).
- [3] OKAZAKI, *Phys. Rev.* **99**, 55 (1955).
- [4] McCORMAC, STEUER, BOND, and HEREFORD, *Phys. Rev.* **104**, 718 (1958).
- [5] CLEMENT, BORELLI, DARDEN, HABERLI, and STRIEBEL, *Nuc. Phys.* **6**, 177 (1958).

- [6] F. BJORKLUND, *Proceedings of the International Conference on the Nuclear Optical Model*, Florida State University (1959).
- [7] F. D.-BROOKS, *Progr. in Nucl. Phys.* *5*, 284, Pergamon Press, London (1956).
- [8] R. B. OWEN, Harwell Report A.E.R.E. EL/R 2712 (1958).
- [9] STRIEBEL, DARDEN, and HABERLI, *Nucl. Phys.* *6*, 188 (1958).
- [10] CRANBERG, L., *Phys. Rev.* *114*, 174 (1959).
- [11] J. E. EVANS, A.E.R.E. Report R. 3347.
- [12] M. WALT, H. H. BARSCHALL, *Phys. Rev.* *93*, 1062 (1954).

Polarization of Elastically Scattered 3.4-MeV Neutrons¹⁾

By FRANK L. HEREFORD, Department of Physics, University of Virginia

In order to determine the suitability of optical model descriptions of the elastic scattering of nucleons by nuclei it is important to measure both the differential cross section and the polarization of the scattered nucleons. In a continuation of a program begun a few years ago at the University of Virginia, we²⁾ have recently measured the polarization of 3.4-MeV neutrons elastically scattered by S, Cu, and Zn. Differential cross sections have been reported for these elements at approximately the same energy (3.7 MeV) by SNOWDEN and his co-workers [1]³⁾. A by-product of the experiment reported here was the accumulation of a considerable amount of data on the polarization of neutrons scattered by C.

Experimental Method

Partially polarized neutrons of mean energy 3.4 MeV were obtained from bombardment of a thick heavy ice target with 1 MeV deuterons. After collimation at 45° (lab) as shown in figure 1, the neutrons were scattered by cylindrical scatterers. The intensities of neutrons scattered to the right and left were recorded simultaneously and the polarization produced by the scatterer inferred from the polarization-asymmetry relation,

$$P_n P_{sc}(\theta) = \frac{R(\theta) - L(\theta)}{R(\theta) + L(\theta)}$$

where P_n and P_{sc} represent the magnitudes of the incident neutron polarization and that produced by the scatterer. In both cases positive polarization is considered to be in the direction of $\mathbf{k}_i \times \mathbf{k}_f$, where \mathbf{k}_i and \mathbf{k}_f are the momenta of incoming and outgoing particles.

¹⁾ Supported by U. S. Atomic Energy Commission and OOR, U. S. Army.

²⁾ The experiments reported here constituted part of the Ph. D. dissertations of Drs. G. C. COBB (now at North Carolina State College), and H. O. FUNSTEN (now at Princeton University). Dr. T. G. WILLIAMSON (now at University of Virginia Nuclear Engineering Department) also participated in the work.

³⁾ Numbers in brackets refer to References, page 310.

The polarization of the $D(d,n)$ neutrons, P_n , is known best from measurements made using $He^4(n,n)$ for analysis [2]. For 1 MeV deuterons on a thick target and for the neutron detector bias used in this experiment, the mean polarization of 45° neutrons was 11.6%. The uncertainty of this value is difficult to assess; we estimate it to be about $\pm 1\%$.

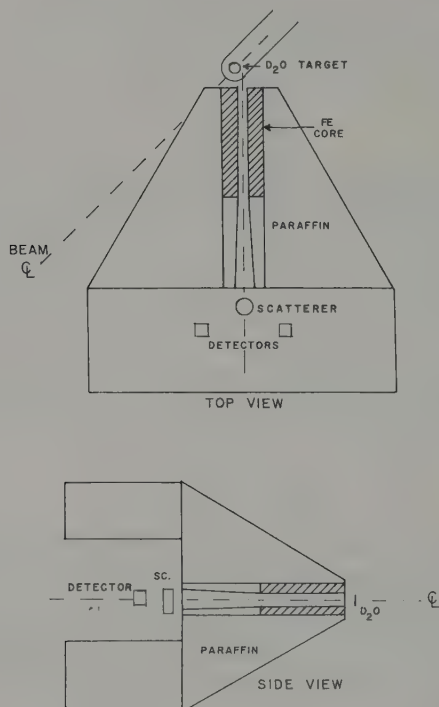


Figure 1

Top view and side view of the collimator, scatterer, and scintillation detectors

Several improvements have been made in the technique used in previous measurements [3]. Specifically these involve the following innovations. Scattered neutrons were detected by pulse-shape discriminating neutron counters [4]. By utilizing the difference in pulse shapes for neutron and gamma induced pulses from stilbene scintillators, it has been possible [5] to achieve neutron to gamma efficiency ratios as high as 1000. At the same time the counters reproduced well the neutron pulse height spectrum making possible discrimination against inelastically scattered neutrons. Neutrons scattered to the right and left were

detected simultaneously and the pulses were displayed on 50-channel sections of a 100-channel pulse analyzer. The analyzer was gated to count only neutrons by 'pulse shape' signals. The scattered neutron intensity was measured as the 'scatterer in minus scatterer out' counting rate. The 'scatterer out' rate could be held to approximately 30% of the 'scatterer in' rate at forward angles, and to 70% at backward angles. Neutron intensity was monitored by a stilbene detector placed above the collimator, viewing the deuterium target at 45°, and with the same bias as the scattered neutron detectors.

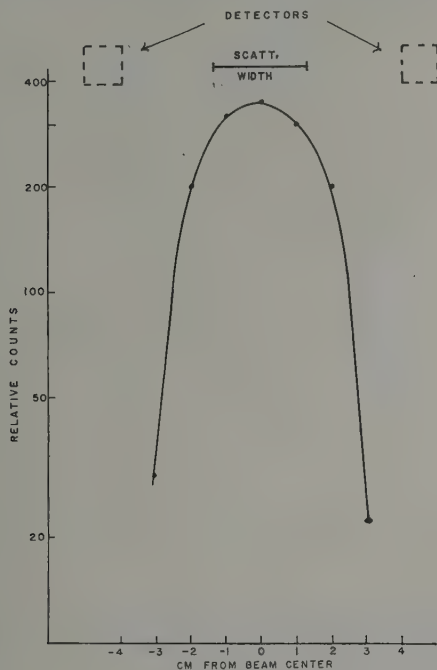


Figure 2

The observed profile of neutron intensity emerging from the collimator. Size and position of the scatterer and detectors are also shown.

The profile of neutrons emerging from the collimator and the energy spectrum of neutrons contributing to the data are shown in figures 2 and 3. The energy spectrum $N(E)$ was calculated from the following expression,

$$dN = C \sigma(E_d) \left(\frac{dE_d}{dx} \right)^{-1} \epsilon(E_n) dE_d$$

where C is a constant, $\sigma(E_d)$ the differential reaction cross section at 45° , dE_d/dx the deuteron energy loss in D_2O , and $\varepsilon(E_n)$ the neutron counter efficiency for neutron energy E_n produced by deuterons of energy E_d .

Instrumental asymmetries were observed and eliminated by taking data alternately with neutrons emitted to the "right" and "left" of the deuteron beam, for which cases the sign of P_n is opposite. The entire apparatus was frequently checked by measuring the right-left asymmetry at 45° for a carbon scatterer, which asymmetry is now well known from previous measurements [3, 6].

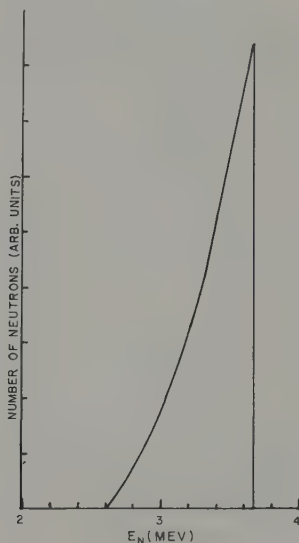


Figure 3

The neutron energy spectrum calculated as described in the text

Recording of the differential pulse spectra of both the right and left counters made possible a determination of the influence of inelastically scattered neutrons. Only pulses occurring above the inelastic energy were accepted. The angular resolution of the scatterer-detector geometry employed varied from 10° to 28° for different scattering angles.

Results

The observed values of polarization, corrected for finite geometry, are shown in figures 4, 5, and 6 for S, Cu, and Zn together with the differential cross sections observed by MACHWE, KENT, and SNOWDEN [1]

(solid lines). It can be seen that the polarization goes through zero near the first diffraction minimum for each of the scatterers. Also, for forward angles the sign of the polarization corresponds to the slope of the cross section. These two features are in accord with RODBERG's approximate calculation [7] which is probably not accurate for large angles. Correspondingly, the polarization produced by Cu and Zn fails to go to zero at the first maximum (100°) and second minimum (140°) although for both elements a slight decrease in the positive polarization is evident near these angles.

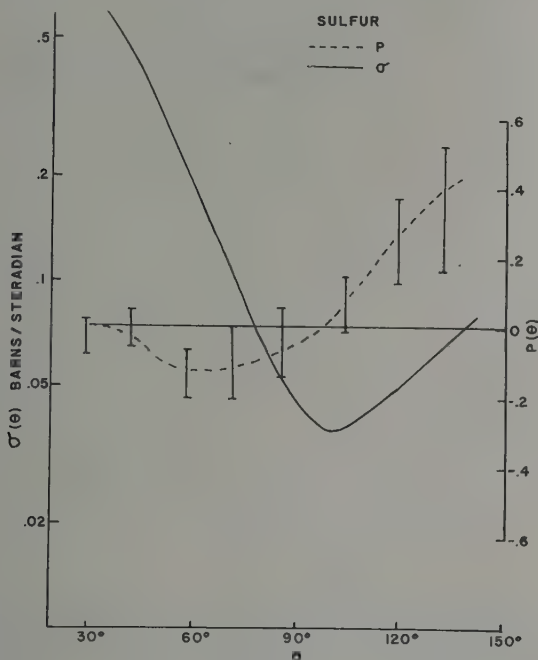


Figure 4

Experimental points and dotted line show the observed polarization produced by sulfur (scale on the right). The solid curve represents the differential cross section measurements of MACHWE *et al.*¹⁾ (scale on the left).

Both the polarizations and differential cross sections for Cu and Zn are very similar, which one expects to be the case for shape elastic scattering by neighbouring elements. The Zn polarization is compared with an optical model calculation made by BJORKLUND⁴⁾ in figure 7. The curve shown is BJORKLUND's curve corrected for finite detector

geometry. Agreement is fair up to about 100° but the predicted change of sign at 110° was not observed. The influence of compound elastic scattering was undoubtedly appreciable. A computed optical model cross section [2] accounts for only about one half of the observed cross section integrated beyond 100° . Comparison of the Cu polarization data with the calculated curve is about as inconclusive as is the case with Zn.

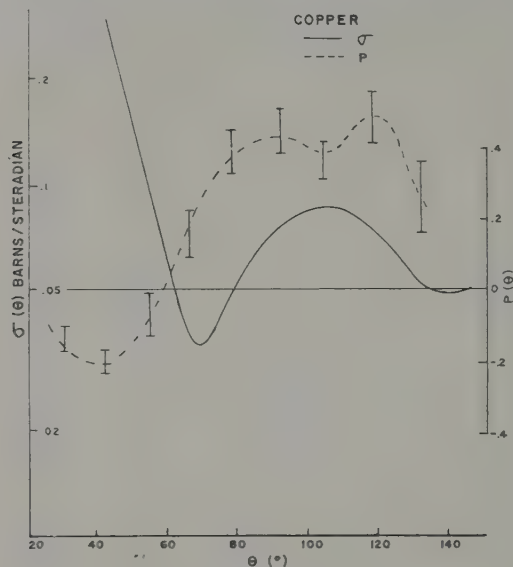


Figure 5

Same as figure 4, but for copper

The frequent checks of the instrumental asymmetry with a carbon scatterer yielded considerable data on the polarization produced by carbon. It is interesting to compare the result with that computed from the phase shifts of MEIER, *et al.* [6] and WILLS, *et al.* [8] for the neutron energy spectrum employed. One finds

$$P_c(45^\circ) = \begin{cases} -0.52, \text{ MEIER, } et\ al. \\ -0.33, \text{ WILLS, } et\ al. \\ -0.64 \pm 0.04, \text{ Observed} \end{cases}$$

⁴) BJORKLUND, private communication. The potential used in these calculations was that described by BJORKLUND and FERNBACH, *Phys. Rev.* 109, 398 (1958) with $V_{CR} = 47$, $V_{CI} = 7$, $V_{SR} = 5$, $V_{SI} = 0$.

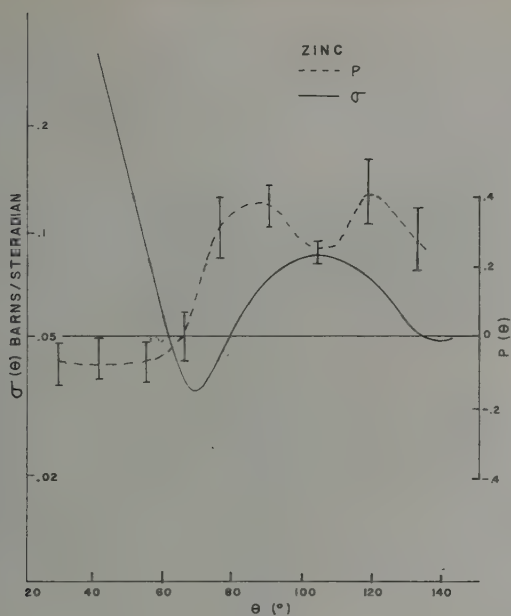


Figure 6

Same as figure 4, but for zinc

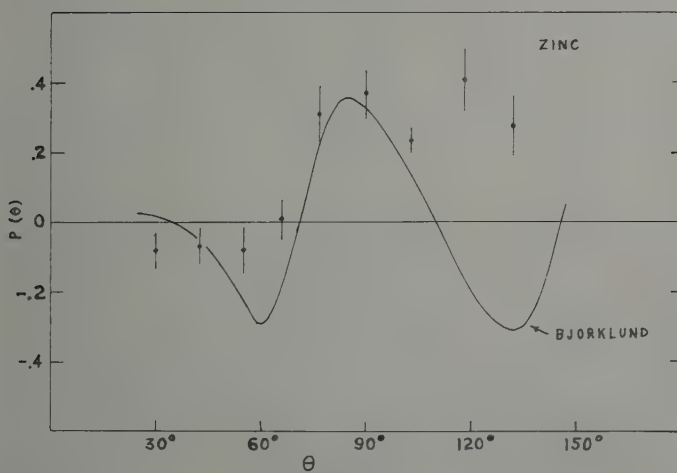


Figure 7

Comparison of the zinc polarization measurements with BJORKLUND's optical model calculation⁴⁾

As in the case of previous results [3, 9], this measurement is in better agreement with the polarization predicted by the Meier phase shifts. Figure 8 shows results obtained previously [3] on the polarization of neutrons scattered at 45° from carbon for neutron energy between 2 and 4 MeV. The uncertainty in knowledge of the $D(d,n)$ neutron polarization introduces possibly a 10% uncertainty in the observed values in addition to the statistical errors. It seems unlikely, however, that the assumed neutron polarization could be in error by a factor of two.

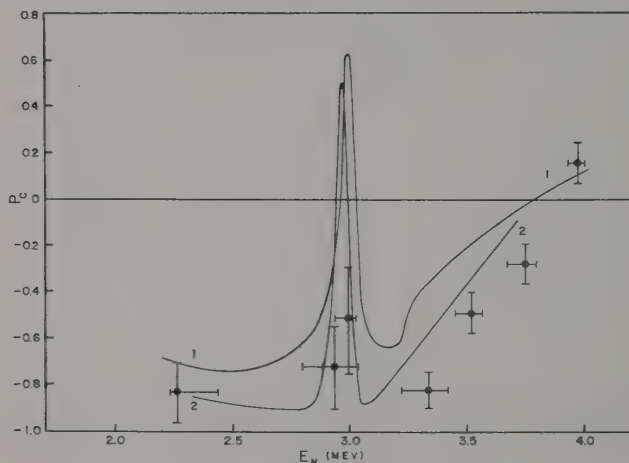


Figure 8

The polarization of neutrons scattered at 45° from carbon. Curve 1 was computed from the phase shifts of WILLS *et al.* [8]; curve 2 from those of MEIER *et al.* [6].

REFERENCES

- [1] MACHWE, KENT, and SNOWDEN, *Phys. Rev.* **114**, 1563 (1959).
- [2] LEVINTOV, MILLER, and SHAMSHEV, *Nucl. Phys.* **3**, 237 (1957); P. J. PASMA, *Nucl. Phys.* **6**, 141 (1958).
- [3] MCCORMAC, STEUER, BOND, and HEREFORD, *Phys. Rev.* **104**, 718 (1956); BUCHER, BEVERLY, COBB, and HEREFORD, *Phys. Rev.* **115**, 961 (1959).
- [4] BROOKS, *Progress in Nuclear Physics*, Vol. 5 (1956); OWEN, AERE Report EL/R2712, Harwell (1958).
- [5] COBB and FUNSTEN, *Rev. Sci. Instr.* **31**, 571 (1960).
- [6] MEIER, SCHERRER, and TRUMPY, *Helv. Phys. Acta* **27**, 577 (1954).
- [7] RODBERG, *Nucl. Phys.* **15**, 72 (1960).
- [8] WILLS, BAIR, COHN, and WILLARD, *Phys. Rev.* **109**, 891 (1958).
- [9] DUBBELDAM, JONKER, and BOERSMA, *Nucl. Phys.* **75**, 452 (1960).

Applications of Millimicrosecond Spectroscopy to Neutron Polarization Studies — Method and Results

By L. CRANBERG, Los Alamos Scientific Laboratory

It is clear that millimicrosecond neutron spectroscopy has an important role to play in connection with neutron polarization studies in several ways. Thus, if one wishes to determine the polarization of one of several neutron groups produced in the target of an accelerator such methods are invaluable if not essential — particularly if one's interest is not restricted to the most energetic or ground-state group. Such use of the method is illustrated by some work already reported at this conference by Dr. SCANLON on behalf of the workers at Harwell. That work is concerned with the limiting case in which the discrete groups corresponding to excitation of single states in the residual nucleus merge into a continuum. We have reported results previously for two groups from the reaction $\text{Li}^7(p, n)\text{Be}^7$ [1¹).

Another case where such methods are clearly useful is that in which one studies polarization in the spectrum of inelastically scattered neutrons. This is a topic of interest from the point of view of theories of nuclear reactions and some information on this item will be presented in what follows.

Less obvious, because it is buried in the quantitative details, is the fact that the pulsed-beam time-of-flight technique is very advantageous even for the study of ground-state neutron groups — the case of special interest in connection with development of the optical model. Most of the new results to be presented are in this category.

There are various possibilities for incorporating millimicrosecond neutron spectroscopy in an arrangement for the study of neutron polarization. The first slide (figure 1) illustrates the arrangement we have chosen. Its most distinctive feature is the fact that the scatterer is very close to the target, in contrast to the usual arrangement which places it close to the detector. The motivation for this choice is that one can, with this plan, do spectroscopy on the products of the neutron-producing reaction

¹) Number in brackets refers to Reference, page 324.

and on the products of the scattering process simultaneously, and it requires only a trivial modification of our usual arrangement for the study of elastic and inelastic neutron scattering – namely, the displacement of the scatterer and of the detector pivot away from the zero-degree direction. The choice of 35° from the proton direction was typical of the reaction angles used in this study.

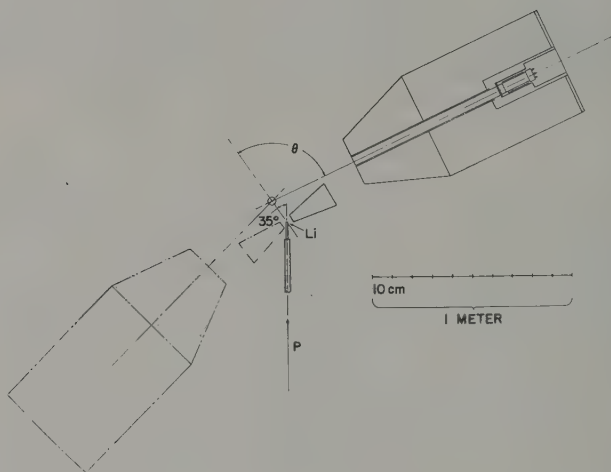


Figure 1

This arrangement is particularly vulnerable to two sources of spurious asymmetry. One is transverse displacement of the proton beam which results in a spurious left-right asymmetry due primarily to a corresponding shift of the zero-degree scattering angle; and the other is the effect associated with the shielding wedge, whose function is to shield the detector from the direct flux from the target. When the detector and the wedge are in the 'right' position the wedge is more strongly illuminated by the neutron flux from the target than when it is in the 'left' position. This gives rise to the possibility that neutrons scattered from the wedge and then scattered again from the scatterer will be more numerous on the right side than on the left side.

The effect of transverse displacement of the proton beam was dealt with in the following way. The beam was sufficiently well focused that it could be transmitted effectively by an aperture of only 2 mm diameter placed close to the target. To check on the positional stability of the beam within this 2 mm aperture the zero-degree neutron scattering direction was determined very frequently, usually between each left and right observation. The procedure for determining zero-degrees follows the plan

described in a paper by CLEMENT, BORELI, DARDEN, HAEBERLI, and STRIEBEL, which will be referred to henceforth as CLEMENT *et al.* This procedure involves measuring the transmission of the sample at small angles in the neighborhood of zero-degrees, and the center of symmetry of the transmission pattern is taken to be zero-degrees. The sensitivity claimed for this method by CLEMENT *et al.* of $\pm 1/4$ of a degree has been confirmed by our experience. In our measurements this angular uncertainty corresponds to an uncertainty in the asymmetry of about 0.01 for forward angles, and less for back angles.

The effect of the wedge in producing spurious asymmetries due to double scattering effects could in fact be observed under sufficiently aggravated conditions. These aggravated conditions correspond to the use of a heavy metal wedge at small scattering angles. By using a polyethylene wedge, however, and restricting the range of observation to angles of 50° or larger, the effect of the wedge was such as to produce substantially less than 1% spurious asymmetry.

Since there is no built-in self-monitoring in this arrangement, accurate monitoring of the neutron flux irradiating the sample on corresponding left and right runs must be done with good accuracy, preferably to 0.1% or better. The next slide (figure 2) illustrates the monitoring arrangement.

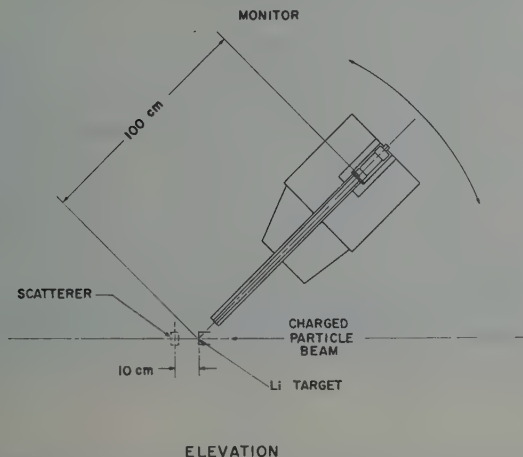


Figure 2

This is an elevation view in the plane of the proton beam and shows the monitoring detector, which is an anthracene scintillator, in its shield and collimator. The essential feature of the arrangement is that with the

aid of tight collimation the field of view of the monitor detector is restricted to a small volume in the vicinity of the neutron-producing target. Thus it is insensitive to the presence of the sample and to the position of the wedge.

The next slide (figure 3) is a photograph which illustrates the arrangement in three dimensions, combining the views of the first and second slides. In the photograph a solid sample is shown in place on a wire which normally supports three samples and may be moved remotely. The next slide (figure 4) illustrates the arrangement which was used when the samples were in the form of compressed gases. Two of the spherical vessels shown contain He^4 and He^3 at pressures of 350 atmospheres, and the third vessel is an evacuated dummy for background subtraction purposes. The large boxes at the corners of the framework are gauges which continuously monitor the pressure in the filled vessels.

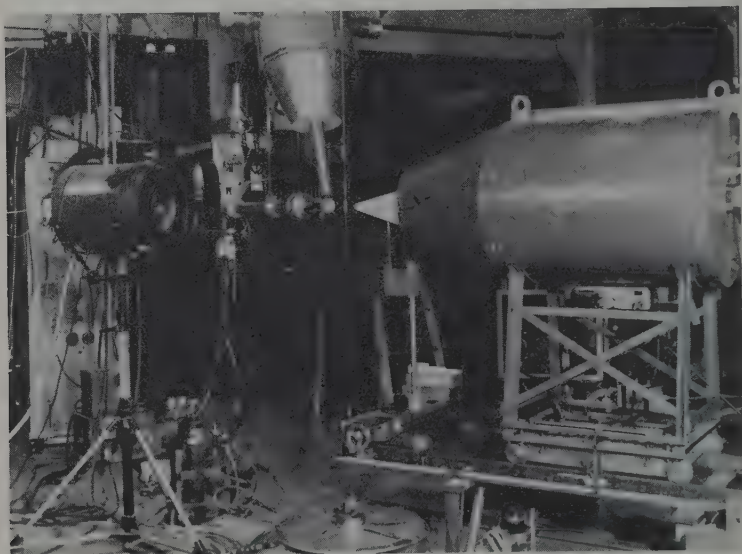


Figure 3

Table I is a summary of the essential performance parameters of the system under the conditions for which most of the measurements which will be reported here were taken.

The accelerator used for this work was the large Los Alamos VAN DE GRAAFF fitted by J. L. McKIBBEN with a terminal pulser of the deflection type.

Let me note parenthetically that I regard the performance characteristics indicated in table I as representative of a state of affairs which can be very radically improved by straightforward procedures, and that one can readily attain the performance indicated by the numbers in parentheses in table I. There are a number of places at which effort is now being directed toward achieving the performance indicated by the numbers given in parentheses, and I think it quite likely that such improvement will have been accomplished before the year is out.



Figure 4

The next slide (figure 5) shows a time spectrum which is typical of those obtained in the course of this work, and illustrates the present state of our technology. The conditions under which this time spectrum was obtained are indicated on the slide. The neutron source was the $\text{Li}^7(p, n)$ reaction giving a ground state group of 2.09 MeV at 35°, and a second group about 10% as strong at about 1.6 MeV. The scatterer was a

sample of titanium. Time increases from right to left. The gamma-ray line is due to de-excitation of Ti^{48} excited to its first state at 1.0 MeV. We then see elastic scattering due to the strong and weak neutron groups, and finally an inelastic neutron line due to the main group from the target. The width of the inelastic line is dominated by the spread in neutron energy due to the target thickness, which was 160 keV. The width of the elastic line is due primarily to the burst duration. This figure indicates we can resolve effectively a neutron group within 500 keV of the 2 MeV ground state group.

Table I

Average Current	1 μA	(10)
Duty Cycle	0.01	(0.001)
Elastic Line Width at Half Max	4.5 ns	(2)
Target-Scatterer Distance	8-12 cm	
Scatterer-Detector Distance	1.2 m	
Signal-Background Ratio	~ 3	
Counting-Rate	10 40 s^{-1}	

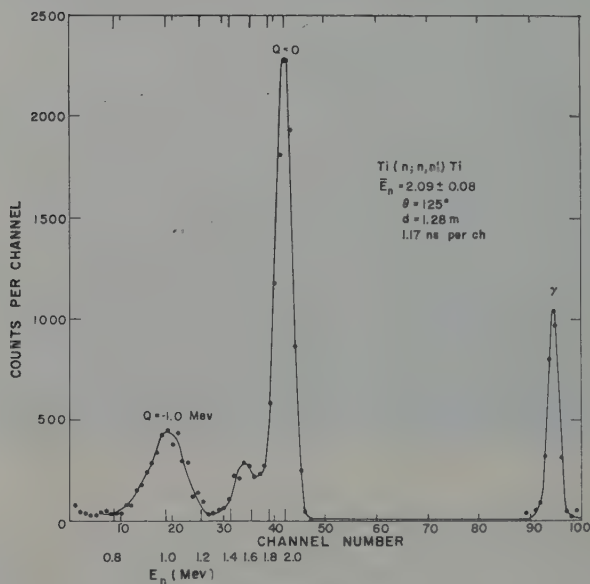


Figure 5

So much for the general features of our method. We turn now to the discussion of the results.

Our first endeavour was to attempt to find a neutron source strongly polarized, at least as prolific as any of those now known, and preferably of an energy substantially higher than 1 MeV, which is the energy of the earlier comprehensive study of CLEMENT *et al.* Following the suggestion of J. MARION, we have investigated the ground state neutron group from the reaction $\text{Be}^9(p, n)\text{B}^9$ which exhibits a strong resonance at 4.5 MeV proton energy. The rather discouraging results are illustrated in the next slide (figure 6), which indicates we have explored this reaction at 45° for proton energies from 4.5 to 5.3 MeV, using carbon as an analyzer, and the values of polarization calculated from the phase shift analysis of MEIER, SCHERRER, and TRUMPY. The polarization obtained is substantially less than that available from the $\text{Li}^7(p, n)$ reaction and the neutron yield is also down. We therefore determined to undertake a systematic investigation of polarization effects at the highest energy at which our previously reported investigation [1] had shown that the $\text{Li}^7(p, n)$ reaction gives substantial polarization. As indicated in the summary given by Professor HAEBERLI earlier at this conference, this energy is in the range of 2 MeV neutron energy, and a systematic investigation of polarization effects in neutron scattering has been carried out at that energy for about 30 nuclear species ranging in mass from deuterium to U^{238} .

$\text{Be}^9(p, n)\text{B}^9 \quad \theta' = 45^\circ$				
$E_p(\text{MeV})$	$E_n(\text{MeV})$	$P_1 P_2$	P_2	P_1
4.49 ± 0.11	2.39	-0.034 ± 0.015	-0.75	0.045 ± 0.02
4.69 ± 0.10	2.58	$+0.078 \pm 0.013$	-0.85	-0.091
4.90 ± 0.10	2.77	$+0.093 \pm 0.015$	-0.97	-0.095
5.30 ± 0.09	3.16	$+0.06 \pm 0.02$	-0.95	-0.101

Figure 6

As a preliminary step the polarization of the $\text{Li}^7(p, n)$ source was re-measured by the same procedure which had been used before, — that is, by scattering from a compressed gas sample of He^4 . Our result for this measurement of $35 \pm 3\%$ compares well with our earlier published result of 38 ± 3 . In the subsequent slides the values of polarization observed in scattering are based on the value 0.38, or the observed value of the asymmetry, ε , only is given. In the latter case the corresponding polarizations are obtained roughly by multiplying the observed values of the asymmetry by three.

One may usefully distinguish four mass intervals (hereafter referred to by Roman numerals) as characterized by special features of theoretical

interest. In group I, which comprises the very lightest nuclei, the chief point of interest is the possibility of obtaining clues with respect to the nucleon-nucleon force itself. In group II are the nuclei whose scattering properties may be interpreted in terms of the excitation of one or two resonances in the compound nucleus. Group IV, which includes the medium-weight and heavy nuclei, is characterized by the excitation of a very large number of states in the compound nucleus and lends itself to description in terms of cross-sections averaged over levels, by the optical model, and by statistical theories of nuclear cross sections such as the Hauser-Feshbach theory. Group III, which is intermediate in mass between groups II and IV is also intermediate with respect to the number of levels excited in the compound nucleus and may be expected to exhibit strong fluctuation effects, that is, a strong and irregular dependence of scattering properties on mass number and on the mean energy and energy spread of the incident neutron beam.

The results in group I have been given for deuterons in earlier work and by previous speakers, and the results obtained on T and He^3 (this was work done in collaboration with J. D. SEAGRAVE and J. E. SIMMONS) were reported at last year's London Conference on the Few Nucleon Problem. They will also appear shortly in the Physical Review. These results may be summarized very simply by saying of all of them that very little polarization is observed. I regard this as our most striking result on polarization to-date. There is a cleancut break with respect to polarization effects at the boundary between mass 4 and mass 5 systems (referring now to the mass of the compound systems) although p -wave effects are equally prominent at an energy of a few MeV for systems of mass 3, 4, and 5. The role of spin-orbit or tensor force in producing a split of p -wave phase shifts is very large for the mass 5 system but is very much smaller for the mass 3 and 4 systems. This is a striking effect which may have a significant unified interpretation, but there is none available at present to the best of my knowledge. I commend this observation to the serious attention of the theorists.

In the mass II region we have observed polarization in scattering from B^{10} , B natural, Be^9 , C^{12} , and Mg^{24} . Here our main motivation for the present has been to look for large polarization effects in the hope that we might find a nucleus suitable for use as an analyzer in our energy range. The largest effect was obtained with carbon, and the results for the polarization of carbon as a function of angle are shown on the next slide (figure 7). Also shown on that slide are the results calculated from the data of MEIER *et al.* at the nearest energies available in their analysis. It is clear that the $\sin 2\theta$ term is the dominant one in describing the polarization as in the results of MEIER *et al.*, but is substantially reduced in magnitude. It is regrettable that we do not have a comparison with the

predictions of WILLS *et al.* which do extend into our energy region, and that our energy coincides with a resonance in C^{13} , so that the analyzing efficiency in carbon is changing rapidly in the energy interval which corresponds to our energy spread. By a crude integration over the relevant energy interval for the prediction of WILLS *et al.* we can say, however, that our result is consistent with WILLS *et al.* to about 15%.

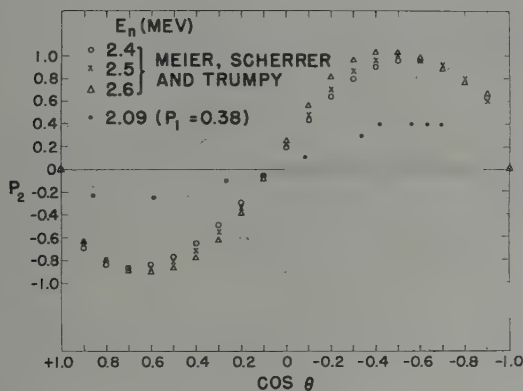


Figure 7

The next pair of slides gives the results obtained for inelastic scattering corresponding to excitation of the first levels in Fe^{56} and Ti^{48} and are, I believe, the first data available on polarization in inelastic neutron scattering.

The first of these slides (figure 8) is for iron. The upper portion of the slide shows the angular distribution of the inelastically scattered neutrons corresponding to the 850 kV level, and the lower portion shows the observed asymmetry. The isotropy of the inelastically scattered neutrons implies the absence of polarization and the experimentally observed result is consistent, within the limits of statistical uncertainty, with the prediction of no polarization. Previous results of LEVIN and myself on inelastic scattering in this nuclide in this energy range have shown, however, that the anisotropy and asymmetry about 90° of inelastically scattered neutrons is rapidly varying with bombarding neutron energy. Hence, the isotropic result, which is consistent with the Hauser-Feshbach prediction of symmetry of about 90° , must be regarded as fortuitous. This interpretation of our result is consistent with the results shown in the next slide for titanium (figure 9) which is similar in mass number to iron and similarly even-even in its predominant isotope. Here we observe substantial asymmetry about 90° in the inelastic scattering,

and the possibility that there is indeed a non-zero polarization of as much as 10%.

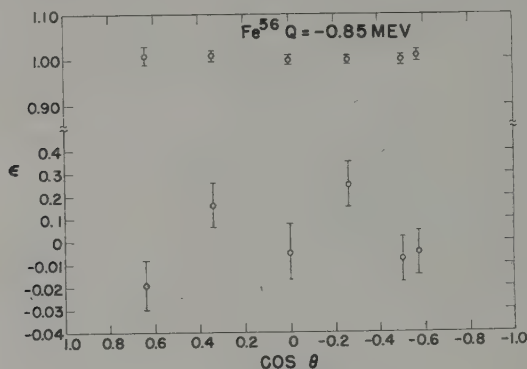


Figure 8

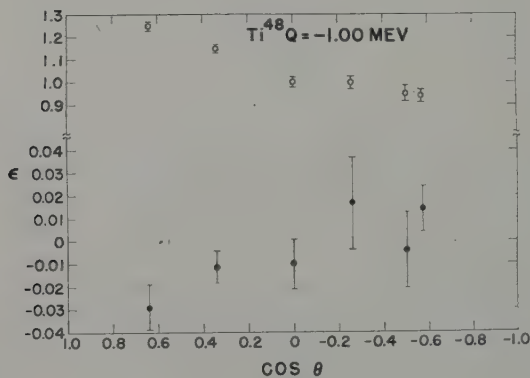


Figure 9

The chief point I want to make here is that at our energy of 2 MeV titanium and iron may be regarded as group III nuclei, that is, nuclei which exhibit marked fluctuation effects associated with the excitation of levels of the compound nucleus which do not satisfy in detail the so-called statistical assumption of the Hauser-Feshbach theory of inelastic scattering, which implies zero polarization.

We come now to the results on elastic scattering for nuclei in groups III and IV. Before giving our results at 2.09 MeV it will be useful to show a slide (figure 10) of the results of CLEMENT *et al.* at 980 keV. In this work

the sign of the polarization convention is not the Basel one, and for comparison with the subsequent slide the sign has been reversed. Let me call your attention to the following two salient features. First, for mass numbers larger than 150 or so, the polarization is positive in the forward direction, decreases at 90° , and essentially vanishes in the back direction. Secondly, we notice a broad negative maximum in the polarization at 90° for nuclei in the neighbourhood of mass 100. This was first pointed out for 400 keV data in the paper which pioneered in this general field, namely, the paper of ADAIR, DARDEN, and FIELDS.

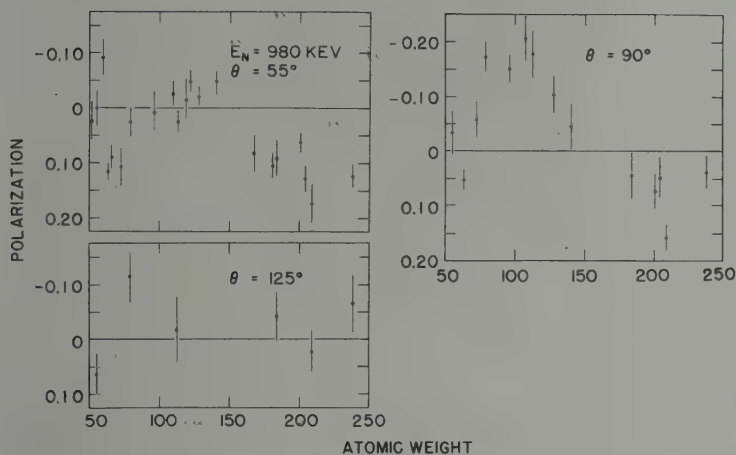


Figure 10

The next slide (figure 11) shows our recent results at 2.09 MeV for 22 nuclei of atomic weight 48 and above, for scattering angles of 50, 90, and 125° . These results do not include corrections for multiple scattering and for unresolved inelastic scattering corresponding to excitation of levels within 500 keV of the ground state, but the corrections will be small and in such a direction as not to modify any of the comments we shall make about the results.

First, we notice, as for the lower energy data, the trend toward diminishing positive polarization for the heaviest nuclei as we go toward the back direction. Secondly, we see again the broad negative maximum at 90° . A new and striking feature, however, is the sharp reversal of the direction of polarization in the back direction in the neighbourhood of mass 100. The paucity of back-angle data at the lower energy precludes

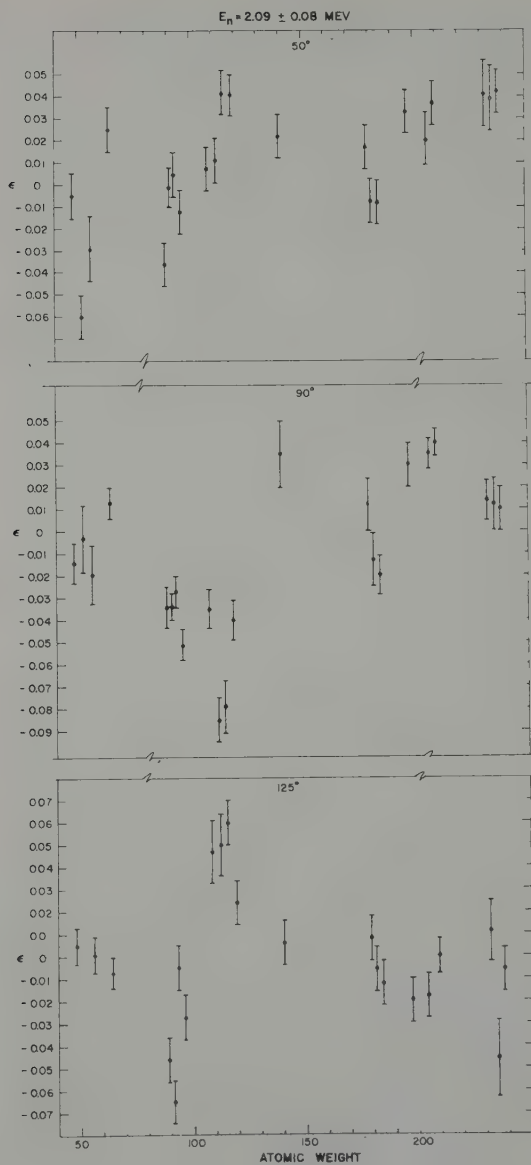


Figure 11

any statement as to whether this effect may not in fact be present also at lower energies.

In sum we see now a pattern of smooth variation among what we feel entitled to call group IV nuclei, with respect both to mass number and energy over a fairly wide range. This result encourages the belief that an optical model fitting of these data can be accomplished. JOHN WILLS at Los Alamos is undertaking to do this. I regret that there are no results to report on this endeavour as yet, but the new data reported here are only a few weeks old. Hopefully, at our higher energy the role of compound elastic scattering, whose evaluation plays a troublesome role in an optical model fitting, is substantially less than in the earlier data taken at lower energy.

It is worth pointing out that it was expected that the reduction of compound elastic scattering would give us substantially higher polarizations than have been observed at lower energies. In this hope we have been somewhat disappointed. The maximum polarization observed of about 27% is not much larger than the maximum of about 20% reported by CLEMENT *et al.* although our expectation of increased polarization has been confirmed.

One special point of interest in these data concerns four adjacent nuclei in the neighbourhood of mass 100, namely, Ag, Cd, In, and Sn. In each of these cases the sign of the polarization changes twice as one goes from 50° to 125°, indium being the most striking case because of the large (greater than 20%) effects observed at each angle. According to the maximum complexity rules of SIMON and WELTON this result implies that there must be a strong contribution of partial waves of l equals 2 or more to the scattering. On the other hand CLEMENT *et al.* have ascribed the structure in the neighbourhood of mass 100 to the effect of splitting of a giant p -wave resonance in this mass interval. The persistence of this structure over a factor of more than 4 in energy, and the clear evidence now that d -waves or higher are important at mass 100 at 2 MeV suggests that another interpretation may be required for a systematic description of the mass 100 effect.

Previous speakers have referred to considerations due to RODBERG which suggest that the polarization in elastic scattering should follow the derivative of the differential scattering cross section. There are too few of the latter data available at 2 MeV to be useful for a check of this matter.

A final point concerns the group III nuclei. In figure 11 the three lightest nuclei shown are titanium, chromium, and iron. At 50° Cr stands out with a polarization of 18%, while the result for the others is small or negligible at all angles. It is tempting to interpret this result as part of the pattern exhibited in the inelastic scattering and in the data reported earlier at this conference by FERGUSON on elastic scattering at 1.6 MeV

and below for similar nuclides. Since few levels are being excited in the residual nucleus, compound elastic scattering is probably strong; and since the level density in the compound nucleus is inadequate to satisfy the statistical assumption of HAUSER and FESHBACH, we are justified in expecting an erratic pattern of polarization effects in the compound elastic scattering.

One would hope for the future that a polarization investigation might be carried out at 4 MeV where BJORKLUND and FERNBACH have had such gratifying success in fitting total and differential scattering cross section data. Such a study will be enormously facilitated by the advent of the improvements in millimicrosecond neutron spectroscopy alluded to earlier.

In conclusion I should like to acknowledge with special thanks the stimulating effect of a visit with Professor HUBER here in Basel in 1952 which directed my interest toward polarization studies.

REFERENCE

- [1] L. CRANBERG, *Phys. Rev.* **114**, 174 (1959).

Polarisation of 9 MeV Protons Elastically Scattered by C, Mg and Al

By G. W. GREENLEES and A. B. ROBBINS,
Department of Physics, University of Birmingham

The polarisation measurements were made using a double scattering technique in which 9.6 MeV protons from the Birmingham 60" cyclotron were scattered first by the target and then by helium. Using the known polarisation properties of helium [1]¹⁾, a measurement of the asymmetry after double scattering gives the polarisation of the protons elastically scattered by the target.

The general arrangement is shown in figure 1. The overall angular definition for scattering by the first target was $\pm 3^\circ$; the target was set to give optimum resolution at each angle of scattering and adjusted so as to present a 1 MeV thickness to the incident beam. The polarisation of protons scattered from helium shows two peaks in this energy region, one of negative sign at about 70° and one of positive sign at about 120° . Photographic plates were used to record the doubly scattered protons and it was arranged that scattering at both 70° and 120° , from helium, was recorded simultaneously. Since the sign of the polarisation differs for the two peaks, they should produce opposite asymmetries. This was a valuable check on the geometrical alignment of the apparatus. A diagram of the helium chamber is shown in figure 2. The direction of the beam through the helium was recorded on a photographic plate at the

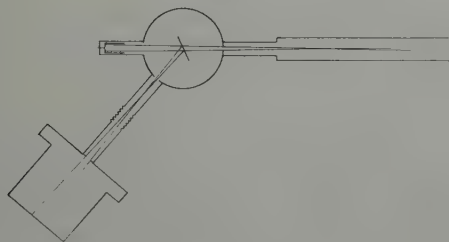


Figure 1

¹⁾ Numbers in brackets refer to References, page 331.

end of the chamber and background plates were placed adjacent to the recording plates (Ilford EI).

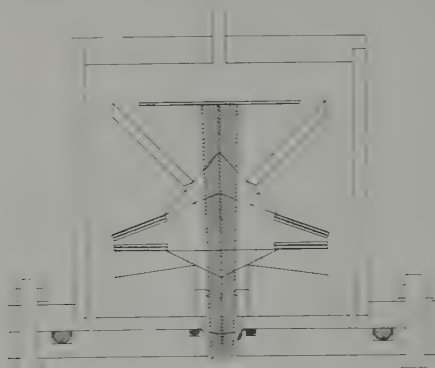


Figure 2

Large solid angles of acceptance were used for the helium scattering corresponding to a range of scattering angles. The distribution of scattering angles corresponding to those tracks used in the asymmetry measurement could be determined from the track orientation and hence, knowing the variation of polarisation with angle of scatter in helium, a mean value for the polarisation of the second scattering could be obtained. Range criteria were used to select the elastically scattered particles. Figure 3 shows the projected range distribution for doubly scattered protons, using Mg and a scattering angle of 60° for the first target. The

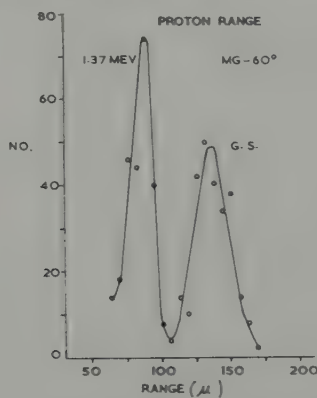


Figure 3

two groups of figure 3 correspond to elastic scattering and to inelastic scattering from the first level at 1.37 MeV excitation. These are clearly resolved and hence the measurements give polarisation for pure elastic scattering without contamination from inelastic groups.

Results

In all three cases studied, C, Mg and Al, elastic scattering angular distributions were also obtained using the same target thickness and an attempt has been made to fit the data with an optical model analysis. The optical model programme was made available by Mr. B. EASLEA of University College, and used on the University of London Mercury Computer. The potential used in the calculations is shown in figure 4 and has a Saxon-Woods form factor, a real spin orbit term of surface form with both surface and volume imaginary potentials. The imaginary potential is specified by the magnitudes at $r = 0$ and $r = R$, W_c and W_s respectively.

$$V(r) = V_{\text{coul.}} + V f(r) + i W g(r) + \sigma \cdot L V_s h(r)$$

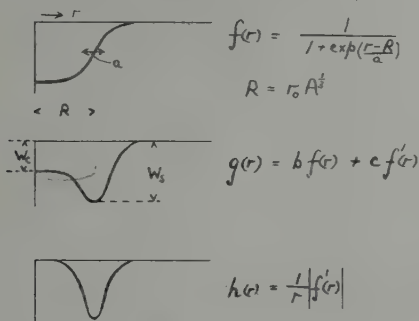


Figure 4

The sign convention used for the polarisation is that $\mathbf{K}_{\text{in}} \cdot \mathbf{K}_{\text{out}}$ is positive.

Carbon

The results for carbon are shown in figure 5. At three angles two points are shown for the polarisation. In each case one of these was taken using forward scattering from helium with a negative polarisation and the other using backward scattering with a positive polarisation. The agreement of these pairs of points indicates the absence of geometrical asymmetries.

The optical model predictions shown in figure 5 (full line) are typical of the results obtained from a number of runs. In all cases the model predicted a negative peak in the polarisation around 60° which was not present experimentally and the cross sections predicted were too low to fit the experimental data.

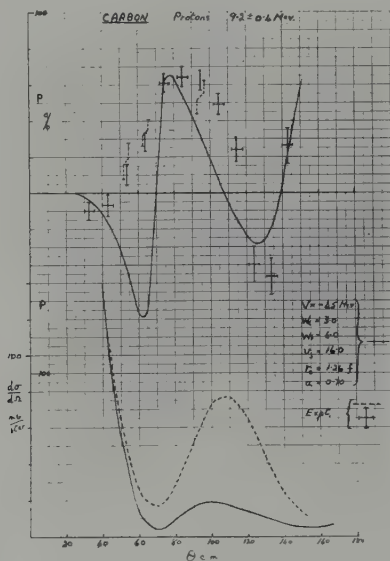


Figure 5

HIRD [2] has observed variations of the polarisation with energy around 9 MeV in the scattering from carbon at 40° . Nevertheless, the shape of HIRD's polarisation angular distribution at 8.2 MeV and ROSEN's [3] at 10 MeV is very similar to the present results. Variations with energy have also been observed in the elastic scattering cross sections for carbon at backward angles [4] which have been attributed to compound nucleus effects but the magnitude of the effects is insufficient to explain the present discrepancy between the model and experiment. One can only conclude that the model as used here is unsatisfactory for carbon in the 10 MeV region.

Magnesium

The elastic scattering cross section angular distribution from magnesium varies markedly with energy around 9 MeV [5]. This is shown in figure 6 where angular distributions are given at five energies between

7.86 and 9.55 MeV. In the present measurements a target thickness of 1 MeV was used so that an experimental average was taken in the energy range 8.6–9.6 MeV. Work by MATSUDA *et al.* [6] has shown that the pattern of the 9.55 MeV curve of figure 6 persists at higher energies and EASLEA [7] has been able to fit the 9.55 MeV data and the higher energy data with the present optical model programme. The fit at 9.55 MeV is shown in figure 7. The departure at backward angles can reasonably be explained in terms of a compound elastic contribution.

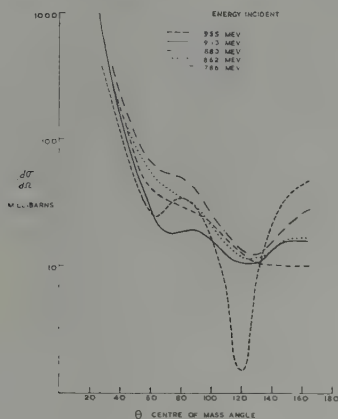


Figure 6

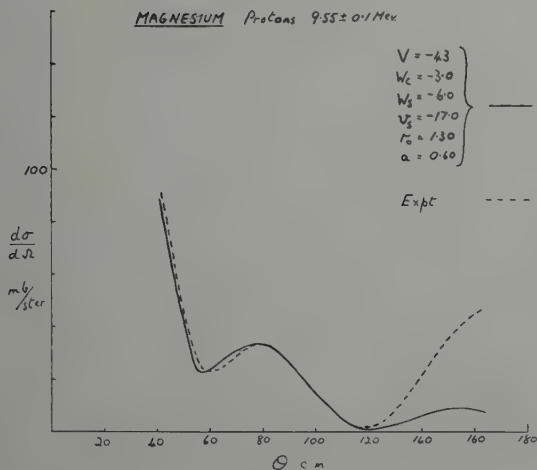


Figure 7

Since the optical model predictions vary slowly with energy, one would not expect a fit to the lower energy data of figure 6 or to the elastic scattering cross sections at 9.1 MeV with a 1 MeV thick target. This is in fact found and must be attributed to some additional process occurring which is not included in the model. The present polarisation and cross section data together with the optical model fits are shown in figure 8. Although, as anticipated, one is not getting a fit to the elastic scattering, the polarisation is reasonably well represented by the model. This polarisation data is very similar in shape to that obtained by ROSEN [3] at 10 MeV; thus in going from 10 MeV to 9.1 MeV the measured polarisation changes little, whereas the cross section angular distribution shows a marked change. One can fit the cross section and the polarisation data at 10 MeV with an optical model but at 9.1 MeV one only fits the polarisation data. This is a surprising result, since, whether the additional elastic scattering process occurring in Mg at about 9 MeV, is polarised or not, one would expect the observed polarisation to change due to its presence.

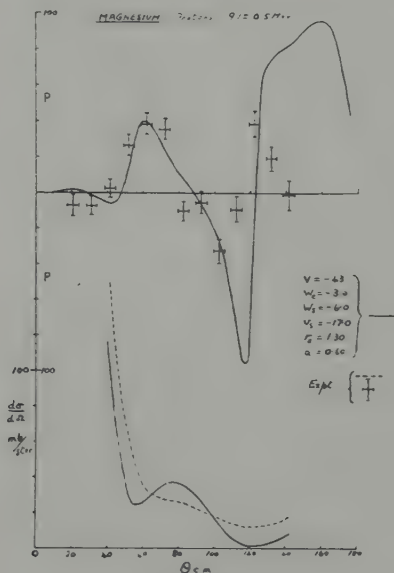


Figure 8

Aluminium

The elastic scattering cross section angular distributions from Al are known to vary smoothly and slowly with energy in the range 7.8–9.6 MeV [8]. It is reasonable therefore to expect a fit to the data with

an optical model analysis. The cross section and polarisation data obtained in the present experiments are shown in figure 9. Apart from one point (51°) which may be in error experimentally, the polarisation data is well represented by the model and a reasonable representation is made of the cross section data. The departure at backward angles might reasonably be attributed to a compound elastic contribution since such effects are known to occur in this energy region [9].

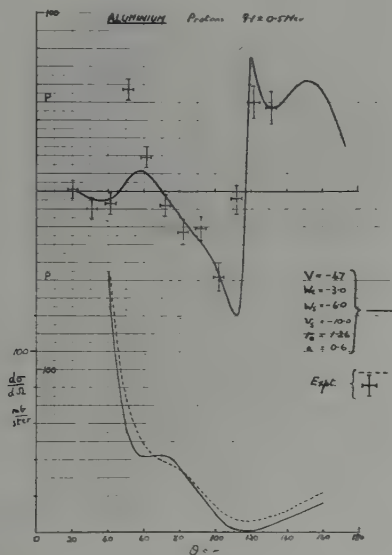


Figure 9

REFERENCES

- [1] K. W. BROCKMAN, P. R. 170, 163 (1958); W. A. BLANPIED, P. R. 173, 1099 (1959).
- [2] A. STRAZAKOWSKI, M. S. BOKHARI, A. AL-JEBOORI, and B. HIRD, Proc. Phys. Soc. 75, 502 (1960).
- [3] L. ROSEN and J. E. BROLLEY, Proceedings of the Second U. N. International Conference on the Peaceful uses of Atomic Energy, Geneva (1958).
- [4] W. M. GIBSON, D. J. PROWSE, and J. ROTBLAT, P. R. S. A243, 237 (1957).
- [5] G. W. GREENLEES, B. C. HAYWOOD, L. G. KUO, and M. PETRAVIC, Proc. Phys. Soc. A70, 331 (1957).
- [6] N. YAMAMURO, S. KOBAYASHI, K. MATSUDA, Y. ODA, and Y. NAGAHARA, Institute for Nuclear Study, Japan, Report INSJ - 29. (1960).
- [7] B. EASLEA, private communication.
- [8] G. W. GREENLEES, L. G. KUO, and M. PETRAVIC, P.R.S., A243, 206 (1957).
- [9] G. W. GREENLEES and P. M. ROLPH, Proc. Phys. Soc. 75, 201 (1960).

A Survey of $p\text{-}\alpha$ Elastic Scattering as a Polarization Analyzer

By M. J. SCOTT, A.E.R.E., Harwell

There at present exist at least three different polar graphs of the polarization to be expected in $p\text{-}\alpha$ elastic scattering as a function of energy and angle [1], [2], [3]¹⁾. Unfortunately, it is not possible for an

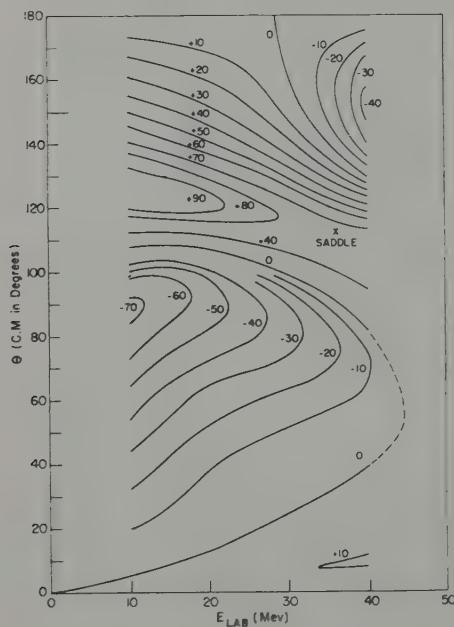


Figure 1

Contour graph of polarization (in %) calculated from a potential [1]

¹⁾ Numbers in brackets refer to References, page 334.

experimental physicist to use these graphs without an error of roughly $\pm 15\%$. For instance, at $\Theta_{\text{lab.}} = 90^\circ$, $E_p = 10$ MeV, the values read from the graphs are 30% [1], 50% [2] and 60%. This is admittedly the worst disagreement found at 10 MeV. In the energy region up to 18 MeV the polar graph of Brockman is probably the best. One of the polar graphs gives the polarization up to 40 MeV (fig. 1). In this paper a polarization measurement at 15.5 MeV is used to choose a set of phase shifts from five possible sets. The measurement is shown on a plot of polarization as a function of angle at 17.5 MeV (fig. 2). The measurement definitely eliminates sets 1, 2 and 3, but lies quite close to sets 4 and 5. Sets 4 and 5 are quite similar, however it is seen that at one angle, at 17.5 MeV, the polarization resulting from set 5 is twice that resulting from set 4. This polar graph is calculated from a potential and using it to extrapolate to 15.5 MeV, it is seen that the agreement of the experimental point with the predicted polarization is indeed excellent. However, the curve of polarization vs. angle for 17.5 MeV read from the polar graph [1]

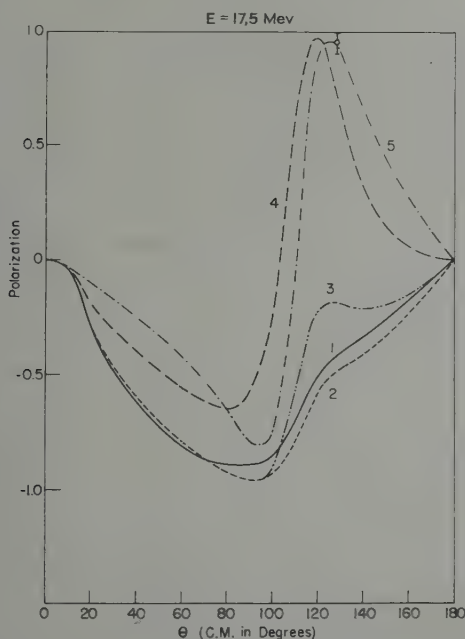


Figure 2

Polarization at 17.5 MeV calculated from five sets of phase shifts. The experimental point is at 15.5 MeV and is due to BROCKMAN

does not agree as well with the experimental data as does a similar curve read from the polar graph of Brockman [2]. It is probable that the polar graph of Gammel and Thaler can be used to choose a region of high polarization in which to make a measurement in order to use p - α elastic scattering as a polarization analyzer.

REFERENCES

- [1] J. L. GAMMEL and R. M. THALER, Phys. Rev. *109*, 2041 (1958).
- [2] K. W. BROCKMAN, JR., Phys. Rev. *110*, 163 (1958).
- [3] G. C. PHILLIPS and P. D. MILLER, Phys. Rev. *115*, 1268 (1959).

D-Phase Dependence of Nucleon-Helium Polarization

By R. E. WHITE, A. E. R. E., HARWELL

Above 10 MeV nucleon energy *D* phases begin to contribute significantly to both the cross-section and the polarization in nucleon-helium scattering [1, 2, 3]¹⁾. At present these *D* phases, while small, are only poorly determined, a collection of assignments made by various workers is shown in figure 1 [2, 4, 5].

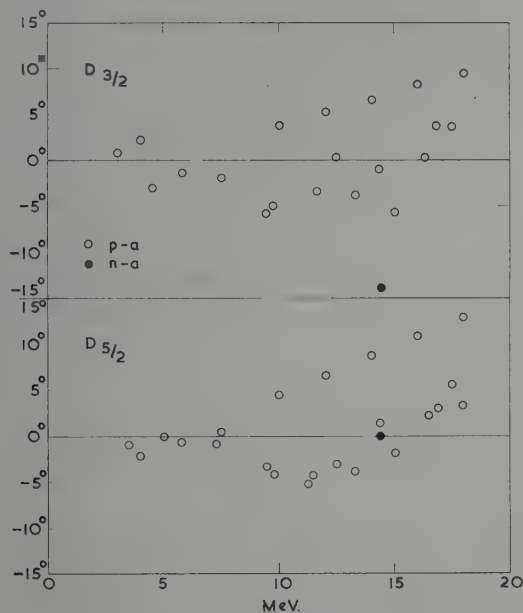


Figure 1

The effect of this uncertainty on the polarization is illustrated for 14 MeV nucleon energy in figure 2 which shows polarization angular

¹⁾ Numbers in brackets refer to References, page 336.

distributions for four extreme sets of D phases consistent with the assignments in figure 1. S and P phases were taken to be $\delta_0 = -92^\circ$, $\delta_1 = 92^\circ$, $\delta_1 = 45^\circ$ in each case. The true polarization angular distribution should lie among these curves, and it is seen that the uncertainty is sufficiently large that above about 10 MeV available polarization graphs [1, 2, 3] should be used with caution.

One point measured at 14.4 MeV [6] is also shown in figure 2, but many more such measurements are needed to remove this ambiguity.

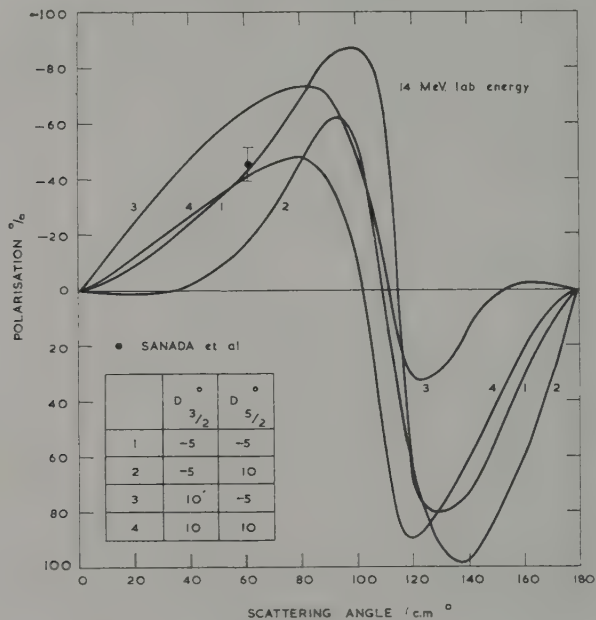


Figure 2

REFERENCES

- [1] G. C. PHILLIPS and P. D. MILLER, *Phys. Rev.* **115**, 1268 (1959).
- [2] J. L. GAMMEL and R. M. THALER, *Phys. Rev.* **109**, 2041 (1958).
- [3] K. W. BROCKMAN, *Phys. Rev.* **110**, 163 (1958).
- [4] P. D. MILLER and G. C. PHILLIPS, *Phys. Rev.* **112**, 2043 (1958).
- [5] P. E. HODGSON, *Phil. Mag.*, Supp. **7**, 1 (1958).
- [6] J. SANADA, K. NISIMURA, S. SUWA, I. HAYASHI, K. FUKUNAGA, N. RYU, and M. SEKI, *Inst. for Nuclear Study Rep. No. 9*, Univ. Tokyo, Tanashi-Machi, Tokyo (also these proceedings).

Observation on the Reaction $\text{Li}^7(p, \alpha)\text{He}^4$ Using Polarized Protons

By K. BEARPARK, I. HALL, R. E. SEGEL, S. M. SHAFROTH and N. W. TANNER
Clarendon Laboratory, Oxford

WOLFENSTEIN [1]¹) in 1949 predicted that the reaction $\text{Li}^7(p, \alpha)\text{He}^4$ would be sensitive to proton polarization which produces an additional term in the angular distribution of the form $\sin 2\Theta \cos \Phi$. The magnitude of the coefficient associated with this term could not be predicted because of the unknown channel spin phase which could not be deduced from the unpolarized angular distribution. However it was clear that a large azimuthal asymmetry would occur at least at some energies.

A polarized proton beam was obtained by scattering 2 to 4 MeV protons from carbon at 60° (lab) at which angle the polarization had been measured [2] as -25 to -35% depending on scattering energy. The scattered beam was allowed to pass through an absorber foil and impinge on a lithium target as shown in figure 1. Alpha particles from the reaction were detected by four CsI scintillation counters at 45° (c.m. angle approximately) to the scattered beam. Using a primary beam of $2\mu\text{A}$, a carbon target 8 mg/cm^2 thick and a lithium target 0.5 mg/cm^2 thick, about 1000 α -counts per hour per counter were recorded for a lithium bombarding energy of 2 MeV. The lithium bombarding energy was varied by appropriate choice of primary bombarding energy, scattering target thickness and carbon absorber thickness. The inherent asymmetry of the chamber was determined by replacing the carbon scatterer with a platinum foil of equivalent thickness.

Figure 2 shows the fractional change r (defined in the same way as WOLFENSTEIN's [1] r) in the intensity of the α -particles at $\Theta = 45^\circ$, $\Phi = 0^\circ$ due to proton polarization (100%).

The immediate consequence of the sign of the asymmetry is that the interpretation of $\text{Li}^7(p, \alpha)\text{He}^4$ in terms of compound states of $J = 0$ and $J = 2$ by INGLIS and by CRITCHFIELD and TELLER [3] is not acceptable. On the other hand two states of $J = 2$ (suggested by CHRISTY and

¹) Numbers in brackets refer to References, page 338.

RUBIN [4] can give the right sign and magnitude. Three curves for the latter case calculated by WOLFENSTEIN [1] for channel spin phase γ are shown in figure 2. Apparently $\gamma \simeq 200^\circ$.

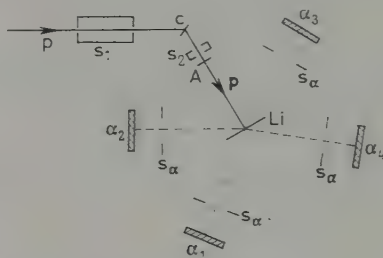


Figure 1

Geometry used for $\text{Li}^7(p, \alpha)\text{He}^4$ measurement: p , primary beam; \bar{p} , polarized beam; S_1, S_2, S_α , collimating slits for primary and polarized beams and α -particles; C , carbon target; Li , lithium target; A , carbon absorber foil; $\alpha_1, \dots, \alpha_4$, CsI counters

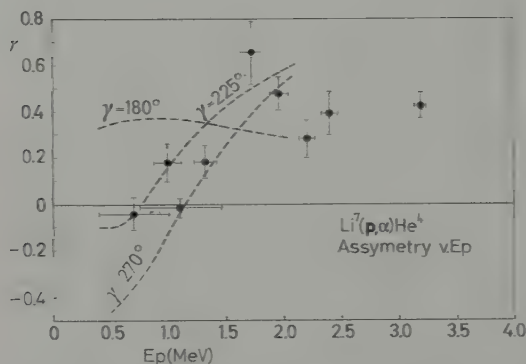


Figure 2

Asymmetry γ as a function of E_p showing measured points and curves calculated by WOLFENSTEIN [1]

REFERENCES

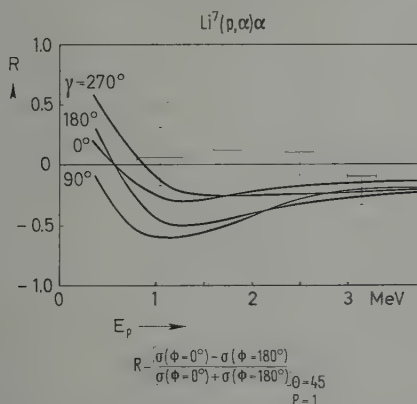
- [1] L. WOLFENSTEIN, Phys. Rev. 75, 1664 (1949).
- [2] J. E. EVANS and M. A. GRACE, Nucl. Phys. 15, 646 (1960).
- [3] D. R. INGLIS, Phys. Rev. 71, 21 (1948). - C. CRITCHFIELD and E. TELLER, Phys. Rev. 60, 10 (1941).
- [4] R. F. CHRISTY and S. RUBIN, Phys. Rev. 71, 275A (1947).

The Reaction $\text{Li}^7(p, \alpha)\alpha$ with Polarized Protons

By C. WEDDIGEN and H. SCHOPPER, University of Mainz

If this reaction is induced by polarized protons one expects a right-left asymmetry for the α -particles emitted in the break up of the Be^8 -compound state. Polarized protons were produced by the $\text{C}^{12}(d, p)$ -stripping reaction ($E_d = 1.06$ MeV). The proton polarization has been measured by JURIĆ and ČIVILOV [1]¹⁾ and is $P = 0.35 \pm 0.12$ for $\theta = 52^\circ$.

Measurements for various proton energies were performed by slowing down the protons in Al-absorbers. An enriched Li^7 -target was used. The α -particles were detected in nuclear emulsions. The experimental results for the relative asymmetry R are shown in the figure. Within the statistical errors no asymmetry was found.



WOLFENSTEIN [2] calculated R using a set of parameters which were deduced from the angular distribution assuming an interference of a very broad resonance with $J = 0$ and a narrow one with $J = 2$. The disagreement of these calculations (curves in the figure) with the measurements is

¹⁾ Numbers in brackets refer to References, page 340.

not surprising as the parameters could not be determined uniquely from the angular distribution alone. The absence of an asymmetry could be understood by assuming that the ($J = 2$)-level is formed by protons with a total angular momentum $j = 1 \pm s = 3/2$ but not by protons with $j = 1/2$.

However the disagreement of our results with those of TANNER communicated in the preceding report could be due to a vanishing proton polarization. The deuteron energy in the work of JURIĆ and ĆIRILOV was not known accurately (private communication) and the proton polarization might change rapidly with this energy. The determination of the proton polarization as a function of the deuteron energy is in progress.

Note added in proof: For the proton polarization a preliminary value of 0.23 ± 0.03 was found for $E_d = 1.06$ MeV. The polarization decreases rapidly for lower and higher deuteron energies.

REFERENCES

- [1] JURIĆ and ĆIRILOV, C. r. du Congr. Int. de Phys. Nucl., Paris 1958.
- [2] WOLFENSTEIN, Phys. Rev. 75, 1664 (1949).

IV.

Theories Concerning Polarization Effects of Nucleons

Nuclear Forces and Polarization Phenomena¹⁾

By G. BREIT, Yale University

Nucleon-nucleon scattering is an important source of information concerning nuclear forces. Additional and at times important information is obtainable from the binding energies of the simpler light nuclei and from nucleon-nucleus scattering. The large value of the pion-nucleon coupling constant in the pseudoscalar meson theory with pseudoscalar coupling (*PSps*) has made it impossible to obtain a practically convergent series for the effective potential and the pseudoscalar theory with pseudovector coupling is not renormalizable. Furthermore, a complete theory must take into account the interactions of *K*-mesons with nuclei which are still poorly understood. The fundamental approaches are thus not available for comparison with experiment.

It would be helpful for data interpretation if it were possible to use a potential describing the interaction between two nucleons. So far no satisfactory potential has been found. The more hopeful approach is, therefore, that of employing phase shifts supplemented by coupling parameters between states with the same total angular momentum $J \hbar$ but different orbital angular momenta $L \hbar$. This description is completely general for energies below meson production as long as only two nucleons are involved, the phase shifts and coupling parameters, phase-parameters for short, describing the scattering phenomena completely. The phase-parameters do not suffice, however, for systems involving more than two nucleons such as the triton and they similarly are only helpful but not definitive in their predictions in such problems as the photodisintegration of the deuteron which involve the participation of a third entity, a photon in this case. Relativistically the phase-parameters can be [1]²⁾ uniquely defined in the center of mass system, by describing the nucleons as Dirac particles with anomalous magnetic moments and employing the 'large-large' combinations of the Dirac spinor for two particles at distances larger than those at which the specifically nuclear forces have an appreciable value.

¹⁾ This research was supported by the Office of Ordnance Research, U. S. Army and by the U. S. Atomic Energy Commission under Contract AT (30-1)-1807.

²⁾ Numbers in brackets refer to References, page 357.

At such distances the 'small' Dirac components are obtainable in terms of the 'large' ones, the particles being uncoupled to each other and the phase-parameters of the large components uniquely define the whole wave function. In the case of p - p scattering there is a slight complication in the Coulomb interaction. For large distances, however, this can be treated [1] relativistically and without ambiguity by first order theory. Coulomb effects are minor at high energies and at low energies where they are important, the relativistic effects are small. The phase-parameters employed in the present discussion are defined in this sense.

In the analysis of low energy (a few MeV) p - p and p - n data, reasonable assumptions regarding the absence of serious effects of $L > 0$ make it possible to obtain reliable values of the 1S_0 phase shift K_0 and the parameters for the $^3S_1 + ^3D_1$ system from measurements of the scattering cross section σ . At higher energies the number of phase-parameters to be considered is so large that their determination from σ alone becomes impossible. The polarization of the scattered particles is of help in restricting the possibilities to a smaller number and in indicating qualitatively the presence or absence of phase shifts. The information derivable from measurements of polarization in the scattering from unpolarized targets is essentially of two types: polarization properties of one or another of the two particles participating in the collision (type A), or else the combined orientation of the spins of the two particles (type B). For a spin $1/2$ particle all information concerning the statistical mixture of spin functions can be summarized in a single vector

$$\mathbf{P} = \overline{\langle \boldsymbol{\sigma} \rangle}.$$

Here $\boldsymbol{\sigma}$ is the vector Pauli spin operator, $\langle \rangle$ denotes the expectation value and $\overline{}$ the statistical average over the statistical mixture of states. Disregarding particle identity all information derivable from experiments with unpolarized targets in category (A) is obviously contained in \mathbf{P} . In category (B) additional information regarding the correlation of the spin directions of particles and recoils is available. This classification is useless for polarized targets.

In a *double scattering* experiment the partly polarized nucleons produced in one scattering are scattered by a second unpolarized target. If the energy change due to recoil is small, the differential scattering cross section is

$$\sigma_D^{(2)} = [\sigma_D^{(2)}]_0 [1 + (\mathbf{P}_1 \cdot \mathbf{P}_2)].$$

Here $[\sigma_D^{(2)}]_0$ is the value of $\sigma_D^{(2)}$ for an unpolarized beam, \mathbf{P}_1 , \mathbf{P}_2 are respectively the polarization vectors produced by scattering unpolarized

beams on the first and second targets. This relation has been proved in the work by WOLFENSTEIN [2], DALITZ [3] and of WOLFENSTEIN and ASHKIN [2]. The proof makes use of invariance of interaction energy to time reversal. The directions of \mathbf{P}_1 and \mathbf{P}_2 are perpendicular to the scattering planes so that

$$\mathbf{P}_1 = P_1 \mathbf{n}_1, \mathbf{P}_2 = P_2 \mathbf{n}_2$$

where the target characterizing quantities P_1 and P_2 are either the absolute values of \mathbf{P}_1 and \mathbf{P}_2 or their negatives. It has been pointed out by R. J. N. PHILLIPS [4] and independently by R. R. LEWIS [5] that on this basis, time reversal invariance could be tested more systematically in nucleon-nucleon scattering. Special tests for time reversal and other symmetries lie outside the scope of the present report. Reference may be made to the work of PHILLIPS and that of BELL and MANDL [6] for theory, ABASHIAN and HAFNER [7] for $p-p$ scattering experiments and to that of L. ROSEN and J. E. BROLLEY [8] who have tested the ' $P-A$ ' relationship in a number of cases. The usual determination of $P = \pm |\mathbf{P}|$ by means of the asymmetry of double scattering rests on the validity of the formula quoted. The knowledge of \mathbf{P}_2 , obtainable for instance by scattering from carbon gives for a known angle between \mathbf{P}_1 and \mathbf{P}_2 the value of P_1 . A double scattering experiment is incapable of giving more than P_1 and its space direction which is known to be perpendicular to the first scattering plane. *Triple scattering* experiments determine what happens to the mean spin $\mathbf{P}/2$ if a beam is scattered. The first scattering produces a polarized beam with known \mathbf{P} , the second changes this \mathbf{P} and the third determines the changed \mathbf{P} . The first and third scatterings serve as polarizer and analyzer respectively. Omitting subscripts on quantities referring to the second scattering, the relation for determining the depolarization parameter D illustrated in figure 1 is

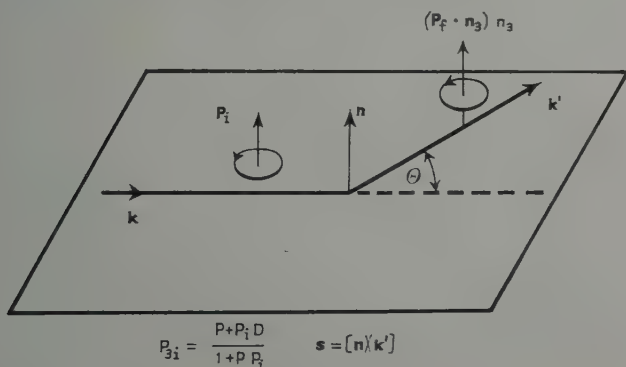


Figure 1

The three scattering planes are the same in this measurement and subscript i indicates incidence. Thus P_{3i} is the P of the beam incident on the third scatterer, P is the inherent P of the second scatterer and P_i is the polarization of the beam incident on the second scatterer.

In this and the following two figures \mathbf{k} and \mathbf{k}' are the initial and final propagation vectors for the second scattering while

$$\mathbf{s} = [\mathbf{n} \times \mathbf{k}'] .$$

The parameter R is measured by having the first and third scattering planes perpendicular to the second. It determines the rotation of \mathbf{P} caused by the second scattering, with \mathbf{P} in the scattering plane and perpendicular to \mathbf{k} . In this case as shown in figure 2

$$P_{3i} = R P_i .$$

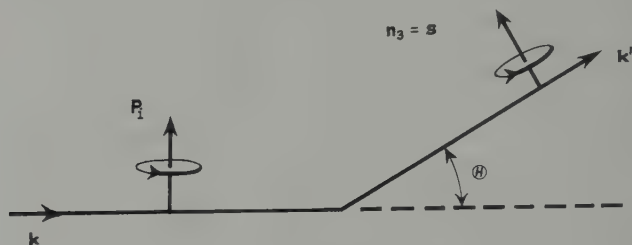


Figure 2

The parameter A is measured by turning the polarization which is produced by the first scattering by means of a magnetic field to be directed along \mathbf{k} . The asymmetry of the third scattering again measures the polarization along \mathbf{s} , the third scattering plane being perpendicular to the second.

The measurement of the triple scattering parameter A is illustrated in figure 3.

$$P_{3i} = A P_i .$$

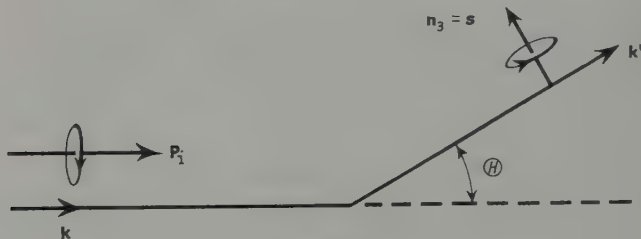


Figure 3

Category (B) type information is derived from spin-correlation experiments and is much less abundant. Double scattering is used in order to determine the spin correlation of the scattered and recoil particles. The theory of such experiments has been first treated by STAPP [9]. The two coefficients most commonly measured are C_{nn} and C_{KP} . Both are concerned with unpolarized targets. The notation is

$$C_{nn} = \langle (\boldsymbol{\sigma}_1 \cdot \mathbf{n}) (\boldsymbol{\sigma}_2 \cdot \mathbf{n}) \rangle, \quad K = \frac{\mathbf{k}' - \mathbf{k}}{|\mathbf{k}' - \mathbf{k}|},$$

$$C_{KP} = \langle (\boldsymbol{\sigma}_1 \cdot \mathbf{K}) (\boldsymbol{\sigma}_2 \cdot \mathbf{P}) \rangle, \quad \mathbf{P} = \frac{\mathbf{k}' + \mathbf{k}}{|\mathbf{k}' + \mathbf{k}|},$$

with \mathbf{k} and \mathbf{k}' standing for the initial and final momenta of the scattered particle in the center of mass system.

The possibilities of deriving information from measurements at a given angle have been considered by SMORODINSKY, OEHME, STAPP, BROWN and KANELLOPOULOS, by PUSIKOV, RYNDIN and SMORODINSKY, by GOLOVIN *et al.* and most completely by R. J. N. PHILLIPS [9] who will report on these matters in more detail later in this session. The report by GAMMEL and BROLLEY is also closely concerned with this phase of the subject. There are 5 complex coefficients entering the expression for the scattering matrix T . Of the 10 real constants that determine the spin properties of the nucleons, one determines the common phase of all terms. The most complete investigation of spin conditions in scattering consists in the determination of the nine remaining parameters. Usual measurements furnish only σ , P , D , R , A and in some cases C_{nn} and C_{KP} giving most frequently 2 in some cases 5 and rarely 6 or 7 pieces of information. In the references quoted experiments with polarized targets are considered. PHILLIPS gives twenty five linearly independent expressions which enter the different measurements. With only nine measurements he finds that the transition matrix T (WOLFENSTEIN's M) is not fully determined. In practice it has not proved possible so far to analyze data by such general procedures.

According to PUSIKOV, RYNDIN and SMORODINSKY if scattering is elastic the unitary character of the scattering matrix makes the measurement of five quantities *at all angles* sufficient for the determination of T . This interesting fact may eventually prove useful. In practice the method involves the solution of an integral equation which has apparently not been applied to data analysis. The errors introduced by lack of knowledge of measured quantities at $\theta \cong 0^\circ$ and $\theta \cong 180^\circ$ are also apparently unknown. In a phase-parameter analysis nearly the equivalent of such information is supplied by reasonable hypotheses concerning phase-parameters with high L and unitarity is automatically satisfied.

Although the systematic determination of T by means of polarization measurements has not proved possible, they are, nevertheless, very useful in restricting the fits obtained through the introduction of phase parameters. Measurements of P at 290 MeV, for example, have shown [10] that phase shifts for $L > 2$ are necessary and [11] that 3F waves in addition to those arising from ${}^3P_2 - {}^3F_2$ coupling are needed at this energy.

Data analysis is carried out either with or without assumed potentials. The employment of potentials [12] has proved only moderately successful. In place of potentials the following methods have also been used: a) boundary value treatment [13], b) dispersion relations [14], c) phenomenological fits [15]. Information derived regarding phase-parameters has been compared [16] with nucleon-nucleus scattering data making use of various forms of the impulse approximation. While satisfactory agreement is obtained, such comparisons have not proved very informative regarding preferences for one or another nucleon-nucleon phenomenologic fit.

The p - p phenomenologic fits indicate at 310 MeV differences in phase shifts for ${}^3P_{0,1,2}$ suggesting $\mathbf{L} \cdot \mathbf{S}$ interaction. If these differences are analyzed in terms of those expected as first order effects of the spin-orbit and tensor potentials, the necessity of including the former becomes apparent. It would be unjustifiable to conclude that there is present in the Hamiltonian a term of the $V_{LS}(\mathbf{r}) (\mathbf{L} \cdot \mathbf{S})$ type because in higher orders the tensor interaction (a multiple of the usual S_{12}) can produce similar effects. The likelihood of the presence of spin-orbit interactions is, nevertheless, increased by this fact.

This situation has a direct connection with polarization. It may in fact be shown [17] that quite generally the first order effect of the tensor interaction gives no polarization as a consequence of the identity

$$\text{Tr} \{ (\sigma_{1z} + \sigma_{2z}) S_{12} \} = 0.$$

If one were sure that higher order effects of S_{12} are sufficiently small, the occurrence of $P \neq 0$ would, therefore, prove the existence of interaction terms in $\mathbf{L} \cdot \mathbf{S}$ within the limitations of the potential concept.

Some comparisons between calculated and observed quantities will be shown. The notation for phase-parameters will first be explained. For singlet states, non-relativistically the phase shift K_L is specified in terms of the asymptotic form of the radial function \mathfrak{F}_L/r by

$$\mathfrak{F}_L \sim \sin \left[k r - \frac{L\pi}{2} - \eta \ln 2kr + \arg \Gamma(L+1+i\eta) + K_L \right]$$

where $k = Mv/2\hbar = 2\pi$ times wave number, $\eta = e^2/\hbar v$, v = relative

velocity, r = relative distance of nucleons. In the case of two states with the same J but different L , different notations are employed in the literature. The results will be presented in terms of the scattering matrix U introduced so that the asymptotic forms at large r for r times the radial function are

$$\begin{cases} [-e^{-i\varphi_L} + U_{L,L} e^{i\varphi_L}] \mathfrak{Y}_\mu^{L,J} + U_{L,L+2} e^{-i\varphi_{L+2}} \mathfrak{Y}_\mu^{L+2,J}, \\ U_{L+2,L} e^{i\varphi_L} \mathfrak{Y}_\mu^{L,J} + [-e^{-i\varphi_{L+2}} + U_{L+2,L+2} e^{i\varphi_{L+2}}] \mathfrak{Y}_\mu^{L+2,J} \end{cases}$$

where

$$\varphi_L = kr - \eta \ln 2kr - \frac{L\pi}{2} + \arg \Gamma(L+1+i\eta), \quad J = L+1.$$

Here the $\mathfrak{Y}_\mu^{L,J}$ are spin angular functions defined in a standard manner. These forms give for an ingoing wave of amplitude -1 in channel with orbital angular momentum L an outgoing wave of amplitude $U_{L,L}$ in the same channel and an outgoing wave of amplitude $U_{L,L+2}$ in the channel with orbital momentum $L+2$. Similarly the second line of the defining form gives the amplitudes in the case of incidence in channel $L+2$. The matrix U is frequently parametrized following BLATT and BIEDENHARN [18] in the form

$$U = \begin{pmatrix} c_\varepsilon^2 e^{2i\delta_\alpha} + s_\varepsilon^2 e^{2i\delta_\beta}, & c_\varepsilon s_\varepsilon (e^{2i\delta_\alpha} - e^{2i\delta_\beta}) \\ c_\varepsilon s_\varepsilon (e^{2i\delta_\alpha} - e^{2i\delta_\beta}), & s_\varepsilon^2 e^{2i\delta_\alpha} + c_\varepsilon^2 e^{2i\delta_\beta} \end{pmatrix},$$

$$c_\varepsilon \equiv \cos \varepsilon, \quad s_\varepsilon \equiv \sin \varepsilon.$$

The quantities $\delta_\alpha, \delta_\beta$ have the significance of eigenphase-shifts while ε determines the coupling between the two eigenstates. For eigenstates α, β the common phase shift in both channels is α or β respectively. In the fits to nucleon-nucleon scattering made by the Yale group the parametrization has been

$$U = \begin{pmatrix} \sqrt{1-\varrho^2} e^{2i\theta_1}, & i\varrho e^{i(\theta_1+\theta_2)} \\ i\varrho e^{i(\theta_1+\theta_2)}, & \sqrt{1-\varrho^2} e^{2i\theta_2} \end{pmatrix}.$$

The second row and column refer to the higher of the two L . The two notations are connected by

$$\theta_1 + \theta_2 = \delta_\alpha + \delta_\beta, \quad \tan(\theta_1 - \theta_2) = \cos 2\varepsilon \tan(\delta_\alpha - \delta_\beta),$$

$$\varrho = \sin(2\varepsilon) \sin(\delta_\alpha - \delta_\beta);$$

this notation was introduced on account of the convenience of possible generalizations. It turned out to be very close to the 'nuclear bar' notation of the Berkeley group and is related to it by

$$\varrho = \sin 2\varepsilon_J, \quad \theta_1 = \delta_{J-1}, \quad \theta_2 = \overline{\delta_{J+1}}.$$

The letter K is reserved for phase shifts of the singlet states and δ_J^L for phase shifts of triplet states with orbital and total angular momenta L and J in the uncoupled cases.

WOLFENSTEIN and ASHKIN [2] making use of invariance considerations have obtained the most general forms of the spin transition matrix T . The requirements were those of invariance of the Hamiltonian to time reversal, space reflections and space rotations. Their form is shown below and so are the relations between elements of S , the submatrix of T referring to triplet states [19]. The first equation follows from time reversal and the last four from space reflections [20].

The most general form is

$$T = A + B (\sigma_1 \cdot \sigma_2) + C ((\sigma_1 + \sigma_2) \cdot \mathbf{n}) + D ((\sigma_1 - \sigma_2) \cdot \mathbf{n}) + \\ + E (\sigma_1 \cdot \mathbf{K}) (\sigma_2 \cdot \mathbf{K}) + F (\sigma_1 \cdot [\mathbf{n} \times \mathbf{K}]) (\sigma_2 \cdot [\mathbf{n} \times \mathbf{K}])$$

where

$$\mathbf{K} = \mathbf{k}_f - \mathbf{k}_i$$

and A, B, C, D, E, F are constants. In the same manner they establish relations between elements of S , the 3×3 submatrix of T referring to triplet states as follows

$$S_{1,1} - S_{0,0} - e^{2i\varphi} S_{1,-1} = 2^{1/2} (e^{-i\varphi} S_{0,1} + e^{i\varphi} S_{1,0}) \cot \theta$$

which follows from time reversal and

$$S_{1,1} = S_{-1,-1}, \quad e^{-i\varphi} S_{-1,0} = -e^{i\varphi} S_{1,0}, \quad e^{-i\varphi} S_{0,1} = \\ = -e^{i\varphi} S_{0,-1}, \quad e^{2i\varphi} S_{1,-1} = e^{2i\varphi} S_{-1,1}$$

which involve the use of space reflections.

The explicit forms of the matrix elements are shown hereafter and so is the way in which the symmetry relations are satisfied by these relations as well. Only 4 of the 5 quantities $\alpha_1, \alpha_2, \alpha_3, \alpha_4, \alpha_5$ are linearly independent. Modifications needed when coupling between states with the same

J and different L is considered are not shown, being readily available in the literature.

$$\begin{aligned}
 k(S_{1,1} - S^c) &= k(S_{-1,-1} - S^c) = \alpha_2 e^{i\Phi} = e^{i\Phi} \sum_L \frac{1}{2} e_{L0} [(L+2) Q_{L,L+1} + \\
 &\quad + (2L+1) Q_{L,L} + (L-1) Q_{L,L-1}] P_L(\cos \theta), \\
 -k S_{0,1} e^{-i\varphi} &= k S_{0,-1} e^{i\varphi} = -2^{-1/2} \alpha_1 \sin \theta e^{i\Phi} = \\
 &= 2^{-1/2} e^{i\Phi} \sum_L e_{L0} [L(L+2) Q_{L,L+1} - \\
 &\quad - (2L+1) Q_{L,L} - (L^2-1) Q_{L,L-1}] \frac{\sin \theta P_L'}{[L(L+1)]}, \\
 k S_{-1,1} e^{-2i\varphi} &= k S_{1,-1} e^{2i\varphi} = \alpha_3 \sin^2 \theta e^{i\Phi} = \\
 &= \frac{1}{2} e^{i\Phi} \sum_L e_{L0} [L Q_{L,L+1} - (2L+1) Q_{L,L} + (L+1) Q_{L,L-1}] \times \\
 &\quad \times \frac{\sin^2 \theta P_L''}{[L(L+1)]}, \\
 k S_{1,0} e^{i\varphi} &= -k S_{-1,0} e^{i\varphi} = 2^{-1/2} \alpha_4 \sin \theta e^{i\Phi} = 2^{-1/2} e^{i\Phi} \times \\
 &\quad \times \sum_L e_{L0} (Q_{L,L+1} - Q_{L,L-1}) \sin \theta P_L', \\
 k(S_{0,0} - S^c) &= \alpha_5 e^{i\Phi} = e^{i\Phi} \sum_L e_{L0} [(L+1) Q_{L,L+1} + L Q_{L,L-1}] P_L, \\
 e_{L0} &= \exp[2i\sigma_{L,0}(\eta)], \quad \sigma_{L,0}(\eta) = \sigma_L(\eta) - \sigma_0(\eta) = \sum_{s=1}^L \arctan \frac{\eta}{s} \\
 \Phi &= \varrho - \eta \log 2\varrho + 2\sigma_0(\eta), \quad Q_{L,J} = Q(\delta_{L,J}) \\
 Q(\delta) &= \frac{e^{2i\delta} - 1}{2i} = e^{i\delta} \sin \delta, \quad s = \sin\left(\frac{\theta}{2}\right).
 \end{aligned}$$

The Wolfenstein-Ashkin relations are obviously satisfied by these explicit expressions and the time reversal condition corresponds to the identity

$$\alpha_2 - \alpha_5 - \alpha_3 \sin^2 \theta = (\alpha_1 + \alpha_4) \cos \theta$$

$$S^c = -\frac{\eta}{2\hbar s^2} e^{i(\Phi - \eta \log s^2)}.$$

For an unpolarized incident beam the polarization component P_1^y and the differential cross section σ_Ω are given by

$$P_1^y = \overline{\langle \sigma_1^y \rangle} = \frac{1}{2^{3/2} \sigma_\Omega} \operatorname{Im} \sum_m (S_{1,m} \overline{S_{-1,m}})^* S_{0,m}$$

$$k^2 P_1^y \sigma_\Omega = \frac{1}{2} \sin \theta \cos \varphi \operatorname{Im} \{ \alpha_1 (\alpha_2 + \alpha_c)^* - \alpha_1 \alpha_3^* \sin^2 \theta + (\alpha_5 + \alpha_c) \alpha_4^* \}$$

$$\alpha_c = -\frac{\eta}{2 s^2} e^{-i\eta \log s^2}$$

$$+ \sigma_\Omega = |T_{00}^s|^2 + \sum_{\mu, \nu} T_{\mu\nu}^2.$$

The statistical average of the expectation value of the component of the spin of one of the particles is readily obtainable as seen in the following. The calculation of other scattering parameters is also straightforward. The fits have been made [21] by employing a gradient search in the space of the phase-parameters to data at all available energies from 9 to 340 MeV and employing one pion exchange potential OPEP values for the higher L , a procedure initiated at selected energies by MORAVCSIK, CZIFFRA, MAC GREGOR and STAPP [15]. The number of phase-parameters searched for in the p - p case was 11 if OPEP was used for $L \geq 5$, but in some searches OPEP parameters were used also for δ_3^F , θ_4^F , ρ_4 and K_4 . For $\tau = 0$ in the n - p case the choice of OPEP parameters was similarly made.

In figure 4 there are shown preliminary versions of phase shifts K_0 , K_2 obtained by fitting p - p data, in figure 5 K_4 and ρ_4 are similarly shown. The notation YRBI refers to searches using as a starting point the Signell-Marshak potential up to 150 MeV and the Stapp, Ypsilantis, Metropolis number 1 fit at 310 MeV, YLA to searches with the Gammel-Thaler potential as a start and YAVG to an average of the searched values. The dashed curves show preliminary error limits and the values shown in the graphs have been improved regarding accuracy of representing data. The width of error bands has also been considerably reduced.

In figure 6 is shown a comparison for p - p of $P(\theta)$ and of triple scattering parameters $A(\theta)$ and $D(\theta)$ with experiment at various energies. At 147 MeV only the Harvard data are shown. The general tendency of the fits has been to give values intermediate between Harvard and Harwell but the improved YLA type fit favors Harvard. The notation 'not searched' in the figures means that the particular datum has not been included in the search. In figure 7 is shown a comparison with experiment of $P(\theta)$ for n - p at 310 MeV. The figure also shows a curve for the same quantity computed for one of the Gammel-Thaler unpublished potential versions for n - p . The same figure shows comparison with data for $\sigma(\theta)$, p - p , at 250 MeV employing fit YLAM and the

Gammel-Thaler published potential. In figure 8 are shown plots of $P(\theta)$, $p-p$ at 20° , 45° and 80° as a function of energy and also $R(\theta)$, $p-p$ at 140, 210, 312 MeV as a function of angle. The plots against energy in these and other cases produce the impression that there may still be present some systematic errors which differ for various groups of observers. Many more comparisons with experiment are available in the work at Yale, only a few of the representative plots having been shown.

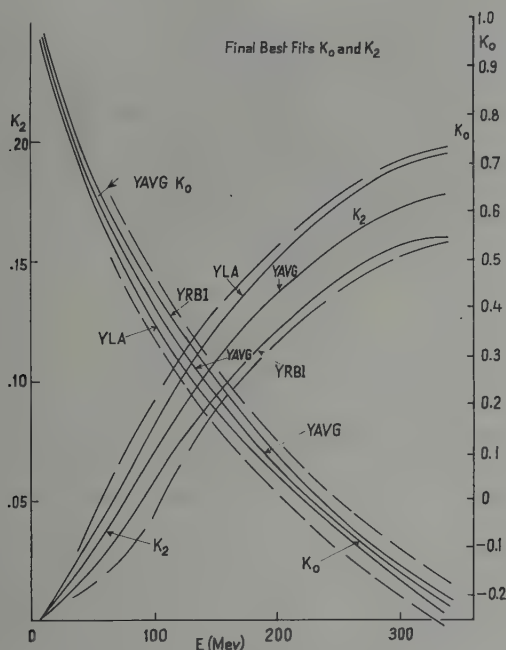


Figure 4

In a phase parameter adjustment it is helpful to know how p -waves behave when they are small. Although low energy (a few MeV) $p-p$ and $n-p$ data can be well represented by means of s -waves alone with due account of vacuum polarization, it has been shown by HULL and SHAPIRO [22] and confirmed by MAC GREGOR [23] that it is possible to represent the data by admitting p -waves in the analysis and that appreciable differences between the three 3P phase shifts are admissible resulting in appreciable polarization. The fits YRBI, YLA and the others mentioned in this report give very small polarizations. Thus at 18.2 MeV and

$\theta = 50^\circ$ the calculated values are 0.06% and 0.08% respectively for a modification of YRB1 and another version of the YRB search procedure. These may be compared with the Blanpied [24] measured value of $(0.6 \pm 0.5)\%$ at 16.0 MeV at $\theta = 12.5^\circ$ and the 3.3 MeV values of ALEXEFF and HAEBERLI [25] of $(0.08 \pm 0.16)\%$ at $\theta = 30^\circ$, $(0.25 \pm 0.16)\%$ at 45° , $(0.59 \pm 0.24)\%$ at 53° . These values have not been included in the searches for phenomenologic fits reported on. There is likely to be difficulty in reconciling the larger values in these difficult experiments with potentials, currently in vogue.

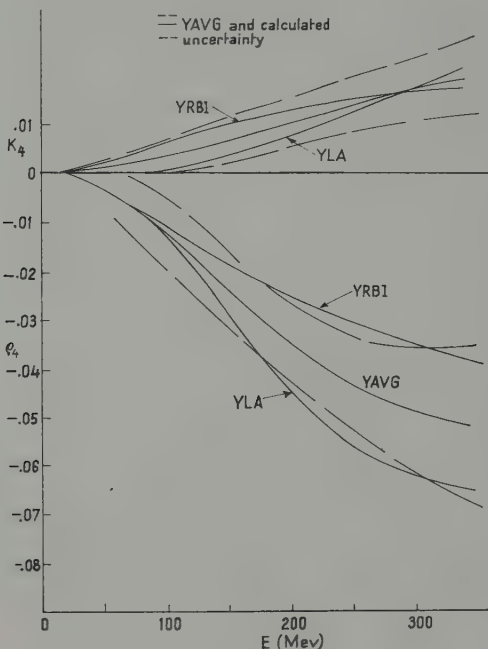


Figure 5

The polarization correlation coefficient C_{nn} according to ALLABY, ASHMORE, DIDDENS and EADES [26] at $\theta = 90^\circ$ and $E = 320$ is 0.75 ± 0.11 . The lower limit of their standard error belt *i.e.*, 0.64 is in agreement with the calculated value 0.63(6) for fit YRB1 but is appreciably higher than the expected value ~ 0.52 for fit YLAM. The latter fit is on the whole, however, the better of the two. The value of $C_{nn}(90^\circ)$ obtained by ASHMORE, DIDDENS and HUXTABLE [27] at 382 MeV is 0.42 ± 0.085 and agrees better with YLAM calculation at 320 MeV but this agreement

is at the wrong energy. Since C_{nn} measurements are available only in a few cases, the disagreements just mentioned are not definite enough to give preference to YRBI over YLAM. Additional measurements of this parameter at more energies and angles would be helpful. According to ASHMORE, DIDDENS, HUXTABLE and SKARSTAD [28], denoting triplets and singlets by t and s ,

$$C_{nn} = \frac{\sigma_t - \sigma_s}{\sigma_t + \sigma_s},$$

an exact relation neglecting the relatively small Coulomb scattering. It should accordingly be possible to resolve the usual σ into σ_s and σ_t . The calculated $C_{KP}(90^\circ)$ changes from 0.44 ± 0.05 for Set 1 of CZIFFRA, MAC GREGOR, MORAVCIK and STAPP [14] to 0.49 ± 0.09 for Set 2 at 310 MeV and appears to be not sensitive to the choice of phase-parameter. The experimentally available value [27] of 0.83 ± 0.10 at 382 MeV is not truly comparable being at an appreciably different energy. The writer is not aware of a systematic set of calculations showing the possibilities of this quantity as a means of distinguishing between phase parameter sets.

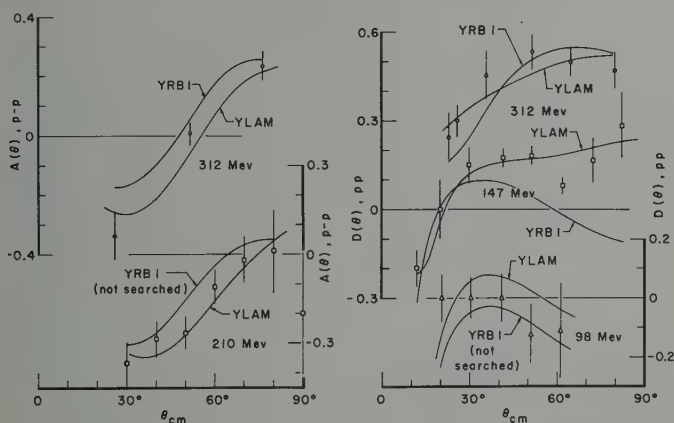


Figure 6

The successful searches with p - p fits obtained from different starting points give essentially the same answer. The availability of triple scattering parameters, the information furnished by the interference with the Coulomb wave for $\sigma(\theta)$ and polarization as well as the relatively high accuracy of the measurements all contribute to this end. In the n - p case there is much less uniqueness in end results. It would be helpful if triple scattering parameters and the polarization correlation

could be measured in this case and if an increase in accuracy of σ and P could be achieved.

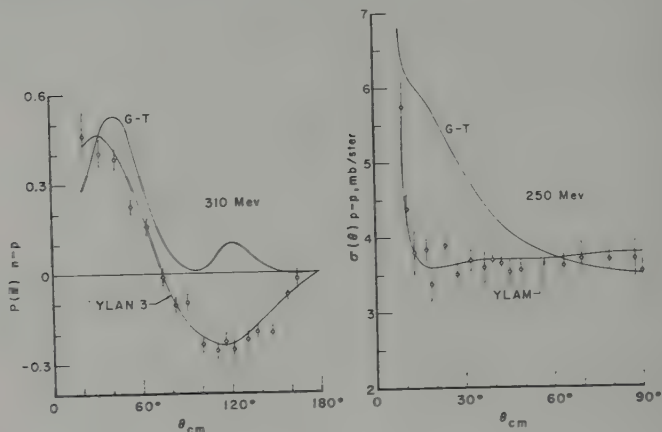


Figure 7

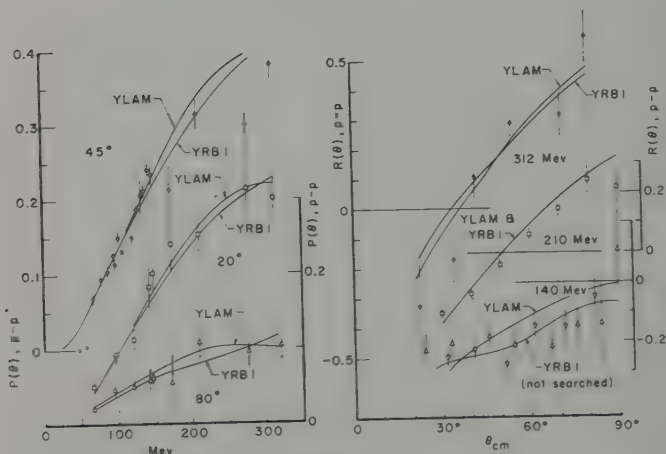


Figure 8

Measurements of nucleon polarization are also promising to be of value in the study of nuclear forces through measurements of polarization of protons and neutrons in the $d(\gamma, n)p$ reaction as first pointed out by ROSENSTVEIG [29]. At the lower energies the polarization measurement is concerned primarily with interference effects of E1 and M1 transitions

and is especially simple regarding theoretical interpretation. One may hope that studies of this type will be especially illuminating regarding properties of ${}^2S_1 + {}^3D_1$, 3P and 1S_0 states, electromagnetic properties combining here with the n - p interaction properties.

The fits of the Yale group to nucleon-nucleon scattering quoted above are the result of collaboration with Messrs. HULL, LASSILA, PYATT, RUPPEL and DEGGES.

REFERENCES

- [1] A. GARREN, Phys. Rev. *96*, 1709 (1954); G. BREIT, Phys. Rev. *99*, 1581 (1955); M. E. EBEL and M. H. HULL, Jr., Phys. Rev. *99*, 1956 (1955); A. GARREN, Phys. Rev. *101*, 419 (1956); G. BREIT, Phys. Rev. *106*, 314 (1957). The inapplicability of Moller's scattering matrix element used in the first and fourth of these references is discussed in the second and limitations caused by presence of non-Coulombian potentials in the fifth. The point referred to in the text is treated in discussion concerned with Equation (8) of the second reference.
- [2] L. WOLFENSTEIN, Phys. Rev. *75*, 1664 (1949); L. WOLFENSTEIN and J. ASHKIN, Phys. Rev. *85*, 947 (1952).
- [3] R. H. DALITZ, Proc. Phys. Soc. (London) *A 65*, 175 (1952).
- [4] R. J. N. PHILLIPS, Nuovo Cim. *8*, 265 (1958).
- [5] R. R. LEWIS (private communication).
- [6] J. S. BELL and F. MANDL, Proc. Phys. Soc. (London) *71*, 272 (1958).
- [7] A. ABASHIAN and E. M. HAFNER, Phys. Rev. Letters *1*, 255 (1958).
- [8] L. ROSEN and J. E. BROLLEY, P/668, Second International Conference on Peaceful Uses of Atomic Energy, Geneva, Switzerland (September 1958).
- [9] H. P. STAPP, UCRL 3098 (1955); PUSIKOV, RYNDIN and SMORODINSKY, Nucl. Phys. *3*, 436 (1957); JETP *32*, 592 (1957); G. E. BROWN and T. V. KANELLOPOULOS, Proc. Phys. Soc. A *70*, 690, 703 (1957); GOLOVIN, DZELEPOV, NADEZH-DIN and SATAROV, JETP, *36*, 302 (1959); R. J. N. PHILLIPS, AERE - R 3143 (1960).
- [10] B. D. FRIED, Phys. Rev. *95*, 851 (1954).
- [11] G. BREIT, J. B. EHRLMAN, A. M. SAPERSTEIN and M. H. HULL, Jr., Phys. Rev. *96*, 807 (1954).
- [12] P. S. SIGNELL and R. E. MARSHAK, Phys. Rev. *109*, 1229 (1958); SIGNELL, ZINN and MARSHAK, Phys. Rev. Letters *1*, 416 (1958); FISCHER, PYATT, HULL and BREIT, Bull. Amer. Phys. Soc. *3*, 183 (1958); HULL, PYATT, FISCHER and BREIT, Phys. Rev. Letters *2*, 264 (1959); GAMMEL, CHRISTIAN and THALER, Phys. Rev. *105*, 311 (1957); J. A. GAMMEL and R. M. THALER, Phys. Rev. *107*, 1337 (1957); R. A. BRYAN, Bull. Amer. Phys. Soc. *5*, 35 (1960), Paper IA 10.
- [13] G. BREIT and W. G. BOURICIUS, Phys. Rev. *75*, 1029 (1949); H. FESHBACH and E. LOMON, Phys. Rev. *102*, 891 (1956); A. M. SAPERSTEIN and LOYAL DURAND, Phys. Rev. *104*, 1102 (1956).
- [14] GOLDBERGER, NAMBU and OEHME, Ann. Phys. *2*, 226 (1957); H. P. NOYES, UCRL - 5921-T.
- [15] R. M. THALER and J. BENGSTON, Phys. Rev. *94*, 679 (1954); THALER, BENGSTON and BREIT, Phys. Rev. *94*, 683 (1954); STAPP, YPSILANTIS and METROPOLIS, Phys. Rev. *105*, 302 (1957); CZIFFRA, MAC GREGOR, MORAVCSIK and STAPP, Phys. Rev. *114*, 880 (1959); G. BREIT, International Conference on Nuclear Forces and the Few Nucleon Problem, University College, London

- (July 1959). This report was based on work done in collaboration with M. H. HULL, Jr., K. D. PYATT, Jr., C. R. FISCHER, K. LASSILA and T. DEGGES; M. H. HULL, Jr., G. BREIT, K. LASSILA, K. D. PYATT, Jr. and H. RUPPEL, Bull. Amer. Phys. Soc. 5, 268 (1960), Paper PA 2.
- [16] S. OHNUMA, Phys. Rev. 108, 400 (1957); H. A. BETHE, Ann. Phys. 3, 190 (1958); and references contained herein.
- [17] G. BREIT, Phys. Rev. 106, 314 (1957).
- [18] J. M. BLATT and L. C. BIEDENHARN, Phys. Rev. 86, 399 (1952).
- [19] G. BREIT and M. H. HULL, Jr., Phys. Rev. 97, 1047 (1955); G. BREIT, J. B. EHRLMAN and M. H. HULL, Jr., Phys. Rev. 97, 1051 (1955); cf. also S. C. WRIGHT, Phys. Rev. 99, 996 (1955); R. OEHME, Phys. Rev. 98, 147, 216 (1955).
- [20] G. BREIT and J. S. MCINTOSH, Encyclopedia of Physics [Handbuch der Physik (Springer-Verlag 1959), 41/1, 466, cf. Eq. (3.54) on p. 485].
- [21] Fifth and sixth references in [15] above.
- [22] M. H. HULL, Jr. and J. SHAPIRO, Phys. Rev. 109, 846 (1958).
- [23] M. H. MAC GREGOR, Phys. Rev. 113, 1559 (1959).
- [24] WILLIAM A. BLANPIED, Phys. Rev. 116, 738 (1959).
- [25] ALEXEFF, BROWN, LUX, MOSS and HAEBERLI, Bull. Amer. Phys. Soc. 4, 253 (1959); paper KA 6. I. ALEXEFF and W. HAEBERLI, Polarization in proton-proton scattering near 3.3 MeV. The writer is grateful to the authors for sending him a preprint of their paper.
- [26] ALLABY, ASHMORE, DIDDENS and EADES, Proc. Phys. Soc. (London) 74, 482 (1959).
- [27] ASHMORE, DIDDENS and HUXTABLE, Proc. Phys. Soc. (London) 73, 957 (1959).
- [28] ASHMORE, DIDDENS, HUXTABLE and SKARSTAD, Proc. Phys. Soc. (London) 72, 289 (1958); cf. H. P. STAPP, UCRL 3098 (1955).
- [29] L. N. ROSENTHAL, JETP 4, 280 (1957); W. Czyz and J. SAWICKI, Nuovo Cim. 5, 45 (1957); Phys. Rev. 110, 900 (1958); Nucl. Phys. 8, 621 (1958); H. KAWAGUCHI, Phys. Rev. 111, 1314 (1958); ZERNIK, RUSTGI and BREIT, Phys. Rev. 114, 1358 (1959).

Stripping Theory in Operator Form¹⁾

By J. L. GAMMEL, Los Alamos Scientific Laboratory

1. Introduction

When considering the possible stripping reaction experiments with beams of polarized deuterons or nucleons, and or aligned nuclei, it is not necessary, or desirable, to consider a detailed model of the stripping process such as the Butler theory [1²⁾]. Rather, it is necessary to write the scattering matrix for stripping reactions in the most general form allowed by rotational invariance and parity conservation arguments; then it is possible to calculate the results of any conceivable experiment using the general methods of WOLFENSTEIN [2]. The most general form allowed within the framework of the shell model is worked out in Section 2 for the case in which the spin of the target nucleus is zero. The form given by the Butler theory is not the most general form.

In Section 3, the expressions for quantities of experimental interest are simplified by the use of operator techniques. A number of theorems, based on a general assumption underlying the Butler theory (but not on its other details), concerning, for example, the connection between (i) the left right asymmetry in the azimuthal distribution of protons produced by polarized deuterons and (ii) the polarization of protons produced by unpolarized deuterons, are proved. These theorems are then criticized on the basis of the more general form of the scattering matrix.

2. General Form of the Scattering Matrix

A. Shell Model

We assume that in a stripping reaction, a deuteron strikes a target nucleus (assumed to have spin zero in the following work), resulting in the production of a proton and a final nucleus in a state of definite total

¹⁾ This work performed under the auspices of the U. S. Atomic Energy Commission.

²⁾ Numbers in brackets refer to References, page 371.

angular momentum J and definite parity p (the same or opposite) relative to the parity of the target nucleus. Thus we write the scattering matrix in the following form

$$M = (m_p J m_J p | m_d) \quad (1)$$

where m_p is the z component of the spin of the proton, m_J is the z component of J , and m_d is the z component of the spin of the deuteron. The operator which connects the initial and final states, is, of course, rotationally invariant and conserves parity, so that it is not explicitly shown in Eq. (1).

Within the framework of the shell model, M will have the form

$$M = \sum C \left(J m_J; L m_L; \frac{1}{2} m_n \right) (m_p m_n | O_L^{m_L}(p) | m_d) \quad (2)$$

where the $O_L^{m_L}(p)$ are operators which transform like the spherical harmonics $Y_L^{m_L}$ under spatial rotations. The C 's are Clebsch-Gordan coefficients; the Σ runs over all m_L and m_n such that $m_L + m_n = m_J$. If the final nucleus has the same parity as the target nucleus, and L is even, $O_L^{m_L}(p)$ must have even parity; if L is odd, $O_L^{m_L}(p)$ must have odd parity. If the final nucleus has opposite parity from the initial nucleus, and L is even, $O_L^{m_L}(p)$ must have odd parity; if L is odd, $O_L^{m_L}(p)$ must have even parity.

That M will have this form follows from the fact that the right hand side of Eqs. (1) and (2) transform in the same way under spatial rotations or parity transformations, and the fact that within the framework of the shell model, J is formed from the orbital angular momentum and spin of the captured neutron. The quantity L which appears in Eq. (2) may be thought of as the orbital angular momentum of the captured neutron.

The operators $O_L^{m_L}(p)$ must be constructed from σ_p , σ_n , k_p , and k_d (the spin operators for the proton and neutron, and the momenta of the proton in the final state and the deuteron in the initial state, respectively).

For $L = 0$, O_0^0 must be a scalar or pseudoscalar. The possible forms are

even parity (scalars)	odd parity (pseudoscalars)
$k_p \cdot k_d^3$	$\sigma_n \cdot k_p$
$\sigma_n \cdot (k_p \times k_d)$	$\sigma_n \cdot k_d$
$\sigma_p \cdot (k_p \times k_d)$	$\sigma_p \cdot k_p$
$(\sigma_n \cdot k_p) (\sigma_p \cdot k_p)$	$\sigma_p \cdot k_d$

³) It is understood that all scattering amplitudes may be functions of $k_p \cdot k_d$.

$$\begin{aligned}
& (\sigma_n \cdot k_p) (\sigma_p \cdot k_p) & (\sigma_n \cdot k_p) (\sigma_p \cdot k_p \times k_d) \\
& (\sigma_n \cdot k_d) (\sigma_p \cdot k_p) & (\sigma_n \cdot k_d) (\sigma_p \cdot k_p \times k_d) \\
& (\sigma_n \cdot k_d) (\sigma_p \cdot k_d) & (\sigma_p \cdot k_p) (\sigma_n \cdot k_p \times k_d) \\
& (\sigma_n \cdot k_p \times k_d) (\sigma_p \cdot k_p \times k_d) & (\sigma_p \cdot k_d) (\sigma_n \cdot k_p \times k_d) .
\end{aligned}$$

For $L = 1$, $O_L^{mL}(p)$ must be related to the components of a vector (or pseudovector) V as follows

$$\begin{aligned}
O_1^1 &= -\frac{V_x - iV_y}{\sqrt{2}}, \\
O_1^0 &= V_z, \\
O_1^{-1} &= \frac{V_x + iV_y}{\sqrt{2}}.
\end{aligned} \tag{4}$$

B. Butler Theory

We characterize the Butler theory by the assumption that the spin of the proton does not appear in the operators O . This single assumption drastically limits the possible form of the operators O .

For $L = 1$, for example, the wave function of the final nucleus may be constructed as follows

$$\sum C(Jm_J; Lm_L; \frac{1}{2} m_n) r_n^{m_L} \chi_{1/2}^{m_n} \psi(r_n) \tag{5}$$

where r_n^1 , r_n^0 , and r_n^{-1} are given by Eq. (4), the χ 's are spin functions for the neutron, and ψ does not depend on the direction of r_n . In its simplest form, the Butler theory gives a matrix element

$$\begin{aligned}
M &\sim \sum C(Jm_J; Lm_L; \frac{1}{2} m_n) \times \\
&\times \int d\mathbf{r}_n d\mathbf{r}_p r_n^{m_L} \psi(r_n) \exp(-i\mathbf{k}_p \cdot \mathbf{r}_p) V(r_n) \varphi(|\mathbf{r}_p - \mathbf{r}_n|) \exp\left(\frac{i\mathbf{k}_d}{2} \cdot (\mathbf{r}_p + \mathbf{r}_n)\right)
\end{aligned} \tag{6}$$

where $V(r_n)$ is the potential the neutron experiences, and φ is the wave function for the ground state of the deuteron. The integral in Eq. (6) is easily evaluated by using r_n and $r_p - r_n$ as coordinates; the result is of the form of Eq. (2) with

$$\mathbf{O} = \mathbf{k}_p + \frac{\mathbf{k}_d}{2}. \tag{7}$$

By using distorted waves in place of

$$\exp(-i\mathbf{k}_p \cdot \mathbf{r}_p) \quad \text{or} \quad \exp\left(i\frac{\mathbf{k}_d}{2} \cdot (\mathbf{r}_p + \mathbf{r}_n)\right),$$

it is possible to obtain a slightly different result; namely,

$$\mathbf{O} = \alpha \mathbf{k}_p + \beta \mathbf{k}_d \quad (8)$$

with α and/or β complex.

To obtain a form in which σ_p appears, it is necessary to allow the proton to experience a spin orbit potential or (what is the same thing) to allow for spin orbit effects in the distorted wave replacing $\exp(-i\mathbf{k}_p \cdot \mathbf{r}_p)$. In referring to the 'Butler theory', we mean that $O_{L^m L}$ does not contain σ_p , or, more explicitly for $L = 1$, that \mathbf{O} has the form Eq. (8).

3. The Experiments

A. Theory of the Experiments

The polarization of the incident deuteron beam may be described in terms of the expectation values of ten operators

$$\begin{aligned} 1 \\ \mathbf{S} = \frac{1}{2} (\sigma_p + \sigma_n) \\ S_{ij} = -\frac{1}{6} \sigma_n \cdot \sigma_p \delta_{ij} + \frac{1}{4} (\sigma_{ni} \sigma_{pj} + \sigma_{nj} \sigma_{pi}). \end{aligned} \quad (9)$$

These are exactly the operators used by STAPP⁴⁾ in his discussion of deuteron polarization.

The polarization of the outgoing proton beam is described by the expectation values of four operators

$$1 \text{ and } \sigma_p. \quad (10)$$

⁴⁾ H. P. STAPP, thesis, UCRL 3098, unpublished. WOLFENSTEIN [2] normalizes these operators so that

$$\text{Tr } S^\mu S^\nu = 3 \delta_{\mu\nu}$$

This is not a necessary assumption. WOLFENSTEIN assumes this normalization so that he can prove

$$\varrho = \sum_\nu \langle S^\nu \rangle \frac{S^\nu}{(2s+1)(2s_\ell+1)}.$$

STAPP shows that this equation remains true for the above definition of the S 's even though the S_{ij} 's are not mutually orthogonal in the sense of the above equation; STAPP finds

$$\varrho = \frac{\langle 1 \rangle + 3/2 \langle \mathbf{S} \rangle \cdot \mathbf{S} + 3 \langle S_{ij} \rangle S_{ij}}{3}.$$

It is *as though* there were normalization factors $\sqrt{3/2}$ multiplying \mathbf{S} , and $\sqrt{3}$ multiplying S_{ij} .

The final nucleus may also be polarized; there exists a set of operators appropriate to the description of its polarization, and the complete set of operators for the state is the direct product of these operators with the proton spin operators; however, the relevant experiments are very difficult at the present time (while it is clear in principle how one might observe the spin of C^{13} by scattering off He^4 (or C^{12}), the high charge and mass of these particles make the experiments difficult; in an inverse experiment it might be more practical to align the spin of Be^9 or C^{13}), so that we do not have to exhibit these operators explicitly.

We need the analogue of Wolfenstein's Eq. (31), p. 62, of his article [2]; namely,

$$I \langle S_f^\mu \rangle = \sum_\nu \frac{\langle S_i^\nu \rangle \text{Tr } M S_i^\nu M^\dagger S_f^\mu}{(2s_i + 1)(2s + 1)} \quad (11)$$

where the S_i^ν and S_f^μ are the spin operators for the initial and final state, respectively. We give the derivation of this analogue now, avoiding unnecessary detail, since the discussion follows Wolfenstein's article very closely.

The discussion beginning on page 60, section 4 (entitled General Formalism) of Wolfenstein's article certainly needs no modification before Eq. (31) (our Eq. (11) above) is obtained, provided the M 's are kept in the form Eq. (1). In detail, Eq. (11) is (omitting the factor $(2s_i + 1)(2s + 1)$)

$$I \langle S_f^\mu \rangle = \sum_\nu \langle S_i^\nu \rangle \sum_{m_p} \sum_{m_J} \sum_{m_d} \sum_{m_d'} \sum_{m_p'} \sum_{m_J'} (m_p J m_J p | M | m_d) \times \quad (12)$$

$$\times (m_d | S_i^\nu | m_d') (m_d' | M^\dagger | m_p' J m_J' p) (m_p' J m_J' p | S_f^\mu | m_p J m_J p).$$

Eq. (2) may be substituted into this Eq. (12) to find $\langle 1_f \rangle$ or $\langle \sigma_{pf} \rangle$ (the only quantities of interest if the spin of the final nucleus is not observed) with the result

$$I \langle 1_f \text{ or } \sigma_{pf} \rangle = \sum_\nu \langle S_i^\nu \rangle \sum_{m_p} \sum_{m_J} \sum_{m_d} \sum_{m_d'} \sum_{m_p'} \sum_{m_J'} \times$$

$$\times \sum C(J m_J; L m_L; \frac{1}{2} m_n) (m_p m_n | O_L^{m_L}(p) | m_d) (m_d | S_i^\nu | m_d') \times \quad (13)$$

$$\times \sum C(J m_J; L m_L'; \frac{1}{2} m_n') (m_d' | O_L^{m_L'}(p) | m_p' m_n')^* (m_p' | 1_f \text{ or } \sigma_{pf} | m_p).$$

For $L = 0$, the result is necessarily simple, since $m_L = m_L' = 0$, $m_n = m_n' = m_J$, and the Clebsch-Gordan coefficients are 1, so that

$$\begin{aligned}
I \langle 1_f \text{ or } \sigma_{pf} \rangle &= \sum_v \langle S_i^v \rangle \sum_{m_p} \sum_{m_n} \sum_{m_p'} \sum_{m_n'} \sum_{m_d} \sum_{m_d'} \times \\
&\times (m_p m_n | O | m_d) (m_d | S_i^v | m_d') (m_d' | O | m_p' m_n')^* \times \\
&\times (m_p' | 1_f \text{ or } \sigma_p | m_p)
\end{aligned} \quad (14)$$

which is formally identical with Eq. (11); that is, it may be written

$$I \langle 1_f \text{ or } \sigma_{pf} \rangle = \sum_v \langle S_i^v \rangle \text{Tr } O S_i^v O^+ (1 \text{ or } \sigma_p) \quad (15)$$

For $L = 1$, it can be proved by use of the explicit values of the Clebsch-Gordan coefficients in Eq. (13), that

$$\text{for } J = \frac{1}{2}, L = 1$$

$$I \langle 1_f \text{ or } \sigma_f \rangle = \frac{1}{3} \sum \langle S_i \rangle \text{Tr } \sigma_n \cdot O S_i^v O^+ \cdot \sigma_n (1 \text{ or } \sigma_p) \quad (16)$$

$$\text{for } J = 3/2, L = 1$$

$$\begin{aligned}
I \langle 1_f \text{ or } \sigma_f \rangle &= \sum \langle S_i \rangle \text{Tr} \left[-\frac{1}{3} \sigma_n \cdot O S_i^v O^+ \cdot \sigma_n + \right. \\
&\quad \left. + O \cdot S_i^v O^+ \right] (1 \text{ or } \sigma_p).
\end{aligned} \quad (17)$$

The term $O \cdot S_i^v O^+$ is written as it is because the O may not commute with S_i^v . Also, the order of the O 's and σ_n 's is correct in case they do not commute.

Since for the experiments of most interest, such as

$$d + C^{12} \rightarrow p + C^{13} \quad (18)$$

$$d + \text{Be}^8 \rightarrow p + \text{Be}^9 \text{ (actually, the inverse)}$$

the spin of the target nucleus is zero, and $J = 1/2$ or $J = 3/2$, it is not of great interest to attempt to generalize Eqs. (15)–(17).

For purposes of calculation, one further modification is convenient; namely, to alter Eq. (14) in such a way that \sum_{m_d} and $\sum_{m_d'}$ are replaced by sums over $m_n m_p$ variables. This modification is easily accomplished by the introduction of the triplet projection operator

$$P_t = \frac{1}{4} (\sigma_n \cdot \sigma_p + 3) \quad (19)$$

All that is necessary is to replace O by OP_t ; the matrix operations shown in Eqs. (15)–(17) are then the usual operations with 2×2 matrices.

B. The experiments in the case that the Butler theory is valid

(see last sentence in Section II B for a precise definition of the 'Butler Theory')

We can prove a series of theorems (some of which are well known).

Theorem 1. In the Butler theory, the proton polarization resulting from an unpolarized deuteron beam vanishes unless α or β is complex.

Proof (for $J = 1/2, L = 1$).

$$3I \langle \sigma_p \rangle = \text{Tr } \sigma_n \cdot (\alpha \mathbf{k}_p + \beta \mathbf{k}_d) \frac{1}{4} (\sigma_n \cdot \sigma_p + 3) \frac{1}{4} (\sigma_n \cdot \sigma_p + 3) \sigma_n \cdot (\alpha^* \mathbf{k}_p + \beta^* \mathbf{k}_d) \sigma_p.$$

The factor 3 is $(2s_t + 1)(2s + 1)$. We take the traces in neutron or proton spin space using

$$\text{Tr } (\mathbf{A} \cdot \boldsymbol{\sigma}) \boldsymbol{\sigma} = 2 \mathbf{A}$$

$$\text{Tr } \mathbf{A} \cdot \boldsymbol{\sigma} \mathbf{B} \cdot \boldsymbol{\sigma} \boldsymbol{\sigma} = 2i \mathbf{A} \times \mathbf{B} \quad (20)$$

$$\text{Tr } \mathbf{A} \cdot \boldsymbol{\sigma} \boldsymbol{\sigma} \mathbf{B} \cdot \boldsymbol{\sigma} = -2i \mathbf{A} \times \mathbf{B}$$

$$\boldsymbol{\sigma} \times \boldsymbol{\sigma} = 2i \boldsymbol{\sigma}.$$

The result is

$$I \langle \sigma_p \rangle = \frac{1}{3} i (\alpha \mathbf{k}_p + \beta \mathbf{k}_d) \times (\alpha^* \mathbf{k}_p + \beta^* \mathbf{k}_d). \quad (21)$$

It is already clear from Eq. (21) that if α and β are both real, $\langle \sigma_p \rangle$ vanishes.

Theorems about the maximum value of the polarization may also be obtained. The calculations are facilitated if we use orthogonal vectors instead of \mathbf{k}_d and \mathbf{k}_p ; namely, if we use

$$\mathbf{O} = \alpha' (\mathbf{k}_d \times \mathbf{k}_p) \times \mathbf{k}_d + \beta' \mathbf{k}_d \quad (22)$$

(we could just as well write $\mathbf{O} = \alpha' \mathbf{i} + \beta' \mathbf{k}$, where \mathbf{i} and \mathbf{k} are unit vectors in the x and z directions, respectively). We find

$$\begin{aligned} \text{for } J = \frac{1}{2} \quad \langle \sigma_p \rangle &= -\frac{1}{3} i \frac{(\alpha' \beta'^* - \beta' \alpha'^*)}{\alpha' \alpha'^* + \beta' \beta'^*} \mathbf{j}, \\ \text{for } J = \frac{3}{2} \quad \langle \sigma_p \rangle &= \frac{1}{6} i \frac{(\alpha' \beta'^* - \beta' \alpha'^*)}{\alpha' \alpha'^* + \beta' \beta'^*} \mathbf{j}, \end{aligned} \quad (23)$$

leading to the theorems.

Theorem 2. For $J = 1/2$, the maximum value of the proton polarization from an unpolarized deuteron beam is $1/3$. For $J = 3/2$, the maximum

value is $1/6$. For the same α', β' (that is, if the $\psi(r_n)$ (see Eq. (5) are not too different for $J = 1/2$ and $J = 3/2$), the polarization from a $J = 1/2$ and $J = 3/2$ state are different in sign.

These results have been obtained by other methods (see reference 1, Chapter IX); the method is novel and the generality of the assumption under which they are obtained is somewhat remarkable.

Theorem 3. In the Butler theory, the tensor components (S_{ij}) of the deuteron spin polarization play no role in the angular distribution of the proton.

Proof: The details of the necessary calculation are given in Appendix A.

Theorem 4. In the Butler theory, the angular distribution of protons produced by polarized deuterons is (for $J = 1/2$)

$$I \langle 1 \rangle_f = I (1 + 3 \mathbf{P}_d \cdot \mathbf{P}_p) \quad (24)$$

where \mathbf{P}_d is the vector polarization of the deuterons (that is $\langle \mathbf{S} \rangle$; see Eq. (9) for the definition of \mathbf{S} and footnote 4 for a warning about its normalization to make the factor 3 come out right), and \mathbf{P}_p is the proton polarization produced by an unpolarized deuteron beam.

This theorem was first given by SATCHLER [3]. The proof follows by calculation from Eq. (16) and Eq. (20).

C. Criticism of the results of the preceding Section III B; the experiments when the Butler theory is not valid

It is known that the proton polarizations sometime exceed the maximum values quoted in Theorem 2 [4], so that the 'Butler theory' is, in fact, *not* valid. The question of most interest is: what happens to the Satchler result, Eq. (24) when the 'Butler theory' is not valid.

If we consider the case $J = 1/2$, $L = 1$ (certainly applicable to the $d + C^{12} \rightarrow p + C^{13}$ reaction), the most general pseudoscalar ($\sigma_n \cdot \mathbf{O}$) that we can write is

$$\sigma_n \cdot \mathbf{O} P_i = \sigma_n \cdot \mathbf{V}_1 + \sigma_p \cdot \mathbf{V}_2 + \sigma_n \cdot \mathbf{V}_3 \sigma_p \cdot \mathbf{n} + \sigma_p \cdot \mathbf{V}_4 \sigma_n \cdot \mathbf{n} \quad (25)$$

where \mathbf{n} is a unit vector in the direction $\mathbf{k}_d \times \mathbf{k}_p$, and $\mathbf{V}_1, \dots, \mathbf{V}_4$ are arbitrary (possibly complex) vectors in the $\mathbf{k}_p, \mathbf{k}_d$ plane. We have included P_i in writing Eq. (25) for computational convenience; for the most general $\sigma_n \cdot \mathbf{O}, \sigma_n \cdot \mathbf{O} P_i$ is less general since it must vanish when applied to a singlet spin function; we find that this restriction implies that

$$-\mathbf{V}_1 + \mathbf{V}_2 + i(\mathbf{V}_3 \times \mathbf{n}) - i(\mathbf{V}_4 \times \mathbf{n}) = 0. \quad (26)$$

We find that the proton polarization (deuteron beam unpolarized) is

$$3I \langle \sigma_p \rangle = 4(V_1 \cdot V_3^* + V_3 \cdot V_1^*) \mathbf{n} + 4i V_2 \times V_2^* + 4i V_4 \times V_4^*. \quad (27)$$

where

$$3I = 4(V_1 \cdot V_1^* + V_2 \cdot V_2^* + V_3 \cdot V_3^* + V_4 \cdot V_4^*). \quad (28)$$

We find that if the incident beam has a vector polarization \mathbf{P} , but no tensor polarization, the azimuthal distribution of the proton is

$$3I \langle 1 \rangle = 3I + \frac{3}{2} \frac{1}{2} \mathbf{P} \cdot \mathbf{P}' \quad (29)$$

where

$$\begin{aligned} \mathbf{P}' = & 4(V_1 \cdot V_3^* + V_3 \cdot V_1^* + V_2 \cdot V_4^* + V_4 \cdot V_2^*) \mathbf{n} - \\ & - 4i V_1 \times V_1^* - 4i V_3 \times V_3^* - 4i V_2 \times V_2^* - 4i V_4 \times V_4^*. \end{aligned} \quad (30)$$

In Eq. (29), the factor $3/2$ comes from the normalization referred to in footnote 4, and the factor $1/2$ comes from the $1/2$ in $\mathbf{S} = \sigma_n + \sigma_p/2$. It is extremely tedious (but possible) to prove that

$$P' < \frac{4}{3} (3I). \quad (31)$$

If Eq. (26) is not taken into account, one finds the obviously absurd possibility $P' = 2 (3I)$.

There is *no connection* between Eq. (27) and Eq. (30) which might give an analogue of SATCHLER's theorem Eq. (24).

There is no point in attempting to prove a connection between \mathbf{P}' and the vector polarization of deuterons produced by unpolarized protons in the inverse reaction, because the scattering amplitude for $d + C^{12} \rightarrow p + C^{13}$ is not the same as the scattering amplitude for $p + C^{13} \rightarrow d + C^{12}$; that is, these 'inverse' reactions are not 'inverse' in this sense. Such a theorem would not be of any use from the experimental point of view anyway.

Finally, we consider the effects of the tensor components of the deuteron polarization in the azimuthal distribution of the protons. If we define the tensor

$$\begin{aligned} t_{ij} \equiv & \text{Tr } M \sigma_{ni} \sigma_{nj} M^+ = \\ & = 4 [V_{1i} V_{2j}^* - i(V_1 \times V_3^*)_i n_j - i(V_1 \times n)_i V_{4j}^* - \\ & - i V_{3i}^* (V_2 \times n)_j - i n_i (V_2 \times V_4^*)_j - (V_3 \times n)_i (n \times V_{4j})] + \\ & + \text{complex conjugate.} \end{aligned} \quad (32)$$

Then

$$T_{ij} \equiv \text{Tr } M S_{ij} M^+ = -\frac{1}{6} \text{Tr } t \delta_{ij} + \frac{1}{4} (t_{ij} + t_{ji}). \quad (33)$$

By choosing coordinate axes N, P, K as STAPP has done

$$\begin{aligned} N &= \mathbf{k}_d \times \mathbf{k}_p \\ P &= \mathbf{k}_p + \mathbf{k}_d / |\mathbf{k}_p + \mathbf{k}_d| \\ K &= \mathbf{k}_p - \mathbf{k}_d / |\mathbf{k}_p - \mathbf{k}_d| \end{aligned} \quad (34)$$

it is possible to write any of the vectors V_1, \dots, V_4 in the form

$$V = V_P P + V_K K \quad (35)$$

and collect Eq. (33) in the form of STAPP'S Eq. (28) (p. 76, ref. 4). It is not necessary to repeat these results here.

One finds

$$\langle 1 \rangle = 1 + \frac{1}{2} tt' + \frac{2}{3} (uu' - vv') \cos \varphi + \frac{1}{6} ww' \cos 2\varphi. \quad (36)$$

Tables of t, u, v, w for $d + \text{He}^4$ scattering have been published elsewhere [5]. Because we do not refer to a specific model in this work, we cannot predict values of t', u', v', w' for the $d + \text{C}^{12}$ reaction (the Butler theory gives $t', v', w' = 0$). Experimentally, one looks for a difference between (left + right) and (up + down) scattering. Also, the total cross section (integral over the azimuth) may be different for polarized deuterons than for unpolarized deuterons.

D. Criticism of the use of C^{12} as an analyzer for the spin polarization of deuterons

The fact that there exists no rigorous analogue of the Satchler theorem means that the stripping reaction is unsuitable as a precision analyzer for the spin polarization of deuteron *before it has been 'calibrated'*. The quantity P' (Eq. (30)) cannot be measured without using deuterons of known vector polarization in an experiment designed to calibrate the reaction. One may, in a *preliminary* experiment, observe a left right asymmetry and use the Satchler theorem to interpret the result; there is no guarantee that the interpretation is correct.

4. Acknowledgement

I thank Professors LEONARD S. RODBERG, JOHN L. McHALE, and R. M. THALER for stimulating discussions.

Appendix A

In this appendix we show that in the 'Butler theory' the T_{ij} defined in Eq. (33) vanish. We have, in the Butler theory, from Eq. (32)

$$t_{ij} = \text{tr } \sigma_n \cdot V \frac{\sigma_n \cdot \sigma_p + 3}{4} \sigma_{ni} \sigma_{pj} \frac{\sigma_n \cdot \sigma_p + 3}{4} \sigma_n \cdot V^*. \quad (\text{A.1})$$

It is best to break this into four terms

$$\begin{aligned} (\text{I}) &= \frac{1}{16} \text{Tr } \sigma_n \cdot V \sigma_n \cdot \sigma_p \sigma_{ni} \sigma_{pj} \sigma_n \cdot \sigma_p \sigma_n \cdot V^* \\ (\text{II}) &= \frac{3}{16} \text{Tr } \sigma_n \cdot V \sigma_n \cdot \sigma_p \sigma_{ni} \sigma_{pj} \sigma_n \cdot V^* \\ (\text{III}) &= \frac{3}{16} \text{Tr } \sigma_n \cdot V \sigma_{ni} \sigma_{pj} \sigma_n \cdot \sigma_p \sigma_n \cdot V^* \\ (\text{IV}) &= \frac{9}{16} \text{Tr } \sigma_n \cdot V \sigma_{ni} \sigma_{pj} \sigma_n \cdot V^* \end{aligned} \quad (\text{A.2})$$

Term (IV) is obviously zero since $\text{Tr } \sigma_{pj} = 0$. Terms II and III are easily calculated by taking the proton trace first and using

$$\text{Tr (proton space)} \sigma_n \cdot \sigma_p \sigma_{pj} = 2\sigma_{nj}. \quad (\text{A.3})$$

We find

$$(\text{II}) + (\text{III}) = \frac{6}{16} \text{Tr } \sigma_n \cdot V (\sigma_{ni} \sigma_{nj} + \sigma_{nj} \sigma_{ni}) \sigma_n \cdot V^*. \quad (\text{A.4})$$

Then using

$$\sigma_{ni} \sigma_{nj} + \sigma_{nj} \sigma_{ni} = 2\delta_{ij} \quad (\text{A.5})$$

and

$$\text{Tr } \sigma_n \cdot V \sigma_n \cdot V^* = 2 V \cdot V^*, \quad (\text{A.6})$$

it follows that

$$(\text{II}) + (\text{III}) = \frac{24}{16} \delta_{ij} V \cdot V^*. \quad (\text{A.7})$$

(I) may be evaluated by using

$$\sigma_n \cdot \sigma_p \sigma_{ni} = (2\sigma_{pi} - \sigma_{ni} \sigma_n \cdot \sigma_p). \quad (\text{A.8})$$

Then

$$\begin{aligned} (\text{I}) &= \frac{1}{16} \text{Tr } \sigma_n \cdot V (2\sigma_{pi} - \sigma_{ni} \sigma_n \cdot \sigma_p) \sigma_{pj} \sigma_n \cdot \sigma_p \sigma_n \cdot V^* = \\ &= (\text{I}_1) + (\text{I}_2) \text{ (the obvious separation into two terms).} \end{aligned} \quad (\text{A.9})$$

Term (I₁) may be evaluated using

$$\sigma_{pi} \sigma_{pj} = \delta_{ij} + ie^{ijk} \sigma_{pk} \quad (\text{A.10})$$

($e^{ijk} = +1$ if ijk even permutation of 123, -1 if odd, 0 otherwise), so that

$$(\text{I}_1) = \frac{2}{16} \text{Tr } \sigma_n \cdot V (\delta_{ij} + ie^{ijk} \sigma_{pk}) \sigma_n \cdot \sigma_p \sigma_n \cdot V^*. \quad (\text{A.11})$$

Taking the trace in the proton space first, the term with δ_{ij} gives nothing because $\text{Tr } \sigma_p = 0$. In the second term, σ_{pk} is replaced by $2\sigma_{nk}$, since

$$\text{Tr } \sigma_p \sigma_p \cdot A = 2 A. \quad (\text{A.12})$$

Therefore

$$(I_1) = \frac{4}{16} \text{Tr } \sigma_n \cdot V i e^{ijk} \sigma_{nk} \sigma_n \cdot V^*. \quad (\text{A.13})$$

Term (I_2) is easily evaluated taking the proton space trace first, using

$$\text{Tr } A \cdot \sigma_p \sigma_{pj} B \cdot \sigma_p = -2i(A \times B)_j \quad (\text{A.14})$$

$$(\sigma_n \times \sigma_n)_j = 2i \sigma_{nj}.$$

The result is

$$(I_2) = -\frac{4}{16} \text{Tr } \sigma_n \cdot V \sigma_{ni} \sigma_{nj} \sigma_n \cdot V^*. \quad (\text{A.15})$$

Applying (A.10) gives

$$(I_2) = -\frac{4}{16} \text{Tr } \sigma_n \cdot V (\delta_{ij} + i e^{ijk} \sigma_{nk}) \sigma_n \cdot V^*. \quad (\text{A.16})$$

The second part of this cancels (I_1) ; the final result is

$$(I_1) + (I_2) = -\frac{8}{16} \delta_{ij} V \cdot V^* \quad (\text{A.17})$$

which, when combined with (A.7) gives

$$t_{ij} = V \cdot V^* \delta_{ij}. \quad (\text{A.18})$$

Eq. (33) leads immediately to

$$T_{ij} = 0. \quad (\text{A.19})$$

It is also possible to obtain this result from Eq. (32) directly, using

$$\begin{aligned} \sigma_n \cdot V \frac{\sigma_n \cdot \sigma_p + 3}{4} &= \frac{3}{4} \sigma_n \cdot V + \frac{1}{4} \sigma_p \cdot V + \\ &+ \frac{i}{4} \sigma_n \cdot (V \times n) \sigma_p \cdot n - \frac{i}{4} p_p \cdot (V \times n) \sigma_n \cdot n. \end{aligned} \quad (\text{A.20})$$

That is, in the 'Butler theory',

$$V_1 = \frac{3}{4} V, \quad V_2 = \frac{1}{4} V, \quad V_3 = \frac{i}{4} (V \times n), \quad V_4 = -\frac{i}{4} (V \times n). \quad (\text{A.21})$$

The algebra is somewhat complicated.

REFERENCES

- [1] S. T. BUTLER and O. H. HITTMAYER, *Nuclear Stripping Reactions*, (John Wiley and Sons, New York 1957).
- [2] L. WOLFENSTEIN, *Annual Reviews of Nuclear Science* 6, 43 (1956).
- [3] G. R. SATCHLER, *Nuclear Physics* 6, 543 (1958).
- [4] J. C. HENSEL and W. C. PARKINSON, *Phys. Rev.* 110, 128 (1957); R. G. ALLAS and F. B. SHULL, *Phys. Rev.* 116, 996 (1959).
- [5] J. L. GAMMEL, B. J. HILL, and R. M. THALER, to appear in *Phys. Rev.*

Polarization Phenomena in Deuteron Stripping Reactions

By L. C. BIEDENHARN¹⁾ and G. R. SATCHLER²⁾

Abstract. Polarization phenomena in the usual theory of (d, p) reactions (i. e., the distorted wave Butler theory without explicit spin-orbit coupling) are shown to have a common origin, which is in effect simply a measurement of the neutron transfer angular momentum direction (multiplied by quantum geometrical factors). The limitations implied by this result are discussed.

The effect of explicit spin-orbit couplings is discussed in detail for the important case where the transfer angular momentum is zero. It is shown that for this case the proton polarization is approximately given by the *derivative* of the (unpolarized) angular distribution. (Conditions are given under which this approximation is useful.)

Symmetry considerations in the distorted wave Butler theory are next discussed, and illustrated by application to Coulomb effects. Various numerical examples are cited to illustrate the qualitative predictions of the present discussion.

The great importance of the stripping process for nuclear reactions lies in the fact that from the *qualitative* features of the angular distribution one may infer, almost directly, information of use in nuclear spectroscopy. Although deuteron induced reactions had previously been considered in much experimental and theoretical detail (e.g., the Oppenheimer-Phillips process) it was the simplicity and usefulness of the Butler stripping theory that led to the widespread attention this process has received since BUTLER's paper [1]³⁾ in 1951. Since that time numerous further developments of the theory have been made, and the whole subject has been treated comprehensively in several reviews and books [2] devoted either exclusively to the stripping process, or else treating it as a special case of the so-called 'direct reaction theory'. Following AUSTERN [2], one may divide the stripping theories into three classes:

(1) the 'crude' Butler theory, which uses plane waves [1], (2) the simple theories, which employ distorted waves in the Born approximation (with or without explicit spin-dependent interactions), and (3) the 'sophisticated' theories which attempt a more or less fundamental treatment from general reaction theory. In surveying these it seems fair to say that two

¹⁾ Department of Physics, Duke University, Durham, North Carolina, USA.

²⁾ Physics Division, Oak Ridge National Laboratory, Oak Ridge, Tenn. U.S.A.

³⁾ Numbers in brackets refer to References, page 400.

points are clear: (1) The Butler theory, even in its simplest form, works surprisingly well and (2) the Butler theory, and all later modifications, are but approximations whose real applicability has yet to be fully assessed. This last point is hardly surprising since the stripping process is an instance of the general three-body rearrangement process, and above the deuteron binding energy, even the general Wigner dispersion theory becomes, in principle at least, inapplicable.

It is not our intention to attempt a discussion of the foundations of the theory; rather we shall accept the general applicability of the distorted wave Born approximation (a development that stems from HOROWITZ and MESSIAH [3]), and try to assess some of the consequences⁴⁾. One of the bothersome difficulties of the distorted wave treatment lies in the fact that it is so general, and contains so many parameters, that it is not easy to know whether agreement (which generally is found sooner or later) is really significant or not. It is, therefore, particularly important to understand intuitively the *qualitative* predictions, and this is the real aim of the present discussion⁵⁾.

The nuclear spectroscopic information obtained from the Butler analysis (in favorable cases) is the orbital angular momentum l (and thus the parity) of the transferred neutron⁶⁾. Further information, such as the total angular momentum of the absorbed neutron, is desirable, and it was quickly pointed out that further measurements on the stripping process could be useful. BOYER [4] for example, suggested angular correlations with any gamma rays emitted; this gives information both for nuclear spectroscopy and the stripping reaction mechanism. It was NEWNS [5] who suggested polarization measurements, and since this conference deals with polarization we shall confine our attention to the information such measurements convey.

⁴⁾ There are some exceptional cases where the observed stripping pattern may be fortuitous or the result of other mechanisms (for example, $B^{10}(d, p)$), but we shall not discuss such cases. It is possible to regard the distorted wave calculations in a more subtle way, and consider that the distorted waves themselves already contain resonant effects in both the elastic and inelastic channels. This latter would then relax the stripping selection rules. For example take $Mg^{24}(d, p)Mg^{25*}$, with the Mg^{25} in the 1.611 MeV, $7/2^+$ state.

The usual selection rules require $l = 4$; but if Mg^{24} were first excited to the $l = 2$ rotational level, then $l = 2$ stripping would now be permitted. This process would, to be sure, be both improbable and not a well defined $l = 2$ stripping pattern. We shall not, however, go further into such extensions of the distorted wave calculations, since they are not directly at issue in polarization processes.

⁵⁾ A quite different approach to the same problem (for stripping, as opposed to polarization) is the 'semi-classical' treatment of AUSTERN [2]. Although marginal in application perhaps, it nonetheless is quite helpful for an intuitive feeling for the stripping process.

⁶⁾ The (d, p) reaction will be considered as the prototype.

In order to understand intuitively the basis for the existence of proton polarization (even in the absence of explicit proton spin orbit coupling) let us consider the (d, p) reaction from the standpoint of the stripping assumption. This we take to mean that the process may be described by the Born approximation, with the transition matrix element:

$$T_{fi} \cong \langle \psi_f^{(-)}(\mathbf{k}_p) | V_{np} | \psi_i^{(+)}(\mathbf{k}_d) \rangle. \quad (1)$$

Here $\psi_i^{(+)}$ is the initial system with (outgoing) deuteron waves, and $\psi_f^{(-)}$ is the final system with (ingoing) proton waves. For simplicity we take the $n-p$ potential, V_{np} , to be of zero range. Whether or not the integral extends over the nuclear volume is a matter of preference; the usual considerations that the stripping process occurs primarily at larger distances exclude the nucleus proper⁷⁾. According to eq. (1), the assumption that the proton spin-orbit coupling is neglected in $\psi_f^{(-)}$ is equivalent to the assumption that the proton spin is not directly involved in the process at all, and is only affected by virtue of its coupling to form the deuteron in the initial state.

If we neglect proton spin-orbit coupling, the angular momentum relationships which govern the proton spin in the stripping process are simply:

$$\begin{aligned} \text{a) } \mathbf{s}_p + \mathbf{s}_n &= \mathbf{s}_d \\ \text{b) } \mathbf{s}_n + \mathbf{l}_n &= \mathbf{j}_n \\ \text{c) } \mathbf{j}_i + \mathbf{j}_n &= \mathbf{j}_f. \end{aligned} \quad (2)$$

That is to say, the proton spin, *by assumption*, is coupled only to the neutron spin to form the incident deuteron, and the neutron spin is coupled to its orbital angular momentum in the final system. Since, by hypothesis, the initial and final spin angular momenta (\mathbf{j}_i and \mathbf{j}_f) are *not* observed (therefore random), one sees from (2c) that the direction of \mathbf{j}_n is similarly *random*. One can now obtain the proton spin polarization distribution quite easily by applying semi-classical correlation techniques [6]. (This is given in detail in Appendix I.) These techniques lead at once to the relation:

$$P_{\text{Proton}} = P_1 (\hat{\mathbf{s}}_p \cdot \hat{\mathbf{s}}_n) P_1 (\hat{\mathbf{s}}_n \cdot \hat{\mathbf{l}}_n) [3/l(l+1)]^{1/2} \langle \mathbf{l}_n \rangle. \quad (3)$$

In other words, the measurement of the proton spin is effectively a measurement of the direction of the neutron's orbital angular momentum, diminished

⁷⁾ T. HONDA and U. NAGASAKI, Proc. Phys. Soc. London, 74, 571 (1959). These authors go further and assume that the proton is completely excluded from the nuclear region, even in the final state wave function.

by the (quantum) geometrical factors $P_1(\hat{s}_n \cdot \hat{s}_p) = 1/3$ from the deuteron spin coupling, and the factor

$$\left[\frac{3}{l(l+2)} \right]^{1/2} P_1(\hat{s}_n \cdot \hat{l}_n) = \begin{cases} (l+1)^{-1} & \text{for } j = l + 1/2 \\ (-l)^{-1} & \text{for } j = l - 1/2 \end{cases}$$

from the neutron spin coupling.

This result for the polarization is even clearer if one takes $l_n = 1$, for then the result may be written in vector notation, instead of the more complicated multipole tensor products. For a zero range np potential and $l_n = 1$, eq. (1) becomes:

$$T_{fi}(l_n = 1) \rightarrow \mathbf{M} \equiv \langle \psi_{\text{proton}}^{(-)}(\mathbf{r}) | \hat{\mathbf{r}} \psi_{\text{neutron}}(\mathbf{r}) | \psi_{\text{deuteron}}^{(+)}(\mathbf{r}) \rangle. \quad (4)$$

With this, one obtains then the simple result:

$$\mathbf{P} = \frac{1}{3} \begin{pmatrix} l/2 \\ -1 \end{pmatrix} \frac{(i) (\mathbf{M} \times \mathbf{M}^*)}{\mathbf{M} \cdot \mathbf{M}^*}. \quad (5)$$

From eq. (5) one can easily see all the qualitative features of the proton polarization process (under the present assumptions). Namely:

a) The maximum polarization is 33%. This is actually a result of the quantization of angular momenta, since the triangle formed by $\mathbf{s}_p + \mathbf{s}_n = \mathbf{s}_d$ —even though the angular momenta are ‘parallel’—still has finite area, and $\hat{\mathbf{s}}_p \cdot \hat{\mathbf{s}}_n \neq 1$.

b) The sign of the polarization distinguishes $j = l + 1/2$ from $j = l - 1/2$ (but one must know the sign of $\mathbf{M} \times \mathbf{M}^*$ to specify either absolutely).

c) There is no polarization if the matrix element is not *complex*, and no polarization if the matrix element is a function of a *single* direction. Either one of these restrictions eliminates any polarization in Butler's original approximation where plane waves are used. (Alternatively one may say that in the plane wave approximation, the neutron is effectively taken from a plane wave along the recoil direction, and since \mathbf{l}_n is equally probable in the plane perpendicular to this direction, $\langle \mathbf{l}_n \rangle = 0$.) *The importance of polarization measurements (for comparison with the theory) lies in the fact that the polarization is solely due to the distortion effects in the absence of $\mathbf{l} \cdot \mathbf{s}$ forces, and is therefore a sensitive test of the stripping mechanism.*

d) Since there are but two physically defined directions in the problem, \mathbf{k}_p and \mathbf{k}_d , it is clear that $i \mathbf{M} \times \mathbf{M}^* = (\mathbf{k}_d \times \mathbf{k}_p) f(\mathbf{k}_p, \mathbf{k}_d, \mathbf{k}_p \cdot \mathbf{k}_d)$. This is the well known general result that \mathbf{P} must lie normal to the scattering plane. (None of these conclusions is in any way affected by our specialization to $l_n = 1$.)

It is quite easy to apply the same techniques to determine the polarization of the final nucleus in the stripping reaction. The angular momentum relationships are exactly the same as before, *except that the experimental observations differ*. Thus s_n is now random (since neither s_p or s_d is observed), but j_n is not random any longer. It follows that the polarization of the final nucleus is given by:

$$\langle \hat{j}_f \rangle = P_1(\hat{j}_f \cdot \hat{j}_n) P_1(\hat{j}_n \cdot \hat{l}_n) \langle \hat{l}_n \rangle. \quad (6)$$

On using the usual definition that the polarization vector P is defined as $\langle \hat{j}_f \rangle / j_f$, one gets:

$$P_{\text{nucleus}} = \left[\frac{j_f + 1}{j_f(l_n)(l_n + 1)} \right]^{1/2} P_1(\hat{j}_f \cdot \hat{j}_n) \cdot P_1(\hat{j}_n \cdot \hat{l}_n) \langle \hat{l}_n \rangle. \quad (7)$$

It will be noted at once that the neutron spin coupling introduces here quite a different result than for proton polarization. Unlike the proton case, here both $j = l \pm 1/2$ have the *same* sign. One sees further that complete polarization can result if $j_i = 0$.

As a final example of the utility of this method of deducing polarizations let us construct the deuteron polarization in the *inverse* reaction. This is, by the same general method,

$$P_{\text{deuteron (inverse)}} = \sqrt{\frac{s_d + 1}{s_d}} P_1(\hat{s}_d \cdot \hat{s}_n) P_1(\hat{s}_n \cdot \hat{l}_n) \langle \hat{l}_n \rangle. \quad (8)$$

However, the angular distribution of the products of a nuclear reaction induced by polarized particles and the polarization of the particles produced in the inverse reaction are related [7] under very general conditions by the equation:

$$\left(\frac{d\sigma}{d\Omega} \right)_{\text{pol.}} = \left(\frac{d\sigma}{d\Omega} \right)_{\text{unpol.}} \left[1 - \frac{3j}{j+1} \mathbf{P}^I \cdot \mathbf{P}^{II} \right]. \quad (9)$$

(Here \mathbf{P}^I and \mathbf{P}^{II} are the polarization vectors of a particle of spin j , with I referring to the particle initiating the reaction and II to the inverse reaction.) We may now substitute eq. (8) in eq. (9) and, if we further recall eq. (3), then one obtains

$$\left(\frac{d\sigma}{d\Omega} \right)_{\text{pol.}} = \left(\frac{d\sigma}{d\Omega} \right)_{\text{unpol.}} \left[1 + 3 \mathbf{P}_{\text{deuteron}} \cdot \mathbf{P}_{\text{proton}} \right]. \quad (10)$$

This relation was first obtained by SATCHLER⁸⁾ and is of interest experimentally in that reactions produced by polarized deuterions may be a

⁸⁾ G. R. SATCHLER, Nucl. Phys. 6, 543 (1958). Note that the sign convention in eq. (10) differs from that given in this reference.

100% effect, as opposed to the 33% limit of the proton polarization. One further notes that *tensor* moments do not enter this relation (eq. (10)). Referring to the angular momentum coupling diagram one sees that this is due *solely to the fact that the angular information on the deuteron spin is coupled through the neutron spin*. Thus $P_\nu(\hat{s}_d \cdot \hat{s}_n)$ enters for the tensor moments, but (because $s_n = 1/2$) ν must be 0 or 1 only.

Finally one may ask as to the generality of the results given by eqs. (3), (7) and (9). It is clear that they are all a direct consequence of the assumption that the proton spin is not directly coupled to the reaction in the stripping approximation without spin-orbit forces, and are no longer valid upon considering spin-orbit couplings⁹⁾. This is important because several examples are already known where $P_p > 1/3$, and hence the Butler theory is not always applicable.

To summarize: *Polarization in the stripping approximation, without explicit spin-orbit coupling on the proton, is essentially a measurement of the transfer angular momentum direction, multiplied by the appropriate quantum geometrical factors.*

Let us turn next to the effects of spin-orbit coupling. The general results that can be obtained using the stripping hypothesis, are quite involved because of the complicated nature of the angular momentum couplings. This general result is given in Appendix II, but will not be discussed otherwise¹⁰⁾. Not many numerical calculations have been carried out with spin-orbit coupling included, but in these [8] the effect is found to be small. (Since $P_{\text{proton}} \leq 1/3$ is not valid here, there can in principle be quite large effects.)

The special case where $l_n = 0$ is of particular interest, because here it is clear that proton spin-orbit effects are the only cause of polarization. In order to obtain most conveniently the desired polarization formula, it is useful to recall that for spin 1/2 particles and photons the polarization can be *formally*¹¹⁾ expressed quite simply in terms of the angular distribution [9]. Thus if the angular distribution is given by:

$$\left(\frac{d\sigma}{d\Omega}\right) = \sum_{\nu l j l' j'} B_\nu(l j l' j') P_\nu(\cos \theta),$$

⁹⁾ Dr. J. GAMMEL has also arrived at similar conclusions in a paper appearing in these Proceedings. The authors are indebted to Dr. GAMMEL for discussions on these topics prior to delivery of this paper.

¹⁰⁾ See also the paper by GOLDFARB, these Proceedings.

¹¹⁾ It is essential to call attention to the formal nature of this result, for the polarization and the angular distribution are in principle independent functions and one cannot be obtained from the other. The difficulty resides in the fact that in eq. (11) only the symmetric (real) part of the dynamical factors in B enters, while in eq. (12) only the anti-symmetric (imaginary) part enters; hence eq. (11) and eq. (12) only formally involve the 'same' dynamical factors.

$$\text{with } B_\nu(l j l' j')^* = B_\nu(l' j' l j), \quad (11)$$

then:

$$P(\theta) = \hat{n} \left(\frac{d\sigma}{d\Omega} \right)^{-1} (i) \sum_{\nu l j l' j'} B_\nu(l j l' j') (-)^{\nu+l'+j'+1/2} \cdot \left[\frac{6(2\nu+1)}{\nu+1} \right]^{1/2} C_{00}^{l l' \nu} X \left(\begin{matrix} l j & 1/2 \\ l' j' & 1/2 \\ \nu & 1 \end{matrix} \right) \cdot W(l j l' j'; \frac{1}{2} \nu)^{-1} \cdot P_\nu^{(0)}(\cos \theta). \quad (12)$$

In eq. (12) the unit vector \hat{n} has the direction $\mathbf{k}_d \times \mathbf{k}_p$, in accord with the 'Basel convention'. An identity [10] for the X coefficient that appears in eq. (12) is given in Appendix III; this simplifies eq. (12) but is less useful for the usual manipulations of the Racah algebra. For the special case that $l_n = 0$, one finds the result¹²⁾ that the angular distribution is:

$$\frac{d\sigma}{d\Omega} = \left(\frac{\lambda_d^2}{2 s_d - 1} \right) \left(\frac{2 j_f + 1}{2 j_i - 1} \right) \sum_\nu B_\nu P_\nu(\hat{\mathbf{k}}_p \cdot \hat{\mathbf{k}}_d), \quad (13)$$

where:

$$B = \frac{1}{4} \sum \bar{Z}(l_p j_p l'_p j'_p; s_p \nu) (-)^{i_p - s_p} \bar{Z}(l_d j_d l'_d j'_d; s_d \nu) (-)^{i_d - s_d} \cdot (-)^{\nu} (2 j_p + 1) (2 j'_p + 1) (2 j_d + 1) (2 j'_d + 1)^{-1/2} W(j'_p \nu j_n i_d; i_p j'_d)$$

$$A_{l_p j_p; l_d j_d}^{l_n j_n} A_{l'_p j'_p; l'_d j'_d}^{* l'_n j'_n}, \quad (14)$$

with,

$$A_{l_p j_p; l_d j_d}^{l_n j_n} \equiv e^{i[\delta(l_p j_p) + \delta(l_d j_d)]} C_{0000}^{l_d l_n l_p}.$$

$$\cdot \left\{ (2 l_n - 1) (2 s_n - 1) X \left(\begin{matrix} l_d s_d j_d \\ l_n s_n j_n \\ l_p s_p j_p \end{matrix} \right) \cdot G_{l_p j_p; l_d j_d}^{l_n j_n} \right\}. \quad (15)$$

$G_{l_p j_p; l_d j_d}^{l_n j_n}$ is discussed following eq. II-3 of the Appendix.

It is convenient now to neglect the spin-orbit coupling on the deuteron, and then:

$$\left(\frac{d\sigma}{d\Omega} \right)_{i_n=0} = \frac{\lambda_d^2}{2 s_d - 1} \cdot \left(\frac{2 j_f + 1}{2 j_i - 1} \right) \sum_\nu B_\nu(l_n = 0) P_\nu(\hat{\mathbf{k}}_p \cdot \hat{\mathbf{k}}_d) \cdot B_\nu(l_n = 0) = \left(\bar{Z}(l j l j; \frac{1}{2} \nu) \right)^2 (A_{lj}) (A_{*lj}),$$

¹²⁾ Here, and elsewhere unless stated otherwise, we are assuming the stripping hypothesis with a zero-range np potential. The further approximation is made that the center of mass is fixed throughout on the target nucleus.

$$A_{lj} \equiv \exp i(\delta_{lj}^{(p)} + \delta_{lj}^{(d)}) G_{lj}^{0, 1/2}. \quad (16)$$

It has been noted many times in the past that the polarization obtained in calculations with the optical model are qualitatively similar to a derivative of the angular distribution. Recently RODBERG [11] has shown that this 'derivative relation' is in fact semi-quantitative for small spin-orbit coupling, and that moreover the ratio

$$|P| \left(\frac{d\sigma}{d\Omega} \right) / \left[\frac{d}{d\theta} \left(\frac{d\sigma}{d\Omega} \right) \right]$$

is a measure of the strength of the spin orbit potential. RODBERG's physical argument is more general, it appears, than his specific application (to the optical model), and it is tempting to apply it to the stripping process as well. For the situation described by eq. (16) it is shown in Appendix IV that for small spin-orbit forces on the proton, the polarization*) is

$$P \cong \hat{n} \left(\frac{d\sigma}{d\Omega} \right)^{-1} \frac{d}{d\theta} \left(\frac{d\sigma}{d\Omega} \right) \cdot \frac{1}{2} \langle \beta_l \rangle, \quad (17)$$

$$\text{where } \langle \beta_l \rangle = \left\langle \left(\frac{-2}{k} \right) e^{-2i\delta_l} \int_0^\infty dr U_l^{(-)*}(r) V_{\text{spin orbit}} U_l^{(+)}(r) \right\rangle.$$

(If one assumes that the deuteron spin-orbit potential is small, then the same result applies at once to the more general case given by eq. (15). Although we do *not* have a proof, it is quite plausible that eq. (17) is approximately correct for the *spin-orbit contribution to P* in the general case. One sees that this is qualitatively correct from examining the results of ref. (15), but the published data do not permit much more than a very rough estimate.)

The origin of the factor of 1/2 in eq. (17) (as opposed to the result of ref. (11) for elastic scattering) comes from the fact that the spin-orbit potential acts on the outgoing wave only.

Qualitatively then one may say that for stripping reactions with $l_n = 0$, a measurement of *P* is approximately the same thing as measuring the proton polarization in the elastic scattering from the final nucleus.

It was early noticed in the numerical calculations involving BUTLER's theory by the use of distorted waves [3, 12] that Coulomb effects and nuclear scattering effects tended to compensate, thus improving the range of applicability of the simpler theory (but no general basis for the cancellation [other than the difference in sign of these potentials] has been given). NEWNS and REFAI [8] gave a qualitative argument to show

*) *Note added in proof:* Recent numerical calculations of Mr. WILLIAM GIBBS for $C^{12}(d, p)C^{13*}$ ($l_n = 0$ case with spin-orbit coupling), indicate good agreement with this "derivative relation", particularly for giving the minima in the polarization.

that absorptive distortion effects on the incident particle tended to cancel absorptive distortion effects on the emergent particle in producing polarization. Recently OKAI [13] and SATCHLER [14] have investigated the origin of this cancellation. It is shown in [14] that if the two conditions: 1) $|\mathbf{k}_p| = |\mathbf{k}_d|$, and 2) $m_p M_f V_{pf} = m_d M_i V_{di}$, hold, then the polarization is *exactly* zero. To understand why this occurs one need only note that the two conditions given are equivalent to eliminating *any* physical distinction—except direction of motion—between the incident and emergent particles, since both have equivalent length scales and equivalent interactions (i.e. same dimensionless strength parameter, and same length scale).

There is, however, now a physical operation which can interchange the role of the two wave functions in the matrix element by interchanging the two directions $\hat{\mathbf{k}}_p$ and $\hat{\mathbf{k}}_d$. This exchange may be accomplished in two steps: 1) a rotation by π about a direction bisecting $\theta = \cos^{-1} \hat{\mathbf{k}}_p \cdot \hat{\mathbf{k}}_d$, and 2) a reversal in the directions $\hat{\mathbf{k}} \rightarrow -\hat{\mathbf{k}}$. These two operations give an invariance operation for the process. But \mathbf{P} reflects under the same process; therefore, \mathbf{P} must vanish. Clearly the vanishing of \mathbf{P} implies that distortions (whether absorptive or not) must give cancelling effects on the polarization. The second condition (above) requires that the deuteron potential, V_{di} , must be about *half as strong* (since $m_p M_f \cong 1/2 m_d M_i$) as that for the proton; since it is usual to take the two potentials to be about of the same strength this supports the general statement that deuteron distortion is the dominant effect in stripping.

For Coulomb effects on the stripping one sees that the second condition is *never* satisfied since this would require $k \eta$ to be the same, whereas $k_d \eta_d = 2 k_p \eta_p$. (It is interesting to note that for the Coulomb field, these two conditions are necessary for the classical limit to exist, as in, for example, Coulomb excitation.)

For $l_n = 0$, stripping calculations using Coulomb distorted 'plane' waves lead to an integral which (for $R = 0$) can be expressed in closed form, and this result can be exploited to give a qualitative understanding of the effects of large Coulomb fields [15]. Unfortunately no similar result can be obtained for $l_n \geq 1$. The best that can be done (without employing series) is the integral for \mathbf{M} given in Appendix V. From this one sees that, *for the special case* $|\mathbf{k}_p| = |\mathbf{k}_d|$, the effect of the Coulomb field is to introduce besides the recoil vector $(\mathbf{k}_d - \mathbf{k}_p)$ a second independent vector: $(\eta_p \mathbf{k}_d - \eta_d \mathbf{k}_p)$ which leads to the result that

$$\mathbf{P} = (\eta_d - \eta_p) (\mathbf{k}_d \times \mathbf{k}_p) f(k_p, k_d, \hat{\mathbf{k}}_p \cdot \hat{\mathbf{k}}_d).$$

This explicitly shows the cancellation of Coulomb distortion effects on

the polarization. Moreover, since $k_d \cong k_p$ implies that $\eta_d = 2\eta_p$ it is clear that the deuteron distortion dominates once again.

With these qualitative results in mind let us look now at some of the numerical results¹³⁾.

Example 1: $B^{10}(d, p)B^{11}$, $Q = 9.24$ MeV, $l = 1$, $j = 3/2$.

The data for this example are taken from the summary of HENSEL and PARKINSON [16] and give the angular distribution of protons for an incident deuteron energy of 8.1 MeV (lab.). The Coulomb parameters are: $\eta_d \cong 0.4$, $\eta_p \cong 0.2$; hence the wave numbers are approximately equal: $k_p \cong k_d$. To carry out a distorted wave calculation the ancillary task of an optical model fit to the elastic deuteron scattering (from B^{10}) and the elastic proton scattering (from B^{11}) must be carried out. These fits (compared to an experiment at approximately the desired energy) are shown in figures 1 and 2. The optical model data are given in table I.

Table I
Parameters characterizing the three examples illustrated

	$B^{10}(d, p)B^{11}$		$Ti^{48}(d, p)Ti^{49*}$	$O^{16}(d, p)O^{17}$
	a	b	c	d
$E_d(\text{MeV})$	8.1	8.1	2.6	19.0
$Q(\text{MeV})$	9.24	9.24	4.46	1.918
l	1	1	1	2
j	3/2	3/2	3/2	5/2
$R(\text{f.})$	5.41	6.15	6.18	3.944
Wood-Saxon well parameters:				
$V_{id}(\text{MeV})$	-60	-50	-44	-40
$W_{id}(\text{MeV})$	-17	-14	-13	-15
$a_{id}(\text{f.})$	0.70	0.68	0.7	0.75
$R_{id}(\text{f.})$	3.66	3.23	5.32	3.8
$V_{fp}(\text{MeV})$	-50	-50	-60	-38
$W_{fp}(\text{MeV})$	-11	-8	-7	-10
$a_{fp}(\text{f.})$	0.4	0.4	0.45	0.5
$R_{fp}(\text{f.})$	2.9	2.9	4.36	3.35

Turning now to the Butler curve (plane waves) first, figure 3, one sees that the shape of the peak is rather well fitted but is quite poor beyond

¹³⁾ Examples 1 and 2 are taken from the paper of W. TOBOCMAN, Phys. Rev. 115, 98 (1959). Example 3 is preliminary, and is taken from the thesis of Mr. WILLIAM GIBBS, Rice Institute (1960), (in preparation). We are indebted to both Dr. TOBOCMAN and Mr. GIBBS for permission to include their examples. (It should be noted that the sign convention used in the paper cited is not explicitly stated, but apparently the $\mathbf{k}_d \times \mathbf{k}_p$ convention is used, judging from the quoted experimental data.)

50°. From the high energy and low Z value one expects the simplest Butler theory to be reasonably applicable although, as suggested by WILKINSON, the relatively high Q value may be a factor opposed to this conclusion.

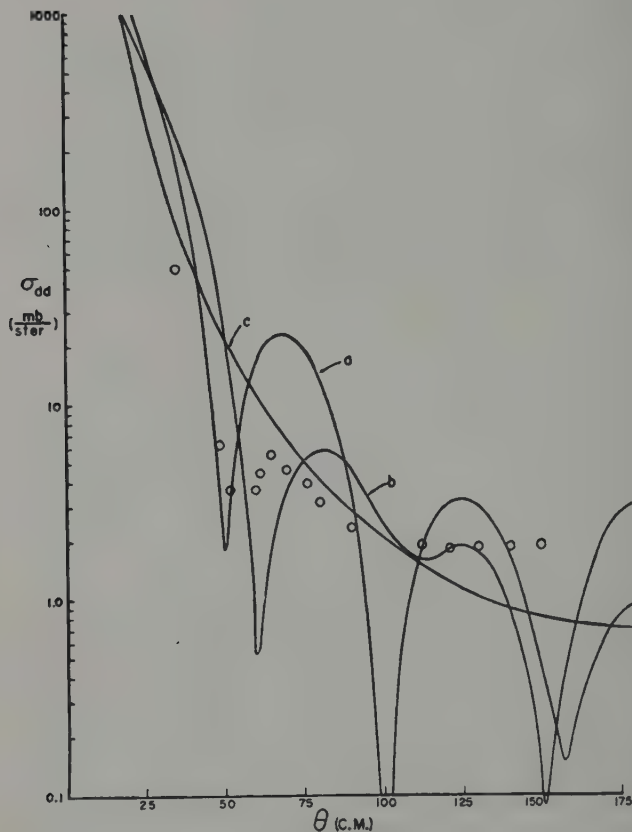


Figure 1

Cross section for the elastic scattering of 8.1 MeV (lab) deuterons on B^{10} . Curves a and b are the cross sections predicted by the potentials a and b given in table I. Curve c is the Rutherford cross section. (The experimental data (circles) are from ref. 16 and represent the elastic scattering of 7.7 MeV (lab) deuterons on Be^9 .)

Introducing now Coulomb effects only we obtain figure 4. Because $\eta_d > \eta_p$; $k_p \cong k_d$; and $j = l + 1/2$ we expect the polarization to be initially positive in the convention adopted. This is borne out by the

numerical results. Note that $P = 0$ at almost precisely the point where the Butler curve has its first zero.

With the optical potentials as well as Coulomb effects, but cutting off the integral at R , we get figure 5. Note that the Coulomb term dominates the (opposing) optical term in the forward direction (as it must) but that otherwise little else can be said about the result in general.

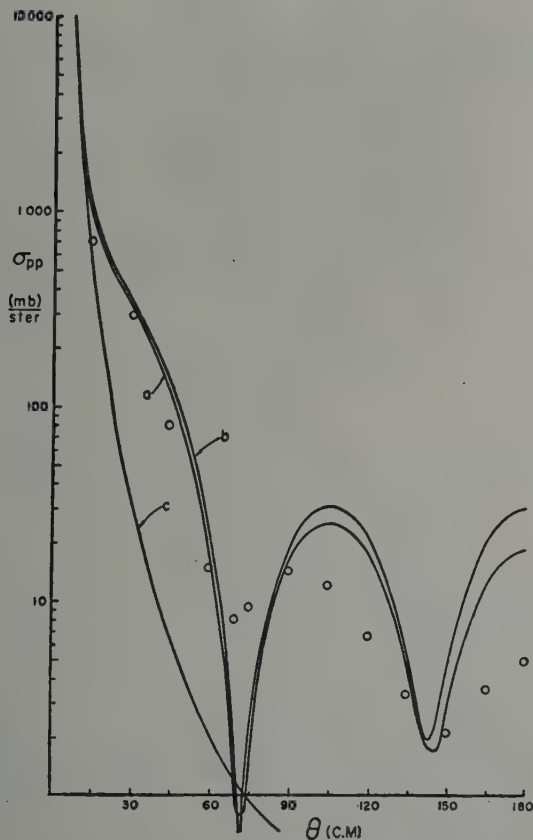


Figure 2

Cross-section for the elastic scattering of 17.44 MeV (lab) protons on B^{11} . Curves a and b are calculated with potentials a and b given in table I. (The circles represent the experimental elastic cross section for 17.0 MeV (lab) protons on B^{10} .)

Finally without cut-off we get figures 6 and 7 for two choices of the deuteron optical potential. The significant points here are 1) the extreme

sensitivity of the polarization in the two cases and 2) the qualitative explanation in terms of cancellation which these potentials suggest. Taking MVR^2 as the appropriate parameter, in case (a) the deuteron to proton parameter is about 4 to 1 and in case (b) about 4 to 3. Thus the latter case should show *less* polarization, which is observed.

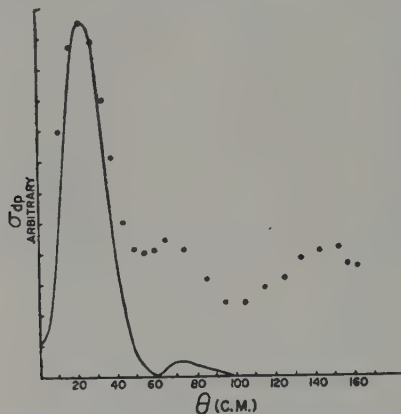


Figure 3

$B^{10}(d, p)B^{11}$ cross section according to the Butler theory for 8.1 MeV (lab) deuterons taking $l = 1$ and $j = 3/2$. (The experimental points are arbitrarily normalized to fit the calculated curve.)

Example 2: $Ti^{48}(d, p)Ti^{49*}$, $Q = 4.46$ MeV, $l = 1$, $j = 3/2$, $R = 6.18 f$.

The angular distribution for 2.6 MeV incident deuterons is taken from PRATT [17]. Figure 8 shows the Butler plane wave curve: this is qualitatively inconsistent with the data. Since this case is chosen to be both low energy and high Z (the Coulomb parameters are $\eta_d \cong 3$, $\eta_p \cong 1.25$), Coulomb effects should be large, and the lack of agreement with a plane wave calculation is to be expected. In figure 9 only the Coulomb effects are introduced, and the fit is improved considerably. Since $k_p \cong k_d$ and $\eta_d > \eta_p$ with $j = l + 1/2$ the polarization should initially be positive as is obtained. Finally in figure 10 the non-cut-off distorted wave theory results are shown, and the agreement seems quite good.

The problem as to whether or not to extend the integrals over the nuclear interior is not clear-cut. In figure 11 we show the effect of various neutron wave functions on the polarization and angular distribution; in figure 12 the corresponding wave functions are shown. The great sensitivity of the results to the interior is disturbing, for stripping is best justifiable as a long range effect.

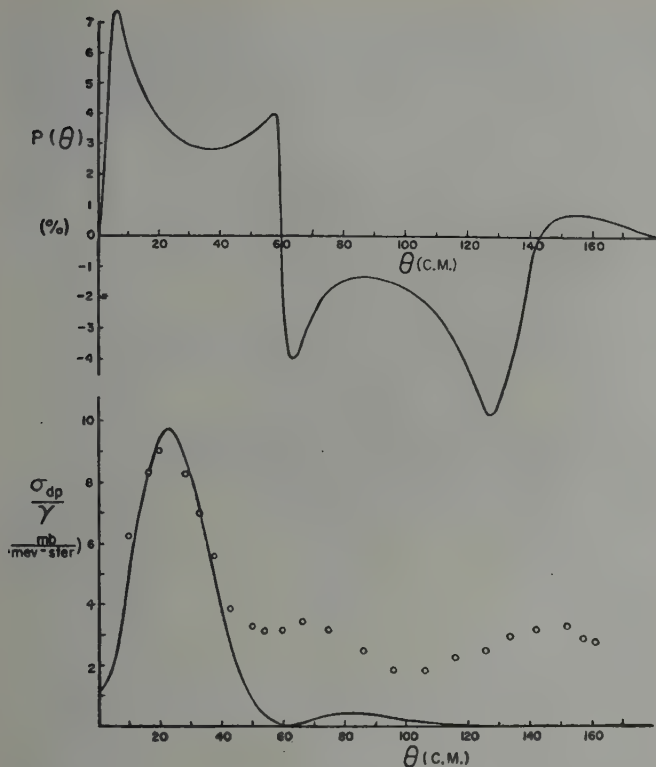


Figure 4

$B^{10}(d, p)B^{11}$ cross section and polarization using the Butler theory modified to include Coulomb effects, with $l = 1$ and $j = 3/2$, 8.1 MeV deuterons.

In this connection it might be well to call attention to an unusual feature of the direct reaction process which has not, to the authors's knowledge, been explicitly discussed¹⁴). Consider the case where the process is at such low energies that the reaction is dominated completely by Coulomb forces. From the asymptotic form of the Coulomb matrix element (as given in Appendix V say, since l is not important in this limit) one can obtain the asymptotic form of the direct reaction cross section. Now for a resonance process, this asymptotic form is simply the product of the two penetration factors, i. e. $\sim e^{-2\pi\eta_d} \cdot e^{-2\pi\eta_p}$. Comparing this to the direct reaction result one may define an enhancement factor (E. F.), i. e., E. F. = Ratio of direct process to resonance process (compound nucleus). One finds that for $E_d \rightarrow 0$, E. F. $\sim \exp \{ \eta f(x) \}$, where $\eta \equiv 4Ze^2 M/\hbar^2 \alpha$ (with α being the reciprocal radius of the

¹⁴) It is implicitly contained, however, in the work of LANDAU and LIFSHITS, J. Exptl. Theor. Phys. 18, 750 (1948); and in the papers of ref. [15].

deuteron ($4.32 f^{-1}$) and $x \equiv k_p \alpha$. The function $f(x)$ is: $f(x) \equiv [(2-x^2)^{1/2} - 1]^{-1} - x^{-1} \tan^{-1} x [2 - (2-x^2)^{1/2}]$. For $Q \rightarrow 0$, E. F. $\rightarrow \exp [2^{1/2}(1+2^{-1/2})^2 \eta_1]$; for $Q \rightarrow \infty$, the enhancement factor becomes $\exp \{\eta_p(4+3\pi)\}$, which approaches 1, as it must. Clearly then, the direct process is considerably enhanced by processes taking place at very large distances, i. e. the deuteron does *not* have to penetrate the barrier to react.

The most striking instance of this occurs for the case where $k_1 \eta_1 = k_2 \eta_2$ (unlike the d, p case). For this case the direct reaction goes as $e^{-2\pi \eta_1 \eta_2}$; in other words for $\eta_1 = \eta_2$ the barrier to the *incoming particle cancels the barrier for the outgoing particle*. Since barriers oppose for either direction this is a surprising, but correct, result¹⁵).

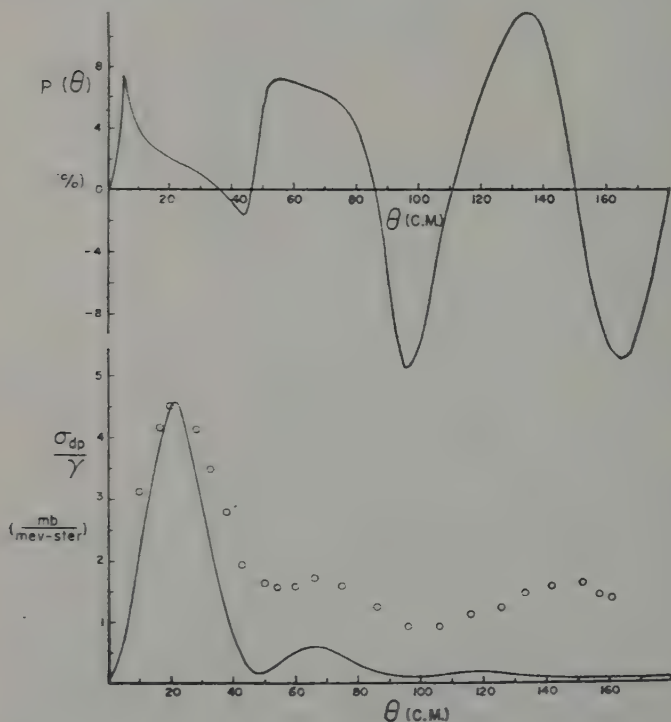


Figure 5

$B^{10} d, p B^{11}$ cross section and polarization using the distorted wave modification of the Butler theory, with cut-off at R . The potentials given in case *a* of table I were used in the calculation.

¹⁵ This effect is well-known in Coulomb excitation, and might be important in, say, Coulomb-induced fission. Data in the barrier inhibited region for protons on U^{235} do not decide for or against such a process. (Unpublished calculations 1956, of R. M. THALER and L. C. BIEDENHARN.)

Example 3: $O^{16}(d, p)^{17}O$, $Q = 1.918$ MeV, $R = 3.944$ f., $l = 2$, $j = 5/2$.

The deuteron energy in this example is 19.0 MeV, and the Coulomb parameters are $\eta_a \cong 0.4$ and $\eta_b \cong 0.25$. Coulomb effects should be quite small. The required fits to the elastic scattering for the deuteron and the

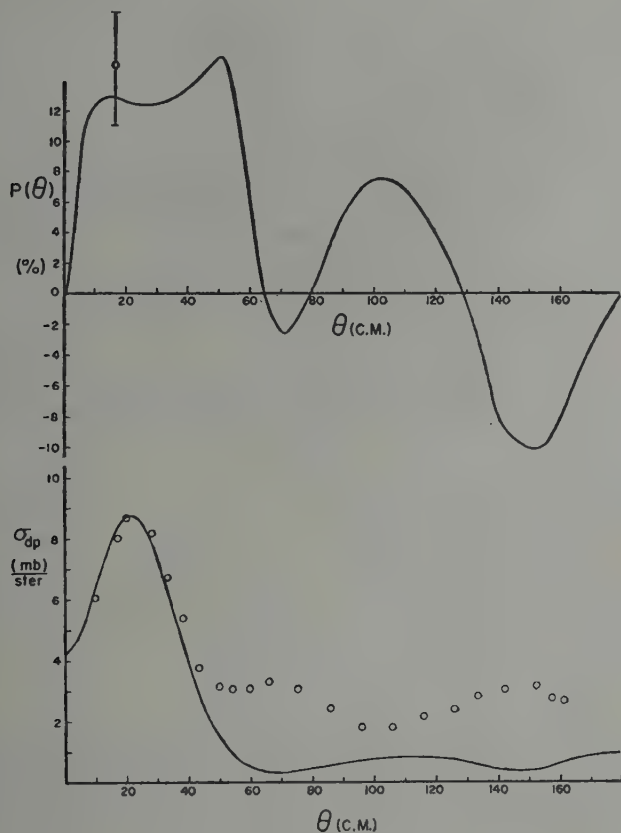


Figure 6

$B^{10}(d, p)B^{11}$ cross section and polarization using the distorted-wave modification of the Butler theory without cut-off. The optical potentials are those of case *a*, table I.

proton are shown in figure 13. The data for the potentials are that for case *d* in table I. The results obtained for the complete distorted wave treatment, with and without cut-off, are shown in figure 14.

The small η approximation discussed in Appendix V ought to be qualitatively applicable to this example (even though the l value is 2). From the results in the appendix one sees that the initial (small θ) polarization due to Coulomb effects can be *negative* for $k_p^2 > k_d^2$ and small k_n^2 , such as obtains in this example. One notes in accord with this that both the cut-off and non-cut-off cases show negative polarization near the forward direction. Note also that in both cases the polarization vanishes almost exactly at the first extremum in the angular distribution.

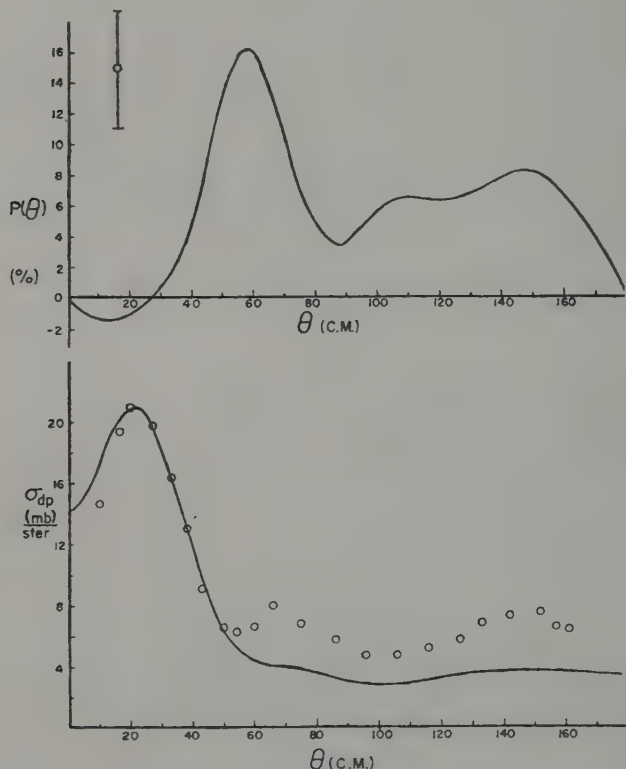


Figure 7

$B^{10}(d, p)B^{11}$ cross-section and polarization using the distorted wave modification of the Butler theory without cut-off. The optical potentials are those of case *b*, table I.

Unlike example 2, where the cut-off greatly varied P but not $(d\sigma/d\Omega)$, this case shows just the opposite behaviour!

To conclude then, it is clear that anything more than a qualitative understanding of the stripping process is a very arduous task. It is equally clear that there is quite a lot of work to be done in this field—experimental, numerical, and theoretical.

Acknowledgements: In the preparation of this paper the authors were greatly helped by many colleagues, in particular Drs. GOLDFARB, IVASH, and TOBOCMAN, and by Messrs. WILLIAM GIBBS and THOMAS GRIFFY.

Appendix I

In the distorted wave Born approximation for stripping reactions the proton polarization (assuming no proton spin orbit coupling) is governed by the angular momentum relations:

$$\mathbf{s}_n + \mathbf{s}_p = \mathbf{s}_d \quad (\text{I-1})$$

$$\mathbf{s}_n + \mathbf{l}_n = \mathbf{j}_n,$$

with the directions of neither \mathbf{s}_d or \mathbf{j}_n being observed.

Using (classical) vectors to represent the angular momenta, one can diagram these relations as shown in figure (I-1).

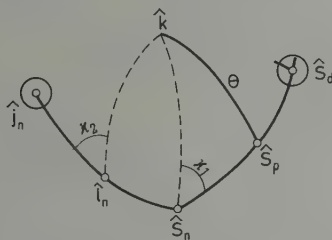


Figure (I-1)

The (classical) angular momentum vectors are represented by their intersection with the surface of a unit sphere with all vectors taken to issue from a common origin. Since $\mathbf{s}_d = \mathbf{s}_n + \mathbf{s}_p$, and $\mathbf{s}_n + \mathbf{l}_n = \mathbf{j}_n$ the representing points for these cases lie along arcs of great circles. The vectors \mathbf{j}_n and \mathbf{s}_d are random (unobserved), and thus the angles χ_1 and χ_2 are random. \mathbf{k} represents an arbitrary direction in space.

Taking an arbitrary axis in space, $\hat{\mathbf{k}}$, the probability that \mathbf{s}_p make an angle (θ, ϕ) with $\hat{\mathbf{k}}$ must be independent of ϕ (cylindrical symmetry), and we, therefore, represent this probability by $W(\theta)$ and develop it as a Legendre series.

$$W(\theta) = \sum_{\nu} \frac{2\nu+1}{2} \langle P_{\nu}(\hat{\mathbf{s}}_p \cdot \hat{\mathbf{k}}) \rangle P_{\nu}(\hat{\mathbf{k}} \cdot \hat{\mathbf{s}}_p). \quad (\text{I-2})$$

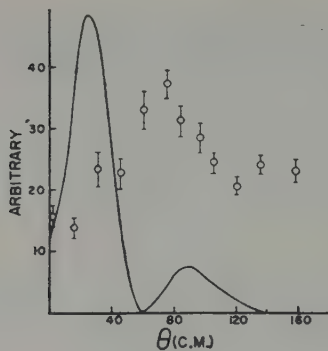


Figure 8

$\text{Ti}^{48}(d, p)\text{Ti}^{49*}$ cross section for 2.6 MeV (lab) deuterons, calculated for the Butler theory with $l = 1$, $j = 3/2$. (The experimental points are arbitrarily normalized.)

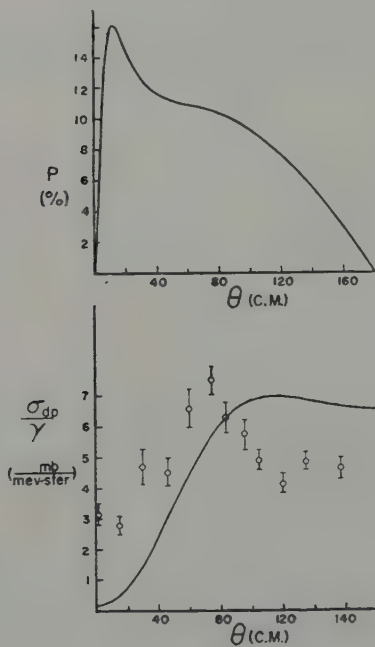


Figure 9

$\text{Ti}^{48}(d, p)\text{Ti}^{49*}$ as in figure 8, except that the Butler theory is modified to include Coulomb effects.

Here $\langle P_\nu \rangle$ represents an average over the random directions of \hat{j}_n and \hat{s}_d . Using the addition theorem to carry out the averages (over χ_1 and χ_2) one finds successively:

$$\begin{aligned} \langle P_\nu (\hat{s}_p \cdot \hat{k}) \rangle &= P_\nu (\hat{s}_p \cdot \hat{s}_n) \langle P (\hat{s}_n \cdot \hat{k}) \rangle \\ &= P_\nu (\hat{s}_p \cdot \hat{s}_n) P_\nu (\hat{s}_n \cdot \hat{l}_n) \langle P_\nu (\hat{l}_n \cdot \hat{k}) \rangle, \end{aligned} \quad (\text{I-3})$$

and hence:

$$W(\theta) = \sum_\nu \left(\frac{2\nu+1}{2} \right) P_\nu (\hat{s}_p \cdot \hat{s}_n) P_\nu (\hat{s}_n \cdot \hat{l}_n) \langle P_\nu (\hat{l}_n \cdot \hat{k}) \rangle P_\nu (\hat{s}_p \cdot \hat{k}). \quad (\text{I-4})$$

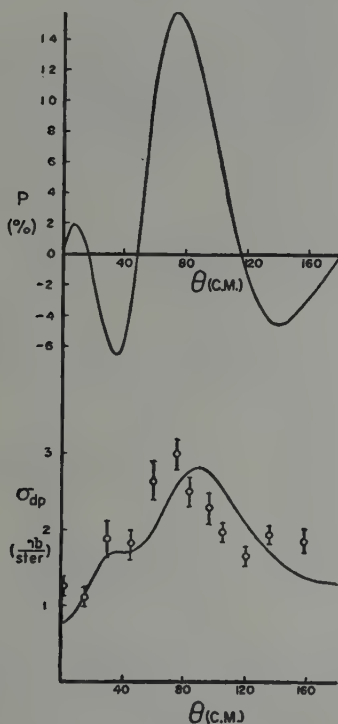


Figure 10

$\text{Ti}^{48}(d, p)\text{Ti}^{49*}$ as in figure 8, except the non-cut-off distorted wave modification of the Butler theory (using the optical potential parameters of case *c*, table I) is employed.

From (I-4) it follows that:

$$\langle P_1 (\hat{s}_p \cdot \hat{k}) \rangle = \langle \hat{s}_p \cdot \hat{k} \rangle = P_1 (\hat{s}_p \cdot \hat{s}_n) P_1 (\hat{s}_n \cdot \hat{l}_n) \langle \hat{l}_n \cdot \hat{k} \rangle,$$

or, since \hat{k} is arbitrary,

$$\langle \hat{s}_p \rangle = P_1 (\hat{s}_p \cdot \hat{s}_n) P_1 (\hat{s}_n \cdot \hat{I}_n) \langle \hat{I}_n \rangle. \quad (I-5)$$

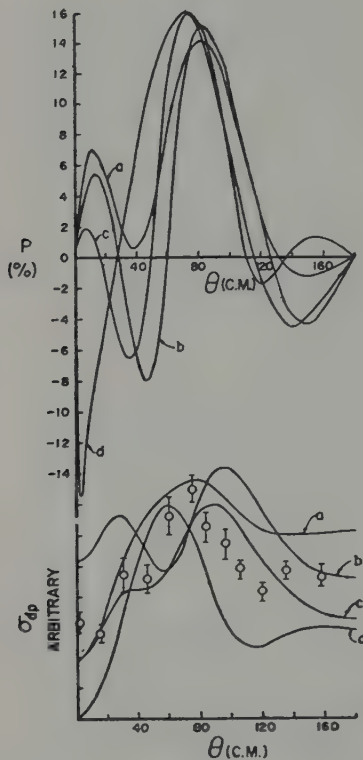


Figure 11

$Ti^{48}(d, p)Ti^{49*}$ as in figure 10, using various choices of the captured neutron wave function. (Note that various scale factors are used in the cross-section curves.)

The neutron wave functions are shown in figure 12.

Replacing the classical quantities in eq. (I-5) by their quantum analogues,

$$(i. e., J \rightarrow \frac{J_{op}}{\sqrt{J(J+1)}} \text{ and } P_\nu (\hat{a} \cdot \hat{b}) \rightarrow (-)^\nu \sqrt{(2a+1)(2b+1)}$$

$$W(a \nu cb; ab) \text{ with } a + b = c).$$

and noting also that the polarization vector \mathbf{P} is defined as the expectation value of \mathbf{s}_p divided by the maximum spin projection, one finds the final result:

$$\begin{aligned}
 P &= \frac{1}{s_p} \cdot \left(\frac{s_p(s_p+1)}{l_n(l_n+1)} \right)^{1/2} \cdot [(-1) \left((2s_p+1)(2s_n+1) \right)^{1/2} W(s_n \ 1 \ s_d \ s_p; s_n \ s_p)] \cdot \\
 &\quad \cdot [(-1) \left((2s_n+1)(2l_n+1) \right)^{1/2} W(s_n \ 1 \ j_n \ l_n; s_n \ l_n)] \cdot \langle \mathbf{l}_n \rangle_{op} = \\
 &= \frac{1}{3} \begin{cases} l_n/(l_n+1) & \text{for } j_n = l_n + 1/2 \\ -1 & \text{for } j_n = l_n - 1/2 \end{cases} \cdot \frac{1}{l_n} \langle \mathbf{l}_n \rangle_{op} = \quad (I-6)
 \end{aligned}$$

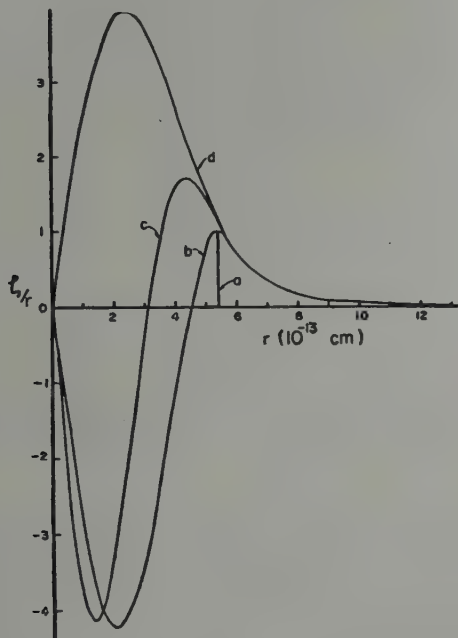


Figure 12

The radial wave functions for the captured neutron used in calculating the results shown in Figure 11.

Appendix II

Using the distorted wave Born approximation ('direct reaction') the angular distribution for the (d, p) reaction is most easily treated in the angular momentum representation, and this leads to a Legendre series

for the proton distribution. This is not a particularly satisfying way to develop the answer—although it seems necessary—for the angular distribution is characteristically peaked at or near the forward direction, and requires (especially for the Coulomb field) a great many terms in the Legendre series. (One might expect that the use of an exact summation of the high l terms could be used to advantage, but this has not yet been carried out except for $l_n = 0$.)

For convenience we make two further approximations: a) a zero range n - p potential and b) we take the target nucleus to be heavy, so that recoil can be neglected.

With these assumptions, the usual techniques [18] lead to the result:

$$\frac{d\sigma}{d\Omega} = \left(\frac{\lambda_a^2}{2s_a+1} \right) \left(\frac{2j_f+1}{2j_i+1} \right) \sum_{\nu} B_{\nu} P_{\nu}(\hat{\mathbf{k}}_p \cdot \hat{\mathbf{k}}_d), \quad (\text{II-1})$$

where:

$$\begin{aligned} B_{\nu} \frac{1}{4} \sum \bar{Z} (l_p j_p l'_p j'_p; s_p \nu) (-)^{j_d-s_d} \\ Z (l_d j_d l'_d j'_d; s_d \nu) (-)^{j_d-s_d} \cdot \\ \cdot (-)^{\nu} [(2j_p+1)(2j'_p+1)(2j_d+1)(2j'_d+1)]^{1/2} W(j'_p \nu j_n j_d; j_p j'_d) \cdot \\ \cdot A_{l_p j_p; l_d j_d}^{l_n j_n} \cdot A_{l'_p j'_p; l'_d j'_d}^{* l'_n j'_n}, \end{aligned} \quad (\text{II-2})$$

and,

$$\begin{aligned} A_{l_p j_p; l_d j_d}^{l_n j_n} = \exp i[\delta(l_p j_p) + \delta(l_d j_d)] C_{0 \ 0 \ 0}^{l_a l_n l_p} \cdot \\ \cdot \sqrt{(2l_n+1)(2s_n+1)} X \left(\begin{matrix} l_d & s_d & j_d \\ l_n & s_n & j_n \\ l_p & s_p & j_p \end{matrix} \right) \cdot G_{l_p j_p; l_d j_d}^{l_n j_n}. \end{aligned} \quad (\text{II-3})$$

In these formulas, the symbols have their usual significance: l = orbital —, s = spin —, j = total — angular momenta; the Z coefficient is defined as in ref. [18] (except that the bar denotes the phase factor is omitted); the δ 's are the phase shifts suffered by the respective proton and deuteron waves; and $C[\dots]$ and $X(\dots)$ denote the Wigner coefficient and $(9-j)$ symbol respectively. The quantity $G[\dots]$ denotes the (cut-off) radial integral over the neutron, proton, and deuteron (considered as a point particle) radial (real) wave functions. This quantity is defined exactly as is the many treatments of the stripping problem in this approximation.

The *structure* of this result, as far as angular correlation effects are concerned, is that of a general (d, p) nuclear reaction in which j_p and j_d play the role of intermediate 'nuclear' states connected by an unobserved 'radiation' of angular momentum j_n . The coefficient $A[\dots]$ plays the role

of the S matrix, and involves a 're-coupling' from $(l-s)$ to $(j-j)$ coupling for the nuclear process.

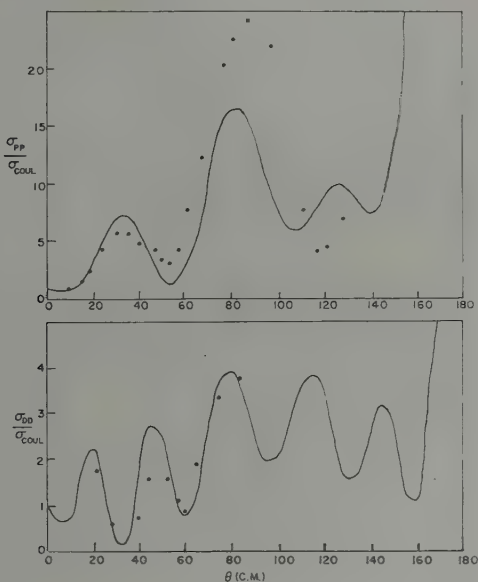


Figure 13

The elastic scattering of 20.9 MeV protons on O^{16} (top curve) and 19.0 MeV deuterons on O^{16} (bottom curve) calculated from the optical potentials listed under case d in table I. (The experimental data are from [19, 20].

The assumption that $l_n = 0$, and that the spin orbit effects on the deuteron may be neglected greatly simplifies the above result. After a little angular momentum algebra, one obtains:

$$\left(\frac{d\sigma}{d\Omega} \right)_{l_n=0} = \left(\frac{\lambda^2_d}{2s_d+1} \right) \cdot \left(\frac{2j_f+1}{2j_i+1} \right) \sum_v B_v(l_n=0) P_v(\hat{\mathbf{k}}_p \cdot \hat{\mathbf{k}}_d),$$

$$B_v(l_n=0) = \left(\bar{Z} \left(l j l j; \frac{1}{2} v \right) \right)^2 A_{lj} A_{lj}^*,$$

$$A_{lj} = e^i \left(\delta_{lj}^{(p)} + \delta_{lj}^{(d)} \right) G_{ij; l}^{0, 1/2}. \quad (\text{II-4})$$

Here l and j refer to the proton's orbital and total angular momentum. Since $l_n = 0$, both l_p and l_d are the same.

Appendix III

To put eq. (12) into the form given by SATCHLER, one needs the identity:

$$C_{00}^{l'l'v} \times \begin{pmatrix} l & j & 1/2 \\ l' & j' & 1/2 \\ v & v & 1 \end{pmatrix} = \frac{(-)^{l'-j'+1/2}}{2 \sqrt{3} v(v+1)} \quad (\text{III-1})$$

$$\cdot [(2j'+1) + (-)^{j+j'+v} (2j+1)] \quad C_{00}^{l'l'v} \times \begin{pmatrix} l & j & 1/2 \\ l' & j' & 1/2 \\ v & v & 0 \end{pmatrix} =$$

$$= \frac{-C_{00}^{l'l'v} W(lj'l'j'; 1/2 v) \cdot [(2j'+1) + (-)^{j+j'+v} (2j+1)]}{2 \sqrt{6} v(v+1) (2v+1)}.$$

Appendix IV

In order to show that the polarization for small spin-orbit coupling is approximately given by the derivative of the angular distribution we assume that eq. (II-4) applies to the process at hand and then use eq. (12) to obtain the polarization.

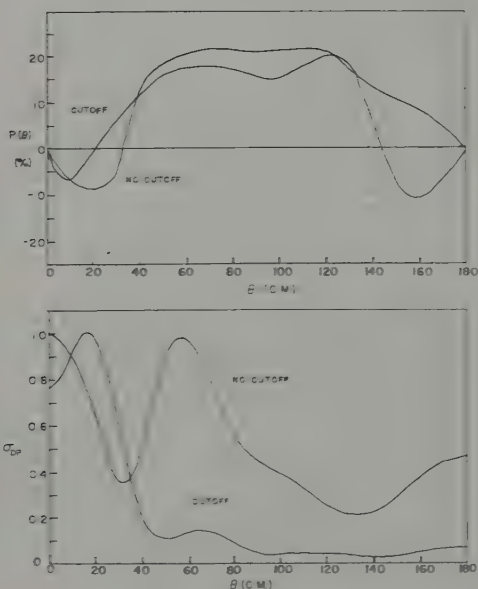


Figure 14

$O^{16}d, pO^{17}$ cross-section and polarization for 19.0 MeV deuterons, calculated from the distorted wave modification of the Butler theory, with and without cut-off.

The various parameters are given under case *d* in table I.)

We further assume that the spin-orbit phase shift splitting is small, so that:

$$A_{lj} \cong e^{i(\delta_l^{(p)} + \delta_l^{(d)})} G_{l,l}^{0,1/2} [1 + (i \Delta \delta_l^{(p)})], \quad (\text{IV-1})$$

with $\Delta \delta_l^{(p)}$ = the spin-orbit proton phase shift splitting

$$= \beta_l \cdot \sqrt{6 l(l+1)(2l+1)} \cdot W(l, 1, j, 1/2; l, 1/2), \quad (\text{IV-2})$$

and

$$\beta_l \equiv -\frac{2}{k} e^{-2i\delta_l} \int_0^\infty dr u_l^{(-)*}(r) V_{\text{spin}}(r) u_l^{(-)}(r). \quad (\text{IV-3})$$

(This definition of β_l is chosen to agree exactly with that used by ROBERG. His choice of radial wave function (in IV-3) differs from ours in that the phase shift $e^{i\delta_l}$ is included.)

(It should be noted explicitly that eq. (IV-1) *assumes* that the radial matrix elements $G_{l,l}$ are *not* effectively different with or without the spin orbit coupling. This assumption seems reasonable in itself, but is actually better than may appear since the variation in G is *real*, and thus leads to only off-diagonal contributions which are small under the same assumption that β_l is slowly varying in l .)

Inserting (III-1, 2) into eq. (12), (using (II-4) for the definition of B_v) one finds for the polarization the expression:

$$\begin{aligned} P(\theta) = & \hat{n} \frac{\lambda_d^2 (2j_f + 1)}{(2s_d + 1)(2j_i + 1)} \left(\frac{d\sigma}{d\Omega} \right)^{-1} \sum_{l,l'} 2 e^{i[\delta_l^{(p)} + \delta_l^{(d)} - \delta_{l'}^{(p)} - \delta_{l'}^{(d)}]} \\ & \cdot \frac{1}{4} \left(G_{l,l}^{0,1/2} \right)^2 \beta_l \sqrt{6 l(l+1)(2l+1)} \left(C_{00}^{l,l^0} \right)^2 (2l+1)(2l'+1) \\ & \cdot \frac{d}{d\theta} (P_v(\cos\theta)) \sqrt{\frac{6(2v+1)}{v(v+1)}} \left\{ \sum_{j,j'} (-)^{v-l'-j'-1/2} (2j+1)(2j'+1) \right. \\ & \cdot X \left(\begin{matrix} l & j & 1/2 \\ l' & j' & 1/2 \end{matrix} \right) W \left(l, j, l', j'; \frac{1}{2}, v \right) W \left(l, 1, j, \frac{1}{2}; l, \frac{1}{2} \right) \Big\}. \end{aligned}$$

$$(\text{This employs the result that } -dP_v/d\theta = P_v^{(1)}.) \quad (\text{IV-4})$$

The bracketed sum in eq. (IV-4) may be carried out using the various sum rules given in ref. [18]. The result is:

$$\left\{ \dots \right\} = \frac{1}{3} W(l, 1, l', v; l, v). \quad (\text{IV-5})$$

Inserting this result (in its explicit algebraic form) in eq. (IV-4) one finds the desired result:

$$P(\theta) = \hat{n} \left(\frac{d\sigma}{d\Omega} \right)^{-1} \frac{\hat{\lambda}_d^2 (2j_f + 1)}{(2s_d + 1)(2j_i + 1)} \cdot \frac{d}{d\theta} \sum_{\nu l l'} \cdot \beta_l \left[\frac{1}{4} (2l + 1)(2l' + 1) \left(C_{00}^{l l' \nu} \right)^2 A_l A_l^* P_\nu(\cos \theta) \right]. \quad (\text{IV-6})$$

If we assume, following RODBERG, that it is justified to regard β_l as slowly varying with l so that $\beta_l \cong \langle \beta_l \rangle$ then one finds that (IV-6) takes the form:

$$P(\theta) \cong \frac{1}{2} \hat{n} \langle \beta_l \rangle \frac{d}{d\theta} \left(\frac{d\sigma}{d\Omega} \right) / \frac{d\sigma}{d\Omega}. \quad (\text{IV-7})$$

(The further approximation that $\langle \beta_l \rangle \cong -\frac{mR}{\hbar^2 k} V_{so}(R)$,

as given in ref. [11], may be of value in obtaining a rough estimate of the spin orbit potential.)

Appendix V

If, in addition to the usual approximation of the direct reaction process with a zero range $n-p$ potential, one neglects all except Coulomb distortions and takes the nucleus to have $R_n = 0$, the stripping integral may be written in the form (for $l_n = 1$):

$$M = \int d^3 r \hat{r} h_1(i k_n r) \psi_p^*(r) \psi_d(r)$$

where:

$$\psi_p^*(r) = \left(\frac{2\pi\eta_p}{e^{2\pi\eta_p} - 1} \right)^{1/2} e^{-i\mathbf{k}_p \cdot \mathbf{r}} {}_1F_1(-i\eta_p, 1; i(\mathbf{k}_p r + \mathbf{k}_p \cdot \mathbf{r}))$$

$$\psi_d(r) \equiv \left(\frac{2\pi\eta_d}{e^{2\pi\eta_d} - 1} \right)^{1/2} e^{i\mathbf{k}_d \cdot \mathbf{r}} {}_1F_1(-i\eta_d, 1; i(\mathbf{k}_d r - \mathbf{k}_d \cdot \mathbf{r})). \quad (\text{V-1})$$

(All factors independent of $k_p, k_d, \eta_p, \eta_d, k_n$ have been eliminated.)

The approximation that $R_n = 0$ is made for convenience, so that SOMMERFELD's techniques may be applied to evaluating this integral. This approximation is of little importance when the reaction is Coulomb-limited; for cases where this is not applicable a rapidly convergent series for the contribution from $0 \leq r \leq R_n$ may be subtracted explicitly from the result in eq. (V-1). The usefulness of the results given below (or in ref. [15] for $l_n = 0$) lies in the fact that the contributions for large values of r and l are treated concisely.

With the application of SOMMERFELD's techniques this integral may be written as:

$$\begin{aligned} \mathbf{M} = & (16 \pi^2 i) \left[\frac{\eta_p \eta_d}{(e^{2\pi \eta_p} - 1)(e^{2\pi \eta_d} - 1)} \right]^{1/2} \\ & \cdot \int_{k_n}^{\infty} ds (s^2 + k_p^2 + k_d^2 - 2 k_p k_d \cos \theta)^{-1-i\eta_p-i\eta_d} \\ & \cdot (k_d + k_p + is)^{-1+i\eta_p+i\eta_d} (k_d - k_p - is)^{-1-i\eta_p} \\ & \cdot (k_p - k_d - is)^{-1+i\eta_d} \{ \dots \}, \end{aligned} \quad (\text{V-2})$$

$$\begin{aligned} \{ \dots \} \equiv & \left\{ \left[\frac{s^2 + (k_d - k_p)^2}{s^2 + (k_d - k_p)^2} (1 + i\eta_p + i\eta_d) (k_p + k_d + is) (k_d - k_p) + \right. \right. \\ & + s (\eta_p k_d - \eta_d k_p) + i (k_p - k_d) (\eta_d k_p + \eta_p k_d) \Big] F + \\ & + 2 \left[(k_p k_d - k_d k_p) + \frac{2 k_p k_d \sin^2 \frac{\theta}{2}}{s^2 + (k_d - k_p)^2} \times \right. \\ & \left. \left. \times i s (k_p - k_d) + (k_p - k_d) (k_p + k_d) \right] F' \right\}, \end{aligned} \quad (\text{V-3})$$

where:

$$F = {}_2F_1(-i\eta_p, -i\eta_d, 1; \left(\frac{-4 k_p k_d \sin^2 \frac{\theta}{2}}{(k_p - k_d)^2 + s^2} \right)),$$

and

$$F' \equiv \frac{d}{d\pi} ({}_2F_1(a, b, c; x)). \quad (\text{V-4})$$

Although this integral is hardly simple, nonetheless it does present certain information. For example, when $|\mathbf{k}_p| = |\mathbf{k}_d|$ there are but two combinations of the vectors \mathbf{k}_p and \mathbf{k}_d that enter: $(\mathbf{k}_d - \mathbf{k}_p)$ and $(\eta_p \mathbf{k}_d - \eta_d \mathbf{k}_p)$. From this one sees that the polarization varies as $(\eta_d - \eta_p) (\mathbf{k}_d \times \mathbf{k}_p)$ and is thus dominated by the deuteron distortion. (The special case where $k_p = k_d$ is amenable to further reduction, but these results will be given elsewhere.)

Since the integral \mathbf{M} decreases essentially exponentially as k_n increases, it is clear also that the integration over s is in effect only the definition of an average value of k_n . Qualitatively then, one may simply dispense with the integral and take $s = \langle k_n \rangle$. Next one notes that $F' \approx \eta^2$ while $F \approx 1$ so that $\{ \dots \}$ may, for small η , be approximated by the first [...] bracket. With these simplifications one obtains for the polarization:

$$P \cong \frac{2}{3} \hat{n} \begin{Bmatrix} 1/2 \\ -1 \end{Bmatrix} \sin \vartheta \left(\frac{k_n^2 + (k_d - k_p)^2}{k_n^2 + (k_d - k_p)^2 + 4k_p^2 \sin^2 \frac{\vartheta}{2}} \right) \frac{1}{|\{\dots\}|^2} \cdot$$

$$\cdot [k_n^2 (\eta_d - \eta_p) + (k_p^2 - k_d^2) (\eta_d + \eta_p)]. \quad (\text{V-5})$$

(small η approximation)

(the bracket $\{\dots\}$ in (V-5) is the same as in (V-3); for $k_p = k_d$ and $\theta \rightarrow 0$, the terms $\theta(\eta^2)$ must be kept in the denominator).

One sees from this approximate result that the polarization is positive (parallel to $\mathbf{k}_d \times \mathbf{k}_p$) for $k_d \approx k_p$, but can become negative as k_p gets sufficiently greater than k_d . In general, one would expect this approximate result to be qualitatively valid in the forward direction, and the examples discussed seem to bear this out.

REFERENCES

- [1] S. T. BUTLER, Proc. Roy. Soc. (London) *A* 208, 559 (1951).
- [2] R. HUBY, *Progress in Nuclear Physics* 3, 177 (1953); W. TOBOCMAN, *Deuteron Stripping Reactions*, U. S. Naval Research Lab. Report (1955) (unpublished); *ibid.*, Case Inst. of Technology Report, No. 29 (1956) (unpublished); S. T. BUTLER and O. H. HITTMAN, *Nuclear Stripping Reactions*, (John Wiley and Sons, Inc., New York 1957); G. R. SATCHLER, *Analysis of Deuteron Stripping Experiments* (1958) (unpublished); N. AUSTERN, Chap. V. D. of *Fast Neutron Physics* (J. L. Fowler and J. B. Marion, Interscience, New York 1961).
- [3] J. HOROWITZ and A. M. L. MESSIAH, J. Phys. Rad. 15, 142 (1954).
- [4] BIEDENHARN, BOYER and CHARPIE, Phys. Rev. 86, 619 (1952); and independently by L. J. GALLAHER and W. B. CHESTON, Phys. Rev. 88, 684 (1952); and by G. R. SATCHLER and J. A. SPIERS, Proc. Phys. Soc. (London) 65A, 980 (1952).
- [5] H. C. NEWNS, Proc. Phys. Soc. (London) 66A, 477 (1953).
- [6] L. C. BIEDENHARN, Chap. V.C in *Nuclear Spectroscopy*, (F. Ajzenberg-Selove, Academic Press, New York 1960).
- [7] G. R. SATCHLER, Nucl. Phys. 8, 65 (1958), and references given there.
- [8] H. C. NEWNS and M. Y. REFAI, Proc. Phys. Soc. (London) 71, 627 (1958); W. B. CHESTON, Phys. Rev. 96, 1590 (1954).
- [9] L. C. BIEDENHARN and M. E. ROSE, Rev. Mod. Phys. 25, 729 (1953); G. R. SATCHLER, Proc. Phys. Soc. A, 118, 1041 (1955).
- [10] M. E. ROSE and L. C. BIEDENHARN, O.R.N.L. 1779, (September 1954) (unpublished).
- [11] LEONARD S. RODBERG, Nucl. Phys. 15, 72 (1960).
- [12] W. TOBOCMAN and M. H. KALOS, Phys. Rev. 97, 132 (1955); J. L. RICHTER and E. V. IVASH, Phys. Rev. 111, 245 (1958); I. B. TEPLOV and B. A. YURIEV, J.E.T.P. 34, 334 (1958); W. TOBOCMAN, Phys. Rev. 115, 98 (1959).
- [13] S. OKAI, Prog. Theor. Phys. 22, 620 (1959).
- [14] G. R. SATCHLER, Nucl. Phys. 18, 110 (1960).

- [15] K. A. TER-MARTIROSYAN, Zhur. Eksptl. i Teort. Fiz. 29, 713 (1955); BIEDENHARN, BOYER, and GOLDSTEIN, Phys. Rev. 104, 383 (1956); J. SAWICKI, Bulletin de l'Academie Polonaise des Sciences, III, 313 (1955).
- [16] J. C. HENSEL and W. C. PARKINSON, Phys. Rev. 110, 128 (1958).
- [17] W. W. PRATT, Phys. Rev. 97, 131 (1954).
- [18] J. M. BLATT and L. C. BIEDENHARN, Rev. Mod. Phys. 24, 258 (1952); L. C. BIEDENHARN, J. M. BLATT and M. E. ROSE, Rev. Mod. Phys. 24, 249 (1952); S. DEVONS and L. J. B. GOLDFARB, Handb. der Phys., Vol. 40 (1959).
- [19] R. H. CHOW and B. T. WRIGHT, Can. J. Phys. 35, 184 (1957).
- [20] FREEMANTLE, GIBSON, PROWSE, and ROTBLAT, Phys. Rev. 92, 1268 (1953).

Selection Rules for Polarization in Direct Interactions and Stripping Processes

By L. J. B. GOLDFARB, Department of Theoretical Physics,
The University, Manchester, England

There exists, by now, quite a variety of direct nuclear reactions. Of these, the most extensively studied is deuteron stripping and its associated pick-up process. Recent studies have been concerned with the stripping of two nucleons, He^3 or H^3 , and pick-up phenomena such as (p, α) , (d, α) , (He^3, α) . Then, there is the phenomenon of heavy-particle stripping where the target nucleus is stripped instead of the projectile. Finally, we have the inelastic scattering of nucleons or heavier particles. All these processes are termed direct so as to create a distinction, with the competitive processes that go by compound-nucleus formation. For these latter reactions, in principle, we need many parameters to give a proper description of the many degrees of freedom of the nuclear system. In contrast to this, direct interactions are typified by very few parameters. These essentially are the quantum numbers associated with a transfer of angular momentum and energy between the system of incoming and outgoing projectiles and that of the target and residual nuclei. If the process is to be easily handled, we expect only a few quantum numbers to play any significant role.

It is convenient for our purposes to illustrate the processes by means of angular-momentum graphs,

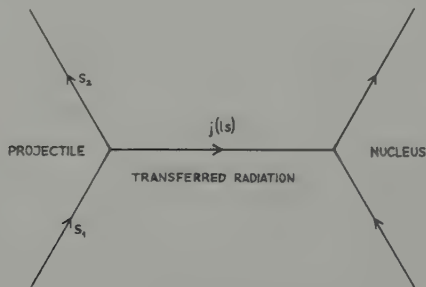


Figure 1

e.g. for d - p processes $s_1 = 1$ and $s_2 = s = 1/2$. The transferred radiation consists of neutrons. On the other hand, for inelastic scattering, there is no exchange of real particles. Rather, the interaction operator can be made to factorise into a part acting on the nuclear configuration and another part acting on the projectile system. These factors are tensors, contragredient to each other, which behave under rotations just like angular-momentum operators. The quantities j , l and s , in fact, incorporate the properties of these tensors under rotation.

To deal with the de-excitation of the residual nucleus, we alter our diagram

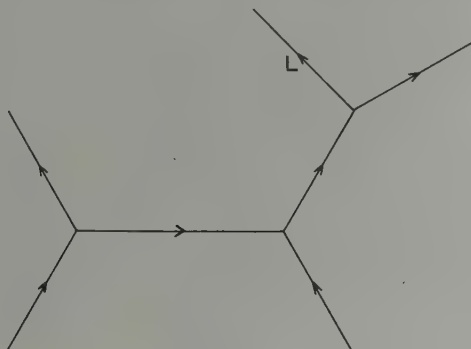


Figure 2

so that L denotes the multipolarity of the γ -radiation.

In principle, measurement of the angular correlations here serves as a measure of the polarization state of the residual nucleus. To typify polarization measurements of the projectiles, we alter the diagram symbolically by breaking up the angular-momentum states of the projectiles into those of orbital angular momentum and intrinsic spin.

It is possible to handle all these possibilities in a systematic fashion by means of the modern analytical techniques of dealing with angular-momentum decoupling, and since these diagrams can be made to apply to all the direct processes, we can treat these together.

The earliest calculations were done in Born approximation. Although, in many cases, particularly in stripping, the angular distributions were well-approximated, the same does not hold for polarization. As is well-known, the Born approximation predicts zero polarization in contrast to large values obtained by more accurate procedures.

These procedures involve use of the distorted-wave Born approximation, where the interactions between the projectiles and nuclei in the incident and outgoing channels are approximated by the use of

optical-model potentials, derived from a study of elastic scattering. However, if one ignores the spin-orbit term in the potential, one finds several restrictive rules for polarization. Thus, as originally found by SATCHLER for deuteron-stripping, second-rank (i.e. tensor) polarization of the deuteron gives rise to no asymmetry in the angular distribution. Also the effects of 1st rank (i.e. vector) polarization are directly correlated to the polarization that would be measured in an identical experiment but where the incoming deuteron-beam is unpolarized. Finally, if $l=0$, we get no polarization nor effects of polarization. This is independent of the complication of the distortion, so long as this distortion is spin-independent.

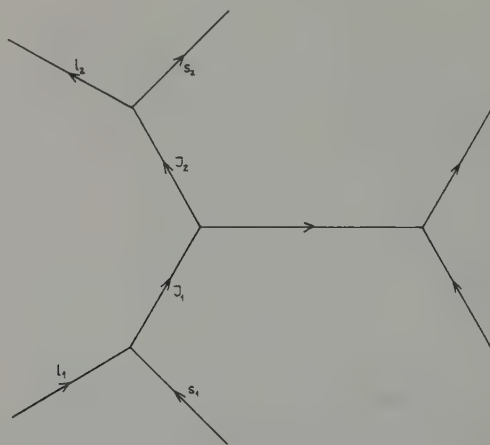


Figure 3

Calculations in this approximation require very elaborate computing programs and for this reason the progress to-date is restricted. TOBOCMAN recently reported the results of some of his analyses of several deuteron stripping processes where he finds in certain cases significant contributions to the cross-sections and, in particular, polarization through the introduction of distorted waves. The same sensitivity has been noticed in numerical calculations of inelastic nucleon scattering. TOBOCMAN ignores the spin-orbit part of the distorting potential in the belief that its magnitude is small compared to the central part, so that its effect should be minor. Still, one should be careful with such a procedure since it is not clear that the effect of the spin-orbit contribution should be the same in elastic scattering and in the quite-different stripping problem. Because of the sensitivity of the polarization to the distortion, it would seem to be safe practice to try and relate the parameters as close as it is possible to

those established by the elastic scattering analyses. The complications, of course, that are added to the computation are great, and would require elaborate use of electronic computers.

I'd like to mention in this context, some calculations we did with BROWN and CASTILLEJO from Birmingham, concerning the inelastic scattering of protons by Ni^{58} for various energies about 9 MeV and higher. Polarization would vanish in the absence of a spin-orbit potential term in the distortion; yet by including this relatively insignificant term, we found polarizations which for certain angles exceeded 50%. At higher energies ~ 15 MeV, polarizations greater than 75% were found.

With this sensitivity of polarization to the spin-dependent distortion in mind, we have arrived at general expressions for angular distributions and polarization for arbitrary types of beams. Certain general rules are obtained which depend on the presence of this distortion.

We deal with a general process with spins s_1 and s_2 for the projectiles and s for the transferred radiation. We make the idealisation that in dealing with composite particles, there is no coupling of the spin to the internal configuration of the particle. This refers to the projectiles or the transferred radiation. Thus, for example, we ignore contributions from the d -state of the deuteron. Also, we ignore any spin-dependence of the direct-reaction potential. This restriction which is not meant to apply to inelastic scattering, is not too serious since to-date only the crudest types of direct interactions have been used, viz., delta-function interactions in coordinate space.

In general, no selection rules are apparent. Of interest, though from the point of view of numerical computation, is the fact that the angular dependence is best expressed in terms of the elements of the rotation matrix, $D_{\lambda\lambda'}^l(0, \theta, 0)$, and not the usual spherical harmonics. This is associated with the introduction of spin-orbit contributions and applies both to cross sections and to polarization. We consider either measurement of the outgoing polarization using unpolarized incident beams, or the asymmetries arising from incident polarized beams. We then limit the spin-dependent distortion to either incoming or outgoing stage or to neither stage.

A particle of spin s has polarization tensors of rank k ranging from 0 up to $2s$. If we let k_1 denote the rank of the incident polarization that is being measured and k_2 that of the outgoing polarization that will be measured, then our first general result is that for no spin-dependent distortion $k_1, k_2 \leq 2l_{\max}$ or $2s_{\max}$ e.g. $l = 0$, gives us neither polarization nor effects of polarization.

Treating $l = 0$, and letting spin-dependent distortion enter in the incoming stage, we find $k_2 \leq 2s_1$, while if it acts only in the outgoing stage, $k_1 \leq 2s_2$. This is all represented in the following table.

Table

No spin-dependent distortion	Spin-dependent distortion of	
	incoming beam only	outgoing beam only
$k_1, k_2 \leq 2 s_{max}$ $\leq 2 l_{max}$		
$(l = 0): k_1 = k_2 = 0$	$k_2 \leq 2 s_1$	$k_1 \leq 2 s_2$
<i>Deuteron stripping</i>		
$(l \neq 0): A = 1 + 3 P_{in} P_{out}$ $(l = 0): = 1$	$1 + P_{in} P_{out}$	$1 + 3/2 P_{in} P_{out}$
$ P_{out} \leq 1/3$ $\leq 1/3(l+1)$ $j = l - 1/2$ $j = l + 1/2$	$ P_{out} \leq 1$	
<i>(He³, p)-(H³, p)-processes etc.</i>		
$(s = 0): A = 1$ $(s = 1) (l \neq 0): = 1 - P_{in} P_{out}$ $(l = 0): = 1$	$1 + P_{in} P_{out}$ $1 - 3 P_{in} P_{out}$	$1 + P_{in} P_{out}$ $1 - 1/3 P_{in} P_{out}$
$(s = 0): P_{out} = 0$ $(s = 1): P_{out} \leq l/(l+1)$ $\leq 1/(l+1)$ ≤ 1 $j = l + 1$ $j = l$ $j = l - 1$		
<i>(α, p)-processes</i>		
$(l \neq 0): P_{out} \leq 1$ $\leq l/(l+1)$ $(l = 0): P_{out} = 0$ $j = l - 1/2$ $j = l + 1/2$		
<i>(α, d)-processes</i>		
$ P_{out} \leq l/(l+1)$ $\leq 1/(l+1)$ ≤ 1 $j = l + 1$ $j = l$ $j = l - 1$		
<i>Inelastic nucleon-scattering</i>		
$A \approx 1 + P_{in} P_{out}$	assuming spin-dependent distortion of incoming and outgoing beam.	

Thus, for deuteron stripping, there are no second rank effects with no spin-orbit distortion for arbitrary l since $s = 1/2$, while if $l = 0$, polarization effects do not show up for no spin-distortion. If, however, there is a spin-dependent distortion acting only on the nucleon, polarization effects occur but these are again limited to first rank only.

Correlations between polarizations can also be established. Suppose in deuteron-stripping, P_{in} is the incident deuteron polarization of 1st rank

normal to the plane of the process. Then the angular distribution is

$$\frac{d\sigma}{d\Omega} = \left(\frac{d\sigma}{d\Omega}\right) A = \left(\frac{d\sigma}{d\Omega}\right)_0 [1 + 3 P_{in} P_{out}], \quad \text{where } \left(\frac{d\sigma}{d\Omega}\right)_0$$

is the unpolarized cross-section, and A , the correlation, takes on the value $1 + 3 P_{in} P_{out}$ for no spin-dependent distortion. The coefficient, P_{out} , is the outgoing polarization as measured in another experiment under identical conditions, except for an unpolarized incident beam. Thus, if in one experiment the incoming polarization is P_{in} , in the other experiment, the left-right asymmetry is equal to $3 P_{in}$. The correlation A for $l = 0$ and spin-dependent distortion in the incoming or outgoing stage or in neither takes on the values $1 + P_{in} P_{out}$, $1 + 3/2 P_{in} P_{out}$, or 1 respectively.

It is clearly of interest, then to examine polarization of $l = 0$ stripping processes.

As already pointed out, the outgoing polarization is never greater than $1/3$ for no spin-dependent distortion (actually only for $j = l - 1/2$, but for $j = l + 1/2$, $|P_{out}| \leq 1/3 l/(l+1)$). This limitation is removed if the distortion is generalised.

Several selection rules obtain when we treat the stripping of two nucleons e.g. (He^3, p) , (H^3, p) etc. Here, $s = 0$ or 1 , although for H^3 , processes we expect only $s = 0$. First consider $s = 0$. Then in the absence of spin-dependent distortion, no polarization effects occur at all, while if this type of distortion acts on only one stage, the correlation function is $A = 1 + P_{in} P_{out}$. This is for arbitrary l .

For $s = 1$, polarization is present even in the absence of spin-dependent distortion where in this case $A = 1 - P_{in} P_{out}$ except that $l = 0$ again gives us no polarization. With $l = 0$ and $s = 1$ and spin-dependent distortion in the incoming or outgoing stage only $A = 1 - 3 P_{in} P_{out}$ or $1 - 1/3 P_{in} P_{out}$ respectively. Again for $s = 1$ and single j and l , then $|P_{out}| \leq l/(l+1)$, $1/(l+1)$, 1 according as $j = l+1$, l , $l-1$ in the absence of spin-dependent distortion.

Furthermore, we no longer necessarily have incoherence over l and s . In all these processes, the summation over j is incoherent, so long as we do not measure the polarization state of the target or residual nuclei. The summation over l is also incoherent for deuteron stripping since $l = j \pm 1/2$ and if two l 's interfere and differ by one, they involve a different parity change for the nuclear system which is not possible. However if $s = 1$, $l = j \pm 1$, j and the l 's can differ by two and contribute coherently. This coherence occurs only if the distortion is spin-dependent.

We can continue our observations and refer to (α, d) , (α, He^3) (α, p) processes. Polarization occurs for $l = 0$, only as a consequence of spin-dependent distortion; but for $l \neq 0$, it occurs without this type of distor-

tion. Also for (α, d) processes the summation over l is generally coherent. In the absence of spin-dependent distortion $|P_{out}| \leq \frac{l(l+1)}{1}$ for (α, p) , (α, He^3) processes according as $j = l + 1/2$ or $l - 1/2$ as found by SATCHLER. For (α, d) processes $|P_{out}| \leq l/(l+1)$, $1/(l+1)$, 1 according as $j = l+1$, l , $l-1$.

Now all these rules, except for the question of coherence in l apply whether or not parity is conserved or time-reversal invariance holds. If we invoke time-reversal invariance, then we get an interesting result for inelastic scattering of nucleons. We find that A is approximately $1 + P_{in} P_{out}$. The difference arises in the radial integration that is involved. The outgoing polarization differs from the asymmetry in that the optical-model eigenfunctions appear in an identical fashion, except for a switching of energies. If the incoming and outgoing optical-model eigenfunctions describing the distortion are not too sensitive to the difference of incoming and outgoing energies, the above result holds. In the limit of no energy loss, we have true equality and the result (called for nucleon-nucleon scattering the polarization-asymmetry theorem) is independent of parity conservation. The same holds true for inelastic scattering. Of practical importance, is the fact that we get little new information by bringing in polarized nucleons as compared to that obtained by measuring the outgoing polarization, since the effects are almost completely correlated.

Finally some remarks about γ -correlations. We find that although correlation studies can give a great deal of independent information, such measurements with $l = 0$ and $s = 0$ or $1/2$ give no information at all if the γ -radiation is of sharp parity. On the other hand if $l \neq 0$, we get contributions with a coherent summation over j and l even if $s = 0$ or $1/2$. In certain cases observation of the complexity of the angular correlation, i.e. the largest value of k in the expansion in terms of $P_k(\cos\theta)$, can single out effects due to $s = 1$, for example in the (He^3, p) processes.

Elastic Scattering of Deuterons by He^4 ¹⁾

By J. L. GAMMEL, B. J. HILL²⁾, and R. M. THALER³⁾

Los Alamos Scientific Laboratory

Abstract. A model of the $d + \text{He}^4$ interaction is developed and compared to the data on the ground state of Li^6 and the $d + \text{He}^4$ elastic scattering data up to 4.5 MeV (deuteron laboratory energy). New phase shift analyses of the 8 and 10.3 MeV elastic scattering data are made, and quantities relevant to the production or analysis of beams of polarized deuteron calculated.

I. Introduction

A model of the $d + \text{He}^4$ interaction is developed. The model is in agreement with the ground state properties of Li^6 as deduced by FOLDY [1]⁴⁾ from the γd reaction in Li^6 . Phase shifts calculated from this model are in agreement with phase shifts found in GALONSKY and McELLI-STREM's [2] analysis of GALONSKY *et al.*'s [3] experimental data on elastic $d + \text{He}^4$ scattering in the energy range up to 4.5 MeV (laboratory deuteron energy). Phase shifts calculated from the model make it possible to extend the phase shift analysis to the experimental data of ALLRED *et al.* at 10.3 MeV, and BURGE *et al.* at 8 MeV [4]. From the phase shifts for 8 and 10.3 MeV, we have calculated the quantities relevant to experiments designed to produce or analyze beams of polarized deuterons.

II. The Model

We reduce the problem to a three body problem by treating He^4 as a 'fundamental particle' or 'lump', and imagining the nucleons in the deuteron to interact with He^4 'lump' via the nucleon- He^4 optical model potential [5] and with each other via the nucleon-nucleon potential. We

¹⁾ This work done under the auspices of the U.S. Atomic Energy Commission and has been published in the Physical Review.

²⁾ Now at the Southwestern State College, Weatherford, Okla.

³⁾ Now at Case Institute of Technology, Cleveland, Ohio.

⁴⁾ Numbers in brackets refer to References, page 421.

solve this three body problem only approximately by applying a no distortion approximation; that is, we imagine the deuteron is not distorted in the course of the $d + \text{He}^4$ interaction.

Thus we neglect the possibility of deuteron break up in the interaction. We hope to estimate the effects of the breakup in future work (in progress with Mr. JOHN H. CHRISTY). Our calculation of the deuteron spin polarization quantities is thus suspect at 8 and 10.3 MeV but may serve as a guide in the planning of experiments.

In order to formulate the model mathematically, we wrote the deuteron wave function in the form

$$\varphi(\mathbf{r}) = \left[u(r) + \frac{1}{\sqrt{8}} w(r) S_{12} \right] \chi_1^m$$

$$S_{12} = \frac{3}{r^2} (\boldsymbol{\sigma}_n \cdot \mathbf{r})(\boldsymbol{\sigma}_p \cdot \mathbf{r}) - 1 \quad (1)$$

where \mathbf{r} is $\mathbf{r}_p - \mathbf{r}_n$, χ_1^m is a triplet spin function, and $\boldsymbol{\sigma}_n$ and $\boldsymbol{\sigma}_p$ are spin operators for neutron and proton, respectively. The total wave function is taken to be

$$\Psi = \varphi(\mathbf{r}) F(\mathbf{q}) \quad (2)$$

where \mathbf{q} is the vector from the He^4 lump to the center of gravity of the deuteron

$$\mathbf{q} = \frac{1}{2} (\mathbf{r}_p + \mathbf{r}_n) - \mathbf{r}_{\text{He}}. \quad (3)$$

Substituting Ψ into the Schrödinger equation, we obtain the no distortion approximation by multiplying by $u(r) + w(r) S_{12}$ and integrating over \mathbf{r} . In this way we obtain an equation for $F(\mathbf{q}) \chi_1^m$, in which $V(\mathbf{q})$ appears as a potential, where

$$V(\mathbf{q}) = \int d\mathbf{r} \left(u + \frac{1}{\sqrt{8}} w S_{12} \right) \left[2V_c + V_{LS} (\boldsymbol{\sigma}_n + \boldsymbol{\sigma}_p) \cdot \left(\mathbf{q} + \frac{1}{2} \mathbf{r} \right) \right] \times \left(\frac{1}{2} \nabla_q - \nabla_r \right) \left(u + \frac{1}{\sqrt{8}} w S_{12} \right). \quad (4)$$

In equation (4), V_c and V_{LS} (the nucleon He^4 optical model potentials) have $|\mathbf{q} + 1/2 \mathbf{r}|$ as argument. Terms with $\mathbf{q} - 1/2 \mathbf{r}$, which may also appear with $1/2 \nabla_q + \nabla_r$, have been transformed by the substitution $\mathbf{r} \rightarrow -\mathbf{r}$ in deriving equation (4).

One may wonder about the question of conservation of total angular momentum. The $V(\mathbf{q})$ given by equation (4) is an operator; we have not yet made a partial wave expansion of $F(\mathbf{q}) \chi_1^m$.

We find by performing the azimuthal integrations in equation (4) (referring \mathbf{r} to \mathbf{q} as polar axis)

$$V(\mathbf{q}) = V_c(q) + V_{LS}(q) (\boldsymbol{\sigma}_n + \boldsymbol{\sigma}_p) \cdot \mathbf{q} \times \nabla_q + V_T(q) \frac{\boldsymbol{\sigma}_n \cdot \mathbf{q} \boldsymbol{\sigma}_p \cdot \mathbf{q}}{q^2} \quad (5)$$

where [6]

$$\left. \begin{aligned} V_C(q) &= 2 \int d\mathbf{r} u'(r) V_C \left(\left| \mathbf{q} + \frac{1}{2} \mathbf{r} \right| \right) u'(r) + \\ &\quad + 2 \int d\mathbf{r} u'(r) V_C \left(\left| \mathbf{q} + \frac{1}{2} \mathbf{r} \right| \right) w'(r), \\ V_{LS}(q) &= \frac{1}{2} \int d\mathbf{r} u'(r) V_{LS} \left(\left| \mathbf{q} + \frac{1}{2} \mathbf{r} \right| \right) u'(r) + \\ &\quad + \frac{1}{4} \int d\mathbf{r} u'(r) V_{LS} \left(\left| \mathbf{q} + \frac{1}{2} \mathbf{r} \right| \right) u'(r) \cos(\mathbf{q}, \mathbf{r}) \frac{r}{q} + \\ &\quad + \frac{1}{2} \int d\mathbf{r} u'(r) V_{LS} \left(\left| \mathbf{q} + \frac{1}{2} \mathbf{r} \right| \right) w'(r) \sin^2(\mathbf{q}, \mathbf{r}), \\ V_T(q) &= 4 \int d\mathbf{r} u'(r) V_C \left(\left| \mathbf{q} + \frac{1}{2} \mathbf{r} \right| \right) w'(r) P_2(\mathbf{q}, \mathbf{r}). \end{aligned} \right\} \quad (6)$$

In equation (6), we have used the substitutions

$$u' = u - \frac{w}{\sqrt{8}}, \quad (7)$$

$$w' = 3 \frac{w}{\sqrt{8}}.$$

Also (\mathbf{q}, \mathbf{r}) means the angle between \mathbf{q} and \mathbf{r} . We have neglected integrals involving w'^2 (because the percent of D state in the deuteron is small).

In calculations, we have used for the deuteron wave function [7]

$$\begin{aligned} u(r) &= N \cos \delta [1 - \exp(-\beta x)] \exp(-x), \\ w(r) &= N \sin \delta [1 - \exp(-\gamma x)] \exp(-x) \\ &\quad \left[1 + \frac{3(1 - \exp(-\gamma x))}{x} + \frac{3(1 - \exp(-\gamma x))^2}{x^2} \right], \end{aligned} \quad (8)$$

$$x = \alpha r$$

$$\begin{array}{lll} N = 0.875041 & \gamma = 2.0170 & \cos \delta = 0.99947 \\ \beta = 4.7533 & \sin \delta = 0.03356 & \alpha = 0.23181750 f^{-1} \end{array}$$

and for the nucleon He^4 optical model potential [5]

$$\left. \begin{aligned} V_C(r) &= V_C / \left[1 + \left(\frac{r}{D} - 1 \right) \exp \left(\frac{r-R}{D} \right) \right], \\ V_{LS}(r) &= \bar{V}_{LS} \exp \left(\frac{r-R}{D} \right) / \left[\dots \right]^2, \end{aligned} \right\} \quad (9)$$

where (these values are rough average values from reference [5])

$$\left. \begin{aligned} V_C &= 57.6 \text{ MeV} \\ V_{LS} &= 16.75 \text{ MeV} \\ R &= 1.775 \text{ f} \\ D &= 0.8875 \text{ f} \end{aligned} \right\} \quad (10)$$

Graphs of $V_C(q)$, $V_{LS}(q)$, and $V_T(q)$ so calculated are shown in figure 1.

III. Qualitative Features of the Model

The nucleon He^4 optical model predicts a bound state of Li^5 (or He^5) if the exclusion principle is not taken into account. When the exclusion principle is taken into account, the bound state disappears because the amplitude of the properly anti-symmetrized wave function formed from the un-anti-symmetrized wave function corresponding to this bound state vanishes. Essentially, one is trying to put three protons (or neutrons) in the 1 S shell in anti-symmetrizing the wave function. These spurious bound states arise in other problems [8] and are well understood.

We must anticipate that spurious bound states will arise from the deep central potential shown in figure 1. In all, two S_1 bound states and one P_0 , one P_1 , and one P_2 bound states (the first and last with admixtures of D_1 and F_2 states, respectively) are found to exist with the potentials shown in figure 1.

The lowest S state is deep (more than 10 MeV of binding), as are the three P states (more than 5 MeV of binding). It is known from the mass defects of d , He^4 , and Li^6 that the binding energy of Li^6 relative to separated d and He^4 is 1.52 MeV, and the binding energy of the second S state agrees closely with this value.

Without further study, we accept the lowest S level and the three P levels as spurious in the sense that if we knew how to anti-symmetrize the corresponding wave functions, we would find the anti-symmetrized wave function to vanish. We accept the 2 S level as the ground state of Li^6 .

From a study of the γd reaction in Li^6 , FOLDY [1] has concluded that $r^{2\lambda}$ in Li^6 is given approximately by the size of a deuteron, and that

$\langle q^2 \rangle$ is much larger than $\langle r^2 \rangle$. We get automatically that $\langle r^2 \rangle$ is given by the size of a deuteron in our model, of course. $\langle q^2 \rangle$ will turn out to be large for two reasons: first, it will be related to the binding energy of d and He^4 relative to Li^6 (1.52 MeV) which is less than the deuteron binding energy (2.22 MeV). The fact that the bound state is a 2 S level means that there is a node in the wave function, which further increases $\langle q^2 \rangle$ over what one might expect. We find

$$\left. \begin{array}{ll} \langle r^2 \rangle = 11 \text{ } f^2 \text{ calculated} & \langle r^2 \rangle = 12 \text{ } f^2 \text{ Foldy} \\ \langle q^2 \rangle = 15 \text{ } f^2 & \langle q^2 \rangle = 22 \text{ } f^2 \end{array} \right\} \quad (11)$$

whereas, as FOLDY points out

$$\left. \begin{array}{ll} \langle r^2 \rangle = 41.80 \text{ } f^2 & \text{shell model} \\ \langle q^2 \rangle = 10.45 \text{ } f^2 & \end{array} \right\} \quad (12)$$

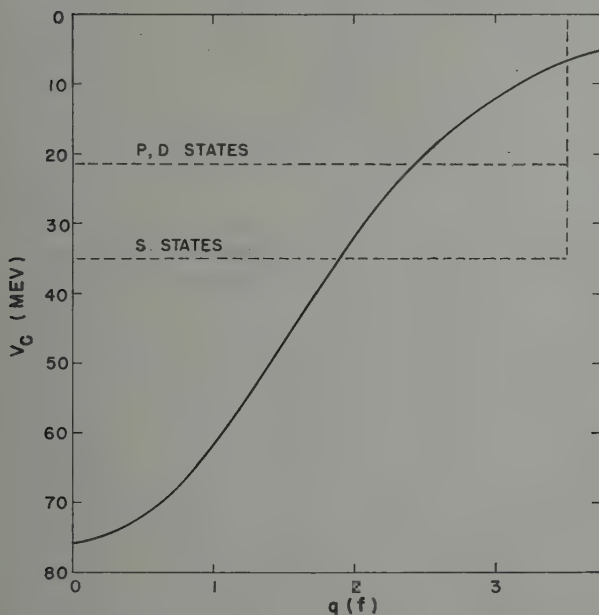


Figure 1a

The central term in the $d + \text{He}^4$ interaction. The solid curve is calculated from the model; the dashed curve is an equivalent square well potential adjusted to fit certain data.

It has to be concluded that the $d + \text{He}^4$ model of Li^6 is superior to the shell model in this respect. We now calculate the location of the virtual (unbound) D levels in order to show that the $d + \text{He}^4$ model also works for these levels. We treat the virtual D levels by calculating scattering phase shifts [9], of course.

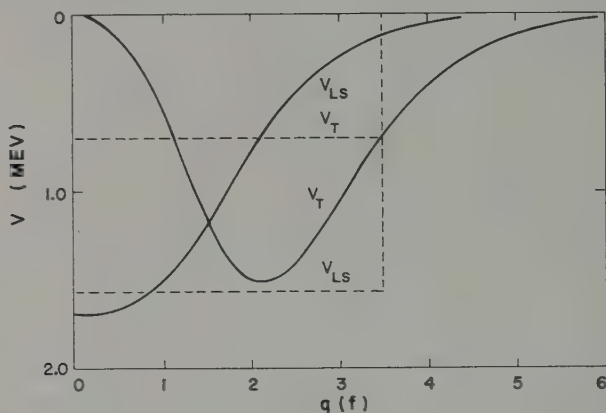


Figure 1b

The tensor and spin orbit terms in the $d + \text{He}^4$ interaction. The solid curves are calculated from the model; the dashed curves are equivalent square well potentials adjusted to fit certain data.

We anticipate the following qualitative features. The S phase shift starts at 2π at zero energy and decreases with energy; that is (when the 2π is subtracted from it) the S phase shift will look something like the S phase shift for hard sphere scattering for some radius hard sphere. This behavior agrees with the result of GALONSKY and McELLISTREM [2]. The P phase shifts start at π at zero energy and decrease with energy. Because the tensor and spin orbit terms shown in figure 1 are weak, compared to the central term, there will not be much J splitting unless there is a resonance. Calculation shows there is no resonance and (as expected) little J splitting. This behaviour also agrees with the results of GALONSKY and McELLISTREM, who found small, negative unsplit P phase shifts.

By inspection of figure 1, and from a knowledge of the interval rules 10 for the spin orbit and tensor terms in equation (5), it can be seen that the order of the D levels as given by GALONSKY and McELLISTREM is the same as the order given by the $d + \text{He}^4$ model.

Only detailed computation can confirm whether or not the magnitude of the S phase shift is correct, whether or not the D phase shifts pass

through 90° at the right energy and with the right level width, and whether or not the tensor coupling of the $^3S_1 + ^3D_1$ state is negligible as GALONSKY and McELLISTREM assumed. We may summarize our calculations very shortly by saying simply that everything calculated from the $d + \text{He}^4$ model does, in fact, agree with the results of GALONSKY and McELLISTREM, and that the $d + \text{He}^4$ model makes it possible to extrapolate their work to 8 and 10.3 MeV, at which energies the tensor coupling is important.

IV. Summary of Calculations Based on the Model

The $^3S_1 + ^3D_1$ phase shifts, including the coupling constant, are shown as a function of energy in figure 2. The coupling parameter 2ϵ is negligible for $E_d < 4.5$ MeV, and the 3S_1 and 3D_1 phase shifts are in reasonable (if not excellent) agreement with the phase shifts of GALONSKY and McELLISTREM.

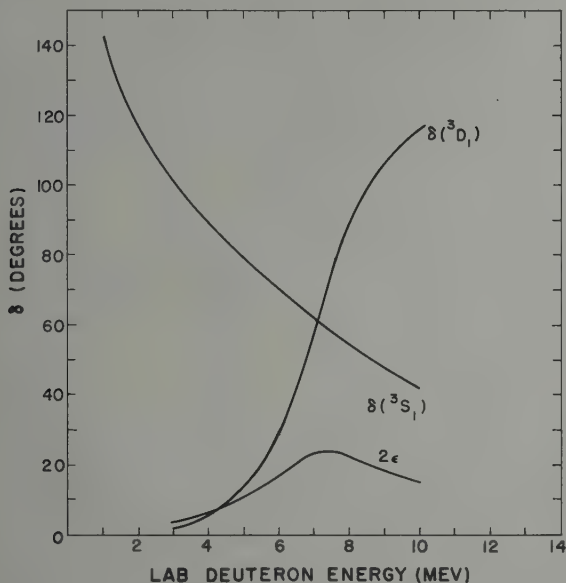


Figure 2

$^3S_1 + ^3D_1$ phase shifts calculated from the model as a function of energy

Rather than calculating the 3D_2 and 3D_3 phase shifts directly from the model, we have adjusted a 'phenomenological' square well potential

central, tensor, and spin orbit terms to fit the following data: the 2 S level must have the right binding energy (1.52 MeV), the 3D_3 and 3D_2 phase shifts must pass through 90° at the energies given by GALONSKY and McELLISTREM, and the width of the 3D_3 resonance must agree with the width given by GALONSKY and McELLISTREM. This last condition determines the range of the square well (we assume that all three terms have the same range) and the first three conditions determine the depth of each term⁵). This square well potential is compared with the model potential in figure 1. The agreement is reasonable. P and 3D_2 and 3D_3 phase shifts calculated from the square well potential are given in table 1 as a function of energy.

We have used phase shifts taken from table 1 and figure 2 as a starting point for a phase shift analysis of the 8 and 10.3 MeV data. The phase shifts which we find to give the best fit to the data are similar to the phase shifts used as a starting point as shown in table 2a; however, the magnitude of the P phase shift is much smaller than expected from table 1, and also smaller than expected from a graphical extrapolation of GALONSKY and McELLISTREM's phase shift. The quality of the fit to the data is shown in tables 2b and 2c; the *rms* deviation is a little over twice the errors assigned by the experimentalists in the case of 10.3 MeV.

The quantities relevant to experiments designed to produce or analyze beams of polarized deuterons are the expectation values of four operators [11]. These four quantities are denoted differently by various authors.

WOLFENSTEIN's notation [12]	=	STAPP's notation	
$\langle T_{20} \rangle$	=	$t/\sqrt{2}$	$\left. \begin{array}{l} \\ \\ \\ \end{array} \right\} \quad (13)$
$\langle T_{11} \rangle$	=	$-u/\sqrt{3}$	
$\langle T_{21} \rangle$	=	$-v/\sqrt{3}$	
$\langle T_{22} \rangle$	=	$-w/2\sqrt{3}$	

The quantities t , u , v , w are given in table 3 as a function of angle for the two energies and also 4.5 MeV. They have been calculated at lower energies (in the vicinity of the 3D_3 resonance, namely 1.1 MeV) by PONDROM [13] and also at 2.5 and 3.5 MeV by PHILLIPS [14]. We have checked these calculations.

⁵) This is not really so since as indicated in fig. 1 we have used different central terms in the S and D states. Thus the square well potential in fig. 1 is 'a' potential (and not 'the' potential) which fits the D_2 and D_3 phase shifts of GALONSKY and McELLISTREM (see also remarks in footnote to table I).

Table 1

Phase shifts versus energy calculated from the square well potentials shown in fig. 1*.

The φ_l are Coulomb phase shifts $\varphi_0 = 0$, $\varphi_l = \varphi_{l-1} + 2 \arctan \eta/l$.

E (MeV)	$\delta(P_0) + \frac{\varphi_1}{2}$	$\delta(P_1) + \frac{\varphi_1}{2}$ (radians)	$\delta(P_2) + \frac{\varphi_1}{2}$	$\delta(D_2) + \frac{\varphi_2}{2}$	$\delta(D_3) + \frac{\varphi_2}{2}$
1	0.3692	0.3749	0.3828	0.6428	0.8114
2	0.1377	0.1530	0.1757	0.4969	0.3531
3	-0.0417	-0.0189	0.0165	0.5509	0.2237
4	-0.1947	-0.1663	-0.1206	1.1065	0.1168
5	-0.3290	-0.2964	-0.2424	-0.9075	0.0226
6	-0.4489	-0.4131	-0.3520	-0.5949	-0.0632
7	-0.5572	-0.5187	-0.4515	-0.5368	-0.1429
8	-0.6558	-0.6150	-0.5422	-0.5435	-0.2178
9	-0.7461	-0.7033	-0.6252	-0.5734	-0.2887
10	-0.8291	-0.7844	-0.7012	-0.6133	-0.3562
11	-0.9057	-0.8592	-0.7710	-0.6576	-0.4207
14	-1.1029	-1.0509	-0.9468	-0.7980	-0.6532

*) The square well potentials in fig. 1 would give the D phase shifts shown; however, the potential actually used in this calculation is $V_C = 22.100$ MeV, $V_{LS} = 1.3667$ MeV, $V_T = 0$, so that the P phase shifts should be slightly different. However, the main point is that the P phase shifts are negative and not much split; their precise magnitude is not important.

Table 2a

Phase shift analysis for 8 and 10.3 MeV

E	8 MeV		10.3 MeV	
	starting point	end point	starting point	end point
$\delta(^3S_1)$	0.9840	0.9489	0.7120	0.7339
$\delta(^3D_1) + \varphi_2/2$	1.5411	1.7764	2.0516	2.2595
2ϵ	0.3990	0.3990	+0.2500	+0.2500
$\delta(^3D_2) + \varphi_2/2$	-0.5435	-1.266	-0.6133	-0.6263
$\delta(^3D_3) + \varphi_2/2$	-0.2178	-0.2965	-0.3562	-0.1760
$\delta(^3P_0) + \varphi_1/2$	-0.6558	+0.1566	-0.8291	+0.4111
$\delta(^3P_1) + \varphi_1/2$	-0.6150	-0.1566	-0.7844	-0.1212
$\delta(^3P_2) + \varphi_1/2$	-0.5422	-0.1566	-0.7012	-0.1627

For 8 MeV, the Coulomb phase shifts are $\varphi_1/2 = 0.1566$ radians, $\varphi_2/2 = 0.2354$ radians, and for 10.5 MeV, $\varphi_1/2 = 0.1383$ radians, $\varphi_2/2 = 0.2077$ radians.

V. Summary

The model we have given for the $d + \text{He}^4$ interaction may be of interest for $d + \text{heavy nucleus}$ interaction.

Table 2b
Quality of fit to differential cross section at 8 MeV

$\theta(\text{cm})$ (degrees)	$\sigma_{exp}(\text{barns})$	$\sigma_{calc}(\text{barns})$
30	0.3300	0.3520
40	0.1760	0.1838
50	0.0920	0.0820
60	0.0395	0.0385
70	0.0415	0.0395
80	0.0660	0.0623
90	0.0830	0.0837
100	0.0950	0.0900
110	0.0860	0.0822
120	0.0730	0.0734
130	0.0750	0.0809
140	0.1070	0.1153
150	0.1860	0.1747
160	0.2400	0.2431

Table 2c
Quality of fit to differential cross section at 10.3 MeV

$\theta(\text{cm})$ (degrees)	σ_{exp} (barns)	$\sigma_{calc}(\text{barns})$	$\theta(\text{cm})$ degrees	$\sigma_{exp}(\text{barns})$	$\sigma_{calc}(\text{barns})$
18.4	0.452	0.5445	100.6	0.0679	0.0713
22.0	0.356	0.3797	101.2	0.0709	0.0710
23.0	0.326	0.3479	103.6	0.0668	0.0694
29.4	0.186	0.2093	109.2	0.0616	0.0629
34.0	0.143	0.1460	110.6	0.0587	0.0608
36.6	0.111	0.1176	112.4	0.0576	0.0580
40.8	0.0761	0.0803	114.6	0.0519	0.0542
43.8	0.0571	0.0593	119.8	0.04447	0.0453
48.2	0.0369	0.0361	120.6	0.0418	0.0440
51.0	0.0223	0.0256	124.6	0.0378	0.0381
55.4	0.0105	0.0155	127.2	0.0362	0.0351
58.4	0.00975	0.0125	129.3	0.0370	0.0332
62.5	0.0118	0.0129	133.6	0.0354	0.0312
65.4	0.0171	0.0158	134.4	0.0371	0.0312
69.4	0.0217	0.0225	137.8	0.0400	0.0320
72.2	0.02535	0.0285	140.6	0.0436	0.0340
76.1	0.0343	0.0377	141.7	0.0473	0.0351
78.8	0.04115	0.0444	145.3	0.04655	0.0401
82.6	0.0481	0.0532	147.4	0.05365	0.0437
85.2	0.0548	0.0586	149.0	0.05845	0.0468
85.4	0.05785	0.0590	152.3	0.0706	0.0540
91.6	0.0629	0.0684	154.1	0.07275	0.0582
95.2	0.0694	0.0712	155.4	0.07425	0.0613
97.7	0.0691	0.0718	157.4	0.0824	0.0662

Table 3a
The function t versus θ

$\theta(\text{cm})$ (degrees)	4.5 MeV	8 MeV	10.3 MeV
20	0.2155	—	-0.005
30	0.3327	-0.1044	-0.045
40	0.1938	-0.2256	-0.115
50	-0.0899	-0.4663	-0.285
60	-0.3618	-0.6060	-0.240
70	-0.2698	-0.0285	0.150
80	0.1778	0.3170	0.220
90	0.4155	0.3712	0.235
100	0.2675	0.3192	0.250
110	-0.0790	0.1777	0.255
120	-0.2920	-0.0621	0.230
130	-0.1749	-0.2526	0.080
140	0.1300	-0.2323	-0.195
150	0.4247	-0.1285	-0.305
160	0.6339	-0.0465	-0.310
170	0.7527	—	-0.310

Table 3b
The function u versus θ

$\theta(\text{cm})$ (degrees)	4.5 MeV	8 MeV	10.3 MeV
20	-0.2449	—	0.23
30	0.4961	0.6615	0.395
40	0.7173	0.9326	0.595
50	0.9201	1.093	0.61
60	0.9944	0.382	-0.40
70	0.7324	-0.740	-0.76
80	0.2773	-0.514	-0.31
90	0	-0.024	0
100	-0.1056	0.433	0.285
110	-0.1726	0.810	0.57
120	-0.2509	0.884	0.875
130	-0.3019	0.423	0.98
140	-0.2934	-0.093	0.52
150	-0.2403	-0.273	0.095
160	-0.1660	-0.243	—
170	-0.0841	—	—

It is our hope that the analysis of the 8 and 10.3 MeV data has led to correct estimates of the quantities required to plan experiments with polarized deuteron beams.

Table 3c
The function v versus θ

$\theta(\text{cm})$ (degrees)	4.5 MeV	8 MeV	10.3 MeV
20	0.1139	—	0
30	0.3292	0.0424	0
40	0.5421	0.0910	0
50	0.7426	0.1650	0
60	0.8433	0.1913	-0.06
70	0.6664	0.0043	-0.11
80	0.2916	-0.1044	-0.115
90	0.	-0.1421	-0.12
100	-0.2155	-0.1762	-0.125
110	-0.4485	-0.2270	-0.115
120	-0.6624	-0.2794	-0.07
130	-0.7369	-0.2647	0.08
140	-0.6596	-0.1812	0.24
150	-0.5074	-0.1060	0.225
160	-0.3363	-0.0577	0.13
170	-0.1664	—	—

Table 3d
The function w versus θ

$\theta(\text{cm})$ (degrees)	4.5 MeV	8 MeV	10.3 MeV
20	-0.0885	—	-0.045
30	-0.3802	-9.2434	-0.163
40	-0.8268	-0.5699	-0.44
50	-1.3568	-1.115	-0.98
60	-1.5953	-1.226	-0.8
70	-0.8091	0.3131	0.60
80	0.6021	1.029	0.73
90	1.2460	1.047	0.65
100	0.8842	0.8240	0.52
110	-0.0782	0.3703	0.315
120	-0.9736	-0.3351	-0.055
130	-1.2392	-0.8482	-0.62
140	-0.9820	-0.7421	-0.85
150	-0.5860	-0.4186	-0.52
160	-0.2615	-0.1743	-0.23
170	-0.0648	—	—

Appendix

The partial wave expansion of $F(\mathbf{q}) x_m^1$ is exactly the same as it is for the triplet state in nucleon-nucleon scattering. The interval rule for

the term $(\sigma_n + \sigma_p) \cdot \mathbf{q} \times \nabla_q$ is the same as the interval rule for the spin orbit term; namely

$$\frac{1}{2} [J(J+1) - L(L+1) - S(S+1)]$$

and since $\sigma_n \cdot \mathbf{q} \sigma_p \cdot \mathbf{q}/q^2$ is $(S_{12} - 1)/3$, its properties when operating on states of definite J and L may be read from a table of the properties of S_{12} (see, for example, ASHKIN and WU, Phys. Rev. 73, 982 (1948) their equation (26)).

We have used the so called nuclear bar phase shifts in parametrizing the scattering matrix. The formulas for the elements of the scattering matrix in terms of these phase shifts are given in H. P. STAPP's thesis (UCRL 3098, unpublished), p. 107, equation A. 20. GALONSKY and McELLISTREM introduce 5 scattering amplitudes A, B, C, D, E and give formulae for these in terms of the elements of the scattering matrix (see their Appendix I, final equation). STAPP, on the other hand, uses only 4 scattering amplitudes a, b, c, d . (See his equation (22), p. 75.) Therefore Galonsky and McEllistrem's amplitudes must be connected; we find

$$\frac{E \sin^2 \theta}{\sqrt{2}} = A - B + \cos \theta (C - D)$$

and

$$b = - \frac{(C+D) \sin \theta i}{2}$$

$$d = \frac{-C+D}{2}$$

$$a = \frac{1}{3} (2A + B)$$

$$c = -2A + 2B - \frac{3}{2} C \cos \theta + \frac{3}{2} D \cos \theta$$

This last formula is, indirectly (via GALONSKY and McELLISTREM's last equation in their Appendix I and STAPP's equation A. 20), an expression for STAPP's amplitudes in terms of the bar phase shifts.

For the calculation of quantities relating to deuteron spin polarization phenomena, we use STAPP's equations on his pp. 76 *et seq.*

REFERENCES

- [1] L. L. FOLDY, to be submitted to Phys. Rev.
- [2] A. GALONSKY and M. T. McELLISTREM, Phys. Rev. 98, 590 (1955).
- [3] GALONSKY, DOUGLAS, HAEBERLI, McELLISTREM, and RICHARDS, Phys. Rev. 98, 586 (1955).

- [4] ALLRED, FROMAN, HUDSON, and ROSEN, Phys. Rev. *82*, 786 (1951); BURGE, BURROWS, and GIBSON, Proc. Roy. Soc. (London) *A270*, 534 (1952).
- [5] J. L. GAMMEL and R. M. THALER, Phys. Rev. *109*, 2041 (1958).
- [6] We use the symbols V_C and V_{LS} in two different ways, but there is no reason to confuse them.
- [7] L. HULTHEN and L. T. HEDIN, Kon. Norske Vidensk. Selsk. Forkand. *37*, No. 3 (1958).
- [8] P. SWAN, Proc. Roy. Soc. (London) *A228*, 10 (1955).
- [9] The literature on the theory of $d + \text{He}^4$ scattering (definition and calculation of phase shifts and connection between phase shifts and scattering amplitudes) is reviewed in the Appendix.
- [10] See the Appendix for the interval rules.
- [11] See the Appendix for an outline of the theory.
- [12] See W. LAKIN, Phys. Rev. *98*, 139 (1955).
- [13] See L. G. PONDROM, Phys. Rev. Letters *2*, 386 (1959).
- [14] R. J. N. PHILLIPS, Phys. Rev. Letters *3*, 101 (1959).

Polarization Contours for $T - \alpha$ and $He^3 - \alpha$ Scattering¹⁾

By J. L. GAMMEL and R. M. THALER²⁾

Los Alamos Scientific Laboratory, University of California

We have made a phase shift analysis of the $T - \alpha$ elastic scattering data of BROLLEY and ROSEN [1] at 9.225 MeV (tritium laboratory energy; actually 12.3 MeV alphas were scattered from tritium). PHILLIPS and MILLER [2] have already analyzed the lower energy $He^3 - \alpha$ data, and found a negative $S_{1/2}$ phase shift, negative and unsplit $P_{1/2}$ and $P_{3/2}$ phase shifts, zero $D_{3/2}$, $D_{5/2}$, and $F_{5/2}$ phase shifts, and a $F_{7/2}$ phase shift which shows a resonance at about 5.5 MeV (laboratory He^3 energy). Our phase shifts for 9.225 MeV are reasonable graphical extrapolations of PHILLIPS' and MILLER's phase shifts. The phase shifts are shown in figure 1 as a function of energy.

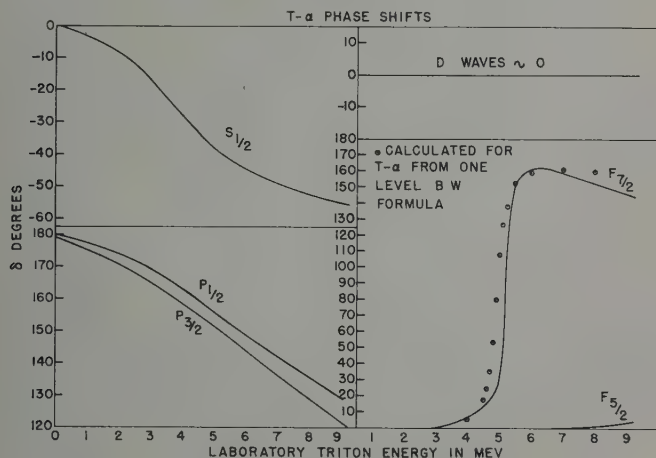


Figure 1

¹⁾ This work done under the auspices of the United States Atomic Energy Commission.

²⁾ Presently at the Case Institute of Technology, Cleveland, Ohio.

The $F_{1/2}$ resonance is given by an optical model potential 22 MeV deep and 4 f wide.

Using the phase shifts shown in figure 1, we have calculated the T- α or He³- α polarization as a function of energy. The results are shown in figure 2. This polarization function is only semi-quantitative, and applies to either T- α or He³- α scattering. It provides a basis for planning the experiment described in the accompanying note by BROLLEY, GAMMEL, and ROSEN.

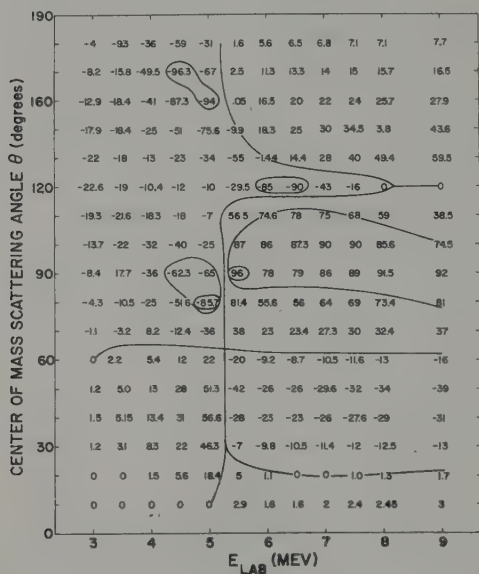


Figure 2

REFERENCES

- [1] E. BROLLEY, Jr. and L. ROSEN, to be published in Phys. Rev.
- [2] T. D. MILLER and G. C. PHILLIPS, Phys. Rev. *112*, 2048 (1958) and *115*, 1268 (1959).

Deuteron Triple-Scattering Experiments¹⁾

By R. J. N. PHILLIPS, A.E.R.E., Harwell

Abstract. Such experiments are needed in general to determine the scattering matrix for deuterons on a spin-0 target. This kind of measurement is familiar in the study of nucleon scattering, but the deuteron spin 1 introduces unfamiliar features.

Introduction

This subject may be unpopular with experimenters, for even double scattering is difficult enough, but sooner or later it will have to be taken seriously.

The scattering amplitude for deuterons at a spinless target is a matrix \mathfrak{M} in spin space, of the form [2]

$$\mathfrak{M} = a + ib N_i S_i + c \left(N_i N_j - \frac{1}{3} \delta_{ij} \right) S_{ij} + d (D_i D_j - E_i E_j) S_{ij}, \quad (1)$$

(assuming parity conservation and time-reversal invariance). S is the deuteron spin operator, and $S_{ij} = 1/2 (S_i S_j + S_j S_i - 2/3 \delta_{ij})$. \mathbf{N} , \mathbf{D} and \mathbf{E} are unit vectors in the directions $\mathbf{k}_i \times \mathbf{k}_f$, $\mathbf{k}_i + \mathbf{k}_f$ and $\mathbf{k}_f - \mathbf{k}_i$, respectively, where \mathbf{k}_i and \mathbf{k}_f are the initial and final deuteron relative momenta (i. e. momenta in the c. m. frame). The complex coefficients a , b , c , and d are functions of energy and scattering angle.

Single- and double-scattering provide five independent measurements at any angle [2, 3], whereas in general²⁾ we need seven to determine \mathfrak{M} (apart from the overall phase, which does not enter). More data may be found by triple-scattering experiments. These measure the effects of initial polarization on final polarization. Thus the second scattering is the interesting one: the first and third just produce and analyze polarization, and may be replaced by other processes with the same effects (e. g. polarized ion source, nuclear reaction).

¹⁾ A fuller account of this work is found in ref. [1]³⁾.

²⁾ If inelastic processes are negligible, unitarity arguments like those of ref. 4 give four integral constraints on a , b , c and d . Four measurements at all angles can then determine \mathfrak{M} , including the phase.

³⁾ Numbers in brackets refer to References, page 428.

It would be tedious to list all possible triple-scattering measurements (various combinations of initial polarization and final analysis), and their values in terms of \mathfrak{M} . Anyway this is straightforward. Instead we briefly discuss how to control initial polarization, and how to analyze with a spin-0 scatterer.

Formalism

To describe the polarization of a deuteron beam we introduce the spherical tensors Ω_{JM} (see e. g. refs [3, 5], spin operators which transform like the spherical harmonics Y_{JM} and obey

$$\frac{1}{3} \text{trace } \Omega_{JM} \Omega_{J'M'}^* = \delta_{JJ'} \delta_{MM'}. \quad (2)$$

If their expectation values are $\langle \Omega_{JM} \rangle$, the density matrix ϱ can be written

$$\varrho = \frac{1}{3} \left\{ 1 + \sum_{\substack{J \\ M \leq J}} \langle \Omega_{JM} \rangle \Omega_{JM}^* \right\}, \quad (3)$$

where we have put $\Omega_{00} = 1$, and normalized $\text{trace } \varrho = 1$. The eight coefficients $\langle \Omega_{JM} \rangle$ specify the polarization completely.

If the density matrix is ϱ_i initially, it becomes $\varrho_f = \mathfrak{M} \varrho_i \mathfrak{M}^*$ after scattering. The final expectation value of any spin operator χ is then $\text{trace } \varrho_f \chi / \text{trace } \varrho_f$. Thus the new quantities measured by triple-scattering are essentially terms, or sums of terms, like

$$\text{trace } \mathfrak{M} \Omega_{JM}^* \mathfrak{M}^* \Omega_{J'M'}, \quad (4)$$

with $J, J' > 0$. Ω_{JM}^* and $\Omega_{J'M'}$, which refer to initial and final polarization, need not have the same axes: we prefer to take the axis OZ along the laboratory direction of motion in each case.

Control of Initial Polarization

For nucleons, polarization is simply a vector which can be rotated into any desired direction by magnetic fields. For deuterons, the polarization of a given beam cannot be adjusted arbitrarily, but some manipulation is still possible.

In a magnetic field the spin axes rotate [3, 6], while the polarization relative to them is unchanged. Suppose these axes rotate right-handedly about the direction of motion (in a solenoidal field) through an angle ϕ . Then the density matrix *referred to the initial axes* is

$$\varrho = \frac{1}{3} \left\{ 1 + \sum_{J,M} \langle \Omega_{JM}^{(i)} \rangle \Omega_{JM}^* e^{iM\phi} \right\}, \quad (5)$$

where $\langle \Omega_{JM}^{(i)} \rangle$ are the initial expectation values.

Hence some components of polarization can in effect be eliminated by averaging over suitable values of ϕ . For instance, we can remove components with $M = \pm 1$ by averaging over $\phi = 0$ and π ; $M = \pm 2$ by using $\phi = 0$ and $\pi/2$; both types simultaneously by using $\phi = 0, \pi/2, \pi$ and $3\pi/2$.

Other effects can be achieved by rotating the spin axis OZ out of the direction of motion; this is harder, since the deuteron g -factor is close to 1.

Analysis with a Spin-0 Scatterer

Consider a spin-0 scatterer which is relatively heavy, so that laboratory and c.m. frames are essentially the same (the case with recoil is similar). Let the incident polarization be given by $\langle \Omega_{JM}^{(0)} \rangle$, with spin axis OZ along the incident motion. Then the differential cross-section proves to be

$$I = I_0 \left\{ 1 - \sum_{J,M} (-1)^M e^{iM\phi} \langle \Omega_{JM}^{(0)} \rangle \langle \Omega_{JM} \rangle \right\}, \quad (6)$$

where I_0 is the unpolarized cross-section, and $\langle \Omega_{JM}^{(0)} \rangle$ is the polarization that would have been set up in an initially unpolarized beam, referred to the outgoing direction as Z -axis and the normal N as Y -axis. ϕ is the angle between N and the Y -axis of the incident polarization, (measured from the latter, right-handedly about the incident motion).

Let us suppose $\langle \Omega_{JM}^{(0)} \rangle$ are known (from double-scattering [2, 3, 7]; they have the property $\langle \Omega_{JM}^{(0)} \rangle = (-1)^{J-M} \langle \Omega_{J,-M}^{(0)} \rangle$. Then Eq. (6) can be re-written

$$\begin{aligned} I = I_0 \{ & 1 - \langle \Omega_{11}^{(0)} \rangle [\langle \Omega_{11} + \Omega_{1-1} \rangle \cos \phi - i \langle \Omega_{11} - \Omega_{1-1} \rangle \sin \phi] \\ & + \langle \Omega_{20}^{(0)} \rangle \langle \Omega_{20} \rangle \\ & - \langle \Omega_{21}^{(0)} \rangle [\langle \Omega_{21} - \Omega_{2-1} \rangle \cos \phi - i \langle \Omega_{21} + \Omega_{2-1} \rangle \sin \phi] \\ & + \langle \Omega_{22}^{(0)} \rangle [\langle \Omega_{22} + \Omega_{2-2} \rangle \cos 2\phi - i \langle \Omega_{22} - \Omega_{2-2} \rangle \sin 2\phi] \}. \end{aligned} \quad (7)$$

Clearly the terms in $\cos \phi$, $\cos 2\phi$, $\sin \phi$, $\sin 2\phi$ and the ϕ -independent term can be separated by measurements at suitable values of the azimuth ϕ (holding the scattering angle fixed). And the contributions to $\sin \phi$ and $\cos \phi$ proportional to $\langle \Omega_{11}^{(0)} \rangle$ and $\langle \Omega_{21}^{(0)} \rangle$ can also be separated, by repeating the measurements at another scattering angle. Thus seven of the eight components of incident polarization can be measured in principle, though of course a particular scatterer may be insensitive to some components.

To measure the last component $\langle \Omega_{10}^{(0)} \rangle$, we need to rotate the spin axis OZ out of the direction of motion.

Conclusions

Triple-scattering or equivalent measurements are needed in general to determine \mathfrak{M} for deuterons on spinless nuclei.

Unlike the nucleon case, it is not feasible to arrange for an arbitrary incident polarization at the scattering of interest. However, some control is possible, and certain components can be «averaged out».

Seven out of eight components of polarization can be analyzed with a calibrated spin-0 scatterer. The eighth requires a magnetic field.

Fortunately, only two new independent measurements⁴⁾ are needed, beside single- and double-scattering data. It will not be necessary to arrange a great variety of incident polarizations, nor to measure many final components.

REFERENCES

1. R. J. N. PHILLIPS, Harwell report AERE-R3306 (1960).
2. H. P. STAPP, California thesis, UCRL-3098 (1955); Phys. Rev. 107, 607 (1957).
3. W. LAKIN, Phys. Rev. 98, 139 (1955).
4. L. PUZIKOV, R. RYNDIN and J. SMORODINSKY, Nucl. Phys. 3, 436 (1957).
5. J. HAMILTON, *Theory of Elementary Particles* (Oxford: Clarendon Press), 1959.
6. G. R. SATCHLER, Oak Ridge report ORNL-2861 (1960).
7. R. J. N. PHILLIPS, Proc. Phys. Soc. 75, 317 (1960).

⁴⁾ Plus perhaps one or two others not algebraically independent, to resolve ambiguities in the solution for \mathfrak{M} .

Nucleon-Nucleon Polarization Experiments¹⁾

By R. J. N. PHILLIPS, A. E. R. E., Harwell

Abstract. Some simple considerations on the set of all possible measurements are given. At any scattering angle there are essentially twenty-five linearly independent measurements (though only nine can be wholly independent), of which only two require a polarized target.

Introduction

Many kinds of polarization experiment have been described and discussed in the literature (e.g. refs [1-6]²⁾ and references therein). We present here some general considerations on the set of all possible measurements at a given scattering angle.

The scattering amplitude for two given nucleons at a given angle is a matrix M in spin space. Assuming parity conservation, time-reversal invariance and charge-symmetry (for the n - p case), it has the form

$$M = a + i c (\sigma_N^{(1)} + \sigma_N^{(2)}) + m \sigma_N^{(1)} \sigma_N^{(2)} + (g + h) \sigma_P^{(1)} \sigma_P^{(2)} + (g - h) \sigma_K^{(1)} \sigma_K^{(2)}. \quad (1)$$

$\sigma^{(1)}$ and $\sigma^{(2)}$ are the nucleon spin operators. N , P and K are unit vectors in the directions $\mathbf{k}_i \times \mathbf{k}_f$, $\mathbf{k}_i + \mathbf{k}_f$ and $\mathbf{k}_f - \mathbf{k}_i$, where \mathbf{k}_i and \mathbf{k}_f are initial and final relative momenta. σ_N denotes $\boldsymbol{\sigma} \cdot \mathbf{N}$, etc. The complex coefficients a , c , m , g and h are functions of energy and angle. This notation follows STAPP [3].

Polarization experiments essentially measure the quantities

$$\text{trace } M X M^* Y \quad (2)$$

(apart from a possible divisor $\text{trace } M M^*$), where X and Y are the density matrix for incident polarization and the efficiency matrix for analyzing final polarization, respectively. In general X and Y contain several terms, but for a given experiment it is instructive to consider only the contribution not given by simpler experiments. These characteristic terms are shown schematically below.

¹⁾ A more detailed account of this work is given in ref. [1].

²⁾ Numbers in brackets refer to References, page 431.

Incident polarization \ Analysis	Cross section	One polarization	Both polarizations
None	$\text{tr } MM^*$	$\text{tr } MM^*\sigma$	$\text{tr } MM^*\sigma\sigma$
One nucleon	$\text{tr } M\sigma M^*$	$\text{tr } M\sigma M^*\sigma$	$\text{tr } M\sigma M^*\sigma\sigma$
Both nucleons . . .	$\text{tr } M\sigma\sigma M^*$	$\text{tr } M\sigma\sigma M^*\sigma$	$\text{tr } M\sigma\sigma M^*\sigma\sigma$

Linearly Independent Measurements

These characteristic terms are linear combination of the twenty-five quantities $|a|^2$, $\text{Re } ac^*$, $\text{Im } ac^*$, etc. However, at most nine³⁾ can be wholly independent, for there are only five independent complex coefficients a , c , etc., and their overall phase does not enter. On the other hand, nine measurements will not in general fix M uniquely. To resolve algebraic ambiguities, further *linearly independent* data are needed (which would also be a useful check on the experiments). Hence there is special interest in measurements which, though not fully independent, are at least linearly independent of each other.

We list the number of linearly independent data contributed by each type of experiment. Details of the characteristic terms themselves may be found in references [1] and [6] (there are a few typographical errors in the latter). For identical nucleons, a measurement at scattering angle Θ is equivalent to some measurement at $\pi - \Theta$; also the values of M at these angles are related. Hence both angles must be considered together, when counting measurements.

- (i) $\text{tr } M M^*$. One measurement.
- (ii) $\text{tr } M \sigma M^*$ or $\text{tr } M M^* \sigma$, (these two are related by time-reversal arguments). One measurement.
- (iii) $\text{tr } M \sigma M^* \sigma$. Eight linearly independent measurements: four from analyzing the «scattered» nucleon, four from the «recoil» nucleon. With identical nucleons, these are related by $\Theta \rightarrow \pi - \Theta$, but we still count eight measurements: see above. (Incidentally, (i) (iii) contain nine fully independent data).
- (iv) $\text{tr } M M^* \sigma \sigma$ or $\text{tr } M \sigma \sigma M^*$, (related by time-reversal). Four linearly independent measurements.

³⁾ When inelastic processes can be ignored, and measurements are made at all angles, unitarity imposes further integral constraints [6]. An appeal to charge independence may also be helpful [7]. Our remarks apply to the general case.

- (v) $\text{tr } M \sigma M^* \sigma \sigma$ or $\text{tr } M \sigma \sigma M^* \sigma$, (related by time-reversal). Ten measurements, but only nine are linearly independent of (i)–(iv).
 (vi) $\text{tr } M \sigma \sigma M^* \sigma \sigma$. Fifteen measurements, but only two are linearly independent of (i)–(v).

Conclusion

Although there are at most nine fully independent measurements at a given angle, further *linearly* independent data will generally be needed to resolve ambiguities in M . (They would also check the internal consistency of experiments, against systematic errors).

There are altogether twenty-five linearly independent measurements.

Experiments of types (i)–(iv), (up to triple-scattering and spin correlation experiments), provide fourteen linearly independent data, which should be more than enough (indeed, (i)–(iii) might suffice). Types (v) and (vi) would then be unnecessary.

In particular, a polarized target should not be necessary⁴). Type (vi) are the only measurements that definitely require one.

REFERENCES

- [1] R. J. N. PHILLIPS, Harwell report AERE-R3141 (1960).
- [2] L. WOLFENSTEIN, Ann. Rev. Nucl. Sci. **6**, 43 (1956).
- [3] H. P. STAPP, California thesis, UCRL-3098 (1955).
- [4] R. J. N. PHILLIPS, Rep. Progr. Phys. **22**, 562 (1959).
- [5] J. L. GAMMEL and R. M. THALER, Progress in Elementary Particle and Cosmic Ray Physics **5**, 99 (1960).
- [6] L. PUZIKOV, R. RYNDIN, and J. SMORODINSKY, Nucl. Phys. **3**, 436 (1957).
- [7] B. M. GOLOVIN, V. P. DZHELEPOV, V. S. NADEZHGIN and V. I. SATAROV, Zh. eksper. teor. Fiz. **36**, 433; see Soviet Physics – J.E.T.P., **36**, 302 (1959).

⁴) This does not mean that such a target would not be useful in performing more familiar measurements.

Optical Model Analysis of Proton-Nucleus Elastic Scattering Data in the Energy Range 8-17 MeV

By F. BJORKLUND, G. CAMPBELL, and S. FERNBACH

Lawrence Radiation Laboratory, Livermore, California

The proton nucleus elastic scattering data in the energy range 8 to 17 MeV have been analyzed using the Coulomb potential of a uniform charge distribution within a sphere of radius R_0 plus the following nuclear potential

$$V = V_{CR} \varrho(r) + i V_{CI} q(r) + V_{SR} \left(\frac{\hbar}{\mu c} \right)^2 \frac{1}{r} \frac{d\varrho(r)}{dr} \boldsymbol{\sigma} \cdot \mathbf{l}$$

where

$$\varrho(r) = \frac{1}{1 + \exp \left(\frac{r - R_0}{a} \right)},$$

and

$$q(r) = \exp \left[- \left(\frac{r - R_0}{b} \right)^2 \right],$$

$$R_0 = r_0 A^{1/3}.$$

The notation used is that of RIESENFELD and WATSON. For all elements and energies $a = 0.65$, $b = 1.2$, $V_{CI} = 11$ and $R_0 = 1.25$. At each energy V_{CR} was increased with increasing mass number in the following way,

$$V_{CR} = V_0(E) + Z/A^{1/3}$$

V_0 decreased smoothly from 44.5 at 8 MeV to 40.7 at 17 MeV. The polarization and differential cross section curves are less sensitive to small changes in V_{SR} than to changes in the other parameters.

At 14 and 17 MeV $V_{SR} = 8 \pm 1$ MeV. At energies below 14 MeV it was necessary to reduce V_{SR} to 5 ± 1 MeV to obtain agreement with the experimental polarization and differential cross section data. Preliminary calculations indicate that the spin-orbit potential may be even smaller below 8 MeV.

The agreement with experimental data is good for medium weight and heavy nuclei becoming very poor for light elements.

For references to experimental data and other theoretical work see the review articles by: HELMUT FAISSNER, *Ergebnisse der exakten Naturwissenschaften*, Bd. XXXII, 1959, E. J. Squires A.E.R.E. t/p. 75.

Basel Convention

In nuclear interactions the positive polarization of particles with spin $1/2$ is taken in the direction of the vector product $\mathbf{k}_i \times \mathbf{k}_0$, where \mathbf{k}_i and \mathbf{k}_0 are the circular wave vectors of the incoming and outgoing particles respectively.

This agreement is called the 'Basel Convention'.